EMERGING INFECTIOUS DISEASES®

CDC Centers for Disease Control and Prevention

Fungal Infections

July 2023

Biho Takashi (active ca. 1890-1930), *Bat in Moon*, ca. 1905. Color woodblock print on paper, 9 1/4 in x 9 9/16 in /23.5 cm x 24.3 cm. Brooklyn Museum, Brooklyn, New York, USA. Gift of the Estate of Dr. Eleanor Z. Wallace, 2007.32.4

EMERGING INFECTIOUS DISEASES®

Emerging Infectious Diseases is published monthly by the Centers for Disease Control and Prevention, 1600 Clifton Rd NE, Mailstop H16-2, Atlanta, GA 30329-4027, USA. Telephone 404-639-1960; email, eideditor@cdc.gov

EMERGING INFECTIOUS DISEASES®

Fungal Infections **July 2023**

On the Cover

Biho Takashi (active ca. 1890–1930), *Bat in Moon*, ca. 1905. Color woodblock print on paper, 9 1/4 in x 9 9/16 in/23.5 cm x 24.3 cm. Brooklyn Museum, Brooklyn, New York, USA. Gift of the Estate of Dr. Eleanor Z. Wallace, 2007.32.4

About the Cover p. 1499

Synopses

Research

Medscape EDUCATION ACTIVITY

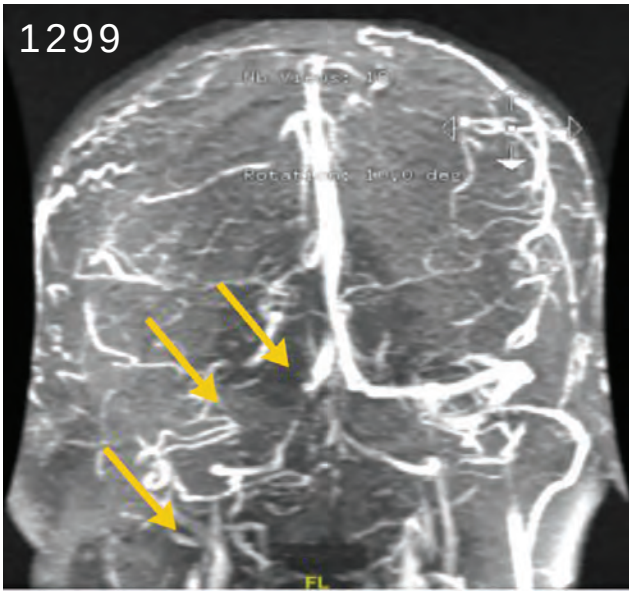

EMERGING INFECTIOUS DISEASES®
July 2023

Dispatches

EMERGING INFECTIOUS DISEASES®
July 2023

Research Letters

Comment Letters

Books and Media

About the Cover

Etymologia

Online Report

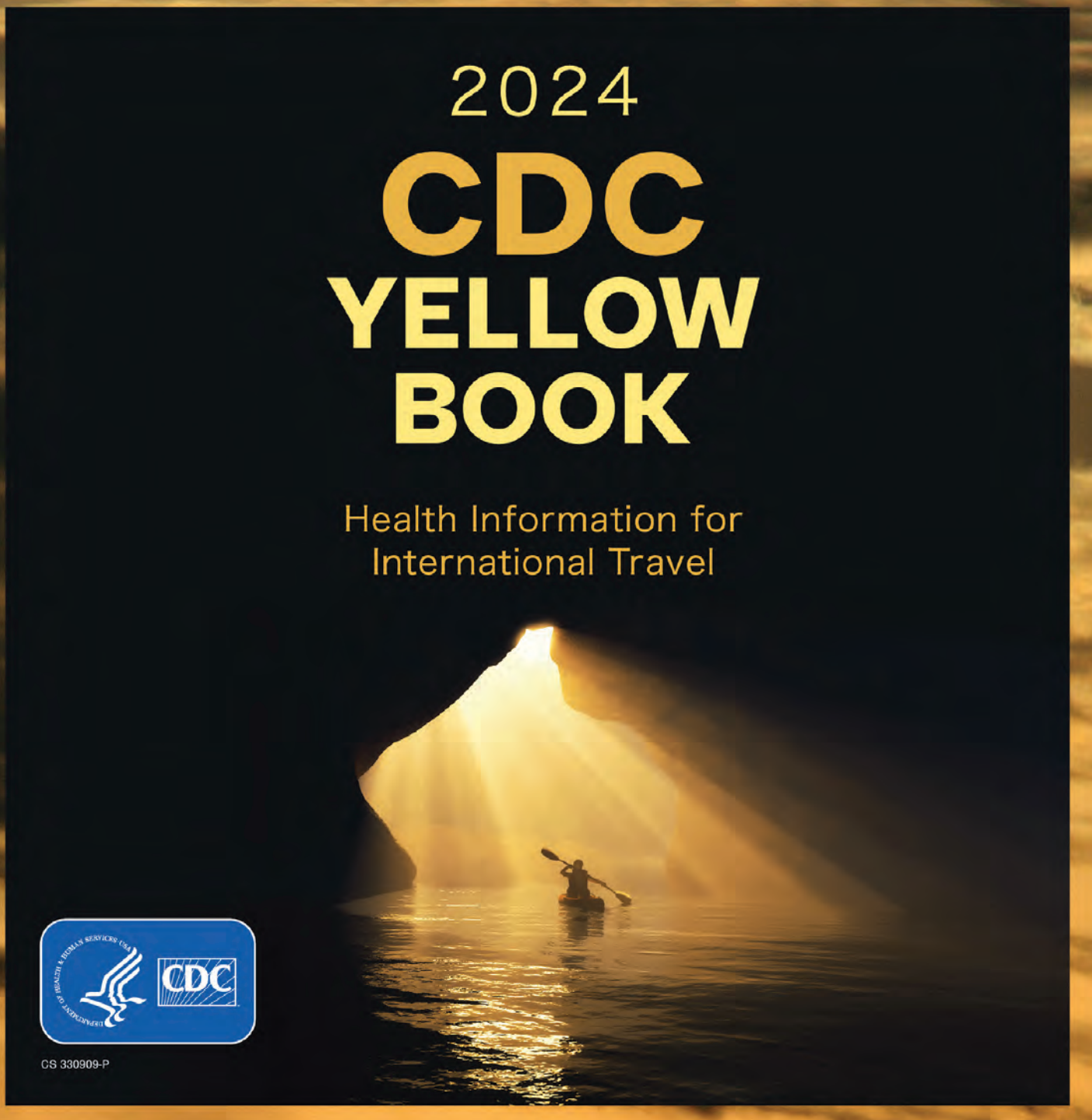

Launch of CDC Yellow Book 2024 – A Trusted Travel Medicine Resource

CDC is pleased to announce the launch of the CDC Yellow Book 2024. The CDC Yellow Book is a source of the U.S. Government's recommendations on travel medicine and has been a trusted resource among the travel medicine community for over 50 years. Healthcare professionals can use the print and digital versions to find the most up-to-date travel medicine information to better serve their patients' healthcare needs.

The CDC Yellow Book is available in print through Oxford University Press and online at www.cdc.gov/yellowbook.

Multicentric Case Series and Literature Review of Coccidioidal Otomastoiditis

Ilan S. Schwartz, Caitlyn Marek, Harleen Sandhu, Ahmed Abdelmonem, Greti Petersen, Emma Dishner, Arash Heidari, George R. Thompson III

Coccidioidomycosis involving the ear, mastoid bone, or both is uncommon. We describe 5 new cases from the United States and review 4 cases reported in the literature of otomycosis and mastoiditis caused by *Coccidioides*. Of the 9 cases, 8 were linked to residence in or travel to California. Two patients had poorly controlled diabetes mellitus, 7 had otomastoiditis, 1 had otitis externa without mastoid involvement, and 1 had mastoiditis without otic involvement. Four patients had concurrent or prior pulmonary coccidioidomycosis. Ipsilateral facial nerve palsies developed in 2 patients. All patients received antifungal treatment for varying durations, and 8 of the 9 patients underwent surgical debridement. Clinicians should consider coccidioidomycosis as a differential diagnosis for otomastoiditis in patients with geographic risks.

The clinical manifestations of coccidioidomycosis, an expanding endemic mycosis caused by *Coccidiodes immitis* and *C. posadasii* (*1*), are notoriously protean (*2*,*3*). Infection occurs primarily by inhalation of aerosolized arthroconidia, which undergo morphologic change within the lungs and turn into spherules (large structures containing endospores) (*4*). Coccidioidomycosis is a highly variable illness and may be asymptomatic or cause a mild respiratory illness in up to 60% of infected persons and an uncomplicated pulmonary infection in most others (*4*). Dissemination or progressive pulmonary disease affects 1%–2% of persons infected with *Coccidioides* spp. (*2*). In those persons, after spherule rupture, endospores may spread hematogenously or through the lymphatic system to virtually all organs, although extrapulmonary clinical disease at sites other than the brain, skin, bone, or psoas muscle is uncommon (*5*). Those infrequently encountered sites of disease may present diagnostic and therapeutic challenges (*2*).

Coccidioidomycosis involving the middle or outer ear, mastoid bone, or both is uncommon. We describe 5 cases of otomycosis and mastoiditis caused by *Coccidioides* spp. in the United States and review 4 cases reported in the literature. Institutional Review Board ethics approval was obtained at Kern Medical Center (Bakersfield, California, USA) and was not required for unidentified case reports at the other medical centers involved.

Author affiliations: Duke University School of Medicine, Durham, North Carolina, USA (I.S. Schwartz); Royal Inland Hospital, Kamloops, British Columbia, Canada (C. Marek); Kern Medical Center, Bakersfield, California, USA (H. Sandhu, G. Petersen, A. Heidari); Valley Fever Institute, Bakersfield (H. Sandhu, A. Heidari); Baylor University Medical Center, Dallas, Texas, USA (A. Abdelmonem, E. Dishner); UC-Davis Medical Center, Davis, California, USA (G.R. Thompson III)

DOI: https://doi.org/10.3201/eid2907.230129

Cases

Case 1

In 2019, a 76-year-old White man from California sought care for left-sided hearing loss that started after an eschar developed on the left tragus and cheek. He had no history of trauma. An otolaryngologist noted a middle ear effusion, which was managed conservatively with topical therapies and tympanostomy tube insertion. Because the effusion persisted despite those interventions, the otolaryngologist sent samples for microbiological analysis, including bacterial and fungal cultures. Bacterial cultures were negative; however, after 3 days of incubation, a mold was isolated, identified by DNA Probe (Hologic, Inc., https://www.hologic.com) as *Coccidioides* spp. A chest radiograph was unremarkable. Oral fluconazole (400 mg/d) was started. Although the effusion decreased, hearing did not improve. After 3 months of therapy, fluconazole was discontinued because of a widespread maculopapular exanthem. Two months thereafter, the unilateral hearing loss persisted. At that time, computed tomography (CT)

of the head showed complete opacification of the left mastoid air cells, a soft tissue infiltrate within the middle ear chambers involving the epitympanic recess, and thinning of the left mastoid bone without obvious bony destruction or intracranial extension. Otoscopic examination revealed extensive debris and discharge throughout the ear canal and tympanic membrane perforation. The ear canal was debrided biweekly for 3 months, which led to healing of the membrane and decreased erythema and discharge from the ear canal. Subsequent treatment was itraconazole (200 mg by mouth 2×/d for 6 months). The patient's hearing partially improved after several weeks of antifungal treatment; improvement reached a plateau at 5 months but did not return to baseline. At the end of therapy, the patient was no longer available for follow-up.

Case 2

In 2015, a 52-year-old man from California sought care for headache and jaw pain. Findings from a physical examination, including the oropharynx and tympanic membranes, were unremarkable. Initially, nonsteroidal antiinflammatories were prescribed, and the condition was managed expectantly. Over the next 4 months, the intensity of the patient's symptoms increased and the pain localized to the left mastoid. Magnetic resonance imaging (MRI) demonstrated left mastoiditis. There was no clinical or radiographic evidence of pulmonary involvement. A biopsy sample was collected from the mastoid; bacterial and fungal cultures were negative, but *Coccidioides* spherules were identified by histopathologic examination. Subsequently, serologic testing demonstrated a *Coccidioides* complement fixation (CF) titer of 1:8, and *Coccidioides* immunodiffusion was positive for IgG. Treatment with oral fluconazole (400 mg/d) was initiated. At a follow-up visit 2 years later, the patient had residual mastoid pain but no other signs or symptoms of disease, and his CF titer had decreased to 1:2. Repeated imaging after 26 months revealed substantial improvement, but radiographic evidence of mastoiditis persisted. Fluconazole was continued indefinitely, although the patient has since been unavailable for follow-up.

Case 3

In 1999, a 42-year-old White man from California sought care for right ear fullness and tinnitus. Examination indicated a right middle ear effusion without erythema. Systemic antihistamines were prescribed; however, the patient returned 1 month later without clinical improvement. Sequential empiric courses of oral prednisone (20 mg/d for 14 days) and amoxicillin/clavulanate (500/125 mg 3×/d for 10 days) also did not lead to improvement. Soon thereafter, ipsilateral facial nerve palsy developed. MRI revealed evidence of an ongoing middle ear effusion and mastoiditis. Tympanocentesis was performed, and *C. immitis* was identified on cultures of the aspirated middle-ear fluid. Serum *Coccidioides* CF titer was 1:4, and *Coccidioides* immunodiffusion was positive for IgG. After further questioning, the patient recalled having had an episode of subacute pneumonia ≈18 months earlier that did not respond to levofloxacin. After *Coccidioides* otomastoiditis was diagnosed, oral fluconazole (800 mg/d) was prescribed. Treatment was continued for 3 years, the ear effusion and tinnitus resolved, the 7th nerve palsy partially improved, the CF titer declined to undetectable, and the radiographic appearance of the mastoiditis improved. After 3 years, the patient self-discontinued fluconazole. He has remained asymptomatic with undetectable CF titers through 21 years of follow-up.

Case 4

In 2014, a 22-year-old Hispanic man from Bakersfield, California, in the *Cocciodioides* epicenter of San Joaquin Valley, who had a medical history of uncontrolled diabetes mellitus type 1, received a diagnosis of pulmonary and osteoarticular coccidioidomycosis but was nonadherent to therapy with fluconazole and then posaconazole (substituted because of liver injury). Peak CF titer was 1:256. After 1 year of nonadherence, he sought care for left ear pain and purulent drainage for 5 days. Symptom onset was gradual, constant, aching, and sharp, with radiation to left jaw and left eye. Left otitis externa was diagnosed and treated with oral amoxicillin and topical neomycin, polymyxin B sulfates, and hydrocortisone otic solutions. He was unavailable for follow-up for another 6 months, at which point he sought care for progressive left-sided hearing loss of 1 week's duration and diffuse pounding headache, nausea, and vomiting for 1 month. Neurologic examination suggested left conductive hearing loss. Results for other cranial nerves were unremarkable. Otoscopic examination revealed that the left tympanic membrane was erythematous and bulging with a middle ear effusion. Results of lumbar puncture were unremarkable. *Coccidioides* CF at this time was 1:64. CT showed complete opacification of the mastoid air cell system on the left side with fluid in the middle ear (Figure 1, panel A). MRI showed left mastoiditis with an extradural collection of fluid. The patient underwent a left myringotomy with insertion of a

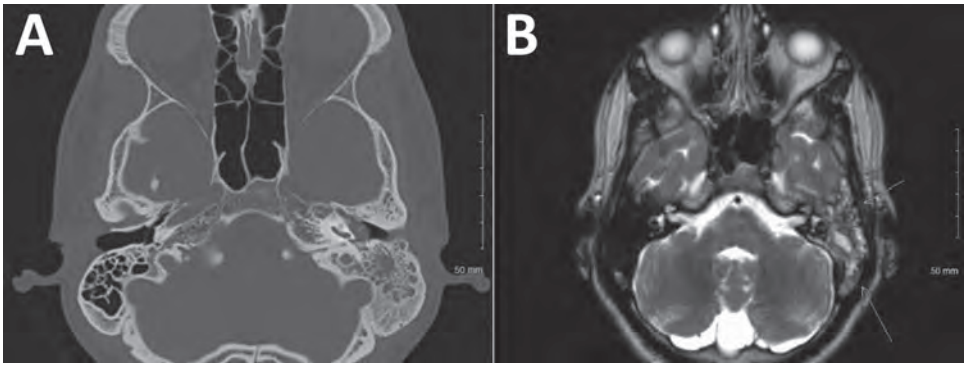

Figure 1. Radiographic findings from 22-year-old Hispanic man from California, USA (case 4), in multicentric case series of coccidioidal otomastoiditis. A) Computed tomography scan of the head, showing opacification of the mastoid. B) Magnetic resonance image of brain, showing mastoiditis.

tympanostomy tube. Ten days postoperatively, he remained symptomatic, reporting a constant headache radiating from his left eye to the occipital area, along with light-headedness and left ear hearing loss. Repeat CT imaging 2 weeks after the myringotomy suggested persistent left otomastoiditis. MRI showed heterogenous signal in the left mastoid and middle ear and discontinuity of the roof of the left mastoid but no temporal lobe or middle cranial fossa involvement (Figure 1, panel B). Because of the lack of response to tympanostomy tube placement, a left mastoidectomy and tympanoplasty were performed. Mastoid tissue was cultured, and *C. immitis* grew after 28 days. The patient was hospitalized, and a 6-week course of intravenous liposomal amphotericin B monotherapy was initiated, which he continued as an outpatient. At 6-week follow-up, his hearing had gradually increased. Antifungals were changed to posaconazole (400 mg/d orally). One year later, *Coccidioides* CF had improved to 1:8, and the patient remained well.

Case 5

In 2021, a 25-year-old Hispanic man from New Mexico with a past medical history of poorly controlled diabetes mellitus type 2 sought care in Texas for right ear pain. Physical examination indicated swelling and tenderness of the right mastoid, along with purulent drainage from the right ear. CT of the temporal bone showed acute right otomastoiditis with thrombophlebitis of the right transverse and sigmoid dural sinuses and right internal jugular vein. The patient also had an associated venous thrombus and abscess under the right mastoid process. He underwent a right mastoidectomy and myringotomy tube placement for his abscess. The abscess cultures grew methicillin-susceptible *Staphylococcus aureus* and later, after the patient was discharged, *Coccidioides*. The patient was discharged with a prescription for intravenous nafcillin for 6 weeks and oral apixaban. However, the abscess and thrombus persisted, and he began to experience shortness of breath 1 month after discharge. He was hospitalized because of disease progression, and chest CT showed septic emboli of the left lower lung lobe and lingula (Figure 2, panel A). Given the lack of improvement, it was thought that the *Coccidioides* infection was playing a larger role in the disease, and intravenous liposomal amphotericin B (5 mg/kg) and oral fluconazole (800 mg/d) were initiated. The right neck abscess was incised and drained, and cultures grew *Coccidioides*. CF titers were 1:32. Magnetic resonance venography showed progression

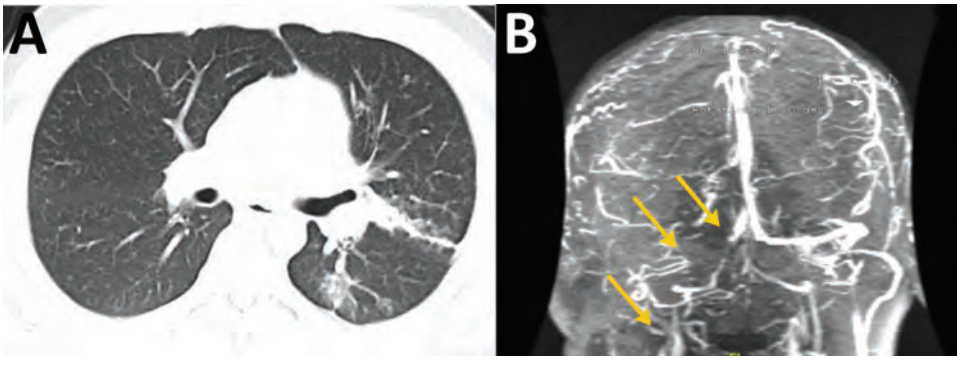

Figure 2. Radiographic findings from 25-year-old Hispanic man from New Mexico, USA (case 5), in multicentric case series of coccidioidal otomastoiditis. A) Computed tomography scan of the chest with contrast, showing septic emboli of the left lower lung lobe and lingula with developing pneumonia. B) Magnetic resonance venogram, showing stable thrombus of the right jugular bulb, right sigmoid and transverse sinuses, and partially occlusive thrombus in the anterior superior sagittal sinus, seen by lack of enhancement (arrows) compared with the left side.

of the thrombus to the sagittal sinus despite anticoagulation therapy. The interventional radiologist attempted a thrombectomy, which was unsuccessful. It was determined that the thrombus progression was most likely caused by *Coccidioide*s thrombophlebitis, and a heparin infusion was started. At 6-week follow-up, the patient was improving with no neurologic dysfunction; repeat magnetic resonance venography showed stability of the thrombus (Figure 2, panel B), and the patient was discharged with prescriptions for voriconazole and apixaban. Repeat CF titers were 1:64 and remained stable for 10 months.

Literature Review and Synthesis

With a literature search, we identified 4 additional cases of coccidioidomycosis involving the ear, mastoid bone, or both (*6*–*8*) and summarized them along with the 5 cases in our series (Table, https://wwwnc.cdc.gov/EID/article/29/7/23-0129-T1.htm). Eight patients for whom details were available had lived in or traveled to California. Ages ranged from 4 to 76 years, and 6 of 9 were male. Ethnicity was known for 7 patients: 4 were Hispanic and 3 were White. Two patients had poorly controlled diabetes mellitus (1 each with types 1 and 2). Another patient had systemic lupus erythematosus, which had been treated with corticosteroids 1 month before the coccidioidal otomastoiditis developed. In retrospect, however, misdiagnosed coccidioidomycosis was probably the cause of the fatigue, fever, and arthralgias (with positive antinuclear and anti-DNA antibodies) attributed to lupus. Seven patients had otomastoiditis, 1 had mastoiditis without otitis, and 1 had otitis without mastoiditis. Ear pain was noted for 5 patients, mastoid swelling or tenderness for 3, and hearing loss for 2. Two patients had cutaneous lesions at the ear.

In addition to the ears or mastoids, 4 patients had previous or concomitant pulmonary disease consistent with coccidioidomycosis, including 1 patient who additionally had osteoarticular coccidioidomycosis. Ipsilateral facial nerve palsies developed in 2 patients, early for one and several months into treatment for the other. In 1 patient, coccidioidal otomastoiditis was complicated by ipsilateral internal jugular thrombosis and septic emboli.

Coccidioides species was cultured from middle ear fluid for 4 patients, mastoid tissue for 2, and both middle ear fluid and mastoid for 1. For 3 patients, diagnosis was based on histopathologic findings of spherules in mastoid tissue and for another, by histopathologic examination of skin. All 9 patients received antifungal drugs: amphotericin B for 2, amphotericin B followed by an azole for 3, and azoles alone for 4. Eight patients underwent surgical irrigation and debridement.

Discussion

Coccidioidomycosis is one of the most common dimorphic fungal diseases encountered in North America; the geographic range on the continent is primarily the southwestern United States and parts of Mexico (*9*). Myriad manifestations have been described (*4*). Ear or mastoid bone involvement, however, is rare with coccidioidomycosis. In addition to the 5 cases in our series, we identified only 4 cases of ear or mastoid coccidioidomycosis in the literature. In a database of 3,000 patients with coccidioidomycosis at Kern Medical Center, only 1 case of otomycosis or otomastoiditis (case 4) was identified, highlighting the uncommon nature of this manifestation.

The mechanism by which coccidioidomycosis involves the ear or mastoid is unclear. Because those structures are contiguous with the upper respiratory tract, primary infection of the ears and mastoids after inhalation of *Coccidioides* arthroconidia is plausible. However, there was evidence of pulmonary disease for only 4 of 9 patients, consistent with the lack of pulmonary signs or symptoms in other patients with disseminated coccidioidomycosis involving sites not contiguous with the airways (*10*). Hematogenous dissemination is also a potential mechanism; Scalarone and Huntington showed in a murine model of coccidioidomycosis that intraperitoneal inoculation (which mimics hematogenous infection) with a low-virulence strain of *C. immitis* can lead to infection that localizes to inner ear structures and mastoids (*11*). It is unclear whether strain virulence or inoculation route differs among patients with this uncommon manifestation.

Although most cases of otitis or mastoiditis are bacterial, the diagnosis of coccidioidomycosis should be considered for patients with otitis or mastoiditis who have resided in or traveled to areas of risk for coccidioidomycosis, especially if the case does not respond to empiric antibacterial therapy. The diagnosis can be suggested by serologic testing, but confirmation requires culture of discharge from the ear or by biopsy of the mastoid for histopathology and fungal culture.

G.R.T. reports grants or contracts from the National Institutes of Health, Astellas, Cidara, Mayne, F2G, Merck, Pfizer, Scynexis, and consulting fees from Astellas, Cidara, Mayne, F2G, Scynexis, all outside of the current work. All other authors declare no conflicts.

About the Author

Dr. Schwartz is an infectious diseases physician and researcher at Duke University School of Medicine. His research interests are emerging fungal infections, endemic mycoses, immunocompromised hosts, and global health.

References

1. Gorris ME, Treseder KK, Zender CS, Randerson JT. Expansion of coccidioidomycosis endemic regions in the United States in response to climate change. Geohealth. 2019;3:308–27. https://doi.org/10.1029/2019GH000209
2. Galgiani JN, Ampel NM, Blair JE, Catanzaro A, Geertsma F, Hoover SE, et al. 2016 Infectious Diseases Society of America (IDSA) clinical practice guideline for the treatment of coccidioidomycosis. Clin Infect Dis. 2016;63:e112–46. https://doi.org/10.1093/cid/ciw360
3. Thompson GR III, Le T, Chindamporn A, Kauffman CA, Alastruey-Izquierdo A, Ampel NM, et al. Global guideline for the diagnosis and management of the endemic mycoses: an initiative of the European Confederation of Medical Mycology in cooperation with the International Society for Human and Animal Mycology. Lancet Infect Dis. 2021;21:e364–74. https://doi.org/10.1016/S1473-3099(21)00191-2
4. Bays DJ, Thompson GR III. Coccidioidomycosis. Infect Dis Clin North Am. 2021;35:453–69. https://doi.org/10.1016/j.idc.2021.03.010
5. Stockamp NW, Thompson GR III. Coccidioidomycosis. Infect Dis Clin North Am. 2016;30:229–46. https://doi.org/10.1016/j.idc.2015.10.008
6. Harvey RP, Pappagianis D, Cochran J, Stevens DA. Otomycosis due to coccidioidomycosis. Arch Intern Med. 1978;138:1434–5. https://doi.org/10.1001/archinte.1978.03630340100037
7. Busch RF. Coccidioidomycosis of the external ear. Otolaryngol Head Neck Surg. 1992;107:491–2. https://doi.org/10.1177/019459989210700331
8. Low WS, Seid AB, Pransky SM, Kearns DB. *Coccidioides immitis* subperiosteal abscess of the temporal bone in a child. Arch Otolaryngol Head Neck Surg. 1996;122:189–92. https://doi.org/10.1001/archotol.1996.01890140073014
9. Ashraf N, Kubat RC, Poplin V, Adenis AA, Denning DW, Wright L, et al. Re-drawing the maps for endemic mycoses. Mycopathologia. 2020;185:843–65. https://doi.org/10.1007/s11046-020-00431-2
10. Bays DJ, Thompson GR III, Reef S, Snyder L, Freifeld AJ, Huppert M, et al. Natural history of disseminated coccidioidomycosis: examination of the Veterans Affairs–Armed Forces database. Clin Infect Dis. 2021;73:e3814–9. https://doi.org/10.1093/cid/ciaa1154
11. Scalarone GM, Huntington RW. Circling syndrome and inner ear disease in mice infected intraperitoneally or intravenously with *Coccidioides immitis* spherule-endospore phase cultures. Mycopathologia. 1983;83:75–86. https://doi.org/10.1007/BF00436887
12. Thompson GR III, Lewis JS II, Nix DE, Patterson TF. Current concepts and future directions in the pharmacology and treatment of coccidioidomycosis. Med Mycol. 2019;57(Supplement_1):S76–84. https://doi.org/10.1093/mmy/myy029

Address for correspondence: Ilan S. Schwartz, Duke University School of Medicine, Hanes House, 315 Trent Dr, Durham, NC 27710, USA; email: ilan.schwartz@duke.edu

Nationwide Outbreak of *Candida auris* Infections Driven by COVID-19 Hospitalizations, Israel, 2021–2022[1]

Roni Biran, Regev Cohen, Talya Finn, Tal Brosh-Nissimov, Galia Rahav, Dafna Yahav, Sharon Amit, Yael Shachor-Meyouhas, Alaa Atamna, Jihad Bishara, Liat Ashkenazi-Hoffnung, Haim Ben Zvi, Mirit Hershman-Sarafov, Shlomo Maayan, Yasmin Maor, Orna Schwartz, Oren Zimhony, Jonathan Lellouche, Meital Elbaz, Ela Burdelova, Naama Mizrahi, Anna Novikov, Oryan Henig, Ronen Ben-Ami

We report an outbreak of *Candida auris* across multiple healthcare facilities in Israel. For the period of May 2014–May 2022, a total of 209 patients with *C. auris* infection or colonization were identified. The *C. auris* incidence rate increased 30-fold in 2021 (p = 0.00015), corresponding in time with surges of COVID-19–related hospitalization. Multilocus sequence typing revealed hospital-level outbreaks with distinct clones. A clade III clone, imported into Israel in 2016, accounted for 48.8% of typed isolates after January 2021 and was more frequently resistant to fluconazole (100% vs. 63%; p = 0.00017) and voriconazole (74% vs. 5.2%; p<0.0001) than were non–clade III isolates. A total of 23% of patients had COVID-19, and 78% received mechanical ventilation. At the hospital level, outbreaks initially involved mechanically ventilated patients in specialized COVID-19 units and then spread sequentially to ventilated non–COVID-19 patients and nonventilated patients.

Candida auris is a drug-resistant fungal pathogen that has emerged over the past decade as a cause of nosocomial outbreaks with substantial mortality rates (*1*–*3*). Widespread resistance to triazole antifungals, rapid spread and persistence within hospital and nursing home environments, and difficulties in accurate identification by standard microbiological methods have prompted the US Centers for Disease Control and Prevention to list *C. auris* as a serious antibiotic-resistant threat (*4*). Recent reports of echinocandin-resistant and pan-resistant *C. auris* isolates in the United States and elsewhere have further heightened these concerns (*5*,*6*).

In 2014 and 2015, five patients with *C. auris* bloodstream infection were identified in 2 hospitals in the Tel Aviv, Israel, metropolitan area (*7*). After that outbreak, laboratory-based surveillance was initiated, and clinical isolates identified or suspected as *C. auris* were sent to the national mycology reference laboratory for sequence-based identification and antifungal drug susceptibility testing. Surveillance showed a stable low incidence of *C. auris* infections and no notable nosocomial clusters. An outbreak in 2016 that was limited to a single hospital originated

Author affiliations: Tel Aviv Sourasky Medical Center, Tel Aviv, Israel (R. Biran, M. Elbaz, E. Burdelova, N. Mizrahi, A. Novikov, O. Henig, R. Ben-Ami); Hillel Yaffe Medical Center, Hadera, Israel (R. Cohen); Technion, Haifa, Israel (R. Cohen, Y. Shachor-Meyouhas, M. Hershman-Sarafov); Sanz Medical Center, Netanya, Israel (T. Finn, J. Lellouche); Samson Assuta Ashdod University Hospital, Ashdod, Israel (T. Brosh-Nissimov); Ben Gurion University in the Negev, Beer Sheba, Israel (T. Brosh-Nissimov); Sheba Medical Center, Tel Hashomer, Israel (G. Rahav, D. Yahav, S. Amit); Tel Aviv University, Tel Aviv (G. Rahav, D. Yahav, A. Atamna, J. Bishara, L. Ashkenazi-Hoffnung, H. Ben Zvi, Y. Maor, R. Ben-Ami); Rambam Medical Center, Haifa (Y. Shachor-Meyouhas); Beilinson Hospital, Rabin Medical Center, Petach-Tikva, Israel (A. Atamna, J. Bishara); Schneider Children's Medical Center, Petach-Tikva (L. Ashkenazi-Hoffnung); Bnai Zion Medical Center, Haifa (M. Hershman Sarafov); Barzilai Medical Center, Ashdod (S. Maayan); Hebrew University of Jerusalem, Jerusalem, Israel (S. Maayan, O. Zimhony); Wolfson Medical Center, Holon, Israel (Y. Maor, O. Schwartz); Kaplan Medical Center, Rehovot, Israel (O. Zimhony); Ariel University, Ariel, Israel (J. Lellouche).

DOI: https://doi.org/10.3201/eid2907.221888

[1]Preliminary results from this study were presented at the 32nd European Congress of Clinical Microbiology and Infectious Diseases, April 23–26, 2022, Lisbon, Portugal.

in a patient transferred to Israel from a hospital in South Africa (*8*).

Since January 2021, a marked increase in the number of *C. auris* isolates referred to the national reference laboratory was noted; many medical centers reported *C. auris* infections for the first time. We conducted a nationwide survey of *C. auris* infections in Israel to assess clinical and microbiological characteristics and to determine drivers of epidemiologic change during 2021–2022.

Methods

Study Design and Population

After the first detection of *C. auris* in Israel in 2014, an alert was issued to all clinical microbiology laboratories to refer yeast isolates identified or suspected as *C. auris* to the national mycology reference laboratory at the Tel Aviv Sourasky Medical Center. Guidance on contact isolation, contact tracing, and environmental disinfection was provided to facilities that reported *C. auris* cases (*9*,*10*).

This nationwide retrospective observational study covered the period January 1, 2014–May 31, 2022. We included all medical facilities that reported ≥1 *C. auris* clinical isolate during the study period. Yeast isolates sent to the reference laboratory underwent confirmatory DNA-sequence based identification, sequence typing, and antifungal susceptibility testing. Demographic and clinical data were collected from each site.

The study was reviewed and approved by the ethics committee of each participating medical center (approval no. for principal site 0543-21-TLV). Requirement for informed consent was waived because of the retrospective observational nature of the study.

Data Collection

We extracted data from the hospital electronic medical records and laboratory computerized database by using a structured form. Collected data included demographics, comorbidities (quantified using the Charlson comorbidity score) (*11*), SARS-CoV-2 infection, previous exposure to antibacterial and antifungal drugs, infection with or carriage of drug-resistant organisms, and mechanical ventilation. Clinical outcomes were all-cause in-hospital death, length of hospitalization, length of stay in intensive care unit (ICU), and duration of mechanical ventilation. *C. auris* was considered a colonizer if growing from respiratory tract, skin, or rectal specimens and potentially clinically significant if isolated from normally sterile specimens.

Microbiological Analyses

The general practice of microbiological laboratories is to identify yeasts cultured from normally sterile sites. Basic identification in participating laboratories was done by using CHROMagar *Candida* plates (CHROMagar, https://www.chromagar.com) and Vitek 2 with the YST ID card (bioMérieux, https://www.biomerieux.com). Hospital H1 implemented measures to identify *C. auris* carriers because of a large outbreak at that site. Those measures included identifying yeast isolates from all specimens and screening patients at admission to ICU and step-down units and at time of transfer from departments where *C. auris* cases were detected. *C. auris* screening was done by swabbing 3 sites (axilla, groin, and throat). Endotracheal aspirates were sampled from intubated patients. Swabs were inoculated onto Sabouraud dextrose agar and incubated at 37°C for 5 days.

Candida species identification at the reference laboratory was done using PCR and sequencing of the ribosomal DNA internal transcribed spacer (ITS) 1–5.8S-ITS2 and D1/D2 regions (*7*,*12*). Antifungal susceptibility testing was performed using broth microdilution according to Clinical and Laboratory Standards Institute guidelines (*13*). Antifungals tested were fluconazole, itraconazole, voriconazole, amphotericin B, and anidulafungin (obtained from Sigma, https://www.sigmaaldrich.com). Tentative *C. auris* susceptibility breakpoints for fluconazole (≥32 mg/L), anidulafungin (≥4 mg/L), and amphotericin B (≥2 mg/L) were used, as proposed by the Centers for Disease Control and Prevention (*14*). Because no breakpoint has been defined for voriconazole, the epidemiologic cutoff (ECOFF) value was calculated from the MIC distribution using the ECOFF Finder program (*15*,*16*).

We determined genetic relatedness among *C. auris* isolates by using multilocus sequence typing, as described previously (*17*,*18*). We used Bayesian inference in MrBayes version 3.2 (*19*) to amplify, concatenate, and compare genomic sequences of RNA polymerase II (RPB)1, RPB2, internal transcribed spacer (ITS), and the D1/D2 region of the 28S nuclear ribosomal large subunit rRNA gene among strains. We used allele sequences reported by Kwon et al. (*17*) as references to classify strains into 4 main clusters (clades). We constructed minimum-spanning trees in R version 4.2.1 (R Foundation for Statistical Computing, https://www.r-project.org) and deposited all sequences into GenBank (Appendix 1, https://wwwnc.cdc.gov/EID/article/29/7/22-1888-App1.xlsx).

Statistical Analyses

We summarized patient characteristics by using descriptive statistics. We determined between-group differences by using the Fisher exact test for categorical variables and Student t or Wilcoxon rank-sum test for normally or nonnormally distributed continuous variables. We measured variance across multiple groups by using the Kruskal-Wallis test. The significance level (type I error) was set at 0.05. We performed all calculations in R.

Results

We recorded 209 patient-specific *C. auris* isolates during the 8-year study period. The first cases of *C. auris* infection in Israel were detected in May 2014 at a tertiary-level medical center in Tel Aviv. During May 2014–December 2020, a total of 24 cases of *C. auris* infection were reported from 7 hospitals (median incidence 4 cases/y, range 1–5 cases/y). The incidence of *C. auris* infection increased dramatically in 2021; an annual incidence of 120 cases was reported from 10 hospitals and 3 long-term care facilities, which represented a 30-fold increase over the previous base annual incidence ($p = 0.00015$; Figure 1). Of 185 patient-specific isolates identified beginning in January 2021, a total of 172 (92.9%) occurred in 4 community hospitals (H1–H4). Hospital H1, located in the Northern Central District of Israel, was the focus of the largest outbreak; 127 patient-specific *C. auris* isolates were reported (Figure 1, panel A). Repeat cultures were performed for 152 patients; colonization was detected for a median of 14 days (interquartile range [IQR] 4–32 days, maximum 210 days) (Appendix 2 Figure).

The incidence of *C. auris* cases during 2021 and 2022 corresponded with surges in COVID-19 cases in Israel during that period (Figure 2). *C. auris* cases peaked in January–March 2021, synchronous with the COVID-19 Alpha variant wave; in June–November 2021, matching the Delta variant wave; and in January–May 2022, during the Omicron wave. During the Alpha wave, 88.0% of patients with *C. auris* (15/17) were infected with SARS-CoV-2. That percentage decreased to 22% (23/103) during the Delta wave and 6.2% (4/65) during the Omicron wave (Figure 2).

Strain Relatedness

We assessed the genetic relatedness and clade designation of *C. auris* strains isolated before 2021 and those from the 2021–2022 outbreak by using multilocus sequence typing. We typed 22 isolates collected during May 2014–December 2020; of those, 18 (81.8%) isolates were clade IV, 3 (13.6%) were clade III, and 1 (4.5%) was clade II (Figures 3, 4). The 3 clade III isolates represented an importation event in 2016 traced

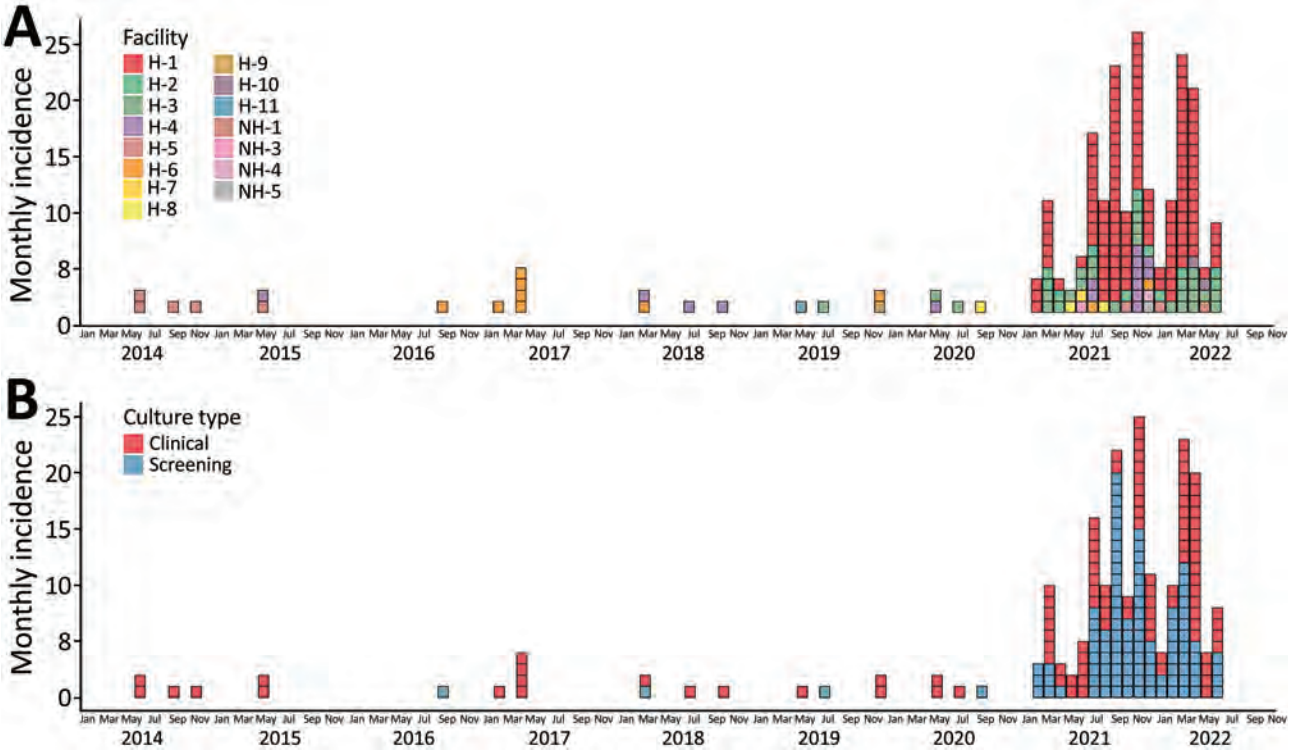

Figure 1. Incidence (no. cases) of *Candida auris* infection by medical facility (A) and type of specimen (B), Israel, 2014–2022. Epidemic plots were constructed with each patient appearing once, on the date of the first *C. auris*–positive specimen. H, hospital; NH, nursing home.

to a patient who acquired a surgical site infection in South Africa before being evacuated to Israel. The population structure changed after January 2021, when localized hospital outbreaks of clade III and clade I occurred. Of 43 isolates typed during January 2021–May 2022, a total of 24 (55.8%) belonged to clade III, 11 (25.5%) to clade IV, and 8 (18.6%) to clade I (Figures 3, 4). All isolates typed from hospital H1 (n = 18) belonged to clade III. Clade I isolates (n = 8) were identified in 2 hospitals (H2 and H3) in Israel's Southern district. Clade III isolates from the 2016 outbreak clustered with the earliest 2021 H1 isolates, suggesting an epidemiologic link.

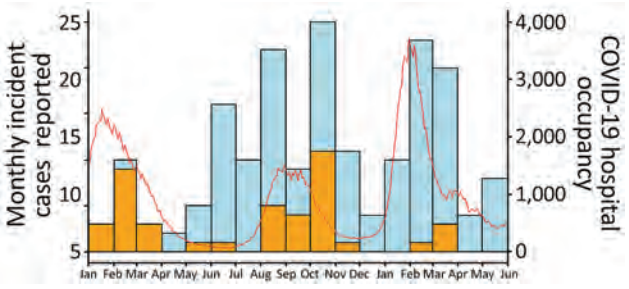

Figure 2. Association of *Candida auris* infection with COVID-19 hospitalization, Israel, January 2021–May 2022. Bars represent monthly *C. auris* incidence (no. cases). Cases with SARS-CoV-2 co-infection are shown in orange, non–co-infected cases are in blue. Red line shows level of hospital occupancy with COVID-19 patients. Scales for the y-axes differ substantially to underscore patterns but do not permit direct comparisons.

Antifungal Susceptibility

Overall rates of antifungal drug susceptibility were 15.5% (32/206) for fluconazole, 79.6% (164/206) for voriconazole, 86.4% (178/206) for amphotericin B, and 98.0% (198/202) for anidulafungin. A total of 21 isolates (10.0%) were resistant to both amphotericin B and fluconazole; 2 (0.95%) were resistant to fluconazole, amphotericin B, and anidulafungin. Clade III

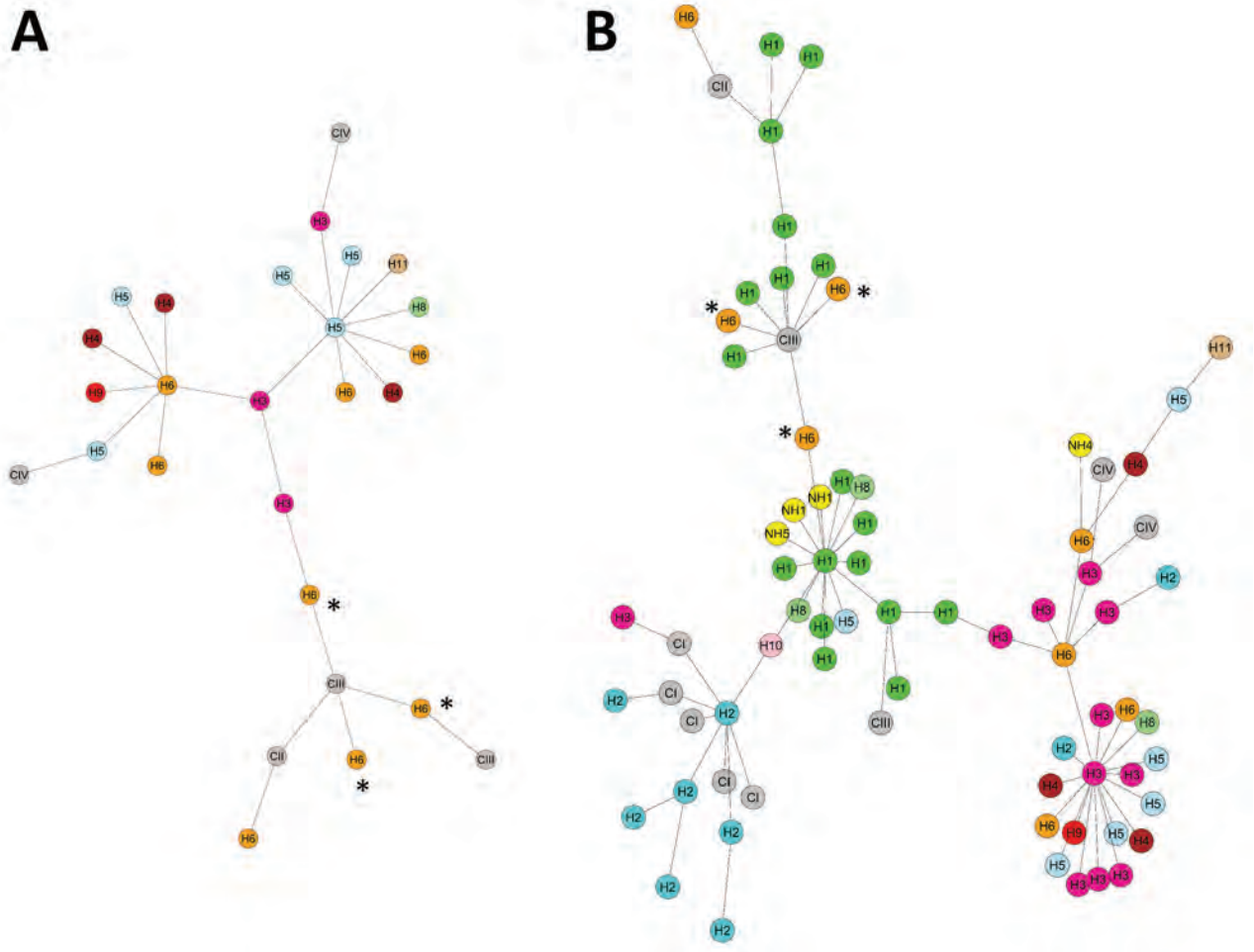

Figure 3. Minnimum-spanning trees of *Candida auris* strains for 2014–2020 (A) and 2014–2022 (B), Israel. Genetic relatedness of *C. auris* isolates was assessed using multilocus sequence typing. Strain cluster designation was determined using sequences published by Kwon et al. (shown in gray nodes) (*17*). Nodes are colored according to the respective medical center. Nodes marked with asterisks represent 2016 importation event from South Africa. C, clade; H, hospital; NH, nursing home.

isolates had significantly higher MICs of fluconazole and voriconazole compared with non–clade III isolates (Figures 4–6). Resistance to fluconazole (MIC ≥32 mg/L) was detected in 100% (27/27) of clade III isolates versus 63.1% (24/38) of non–clade III isolates (p = 0.00017). Voriconazole MIC values above the calculated ECOFF (MIC ≥4 mg/L) were detected in 74.0% (20/27) of clade III isolates versus 5.2% (2/38) of non–clade III isolates (p<0.0001).

Clinical Characteristics and Outcomes

Clinical data were available for 177 patients (86.7%) (Table). Patients were predominantly men (68.3%); median age was 70 years (IQR 55–80 years). Patients had multiple comorbidities; 50% had significant functional impairment and 30% had dementia. Most patients (78%) required mechanical ventilation during the same hospitalization, and 67% had a central venous catheter. Carriage or infection with other drug-resistant organisms was detected in 55% of patients.

Forty-one patients (23.2%) had received a COVID-19 diagnosis before acquiring *C. auris* in the same hospital stay. Most of those patients (73.1%) had critical COVID-19. Almost all patients with COVID-19 received corticosteroids, and half were treated with remdesivir. The median time from detection of SARS-CoV-2 infection to recovery of *C. auris* was 25 days (IQR 11–38.5 days). Patients with and without COVID-19 had similarly high rates of mechanical ventilation (78%), but patients with COVID-19 had better baseline functional status, fewer comorbidities, and lower rates of dementia (Table).

Of 177 patients, 82 (46.3%) had positive clinical specimens, and 95 (53.6%) were colonized with *C. auris* with no evidence of invasive candidiasis. The proportion of colonized versus infected patients was significantly greater for patients with COVID-19 (70.7% vs. 48%; p = 0.013) and in hospital H1, where screening was implemented (77.7% vs. 14.9% in other hospitals; p<0.0001). Clinical specimens consisted of urine (59.8%, n = 49), blood (36.6%, n = 30), and wounds (17.1%, n = 14). In-hospital death occurred in 70 (39.5%) patients. The in-hospital mortality rate did not differ significantly between patients with clinical infections, including those with *C. auris* bloodstream infections, and patients who were only colonized with *C. auris*. Increasing age and comorbidity (Charlson score) were predictors of in-hospital death (Appendix 2,

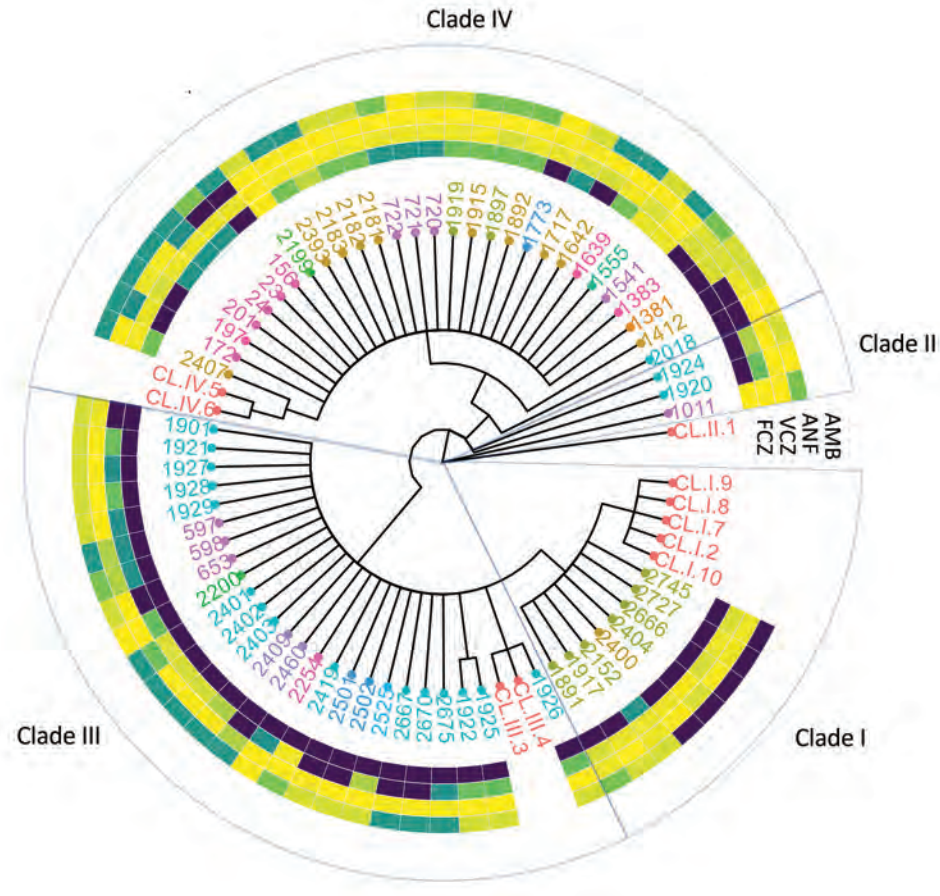

Figure 4. Association of population strain clustering with antifungal drug MIC and medical facility for *Candida auris* strains, Israel. A phylogenetic tree of *C. auris* isolates was constructed using multilocus sequence typing and Bayesian inference. Text colors represent different medical centers. Heat map colors represent MIC of each drug, ranging from fully susceptible (yellow) to resistant (dark blue). AMB, amphotericin B; ANF, anidulafungin; FCZ, fluconazole; VCZ, voriconazole.

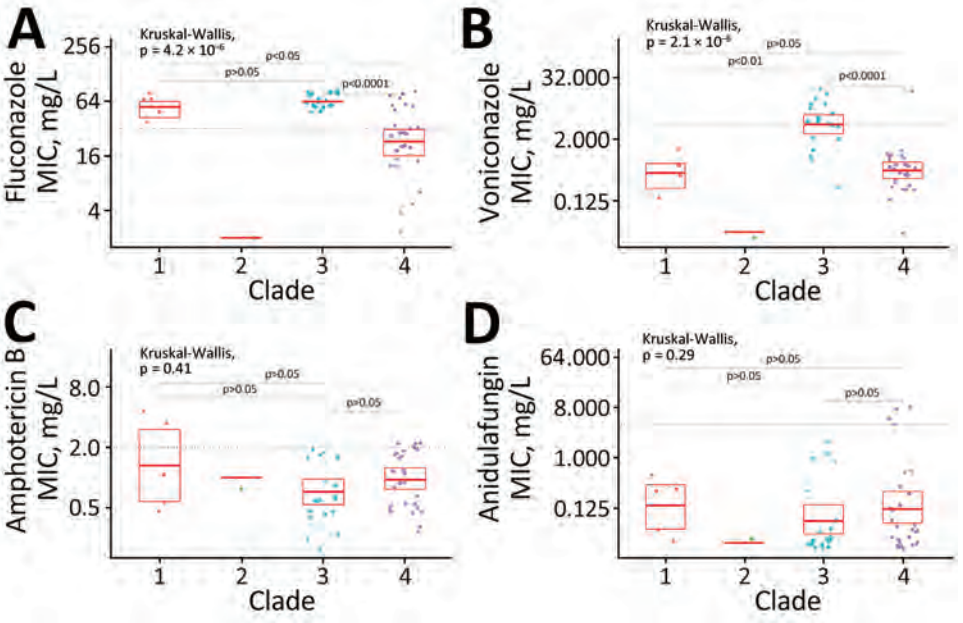

Figure 5. Comparison of antifungal MIC distribution among *Candida auris* clades, Israel. Antifungal MICs were determined using Clinical Laboratory Standards Institute M27A3/S4 methodology, for fluconazole (A), voriconazole (B), amphotericin B (C), and anidulafungin (D). Comparison among *C. auris* clades was done using the Kruskal-Wallis test and the pairwise Wilcoxon post-hoc test. Each dot represents a patient-specific isolate. Horizontal bars within box plots indicate medians, box tops and bottoms represent 95% confidence interval. NS, not significant.

https://wwwnc.cdc.gov/EID/article/29/7/22-1888-App2.pdf). Of the surviving patients, 27 (29.0%) were discharged to home, 27 (29.0%) to ventilator-capable skilled nursing facilities, 19 (20.4%) to rehabilitation facilities, and 17 (18.2%) to long-term care facilities.

Time Course of *C. auris* Hospital Outbreaks

We analyzed the evolution of the *C. auris* outbreaks in hospitals H1, H2, and H3 (Figure 7). In H1, *C. auris* infections were first detected among 10 mechanically ventilated COVID-19 patients; 9 of these infections occurred over a period of 13 days in February 2021 (cluster 1). Next, *C. auris* infections were detected in mechanically ventilated patients with no history of COVID-19 (cluster 2). Infections were first detected in May 2021 in intermediate care unit A, to which convalescing COVID-19 patients had been transferred, and in the adjacent general ICU. The first of the non–COVID-19 cases was a patient admitted 52 days after the last of the COVID-19 patients had been discharged. Additional cases were detected in intermediate care unit B starting in July 2021, after that unit became a destination for recovering COVID-19 patients. Overall, 65 mechanically ventilated patients were infected with *C. auris* in cluster 2.

A similar pattern, in which a cluster of *C. auris* cases in mechanically ventilated patients with COVID-19 was followed by spread to ventilated patients without COVID-19, was observed in hospital H2, albeit on a smaller scale. The gap between discharge of the last cluster 1 patients and admission of the first cluster 2 patient was 67 days. Cluster 1 strains included 2 sequence types belonging to clade I and clade IV, whereas only the clade I sequence type was identified in cluster 2. In hospital H3, *C. auris* infection was detected predominantly in ventilated patients, with or without COVID-19, with no temporal clustering over the study period (Figure 7).

Discussion

We report an ongoing nationwide outbreak of *C. auris* colonization and infection in hospitals in Israel. The introduction of distinct clones of clade I and clade III into 3 hospitals, as well as increased circulation of clade IV,

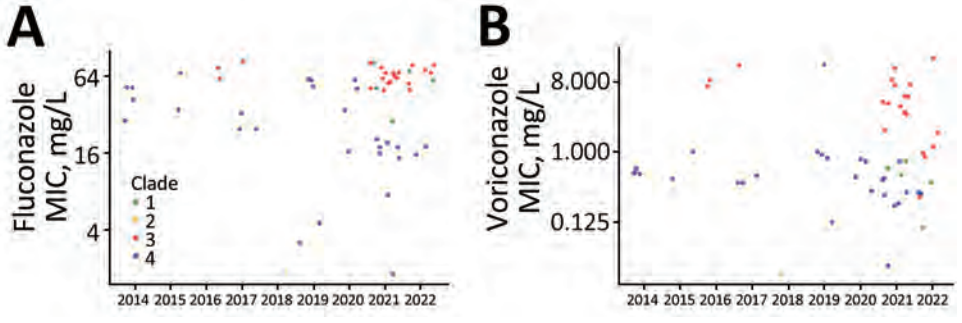

Figure 6. Temporal distribution of *Candida auris* clades and their respective MIC values, Israel. Distribution of *C. auris* fluconazole and voriconazole MIC is shown for January 2014–May 2022. Each dot represents a patient-specific isolate. High fluconazole and voriconazole MIC associated with clade III is noted in 2021 and 2022.

resulted in a 30-fold increase in the annual *C. auris* incidence rate in 2021. Neither clade I nor clade III had circulated in Israel before 2021, suggesting they arose through importation events into the country. Further, phylogenetic analyses showed that the clade III isolates collected during the current outbreak were related to those imported into Israel from South Africa in 2016 (*8*). The shift in clade distribution was associated with a change in the azole MIC range; specifically, clade III strains had higher fluconazole and voriconazole MICs compared with those for clade IV strains. Thus, the continuing expansion of clade III in Israel and its spread beyond H1 to other medical facilities might limit the already constrained treatment options for *C. auris*.

We identified 2 main drivers of *C. auris* healthcare-associated dissemination in this outbreak. The first was COVID-19. Almost one quarter of patients with *C. auris* infection or colonization were infected with SARS-CoV-2 and received care in designated COVID-19 units. *C. auris* incidence rates corresponded in time with COVID-19–related surges in hospitalization. Cases of *C. auris* infection in COVID-19 wards tended to be tightly clustered (Figure 7), suggesting efficient healthcare-associated transmission within those units. Multiple genotypes of *C. auris* were found in COVID-19 units in hospitals H1 and H2, and 1 dominant clone carried over to non–COVID-19 patients in other departments. Outbreaks of *C. auris* have been reported in COVID-19 care units in the United States, India, Mexico, and Columbia, resulting in colonization or infection rates as high as 50% (*20*–*24*). Potential reasons for the susceptibility of COVID-19 units to such outbreaks include the use of double gloving (wearing 2 pairs of gloves), poor adherence to hand hygiene, and inadequate disinfection of shared medical devices and equipment (*20*).

Table. Clinical characteristics of patients infected or colonized with *Candida auris*, Israel*

Characteristic	COVID-19	Non–COVID-19	p value	Total
No. patients	41 (23.2)	136 (76.8)		177 (100)
Median age, y (IQR)	67 (53–75)	72 (56–82)	0.16	70 (55–80)
Sex				
M	24 (58.5)	97 (71.3)	0.13	121 (68.3)
F	17 (41.4)	39 (28.6)		56 (31.6)
Long-term care facility	5 (12.1)	33 (24.2)	0.12	38 (21.5)
Functional status			0.0036	
Independent	30 (73.1)	59 (43.3)		89 (50.3)
Requires assistance	4 (9.7)	21 (15.4)		25 (14.1)
Complete dependence	7 (17.0)	56 (41.1)		63 (35.6)
Comorbidities				
Dementia	6 (14.6)	46 (33.8)	0.019	52 (29.4)
Malignancy	3 (7.3)	18 (13.2)	0.41	21 (11.8)
Median Charlson comorbidity score (IQR)	2 (0–3)	3 (1–4)	0.00016	2 (1–4)
Drug-resistant organism carriage/infection				
Any	21 (51.2)	76 (55.8)	0.72	97 (54.8)
Vancomycin-resistant *Enterococcus*	5 (12.1)	17 (12.5)	1.0	22 (12.4)
Methicillin-resistant *Staphylococcus aureus*	10 (24.3)	25 (18.3)	0.38	35 (19.8)
Carbapenem-resistant Enterobacteriaceae	8 (19.5)	31 (22.7)	0.83	39 (22.0)
Clostridioides difficile	0	6 (4.4)	0.33	6 (3.4)
Exposure to antimicrobials				
Antibacterial	37 (90.2)	119 (87.5)	0.78	156 (88.1)
Azole	5 (12.1)	11 (8.0)	0.53	16 (9.0)
Echinocandin	2 (4.8)	3 (2.2)	0.32	5 (2.8)
Amphotericin B	0	0	1.0	0
COVID-19 severity and treatment				
Critical	30 (73.1)	NA		30 (76.9)
Severe	8 (19.5)	NA		8 (20.5)
Mild	1 (2.4)	NA		1 (2.5)
Corticosteroids	38 (97.4)	NA		38 (97.4)
Remdesivir	17 (43.5)	NA		17 (43.5)
Treatment required				
Intensive care unit	14 (34.1)	34 (25.0)	0.31	48 (27.1)
Mechanical ventilation	32 (78.0)	106 (77.9)	1.0	138 (78.0)
Central venous catheter	30 (73.1)	89 (65.4)	0.44	119 (67.2)
Outcome				
Median hospital stay, d (IQR)	36 (24–52)	36 (21–54)	0.98	36 (21.5–54)
Median ICU stay, d (IQR)	24 (18.5–38)	21 (11.2–28.8)	0.08	21.5 (13–33)
Median mechanical ventilation duration, d (IQR)	35.5 (19.8–46)	35 (17.8–51.2)	0.60	35 (18–50)
In-hospital death	15 (36.5)	55 (40.4)	0.71	70 (40.0)

*Values are no. (% within COVID-19 group) except as indicated. IQR, interquartile range; NA, not applicable.

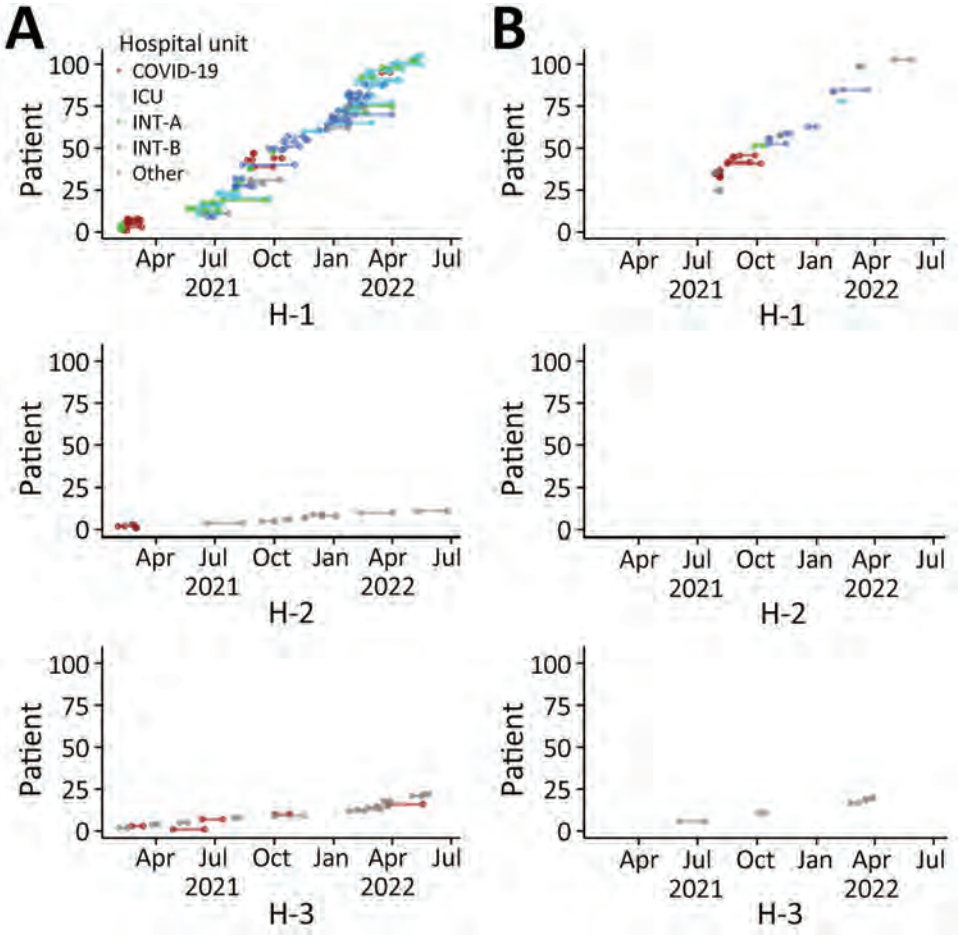

Figure 7. Hospital-level outbreak time course for the 3 hospitals with the largest *Candida auris* case numbers, Israel. Time course of *C. auris* hospital outbreaks is shown for patients receiving mechanical ventilation (A) and patients not receiving mechanical ventilation (B). Individual patients are displayed in bottom to top order according to the first date they became infected. Bars are plotted from the date of first *C. auris*–positive specimen to the date of hospital discharge. Colors represent hospital unit at the time *C. auris* was recovered. COVID-19, specialized COVID-19 unit; H, hospital; ICU, intensive care unit; INT-A, intermediate care unit A; INT-B, intermediate care unit B

A second crucial driver appeared to be mechanical ventilation. Patients with and without COVID-19 had similarly high rates of mechanical ventilation (78%). Moreover, within specific hospitals, *C. auris* spread first among mechanically ventilated COVID-19 patients and then infected non–COVID-19 patients in intermediate care units shared by both recovered COVID-19 and non–COVID-19 patients. This second population included patients with multiple comorbidities, high rates of dementia, and long-term mechanical ventilation. *C. auris* moved between those patient populations asynchronously; gaps of >6 weeks were observed in 2 hospitals between discharge of the last infected COVID-19 patient and admission of a ventilated non–COVID-19 patient who later acquired *C. auris*. Possible explanations include persistence of *C. auris* in the patient environment and on shared medical equipment, as well as undetected carriage by colonized patients or healthcare workers. *C. auris* was previously isolated from 70% of environmental samples at a ventilator-capable skilled nursing facility, including those from handrails, doorknobs, and windowsills (*25*). In vitro studies found that *C. auris* forms biofilm on plastic surfaces and is able to persist in viable colonies for ≥2 weeks and as viable nonculturable cells for ≥4 weeks (*26*).

Among the study cohort, 46% had clinical *C. auris* infection, including 30 patients with candidemia. The in-hospital mortality rate was 40% and was similar for patients colonized and infected with *C. auris*, likely reflecting the multiple acute and chronic comorbidities in this patient population. Of the surviving patients, only 30% were discharged home; the rest were transferred to ventilator-capable skilled nursing facilities, rehabilitation facilities, and long-term care facilities, potentially establishing reservoirs of *C. auris* carriage.

Limitations of this study include lack of systematic active surveillance and environmental sampling in most medical centers. In addition, hospitals differed in some key areas, including criteria for performing yeast species identification and screening for *C. auris* colonization.

In summary, *C. auris* is spreading in multiple hospitals in Israel, and appears set to become endemic in some facilities. The emergence and amplification of

new *C. auris* clones was traced to patients receiving mechanical ventilation in COVID-19 isolation units. *C. auris* was transmitted from this population to non–COVID-19 patients in shared intermediate care units and from there disseminated to nonventilated patient populations. New guidelines addressing this public health threat were recently published by the Israeli Ministry of Health (*27*). Continued surveillance and implementation of infection control measures, focusing on debilitated patients and those receiving mechanical respiratory support, are essential to control the spread of *C. auris*.

Acknowledgments

We thank Miriam Weinberger for her help in preparing the manuscript.

This work was supported by Israeli Science Foundation Moked grant 442/18.

About the Author

Dr. Biran is a resident in internal medicine at the Tel Aviv Sourasky Medical Center, Tel Aviv, Israel. Her primary research interest is the epidemiology of hospital-acquired infections.

References

1. Du H, Bing J, Hu T, Ennis CL, Nobile CJ, Huang G. *Candida auris*: epidemiology, biology, antifungal resistance, and virulence. PLoS Pathog. 2020;16:e1008921. https://doi.org/10.1371/journal.ppat.1008921
2. Lockhart SR, Etienne KA, Vallabhaneni S, Farooqi J, Chowdhary A, Govender NP, et al. Simultaneous emergence of multidrug-resistant *Candida auris* on 3 continents confirmed by whole-genome sequencing and epidemiological analyses. Clin Infect Dis. 2017;64:134–40. https://doi.org/10.1093/cid/ciw691
3. Borman AM, Johnson EM. Candida auris in the UK: introduction, dissemination, and control. PLoS Pathog. 2020;16:e1008563.
4. Centers for Disease Control and Prevention. 2019 AR threats report. 2021 [cited 2021 Jul 24]. https://www.cdc.gov/drugresistance/biggest-threats.html
5. Biagi MJ, Wiederhold NP, Gibas C, Wickes BL, Lozano V, Bleasdale SC, et al. Development of high-level Echinocandin resistance in a patient with recurrent *Candida auris* Candidemia secondary to chronic Candiduria. Open Forum Infect Dis. 2019;6:ofz262. https://doi.org/10.1093/ofid/ofz262
6. Ostrowsky B, Greenko J, Adams E, Quinn M, O'Brien B, Chaturvedi V, et al.; C. auris Investigation Work Group. Candida auris isolates resistant to three classes of antifungal medications—New York, 2019. MMWR Morb Mortal Wkly Rep. 2020;69:6–9. https://doi.org/10.15585/mmwr.mm6901a2
7. Ben-Ami R, Berman J, Novikov A, Bash E, Shachor-Meyouhas Y, Zakin S, et al. Multidrug-resistant *Candida haemulonii* and *C. auris*, Tel Aviv, Israel. Emerg Infect Dis. 2017;23:195–203. https://doi.org/10.3201/eid2302.161486
8. Belkin A, Gazit Z, Keller N, Ben-Ami R, Wieder-Finesod A, Novikov A, et al. *Candida auris* infection leading to nosocomial transmission, Israel, 2017. Emerg Infect Dis. 2018;24:801–4. https://doi.org/10.3201/eid2404.171715
9. Centers for Disease Control and Prevention. Infection prevention and control for *Candida auris*. 2018 [cited 2018 May 23]. https://www.cdc.gov/fungal/candida-auris/c-auris-infection-control.html
10. Tsay S, Kallen A, Jackson BR, Chiller TM, Vallabhaneni S. Approach to the investigation and management of patients with *Candida auris*, an emerging multidrug-resistant yeast. Clin Infect Dis. 2018;66:306–11. https://doi.org/10.1093/cid/cix744
11. Charlson ME, Pompei P, Ales KL, MacKenzie CR. A new method of classifying prognostic comorbidity in longitudinal studies: development and validation. J Chronic Dis. 1987;40:373–83. https://doi.org/10.1016/0021-9681(87)90171-8
12. Satoh K, Makimura K, Hasumi Y, Nishiyama Y, Uchida K, Yamaguchi H. *Candida auris* sp. nov., a novel ascomycetous yeast isolated from the external ear canal of an inpatient in a Japanese hospital. Microbiol Immunol. 2009;53:41–4. https://doi.org/10.1111/j.1348-0421.2008.00083.x
13. Clinical and Laboratory Standards Institute. Reference method for broth dilution antifungal susceptibility testing of yeasts: 4th informational supplement (M27–S4). Wayne (PA): The Institute; 2012.
14. Centers for Disease Control and Prevention. Antifungal susceptibility testing and interpretation. 2020 [cited 2021 Jul 24]. https://www.cdc.gov/fungal/candida-auris/c-auris-antifungal.html
15. Arendrup MC, Prakash A, Meletiadis J, Sharma C, Chowdhary A. Comparison of EUCAST and CLSI reference microdilution MICs of eight antifungal compounds for *Candida auris* and associated tentative epidemiological cutoff values. Antimicrob Agents Chemother. 2017;61:e00485–17. https://doi.org/10.1128/AAC.00485-17
16. Turnidge J, Kahlmeter G, Kronvall G. Statistical characterisation of bacterial wild-type MIC value distributions and the determination of epidemiological cut-off values. Clin Microbiol Infect. 2006;12:418–25. https://doi.org/10.1111/j.1469-0691.2006.01377.x
17. Kwon YJ, Shin JH, Byun SA, Choi MJ, Won EJ, Lee D, et al. *Candida auris* clinical isolates from South Korea: identification, antifungal susceptibility, and genotyping. J Clin Microbiol. 2019;57:e01624-18. https://doi.org/10.1128/JCM.01624-18
18. Prakash A, Sharma C, Singh A, Kumar Singh P, Kumar A, Hagen F, et al. Evidence of genotypic diversity among *Candida auris* isolates by multilocus sequence typing, matrix-assisted laser desorption ionization time-of-flight mass spectrometry and amplified fragment length polymorphism. Clin Microbiol Infect. 2016;22:277.e1–9.
19. Huelsenbeck JP, Ronquist F. MRBAYES: Bayesian inference of phylogenetic trees. Bioinformatics. 2001;17:754–5. https://doi.org/10.1093/bioinformatics/17.8.754
20. Prestel C, Anderson E, Forsberg K, Lyman M, de Perio MA, Kuhar D, et al. *Candida auris* outbreak in a COVID-19 specialty care unit—Florida, July–August 2020. MMWR Morb Mortal Wkly Rep. 2021;70:56–7. https://doi.org/10.15585/mmwr.mm7002e3
21. Rodriguez JY, Le Pape P, Lopez O, Esquea K, Labiosa AL, Alvarez-Moreno C. *Candida auris*: a latent threat to critically ill patients with coronavirus disease 2019. Clin Infect Dis. 2021;73:e2836–7. https://doi.org/10.1093/cid/ciaa1595

22. Villanueva-Lozano H, Treviño-Rangel RJ, González GM, Ramírez-Elizondo MT, Lara-Medrano R, Aleman-Bocanegra MC, et al. Outbreak of *Candida auris* infection in a COVID-19 hospital in Mexico. Clin Microbiol Infect. 2021;27:813–6. https://doi.org/10.1016/j.cmi.2020.12.030
23. Chowdhary A, Tarai B, Singh A, Sharma A. Multidrug-resistant *Candida auris* infections in critically ill coronavirus disease patients, India, April–July 2020. Emerg Infect Dis. 2020;26:2694–6. https://doi.org/10.3201/eid2611.203504
24. Magnasco L, Mikulska M, Giacobbe DR, Taramasso L, Vena A, Dentone C, et al. Spread of carbapenem-resistant gram-negatives and *Candida auris* during the COVID-19 pandemic in critically ill patients: one step back in antimicrobial stewardship? Microorganisms. 2021;9:95. https://doi.org/10.3390/microorganisms9010095
25. Sexton DJ, Bentz ML, Welsh RM, Derado G, Furin W, Rose LJ, et al. Positive correlation between *Candida auris* skin-colonization burden and environmental contamination at a ventilator-capable skilled nursing facility in Chicago. Clin Infect Dis. 2021;73:1142–8. https://doi.org/10.1093/cid/ciab327
26. Welsh RM, Bentz ML, Shams A, Houston H, Lyons A, Rose LJ, et al. Survival, persistence, and isolation of the emerging multidrug-resistant pathogenic yeast *Candida auris* on a plastic health care surface. J Clin Microbiol. 2017;55:2996–3005. https://doi.org/10.1128/JCM.00921-17
27. Israeli Ministry of Health Medical Division. Management of multidrug resistant organisms of special epidemiological importance in medical facilities [in Hebrew]. 2022 [cited 2023 May 25]. https://www.gov.il/he/departments/policies/mr15-2022

Address for correspondence: Ronen Ben-Ami, Department of Infectious Diseases, Tel Aviv Sourasky Medical Center, 6 Weizmann, Tel Aviv 64239, Israel; email: ronenba@tlvmc.gov.il

etymologia

Fonsecaea pedrosoi [fon-se-se′ə pedro´soi]

Dayane Moraes, Alexandre Melo Bailão, Mirelle Garcia Silva-Bailão

Chromoblastomycosis (CBM) is a neglected tropical disease caused by dematiaceous fungi, mainly *Fonsecaea pedrosoi*. This disease resembles blastomycosis in the Americas; the prefix indicates causative microorganisms' pigmentation. In 1911, Pedroso observed histologic pathognomonic findings for CBM. He also observed rounded and brownish elements, now called muriform cells, in skin biopsy specimens from a patient in Goiás, Brazil. In 1915, Medlar described a similar cutaneous infection on the basis of culture and histologic analyses. In 1922, Brumpt reported Pedroso's findings as *Hormodendrum pedrosoi*. Genus description referred to dendroidal conidial chains.

Subsequent publications classified this fungus into different genera (*Botrytoides*, *Phialophora*, *Phidoconidiophora*, and *Trichosporium*) on the basis of type of sporulation. Multiple forms of conidiation in dematiaceous fungi contributed to frequent genus changes. Terra et al. described this fungus as *Acrotheca pedrosoi*. In 1936, Negroni renamed this microorganism *Fonsecaea pedrosoi* because *Hormodendrum* and *Acrotheca* reproductive structures were recognized in samples. The genus was named in honor of Fonseca Filho, a Brazilian investigator who made notable contributions to dermatomycoses.

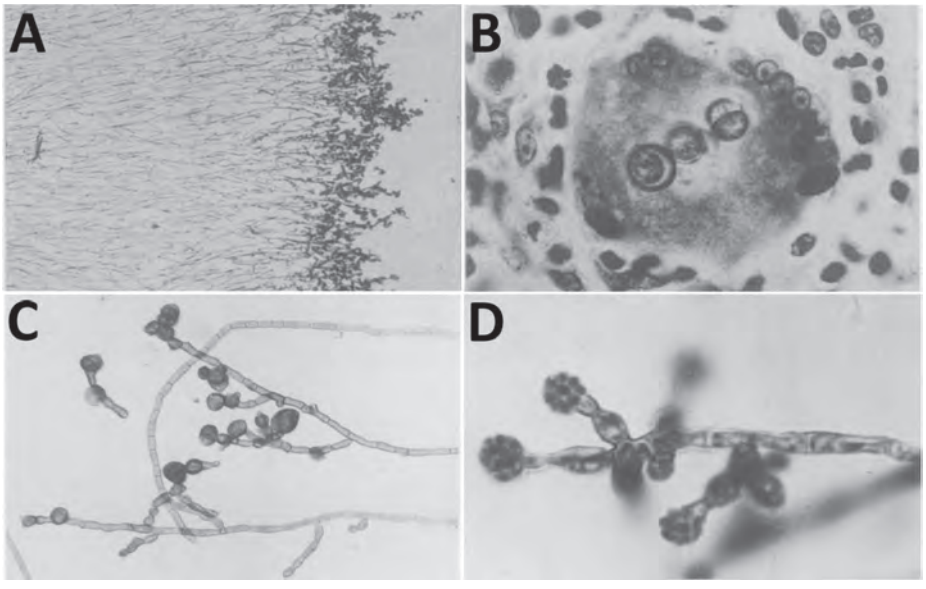

Figure. Micrographs showing tissue and culture analyses of a fungal infection case described by Medlar in 1915. A) Section of 5-week-old colony. B) Muriform bodies inside a giant cell. C) Hyphae in a 4-week-old colony. D) Aerial hypha showing numerous, typical sporogenous cells.

Sources

1. Brumpt E. *Hormodendrum pedrosoi* Brumpt. In: Précis de parasitology [in French]. Paris: Masson and Cie; 1922. p. 1105 [cited 2023 Apr 29]. https://agris.fao.org/-search/search.do?recordID=US201300541075
2. Medlar EM. A cutaneous infection caused by a new fungus, *Phialophora verrucosa*, with a study of the fungus. J Med Res. 1915;32:507–22.9.
3. Negroni P. Study of the first Argentine case of chromomycosis, *Fonsecaea* (Neg.) *pedrosoi* (Brump) 1921 [in Portuguese]. Rev Inst Bacteriol. 1936;7:424.
4. Pedroso A, Gomes JM. About four cases of verrucous dermatitis produced by *Phialophora verrucosa* [in Portuguese]. An Paul Med Cir. 1920;11:53–61.
5. Terra F, Torres M, Fonseca FO, Arêa-Leão A. New type of verrucous dermatitis: *Acrotheca* mycosis associated with leishmaniasis [in Portuguese]. Bras Med. 1922;36:363–8.

Address for correspondence: Mirelle Garcia Silva-Bailão, Laboratório de Biologia Molecular, Universidade Federal de Goiás, Avenida Esperança s/n ICB2, Sala 217, Goiânia, Brazil; email: mgsbailao@ufg.br

Author affiliation: Universidade Federal de Goiás, Goiânia, Goiás, Brazil

DOI: https://doi.org/10.3201/eid2907.230014

Clinical and Mycologic Characteristics of Emerging Mucormycosis Agent *Rhizopus homothallicus*

Shivaprakash M. Rudramurthy,[1] Shreya Singh,[1,2] Rimjhim Kanaujia, Hansraj Chaudhary,[3] Valliappan Muthu, Naresh Panda, Abhishek Pandey, Sheetal Thakur, Harsimran Kaur, Anup Ghosh, Ritesh Agarwal, Arunaloke Chakrabarti[4]

Medscape CME Activity

In support of improving patient care, this activity has been planned and implemented by Medscape, LLC and Emerging Infectious Diseases. Medscape, LLC is jointly accredited with commendation by the Accreditation Council for Continuing Medical Education (ACCME), the Accreditation Council for Pharmacy Education (ACPE), and the American Nurses Credentialing Center (ANCC), to provide continuing education for the healthcare team.

Medscape, LLC designates this Journal-based CME activity for a maximum of 1.00 ***AMA PRA Category 1 Credit(s)™***. Physicians should claim only the credit commensurate with the extent of their participation in the activity.

Successful completion of this CME activity, which includes participation in the evaluation component, enables the participant to earn up to 1.0 MOC points in the American Board of Internal Medicine's (ABIM) Maintenance of Certification (MOC) program. Participants will earn MOC points equivalent to the amount of CME credits claimed for the activity. It is the CME activity provider's responsibility to submit participant completion information to ACCME for the purpose of granting ABIM MOC credit.

All other clinicians completing this activity will be issued a certificate of participation. To participate in this journal CME activity: (1) review the learning objectives and author disclosures; (2) study the education content; (3) take the post-test with a 75% minimum passing score and complete the evaluation at http://www.medscape.org/journal/eid; and (4) view/print certificate. For CME questions, see page 1501.

NOTE: It is Medscape's policy to avoid the use of Brand names in accredited activities. However, in an effort to be as clear as possible, the use of brand names should not be viewed as a promotion of any brand or as an endorsement by Medscape of specific products.

Release date: June 20, 2023; Expiration date: June 20, 2024

Learning Objectives

Upon completion of this activity, participants will be able to:

- Assess the proportion of *Rhizopus homothallicus* infection and clinical characteristics, including 30-day mortality in rhino-orbital mucormycosis from *R. homothallicus* vs *Rhizopus arrhizus*, of emerging *R. homothallicus* reported from a tertiary care center in India, based on a retrospective review of consecutive mucormycosis cases
- Evaluate the mycological characteristics, including antifungal susceptibility testing and amplified length polymorphism of emerging *Rhizopus homothallicus* reported from a tertiary care center in India, based on a retrospective review of consecutive mucormycosis cases
- Determine the clinical implications of the clinical and mycological characteristics of emerging *Rhizopus homothallicus* reported from a tertiary care center in India, based on a retrospective review of consecutive mucormycosis cases

CME Editor

Jude Rutledge, BA, Technical Writer/Editor, Emerging Infectious Diseases. *Disclosure: Jude Rutledge, BA, has no relevant financial relationships.*

CME Author

Laurie Barclay, MD, freelance writer and reviewer, Medscape, LLC. *Disclosure: Laurie Barclay, MD, has no relevant financial relationships.*

Authors

Shivaprakash M. Rudramurthy, MD, PhD; Shreya Singh, MD; Rimjhim Kanaujia, MD; Hansraj Chaudhary, MSc, PhD scholar; Valliappan Muthu, MD; Naresh Panda, MS; Abhishek Pandey, MSc; Sheetal Thakur, MSc, PhD scholar; Harsimran Kaur, MD; Anup Ghosh, PhD; Ritesh Agarwal, MD; and ***Arunaloke Chakrabarti, MD.***

Author affiliation: Postgraduate Institute of Medical Education and Research, Chandigarh, India

DOI: https://doi.org/10.3201/eid2907.221491

[1]These first authors contributed equally to this article.

[2]Current affiliation: Dr. B R Ambedkar State Institute of Medical Sciences, Mohali, India.

[3]Current affiliation: Indian Council of Medical Research, New Delhi, India.

[4]Current affiliation: Doodhadhari Burfani Hospital, Haridwar, India.

We retrospectively reviewed consecutive cases of mucormycosis reported from a tertiary-care center in India to determine the clinical and mycologic characteristics of emerging *Rhizopus homothallicus* fungus. The objectives were ascertaining the proportion of *R. homothallicus* infection and the 30-day mortality rate in rhino-orbital mucormycosis attributable to *R. homothallicus* compared with *R. arrhizus. R. homothallicus* accounted for 43 (6.8%) of the 631 cases of mucormycosis. *R. homothallicus* infection was independently associated with better survival (odds ratio [OR] 0.08 [95% CI 0.02–0.36]; p = 0.001) than for *R. arrhizus* infection (4/41 [9.8%] vs. 104/266 [39.1%]) after adjusting for age, intracranial involvement, and surgery. We also performed antifungal-susceptibility testing, which indicated a low range of MICs for *R. homothallicus* against the commonly used antifungals (amphotericin B [0.03–16], itraconazole [0.03–16], posaconazole [0.03–8], and isavuconazole [0.03–16]). 18S gene sequencing and amplified length polymorphism analysis revealed distinct clustering of *R. homothallicus*.

Mucormycosis is an angioinvasive disease caused by the saprophytic fungi of the order Mucorales. The estimated prevalence of mucormycosis is ≈70 times higher in India than elsewhere (*1*). *Rhizopus arrhizus* is the most common etiologic agent of mucormycosis in India and worldwide (*2*). Other reported Mucorales include *Apophysomyces variabilis*, *Cunnighamella* spp., *Lichtheimia* spp., *Mucor* spp., *Rhizomucor* spp., *Rhizopus microsporus*, *Rhizopus homothallicus*, *Saksenaea vasiformis*, *Syncephalastrum* spp., and *Thamostylum lucnowense* (*3*–*7*). *R. arrhizus* was the most common causative agent even during the recent outbreak of COVID-19–associated mucormycosis (CAM) in India (*8*). Although infection with *R. homothallicus* was also reported in a few patients (*9*), the importance of mucormycosis caused by *R. homothallicus* is unclear. We report the percentage of patients with mucormycosis caused by *R. homothallicus* at our center (Postgraduate Institute of Medical Education and Research [PGIMER], Chandigarh, India) and describe clinical features, mycologic characteristics, antifungal susceptibility, treatment, and mortality rates. We also assess whether the mortality rate from rhino-orbital mucormycosis (ROM) caused by *R. homothallicus* is different from that of *R. arrhizus* disease.

The primary objectives of this study were to assess the proportion of patients with mucormycosis caused by *R. homothallicus* and 30-day mortality rate from ROM caused by *R. homothallicus* and to determine whether the species of Mucorales (*R. homothallicus* vs. *R. arrhizus*) was an independent predictor of death from ROM. The secondary objectives were to compare the profile of patients infected with *R. homothallicus* versus *R. arrhizus* and to ascertain the mycologic characteristics of *R. homothallicus* isolates by conducting antifungal-susceptibility testing (AFST) and amplified fragment length polymorphism (AFLP) analysis.

Methods

Study Design and Setting

We performed a retrospective study at PGIMER on a 10-month period (January–October 2021). Our center's institutional ethics committee approved the study protocol. We were granted a consent waiver because the study was a retrospective analysis of anonymized patient data. We report the study according to the Strengthening the Reporting of Observational Studies in Epidemiology statement (*10*). Data for a few participants published in this study have been reported in previous studies (*11*–*13*). We conducted the study in accordance with Declaration of Helsinki guidelines; the study was approved by the PGIMER Institutional Review Board (approval no. PGI/IEC/2021/001101) in August 2021.

Study Participants

We enrolled consecutive patients with ROM caused by *R. homothallicus* and *R. arrhizus*. The patients in whom mucormycosis caused by *R. homothallicus* and *R. arrhizus* was diagnosed were identified from our mycology laboratory records; we collected relevant clinical data from the patient records. We followed the study participants until discharge or 30 days after their mucormycosis was diagnosed. We sought any missing information for the study by contacting patients by telephone. We excluded patients for whom information was not adequate or not available. We obtained informed consent from all patients involved in the study.

Data Collection and Variables

For eligible patients with ROM, we retrieved data on age, sex, and risk factors for mucormycosis (e.g., diabetes mellitus, COVID-19 infection, organ transplantation, immunosuppressive therapy, hematologic malignancies). We defined diabetes mellitus as recently diagnosed if the disease was detected (hyperglycemia and glycated hemoglobin >6.5%) during the current illness. We also retrieved clinical details, including signs and symptoms of ROM, treatment, and outcome of all patients (noted on follow up at 30 days after mucormycosis diagnosis, irrespective of discharge from hospital). All the study participants received the standard of care treatment in accordance with our institutional protocol.

Study Definitions

Mucormycosis was diagnosed in patients with compatible clinical and radiologic features and confirmed

by histopathologic or microbiologic methods, as previously described (*8*). We arbitrarily defined COVID-19–associated mucormycosis as mucormycosis diagnosed simultaneously with or within 3 months of virologically confirmed COVID-19 (*14*).

Phenotypic Identification of the Isolates

We inoculated tissue samples collected from patients on Sabouraud dextrose agar and dichloran rose bengal chloramphenicol (both from HiMedia, India) with benomyl. We isolated the Mucorales from the culture and confirmed them by demonstrating broad aseptate ribbon-shaped hyphae on direct microscopic examination of the samples. We performed phenotypic identification on the basis of the colony morphology (e.g., texture, growth rate, and color) and microscopic findings (i.e., lactophenol cotton blue mount prepared from slide culture) (*15*). We then summarized the distinctive features of *R. arrhizus* and *R. homothallicus* (Table 1; Figure 1).

Molecular Identification of the Isolates

We confirmed identification of all *R. homothallicus* isolates from ROM cases and 6 additional *R. homothallicus* isolates from pulmonary mucormycosis cases by using a molecular sequencing method. In addition, we used sequences of 2 environmental isolates of *R. homothallicus* for comparison with clinical strains. We submitted to GenBank and included for phylogenetic analysis only isolates with good-quality sequences (Appendix Table 1, https://wwwnc.cdc.gov/EID/article/29/7/22-1491-App1.pdf). We included the DNA sequences of 1 isolate each of *R. microsporus* and *R. arrhizus* from our culture collection as controls. For DNA extraction, we used freshly grown sporulated culture suspended in 500 µL of lysis buffer and incubated for 5 minutes at 56°C. We then extracted DNA by using the phenol–chloroform–isoamyl alcohol (25:24:1) method, as previously described (*16*). We used PCR-based amplification of the 18S, internal transcribed spacer, and 28S genes, followed by sequencing using previously published primers for molecular identification (*17*). Because we obtained mixed chromatograms in most isolates of *R. homothallicus* by sequencing the internal transcribed spacer and 28S regions, we used the sequences of 18S for phylogenetic analysis. We aligned all sequences of the study isolates and reference sequences of various *Rhizopus* species obtained from GenBank by using MEGA 7.0 (*18*). We studied the evolutionary relationship of isolates by constructing a phylogenetic tree by using neighbor-joining analysis in MEGA 7.0.

Table 1. Mycologic characteristics of *Rhizopus arrhizus* and *R. homothallicus* based on macroscopic and microscopic findings of tissue samples from patients enrolled in a 10-month retrospective study, Chandigarh, India, January–October 2021*

Characteristic	*R. homothallicus*	*R. arrhizus*
Macroscopic appearance		
Growth rate	Fast-growing colonies and sporulation relatively slower than *R. arrhizus*	Fast-growing colonies and sporulation relatively faster than *R. homothallicus*
Obverse surface growth	Cottony, white colonies that turn **grayish to olive brown** with a variegated appearance; because of the large-sized zygospores, brownish tufts can be seen unevenly distributed throughout the mycelial growth	Cottony, white colonies that turn gray with **typical salt and pepper appearance**
Reverse macroscopic findings	Reverse surface has no pigment	Reverse surface has no pigment
Microscopic findings		
Hyphae	Aseptate hyphae, less prominent rhizoids; smooth and thick-walled intercalary chlamydospore	Aseptate hyphae, well-developed nodal rhizoids with occasional intercalary chlamydospores
Sporangiophore	Erect, unbranched, or dichotomously branched (length 300–2,000 µm, width 5–30 µm)	Single or tufts of mostly unbranched sporangiophores (length 1,000–2,000 µm, width 7–18 µm)
Sporangium	Sparsely noted in cultures; when present, appears spherical and greyish brown (20–140 µm) with conspicuous dark apophysis and subspherical columella	Spherical sporangia (20–250 µm) with short apophysis and spherical columella occupying 50% of sporangium
Sporangiospores	Spherical to broadly ellipsoidal (3–5 × 4–8 µm), hyaline, and thick-walled with less prominent striations	Lemon-shaped or subspherical to ellipsoidal (6–8 × 4.5–5 µm) with striations, rough surface
Zygospores	Homothallic;† **abundant golden brown zygospores** (60–100 µm) with stellate spinous projections, attached to large globose suspensor cells that are unequal in size	Heterothallic **zygospores not seen on primary culture**; red-brown spherical or laterally flattened (60–140 µm) with flat projections; suspensors are unequal, spherical to conical

*Key features highlighted in bold.
†Differentiation from other homothallic *Rhizopus* species that produce abundant zygospores (e.g., *R. sexualis* and *R. azygosporus*) is done based on size of the suspensor cells of the zygospore and by molecular identification using the internal transcribed spacer and 28S sequences of rDNA.

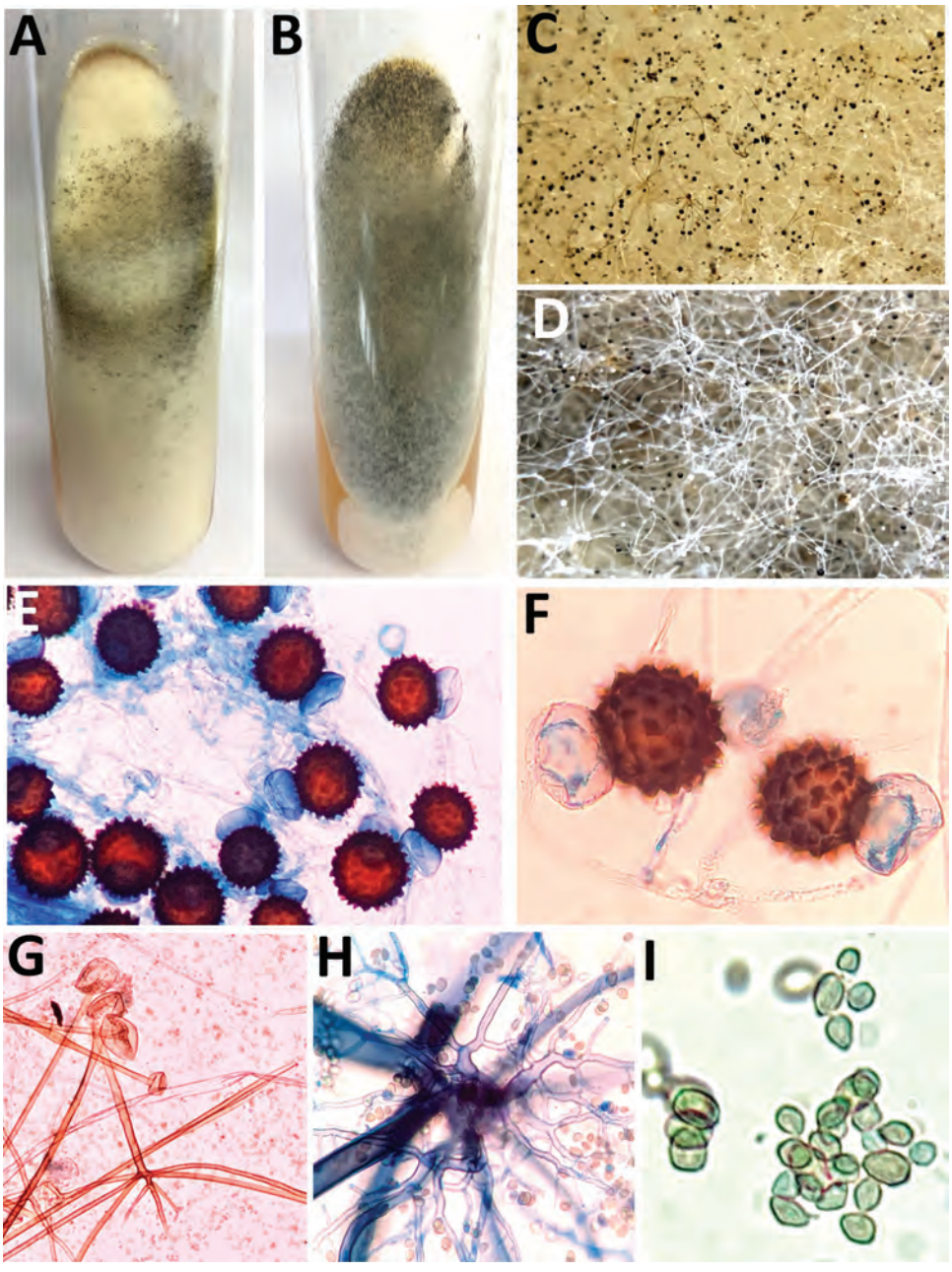

Figure 1. Macroscopic and microscopic characteristics of *Rhizopus arrhizus* and *R. homothallicus* isolated from tissue samples from patients enrolled in a 10-month retrospective study, Chandigarh, India, January–October 2021. A, B) Macroscopic appearance of colonies of *R. homothallicus* (A) and *R. arrhizus* (B) fungi. C, D) Macro lens image of the colonies showing dark-brown specks in *R. homothallicus* (C) and black and white dots (salt and pepper appearance) in *R. arrhizus* (D). E) Photomicrograph from a lactophenol cotton blue mount of *R. homothallicus* showing multiple reddish brown ornamented zygospores (original magnification ×400). F) Magnified image of panel E showing unequal suspenser cells and zygospore with prominent spinous projections. G) *R. arrhizus* showing long, unbranched sporangiophore with nodal rhizoids (original magnification ×200). H) Magnified image of extensively branched rhizoid seen in *R. arrhizus*. I) Magnified image of sporangiospores of *R. arrhizus*.

AFST

We performed AFST of the isolates for amphotericin B, itraconazole, posaconazole, isavuconazole, and terbinafine in accordance with Clinical and Laboratory Standards Institute (CLSI) standards (*19*). In brief, we diluted the drugs in the standard Roswell Park Memorial Institute 1640 medium and then dispensed 100 µL into each well of 96-well microdilution trays. We tested MICs in the range of 0.03–16 µg/mL. We prepared the inoculum by harvesting the zygospores in 0.85% normal saline and adjusted spore counts by using a spectrophotometer at an absorbance of 530 nm. On adjusting the optical density (OD) to limits of 0.15–0.17 (0.4–5.0 × 10^4 zygospores/mL), we observed no growth on subsequent incubation; hence, we used a higher OD of 0.2–0.3 (0.3–5.0 × 10^6 zygospores/mL, confirmed by counting on hemocytometer). We diluted the suspensions to 1:50 in Roswell Park Memorial Institute 1640 medium and incubated the microtiter plates at 35°C for 4–8 days until visible growth was observed in the growth control. We defined MIC endpoints as the lowest drug concentration that inhibited any recognizable growth. We used *Candida krusei* (ATCC 6258)

and *Aspergillus flavus* (ATCC 204304) as the quality-control strains.

Because of the absence or presence of fewer sporangiospores in *R. homothallicus*, performing AFST was challenging, and we modified the standard CLSI guidelines of AFST for this study. We used a higher OD with more inoculum containing both zygospores and hyphal fragments; performed intermittent vortexing of the inoculum for up to 45 minutes to ensure homogenous suspension (because zygospores tend to settle fast and are sometimes unevenly distributed between the wells); and conducted reading of AFST results up to 7 days (because zygospores take longer time to germinate or multiply compared with sporangiospores). The last step is in contrast to the standard protocol of reading the results at 24 hours for other medically important Mucorales, according to CLSI (*19*).

AFLP Analysis

We performed AFLP typing of *R. homothallicus* isolates as previously described (*20*). We used ≈50 ng of genomic DNA for the combined restriction–ligation procedure. We fragmented the DNA by using the 5 units each of restriction enzymes *Eco*RI and *Hin*dIII (New England Biolabs). For the preselective amplification, we used 10 μmol/L each of preselective primers of *Eco*RI primer (5′-GACTGCGTACCAATTC-3′) and *Hin*dIII (5′-GACTGCGTACCAGCTT-3′). We used the 6-carboxyfluorescein (6-FAM) labeled primers for selective amplification. We used 10 μmol/L each of *Hin*dIII primer (5′-ACTGCGTACCAGCTTT-3′) and *Eco*RI primer (5′-GACTGCGTACCAATTCAC-3′) for selective amplification. We performed capillary electrophoresis to identify the restricted DNA fragments and reference marker (LIZ 500) in a genetic analyzer (3500 Genetic Analyzer 8 Capillary Array; Applied Biosystems). We imported the fingerprint data into BioNumerics 6.6 (Applied Maths) and converted curves into bands for analysis. We calculated the genetic diversity by using the Pearson correlation coefficient and clustered the isolates by using the unweighted pair group method with arithmetic mean. Although no definite cutoff for differentiating between strains exists, we used an arbitrary cutoff of <70% for genus differentiation and >70% for species differentiation. We defined clonal isolates when the similarity was in the range of 95%–99%.

Statistical Analysis

For statistical analysis, we used SPSS Statistics 22.0 (IBM) and GraphPad Prism 9.0 (GraphPad

Table 2. Comparison of mucormycosis caused by *Rhizopus homothallicus* versus *R. arrhizus* in patients enrolled in a 10-month retrospective study, Chandigarh, India, January–October 2021*

Parameter	*R. homothallicus*, n = 41	*R. arrhizus*, n = 266	p value
Mean age, y (± SD)	45.9 (± 12.8)	52.5 (± 12.7)	0.002
Sex			
M	23/41 (56.1)	182/266 (68.4)	0.15
F	18/41 (43.9)	84/266 (31.6)	
Risk factors			
CAM	23/41 (56.1)	256/266 (96.2)	0.0001
Duration after COVID-19, d (± SD)	6.13 (± 13.5)	11.9 (± 14.8)	0.07
Diabetes mellitus	39/41 (95.1)	223/238 (93.7)	0.72
Recently diagnosed diabetes mellitus	9/39 (23.1)	54/223 (24.2)	
Renal transplantation	0	1/238 (0.4)	1.00
Intracranial involvement	3/41 (7.3)	13/266 (4.9)	0.46
Clinical features			
Fever	4/41 (9.8)	3/55 (5.5)	0.42
Headache	4/41 (9.8)	10/55 (18.2)	0.38
Toothache	4/41 (9.8)	5/55 (9.1)	0.91
Eye swelling	27/41 (65.9)	27/55 (49.1)	0.10
Facial pain	11/41 (26.8)	22/55 (40)	0.18
Facial swelling	16/41 (39)	22/55 (40)	0.92
Proptosis	3/41 (7.3)	0	0.08
Visual disturbance	18/41 (43.9)	7/55 (12.7)	0.0005
Oral ulcer	3/41 (7.3)	10/55 (18.2)	0.12
Nasal crust	5/41 (12.2)	5/55 (9.1)	0.62
Palatal eschar	5/41 (12.2)	10/55 (18.2)	0.42
Management			
Amphotericin therapy	38/41 (92.7)	212/218 (97.2)	0.14
LAMB	36/38 (94.7)	196/212 (92.5)	
Conventional AMB	2/38 (5.3)	16/212 (7.5)	
Surgery	24/36 (66.7)	184/245 (75.1)	0.31
30-day mortality	4/41 (9.8)	104/266 (39.1)	0.0001

*Values are no. patients/no. with data available (%) except as indicated. CAM, COVID-19–associated mucormycosis; LAMB, liposomal amphotericin B; AMB, amphotericin.

Table 3. Binary logistic regression analysis demonstrating the factors associated with death among patients with rhino-orbital mucormycosis enrolled in a 10-month retrospective study, Chandigarh, India, January–October 2021*

Variable	Survivors	Nonsurvivors	Odds ratio (95% CI)	p value
Mean age, y (± SD)	55.8 (± 12.4)	49.4 (± 12.6)	1.06 (1.03–1.08)	0.0001
Male sex	124/199 (62.3)	81/108 (75)	1.38 (0.75–2.53)	0.31
Intracranial involvement	4/199 (2)	12/108 (11.1)	22.7 (4.03–128.1)	0.0001
Surgery for ROM	144/173 (83.2)	64/108 (59.3)	0.22 (0.11–0.43)	0.0001
R. homothallicus infection	37/199 (18.6)	4/108 (3.7)	0.08 (0.02–0.36)	0.001

*Values are no. patients/no. with data available (%) except as indicated. ROM, rhino-orbital mucormycosis.

Software). We present the descriptive data as mean ±SD for continuous variables and frequencies with percentages for categorical variables. We compared differences between the 2 groups by using the χ^2 test and Fisher exact test for categorical variables, as appropriate, and used the Student *t*-test test to compare continuous data. We performed a binary logistic regression analysis of variables (age, sex, presence of brain involvement, combined medical–surgical therapy for ROM, and causative species [*R. homothallicus* vs. *R. arrhizus*]) that influenced the mortality rate for ROM and reported the adjusted odds ratio (aOR) and 95% CI. All the statistical tests were 2-sided, and we considered a p value <0.05 to be statistically significant.

Results

Of the 631 patients with culture-confirmed mucormycosis, 43 (6.8%) had infection attributable to *R. homothallicus*. We excluded 324 cases from the study (262 because of inadequate information [e.g., lost to follow up], 35 because of non–*R. arrhizus* and non–*R. homothallicus* mucormycosis, and 27 non-ROM cases). We analyzed 41 ROM cases caused by *R. homothallicus* and 266 consecutive ROM cases attributable to *R. arrhizus*.

The mean ±SD age of the 307 patients with ROM was 51.6 years ±12.8 years, and most were men (205 [66.8%]). The mean age of patients with *R. arrhizus* infection was significantly higher than that for patients with ROM caused by *R. homothallicus*. Data on diabetes status were available for 279 patients; 93.9% had diabetes, and of those, 45 (16.1%) had diabetic ketoacidosis during the initial encounter. We observed no statistically significant difference between the risk factors proportion of patients with intracranial involvement or medical and surgical management in the 2 study groups (Table 2). The overall mortality rate was 35.2% (108/307) and was significantly higher among patients infected with *R. arrhizus* compared with *R. homothallicus* (39.1% vs. 9.8%; p = 0.0001). The mortality rate of patients with ROM caused by *R. homothallicus* was not significantly different between CAM and non-CAM subgroups (Appendix Table 2).

On multivariate analysis, infection with *R. homothallicus* and surgery for ROM were independently associated with lower odds of death. A higher age (odds ratio [OR] 1.01 [95% CI 1.03–1.08]) and the presence of brain involvement (OR 22.7 [95% CI 4.03–128.10]) were independently associated with higher mortality rates among ROM cases (Table 3).

We performed AFST for 34 *R. homothallicus* isolates. We calculated the geometric mean, range, and MICs at which 50% (MIC_{50}) and 90% (MIC_{90}) of isolates are inhibited for amphotericin B, itraconazole, posaconazole, isavuconazole, and terbinafine (Table 4).

The phylogram constructed using 18S sequences (40 clinical and 2 environmental isolates of *R. homothallicus* and 1 each of *R. arrhizus* and *R. microsporus*) (Figure 2; Appendix Table 1) and the AFLP results (Appendix Figure) both revealed distinct clustering of *R. homothallicus* from the other tested species. We observed no prominent clades among isolates of *R. homothallicus* from patients with CAM versus non-CAM.

Discussion

We report a 6.8% prevalence of *R. homothallicus* infection among culture-confirmed mucormycosis cases. The mortality rate for ROM caused by *R. homothallicus* was significantly less than that for *R. arrhizus* (9.8% vs. 39.1%) after adjusting for age, sex, intracranial extension of the disease, and surgery for mucormycosis in the binary logistic regression model. The AFST data indicated good susceptibility to the common antifungal drugs and the newer agent isavuconazole.

Table 4. Distribution of MICs of 34 *Rhizopus homothallicus* isolates from patients enrolled in a 10-month retrospective study, Chandigarh, India, January–October 2021*

Antifungal agent	Geometric mean (range), mg/L	MIC_{50}, mg/L	MIC_{90}, mg/L
Amphotericin B	0.75 (0.03–16)	2	4
Itraconazole	0.51 (0.03–16)	0.5	8
Posaconazole	0.24 (0.03–8)	0.12	2
Isavuconazole	0.32 (0.03–16)	0.25	2
Terbinafine	0.34 (0.03–16)	0.25	4

*MIC_{50}, MIC at which 50% of isolates are inhibited; MIC_{90}, MIC at which 90% of isolates are inhibited.

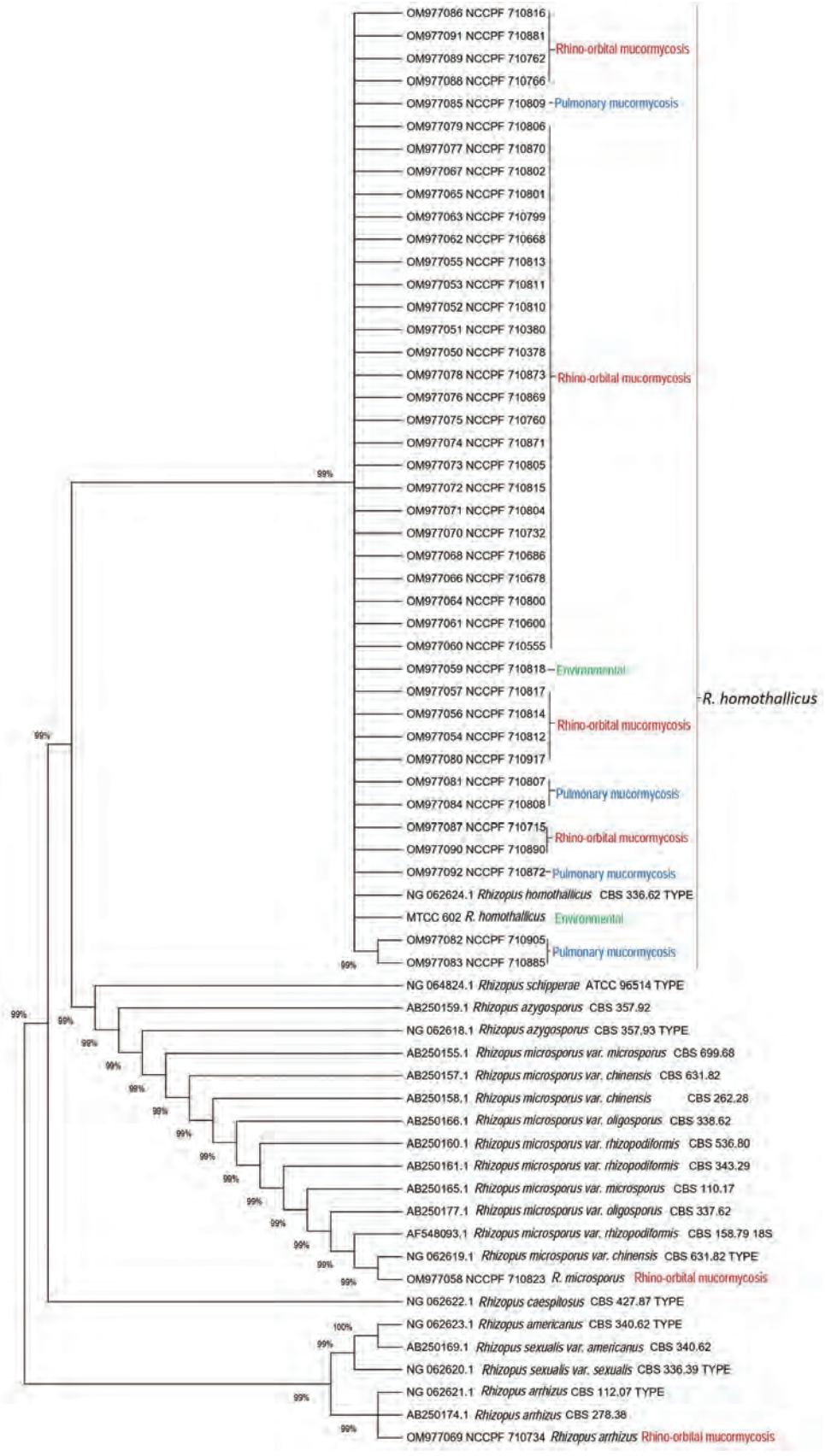

Figure 2. Evolutionary relationships of 40 *Rhizopus homothallicus* isolates from patients in a 10-month study, Chandigarh, India, January–October 2021, and 2 environmental isolates.January–October 2021. GenBank accession numbers of 41 clinical and 1 environmental–MTCC 602 isolate of *R. homothallicus* from India are shown. Tree generated using neighbor-joining algorithm with 1,000 bootstrap replicates.

The 18S gene sequencing and AFLP revealed distinct clustering of *R. homothallicus* from the common species implicated in ROM.

Human infection with *R. homothallicus* was first reported from North India (*4*) in a case of pulmonary mucormycosis and was followed by a few more reports (*5*,*21*). In 2 prospective multicenter studies from India, *R. homothallicus* accounted for 2.5% (6/239) (*22*) and 7.6% (22/290) (*23*) of the cases where the causative organism could be identified. Despite a higher prevalance of mucormycosis cases (associated with the CAM outbreak) in our study, the prevalence of *R. homothallicus* mucormycosis (6.8%) was similar to that in the previous reports.

R. homothallicus, a homothallic fungus, produces more heavy sexual spores than asexual spores (sporangiospores) and undergoes less dispersion in the air. The relative amount of sporangiospores is considerably lower in *R. homothallicus* than in the heterothallic *Rhizopus* species (*24*). Consequently, the chances of acquiring infection with *R. homothallicus* are expected to be low. Thus, *R. homothallicus* infections probably indicate the presence of some unidentified environmental niche where this agent can produce asexual spores abundantly and disperse them in the air. Recent studies have shown *R. homothallicus* in the hospital air and air samples obtained from the residence of patients with mucormycosis (*25*,*26*).

The mortality rate for mucormycosis may vary with the causative species. For instance, 2 systematic reviews have shown higher mortality rates for infections with *Cunninghamella* spp. than those with *R. arrhizus* (*2*,*27*). We observed a significantly better survival rate with *R. homothallicus* infection compared with *R. arrhizus*. A substantially higher proportion of patients with *R. homothallicus* infection had visual disturbance (44% vs. 13% for *R. arrhizus*), and this difference could have led to earlier detection. The duration of symptoms in CAM patients with mucormycosis caused by *R. homothallicus* and *R. arrhizus* was also different, although not significantly (6 vs. 12 days; p = 0.07). The timely initiation of antifungal therapy, intracranial spread of disease, and surgery for mucormycosis are important factors determining the outcome of mucormycosis (*28*,*29*). We conducted a preliminary growth curve analysis at 25°C, 37°C, and 40°C (data not shown) to determine whether the 2 species had a difference in growth rate. We observed an overall faster time to log phase at all temperatures for *R. arrhizus* compared with *R. homothallicus* (6 h vs. 27 h at 25°C, 5 h vs. 32 h at 37°C, and 6 h vs. 25 h at 40°C). However, further in vivo studies are required to identify the different pathogenic potentials of these 2 Mucorales species.

The first limitation of our study was that it was retrospective and conducted at a single center, limiting generalizability. We do not have information on all patients with ROM caused by *R. arrhizus*, and the proportion of patients with CAM was much higher in the *R. arrhizus* group than in the *R homothallicus* group. However, data from our center and another large multicenter study from India showed similar mortality rates for ROM with or without COVID-19 co-infection (*8*,*11*). Because our study focused exclusively on ROM cases, future studies should explore pulmonary or other sites of involvement, which are inherently associated with higher mortality rates (*30*). Although we noted a lower mortality rate from *R. homothallicus* infection on multivariate analysis, we cannot exclude residual confounding factors that could have resulted in improved survival with *R. homothallicus* infection. Also, we do not have a detailed evaluation of risk factors or genetic analysis to ascertain whether specific factors predispose persons to infection with *R. homothallicus*. Alhough the AFLP method is known for poor reproducibility, the results may be within an acceptable range when the test is repeated with the same batch of reagents, as we observed with our *R. homothallicus* isolates. Moreover, modification of the AFST protocol makes the results difficult to interpret and compare with published data.

In conclusion, our results show that *R. homothallicus* is an important agent of mucormycosis with epidemiologic and clinical significance. *R. homothallicus* may be less virulent or manifest earlier than *R. arrhizus*, thus resulting in better survival. Identifying *R. homothallicus* based on macroscopic and microscopic appearance is not difficult and should be emphasized. Most *R. homothallicus* isolates are uniformly susceptible to the commonly used antifungal agents to manage mucormycosis.

The Indian Council of Medical Research partially funded this work (grant no. ref no. AMR/149/2018-ECD-II).

Author contributions: conceptualization (S.M.R. and A.C.); methodology (S.S., R.K., N.P., H.C., A.P., and S.T.); formal analysis (S.S. and R.K.); investigations (H.C., A.P., R.K., and H.K.); resources (S.M.R. and A.C.); data curation (R.K., S.T., N.P., and V.M.); data interpretation (A.C., S.M.R., S.S., and V.M.); writing original draft (S.S.); writing review and editing (A.C., S.M.R., R.K., H.K., A.G., V.M., and R.A.); visualization (S.S.); and project administration (A.C.).

About the Author

Dr. Rudramurthy is professor and heads the Mycology Division of the Medical Microbiology Department at the Postgraduate Institute of Medical Education and Research in Chandigarh, India. His primary research interests include epidemiology, antifungal resistance, and molecular diagnosis of fungal infections. Dr. Singh is an assistant professor at the Dr. B R Ambedkar State Institute of Medical Sciences in Mohali, India. Her primary research interests include medial mycology, fungal diagnostics, and invasive fungal diseases.

References

1. Prakash H, Chakrabarti A. Epidemiology of mucormycosis in India. Microorganisms. 2021;9:523. https://doi.org/10.3390/microorganisms9030523
2. Jeong W, Keighley C, Wolfe R, Lee WL, Slavin MA, Kong DCM, et al. The epidemiology and clinical manifestations of mucormycosis: a systematic review and meta-analysis of case reports. Clin Microbiol Infect. 2019;25:26–34. https://doi.org/10.1016/j.cmi.2018.07.011
3. Singh S, Pal N, Chander J, Sardana R, Mahajan B, Joseph N, et al. Mucormycosis caused by *Syncephalastrum* spp.: clinical profile, molecular characterization, antifungal susceptibility and review of literature. Clin Infect Pract. 2021;11:100074. https://doi.org/10.1016/j.clinpr.2021.100074
4. Chakrabarti A, Marak RS, Shivaprakash MR, Gupta S, Garg R, Sakhuja V, et al. Cavitary pulmonary zygomycosis caused by *Rhizopus homothallicus*. J Clin Microbiol. 2010;48:1965–9. https://doi.org/10.1128/JCM.01272-09
5. Kokkayil P, Pandey M, Agarwal R, Kale P, Singh G, Xess I. *Rhizopus homothallicus* causing invasive infections: series of three cases from a single centre in North India. Mycopathologia. 2017;182:921–6. https://doi.org/10.1007/s11046-017-0153-5
6. Chakrabarti A, Ghosh A, Prasad GS, David JK, Gupta S, Das A, et al. *Apophysomyces elegans*: an emerging zygomycete in India. J Clin Microbiol. 2003;41:783–8. https://doi.org/10.1128/JCM.41.2.783-788.2003
7. Chakrabarti A, Shivaprakash MR, Curfs-Breuker I, Baghela A, Klaassen CH, Meis JF. *Apophysomyces elegans*: epidemiology, amplified fragment length polymorphism typing, and in vitro antifungal susceptibility pattern. J Clin Microbiol. 2010;48:4580–5. https://doi.org/10.1128/JCM.01420-10
8. Patel A, Agarwal R, Rudramurthy SM, Shevkani M, Xess I, Sharma R, et al.; MucoCovi Network3. Multicenter epidemiologic study of coronavirus disease-associated mucormycosis, India. Emerg Infect Dis. 2021;27:2349–59. https://doi.org/10.3201/eid2709.210934
9. Kaur H, Kanaujia R, Rudramurthy SM. *Rhizopus homothallicus*: an emerging pathogen in era of COVID-19 associated mucormycosis. Indian J Med Microbiol. 2021;39:473–4. https://doi.org/10.1016/j.ijmmb.2021.06.013
10. Vandenbroucke JP, von Elm E, Altman DG, Gøtzsche PC, Mulrow CD, Pocock SJ, et al.; STROBE Initiative. Strengthening the Reporting of Observational Studies in Epidemiology (STROBE): explanation and elaboration. Int J Surg. 2014;12:1500–24. https://doi.org/10.1016/j.ijsu.2014.07.014
11. Muraleedharan M, Panda NK, Angrish P, Arora K, Patro SK, Bansal S, et al. As the virus sowed, the fungus reaped! A comparative analysis of the clinico-epidemiological characteristics of rhino-orbital mucormycosis before and during COVID-19 pandemic. Mycoses. 2022;65:567–76. https://doi.org/10.1111/myc.13437
12. Muthu V, Dhaliwal M, Sharma A, Nair D, Kumar HM, Rudramurthy SM, et al. Serum glucose-regulated protein 78 (GRP78) levels in COVID-19–associated mucormycosis: results of a case-control study. Mycopathologia. 2022;187:355–62. https://doi.org/10.1007/s11046-022-00645-6
13. Kumar H M, Sharma P, Rudramurthy SM, Sehgal IS, Prasad KT, Pannu AK, et al. Serum iron indices in COVID-19–associated mucormycosis: a case-control study. Mycoses. 2022;65:120–7. https://doi.org/10.1111/myc.13391
14. Muthu V, Agarwal R, Patel A, Kathirvel S, Abraham OC, Aggarwal AN, et al. Definition, diagnosis, and management of COVID-19–associated pulmonary mucormycosis: Delphi consensus statement from the Fungal Infection Study Forum and Academy of Pulmonary Sciences, India. Lancet Infect Dis. 2022;22:e240–53. https://doi.org/10.1016/S1473-3099(22)00124-4
15. de Hoog GS, Guarro J, Gene J, Ahmed SA, Al-Hatmi AMS, Figueras MJ, et al. Atlas of clinical fungi. 4th edition. Hilversum: Foundation Atlas of Fungi; 2020
16. Shivaprakash MR, Appannanavar SB, Dhaliwal M, Gupta A, Gupta S, Gupta A, et al. *Colletotrichum truncatum*: an unusual pathogen causing mycotic keratitis and endophthalmitis. J Clin Microbiol. 2011;49:2894–8. https://doi.org/10.1128/JCM.00151-11
17. White TJ, Bruns S, Lee S, Taylor J. Amplification and direct sequencing of fungal ribosomal RNA genes for phylogenetics. In: Innis MA, Gelfand DH, Sninsky JJ, White TJ, editors. PCR protocols: a guide to methods and applications. London: Academic Press; 1990. p. 315–22.
18. Kumar S, Stecher G, Tamura K. MEGA7: Molecular Evolutionary Genetics Analysis version 7.0 for bigger datasets. Mol Biol Evol. 2016;33:1870–4. https://doi.org/10.1093/molbev/msw054
19. Clinical and Laboratory Standards Institute. Reference method for broth dilution antifungal susceptibility testing of filamentous fungi. 3rd edition. 2017 Nov 30 [cited 2018 Aug 2]. https://clsi.org/standards/products/microbiology/documents/m38
20. Prakash H, Ghosh AK, Rudramurthy SM, Paul RA, Gupta S, Negi V, et al. The environmental source of emerging *Apophysomyces variabilis* infection in India. Med Mycol. 2016;54:567–75. https://doi.org/10.1093/mmy/myw014
21. Compain F, Aït-Ammar N, Botterel F, Gibault L, Le Pimpec Barthes F, Dannaoui E. Fatal pulmonary mucormycosis due to *Rhizopus homothallicus*. Mycopathologia. 2017;182:907–13. https://doi.org/10.1007/s11046-017-0151-7
22. Prakash H, Ghosh AK, Rudramurthy SM, Singh P, Xess I, Savio J, et al. A prospective multicenter study on mucormycosis in India: epidemiology, diagnosis, and treatment. Med Mycol. 2019;57:395–402. https://doi.org/10.1093/mmy/myy060
23. Patel A, Kaur H, Xess I, Michael JS, Savio J, Rudramurthy S, et al. A multicentre observational study on the epidemiology, risk factors, management and outcomes of mucormycosis in India. Clin Microbiol Infect. 2020;26:944.e9–15.
24. Kaerger K, Schwartze VU, Dolatabadi S, Nyilasi I, Kovács SA, Binder U, et al. Adaptation to thermotolerance in *Rhizopus* coincides with virulence as revealed by avian and invertebrate infection models, phylogeny, physiological and metabolic flexibility. Virulence. 2015;6:395–403. https://doi.org/10.1080/21505594.2015.1029219

25. Biswal M, Gupta P, Kanaujia R, Kaur K, Kaur H, Vyas A, et al. Evaluation of hospital environment for presence of Mucorales during COVID-19-associated mucormycosis outbreak in India: a multi-centre study. J Hosp Infect. 2022;122:173–9. https://doi.org/10.1016/j.jhin.2022.01.016
26. Ghosh AK, Singh R, Reddy S, Singh S, Rudramurthy SM, Kaur H, et al. Evaluation of environmental Mucorales contamination in and around the residence of COVID-19-associated mucormycosis patients. Front Cell Infect Microbiol. 2022;12:953750. https://doi.org/10.3389/fcimb.2022.953750
27. Roden MM, Zaoutis TE, Buchanan WL, Knudsen TA, Sarkisova TA, Schaufele RL, et al. Epidemiology and outcome of zygomycosis: a review of 929 reported cases. Clin Infect Dis. 2005;41:634–53. https://doi.org/10.1086/432579
28. Cornely OA, Alastruey-Izquierdo A, Arenz D, Chen SCA, Dannaoui E, Hochhegger B, et al.; Mucormycosis ECMM MSG Global Guideline Writing Group. Global guideline for the diagnosis and management of mucormycosis: an initiative of the European Confederation of Medical Mycology in cooperation with the Mycoses Study Group Education and Research Consortium. Lancet Infect Dis. 2019; 19:e405–21. https://doi.org/10.1016/S1473-3099(19)30312-3
29. Muthu V, Rudramurthy SM, Chakrabarti A, Agarwal R. Epidemiology and pathophysiology of COVID-19-associated mucormycosis: India versus the rest of the world. Mycopathologia. 2021;186:739–54. https://doi.org/10.1007/s11046-021-00584-8
30. Muthu V, Agarwal R, Dhooria S, Sehgal IS, Prasad KT, Aggarwal AN, et al. Has the mortality from pulmonary mucormycosis changed over time? A systematic review and meta-analysis. Clin Microbiol Infect. 2021;27:538–49. https://doi.org/10.1016/j.cmi.2020.12.035

Address for correspondence: Arunaloke Chakrabarti, Director Office, Doodhadhari Burfani Hospital, Haridwar, Uttarakhand, India; email: arunaloke@hotmail.com

Trajectory and Demographic Correlates of Antibodies to SARS-CoV-2 Nucleocapsid in Recently Infected Blood Donors, United States

James M. Haynes, Roger Y. Dodd, Lauren A. Crowder, Edward P. Notari, Susan L. Stramer

We evaluated antibodies to the nucleocapsid protein of SARS-CoV-2 in a large cohort of blood donors in the United States who were recently infected with the virus. Antibodies to the nucleocapsid protein of SARS-CoV-2 indicate previous infection but are subject to waning, potentially affecting epidemiologic studies. We longitudinally evaluated a cohort of 19,323 blood donors who had evidence of recent infection by using a widely available serologic test to determine the dynamics of such waning. We analyzed overall signal-to-cutoff values for 48,330 donations (average 2.5 donations/person) that had an average observation period of 102 days. The observed peak signal-to-cutoff value varied widely, but the waning rate was consistent across the range, with a half-life of 122 days. Within the cohort, only 0.75% of persons became seronegative. Factors predictive of higher peak values and longer time to seroreversion included increasing age, male sex, higher body mass index, and non-Caucasian race.

Blood donors are a healthy subset of the population, and data collected from testing their donations for infectious disease markers provides opportunities for monitoring epidemiologic characteristics translatable to the general population (*1*,*2*). Most blood donors return to donate frequently and at somewhat regular intervals, which offers a unique opportunity for longitudinal studies. In June 2020, the American Red Cross and many other large blood centers began testing donors in the United States for antibodies against SARS-CoV-2 as a means to identify sources for convalescent-phase plasma and to attract potential donors (*3*).

Natural decay of SARS-CoV-2 antibodies is expected after vaccination and natural infection and can be quantified by serosurveillance over time. Specifically, antibodies to the spike protein develop after vaccination or infection and can take a relatively long time to decrease, but antibodies to the nucleocapsid protein develop only after natural infection and wane at a faster rate, which is particularly detectable with testing by using an IgG assay format versus a total antibody assay format (*3*–*8*).

In this study, over ≈1 year, every blood donation was tested for antibodies to SARS-CoV-2 spike protein antigens. Donations that had a reactive result were further tested for antibodies to nucleocapsid antigens. A subset of donors who seroconverted during the study period and who donated at least once more were investigated. Signal levels and waning rates for nucleocapsid antibodies were modeled, and demographic correlates, including age, sex, body mass index (BMI), and race, were sought.

Methods

During June 2020–June 2021, the American Red Cross tested >5.2 million blood donations from 2.4 million blood donors for the presence of total antibodies to the SARS-CoV-2 S1 protein by using the Ortho-Clinical Diagnostics VITROS Anti-SARS-CoV-2 Total Reagent Pack test system (Thermo Fisher Scientific, https://www.thermofisher.com). Reactive samples were tested for total nucleocapsid antibodies by using the Roche Elecsys Anti-SARS-CoV-2 test (Roche, https://www.roche.com), as described elsewhere (*3*,*9*). By manufacturer guidelines, a signal-to-cutoff (S/CO) value ≥1 was considered reactive. A total of 1,527,776 donations were spike protein reactive, of which 475,943 (31%) were subsequently classified as nucleocapsid reactive.

The cohort selected for the study was nonreactive donors who seroconverted to reactive for

Author affiliations: American Red Cross, Rockville, Maryland, USA

DOI: https://doi.org/10.3201/eid2907.230173

Table 1. Cohort selection process for study of trajectory and demographic correlates of antibodies to SARS-CoV-2 nucleocapsid in recently infected blood donors, United States, June 2020–June 2021*

Characteristic	No. donors (no. donations)
Donations received during June 2020–June 2021	2,448,127 (5,221,553)
S1 reactive tested for N antibody	1,092,736 (1,527,776)
N reactive	321,387 (475,943)
Seroconverters, N antibody reactive after N antibody nonreactive	54,414 (190,983)
Period to observed N antibody peak value ≤120 d from N antibody nonreactive	32,376 (126,227)
Donations with N antibody signal value reported	32,376 (89,682)
Observations at and after observed peak	32,376 (61,432)
Donors with ≥1 observation after observed peak	19,326 (48,382)
Observations that were valid or without apparent reinfection	19,323 (48,330)

*N, nucleocapsid; S, spike.

antibodies to spike protein and to nucleocapsid at the same time, or within no more than 120 days, and who had at ≥1 donation after seroconversion (Table 1) (*3*). We identified persons only by code and were advised of reactive test results; individual characteristics were self-reported and obtained from routine blood donation records. This study was approved by the American Red Cross Biomedical Services Institutional Review Board.

Peak Signal/Cutoff Measurement and Antibody Waning

For this study, we analyzed S/CO values from the nucleocapsid antibody test starting from the day of the highest observed value (i.e., peak) (Figure 1). We converted all nucleocapsid antibody S/CO values to the natural log scale to capture the exponential decay as a linear function of the percentage change in S/CO per day. We classified donors as seroreverting if any donation crossed into nonreactivity (S/CO <1) at any point after their observed peak S/CO date.

To evaluate the consistency of the slope of decrease of S/CO values and to demonstrate the relationship of observed peak value to negative signal, we placed donors into deciles based on the natural log of their observed peak S/CO. We calculated days to seroreversion as the natural log of the peak S/CO divided by the estimated slope.

Statistical Considerations

We used linear mixed effects regression to estimate the slope of nucleocapsid S/CO values from the observed peak. Demographic covariates serving as fixed effects were sex, age, and BMI at observed peak S/CO and binary race variable (Caucasian vs. non-Caucasian). We considered the intercept and days after peak S/CO as random effects to account for variations in observed peak S/CO values and follow-up time between donations, respectively. We used model influence diagnostics (restricted likelihood distance) to identify data points with large deviations from predicted values. We matched donors to those data points and their historical serology. We removed large increases in antibody nucleocapsid S/CO after an observed pattern of decrease from analysis, along with subsequent observations, because they were assumed to indicate reinfection.

We compared demographics of seroreverting donors at the time of peak donation (with BMI calculated from height and weight measurements) to nonseroreverting donors by using the G-test of in-

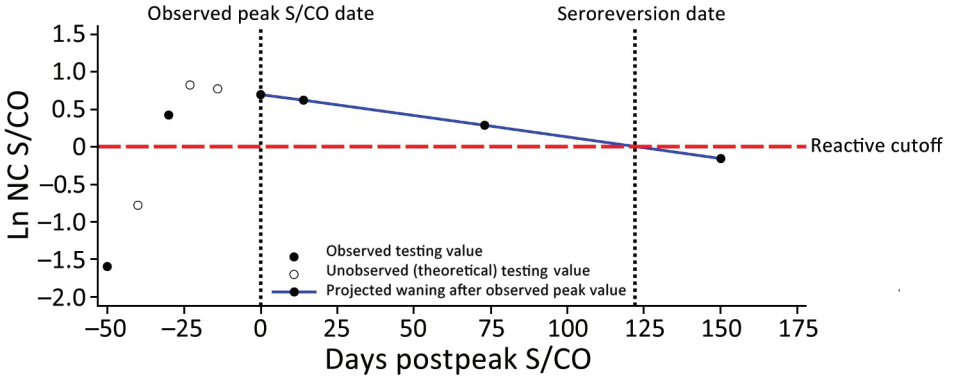

Figure 1. Potential nucleocapsid antibody test signal over time, showing likely sequence of S/CO values and seroconversion and seroreversion for nucleocapsid antibodies, in study of trajectory and demographic correlates of antibodies to SARS-CoV-2 nucleocapsid in recently infected blood donors, United States, June 2020–June 2021. Each circle shows a potential value; solid circles indicate observed testing values and open circles theoretical unobserved points. The observed peak value is likely to be less than the true peak value and could occur before the true peak, in which case the slope could be affected. Blue line indicates the projected waning after the observed peak value. Ln, natural log; NC, nucleocapsid; S/CO, signal-to-cutoff value.

Table 2. Study sample donor demographics stratified by seroreversion status during the follow-up period for study of trajectory and demographic correlates of antibodies to SARS-CoV-2 nucleocapsid in recently infected blood donors, United States, June 2020–June 2021*

Characteristic	Total, n = 19,323	Nonseroreverter, n = 19,178	Seroreverter,† n = 145	Significance‡
Sex				NS
F	9,965 (51.6)	9,890 (51.6)	75 (51.7)	
M	9,358 (48.4)	9,288 (48.4)	70 (48.3)	
Race/ethnicity				NS
Caucasian	18,285 (94.6)	18,143 (94.6)	142 (97.9)	
African American	221 (1.1)	220 (1.2)	1 (0.7)	
Hispanic	429 (2.2)	428 (2.2)	1 (0.7)	
American Indian	46 (0.2)	46 (0.2)	0	
>1 race	101 (0.5)	101 (0.5)	0	
Other	53 (0.3)	53 (0.3)	0	
Asian	159 (0.8)	159 (0.8)	0	
Missing	29 (0.2)	28 (0.2)	1 (0.7)	
Region				NS
Northeast	2,228 (11.5)	2,215 (11.6)	13 (8.9)	
Midwest	10,274 (53.2)	10,199 (53.2)	75 (51.7)	
South	3,998 (20.7)	3,965 (20.7)	33 (22.8)	
West	2,818 (14.6)	2,794 (14.6)	24 (16.6)	
Missing	5 (0.03)	5 (0.03)	0	
Mean age, y (SD)	52.3 (13.9)	52.3 (13.9)	49.6 (13.6)	p = 0.01
BMI, kg/m^2 (SD)	28.8 (5.7)	28.8 (5.7)	27.4 (5.4)	p<0.01

*Values are no. (%) unless otherwise indicated. BMI, body mass index; NS, not significant; S/CO, signal-to-cutoff value.
†Donor with any donation after the peak S/CO with loss of nucleocapsid reactivity (S/CO <1.0).
‡G-test of independence was used for categorical significance tests comparing demographics of seroreverting and nonseroreverting donors.

dependence for categorical variables and t-tests for continuous variables. We manually selected variables by using a forward stepwise process where each variable was first entered into a model with only days postpeak, after which significant variables were added one-by-one to build the final model. Vaccination status at peak S/CO was initially significant but was no longer significant after addition of the age, male, and Caucasian variables.

We evaluated the validity of the linear model by comparing model outcomes with actual observations among 3 groups of 10 randomly selected donors from different quartiles of observed peak values. We used SAS version 9.4 (SAS Institute Inc., https://www.sas.

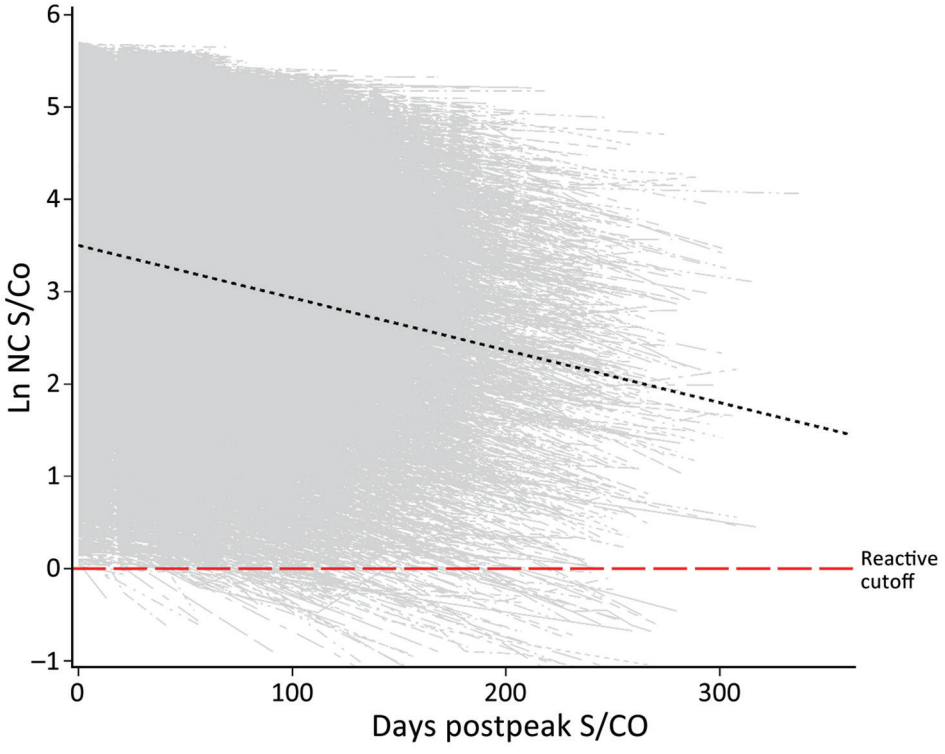

Figure 2. Longitudinal plot of all nucleocapsid-reactive donors with predicted slope (black dashed line) at mean observed peak S/CO in study of trajectory and demographic correlates of antibodies to SARS-CoV-2 nucleocapsid in recently infected blood donors, United States, June 2020–June 2021. Shown are the overall dataset and a spaghetti plot of regression lines of S/CO values for each donor in the cohort. The natural log of observed peak values covered a range from ≈0 to ≈5.7, and the mean observation time was 101.7 days. Ln, natural log; NC, nucleocapsid; S/CO, signal-to-cutoff value.

Table 3. Parameter estimates modeling repeat donor nucleocapsid S/CO for study of trajectory and demographic correlates of antibodies to SARS-CoV-2 nucleocapsid in recently infected blood donors, United States, June 2020–June 2021*

Parameter	Estimate (SE)	p value
Intercept	2.3278 (0.06794)	<0.0001
Days postpeak S/CO	−0.00656 (0.00009)	<0.0001
Male sex	0.2901 (0.08703)	0.0009
Caucasian race	−0.2856 (0.02960)	<0.0001
Age at peak S/CO	0.01445 (0.00061)	<0.0001
BMI at peak S/CO	0.03441 (0.00193)	<0.0001
Male† BMI at peak S/CO	−0.00834 (0.00295)	0.0047
Days postpeak† age at peak S/CO	0.000017 (0.000002)	<0.0001

*BMI, body mass index; S/CO, signal-to-cutoff value.
†Multiply estimates by 100 to obtain percentage change per unit increase. Only effects that include days postpeak S/CO affect the slope of decrease where others effect peak S/CO.

com) for all analyses.

Results

Study Population

A total of 51,414 donors (190,983 donations) seroconverted to nucleocapsid antibody reactivity during the universal screening period, of which 48,330 donations from 19,323 donors remained eligible for analysis (Tables 1, 2). The population had slightly more female than male donors (51.6% vs. 48.4%), a mean age of 52.3 years (SD 13.9 years), and was primarily of Caucasian race (94.6%); most (53.2%) persons resided in the Midwest United States and were overweight (mean BMI 28.8 kg/m^2, SD 5.75 kg/m^2). A significant difference was found in mean follow-up time between male donors (99.9 days, SD 48.05 days) and female donors (103.3 days, SD 48.08 days) (p<0.0001) although such a small difference is unlikely to have any effect in the model. A total of 145 (0.75%) persons seroreverted during the study. Persons who were older and had higher BMIs had higher S/CO values (albeit minor) when seroreverters and persons who did not serorevert were compared (Table 2). The effect of vaccination on seroreversion was not apparent in the model.

Table 4. Days to seroreversion by peak nucleocapsid S/CO at a mean age of 52 for study of trajectory and demographic correlates of antibodies to SARS-CoV-2 nucleocapsid in recently infected blood donors, United States, June 2020–June 2021*

Percent decile	Peak S/CO Ln (raw)	Days to 100% seroreversion
100	5.71 (301.87)	1,005
90	5.19 (179.47)	914
80	4.91 (135.64)	865
70	4.64 (103.54)	817
60	4.34 (76.71)	765
50	4.03 (56.26)	709
40	3.70 (40.45)	652
30	3.29 (26.84)	580
20	2.80 (16.44)	494
10	2.11 (8.25)	372

*Ln, natural log; S/CO, signal-to-cutoff value.

Observed Peak S/CO and Rate of Waning

The observed peak S/CO varied greatly between donors; on the natural log scale, the overall mean peak S/CO was 3.8 (SD 1.19), translating to a raw value of 44.7 (Figure 2), which also showed a relatively constant rate of waning across all donors. The mean observation period postpeak for all donors was 101.7 days. Using our linear model, we estimated peak values and identified differences by demographics in estimated peak S/CO values. For every additional year of age, the estimated peak S/CO increased by 1.4%. Caucasian persons were estimated to have a 28.6% lower peak S/CO than persons of other races. Every point increase in BMI was associated with an increased estimated peak S/CO by 3.4%. Male donors were estimated to have a 29.0% higher peak S/CO than female donors.

Linear mixed effects regression (Table 3) adjusting for age, sex, race, and BMI at peak S/CO estimated the population mean nucleocapsid antibody slope of decrease to be −0.656% (95% CI −0.64% to −0.67%) per day (p<0.0001). An interaction between age and days postpeak S/CO indicates the estimated S/CO decrease is slower as age increases, reducing the slope by 0.0017% (95% CI 0.0013%–0.0021%) with each additional year of age. Donors were placed into deciles (Table 4) based on the natural log of their observed peak S/CO with days to seroreversion calculated as the natural log of the peak S/CO divided by the estimated slope using the sum of the population mean slope (−0.00656) and the age interaction slope using the mean age (0.000017 × 52), resulting in a slope of −0.568% per day, or a 122-day half-life.

On the basis of the estimated decrease, donors are projected to remain reactive between 1 year and 2.75 years postpeak. To evaluate the efficacy of the linear model, we assigned donors to quartile groups based on peak S/CO. Ten donors from each quartile group were randomly selected, and their data were plotted with their observed and predicted serology values. We compiled raw model estimates of peak S/CO

values (Figure 3, panel A) and adjustments of each of the estimated values by the difference in the observed and predicted peak S/CO to better depict the accuracy of the projected slope (Figure 3, panel B).

Seroreversion

Nucleocapsid antibody serology for all seroreverters (n = 145, 0.75%) during the study period (Figure 4) showed 98% had peak S/CO values within the first decile (raw nucleocapsid antibody S/CO≤8.25). The remaining values fell within the second decile (raw nucleocapsid antibody S/CO ≤16.44). We also determined the estimated time of waning to a negative test signal for 100% of donors in each decile (Table 4).

Discussion

This large study supports the finding that, using the VITROS Anti-SARS-CoV-2 total nucleocapsid antibody test, the signal decreases with time, but the degree of decrease varies with donor age, as indicated by the age and days interaction. All other variables in the model contribute solely to the estimated peak. Therefore, using a linear model, we estimated the rate of decrease to be 0.656%/day, or a half-life of ≈106 days, or 122 days if correction is made for the age interaction (i.e., as age increases, waning decreases), using the average donor age in the study. Direct observation of the study population showed that only 0.75% of study participants seroreverted, all of whom had an observed peak value within the 2 lowest deciles for the population. The validation study of the linear model did not accurately define the peak signal level (Figure 3, panel A), indicating that peak signal levels are inherently variable over a wide range. However, when the model was adjusted to compare the waning slopes, these slopes were found to be consistent across a range of different observed peak values (Figure 3, panel B).

Our results are similar to those from a longitudinal study of employees at Brigham and Women's Hospital (Boston, MA, USA), where it was estimated that the nucleocapsid antibody half-life was 128 days (*8*), compared to our study value of 122 days. We also observed a similar interaction effect between nucleocapsid antibody levels and BMI in men as that reported by Yamamoto et al. (*10*). Our study

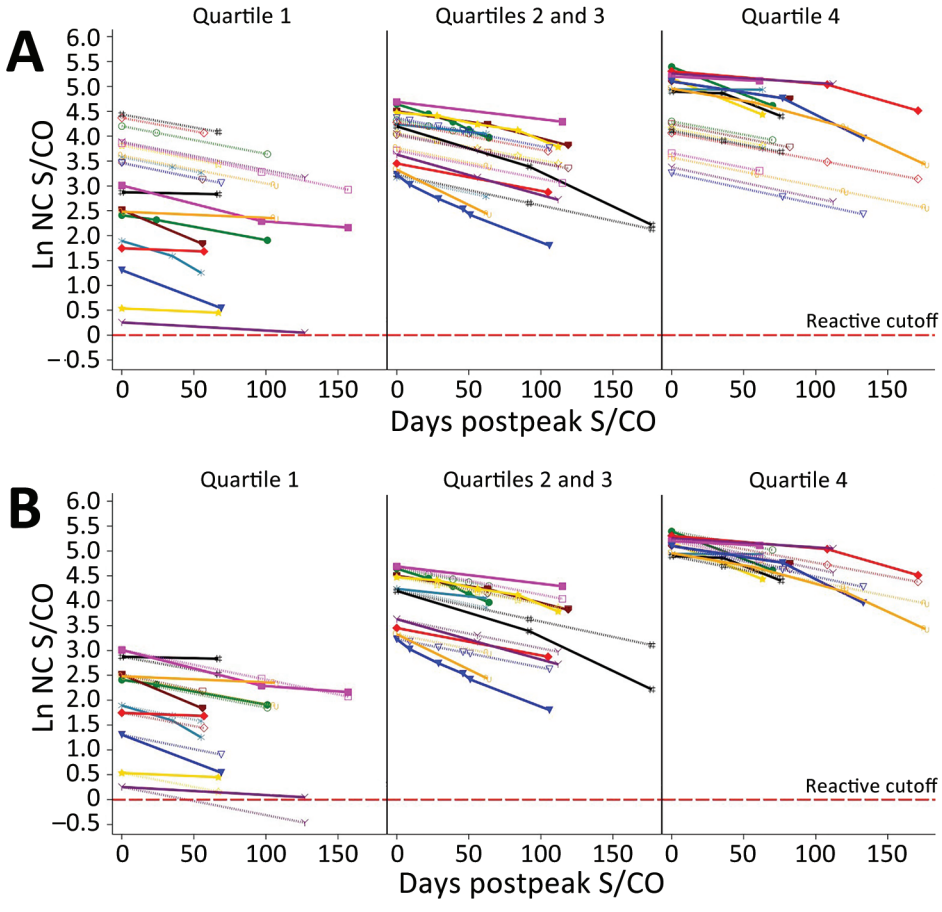

Figure 3. Predicted values and actual S/CO values. A) Raw predicted peak S/CO values and actual donor serologic values by peak S/CO quartile (n = 30); B) intercept-adjusted predicted S/CO values and actual donor serologic values by peak S/CO quartile (n = 30). Dotted lines indicate predicted values and solid lines observed values. Quartiles were defined on the basis of their observed peak value. Samples were randomly chosen. Ln, natural log; NC, nucleocapsid; S/CO, signal-to-cutoff value.

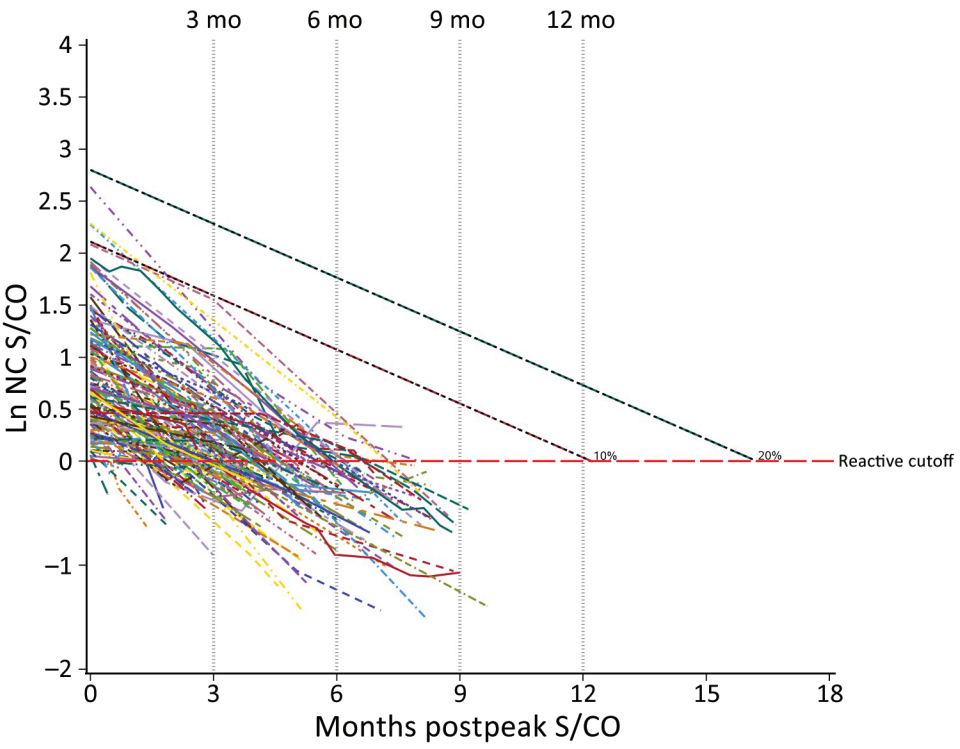

Figure 4. Longitudinal plot of nucleocapsid reactive seroreverting donors in study of trajectory and demographic correlates of antibodies to SARS-CoV-2 nucleocapsid in recently infected blood donors, United States, June 2020–June 2021. All seroreverting donors are plotted by their observed testing values. Black dashed lines are overlaid as indicators of the first and second deciles of peak S/COs across all donors to show low starting values of those who seroreverted. Decile lines are plotted by using the mean age (52 years) of donors, but seroreverting donors were slightly younger (49 years) and showed faster waning. Ln, natural log; NC, nucleocapsid; S/CO, signal-to-cutoff value.

demonstrated that the Roche Elecsys Total Ig nucleocapsid test for serosurveillance of SARS-CoV-2 as antibody reactivity remains detectable for >1 year in 90% and >2 years in 50% of donors in our cohort. Our results contrast those of Alfego et al., who found a decrease of 31.8% nucleocapsid seropositivity by using a qualitative assay after 293 days in a population-based analysis (*11*). The explanation for this difference is probably low peak antibody levels in that study's population.

Although immunity to SARS-CoV-2 wanes over time, the extent to which this waning is linked to nucleocapsid antibody signal strength is unknown and should not be assumed. However, the trajectory of antibody levels is such that an estimate of seroreversion may be made for any given population if the distribution of observed peak values is known. In addition, the same information could be used to estimate the number of persons who seroconverted at a given time in the past.

Strengths of our study include a large geographically dispersed sample within the United States, with almost equal representation by sex, and the ability to isolate incident infections on the basis of previous nonreactive results. Limitations of the study include that blood donors are mostly Caucasian, are healthy at the time of donation, and are not fully representative of the general US population. In addition, during the study period, a higher proportion of blood donors were vaccinated relative to the population at large (*2*). Nevertheless, donors have been used in this context for previous research (*2*). A second limitation is that although a linear model appears to be appropriate, there was some deviation from linearity among donors who had the highest and lowest antibody S/CO signal levels. For donors who had low levels, this finding may reflect the inherent variability of signal levels close to the cutoff value of the test used. Geography, grouped by US census region, was not considered for the model because it was believed to only affect the timing of infection onset, as opposed to providing a biologic effect on S/CO values. In addition, the method did not necessarily identify true peak signal levels. Nevertheless, it is clear that the range of signal levels was highly variable, but the slope of decrease was similar across all observed peak levels.

In conclusion, we evaluated the waning of signal levels for SARS-CoV-2 nucleocapsid antibodies in a large cohort of blood donors by using a widely available total antibody test. Waning rates were consistent across a wide range of observed signal peaks. Rates differed somewhat by age and BMI. The overall half-life of the antibody signal was 106 days uncorrected and 122 days when corrected for age and BMI distribution in the study cohort. We believe that the method reported here may be generalized to other antibody systems.

Acknowledgments

We thank those persons in Scientific Affairs of the American Red Cross, including Bryan Spencer and Paula Saa, and members of the Nationwide Blood Donor Cohort Program for reviewing and providing comments on the analysis.

Antibody testing was partially supported by the Centers for Disease Control and Prevention (contract no. 75D30120C08170).

About the Author

Mr. Haynes is an epidemiologist at the American Red Cross, Rockville, MD. His primary research interests are multiple infectious disease surveillance that monitors the blood supply through donor surveys and analyzing data from routine blood collections.

References

1. Steele WR, Dodd RY, Notari EP, Xu M, Nelson D, Kessler DA, et al.; Transfusion-Transmissible Infections Monitoring System (TTIMS). Prevalence of human immunodeficiency virus, hepatitis B virus, and hepatitis C virus in United States blood donations, 2015 to 2019: the Transfusion-Transmissible Infections Monitoring System (TTIMS). Transfusion. 2020;60:2327–39. https://doi.org/10.1111/trf.16005
2. Jones JM, Stone M, Sulaeman H, Fink RV, Dave H, Levy ME, et al. Estimated US infection- and vaccine-induced SARS-CoV-2 seroprevalence based on blood donations, July 2020–May 2021. JAMA. 2021;326:1400–9. https://doi.org/10.1001/jama.2021.15161
3. Dodd RY, Spencer BR, Xu M, Foster GA, Saá P, Brodsky JP, et al. Characterisitics of US blood donors testing reactive for antibodies to SARS-CoV-2 prior to the availability of authorized vaccines. Transfus Med Rev. 2021;35:1–7. https://doi.org/10.1016/j.tmrv.2021.07.001
4. Van Elslande J, Oyaert M, Lorent N, Vande Weygaerde Y, Van Pottelbergh G, Godderis L, et al. Lower persistence of anti-nucleocapsid compared to anti-spike antibodies up to one year after SARS-CoV-2 infection. Diagn Microbiol Infect Dis. 2022;103:115659. https://doi.org/10.1016/j.diagmicrobio.2022.115659
5. Krutikov M, Palmer T, Tut G, Fuller C, Azmi B, Giddings R, et al. Prevalence and duration of detectable SARS-CoV-2 nucleocapsid antibodies in staff and residents of long-term care facilities over the first year of the pandemic (VIVALDI study): prospective cohort study in England. Lancet Healthy Longev. 2022;3:e13–21. https://doi.org/10.1016/S2666-7568(21)00282-8
6. Levin EG, Lustig Y, Cohen C, Fluss R, Indenbaum V, Amit S, et al. Waning immune humoral response to BNT162b2 COVID-19 vaccine over 6 months. N Engl J Med. 2021;385:e84. https://doi.org/10.1056/NEJMoa2114583
7. Shrotri M, Navaratnam AM, Nguyen V, Byrne T, Geismar C, Fragaszy E, et al.; Virus Watch Collaborative. Spike-antibody waning after second dose of BNT162b2 or ChAdOx1. Lancet. 2021;398:385–7. https://doi.org/10.1016/S0140-6736(21)01642-1
8. Loesche M, Karlson EW, Talabi O, Zhou G, Boutin N, Atchley R, et al. Longitudinal SARS-CoV-2 nucleocapsid antibody kinetics, seroreversion, and implications for seroepidemiologic studies. Emerg Infect Dis. 2022;28:1859–62. https://doi.org/10.3201/eid2809.220729
9. Riester E, Majchrzak M, Mühlbacher A, Tinguely C, Findeisen P, Hegel JK, et al. Multicentre performance evaluation of the Elecsys anti-SARS-CoV-2 immunoassay as an aid in determining previous exposure to SARS-CoV-2. Infect Dis Ther. 2021;10:2381–97. https://doi.org/10.1007/s40121-021-00504-9
10. Yamamoto S, Mizoue T, Tanaka A, Oshiro Y, Inamura N, Konishi M, et al. Sex-associated differences between BMI and SARS-CoV-2 antibody titers following the BNT162b2 vaccine. Obesity (Silver Spring). 2022;30:999–1003. https://doi.org/10.1002/oby.23417
11. Alfego D, Sullivan A, Poirier B, Williams J, Adcock D, Letovsky S. A population-based analysis of the longevity of SARS-CoV-2 antibody seropositivity in the United States. EClinicalMedicine. 2021;36:100902. https://doi.org/10.1016/j.eclinm.2021.100902

Address for correspondence: Susan L. Stramer, American Red Cross, 15601 Crabbs Branch Way, Rockville, MD 20855, USA; email: susan.stramer@redcross.org

Rising Incidence of *Sporothrix brasiliensis* Infections, Curitiba, Brazil, 2011–2022

Regielly C.R. Cognialli, Diego H. Cáceres, Fernanda de A.G.D. Bastos, Francelise B. Cavassin, Bruno P.R. Lustosa, Vânia A. Vicente, Giovanni L. Breda, Izabella Santos-Weiss, Flávio Queiroz-Telles

Medscape CME Activity

In support of improving patient care, this activity has been planned and implemented by Medscape, LLC and Emerging Infectious Diseases. Medscape, LLC is jointly accredited with commendation by the Accreditation Council for Continuing Medical Education (ACCME), the Accreditation Council for Pharmacy Education (ACPE), and the American Nurses Credentialing Center (ANCC), to provide continuing education for the healthcare team.

Medscape, LLC designates this Journal-based CME activity for a maximum of 1.00 ***AMA PRA Category 1 Credit(s)™***. Physicians should claim only the credit commensurate with the extent of their participation in the activity.

Successful completion of this CME activity, which includes participation in the evaluation component, enables the participant to earn up to 1.0 MOC points in the American Board of Internal Medicine's (ABIM) Maintenance of Certification (MOC) program. Participants will earn MOC points equivalent to the amount of CME credits claimed for the activity. It is the CME activity provider's responsibility to submit participant completion information to ACCME for the purpose of granting ABIM MOC credit.

All other clinicians completing this activity will be issued a certificate of participation. To participate in this journal CME activity: (1) review the learning objectives and author disclosures; (2) study the education content; (3) take the post-test with a 75% minimum passing score and complete the evaluation at http://www.medscape.org/journal/eid; and (4) view/print certificate. For CME questions, see page 1502.

NOTE: It is Medscape's policy to avoid the use of Brand names in accredited activities. However, in an effort to be as clear as possible, the use of brand names should not be viewed as a promotion of any brand or as an endorsement by Medscape of specific products.

Release date: June 16, 2023; Expiration date: June 16, 2024

Learning Objectives

Upon completion of this activity, participants will be able to:

- Assess cat-transmitted sporotrichosis disease incidence, demographics, and clinical and laboratory findings, based on a medical record review of 216 sporotrichosis cases diagnosed during 2011 to 2022 in Curitiba, Brazil
- Evaluate cat-transmitted sporotrichosis geographic distribution and incidence trends, based on a medical record review of 216 sporotrichosis cases diagnosed during 2011 to 2022 in Curitiba, Brazil
- Determine the clinical and public health implications of cat-transmitted sporotrichosis disease incidence, clinical syndromes, and geographic distribution, based on a medical record review of 216 sporotrichosis cases diagnosed during 2011 to 2022 in Curitiba, Brazil

CME Editor

Tony Pearson-Clarke, MS, Technical Writer/Editor, Emerging Infectious Diseases. *Disclosure: Tony Pearson-Clarke, MS, has no relevant financial relationships.*

CME Author

Laurie Barclay, MD, freelance writer and reviewer, Medscape, LLC. *Disclosure: Laurie Barclay, MD, has no relevant financial relationships.*

Authors

Regielly C.R. Cognialli, MS; Diego H. Cáceres, MS; Fernanda de A.G.D. Bastos, MS; Francelise B. Cavassin, PhD; Bruno P.R. Lustosa, MS; Vânia A. Vicente, PhD; Giovanni L. Breda, MS; Izabella Santos-Weiss, PhD; and ***Flávio Queiroz-Telles, PhD.***

Author affiliations: Federal University of Paraná Program in Internal Medicine and Health Science, Curitiba, Brazil (R.C.R. Cognialli, F. de A.G.D. Bastos); Federal University of Paraná Hospital de Clínicas, Curitiba (R.C.R. Cognialli, G.L. Breda); Center of Expertise in Mycology Radboudumc/CWZ, Nijmegen, the Netherlands (D.H. Cáceres); Universidad del Rosario Studies in Translational Microbiology and Faculty of Medical Sciences, Emerging Diseases Research Group, Bogota, Colombia (D.H. Cáceres); Faculdades Pequeno Príncipe, Curitiba (F.B. Cavassin); Federal University of Paraná Basic Pathology Department, Curitiba (B.P.R. Lustosa, V.A. Vicente); Federal University of Paraná Department of Clinical Analysis, Curitiba (I. Santos-Weiss); Federal University of Paraná Department of Public Health, Curitiba (F Queiroz-Telles)

DOI: https://doi.org/10.3201/eid2907.230155

Zoonotic outbreaks of sporotrichosis are increasing in Brazil. We examined and described the emergence of cat-transmitted sporotrichosis (CTS) caused by the fungal pathogen *Sporothrix brasiliensis*. We calculated incidence and mapped geographic distribution of cases in Curitiba, Brazil, by reviewing medical records from 216 sporotrichosis cases diagnosed during 2011–May 2022. Proven sporotrichosis was established in 84 (39%) patients and probable sporotrichosis in 132 (61%). Incidence increased from 0.3 cases/100,000 outpatient visit-years in 2011 to 21.4 cases/100,000 outpatient visit-years in 2021; of the 216 cases, 58% (n = 126) were diagnosed during 2019–2021. The main clinical form of sporotrichosis was lymphocutaneous (63%), followed by localized cutaneous (24%), ocular (10%), multisite infections (3%), and cutaneous disseminated (<0.5%). Since the first report of CTS in Curitiba in 2011, sporotrichosis has increased substantially, indicating continuous disease transmission. Clinician and public awareness of CTS and efforts to prevent transmission are needed.

Sporotrichosis, the most prevalent implantation mycosis worldwide, is caused by fungi of genus *Sporothrix* (*1*–*4*). In some regions of Brazil, sporotrichosis has been referred to as cat disease because of its zoonotic transmission from felines. Since 1990, a new *Sporothrix* species, *S. brasiliensis*, has emerged rapidly as an agent of cat-transmitted sporotrichosis (CTS) (*5*). Initially identified primarily in Rio de Janeiro, highly virulent S. brasiliensis causes a notable level of epizootic disease involving cats, dogs, and humans (*5*–*12*) that is emerging and expanding geographically across Brazil (*7*–*9*,*11*) and is now a major public health problem (*12*). Originally, CTS was reported primarily in the South and Southeast regions of Brazil, but by 2022, CTS was reported in 25 of its 26 states, as well as in neighboring Argentina, Chile, and Paraguay (Figure 1) (*2*,*9*,*13*–*18*). In 2022, a case of cutaneous CTS caused by *S. brasiliensis* was reported in a veterinarian in the United Kingdom who was infected by an imported cat with sporotrichosis (*19*,*20*).

Rio de Janeiro state, in the Southeast region of Brazil, has the highest prevalence of CTS, >8,900 human cases reported since the beginning of the outbreak, followed by Rio Grande do Sul (South region) with 181 human cases (*14*,*15*,*21*). In Paraná state, also in the South region, public health officials and clinicians have been alarmed by the emergence of CTS, but epidemiologic and clinical data on this disease in this jurisdiction are lacking because reporting is not mandatory (*11*,*22*). Therefore, we performed a retrospective, descriptive study of human CTS to describe the characteristics of patients with sporotrichosis, based on a decade of experience in a single medical institution, the Hospital de Clínicas of the Federal University of Paraná (HC/UFPR), a tertiary referral hospital in Curitiba, Paraná's largest city. Our study was approved by the HC/UFPR ethical committee (registration no. 12379819.4.0000.0096).

Methods

Study Design

We identified cases from the hospital database by using code B42 from the International Classification of Diseases, 10th Revision. Our study analyzed data from all proven and probable CTS cases from HC/UFPR during January 2011–May 2022.

Case Definition

We used case definitions approved by the Brazilian Ministry of Health (*23*–*25*). Proven human CTS was defined as microbiologic evidence (positive culture or histopathology) of sporotrichosis, presence of lesions or other symptoms compatible with sporotrichosis, and evidence of CTS transmission, including cat scratches or bites, contact with feline exudates, or exposure to sneezing by cats (Table 1) (*23*–*26*). Probable human CTS was defined as presence of compatible clinical manifestations after traumatic injury from or close contact with infected cats but lacking microbiologic evidence of sporotrichosis (Table 1) (*23*–*25*). We excluded patients with possible CTS or among whom CTS was ruled out.

Sporothrix Isolate Molecular Typing

We molecularly identified at the species level all *Sporothrix* isolates obtained from patients and extracted DNA from isolates using MasterPure Yeast DNA Purification Kit (Thermo Fisher Scientific). We amplified the calmodulin (*CAL*) locus region using the degenerate primers CL1 (5′-GAR TWC AAG GAG GCC TTC TC-3′) and CL2A (5′-TTT TTG CAT CAT GAG TTG GAC-3′), then sequenced amplicons using a BigDye Terminator v3.1 Cycle Sequencing Kit (Applied Biosystems). We visually inspected sequences using the BioEdit version 7.2.5 sequence alignment editor and used MAFFT version 7 to align sequences with reference strains from the National Center for Biotechnology Information databank and MEGA version 7.0.26 software with Tamura Nei method with 1,500 bootstraps to calculate evolutionary distance.

Data Collection and Statistical Analysis

From hospital clinical records we collected clinical, laboratory, and epidemiologic data from cases and stored them using a standardized Microsoft Excel form. We

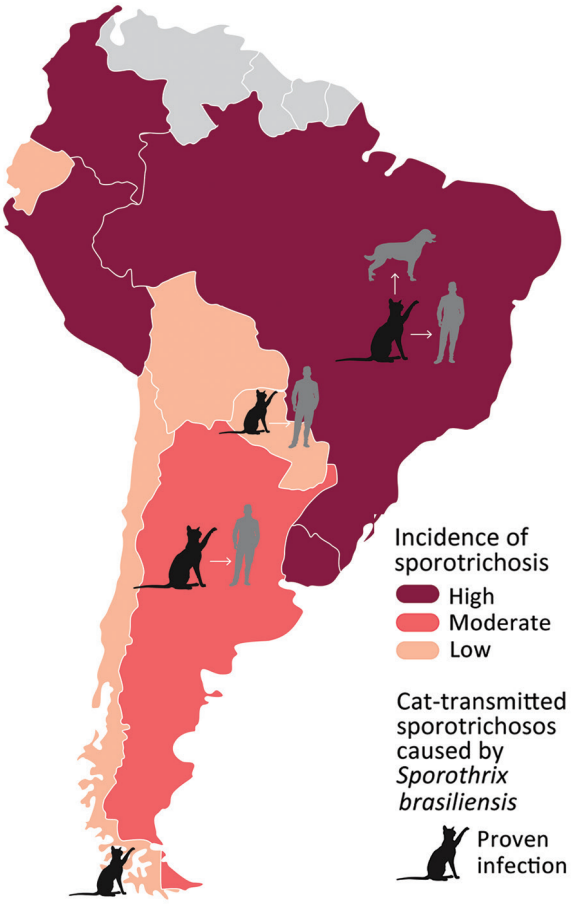

Figure 1. Burden of sporotrichosis in South America and distribution of cat-transmitted sporotrichosis in humans caused by *Sporothrix brasiliensis*, 2022. Cat icons indicate countries where cases of cat-transmitted sporotrichosis caused by *S. brasiliensis* have been reported; arrows indicate transmission from cats to cats, humans, and dogs.

calculated descriptive statistics to record the characteristics of the cases. We also calculated the incidence rate per 100,000 outpatient all-reason visits per year (outpatient visit-years [OPVY]). We performed analyses using Medcalc version 19.0 statistical software and used Qgis version 3.28.3 to map distribution of CTS cases by residence coordinates (latitude and longitude). We obtained graphic sources of the vector layer from the Instituto de Pesquisa e Planejamento Urbano de Curitiba, Instituto Ambiental do Paraná, and Coordenação da Região Metropolitana de Curitiba. We created kernel density maps to show hotspot areas for sporotrichosis in Curitiba; for this analysis, we established a search radius of 750 m.

Results

We included 216 CTS cases in this analysis. Case-patients were more frequently female than male (ratio 1.8:1) except in the 11–17 year age group (Figure 2). Median age among CTS case-patients was 40 years (interquartile range 22.5–56.0 years) (Table 2); 29 (13%) patients were <18 years of age. Overall, 11% of patients had occupations with disease-related risk factors, including 9 veterinarians, 5 veterinary students, 3 pet sitters, and 2 gardeners. The most frequent clinical form of sporotrichosis was lymphocutaneous (n = 136, 63%), followed by fixed cutaneous (n = 53, 25%), ocular (n = 21, 10%), mixed forms (n = 5, 2%), and cutaneous disseminated (n = 1, <0.5%). We observed that some CTS case-patients had unusual clinical manifestations (Figure 3).

Overall, 84 (39%) patients had proven CTS and 132 (61%) had probable CTS. Among probable CTS cases, we tested 18 patients by microscopy and culture, and all tested negative. Laboratory testing was not requested for the 14 remaining probable CTS case-patients; the main causes for not testing were specimen unavailability for microbiology testing and previous initiation of antifungal treatment. Among the proven CTS cases, *Sporothrix* isolates were collected from direct swabbing of lesion secretions for 50 patients, skin biopsy for 29, and aspirate from abscesses for 5. Average times for positive *Sporothrix* culture results varied by specimen type: specimens collected using the swab method averaged 6 days (range 3–17 days), compared with 13 days (range 4–30 days) for

Table 1. Cat-transmitted sporotrichosis case definitions used in study of human cases in Curitiba, Brazil, 2011–2021*

Definition	Epidemiology	Clinical	Laboratory
Proven	History of trauma or contact with a cat with sporotrichosis	Lesions compatible with sporotrichosis	Positive culture and/or histopathology (microbiological evidence)
Probable	History of trauma or contact with a cat with sporotrichosis	Lesions compatible with sporotrichosis	Human: Negative culture and/or histopathology.† Sick cat: A) sporotrichosis diagnosed by culture and/or histopathology in a veterinarian laboratory; B) cat resident in a region with confirmed presence of cats with sporotrichosis (data verified by public health authorities)
Possible	History of trauma or contact with a cat with sporotrichosis	Lesions compatible with sporotrichosis	Absent
Non-CTS	History of trauma or contact with a cat with sporotrichosis	Lesions compatible with sporotrichosis	Negative culture and/or histopathology for *Sporothrix* spp.† Definition of other case of disease (infectious or noninfectious)

*Adapted from Guide to Health Surveillance, 5th ed (*23*–*25*). CTS, cat-transmitted sporotrichosis.
†Negative culture for *Sporothrix* spp. alone does not rule out diagnosis (limitation of the culture).

specimens collected by biopsy (p<0.0001). On the basis of phylogenetic analysis of calmodulin sequence genes of 38 *Sporothrix* isolates from patients, we identified *S. brasiliensis* as the only etiologic agent (38/38 cases) of CTS during the study period (Figure 4).

In 98% (212) of the 216 total CTS cases, infection was associated with zoonotic transmission; in those cases, the patient had direct or indirect contact with a cat with diagnosed sporotrichosis. In 4 (2%) sporadic cases, occurring in 2016, 2017, 2019, and 2021, infection was associated with saprozoic exposure with traumatic implantation from an environmental source. The first observed substantial increase in cases was from 1 in 2015 (0.3 cases/100,000 OPVY) to 12 in 2016 (3.5 cases/100,000 OPVY) (Figure 5), and incidence rates continued to increase thereafter. There were 34 cases (8.3 cases/100,000 OPVY) in 2018, almost 3 times as many as in 2016, and 61 cases (21.4 cases/100,000 OPVY) in 2021 (Figure 5). During January–May 2022, we identified 20 cases from 142,873 outpatient visits (14 cases/100,000 OPVY) (Figure 5).

CTS cases were reported in 15 of the 399 municipalities in the state of Paraná (Figure 6, panels A, B) and in 11 of the 29 municipalities comprising the metropolitan region of Curitiba (Figure 6, panel C). Among the 216 CTS cases identified in the state of Paraná, the metropolitan region of Curitiba accounted for 205 (95%), the city of Curitiba alone for 170 (79%) (Figure 6, panel D). We also tracked triennial distribution of cases in the city of Curitiba during 2011–2013, 2014–2016, 2017–2019, and 2020–May 2022. The first case of CTS in Paraná was identified in 2011 in Campina Grande do Sul, a municipality located in the metropolitan region of Curitiba. The first case of CTS in the city of Curitiba was identified in 2012 in the Mercês neighborhood, located in the north-central part of the city (Figure 6, panel E). Since 2016, cases have spread across the city of Curitiba and been reported in 41 of 75 districts; most cases have been identified in the northwest region of the city, but during 2020–May 2022, incidence spread throughout the city (Figure 6, panels F, G, H). We also observed clusters of CTS cases involving members of the same household. Since 2011, a total of 10 clusters involving 21 cases were identified; 7/10 CTS clusters (15 cases) occurred after the COVID-19 pandemic began in 2020.

Kernel density maps identified hotspots for sporotrichosis in the city of Curitiba (Figure 7). The most critical hotspots were identified in the western part, mainly the Cidade Industrial de Curitiba (CIC) neighborhood, and north-central (city center) areas of Curitiba. CIC has an area of 44,588 km^2 and a population

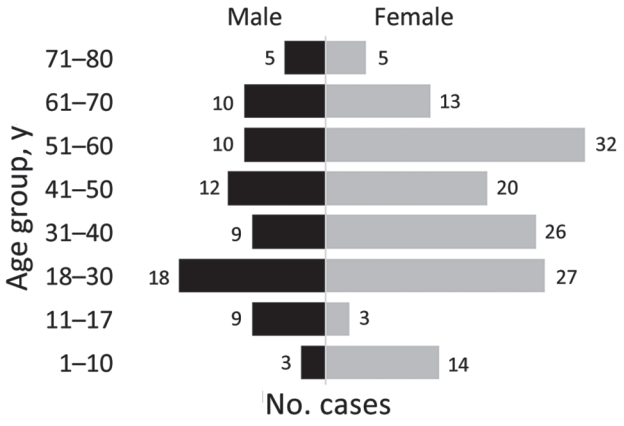

Figure 2. Age–sex pyramid showing the distribution of cat-transmitted sporotrichosis cases in patients treated at Hospital de Clínicas, Federal University of Paraná, Curitiba, Brazil, 2011–May 2022.

of 172,909 inhabitants (density 3.9 habitants/km^2); it is largely residential, and most residents live in houses. CIC is economically characterized as a lower middle–income area, with an average daily income of USD $4.7 (*27*). The second hotspot, in downtown Curitiba, is a combination of commercial and residential areas, composed mostly of apartment buildings. Curitiba city center comprises 3,310 km^2 and is the most densely populated (37,234 inhabitants; density 11.2 inhabitants/km^2) part of the city. Average daily income among residents is USD $20 (*27*). The kernel density maps of Curitiba show additional medium-density hotspots for CTS throughout other parts of the city, especially in the south, southeast, and northeast parts.

Table 2. Sociodemographic characteristics in study of human sporotrichosis cases in Curitiba, Brazil, 2011–2022

Characteristic	No. (%) patients
Sex	
F	140 (65)
M	76 (35)
Age range, y	
≤10	17 (8)
11–17	12 (6)
18–30	45 (21)
31–60	109 (50)
>60	33 (15)
Occupation	
Unemployed	42 (19)
Student	42 (19)
Retired	23 (11)
Domestic worker	17 (8)
Veterinarian or veterinary student	17 (8)
Administrator	11 (5)
Teacher	3 (1)
Pet sitter	3 (1)
Gardener	2 (1)
Butcher	2 (1)
Others	54 (26)

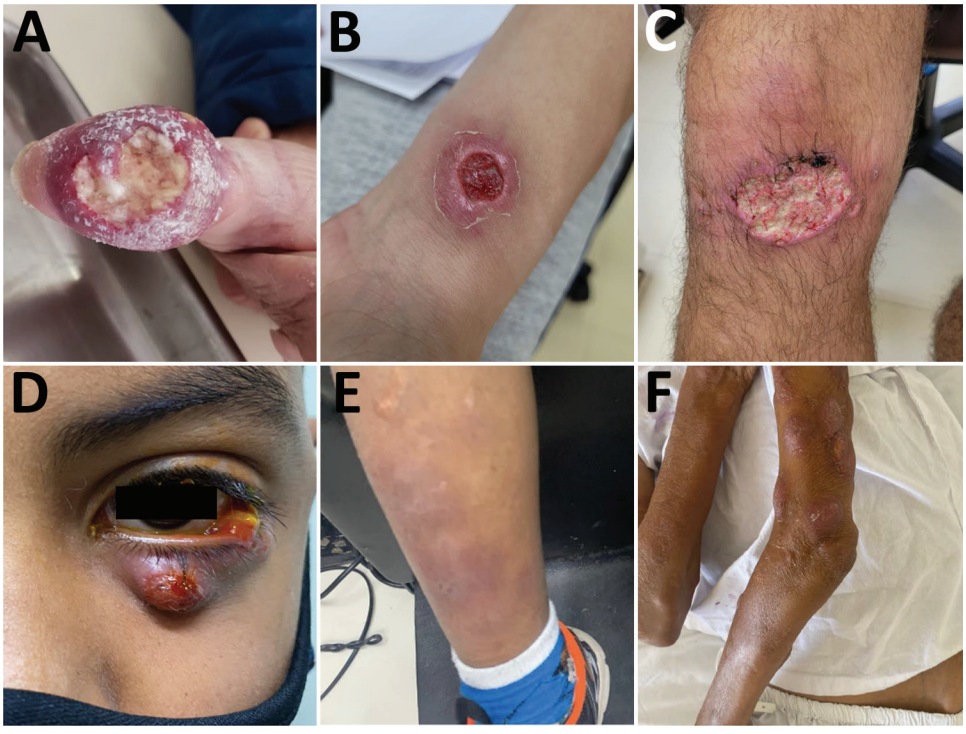

Figure 3. Unusual clinical manifestations of cat-transmitted sporotrichosis in patients treated at Hospital de Clínicas, Federal University of Paraná, Curitiba, Brazil, 2011–May 2022. A) Fixed cutaneous manifestation in the thumb with osteoarticular involvement. B) Fixed cutaneous manifestation in forearm with ulcer similar to primary cutaneous leishmaniasis. C) Lymphocutaneous manifestation in the knee with a large ulceration, mimicking cutaneous leishmaniasis. D) Ocular form with Parinaud ocular-glandular syndrome and dacryocystitis. E) Erythema nodosum resulting from immunoreactive sporotrichosis manifestation in the leg (same patient from panel D). F) Cutaneous disseminated manifestation in immunocompromised patient.

Discussion

During the 10-year study period, sporotrichosis incidence increased substantially, suggesting uncontrolled spread in the city of Curitiba. Brazil is facing the largest reported current zoonotic outbreak of CTS globally (*9*,*11*,*13*,*28*). CTS is a public health issue exacerbated by insufficient public health activities, such as case surveillance, animal control, and diagnostic capacity, and by lack of disease awareness among health professionals and the general population (*9*,*13*,*25*,*29*). Our study adds relevant epidemiologic information to promote better understanding of CTS in the state of Paraná, Brazil.

We found a higher prevalence of CTS among female patients, especially in adult women involved in domestic activities. This finding is similar to those of other previous reports and is likely related to close contact with infected domestic cats (*30*–*33*). In this study, we observed an increased proportion of pediatric CTS cases; 29 cases (13%) occurred in patients <18 years of age, likely reflecting the close nature of interactions between children and domestic pets, especially cats (*23*). In addition, we found that >10% of cases occurred in persons working in professional animal care disciplines (*2*,*11*,*22*), who are at increased risk for CTS because of close contact with and exposure to contaminated body fluids from infected animals. Those professionals would benefit from increased awareness that infection in humans can occur through direct contact with body fluids from cats contaminated with *S. brasiliensis* yeast (*26*).

Lymphocutaneous and fixed cutaneous forms were the most frequently identified clinical manifestations of sporotrichosis, consistent with findings in previous literature (*1*,*22*). However, since the sporotrichosis epidemic in Brazil began, reports of unusual clinical manifestations have been increasing (*1*,*6*,*34*). It should be highlighted that cutaneous disseminated sporotrichosis is a rare manifestation that mostly occurs in immunocompromised persons; it differs from cutaneous manifestations caused by multiple traumatic implantations, as also happens in CTS cases (*35*–*37*). We also found a relatively high frequency of ocular sporotrichosis, which occurred in 10% of cases. Ocular sporotrichosis occurs mainly because of direct contact of the ocular mucosa of a person with secretions from an infected cat, usually because of cutaneous exudates or respiratory droplets expelled during cat sneezing (*5*,*12*,*26*). Ocular sporotrichosis is characterized by acute or chronic conjunctivitis, including Parinaud ocular syndrome and dacryocystitis (*2*,*12*,*38*–*41*). We also observed that unusual clinical manifestations of CTS increased from 2018 onward, coinciding with the epidemic increase in the number of cases of the disease. On the basis of those findings, the current guidelines in Brazil recommend use of personal protective equipment, including glasses or a face shield, during contact with sick cats (*24*).

Proven cases of CTS in this study made up slightly more than one third (39%) of all cases, compared with

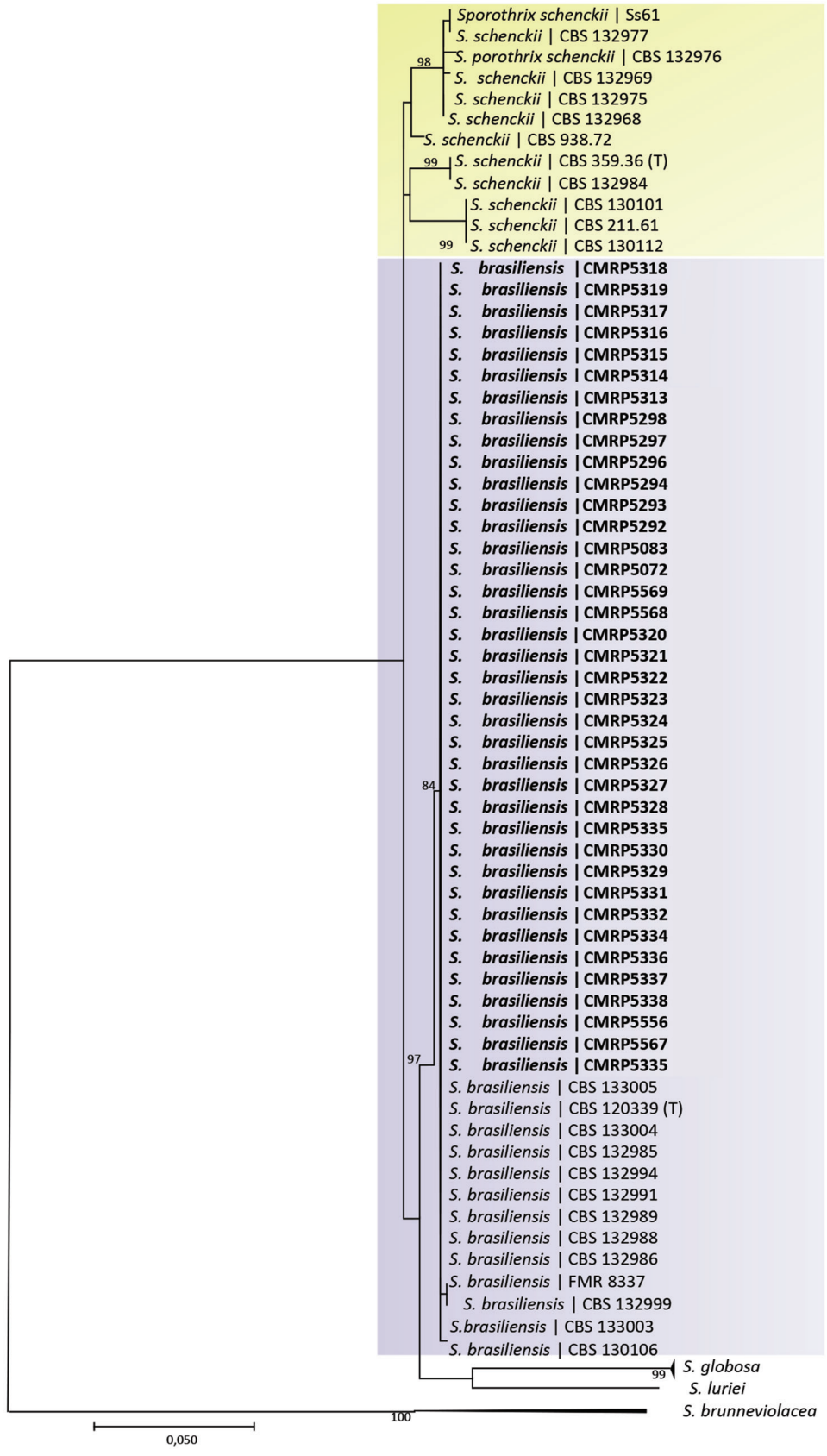

Figure 4. Phylogenetic analysis of *Sporothrix* spp. isolates from cat-transmitted sporotrichosis patients treated at Hospital de Clínicas, Federal University of Paraná, Curitiba, Brazil, 2011–May 2022. Tree shows analysis of clades based on calmodulin near-complete genes constructed with maximum-likelihood implemented in MEGA 7.0.26. Bootstrap values >80 from 1,500 resampled datasets are shown. Bold indicates strains isolated in this study; yellow shading represents *S. schenckii* isolates and *S. brasiliensis* isolates. GenBank accession numbers are shown in Appendix Table 1 (https://wwwnc.cdc.gov/EID/article/29/7/23-0155-App1.pdf). Scale bar represents number of substitutions per site.

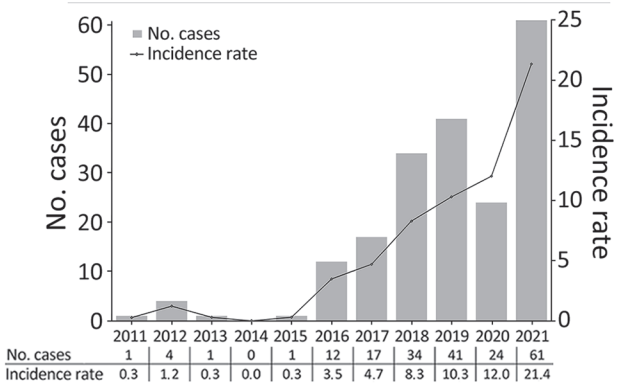

Figure 5. Epidemiologic curve and incidence rate (cases/100,000 outpatient visit-years) of cat-transmitted sporotrichosis patients treated at Hospital de Clínicas, Federal University of Paraná, Curitiba, Brazil, 2011–2021.

65.3% in other case-series studies of sporotrichosis (*22*,*23*). This difference may have resulted from using a case definition not based solely on culture and microscopy results, which are suboptimal assays for detecting sporotrichosis in humans. Cultures from pus or secretion from lesions could be a feasible alternative; that type of test shows good performance and generates results in half the time compared with testing specimens obtained by biopsy. In addition, that type of sample is noninvasive, simple, and inexpensive. HC/UFPR has a medical institute with extensive experience in the diagnosis of sporotrichosis, and its medical professionals consequently have a high index of suspicion for this disease, increasing the chances of early detection of cases in which culture and microscopy are generally negative. On the basis of this experience, we highlight the importance of the probable case classification, because recognizing probable CTS enables rapid initiation of treatment, resulting in a positive effect on the quality of life of patient with sporotrichosis (*23*,*25*).

Molecular typing identified a single species, *S. brasiliensis*, in all proven cases in our study. The isolates were related to the species that caused the CTS outbreak in the state of Rio de Janeiro in the early 2000s and is primarily causing outbreaks throughout Brazil (*5*,*11*,*13*,*17*, *42*–*44*). Those isolates were identified by phylogenetic analysis of the near-complete calmodulin gene sequencing, showing a high degree of similarity with previously sequenced isolates from Rio de Janeiro. Additional analyses, such as microsatellite typing, multilocus sequence typing, and amplified

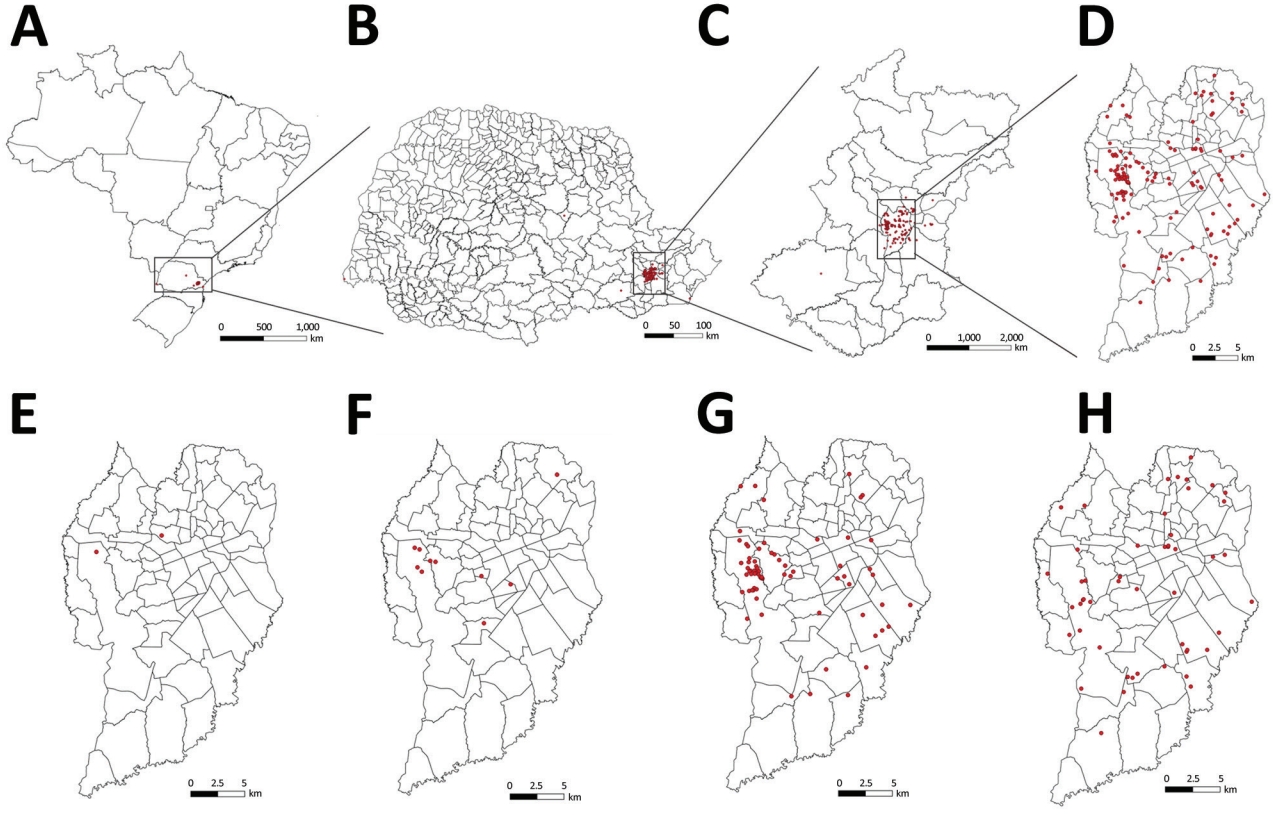

Figure 6. Locations of human cat-transmitted sporotrichosis cases (red dots) treated at Hospital de Clínicas, Federal University of Paraná, Curitiba, Brazil, during 2011–May 2022, and evolution of spatial distribution of cases in the city of Curitiba. A–D) Locations of all human cases in Brazil (A), Paraná state (B), Metropolitan Region of Curitiba (C), and Curitiba (D). E–H) Distribution of new human cases in Curitiba during 2011–2013 (E), 2014–2016 (F), 2017–2019 (G), and 2020–May 2022 (H).

fragment-length polymorphic fingerprinting, can improve understanding of the expansion of cases in Paraná and the city of Curitiba (*13*,*45*). Moreover, analysis of whole-genome sequencing results is a tool relevant for elucidating central concerns about the differences in infectious potential between closely related species. Comparative genomic analysis of data on tissue invasion and transmission of pathogenic sibling species has been applied to highlight genes involved in fungal adaptation to an animal-associated lifestyle (*11*,*46*,*47*).

We observed an exponential increase in the incidence rate of sporotrichosis, from 0.3 OPVY in 2011 to 21.4 OPVY in 2021, a trend similar to that for data reported recently in a review of the burden of sporotrichosis in Brazil (*9*,*15*,*22*,*29*,*30*,*48*). In Brazil, the largest number of CTS cases is concentrated in the southwest and south of Brazil, including the states of Rio de Janeiro, Rio Grande do Sul, São Paulo, Espírito Santo, and Minas Gerais. However, cases of CTS have also been described in the Midwest, Federal District, and Northeast regions and in Pernambuco and Rio Grande do Norte states, clearly showing the spread of the disease throughout Brazil (*22*,*32*,*49*).

Most cases in this study occurred in the city of Curitiba. The first case identified at HC/UFPR was in the center-north part of the city in 2012, but the first substantial increase in the number of cases, a trend that continued, was observed in 2016. After the World Health Organization declared COVID-19 a pandemic in March 2020 and lockdowns started, we observed a 37% increase in cases and also an increase in CTS clusters. The increase may have been related to higher rates of pet adoption aimed at reducing anxiety and depression because of the lockdowns (*23*). We identified 2 areas of the city of Curitiba as CTS hotspots, one area characterized by high population density and the other by social inequalities. In addition, the kernel density estimate showed low or medium CTS expanded practically throughout the city, especially during 2020–2022; areas of medium density were located in the south, southeast, and northeast parts of the city.

The main limitation of our study was that data came from a single center; however, the data covered a decade of experience, and our findings add information based on actual case numbers rather than estimates. Since March 7, 2022, the State Department of Health of Paraná, has provided guidelines (resolution no. 093/2022) for mandatory notification of human and animal sporotrichosis cases in the state.

Because of the zoonotic transmission of this disease, a One Health approach is necessary to control the public health effects of CTS. Integrating human, animal, and environmental health approaches through coordinated actions among microbiologists, veterinarians, physicians, epidemiologists, and surveillance authorities could benefit control efforts. Potential actions include owners restricting cats from going outside homes and having contact with street cats, providing no-cost neutering of cats in regions where *S. brasiliensis* is endemic to prevent expansion of feral cat populations, widely establishing compulsory notification of CTS cases, increasing awareness of the disease among clinicians and the public, providing easy access to treatment in human and animal cases, and cremating cat remains (*12*,*36*,*50*). Additional interventions to control CTS outbreaks could include providing access to rapid, accurate diagnostic assays and antifungal drugs, developing vaccines specifically for cats, and evaluating novel treatment strategies, particularly for treating feline sporotrichosis. Enacting

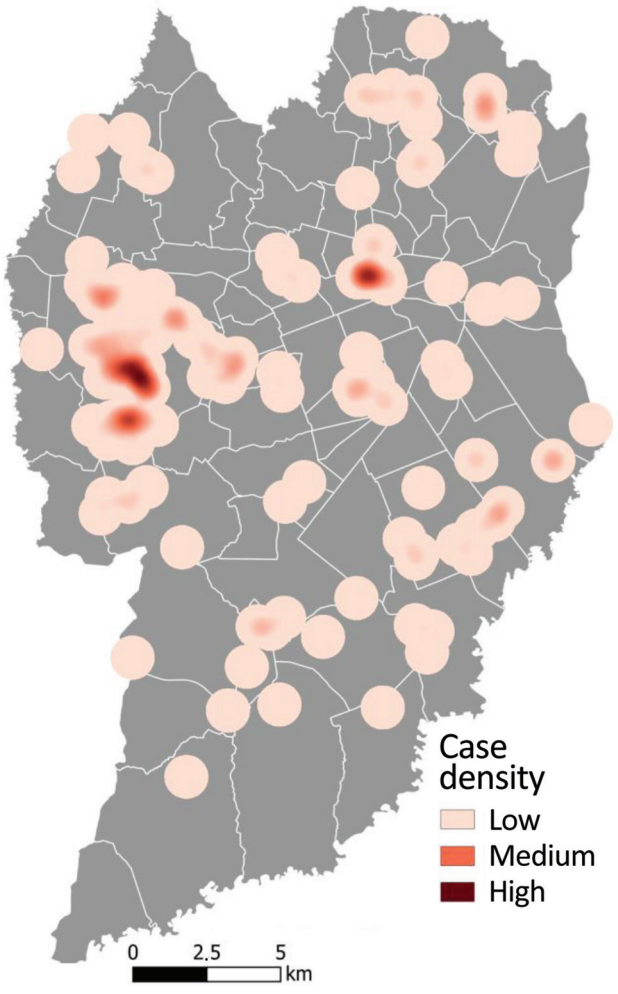

Figure 7. Heatmap of human cat-transmitted sporotrichosis cases using kernel density estimation in Curitiba, Brazil, 2011–May 2022. Kernel density map was created using a search radius of 750 m.

those and other prevention and control measures in a timely manner is urgently needed to repress the increased incidence and spread of this serious health condition.

Acknowledgments

We thank Lili Volochen Lopuch and Adriana de Fátima Gabriel for all support with collecting and preparing samples and Regiane Cognialli Born for the map design. We also thank Jeremy Gold for reviewing the manuscript.

About the Author

Ms. Cognialli is a mycologist at Hospital de Clínicas of Federal University of Paraná and a PhD student at Federal University of Paraná, Curitiba, Paraná, Brazil. Her primary interest is in neglected endemic mycosis.

References

1. Orofino-Costa R, Macedo PM, Rodrigues AM, Bernardes-Engemann AR. Sporotrichosis: an update on epidemiology, etiopathogenesis, laboratory and clinical therapeutics. An Bras Dermatol. 2017;92:606–20. https://doi.org/10.1590/abd1806-4841.2017279
2. Queiroz-Telles F, Bonifaz A, Rossow J, Chindamporn A. *Sporothrix* and sporotrichosis. In: Encyclopedia of infection and immunity. New York: Elsevier Science; 2021.
3. Queiroz-Telles F, Fahal AH, Falci DR, Caceres DH, Chiller T, Pasqualotto AC. Neglected endemic mycoses. Lancet Infect Dis. 2017;17:e367–77. https://doi.org/10.1016/S1473-3099(17)30306-7
4. Chakrabarti A, Bonifaz A, Gutierrez-Galhardo MC, Mochizuki T, Li S. Global epidemiology of sporotrichosis. Med Mycol. 2015;53:3–14. https://doi.org/10.1093/mmy/myu062
5. Gremião ID, Miranda LH, Reis EG, Rodrigues AM, Pereira SA. Zoonotic epidemic of sporotrichosis: cat to human transmission. PLoS Pathog. 2017;13:e1006077. https://doi.org/10.1371/journal.ppat.1006077
6. Schechtman RC, Falcão EMM, Carard M, García MSC, Mercado DS, Hay RJ. Sporotrichosis: hyperendemic by zoonotic transmission, with atypical presentations, hypersensitivity reactions and greater severity. An Bras Dermatol. 2022;97:1–13. https://doi.org/10.1016/j.abd.2021.07.003
7. Barros MB, Schubach AO, do Valle AC, Gutierrez Galhardo MC, Conceição-Silva F, Schubach TM, et al. Cat-transmitted sporotrichosis epidemic in Rio de Janeiro, Brazil: description of a series of cases. Clin Infect Dis. 2004;38:529–35. https://doi.org/10.1086/381200
8. de Lima Barros MB, Schubach TM, Galhardo MC, de Oliviera Schubach A, Monteiro PC, Reis RS, et al. Sporotrichosis: an emergent zoonosis in Rio de Janeiro. Mem Inst Oswaldo Cruz. 2001;96:777–9. https://doi.org/10.1590/S0074-02762001000600006
9. Gremião IDF, Oliveira MME, Monteiro de Miranda LH, Saraiva Freitas DF, Pereira SA. Geographic expansion of sporotrichosis, Brazil. Emerg Infect Dis. 2020;26:621–4. https://doi.org/10.3201/eid2603.190803
10. Pereira SA, Gremião ID, Kitada AA, Boechat JS, Viana PG, Schubach TM. The epidemiological scenario of feline sporotrichosis in Rio de Janeiro, state of Rio de Janeiro, Brazil. Rev Soc Bras Med Trop. 2014;47:392–3. https://doi.org/10.1590/0037-8682-0092-2013
11. Rodrigues AM, Della Terra PP, Gremião ID, Pereira SA, Orofino-Costa R, de Camargo ZP. The threat of emerging and re-emerging pathogenic *Sporothrix* species. 2020;185:813–42.
12. Rossow JA, Queiroz-Telles F, Caceres DH, Beer KD, Jackson BR, Pereira JG, et al. A One Health approach to combatting *Sporothrix brasiliensis*: narrative review of an emerging zoonotic fungal pathogen in South America. J Fungi (Basel). 2020;6:247. https://doi.org/10.3390/jof6040247
13. Rodrigues AM, Gonçalves SS, de Carvalho JA, Borba-Santos LP, Rozental S, Camargo ZP. Current progress on epidemiology, diagnosis, and treatment of sporotrichosis and their future trends. J Fungi (Basel). 2022;8:776. https://doi.org/10.3390/jof8080776
14. Brandolt TM, Madrid IM, Poester VR, Sanchotene KO, Basso RP, Klafke GB, et al. Human sporotrichosis: a zoonotic outbreak in southern Brazil, 2012–2017. Med Mycol. 2018;57:myy082. https://doi.org/10.1093/mmy/myy082
15. Poester VR, Mattei AS, Madrid IM, Pereira JTB, Klafke GB, Sanchotene KO, et al. Sporotrichosis in southern Brazil, towards an epidemic? Zoonoses Public Health. 2018;65:815–21. https://doi.org/10.1111/zph.12504
16. Etchecopaz AN, Lanza N, Toscanini MA, Devoto TB, Pola SJ, Daneri GL, et al. Sporotrichosis caused by *Sporothrix brasiliensis* in Argentina: case report, molecular identification and in vitro susceptibility pattern to antifungal drugs. J Mycol Med. 2020;30:100908. https://doi.org/10.1016/j.mycmed.2019.100908
17. Etchecopaz A, Toscanini MA, Gisbert A, Mas J, Scarpa M, Iovannitti CA, et al. *Sporothrix brasiliensis*: a review of an emerging South American fungal pathogen, its related disease, presentation and spread in Argentina. J Fungi (Basel). 2021;7:170. https://doi.org/10.3390/jof7030170
18. Thomson P, González C, Blank O, Ramírez V, Río Cd, Santibáñez S, et al. Sporotrichosis outbreak due to *Sporothrix brasiliensis* in domestic cats in Magallanes, Chile: a One-Health-approach study. J Fungi (Basel). 2023;9:226. https://doi.org/10.3390/jof9020226
19. Rachman R, Ligaj M, Chinthapalli S, Serafino Wani R. Zoonotic acquisition of cutaneous *Sporothrix braziliensis* infection in the UK. BMJ Case Rep. 2022;15:e248418. https://doi.org/10.1136/bcr-2021-248418
20. Barnacle JR, Chow YJ, Borman AM, Wyllie S, Dominguez V, Russell K, et al. The first three reported cases of *Sporothrix brasiliensis* cat-transmitted sporotrichosis outside South America. Med Mycol Case Rep. 2022;39:14–7. https://doi.org/10.1016/j.mmcr.2022.12.004
21. Marinho Falcão EMM, Rocha Romão A, de Avelar Figueiredo Mafra Magalhães M, de Lima Filho JB, Francesconi do Valle AC, Bastos FI, et al. A spatial analysis of the spread of hyperendemic sporotrichosis in the state of Rio de Janeiro, Brazil. J Fungi (Basel). 2022;8:434. https://doi.org/10.3390/jof8050434
22. Rabello VBS, Almeida MA, Bernardes-Engemann AR, Almeida-Paes R, de Macedo PM, Zancopé-Oliveira RM. The historical burden of sporotrichosis in Brazil: a systematic review of cases reported from 1907 to 2020. Braz J Microbiol. 2022;53:231–44. https://doi.org/10.1007/s42770-021-00658-1
23. Queiroz-Telles F, Bonifaz A, Cognialli R, Lustosa BPR, Aparecida Vicente V, Ramírez-Marín HA. Sporotrichosis in

children: case series and narrative review. Curr Fungal Infec Rep. 2022;33–46.
24. Ministry of Health of Brazil. Guide to health surveillance [in Portuguese]. 5th ed. Brasilia (Brazil): Ministry of Health of Brazil; 2022.
25. Cognialli R, Bloss K, Weiss I, Caceres DH, Davis R, Queiroz-Telles F. A lateral flow assay for the immunodiagnosis of human cat-transmitted sporotrichosis. Mycoses. 2022;65:926–34. https://doi.org/10.1111/myc.13516
26. de Andrade Galliano Daros Bastos F, Raimundo Cognialli RC, Rodrigues de Farias M, Dos Santos Monti F, Wu K, Queiroz-Telles F. Spread of *Sporothrix* spp. through respiratory droplets from infected cats: a potential route of transmission. Med Mycol. 2022;60:myac079.
27. Viezzer J, Moraes E, Biondi D, Martini A, Scarano F. Green areas, population and income in Curitiba, PR, Brasil [in Portuguese]. Rev Soc Bras Arb Urb. 2022;17:37–49. https://doi.org/10.5380/revsbau.v17i2.85848
28. Queiroz-Telles F, Buccheri R, Benard G. Sporotrichosis in immunocompromised hosts. J Fungi (Basel). 2019;5:8. https://doi.org/10.3390/jof5010008
29. Munhoz LS, Poester VR, Severo CB, Trápaga MR, Madrid IM, Benelli JL, et al. Update of the epidemiology of the sporotrichosis epidemic in the state of Rio Grande do Sul, Brazil. Mycoses. 2022;65:1112–8. https://doi.org/10.1111/myc.13497
30. Alzuguir CLC, Pereira SA, de Avelar Figueiredo Mafra Magalhães, Almeida-Paes R, Freitas DFS, Oliveira LFA, et al. Geo-epidemiology and socioeconomic aspects of human sporotrichosis in the municipality of Duque de Caxias, Rio de Janeiro, Brazil, between 2007 and 2016. Trans R Soc Trop Med Hyg. 2020;114:99–106.
31. Barros MB, de Almeida Paes R, Schubach AO. *Sporothrix schenckii* and sporotrichosis. Clin Microbiol Rev. 2011;24:633–54. https://doi.org/10.1128/CMR.00007-11
32. de Oliveira Bento A, de Sena Costa AS, Lima SL, do Monte Alves M, de Azevedo Melo AS, Rodrigues AM, et al. The spread of cat-transmitted sporotrichosis due to *Sporothrix brasiliensis* in Brazil towards the northeast region. PLoS Negl Trop Dis. 2021;15:e0009693. https://doi.org/10.1371/journal.pntd.0009693
33. Barros MB, Schubach AO, Schubach TM, Wanke B, Lambert-Passos SR. An epidemic of sporotrichosis in Rio de Janeiro, Brazil: epidemiological aspects of a series of cases. Epidemiol Infect. 2008;136:1192–6. https://doi.org/10.1017/S0950268807009727
34. Mialski R, de Almeida JN Jr, da Silva LH, Kono A, Pinheiro RL, Teixeira MJ, et al. Chronic meningitis and hydrocephalus due to *Sporothrix brasiliensis* in immunocompetent adults: a challenging entity. Open Forum Infect Dis. 2018;5:ofy081. https://doi.org/10.1093/ofid/ofy081
35. Bonifaz A, Tirado-Sánchez A. Cutaneous disseminated and extracutaneous sporotrichosis: current status of a complex disease. J Fungi (Basel). 2017;3:6. https://doi.org/10.3390/jof3010006
36. Orofino-Costa R, Freitas DFS, Bernardes-Engemann AR, Rodrigues AM, Talhari C, Ferraz CE, et al. Human sporotrichosis: recommendations from the Brazilian Society of Dermatology for the clinical, diagnostic and therapeutic management. An Bras Dermatol. 2022;97:757–77. https://doi.org/10.1016/j.abd.2022.07.001
37. Queiroz-Telles F, Cognialli RC, Salvador GL, Moreira GA, Herkert PF, Hagen F. Cutaneous disseminated sporotrichosis in immunocompetent patient: case report and literature review. Med Mycol Case Rep. 2022;36:31–4. https://doi.org/10.1016/j.mmcr.2022.05.003
38. Arinelli A, Aleixo A, Freitas DFS, do Valle ACF, Almeida-Paes R, Gutierrez-Galhardo MC, et al. Ocular sporotrichosis: 26 cases with bulbar involvement in a hyperendemic area of zoonotic transmission. Ocul Immunol Inflamm. 2019;28:764–71.
39. Ferreira TA, Sodré CT, Costa JM, Setta CRP, Ramos-E-Silva M. Primary conjunctival sporotrichosis: an atypical presentation of the disease. JAAD Case Rep. 2018;4:497–9. https://doi.org/10.1016/j.jdcr.2018.01.022
40. Lacerda Filho AM, Cavalcante CM, Da Silva AB, Inácio CP, de Lima-Neto RG, Liete de Andrade MC, et al. High-virulence cat-transmitted ocular sporotrichosis. Mycopathologia. 2019;184:547–9. https://doi.org/10.1007/s11046-019-00347-6
41. Aidar MN, Rebeschini BM, Salgado Silveira da Mata CT, Borges TC, Dos Santos Araújo MEX. The importance of considering the possibility of ocular sporotrichosis in areas with high incidence rates of sporotrichosis. Arq Bras Oftalmol. 2022: S0004-27492022005006208.
42. Marimon R, Cano J, Gené J, Sutton DA, Kawasaki M, Guarro J. *Sporothrix brasiliensis, S. globosa*, and *S. mexicana*, three new *Sporothrix* species of clinical interest. J Clin Microbiol. 2007;45:3198–206. https://doi.org/10.1128/JCM.00808-07
43. Della Terra PP, Rodrigues AM, Fernandes GF, Nishikaku AS, Burger E, Pires de Camargo Z. Exploring virulence and immunogenicity in the emerging pathogen *Sporothrix brasiliensis*. PLoS Negl Trop Dis. 2017;11:e0005903. https://doi.org/10.1371/journal.pntd.0005903
44. Almeida-Paes R, de Oliveira MM, Freitas DF, do Valle AC, Zancopé-Oliveira RM, Gutierrez-Galhardo MC. Sporotrichosis in Rio de Janeiro, Brazil: *Sporothrix brasiliensis* is associated with atypical clinical presentations. PLoS Negl Trop Dis. 2014;8:e3094. https://doi.org/10.1371/journal.pntd.0003094
45. de Carvalho JA, Hagen F, Fisher MC, de Camargo ZP, Rodrigues AM. Genome-wide mapping using new AFLP markers to explore intraspecific variation among pathogenic *Sporothrix* species. PLoS Negl Trop Dis. 2020;14:e0008330. https://doi.org/10.1371/journal.pntd.0008330
46. Teixeira MM, Almeida-Paes R, Bernardes-Engemann AR, Nicola AM, de Macedo PM, Valle ACF, et al. Single nucleotide polymorphisms and chromosomal copy number variation may impact the *Sporothrix brasiliensis* antifungal susceptibility and sporotrichosis clinical outcomes. Fung Gen Biol 2022;163:103743.
47. Huang M, Ma Z, Zhou X. Comparative genomic data provide new insight on the evolution of pathogenicity in *Sporothrix* species. Front Microbiol. 2020;11:565439. https://doi.org/10.3389/fmicb.2020.565439
48. Sanchotene KO, Madrid IM, Klafke GB, Bergamashi M, Della Terra PP, Rodrigues AM, et al. *Sporothrix brasiliensis* outbreaks and the rapid emergence of feline sporotrichosis. Mycoses. 2015;58:652–8. https://doi.org/10.1111/myc.12414
49. Valeriano CAT, Ferraz CE, Marques Evangelista Oliveira M, Inácio CP, de Oliveira EP, Lacerda AM, et al. Cat-transmitted disseminated cutaneous sporotrichosis caused by *Sporothrix brasiliensis* in a new endemic area: case series in the northeast of Brazil. JAAD Case Rep. 2020;6:988–92. https://doi.org/10.1016/j.jdcr.2020.07.047
50. Andrade EHP, Bastos CV, Silva AVD, Moreira SM, Costa TGA, Salvato LA, et al. Household outbreak of sporotrichosis: towards the One Health approach. Rev Soc Bras Med Trop. 2022;55:e0021. https://doi.org/10.1590/0037-8682-0021-2022

Address for correspondence: Flávio Queiroz-Telles, Federal University of Paraná, 280 Padre Camargo, Curitiba, Paraná, Brazil; email: queiroz.telles@uol.com.br

Triplex ELISA for Assessing Durability of *Taenia solium* Seropositivity after Neurocysticercosis Cure

Nina L. Tang, Theodore E. Nash, Madelynn Corda, Thomas B. Nutman, Elise M. O'Connell

Neurocysticercosis prevalence estimates often are based on serosurveys. However, assessments of *Taenia solium* seropositivity durability in patients with various neurocysticercosis types are lacking. We optimized a triplex serologic ELISA by using synthetic GP50, T24H, and Ts18var3 antigens for *T. solium*. We used that assay to test sequential serologic responses over several years after neurocysticercosis cure in 46 patients, 9 each with parenchymal or ventricular neurocysticercosis and 28 with subarachnoid disease. Triplex results were concordant with 98% of positive and 100% of negative enzyme-linked immunoelectrotransfer blots. Eight years after neurocysticercosis cure, 11.1% of patients with parenchymal, 47.3% with subarachnoid, and 41.7% with ventricular disease were still seropositive. Median time to seroreversion after cure in this cohort in a *T. solium* nonendemic area was 2 years for parenchymal disease, 4 years for ventricular disease, and 8 years for subarachnoid disease. Our findings can inform epidemiologic models that rely on serosurveys to estimate disease burden.

Neurocysticercosis is a parasitic disease caused by infection with larval cysts of the pork tapeworm, *Taenia solium*. Serosurveys are crucial tools for understanding the epidemiology of *T. solium* infection and populations at risk for neurocysticercosis. However, even in highly disease-endemic communities, concurrent neuroimaging reveals that few *T. solium*–seropositive neurocysticercosis patients have viable cysts at any given time (*1*,*2*). The discrepancy between seropositivity and evidence of central nervous system infection is likely the result of a combination of factors. One contributor is certainly persisting antibody response after intracranial cysts have resolved. However, the kinetics of serologic reactivity of patients after neurocysticercosis cure has not been demonstrated in follow-up beyond 1 year after treatment (*3*). Because serologic responses to any antigen can be boosted by repeat exposure, assessing long-term responses in a population that has left an endemic area and has little possibility of reexposure can be particularly useful.

The reference standard serologic diagnostic assay for neurocysticercosis is the enzyme-linked immunoelectrotransfer blot (EITB). EITB uses *T. solium* glycoproteins purified with lentil lectin to detect *Taenia*-specific antibodies, and positivity to any of 7 glycoproteins of interest is considered a positive result. EITB has a universally high sensitivity for detecting viable neurocysticercosis cysts, except in the case of a single parenchymal cyst. However, EITB testing is extremely labor intensive, requires parasite material, depends on expertise to accurately interpret the results, and has low throughput (*4*). Previous studies identified the 7 glycoproteins detected by EITB, which encompass 3 families of proteins, GP50, T24, and 8kD (*5*–*8*). Using QuickELISA (Immunetics Inc., https://immunetics.com) and a synthetic or recombinant antigen from each family has been previously reported to have high sensitivity for each component (*9*). That finding contrasts with ELISAs that use crude *Taenia* antigens and have reduced sensitivity and specificity (*10*,*11*).

We assessed the sensitivity of a slightly different combination of antigens representing the 3 families of proteins (GP50, T24H, and Ts18var3) used in the EITB assay in a traditional ELISA by using samples known to be EITB-positive or EITB-negative. We subsequently assessed the durability of seroreactivity after cure in a well-characterized group of patients with parenchymal, ventricular, and subarachnoid neurocysticercosis followed longitudinally in a nonendemic setting.

Author affiliation: National Institutes of Health, Bethesda, Maryland, USA

DOI: https://doi.org/10.3201/eid2907.230364

Methods

Samples

To define assay cutoffs, we obtained samples from 2 sources. First, we obtained samples from patients with known neurocysticercosis enrolled in an Institutional Review Board–approved neurocysticercosis natural history protocol (no. NCT00001205) at the National Institutes of Health Clinical Center, (Bethesda, Maryland, USA). All persons in that protocol provided written consent and were confirmed to be serologically positive by EITB performed at the Centers for Disease Control and Prevention (Atlanta, Georgia, USA). A second source of serum and plasma was deidentified samples left over from clinical testing that would otherwise have been discarded and that had quantitative PCR–detectable levels of circulating *T. solium* antigen (*12*), *T. solium* DNA, or both (*13*). Patients with positive results by those assays had a large burden of viable *T. solium* and were universally positive by EITB (*14*), here referred to as putative positives. To establish the optimal cutoffs for our triplex assay, we used serum or plasma from 100 known EITB-positive or putative positive patients and 52 persons from an endemic area, 29 of whom were known to be EITB-negative and 23 of whom were healthy blood bank controls without epidemiologic exposures. We collected samples from EITB-positive patients ≤18 months after their positive EITB. The pool of neurocysticercosis patients included cases of various cyst locations and represented a diverse range of geographic exposure (Table).

Patients from the neurocysticercosis natural history protocol that were serologically positive during active infection by the triplex assay and had banked samples with at least 2 years of follow-up after cure also underwent sequential sample testing. Cure for subarachnoid neurocysticercosis was defined as the first timepoint at which *T. solium* DNA was undetectable in cerebrospinal fluid (CSF) (n = 11) by qPCR (*13*) or *T. solium* antigen testing (*12*). For patients who did not have CSF available for testing (n = 17), we defined cure as the date anthelmintics were stopped; all patients in that group had ≥3 years of clinical follow-up with brain magnetic resonance imaging (MRI) after anthelmintics were discontinued. For patients with ventricular disease, we defined time of cure as the date on which the lesion was calcified on computed tomography (CT) imaging or susceptibility-weighted MRI images or when T2-weighted MRI sequences became dark, or at the time of surgical resection if the cyst was removed. Patients with parenchymal disease had to have noncalcified cysts at study entry to be included in this cohort. We defined time of cure for parenchymal disease as the date that imaging first demonstrated calcification or complete lesion resolution. Most patients were able to provide samples from both before and after cure. Year after cure was calculated as the date of serum collection minus the date of cure and rounded to the closest year.

Triplex *T. solium* Assay

The triplex *T. solium* assay used recombinant T24H and GP50 proteins. T24H (8) was expressed in a High Five (BTI-Tn-5B1-4) (Kempbio, http://www.kempproteins.com) baculovirus expression system (*8*). GP50 was produced (Genscript, https://www.genscript.com) as previously described (*7*). The synthetically produced 74 amino acid polypeptide Ts18var3 (LifeTein, https://www.lifetein.com) was derived from a *T. solium* DNA sequence (Genbank accession no. AF098075) (*5*,*6*) (Appendix, https://wwwnc.cdc.gov/EID/article/29/7/23-0364-App1.pdf). We tested additional proteins, TsRS1 (*6*) and NC3 (*15*), but preliminary tests on those 2 proteins were not as sensitive as the 3 proteins used (data not shown), and we did not pursue those 2 proteins further.

Statistical Analysis

We used Prism 9 (Graphpad, https://www.graphpad.com) to perform statistical analyses. We

Table. Demographics of a cohort of neurocysticercosis patients who underwent serial ELISA testing for reactivity to *Taenia solium* antigens GP50, T24H, and Ts18var3 to assess seropositivity after cure*

Characteristic	Value
Sex	
M	28
F	18
Age at cure, y	
19–29	15
30–60	30
>60	1
Region of birth	
Asia	4
Central America	29
Mexico	8
South America	4
United States	1
Neurocysticercosis type†	
Parenchymal	
Single cyst	3
>1 cyst	6
Extraparenchymal	
Subarachnoid	28
Ventricular	9
Total cohort size	46
Median length of follow-up, y (range)	
Parenchymal	8.5 (4–17.5)
Subarachnoid	6.6 (1.2–16.6)
Ventricular	8.4 (2.6–12.1)

*Values are no. patients except as indicated.
†Patients were classified by their most severe form of disease: subarachnoid, ventricular, then parenchymal.

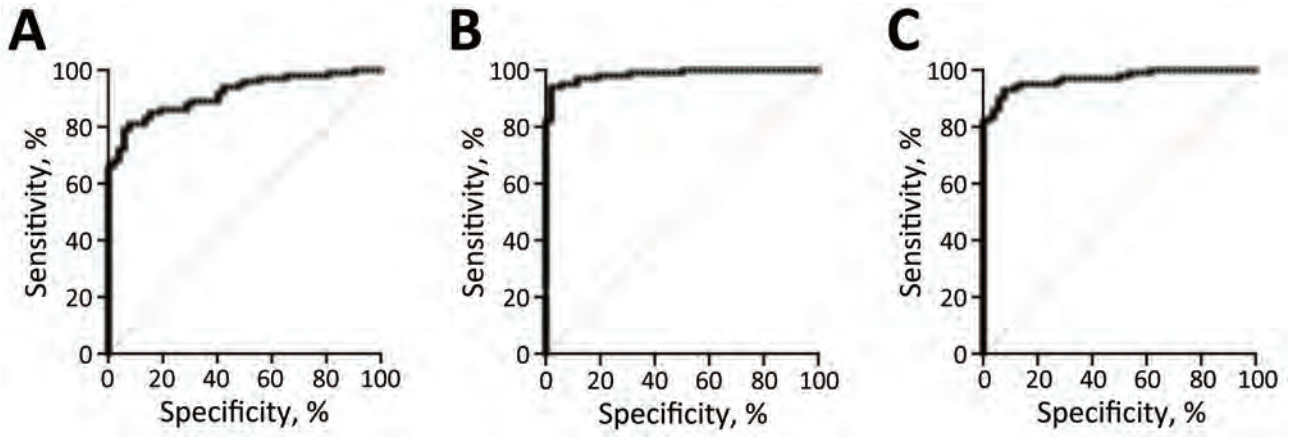

Figure 1. Sensitivity and specificity of a triplex assay to determine durability of *Taenia solium* seropositivity after neurocysticercosis cure. The assay combines 3 families of *T. solium* antigens: A) T24H; B) GP50; and C) Ts18var3. Receiver operating characteristic curves were produced by testing serum from 52 persons who were *T. solium*–negative and 100 neurocysticercosis patients with positive enzyme-linked immunoelectrotransfer blot results: 17 with parenchymal disease, 16 with ventricular disease, 35 with subarachnoid disease, and 32 putative positives (patients with detectable levels of circulating *T. solium* antigen, *T. solium* DNA, or both).

produced receiver operating characteristic (ROC) curves by using the Wilson-Brown method for sensitivity and specificity and set 95% CIs. We calculated the J-index at various signal-to-noise cutoffs by adding sensitivity and specificity and subtracting 1. To compare the seroreactivity of different disease types to T24H, GP50, and Ts18var3, we used Kruskal-Wallis analysis of variance and Dunn multiple comparisons tests with adjusted p values. We used Fisher exact tests and Baptista-Pike odds ratios (ORs) to determine the specificity of various seroreactivity patterns for different forms of neurocysticercosis. We used Fisher exact tests to determine differences in seropositivity at cure among neurocysticercosis groups. We used nonparametric Wilcoxon matched pairs signed-rank tests to compare the seroreactivity to T24H, GP50, and Ts18var3 at the time of cure and 4 years after cure. We used Kaplan-Meier simple survival analyses to describe the annual prevalence of seroreversion after cure and log-rank Mantel-Cox tests to analyze differences between survival curves.

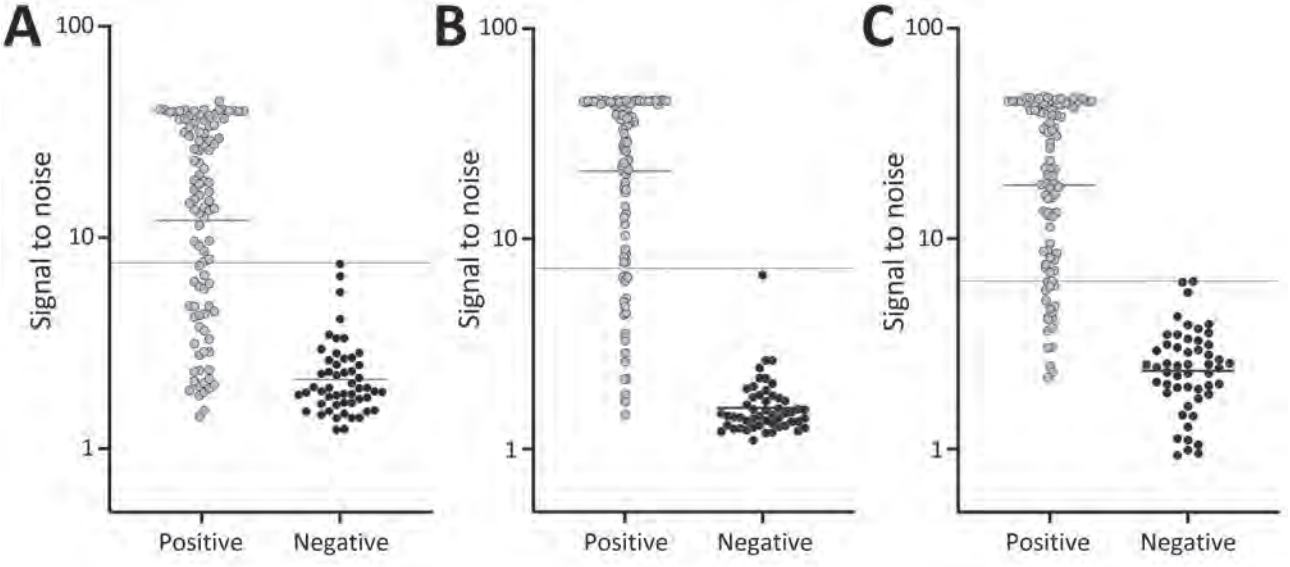

Figure 2. Signal-to-noise results of a triplex assay to determine durability of *Taenia solium* seropositivity after neurocysticercosis cure. The assay combines 3 families of *T. solium* antigens: A) T24H; B) GP50; and C) Ts18var3. Samples from neurocysticercosis positive and negative persons were compared; each circle represents 1 person. Horizontal bars indicate geometric mean; dotted horizontal lines indicate signal-to-noise cutoffs that provided the highest sensitivity while maintaining 100% specificity for each protein.

Results

Sensitivity and Specificity of *T. solium* Triplex Assay

For all proteins, we compared the sensitivity and specificity produced by various signal-to-noise cutoffs determined using ROC curves (Figure 1). We defined sensitivity as the percent positive by the triplex assay out of the 100 samples known to be positive by EITB or antigen testing. We defined specificity as the percent of the 52 samples known to be EITB-negative that were also negative by the triplex assay. The J-index cutoffs for signal-to-noise were 3.547 (J = 0.7331) for T24H, 2.742 (J = 0.9208) for GP50, and 4.019 (J = 0.8531) for Ts18var3. Those cutoffs resulted in sensitivity of 81% (95% CI 72%–88%) and specificity of 92% (95% CI 82%–97%) for T24H, sensitivity of 94% (95% CI 88%–97%) and specificity of 98% (95% CI 90%–100%) for GP50, and sensitivity of 93% (95% CI 86%–97%) and specificity of 92% for Ts18var3 (95% CI 82%–97%). In addition to the J-index, we used ROC curves for each protein to determine cutoffs that yielded 100% specificity. This approach resulted in signal-to-noise thresholds of 7.6 for T24H, 7.206 for GP50, and 6.261 for Ts18var3. With those cutoffs, each protein independently achieved moderate sensitivity, 66% for T24H and 82% for both GP50 and Ts18var3 (Figure 2).

To improve the diagnostic capacity of the individual proteins, we combined the results of each assay and defined *T. solium* positivity as positivity to any of the 3 proteins. Using this approach, the sensitivity of the combined triplex assay exceeded that of any individual protein (Figure 3). When we used cutoffs that yielded 100% specificity, the triplex assay achieved a sensitivity of 98% (95% CI 93%–100%), a major improvement over the sensitivities of each assay in isolation, demonstrating the power of this triplex approach.

Differential Seroreactivity to Antigens

In addition to binary detection of *Taenia*-specific antibodies, we found the triplex assay provided information on disease type by assessing the differential reactivity of serum to the assays' components. We noted no difference in reactivity (H2) between patients with subarachnoid and ventricular disease for T24H (H2 adjusted p>0.9999), GP50 (H2 adjusted p = 0.3676), or Ts18var3 (H2 adjusted p>0.9999), suggesting that extraparenchymal disease drives reactivity to all 3 proteins (Figure 4). We also saw no significant difference in seroreactivity toward Ts18var3 between patients with parenchymal and subarachnoid disease (H2 adjusted p = 0.5396) or parenchymal and ventricular disease (H2 p>0.9999).

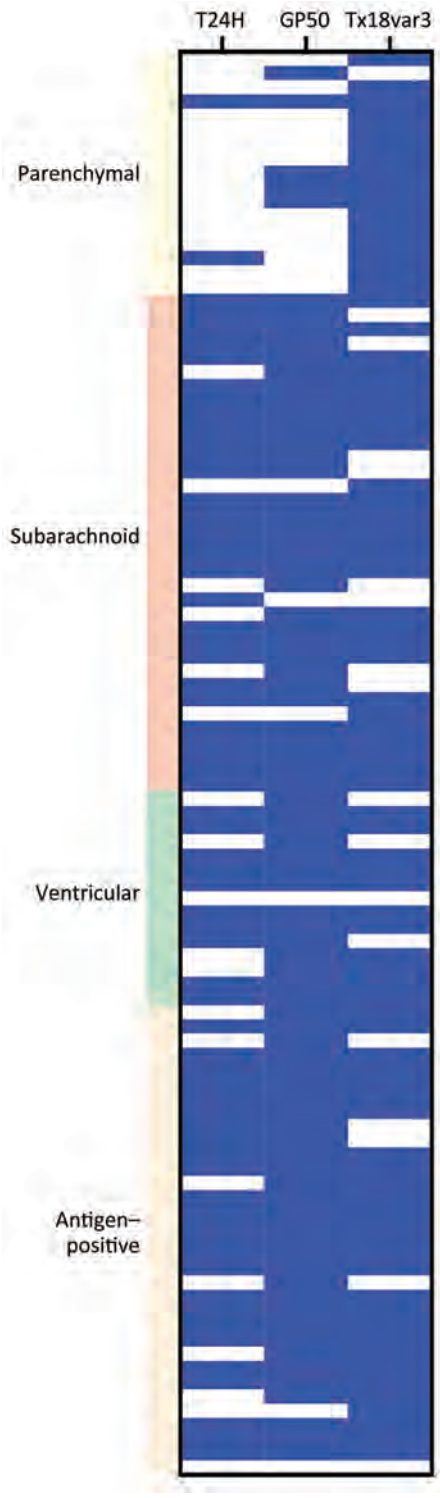

Figure 3. Comparison of positive and negative results of a triplex assay to determine durability of *Taenia solium* seropositivity after neurocysticercosis cure. The assay combines 3 families of *T. solium* antigens: T24H, GP50, and Ts18var3. The graph shows results for each antigen from 100 persons with and without neurocysticercosis, by disease type. Blue indicates positive results; white indicates negative results.

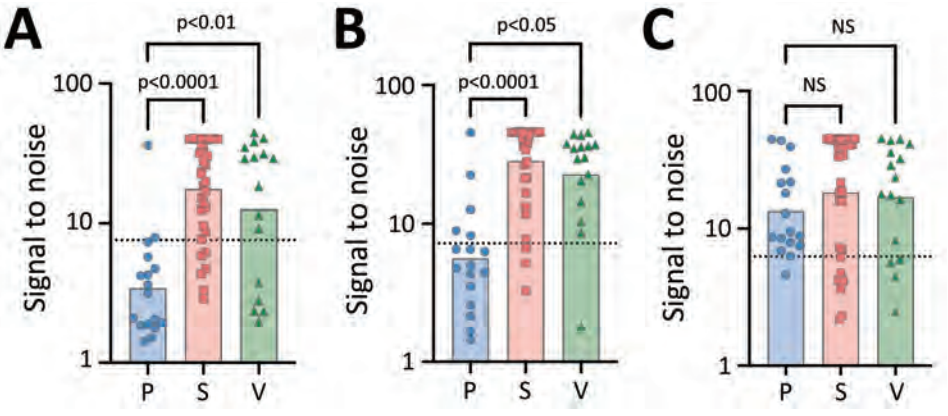

Figure 4. Positivity patterns per cyst location for a triplex assay to determine durability of *Taenia solium* seropositivity after neurocysticercosis cure. The assay combines 3 families of *T. solium* antigens: A) T24H; B) GP50; and C) Ts18var3. Graphs display signal-to-noise reactivity to T24H, GP50, and Ts18var3 by neurocysticercosis disease type. We assessed differential reactivity to *T. solium* antigens in samples from 68 neurocysticercosis-positive persons, 17 with parenchymal, 16 with ventricular, and 35 with subarachnoid neurocysticercosis. Dotted horizontal lines indicate 100% specificity cutoff each protein. NS, not statistically significant; P, parenchymal; S, subarachnoid; V, ventricular.

However, the divergent patterns of seroreactivity between extraparenchymal and parenchymal cases became clear when comparing reactivity to T24H and GP50. Subarachnoid patients exhibited higher reactivity than parenchymal patients to both T24H (H2 adjusted p<0.0001) and GP50 (H2 adjusted p<0.0001). Similarly, ventricular patients were also significantly more reactive than parenchymal patients to T24H (H2 adjusted p = 0.0046) and GP50 (H2 adjusted p = 0.0108). Odds ratio analysis using Fisher exact tests and Baptista-Pike ORs demonstrated the predictive capacity of those seroreactivity patterns; seropositivity to T24H resulted in 25.91 (95% CI 4.931–120.1; p<0.0001) times the odds of extraparenchymal over parenchymal disease and positivity to GP50 resulted in 27.00 (95% CI 6.531–93.71; p<0.0001) times the odds in the same direction (Figure 5). Meanwhile, positivity to only Ts18var3 resulted in nonsignificant odds of 5.189 (95% CI 0.7467–58.76; p = 0.1574) in favor of parenchymal over extraparenchymal neurocysticercosis.

Although positivity to Ts18var3 did not confer any statistically significant predictive capacity to the triplex assay, it was the main driver of the triplex assay's sensitivity for parenchymal neurocysticercosis. When we used only Ts18var3 with the 100% specificity cutoff of 6.261 signal-to-noise, we detected 94.1% (16/17) of patients with parenchymal disease, compared with 11.8% (2/17) when we only used T24H and 29.4% (5/17) when we only used GP50 (Figure 6). Therefore, to maximize detection of parenchymal disease, Ts18var3 is a necessary component of the assay.

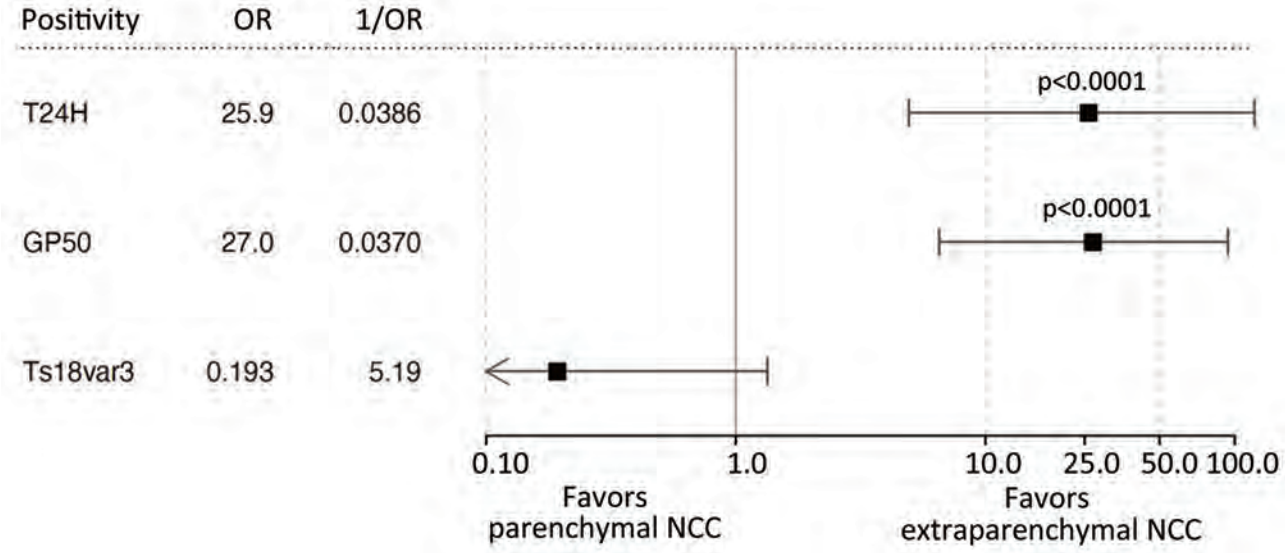

Figure 5. Odds ratios of seropositivity of a triplex assay to determine durability of *Taenia solium* seropositivity after neurocysticercosis cure. The assay combines 3 families of *T. solium* antigens: T24H, GP50, and Ts18var3. We assessed seropositivity in extraparenchymal and parenchymal disease. Error bars indicate 95% CIs; arrows indicate that the end of a CI exceeds the range of the graph axis. NCC, neurocysticercosis; 1/OR, reciprocal odds ratio; OR, odds ratio.

Persistence of Seropositivity after Neurocysticercosis Cure

To evaluate the persistence of seropositivity after cure, we longitudinally collected serum from 46 neurocysticercosis patients and evaluated samples by using the triplex *T. solium* assay. The patient cohort included 9 persons with active parenchymal neurocysticercosis, all of whom subsequently had calcified disease; 28 subarachnoid patients; and 9 ventricular patients. The median follow-up time was 8.5 (range 4–17.5) years for parenchymal disease, 6.6 (range 1.2–16.6) years for subarachnoid disease, and 8.4 (range 2.6–12.1) years for ventricular disease (Table).

At the time of cure, 67% of patients with parenchymal, 100% with subarachnoid, and 89% with ventricular disease were seropositive (Figure 7, panel A). In the first 4 years after cure, we noted all groups had statistically significant reductions in seroreactivity toward T24H ($p<0.0001$), GP50 ($p<0.0001$), and Ts18var3 ($p = 0.0002$) (Figure 7, panels B–D). This finding suggests a reduction in *T. solium* antibodies after disease resolution. However, the rate at which reactivity decreases to the individual antigens of the triplex assay is different. Kaplan-Meier survival analysis showed that, by 4 years after cure, 80% of patients with parenchymal, 90.5% with subarachnoid, and 100% with ventricular disease were no longer reactive to Ts18var3 (Figure 8, panels A–C). Insufficient numbers of patients with parenchymal disease were available to perform survival analysis for T24H and GP50. However, 4 years after cure, 69.4% of patients with subarachnoid disease seroreverted to T24H and 52% seroreverted to GP50. Meanwhile, 70% of patients with ventricular disease seroreverted to T24H and 78% seroreverted to GP50 over the same period. Log-rank Mantel-Cox analysis showed a significant difference in annual seroreversion between T24H, GP50, and Ts18var3 in both subarachnoid ($p = 0.03$) and ventricular patients ($p = 0.04$), and reactivity to Ts18var3 was the first to decline, then GP50 and T24H.

We used additional Kaplan-Meier survival analysis to determine the probability of complete seroreversion for each disease type, meaning that patients would achieve seronegativity to all proteins. That analysis demonstrated significant differences in seroreversion over time ($p = 0.025$) among the 3 different categories of neurocysticercosis. Median seropositivity was 2 years after cure for parenchymal disease, 8 years for subarachnoid disease, and 4 years for ventricular disease (Figure 8, panel D). Overall seropositivity at year 8 after cure was 11% for parenchymal disease, 47.3% for subarachnoid disease, and 41.7% for ventricular disease.

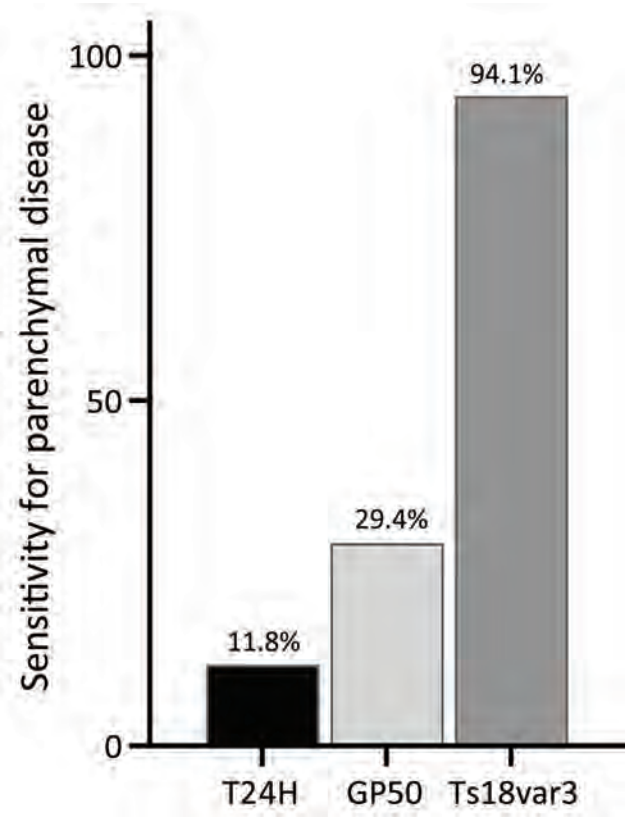

Figure 6. Sensitivity for parenchymal disease of a triplex assay to determine durability of *Taenia solium* seropositivity after neurocysticercosis cure. The assay combines 3 families of *T. solium* antigens: T24H, GP50, and Ts18var3. The graph shows that sensitivity is primarily dependent on Ts18var3; numbers at tops of bars indicate percentages of parenchymal cases (n = 17) found to be positive by each protein.

Discussion

Although brain imaging is required to diagnose neurocysticercosis, serologic testing often confirms the diagnosis, and *T. solium* serosurveys often are performed to assess the burden of *T. solium* exposure in a population. We optimized a serologic ELISA by using 3 proteins in a triplex assay. The triplex *T. solium* assay was able to detect 98% of EITB-positive or antigen-positive cases and agreed 100% with EITB test negativity. Although recombinant T24H has been reported to have a high sensitivity and specificity when used in an ELISA for serologic detection (*9*), our study did not find T24H was an essential driver of overall positivity. In fact, of the 98 samples that were positive by the optimized triplex assay, 97 would still have been positive by relying only on GP50 and Ts18var3 without sacrificing specificity. This finding suggests that future diagnostic assays might be able to rely on only 2 antigens, but because neurocysticercosis involving a single parenchymal lesion has diminished seroreactivity, a larger scale

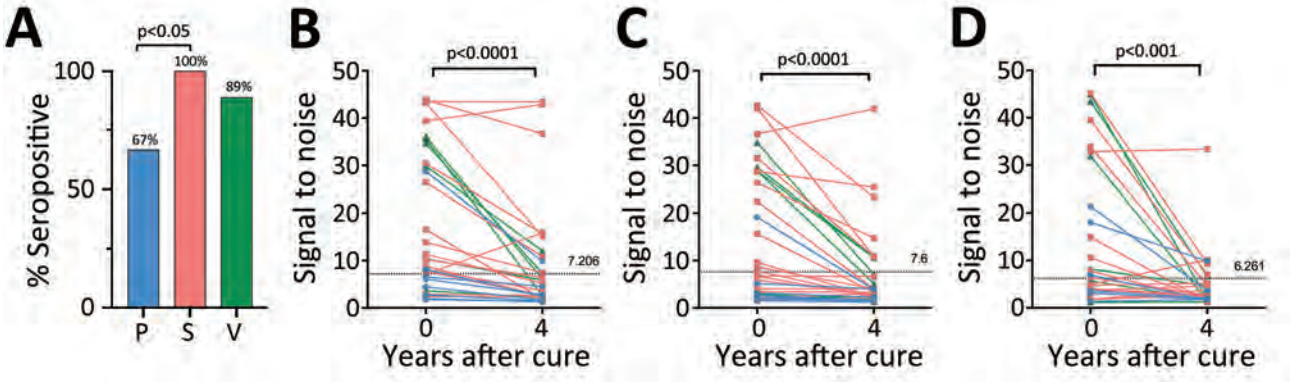

Figure 7. *Taenia solium* seropositivity over time by a triplex assay to determine durability of *T. solium* seropositivity after neurocysticercosis cure. The triplex assay combines 3 families of *T. solium* antigens: T24H, GP50, and Ts18var3. A) Seropositivity at time of cure. B–D) Seropositivity at year 4 by neurocysticercosis disease type: B) parenchymal (n = 9); C) subarachnoid (n = 28); and D) ventricular disease (n = 9). Line colors in panels B–D correspond to bar colors in panel A. Horizonal dotted lines indicate the 100% specificity cutoff used for that protein. Statistically significant differences in seropositivity were seen between patients with parenchymal disease (67%) and subarachnoid disease (100%) (p = 0.011), but not for ventricular disease (89% at the time of cure). Patients seropositive at time of cure (parenchymal n = 6, subarachnoid n = 28, ventricular n = 8) underwent testing of paired samples at time of cure (day 0) and 4 years after cure. For each subgroup, reactivity to GP50, T24H, and Ts18var3 showed statistically significant decreases by year 4. P, parenchymal; S, subarachnoid; V, ventricular.

study in a population more representative of those patients will be needed to verify that finding (*16*). In addition, EITB banding patterns have been reported to be somewhat different in small assessments in Asia (*17*). In ROC curve development for this study, we had 5 patients from countries in Asia, namely India, South Korea, and Laos. All those patients were *T.* solium–positive by the triplex assay without exception to any antigen. High quality evidence from serologic assessments in Asia also showed that reactivity to T24 and to the 8kDa family, of which Ts18var3 is a member, was maintained (*17*,*18*). However, because of the small representation of patients from Asia, formal validation of our triplex assay should be undertaken in endemic areas of Asia before deploying it in that setting.

In this group of patients, responsiveness to GP50 and T24H greatly increased the odds that the patient had extraparenchymal disease. In a previous study that analyzed EITB assay banding patterns, positivity to GP50 or T24 was associated with intraparenchymal infections (*19*). In that same study, reactivity to GP50, T24, and the 8kDa protein family were observed more frequently in extraparenchymal disease and patients with multiple intraparenchymal lesions (*19*). However,

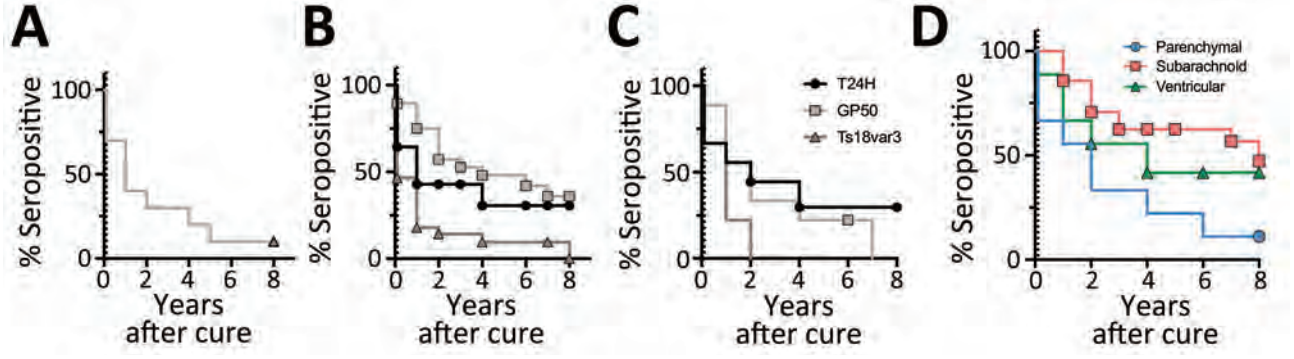

Figure 8. Degradation of *Taenia solium* seropositivity over time by a triplex assay to determine durability of *T. solium* seropositivity after neurocysticercosis cure. The assay combines 3 families of *T. solium* antigens: T24H, GP50, and Ts18var3. Kaplan-Meier survival curves show seropositivity by disease type for each protein over 8 years after neurocysticercosis cure. A) Parenchymal disease; B) subarachnoid disease; C) ventricular disease; D) all disease types. Time 0 represents time during treatment when all subjects were seropositive; dotted vertical line indicates time of cure. Symbols indicate years containing censored data for each disease type. The sample size for patients with parenchymal disease testing positive to T24H, GP50, or both, at cure were too few to plot. Therefore, these curves were excluded in this analysis. Log-rank Mantel-Cox analysis found significant differences in seroreversion in Ts18var3 compared with T24H and GP50 for both subarachnoid (p = 0.03) and ventricular disease (p = 0.04). Log-rank Mantel-Cox analysis for all survivors (D) demonstrates significant differences between the curves (p = 0.025); 11.1% of patients with parenchymal disease, 47.3% with subarachnoid disease, and 41.7% with ventricular disease were seropositive 8 years after cure.

those differences likely are a result of the different platforms used for antibody detection. Such differences include the sensitivity in detecting antibodies to various antigens because of the different methods and because the positivity threshold for ELISA is artificially set by choosing a signal-to-noise ratio that maximizes sensitivity and specificity. EITB also might be limited by what can be visually observed in grading reactivity.

Clarifying the kinetics of seroreactivity to *T. solium* infection in neurocysticercosis patients is vital for determining the clinical utility these tests and epidemiologic studies that involve their use (*3*,*20*). Serial serosurveys without concurrent brain imaging in Peru and Ecuador have shown that, over the course of a year, ≈30% of serologically positive patients will revert to negative (*21*,*22*). Another study in Peru followed patients with parenchymal neurocysticercosis after therapy and demonstrated that only 7% of all treated patients became seronegative 1 year after treatment, and only 23% (3/13) of cured patients became seronegative (*3*). Here, we studied patients that had ≥1 positive serologic response during active disease and assessed what happened over time. By the time of cure, determined by CSF antigen negativity, calcification, or surgical removal, depending on disease type and sample availability, only 33% (3/9) of patients with parenchymal disease, 11% (1/9) with ventricular disease, and none (0/28) with subarachnoid disease seroreverted. The time parameters of our study are not completely comparable to the studies from Peru and Ecuador because it can take >1 year from the time of treatment for an intraparenchymal cyst to start to calcify, which we used as a criterium for cure in this study. However, we used cure to standardize the durability of seropositivity because in some cases viable cysts begin to die before treatment is begun, and some patients require multiple treatment courses. Regardless of the timeframe used for assessing seroreversion, serologic negativity is unreliable for determining disease activity in neurocysticercosis, as others have also demonstrated (*3*), and should not be used to assess treatment efficacy nor disease activity.

Our data show a major decrease in antibody reactivity to each antigen in the triplex assay for all neurocysticercosis disease states over time. However, the overall durability of seropositivity was striking; the median seropositivity for patients with parenchymal disease was 2 years, for subarachnoid disease was 8 years, and for ventricular disease was 4 years. Those differences appear to be driven by the difference in the kinetics of disappearance of the antibodies to the individual antigens. Reactivity to Ts18var3 was the most short-lived for each disease type. However, Ts18var3 is the main driver of positivity among patients with parenchymal disease; thus, the overall seropositivity for those with parenchymal disease was shorter. By comparison, patients with ventricular disease were reactive to Ts18var3 for a median of 1 year after cure, but >50% of patients with subarachnoid disease had already seroconverted to Ts18var3 at 1 year after cure.

A few aspects of this study should be considered when interpreting these data in a larger epidemiologic context. Our population is skewed toward more heavily infected patients, and most of the included patients had extraparenchymal neurocysticercosis. Our parenchymal disease cohort was relatively small, and most patients had >1 cyst. However, those data are particularly useful for demonstrating durability of seropositivity among patients with extraparenchymal disease, and nearly half of those patients were still seropositive 8 years after cure. That finding is notable because extraparenchymal disease is likely underdiagnosed, and the true prevalence likely is unknown and higher than previously appreciated (*23*). Moreover, symptoms of extraparenchymal disease are often not captured when screening populations by history because patients without parenchymal cysts do not have seizures, and a history of headaches is very nonspecific. Finally, CT imaging often misses extraparenchymal cysts and cannot be relied on for making that diagnosis. Thus, the contribution of extraparenchymal disease to the seropositivity of a population remains an area of active investigation. We did not address the contribution of cysts outside the central nervous system to overall seropositivity or the duration of seropositivity in those patients.

In conclusion, seroreversion in neurocysticercosis patients is often delayed for years after cure. We described the kinetics of serologic responses against 3 diagnostic antigens for *T. solium* from neurocysticercosis diagnosis to cure in persons who likely did not have further exposure to the parasite. These data could help inform epidemiologic models that rely on serosurveys to estimate disease burden.

This work was supported by the Intramural Research Program of the National Institutes of Health, National Institute of Allergy and Infectious Diseases.

About the Author

Ms. Tang is a MD-PhD candidate at the Baylor College of Medicine in Houston, Texas, USA. Her primary research interest is human helminth infections.

References

1. Goodman KA, Ballagh SA, Carpio A. Case-control study of seropositivity for cysticercosis in Cuenca, Ecuador. Am J Trop Med Hyg. 1999;60:70–4. https://doi.org/10.4269/ajtmh.1999.60.70
2. Fleury A, Gomez T, Alvarez I, Meza D, Huerta M, Chavarria A, et al. High prevalence of calcified silent neurocysticercosis in a rural village of Mexico. Neuroepidemiology. 2003;22:139–45. https://doi.org/10.1159/000068748
3. Garcia HH, Gilman RH, Catacora M, Verastegui M, Gonzalez AE, Tsang VC; Cysticercosis Working Group in Peru. Serologic evolution of neurocysticercosis patients after antiparasitic therapy. J Infect Dis. 1997;175:486–9. https://doi.org/10.1093/infdis/175.2.486
4. Tsang VC, Brand JA, Boyer AE. An enzyme-linked immunoelectrotransfer blot assay and glycoprotein antigens for diagnosing human cysticercosis (*Taenia solium*). J Infect Dis. 1989;159:50–9. https://doi.org/10.1093/infdis/159.1.50
5. Greene RM, Hancock K, Wilkins PP, Tsang VC. *Taenia solium*: molecular cloning and serologic evaluation of 14- and 18-kDa related, diagnostic antigens. J Parasitol. 2000;86:1001–7. https://doi.org/10.1645/0022-3395(2000)086[1001:TSMCAS]2.0.CO;2
6. Hancock K, Khan A, Williams FB, Yushak ML, Pattabhi S, Noh J, et al. Characterization of the 8-kilodalton antigens of *Taenia solium* metacestodes and evaluation of their use in an enzyme-linked immunosorbent assay for serodiagnosis. J Clin Microbiol. 2003;41:2577–86. https://doi.org/10.1128/JCM.41.6.2577-2586.2003
7. Hancock K, Pattabhi S, Greene RM, Yushak ML, Williams F, Khan A, et al. Characterization and cloning of GP50, a *Taenia solium* antigen diagnostic for cysticercosis. Mol Biochem Parasitol. 2004;133:115–24. https://doi.org/10.1016/j.molbiopara.2003.10.001
8. Hancock K, Pattabhi S, Whitfield FW, Yushak ML, Lane WS, Garcia HH, et al. Characterization and cloning of T24, a *Taenia solium* antigen diagnostic for cysticercosis. Mol Biochem Parasitol. 2006;147:109–17. https://doi.org/10.1016/j.molbiopara.2006.02.004
9. Lee Y-M, Handali S, Hancock K, Pattabhi S, Kovalenko VA, Levin A, et al. Serologic diagnosis of human *Taenia solium* cysticercosis by using recombinant and synthetic antigens in QuickELISA™. Am J Trop Med Hyg. 2011;84:587–93. https://doi.org/10.4269/ajtmh.2011.10-0079
10. Ramos-Kuri M, Montoya RM, Padilla A, Govezensky T, Díaz ML, Sciutto E, et al. Immunodiagnosis of neurocysticercosis. Disappointing performance of serology (enzyme-linked immunosorbent assay) in an unbiased sample of neurological patients. Arch Neurol. 1992;49:633–6. https://doi.org/10.1001/archneur.1992.00530300069012
11. Montenegro T, Gilman RH, Castillo R, Tsang V, Brandt J, Guevara A, et al. The diagnostic importance of species specific and cross-reactive components of *Taenia solium*, *Echinococcus granulosus*, and *Hymenolepis nana*. Rev Inst Med Trop São Paulo. 1994;36:327–34. https://doi.org/10.1590/S0036-46651994000400005
12. Corda M, Sciurba J, Blaha J, Mahanty S, Paredes A, Garcia HH, et al. A recombinant monoclonal-based *Taenia* antigen assay that reflects disease activity in extra-parenchymal neurocysticercosis. PLoS Negl Trop Dis. 2022;16:e0010442. https://doi.org/10.1371/journal.pntd.0010442
13. O'Connell EM, Harrison S, Dahlstrom E, Nash T, Nutman TBA. A novel, highly sensitive quantitative polymerase chain reaction assay for the diagnosis of subarachnoid and ventricular neurocysticercosis and for assessing responses to treatment. Clin Infect Dis. 2020;70:1875–81. https://doi.org/10.1093/cid/ciz541
14. White AC Jr, Coyle CM, Rajshekhar V, Singh G, Hauser WA, Mohanty A, et al. Diagnosis and treatment of neurocysticercosis: 2017 clinical practice guidelines by the Infectious Diseases Society of America (IDSA) and the American Society of Tropical Medicine and Hygiene (ASTMH). Clin Infect Dis. 2018;66:e49–75. https://doi.org/10.1093/cid/cix1084
15. Hubert K, Andriantsimahavandy A, Michault A, Frosch M, Mühlschlegel FA. Serological diagnosis of human cysticercosis by use of recombinant antigens from *Taenia solium* cysticerci. Clin Diagn Lab Immunol. 1999;6:479–82. https://doi.org/10.1128/CDLI.6.4.479-482.1999
16. Wilson M, Bryan RT, Fried JA, Ware DA, Schantz PM, Pilcher JB, et al. Clinical evaluation of the cysticercosis enzyme-linked immunoelectrotransfer blot in patients with neurocysticercosis. J Infect Dis. 1991;164:1007–9. https://doi.org/10.1093/infdis/164.5.1007
17. Sato MO, Sako Y, Nakao M, Yamasaki H, Nakaya K, Ito A. Evaluation of purified *Taenia solium* glycoproteins and recombinant antigens in the serologic detection of human and swine cysticercosis. J Infect Dis. 2006;194:1783–90. https://doi.org/10.1086/509262
18. Arora N, Kaur R, Rawat SS, Kumar A, Singh AK, Tripathi S, et al. Evaluation of *Taenia solium* cyst fluid-based enzyme linked immunoelectro transfer blot for neurocysticercosis diagnosis in urban and highly endemic rural population of North India. Clin Chim Acta. 2020;508:16–21. https://doi.org/10.1016/j.cca.2020.05.006
19. Arroyo G, Rodriguez S, Lescano AG, Alroy KA, Bustos JA, Santivañez S, et al.; Cysticercosis Working Group in Peru. Antibody banding patterns of the enzyme-linked immunoelectrotransfer blot and brain imaging findings in patients with neurocysticercosis. Clin Infect Dis. 2018;66:282–8. https://doi.org/10.1093/cid/cix774
20. Dixon MA, Winskill P, Harrison WE, Whittaker C, Schmidt V, Flórez Sánchez AC, et al. Global variation in force-of-infection trends for human *Taenia solium* taeniasis/cysticercosis. eLife. 2022;11:e76988. https://doi.org/10.7554/eLife.76988
21. Garcia HH, Gonzalez AE, Gilman RH, Palacios LG, Jimenez I, Rodriguez S, et al.; Cysticercosis Working Group in Peru. Short report: transient antibody response in *Taenia solium* infection in field conditions-a major contributor to high seroprevalence. Am J Trop Med Hyg. 2001;65:31–2. https://doi.org/10.4269/ajtmh.2001.65.31
22. Coral-Almeida M, Rodríguez-Hidalgo R, Celi-Erazo M, García HH, Rodríguez S, Devleesschauwer B, et al. Incidence of human *Taenia solium* larval infections in an Ecuadorian endemic area: implications for disease burden assessment and control. PLoS Negl Trop Dis. 2014;8:e2887. https://doi.org/10.1371/journal.pntd.0002887
23. McCleery E, Allen SE, Moyano LM, Gamboa R, Vilchez P, Muro C, et al.; Cysticercosis Working Group in Peru. Population screening for urine antigens to detect asymptomatic subarachnoid neurocysticercosis: a pilot study in northern Peru. Am J Trop Med Hyg. 2020;103:1125–8. https://doi.org/10.4269/ajtmh.20-0196

Address for correspondence: Elise O'Connell, Laboratory of Parasitic Diseases, National Institute of Allergy and Infectious Diseases, 4 Center Dr. Bldg 4 Rm. 424, Bethesda, MD 20892, USA; email: oconnellem@niaid.nih.gov

Effect of Norovirus Inoculum Dose on Virus Kinetics, Shedding, and Symptoms

Yang Ge, W. Zane Billings, Antone Opekun, Mary Estes, David Graham, Juan Leon, Katia Koelle, Ye Shen, Robert Atmar, Benjamin Lopman, Andreas Handel

The effect of norovirus dose on outcomes such as virus shedding and symptoms after initial infection is not well understood. We performed a secondary analysis of a human challenge study by using Bayesian mixed-effects models. As the dose increased from 4.8 to 4,800 reverse transcription PCR units, the total amount of shed virus in feces increased from 4.5×10^{11} to 3.4×10^{12} genomic equivalent copies; in vomit, virus increased from 6.4×10^{5} to 3.0×10^{7} genomic equivalent copies. Onset time of viral shedding in feces decreased from 1.4 to 0.8 days, and time of peak viral shedding decreased from 2.3 to 1.5 days. Time to symptom onset decreased from 1.5 to 0.8 days. One type of symptom score increased. An increase in norovirus dose was associated with more rapid shedding and symptom onset and possibly increased severity. However, the effect on virus load and shedding was inconclusive.

Norovirus is a major cause of foodborne disease and causes a large number of cases, hospitalizations, and deaths in the United States and globally (*1*–*4*). Specific treatments are not available, and vaccines are still under development (*4*,*5*). Generic infection control measures are the best approaches to minimizing disease burden (*6*–*10*).

An increase in exposure dose (number of virus particles) is associated with an increased risk for infection; this principle applies to norovirus (*11*–*14*) and many other pathogens (*15*,*16*). Less is known about the possible effect of dose on infection outcomes after infection has occurred. For acute infections such as influenza, infectious bronchitis virus, and parainfluenza virus, animal studies and models suggest that dose influences the virus load kinetics (*17*–*19*). For norovirus, some evidence from experimental challenge studies suggests that dose is associated with more rapid onset of symptoms (*20*). To further elucidate the effect of inoculum dose on infection outcomes such as virus shedding and symptom severity, we performed a secondary analysis of data from a human norovirus challenge study (*20*).

Methods

In this article, we will give brief descriptions of our methods. We have also provided complete modeling and analysis details, including all data and code needed to reproduce our results (Appendix, https://wwwnc.cdc.gov/EID/article/29/7/23-0117-App1.pdf).

Data

The data we used for our analyses are from a human challenge study registered at ClinicalTrials.gov (trial no. NCT00138476) (*20*–*24*). The clinical protocol was reviewed and approved by the institutional review boards of the Baylor College of Medicine and The Houston Methodist Hospital, and written informed consent was obtained from each study participant.

In the challenge study, 57 healthy persons (18–50 years of age) were randomly inoculated with either placebo or norovirus genogroup I genotype 1 strain (GI.1 NV) at 4 different doses (0.48, 4.8, 48, or 4,800 reverse transcription PCR [RT-PCR] units). Of the 21 persons who became infected, 1 person was unavailable for follow-up, and thus we excluded that patient from all analyses. In addition, only 1 person in the 0.48-unit dose group became infected, so we excluded this person from our main analyses. Therefore, remaining for our analysis were 6 persons in the

Authors affiliations: University of Southern Mississippi School of Health Professions, Hattiesburg, Mississippi, USA (Y. Ge); University of Georgia, Athens, Georgia, USA (W.Z. Billings, Y. Shen, A. Handel); Baylor College of Medicine, Houston, Texas, USA (A. Opekun, M. Estes, D. Graham, R. Atmar); Emory University Rollins School of Public Health, Atlanta, Georgia, USA (J. Leon, B. Lopman); Emory University, Atlanta (K. Koelle)

DOI: https://doi.org/10.3201/eid2907.230117

4.8-unit dose group, 7 persons in the 4.8-unit dose group, and 6 persons in the 4,800-unit dose group. We provide analyses that include the 1 person who was infected at the 0.48-dose level (Appendix).

All persons were isolated in the research center for ≥4 days (96 hours) after inoculation. The study personnel collected samples of feces and vomit and recorded clinical symptoms.; samples were also collected for 4–8 weeks postinoculation. For some of our analyses, we focused on the 96 hours during which persons were under clinical observation. For other analyses, we included the data collected after persons returned home. We state which data are used for each analysis.

Overall Analysis Approach and Implementation

Because we performed a secondary data analysis, a strict null hypothesis significance testing framework using p values was not suitable, so we performed all analyses in a Bayesian framework. For all analyses, we used Bayesian mixed-effects models. We treated the dose as a continuous variable for the results shown in the article. We also provide a sensitivity analysis with dose modeled as categorical (Appendix). We report the mean of the estimated posterior distribution with 95% equal-tailed credible intervals (CrIs) for all model results (*25*). We conducted all analyses using R version 4.2.3 (*26*), and Stan (*27*), accessed through the brms package in R (*28*). We used Rhat values to diagnose convergence (*28*).

Analysis of Virus Shedding Outcomes

We measured virus shedding concentration in samples by either an immunomagnetic capture (IMC) RT-PCR, which provided a qualitative readout (positive or negative), or real-time quantitative RT-PCR (qRT-PCR), which provided a quantitative readout in genomic equivalent copies (GEC) (*21*). Those 2 methods had limits of detection (LOD) at 15,000 GEC/g of stool (LOD1) and 40,000,000 GEC/g of stool (LOD2). Therefore, the virus shedding concentration could be between 0 and LOD1 (negative IMC, negative qRT-PCR), between LOD1 and LOD2 (positive IMC, negative qRT-PCR), or a quantitative measurement above LOD2 (positive qRT-PCR). We reported vomit shedding data similarly, with either a numeric value or a positive or negative readout. We accounted for this censored data structure in our models (Appendix).

We obtained the total virus contained in each sample by multiplying virus concentration by sample weight for feces (GEC/g × weight of feces in grams) or sample volume for vomit (GEC/mL × volume of vomit in mL). We calculated each participant's total amount of virus shedding in feces and vomit by summing virus shedding values for all samples per participant. We used a linear model structure to analyze associations between inoculum dose and the total amount of virus shedding.

In a further analysis, we modeled the longitudinal time-series of virus concentration in feces, $V(t)$, using the 4-parameter equation

$$V(t) = \frac{2p}{\exp\left(-g(t-T)\right) + \exp\left(d(t-T)\right)}$$

which was shown to accurately describe trajectories of acute viral infections (*17*,*29*). We fitted the trajectories by using a Bayesian nonlinear mixed-effects model in which the mean of the response was described using this equation. We used the comparison between the parameter's prior and posterior distributions to ensure that the choice of prior distribution had no significant effect on our results. We sampled from the posterior distribution of the estimated parameters to obtain predicted trajectories of virus concentration kinetics. From those time-series, we computed several summary quantities: virus shedding onset (time at which the trajectory crossed LOD1); time to peak virus shedding; shedding duration, defined as the total amount of time at which virus concentration was above LOD1; and total amount of virus shed, defined as the area under the virus concentration curve.

Vomiting episodes were too few (11 persons with 26 samples of vomit) to enable a time-series analysis similar to the one we performed for virus shedding in feces. We have compiled vomit event time-series data (Appendix).

Analysis of Symptom Outcomes

The study recorded 10 kinds of symptoms: body temperature, malaise, muscle aches, headache, nausea, chills, anorexia, cramps, unformed or liquid feces, and vomiting. Clinical symptom scores (except feces and vomit) were reported as none = 0, mild = 1, moderate = 2, or severe = 3. For feces, we used a scoring of solid = 0, unformed = 1, and liquid = 2. Vomit was reported as absent = 0 or present = 1.

We considered time to symptom onset (incubation period) and 2 symptom scores as outcomes of interest. We defined time to system onset as the time from inoculation to the first reported symptom of any type. For the first symptom score, we used a modified Vesikari score (MVS) that was previously applied to measure norovirus severity (*5*,*30*–*33*). We computed the MVS by using a limited number of symptoms (i.e., fever, diarrhea, and vomiting). We also developed an additional score, which we call the comprehensive symptom score (CSS), which encompasses all

Table. Selected characteristics of patients in in study of the effect of norovirus inoculum dose on virus kinetics, shedding, and symptoms*

Characteristic	Dose, RT-PCR units			
	0.48	4.8	48	4,800
No. participants	1	6	7	6
Age, y, median (range)	24 (24–24)	30 (21–39)	24 (22–34)	28 (22–47)
Sex				
F	1 (100)	2 (33)	4 (57)	2 (33)
M	0	4 (67)	3 (43)	4 (67)
Blood type group				
A	0	2 (33)	2 (29)	3 (50)
O	1 (100)	4 (67)	5 (71)	3 (50)

*Values are no. (%) except as indicated. RT-PCR, reverse transcription PCR.

reported 10 symptoms in this study. Additional details of score computation, scores for each individual, and further model details are provided (Appendix).

Sensitivity Analyses

We performed 2 sensitivity analyses. In the first analysis, we treated dose as categorical rather than continuous. In the second analysis, we included 1 person who became infected after exposure to a dose of 0.48 RT-PCR units.

Results

Data Description

Detailed descriptions of the study can be found in previous publications (*20*–*24*). We summarized characteristics of the infected persons included in our analyses (Table). Distributions of age, sex, and ABO blood group status were generally similar across dose groups.

Association between Dose and Total Virus Shedding

We computed total virus shedding in either feces or vomit by summing the amount of shed virus in all samples for each person. We focused on fecal shedding during the first 96 hours of the study, when patients were under clinical observation. Almost all viral shedding events that occurred during this timeframe were recorded. Every person shed virus in ≥1 fecal sample. All vomiting events occurred within the first 96 hours, and only 11 persons vomited. Virus shedding showed some association with dose, although with a fair amount of uncertainty (Figure 1), leading to overall inconclusive results. We developed an alternative analysis using fecal shedding that includes the self-reported data after persons returned to their homes (Appendix). In that case, we observed no noticeable association.

Association between Dose and Viral Kinetics

Next, we fitted the virus concentration model to the time-series data for virus load for each person. The parameter's prior and posterior distributions showed that the choice of prior distribution had no significant effect on our results (Appendix).

We calculated the population-level curves per dose group for the estimated virus load trajectories (Figure 2) and developed fitted curves for each person (Appendix). The curves show a trend toward more rapid onset and earlier virus peak as dose increases (Figure 2, panel B) but little effect on shedding duration and total viral load (Figure 2, panel A). To further quantify these results, we sampled trajectories from the posterior distributions. For each trajectory, we computed 4 quantities (indicated in Figure 2, panel A): shedding onset (i.e., time at which virus became detectable), time of peak virus shedding, duration of virus shedding, and the total amount of virus shed (computed as area under the curve). We then examined the distribution of each of these quantities.

We calculated the model-predicted relationship between dose and those 4 quantities (Figure 3). As the dose increased from 4.8 to 4,800 RT-PCR units, average onset time decreased from 1.4 (95% CrI 1.1–1.8) to 0.8 (95% CrI 0.5–1.1) days, and the time of virus peak decreased from 2.3 (95% CrI 2–2.8) to 1.5 (95% CrI 1.3–1.8) days. We observed a very slight trend toward increased duration of shedding, from 23.7 (95% CrI 17.8–30.6) to 26.4 (95% CrI 19–35.8) days. Total virus load barely changed, from 1.5×10^{10} (95% CrI 2.2×10^{9}–5.2×10^{10}) to 1.7×10^{10} (95% CrI 1.9×10^{9}–6.6×10^{10}) GEC × days/g.

Association between Dose and Symptoms

We investigated associations between dose and symptom related outcomes next. A higher inoculum dose was associated with a shorter incubation period (more rapid symptoms onset) (Figure 4). The incubation period decreased from 1.5 (95% CrI 0.9–2.5) to 0.8 (95% CrI 0.4–1.4) days as dose increased (Figure 4, panel A).

Our model estimated a slight increase in symptoms as measured by the MVS, from 2.9 (95% CrI 1.4–5.2) to 3.3 (95% CrI 1.4–6.5) as dose increased (Figure 4, panel B). The CSS showed a more pronounced

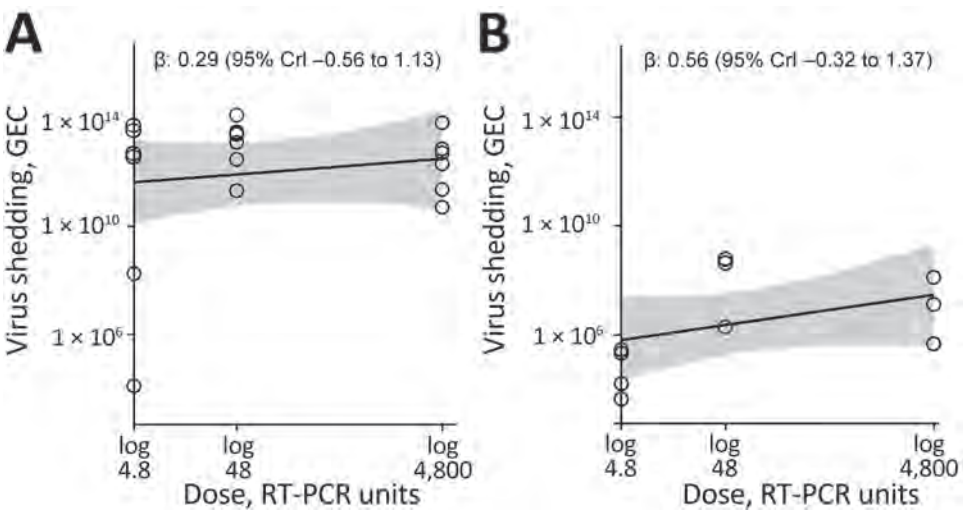

Figure 1. Total virus shedding in feces and vomit of patients challenged with norovirus in study of the effect of norovirus inoculum dose on virus kinetics, shedding, and symptoms. A) Cumulative virus shedding in feces. B) Cumulative virus shedding in vomit. Open circles represent raw data points. Lines and shaded regions indicate means and 95% CrIs of the fitted Bayesian model. Missing values attributable to limits of detection were replaced with fixed values (Appendix, https://wwwnc.cdc.gov/EID/article/29/7/23-0117-App1.pdf). CrI, credible interval; GEC, genomic equivalent copies; RT-PCR, reverse transcription PCR.

increase, from 9.4 (95% CrI 6.1–13.6) to 18.7 (95% CrI 11.8–28.3) (Figure 4, panel C). A further analysis suggests that the different pattern seen for the MVS and CSS might be attributable to those symptoms that are part of the MVS not showing an association with dose, whereas a few symptoms (e.g., cramps, malaise, nausea) that are part of the CSS but not the MVS do show a correlation with dose (Appendix).

Sensitivity Analyses

We performed 2 main sensitivity analyses (Appendix). In the first sensitivity analysis, we treated dose as categorical (low, medium, or high) instead of continuous. For this analysis, total virus shedding in feces and vomit was highest at the intermediate dose, though with overlap of the credible intervals for all doses. Similar to results for the main analysis, an increase in dose led to earlier onset and peak of shedding. Duration of shedding and total virus load concentration also suggested the highest levels at intermediate doses, although again with overlap in uncertainty estimates. Symptom onset was earlier, and the CSS measure increased, with no noticeable effect on the MVS measure.

In the second sensitivity analysis, we included 1 person infected after receiving the lowest dose (0.48 RT-PCR units). For this dataset, we found similar patterns of increasing total virus shedding in feces and vomit as dose increased. Also consistent with those results, onset and peak of shedding occurred earlier

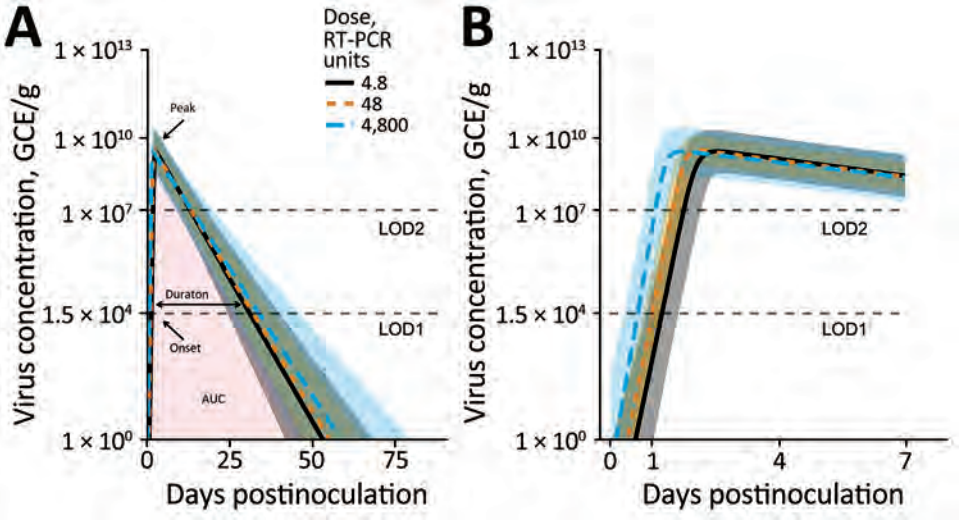

Figure 2. Fitted virus concentration (GEC/g) in feces of patients challenged with norovirus in study of the effect of norovirus inoculum dose on virus kinetics, shedding, and symptoms. A) Fitted curves showing the full infection time-course. Onset is time at which virus load rose to the LOD1 level. Duration is amount of time where virus load was above the LOD1 level. Peak is time to virus peak shedding. B) Zoomed in plot of the first 7 days to better show the initial increase and peak. Curves and shaded regions indicate means and credible intervals of the fitted time series Bayesian model. LOD1 and LOD2 lines indicate the 2 different limits of detection. Missing values attributable to limits of detection were treated as censors (Appendix, https://wwwnc.cdc.gov/EID/article/29/7/23-0117-App1.pdf). AUC, area under virus concentration curve; GEC, genomic equivalent copies; LOD, limit of detection; RT-PCR, reverse transcription PCR.

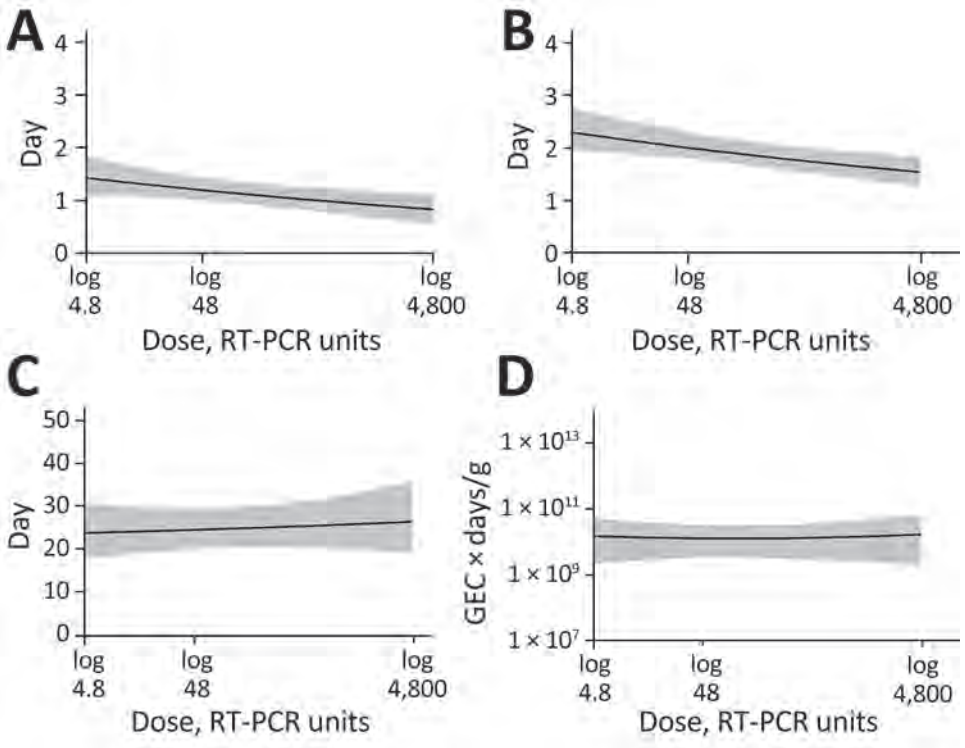

Figure 3. Associations between 4 characteristics of fecal viral shedding kinetics and levels of inoculum dose in patients in study of the effect of norovirus inoculum dose on virus kinetics, shedding, and symptoms. A) Shedding onset (time at which virus load reaches limit of detection 1). B) Time to virus peak shedding. C) Shedding duration (amount of time where virus load was above limit of detection 1). D) Total virus load (area under the fitted trajectory). Lines and shaded regions indicate means and 95% credible intervals of the posterior samples of the fitted time series model. RT-PCR, reverse transcription PCR.

but duration of shedding and total virus load concentration did not change noticeably. Symptom onset was earlier and stronger based on the CSS measure, with no noticeable effect on the MVS.

The categorical analysis suggested similar patterns but supported, albeit very tentatively, that intermediate dose might be associated with the highest level of shedding. However, because only a single person fell into the lowest-dose category, a categorical analysis that included that person did not seem to be useful, so we did not perform such an analysis.

In time series models, we treated values below the limits of detection as censors. In other virus shedding models, we additionally performed 2 sensitivity analyses to explore the effect of choices for the values that are below the limits of detection. The conclusions remained consistent (Appendix).

Discussion

We explored the effect of norovirus inoculum dose on infection and disease outcomes, an important gap in the literature. We found that an increased dose was associated with a faster onset and peak of virus shedding in feces (Figure 3, panel A, B) but not with fecal shedding duration and total virus concentration (Figure 3, panel C, D). A trend toward increased total shedding was noted for both feces and vomit (Figure 1). Our analysis also showed a pattern of accelerated onset of symptoms. Symptom severity showed an increase with inoculum dose for the CSS measure but not the MVS measure (Figure 4), possibly because only some symptoms are affected by dose, and those symptoms are captured by CSS but not MVS (Appendix). An increase in symptoms despite no noticeable change in virus load suggests that symptoms are mostly immune-mediated. We found mild evidence that a high virus growth rate associated with increased symptoms (Appendix); thus, a more rapid initial virus growth might trigger a stronger immune response. This finding could be tested in studies that measure components of the ensuing immune response.

Findings similar to ours have been reported for other enteric pathogens. The clinical manifestation of typhoid illness appears to be independent of inoculum dose, whereas the onset of symptoms was more rapid after a higher infectious dose (*34*). More rapid onset of symptoms after a larger infectious dose has also been observed with cholera infections (*35*). This finding could suggest a general pattern of dose-dependent incubation periods for enteric diseases. We did not find evidence of presymptomatic virus shedding, which could be attributable to the fact that diarrhea and vomit were considered as symptoms in our research, which explains the similar time of virus shedding onset time and incubation period.

The association between dose and severity might partially explain the results of several recent

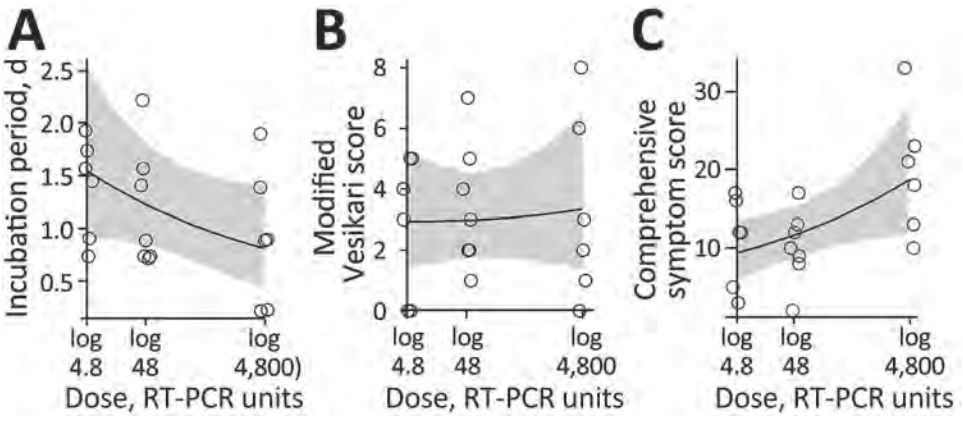

Figure 4. Association between inoculum dose and symptoms in patients in study of the effect of norovirus inoculum dose on virus kinetics, shedding, and symptoms. A) Incubation period (i.e., time between infection and onset of first symptoms). B) Severity using the modified Vesikari score. C) Severity using the comprehensive symptom score. Circles show raw data for participants. Lines and shaded regions indicate means and 95% credible intervals of the fitted Bayesian model. RT-PCR, reverse transcription PCR.

norovirus vaccine candidates. Those vaccines have shown limited effectiveness at reducing the risk for infection but do seem to reduce disease outcomes (*5*,*36*). Perhaps protection induced by current vaccine candidates (assumed to be mainly mediated by antibodies) is not enough to provide sterilizing immunity and thus prevent infection but can reduce the effective dose that starts an infection and thereby reduce symptoms. This pattern would be consistent with our findings here.

However, it is unclear what the typical norovirus dose is for natural infections and how that dose compares with the doses chosen in the challenge study data we analyzed. This uncertainty limits any possibility to generalize results obtained from challenge studies to natural infections or the potential role of vaccine candidates at influencing the effective inoculum size that starts an infection. Thus, potential clinical or epidemiologic implications of changes in dose for natural infections will need to await further investigations to determine the potential applicability of challenge study results to such natural infection settings.

Our analysis was a secondary data analysis of a limited number of persons, which resulted in wide credible intervals and constrained further explorations of nonlinear models. The associations we found may not equal to causality. As such, our results should be considered exploratory and need to be confirmed in future studies. Further studies, ideally with larger sample sizes, are needed. Larger sample sizes might also allow for stratification on the basis of host characteristics, which could yield information regarding possible interactions between host characteristics and dose–outcome relationships.

In conclusion, if we can assume that the associations we found have an underlying causal relation (something that needs to be confirmed in future studies), our results suggest that norovirus dose might affect some infection outcomes while not influencing others. Thus, when comparing results across challenge studies or trying to combine data from multiple studies for analysis, some care must be taken if doses are different. In some instances, combining data across studies seems reasonable, such as combining data from multiple studies to focus on viral shedding. However, for symptom-related outcomes and quantities that focus on norovirus infection kinetics, dose differences might lead to differences between studies that prohibit easy comparison.

Y.G., J.L., K.K., B.L., and A.H. are partially supported by National Institutes of Health grant no. R01 GM124280. Y.G. was supported by the Start-Up Grant from the University of Southern Mississippi. J.L. is partially supported by the National Institute of Food and Agriculture at the US Department of Agriculture (grant no. 2019-67017-29642). Z.B. is supported by the University of Georgia Graduate School. Y.S. is partially supported by National Institutes of Health grant no. R35 GM146612. D.G. and A.O. are partially supported by the Office of Research and Development Medical Research Service Department of Veterans Affairs, Public Health Service (grant no. DK56338), which funds the Texas Medical Center Digestive Diseases Center.

About the Author

Dr. Ge is an assistant professor at the University of Southern Mississippi. His research focuses on infectious disease epidemiology, covering pathogens like influenza, norovirus, SARS-CoV-2, and tuberculosis.

References

1. Patel MM, Widdowson M-A, Glass RI, Akazawa K, Vinjé J, Parashar UD. Systematic literature review of role of noroviruses in sporadic gastroenteritis. Emerg Infect Dis. 2008;14:1224–31. https://doi.org/10.3201/eid1408.071114

2. Lozano R, Naghavi M, Foreman K, Lim S, Shibuya K, Aboyans V, et al. Global and regional mortality from 235 causes of death for 20 age groups in 1990 and 2010: a systematic analysis for the Global Burden of Disease Study 2010. Lancet. 2012;380:2095–128. https://doi.org/10.1016/S0140-6736(12)61728-0
3. Bartsch SM, Lopman BA, Ozawa S, Hall AJ, Lee BY. Global economic burden of norovirus gastroenteritis. PLoS One. 2016;11:e0151219. https://doi.org/10.1371/journal.pone.0151219
4. Scallan E, Hoekstra RM, Angulo FJ, Tauxe RV, Widdowson MA, Roy SL, et al. Foodborne illness acquired in the United States—major pathogens. Emerg Infect Dis. 2011;17:7–15. https://doi.org/10.3201/eid1701.P11101
5. Atmar RL, Bernstein DI, Harro CD, Al-Ibrahim MS, Chen WH, Ferreira J, et al. Norovirus vaccine against experimental human Norwalk virus illness. N Engl J Med. 2011;365:2178–87. https://doi.org/10.1056/NEJMoa1101245
6. Johnston CP, Qiu H, Ticehurst JR, Dickson C, Rosenbaum P, Lawson P, et al. Outbreak management and implications of a nosocomial norovirus outbreak. Clin Infect Dis. 2007;45:534–40. https://doi.org/10.1086/520666
7. Isakbaeva ET, Widdowson M-A, Beard RS, Bulens SN, Mullins J, Monroe SS, et al. Norovirus transmission on cruise ship. Emerg Infect Dis. 2005;11:154–8. https://doi.org/10.3201/eid1101.040434
8. Carling PC, Bruno-Murtha LA, Griffiths JK. Cruise ship environmental hygiene and the risk of norovirus infection outbreaks: an objective assessment of 56 vessels over 3 years. Clin Infect Dis. 2009;49:1312–7. *PMID 19814610*
9. Wikswo ME, Cortes J, Hall AJ, et al. Disease transmission and passenger behaviors during a high morbidity norovirus outbreak on a cruise ship, January 2009. Clin Infect Dis. 2011;52:1116–22. *PMID 21429864*
10. Bitler EJ, Matthews JE, Dickey BW, Eisenberg JNS, Leon JS. Norovirus outbreaks: a systematic review of commonly implicated transmission routes and vehicles. Epidemiol Infect. 2013;141:1563–71. *PMID 23433247*
11. Teunis PFM, Moe CL, Liu P, Miller SE, Lindesmith L, Baric RS, et al. Norwalk virus: how infectious is it? J Med Virol. 2008;80:1468–76. https://doi.org/10.1002/jmv.21237
12. Van Abel N, Schoen ME, Kissel JC, Meschke JS. Comparison of risk predicted by multiple norovirus dose-response models and implications for quantitative microbial risk assessment. Risk Anal. 2017;37:245–64. https://doi.org/10.1111/risa.12616
13. Messner MJ, Berger P, Nappier SP. Fractional Poisson—a simple dose-response model for human norovirus. Risk Anal. 2014;34:1820–9. https://doi.org/10.1111/risa.12207
14. Schmidt PJ. Norovirus dose-response: are currently available data informative enough to determine how susceptible humans are to infection from a single virus? Risk Anal. 2015;35:1364–83. https://doi.org/10.1111/risa.12323
15. Haas CN. Estimation of risk due to low doses of microorganisms: a comparison of alternative methodologies. Am J Epidemiol. 1983;118:573–82. https://doi.org/10.1093/oxfordjournals.aje.a113662
16. Teunis PFM, Nagelkerke NJD, Haas CN. Dose response models for infectious gastroenteritis. Risk Anal. 1999;19:1251–60. https://doi.org/10.1111/j.1539-6924.1999.tb01143.x
17. Li Y, Handel A. Modeling inoculum dose dependent patterns of acute virus infections. J Theor Biol. 2014;347:63–73. https://doi.org/10.1016/j.jtbi.2014.01.008
18. Handel A, Li Y, McKay B, Pawelek KA, Zarnitsyna V, Antia R. Exploring the impact of inoculum dose on host immunity and morbidity to inform model-based vaccine design. PLoS Comput Biol. 2018;14:e1006505. *PMID 30273336*
19. Moore JR, Ahmed H, Manicassamy B, Garcia-Sastre A, Handel A, Antia R. varying inoculum dose to assess the roles of the immune response and target cell depletion by the pathogen in control of acute viral infections. Bull Math Biol. 2020;82:35. https://doi.org/10.1007/s11538-020-00711-4
20. Atmar RL, Opekun AR, Gilger MA, Estes MK, Crawford SE, Neill FH, et al. Determination of the 50% human infectious dose for Norwalk virus. J Infect Dis. 2014;209:1016–22. https://doi.org/10.1093/infdis/jit620
21. Atmar RL, Opekun AR, Gilger MA, Estes MK, Crawford SE, Neill FH, et al. Norwalk virus shedding after experimental human infection. Emerg Infect Dis. 2008;14:1553–7. https://doi.org/10.3201/eid1410.080117
22. Kavanagh O, Estes MK, Reeck A, Raju RM, Opekun AR, Gilger MA, et al. Serological responses to experimental Norwalk virus infection measured using a quantitative duplex time-resolved fluorescence immunoassay. Clin Vaccine Immunol. 2011;18:1187–90. https://doi.org/10.1128/CVI.00039-11
23. Czakó R, Atmar RL, Opekun AR, Gilger MA, Graham DY, Estes MK. Serum hemagglutination inhibition activity correlates with protection from gastroenteritis in persons infected with Norwalk virus. Clin Vaccine Immunol. 2012;19:284–7. https://doi.org/10.1128/CVI.05592-11
24. Ajami NJ, Barry MA, Carrillo B, Muhaxhiri Z, Neill FH, Prasad BV, et al. Antibody responses to norovirus genogroup GI.1 and GII.4 proteases in volunteers administered Norwalk virus. Clin Vaccine Immunol. 2012;19:1980–3. https://doi.org/10.1128/CVI.00411-12
25. McElreath R. Statistical rethinking: a Bayesian course with examples in R and Stan. 2nd edition. Boca Raton: Taylor and Francis, CRC Press; 2020.
26. R Core Team. R: a language and environment for statistical computing. 2017 [cited 2023 Apr 22]. https://www.r-project.org
27. Carpenter B, Gelman A, Hoffman MD, Lee D, Goodrich B, Betancourt M, et al. Stan: a probabilistic programming language. J Stat Softw. 2017;76:1–32.
28. Burkner P-C. Brms: an R Package for Bayesian multilevel models using Stan. J Stat Softw. 2017;80. https://doi.org/10.18637/jss.v080.i01
29. Holder BP, Beauchemin CA. Exploring the effect of biological delays in kinetic models of influenza within a host or cell culture. BMC Public Health. 2011;11(Suppl 1):S10. https://doi.org/10.1186/1471-2458-11-S1-S10
30. Ruuska T, Vesikari T. Rotavirus disease in Finnish children: use of numerical scores for clinical severity of diarrhoeal episodes. Scand J Infect Dis. 1990;22:259–67. https://doi.org/10.3109/00365549009027046
31. Freedman SB, Eltorky M, Gorelick M; Pediatric Emergency Research Canada Gastroenteritis Study Group. Evaluation of a gastroenteritis severity score for use in outpatient settings. Pediatrics. 2010;125:e1278–85. https://doi.org/10.1542/peds.2009-3270
32. Bierhoff M, Arvelo W, Estevez A, Bryan J, McCracken JP, López MR, et al. Incidence and clinical profile of norovirus disease in Guatemala, 2008–2013. Clin Infect Dis. 2018;67:430–6. https://doi.org/10.1093/cid/ciy091
33. Shim DH, Kim DY, Cho KY. Diagnostic value of the Vesikari scoring system for predicting the viral or bacterial pathogens in pediatric gastroenteritis. Korean J Pediatr. 2016;59:126–31. https://doi.org/10.3345/kjp.2016.59.3.126

34. Hornick RB, Greisman SE, Woodward TE, DuPont HL, Dawkins AT, Snyder MJ. Typhoid fever: pathogenesis and immunologic control. N Engl J Med. 1970;283:686–91. https://doi.org/10.1056/NEJM197009242831306
35. Hornick RB, Music SI, Wenzel R, Cash R, Libonati JP, Snyder MJ, et al. The Broad Street pump revisited: response of volunteers to ingested Cholera vibrios. Bull N Y Acad Med. 1971;47:1181–91.
36. Bernstein DI, Atmar RL, Lyon GM, Treanor JJ, Chen WH, Jiang X, et al. Norovirus vaccine against experimental human GII.4 virus illness: a challenge study in healthy adults. J Infect Dis. 2015;211:870–8. https://doi.org/10.1093/infdis/jiu497

Address for correspondence: Yang Ge, 118 College Dr, School of Health Professions, University of Southern Mississippi, Hattiesburg, MS 39402, USA; email: yang.ge@usm.edu; or Andreas Handel, 124 B.S. Miller Hall, Health Sciences Campus, University of Georgia, Athens, GA 30602, USA; email: ahandel@uga.edu

Estimating Waterborne Infectious Disease Burden by Exposure Route, United States, 2014

Megan E. Gerdes,[1] Shanna Miko,[1] Jasen M. Kunz, Elizabeth J. Hannapel, Michele C. Hlavsa, Michael J. Hughes, Matthew J. Stuckey, Louise K. Francois Watkins, Jennifer R. Cope, Jonathan S. Yoder, Vincent R. Hill, Sarah A. Collier

More than 7.15 million cases of domestically acquired infectious waterborne illnesses occurred in the United States in 2014, causing 120,000 hospitalizations and 6,600 deaths. We estimated disease incidence for 17 pathogens according to recreational, drinking, and nonrecreational nondrinking (NRND) water exposure routes by using previously published estimates. In 2014, a total of 5.61 million (95% credible interval [CrI] 2.97–9.00 million) illnesses were linked to recreational water, 1.13 million (95% CrI 255,000–3.54 million) to drinking water, and 407,000 (95% CrI 72,800–1.29 million) to NRND water. Recreational water exposure was responsible for 36%, drinking water for 40%, and NRND water for 24% of hospitalizations from waterborne illnesses. Most direct costs were associated with pathogens found in biofilms. Estimating disease burden by water exposure route helps direct prevention activities. For each exposure route, water management programs are needed to control biofilm-associated pathogen growth; public health programs are needed to prevent biofilm-associated diseases.

Waterborne infectious diseases substantially affect public health in the United States, despite widespread treatment and disinfection of drinking water systems and recreational water venues such as swimming pools and hot tubs. Cases of waterborne infections are estimated at >7.15 million annually in the United States, causing 120,000 hospitalizations and 6,600 deaths (*1*). Pathogens found in biofilms, such as nontuberculous mycobacteria (NTM) and *Legionella* bacteria, are predominant causes of hospitalizations and deaths from waterborne diseases in the United States. Waterborne pathogen exposure routes include swimming, drinking water, bathing, or breathing in aerosolized water.

Before widespread application of drinking water disinfection treatments, cholera and typhoid were major causes of death in the United States. Supplying treated, safe drinking water dramatically reduced the incidence of those diseases; in the past 50 years, outbreaks from large public drinking water systems have occurred less frequently (*2*–*4*), likely because of operational regulations and improvements. However, aging infrastructures and climate change negatively affect drinking water systems (*5*). Furthermore, 43 million US residents are served by private wells or domestic water systems that are not regulated by the Environmental Protection Agency Safe Drinking Water Act, leaving homeowners responsible for maintaining and monitoring water quality in their wells (*6*). During 1971–2008, one third of reported disease outbreaks from drinking water were linked to private wells (*7*). The complexity of water distribution has also increased; 6 million miles of plumbing inside buildings (known as premise plumbing) support drinking water, sanitation, hygiene, cooling, and heating needs in the United States (*8*,*9*). Premise plumbing water quality can be compromised when water is stagnant or disinfectant concentrations are reduced, thereby promoting microbial pathogen growth and biofilm formation (*10*). Exposure to biofilm-related pathogens can occur through contact with, ingestion of, or aerosol inhalation of contaminated water from different sources, such as showerheads, hot tubs, building cooling towers, or decorative fountains.

Filtration and chlorination of water in swimming pools to remove and inactivate pathogens were

Author affiliations: Chenega Corporation, Atlanta, Georgia, USA (M.E. Gerdes); Centers for Disease Control and Prevention, Atlanta (M.E. Gerdes, S. Miko, J.M. Kunz, E.J. Hannapel, M.C. Hlavsa, M.J. Hughes, M.J. Stuckey, L.K. Francois Watkins, J.R. Cope, J.S. Yoder, V.R. Hill, S.A. Collier)

DOI: https://doi.org/10.3201/eid2907.230231

[1]These first authors contributed equally to this article.

introduced in the early 1900s. Illnesses caused by recreational water contact still occur, partly because of lack of national standards across the United States for treated recreational water venues, such as pools, hot tubs, and splash pads, and design innovations that have increased venue sizes and complexity and have changed how persons are exposed (e.g., increased hot tub water aerosols).

Swimming in untreated recreational water venues (lakes, rivers, and oceans) can cause outbreaks predominantly linked to norovirus, Shiga toxin–producing *Escherichia coli*, *Cryptosporidium* spp., and *Shigella* spp. (*11*,*12*). Those enteric pathogens can be introduced into untreated recreational water through human feces or vomit, stormwater runoff, sewage or septic system malfunctions, or animal waste and can then be transmitted to persons who ingest the contaminated water.

Annual incidences of illness associated with drinking water in community drinking water systems have been estimated at 4–20 million (*13*–*16*). Illnesses associated with recreational contact with untreated or natural waters have also been estimated (*17*,*18*), and 1 study reported 90 million illnesses annually attributable to recreational water exposure. We previously estimated the overall burden of waterborne diseases in the United States (*1*). In this study, we quantified exposure-specific diseases from 3 water sources—recreational, drinking, and nonrecreational nondrinking (NRND) water—by using a multiplier model of surveillance data from 2014. Our goals were to estimate disease burdens by water exposure route, help guide disease prevention measures, determine key prevention partners, and prioritize limited resources.

Methods

We apportioned waterborne diseases to recreational, drinking, or NRND water categories as previously described in a structured expert judgment study (*19*) (Appendix Table 1, https://wwwnc.cdc.gov/EID/article/29/7/23-0231-App1.pdf). Recreational water is defined as water used for recreational activities, such as aquatic venues or natural bodies of water. Drinking water is used primarily for drinking but can include other domestic uses, such as washing or showering. Drinking water can come from a public water system, private well, or commercially bottled sources. NRND water is used for purposes other than recreation or consumption, such as agriculture, manufacturing or cooling equipment, or medical treatment; this category also includes backcountry streams and flood waters. Examples of diseases transmitted by NRND water include Legionnaires' disease associated with a cooling tower, giardiasis transmitted by drinking untreated water from a stream, and *Vibrio* spp. wound infections after wading through flood waters.

We estimated the total number of cases for 17 diseases or syndromes in 2014 in the United States (Appendix): acute otitis externa, campylobacteriosis, cryptosporidiosis, giardiasis, Legionnaires' disease, NTM infection, norovirus infection, *Pseudomonas* pneumonia, *Pseudomonas* septicemia, salmonellosis (nontyphoidal), Shiga toxin–producing *Escherichia coli* infection with an O157 or non-O157 serogroup, shigellosis, and vibriosis caused by *Vibrio alginolyticus*, *V. parahaemolyticus*, *V. vulnificus*, and other non–*V. cholerae* spp. (*1*) (Appendix Table 2). We divided total waterborne disease estimates previously reported (*1*) by structured expert judgment study estimates (*19*) to produce 2014 burden estimates for recreational, drinking, and NRND water exposure (Appendix Table 3). We quantified direct healthcare costs of treat-and-release emergency department (ED) visits and hospitalizations, measured by insurers and out-of-pocket payments, by using MarketScan data, as previously described (*1*).

We used anonymized administrative surveillance and literature data from 2000–2015 and based all estimates on the 2014 US population (318.6 million persons); at the time of analysis, 2014 was the most recent year for which all data were available. Data sources have been described previously (*1*). We estimated values by using probabilistic multiplier models (Appendix); each model input had an associated uncertainty estimate represented by a distribution of plausible values (Appendix Figure). Uncertainty in final estimates for each type of water exposure was a cumulative effect, incorporating the uncertainties of each model input (*1*,*19*). We obtained count distributions by using 100,000 iterations to generate point estimates of means and corresponding 95% credible intervals (CrIs; the 2.5th–97.5th percentiles of empirical distribution). We generated all-disease totals for each outcome by sampling from the distributions generated for each disease. We used SAS version 9.4 (SAS Institute, https://www.sas.com) and R version 3.5.1 (The R Project for Statistical Computing, https://www.r-project.org) for analyses.

Results

Illnesses

In 2014, a total of 5.61 million (95% CrI 2.97–9.00 million) domestically-acquired infectious waterborne illnesses were associated with recreational water,

1.13 million (95% CrI 255,000–3.54 million) with drinking water, and 407,000 (95% CrI 72,800–1.29 million) with NRND water (Table 1). Acute otitis externa caused most illnesses associated with recreational water (79%) and NRND water (27%), and norovirus infection was the leading illness associated with drinking water (53%).

ED visits

Recreational water exposure was linked to ≈552,000 (95% CrI 320,000–808,000) ED visits, drinking water to 31,600 (95% CrI 4,070–133,000) visits, and NRND water exposure to 17,200 (95% CrI 951–69,400) visits (Table 2). Acute otitis externa caused the most ED visits for each water exposure: 97% of those associated with recreational water, 48% associated with drinking water, and 78% associated with NRND water.

Hospitalizations

Recreational water was linked to ≈42,300 (95% CrI 26,500–63,000), drinking water to 47,700 (95% CrI 24,600–72,800), and NRND water to 27,900 (95% CrI 13,200–48,900) hospitalizations (Table 3). Acute otitis externa caused most (52%) hospitalizations associated with recreational water exposure; NTM infections caused most hospitalizations associated with drinking water (73%) and NRND water (37%) exposures.

Deaths

Recreational water exposure was linked to ≈1,290 (95% CrI 591–2,520) deaths, drinking water to 3,300 (95% CrI 1,630–5,180) deaths, and NRND water exposure to 2,040 (95% CrI 909–3,690) deaths (Table 4). NTM infections caused most deaths for each water exposure type; 37% of NTM-related deaths were associated with recreational water, 78% with drinking water, and 37% with NRND water.

Direct healthcare costs for ED visits and hospitalizations

Illnesses associated with drinking water represented the largest portion (42%) of combined costs, totaling $1.39 billion (95% CrI $364.00 million–$4.81 billion) (Figure; Appendix Tables 4, 5). Illnesses associated with recreational water exposures represented 32%, totaling $1.07 billion (95% CrI $439.00 million–$2.67 billion) of combined costs; illnesses associated with NRND exposures made up 26%, totaling $871.00 million (95% CrI $240.00 million–$2.64 billion) of combined costs. Four infection types accounted for 89% of $3.33 billion total costs; NTM infection was responsible for 46%, acute otitis externa for 17%, *Pseudomonas* pneumonia for 14%, and Legionnaires' disease for 12% of combined costs (Appendix Tables 4, 5).

Discussion

Of the estimated 7.15 million infectious waterborne illnesses in 2014 in the United States, 78% of illnesses were attributed to recreational water, 16% to drinking water, and 6% to NRND water. Drinking water exposure caused 40% of hospitalizations and 50% of deaths, recreational water exposure 36% of hospitalizations and 20% of deaths, and NRND exposure 24% of hospitalizations and 30% of deaths. ED visits and hospitalizations from exposure to drinking or recreational water exposure cost >$2 billion annually.

Acute otitis externa, which can be acutely painful and cause itchiness, drainage, and swelling, was the most common recreational water–associated illness. Risks for acute otitis externa have been correlated with water quality measures, levels of *Pseudomonas* and other pathogens in water, and increased bather load in recreational water venues in some studies but not others (*20*–*23*). Water can displace the protective coating of cerumen (ear wax) in the ear canal, leaving the outer ear more vulnerable to infection by endogenous flora. Whether otitis externa is caused by endogenous flora or contamination introduced by water remains unclear. In the structured expert judgment study (*19*), experts were asked to consider this question while estimating the proportion of otitis externa transmitted through water versus other pathways. They estimated 81% (95% uncertainty interval 67%–95%) of *Pseudomonas* otitis externa was transmitted through water (*19*). In response to the absence of national standards for recreational water venues, the Centers for Disease Control and Prevention (CDC) participated in the development and updating of the Model Aquatic Health Code (MAHC) (*24*). For treated water venues, the MAHC includes guidance for health authorities and aquatics sector to minimize risks for acute otitis externa and other illnesses and injuries (*24*,*25*). For both treated and untreated venues, risk for acute otitis externa can be minimized by keeping ears as dry as possible when swimming and ensuring ears are dry after swimming. Recreational swimmers and parents of young swimmers can educate themselves about steps to minimize the risks for infection from enteric pathogens at trusted sites, such as the CDC's healthy swimming webpage (*26*). Signage at treated and untreated recreational water venues (*12*) and adoption of CDC's MAHC for treated public recreational water venues can further improve prevention. The number of

illnesses and ED visits for acute otitis externa caused by drinking water exposure might seem counterintuitive, but drinking water was defined as water used for drinking, bathing, or showering.

Cryptosporidium and *Legionella* spp. infections in humans were identified in the late 1970s, and outbreaks associated with those pathogens in treated recreational water venues were identified soon after. In subsequent decades, reported incidences of treated recreational water–associated outbreaks increased substantially; *Cryptosporidium*, *Legionella*, and *Pseudomonas* spp. were the predominant etiologies (*27*). *P. aeruginosa* is a major cause of acute otitis externa and folliculitis or hot tub rash in addition to pneumonia and septicemia (*28*). Infectious *Cryptosporidium* sp. oocysts have tough outer shells that provide extreme chlorine tolerance, whereas *Legionella* and *Pseudomonas* spp. thrive in biofilms, where they are protected from chlorine inactivation.

Reported infectious disease outbreaks associated with public drinking water systems have decreased since the 1970s, likely because of federal management and treatment regulations that address enteric pathogens (*3*). However, outbreaks associated with individual water systems, such as private wells, and premise plumbing deficiencies have not decreased (*3*). Our analysis affirms that most hospitalizations and deaths associated with drinking water exposure were linked to biofilm-associated pathogens, not to pathogens causing enteric disease. *Legionella* bacteria are biofilm-associated pathogens and have become the most frequently reported cause of disease outbreaks associated with drinking water. Our analysis revealed that NTM infections were the leading cause of drinking water–associated illnesses, ED visits, hospitalizations, and deaths; NTM infections were the most common cause of death associated with all 3 water exposure routes. However, NTM infections are not nationally notifiable diseases; thus, cases are not consistently reported to public health authorities and outbreaks might remain undetected. Improving NTM illness reporting could lead to greater outbreak detection and inform disease prevention strategies for water systems. The Council of State and Territorial Epidemiologists has a standardized case definition for extrapulmonary NTM infections (opportunistic infections of wounds, soft tissue, or joints) to increase reportability, ensure consistency in reporting, and help identify outbreaks (*29*). Thus far, the state of Oregon has adopted this definition for their surveillance program (*30*), and other sites are piloting NTM surveillance programs (*31*).

NRND water includes water used for agriculture, such as for irrigation or livestock; industry, such as manufacturing or cooling equipment; medical procedures, such as medical devices, washing surgical

Table 1. Number of cases of selected domestically acquired illnesses from different water sources in study estimating waterborne infectious disease burden by exposure route, United States, 2014*

	Water exposure route, no. cases (95% CrI)		
Disease or syndrome	Recreational water†	Drinking water‡	NRND water§
Acute otitis externa	4,430,000 (2,170,000–7,020,000)	126,000 (0–891,000)	111,000 (0–521,000)
Campylobacteriosis	54,900 (0–307,000)	75,400 (40–366,000)	40,900 (0–257,000)
Cryptosporidiosis	211,000 (27,700–718,000)	76,400 (957–362,000)	34,400 (37–177,000)
Giardiasis	204,000 (26,900–552,000)	137,000 (6,070–445,000)	74,100 (41–329,000)
Legionnaires' disease	1,000 (174–3,810)	5,760 (2,030–9,160)	4,250 (1,360–7,890)
NTM infection	8,630 (0–29,700)	46,400 (17,400–78,200)	13,800 (0–38,200)
Norovirus infection	626,000 (1,930–2,960,000)	604,000 (1,800–2,890,000)	102,000 (2–792,000)
Pseudomonas pneumonia	7,600 (996–16,200)	935 (62–4,750)	7,380 (1,330–15,900)
Pseudomonas septicemia	417 (23–1,940)	929 (25–3,710)	4,410 (481–11,500)
Salmonellosis, nontyphoidal	14,000 (343–67,500)	57,700 (3,050–214,000)	5,320 (72–31,000)
STEC infection			
O157 serotype	2,300 (188–9,260)	887 (33–4,220)	163 (0–1,050)
Non-O157 serotype	5,780 (0–23,600)	1,360 (0–8,820)	4,300 (0–18,000)
Shigellosis	13,200 (667–60,900)	586 (0–3,920)	3,450 (71–18,800)
Vibrio spp. infections	33,500 (184–20,300)	342 (2–210)	759 (3–277)
V. alginolyticus	12,300 (3,500–24,900)	93 (0–564)	248 (0–2,330)
V. parahaemolyticus	20,300 (4,950–38,600)	210 (0–1,900)	277 (0–2,490)
V. vulnificus	184 (82–274)	2 (0–18)	3 (0–45)
Other *Vibrio* spp.	610 (0–5,050)	38 (0–270)	231 (0–1,350)
Total illnesses	5,610,000 (2,970,000–9,000,000)	1,130,000 (255,000–3,540,000)	407,000 (72,800–1,290,000)

*Estimates are rounded to 3 significant figures. CrI, credible interval; NRND, nonrecreational nondrinking; NTM, nontuberculous mycobacteria; STEC, Shiga toxin–producing *Escherichia coli.*
†Recreational water is used for recreational activities, such as swimming, in treated (e.g., pools, hot tubs, and splash pads) or untreated (e.g., lakes, rivers, and oceans) venues (*19*).
‡Drinking water is used primarily for drinking but can also be used for maintaining hygiene, such as for washing or showering, and can come from public water systems, private wells, or commercially bottled sources (*19*).
§NRND water is used for purposes other than recreation or drinking (e.g., for agriculture, industry, or medical procedures) and can come from backcountry streams or flood waters (*19*).

Table 2. Number of emergency department visits for selected domestically acquired illnesses from different water sources in study estimating waterborne infectious disease burden by exposure route, United States, 2014*

	Water exposure route, no. visits (95% CrI)		
Disease or syndrome	Recreational water†	Drinking water‡	NRND water§
Acute otitis externa	538,000 (309,000–793,000)	15,300 (0–111,000)	13,500 (0–63,500)
Campylobacteriosis	102 (0–534)	140 (0–630)	76 (0–468)
Cryptosporidiosis	323 (69–732)	117 (2–413)	53 (0–228)
Giardiasis	278 (36–755)	187 (8–615)	102 (0–453)
Legionnaires' disease	61 (8–234)	349 (96–722)	257 (66–585)
NTM infection	636 (0–2,200)	3,420 (1,240–5,980)	1,020 (0–2,850)
Norovirus infection	12,300 (39–57,200)	11,900 (36–56,100)	2,020 (0–15,700)
Pseudomonas pneumonia	139 (18–307)	17 (1–87)	135 (24–301)
Pseudomonas septicemia	3 (0–12)	6 (0–26)	28 (1–85)
Salmonellosis, nontyphoidal	35 (0–168)	145 (8–514)	14 (0–78)
STEC infection			
O157 serotype	8 (0–25)	3 (0–12)	0 (0–3)
Non–O157 serotype	2 (0–9)	0 (0–3)	2 (0–7)
Shigellosis	49 (3–236)	2 (0–15)	13 (0–62)
Vibrio spp. infections¶	NA	NA	NA
Total visits	552,000 (320,000–808,000)	31,600 (4,070–133,000)	17,200 (951–69,400)

*Estimates are rounded to 3 significant figures. CrI, credible interval; NA, not applicable; NRND, nonrecreational nondrinking; NTM, nontuberculous mycobacteria; STEC, Shiga toxin–producing *Escherichia coli.*
†Recreational water is used for recreational activities, such as swimming, in treated (e.g., pools, hot tubs, and splash pads) or untreated (e.g., lakes, rivers, and oceans) venues (*19*).
‡Drinking water is used primarily for drinking but can also be used for maintaining hygiene, such as for washing or showering, and can come from public water systems, private wells, or commercially bottled sources (*19*).
§NRND water is used for purposes other than recreation or drinking (e.g., for agriculture, industry, or medical procedures) and can come from backcountry streams or flood waters (*19*).
¶No codes from the International Classification of Diseases, 9th Revision, Clinical Modification, are available for *Vibrio* spp. infections, only a general code for vibriosis and cholera combined. Emergency department visit estimates relied on administrative data that used those codes and are available only for *Vibrio* infections overall.

tools and equipment, and hydrotherapy; and backcountry streams or floodwaters (*19*). NRND water made up 87% of the 322 billion gallons of water used each day in the United States in 2015; of that volume, 2 billion gallons were used for livestock, 118 billion gallons for irrigation, 7.55 billion gallons for aquaculture, and 133 billion gallons for thermoelectric power (*6*). NRND water is associated with a small portion of

Table 3. Number of hospitalizations for selected domestically acquired illnesses from different water sources in study estimating waterborne infectious disease burden by exposure route, United States, 2014*

	Water exposure route, no. hospitalizations (95% CrI)		
Disease or syndrome	Recreational water†	Drinking water‡	NRND water§
Acute otitis externa	22,000 (12,700–32,400)	628 (0–4,590)	553 (0–2,630)
Campylobacteriosis	690 (0–3,700)	947 (0–4,410)	513 (0–3,190)
Cryptosporidiosis	734 (56–2,560)	265 (3–1,260)	119 (0–625)
Giardiasis	540 (71–1,470)	362 (16–1,180)	196 (0–870)
Legionnaires' disease	985 (171–3,740)	5,650 (1,990–8,990)	4,170 (1,340–7,740)
NTM infection	6,440 (0–22,200)	34,600 (13,000–58,000)	10,300 (0–28,400)
Norovirus infection	2,240 (7–10,300)	2,170 (7–10,100)	367 (0–2,840)
Pseudomonas pneumonia	7,390 (970–15,700)	909 (60–4,620)	7,170 (1,290–15,400)
Pseudomonas septicemia	405 (22–1,890)	903 (24–3,600)	4,290 (468–11,100)
Salmonellosis, nontyphoidal	275 (6–1,360)	1,140 (56–4,400)	105 (1–617)
STEC infection			
O157 serotype	95 (8–364)	36 (1–165)	7 (0–42)
Non-O157 serotype	38 (0–165)	9 (0–61)	28 (0–126)
Shigellosis	188 (8–886)	8 (0–56)	49 (0–264)
Vibrio spp. infections	243 (3–157)	2 (0–1)	5 (0–3)
V. alginolyticus	25 (7–57)	0 (0–1)	0 (0–5)
V. parahaemolyticus	58 (14–111)	0 (0–5)	0 (0–7)
V. vulnificus	157 (69–239)	1 (0–15)	3 (0–38)
Other *Vibrio* spp.	3 (0–27)	0 (0–2)	1 (0–7)
Total hospitalizations	42,300 (26,500–63,000)	47,700 (24,600–72,800)	27,900 (13,200–48,900)

*Estimates are rounded to 3 significant figures. CrI, credible interval; NRND, nonrecreational nondrinking; NTM, notuberculous mycobacteria; STEC, Shiga toxin–producing *Escherichia coli*.
†Recreational water is used for recreational activities, such as swimming, in treated (e.g., pools, hot tubs, and splash pads) or untreated (e.g., lakes, rivers, and oceans) venues (*19*).
‡Drinking water is used primarily for drinking but can also be used for maintaining hygiene, such as for washing or showering, and can come from public water systems, private wells, or commercially bottled water sources (*19*).
§NRND water is used for purposes other than recreation or drinking (e.g., agriculture, industry, or medical procedures) and can come from backcountry streams or flood waters (*19*).

Table 4. Number of deaths from selected illnesses domestically acquired from different water sources in study estimating waterborne infectious disease burden by exposure route, United States, 2014*

	Water exposure route, no. deaths (95% CrI)		
Disease or syndrome	Recreational water†	Drinking water‡	NRND water§
Acute otitis externa	208 (98–352)	6 (0–41)	5 (0–24)
Campylobacteriosis	9 (0–65)	12 (0–81)	6 (0–49)
Cryptosporidiosis	16 (0–96)	6 (0–46)	3 (0–22)
Giardiasis	0 (0–3)	0 (0–2)	0 (0–2)
Legionnaires' disease	91 (15–347)	520 (180–858)	384 (122–727)
NTM infection	476 (0–1,650)	2,560 (950–4,370)	763 (0–2,110)
Norovirus infection	25 (0–116)	25 (0–114)	4 (0–32)
Pseudomonas pneumonia	349 (44–795)	43 (3–213)	339 (58–779)
Pseudomonas septicemia	50 (3–236)	112 (3–449)	532 (58–1,390)
Salmonellosis, nontyphoidal	4 (0–24)	18 (0–79)	2 (0–11)
STEC infections			
O157 serotype	1 (0–12)	0 (0–5)	0 (0–0)
Non-O157 serotype	0 (0–6)	0 (0–1)	0 (0–4)
Shigellosis	0 (0–7)	0 (0–0)	0 (0–2)
Vibrio spp. infections	58 (0–53)	0 (0–0)	1 (0–0)
V. alginolyticus	1 (0–4)	0 (0–0)	0 (0–0)
V. parahaemolyticus	4 (0–9)	0 (0–0)	0 (0–0)
V. vulnificus	53 (21–84)	0 (0–5)	0 (0–13)
Other *Vibrio* spp.	0 (0–2)	0 (0–0)	0 (0–0)
Total deaths	1,290 (591–2,520)	3,300 (1,630–5,180)	2,040 (909–3,690)

*Estimates are rounded to 3 significant figures. CrI, credible interval; NRND, nonrecreational nondrinking; NTM, nontuberculous mycobacteria; STEC, Shiga toxin–producing *Escherichia coli.*
†Recreational water is used for recreational activities (e.g., swimming) in treated (e.g., pools, hot tubs, and splash pads) or untreated (e.g., lakes, rivers, and oceans) venues (*19*).
‡Drinking water is used primarily for drinking but can also be used for hygiene activities, like washing or showering, and can come from a public water system, a private well, or commercially bottled sources (*19*).
§NRND water is used for purposes other than recreation or drinking (e.g., for agriculture, industry, medical treatment, backcountry streams, or flood waters) (*19*).

reported waterborne illnesses but is responsible for one quarter of waterborne disease–associated hospitalizations and one third of associated deaths.

Waterborne pathogens, such as NTM, *Pseudomonas* spp., and *Legionella* spp., occur naturally in freshwater and can colonize other environments, particularly large complex equipment that is not properly maintained. Those pathogens are aerosolized in water droplets produced during use, which can be inhaled. Water management programs are recommended to minimize growth and spread of pathogens in engineered systems (*32*–*34*). Resources can be found on the CDC Environmental Health Services safe water program webpage (*35*), guide for developing a water management program to reduce *Legionella* growth and spread in buildings (*36*), *Legionella* control toolkit (*37*), and guide for reducing risk from water (*38*). Water management programs in healthcare facilities are also critical for protecting vulnerable patient populations, staff, and visitors and might require specific considerations for a wide range of biofilm-associated pathogens, including NTM, *Pseudomonas*, and *Legionella* spp. (*39*–*42*). Interdisciplinary collaboration is needed for planning future management of complex water systems and investigating illnesses and outbreaks.

Reducing risks for illness from biofilms in water systems is difficult. Biofilms can persist despite standard water treatment processes. Biofilms are complex ecosystems; control is complicated by structural issues (e.g., pipe characteristics), system operational issues (e.g., water age, temperature, and residual disinfectants), and water end-user behaviors. Changes designed to reduce prevalence of 1 microbial constituent can sometimes produce unintended consequences, such as proliferation of NTM, if a comprehensive approach to biofilm control is not considered (*43*). NTM are persistent pathogens; despite standard treatment, NTM species have been recovered from surface water treatment plants, biofilms in sand filters, ozonated water, biofilms from granular activated carbon filters, and activated carbon-filtered water. Even municipal systems that incorporate full treatment chains, including 2 filtration and 2 disinfection stages, might not effectively prevent NTM growth (*44*). Because climate change continues to create extreme weather events and increase water temperatures, more stress will be placed on aging water infrastructure; biofilm-associated pathogens will continue to proliferate (*5*), highlighting the need for biofilm-focused control programs.

Prevention of biofilm-associated organisms is an emerging field, and more scientific evidence is needed to determine best practices for public water systems and premise plumbing and identify effective prevention strategies for homeowners and building

managers. Persons can reduce their risk for illness from a biofilm-associated pathogen by flushing rarely used faucets and showerheads, flushing water heaters, and maintaining specific water heater temperatures. Resources for risk reduction can be found on CDC's Preventing Waterborne Germs at Home webpage (*45*).

Most previous waterborne infectious disease estimates are not directly comparable with results from this study because of differing methods used to generate estimates. Many studies have attempted to estimate a burden for 1 disease or aspect of drinking or recreational water exposure. Two studies from a workshop convened by CDC and the Environmental Protection Agency used 2 different methods to estimate the number of cases of acute gastrointestinal illness in public drinking water systems only. Those studies estimated 4–16 million acute gastrointestinal illness cases per year (*13*,*16*). A 2008 study estimated all illnesses associated with public drinking water systems at 19 million cases per year (*14*). Previous publications have used cohort studies to estimate gastrointestinal illness from water recreational activities and percentages of economic burden from recreational water exposure (*17*,*46*). In Canada, rates for waterborne disease per 100,000 persons were estimated by using literature, clinical input, and administrative data (*47*). Our estimates differ from previous work because we focused on specific pathogens, including those causing nongastrointestinal diseases, and we provide estimates for recreational water, drinking water, and NRND water exposure routes.

The first limitation of our study is that the estimates relied on a series of multipliers. Although we attempted to account for uncertainty in the multiplier estimates, biased multipliers will yield biased estimates. We used attribution estimates for proportions of disease caused by each water exposure route, derived from a structured expert judgment study. Structured expert judgment is used when data are sparse and relies on expert opinion. Statistical techniques are used to combine expert opinions into a single estimate with an uncertainty interval. Various weighting techniques can be used to increase accuracy or informativeness (narrowness of the uncertainty interval), but tradeoffs between accuracy and informativeness occur. For some individual estimates, including norovirus infection, NTM infection, and acute otitis externa, uncertainty intervals were wide, reflecting uncertainty about the proportion of disease transmitted via water. Second, as with previous waterborne disease burden estimates (*1*), we included estimates of 17 infectious diseases that had adequate data available. Other waterborne infectious diseases were excluded, such as *Pseudomonas* folliculitis or viral gastroenteritis not caused by norovirus. We also excluded noninfectious diseases caused by exposure to contaminated water, such as from lead or harmful algae-derived toxins, and did not evaluate long-term chronic effects of infectious or noninfectious diseases. In addition, we excluded foodborne illnesses, such as salmonellosis from lettuce or norovirus disease

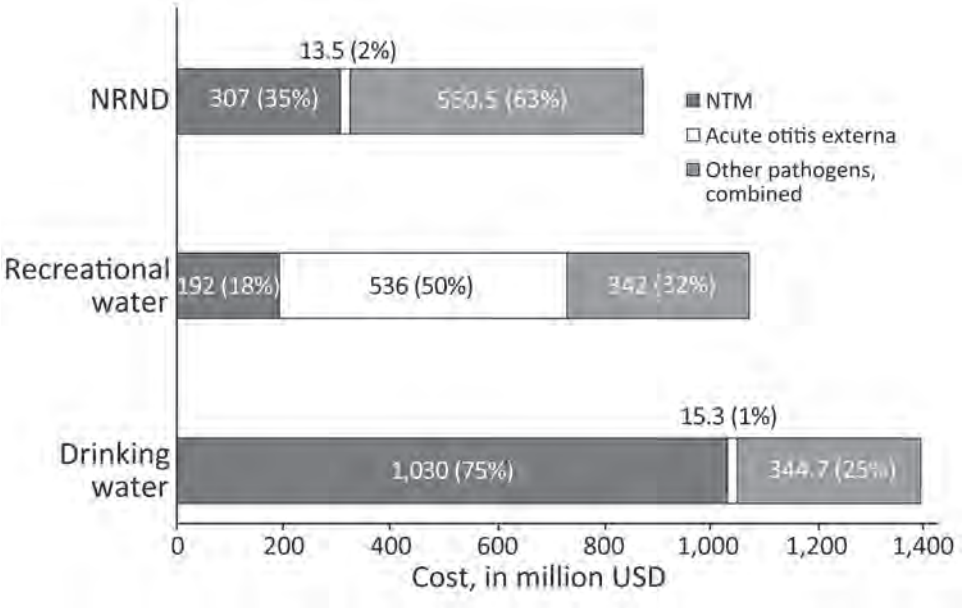

Figure. Direct healthcare costs for emergency department visits and hospitalizations in study estimating waterborne infectious disease burden by exposure route, United States, 2014. Estimated combined costs are shown in US dollars for selected domestically acquired waterborne illnesses for each exposure route. Estimates were rounded to 3 significant figures. NRND water is used for purposes other than recreation or drinking (e.g., agriculture, industry, medical treatment, backcountry streams, or flood waters); recreational water is used for recreational activities in treated (e.g., pools, hot tubs, and splash pads) or untreated (e.g., lakes, rivers, and oceans) venues; drinking water is used for drinking, washing, or showering and can come from a public water system, private well, or commercially bottled sources (*19*). NRND, nonrecreational nondrinking; NTM, nontuberculous mycobacteria.

from shellfish, where contaminated water might have been responsible. Third, this study used data from hospital and ED billing databases. Billing records are not medical records and might reflect diagnoses that result in reimbursement from insurance companies rather than true assessments by clinicians. Fourth, those billing databases use International Classification of Diseases, 9th Revision, Clinical Modification, coding to classify diagnoses; some illnesses might not perfectly match existing codes. Fifth, we provide estimates for 2014, and illness burdens, healthcare costs, and clinical practices have likely changed since then. Sixth, we assumed that severity of illness was independent of exposure route. For example, if salmonellosis was more severe when transmitted by drinking water than by recreational water, the multipliers used in calculating estimates did not account for this. Seventh, many diseases in this analysis might be more severe in persons with compromised immunity, but we did not attempt to apportion the burden of illness between waterborne illnesses and immune status. Finally, reliably distinguishing between illnesses linked to premise plumbing water exposure and distribution system exposure was difficult, which was reflected in 95% CrI widths for drinking water and NRND estimates for some pathogens, including NTM. More research is needed in this area because federal regulations for distribution systems differ from building codes and state and local laws that regulate premise plumbing.

In conclusion, quantifying the burden of illness linked to drinking, recreational, and NRND water is an essential factor for addressing biofilm-associated pathogens, because prevention measures and vital partners differ for each exposure route. Estimating disease burden by water exposure route will help direct prevention activities and prioritize limited resources. Measures for preventing illnesses from recreational water use, such as those in the MAHC for treated recreational water venues, could reduce disease burden associated with recreational water exposure. Incorporating water management programs and control measures for systems that are common sources of biofilm pathogen exposure into building and public health codes is crucial for reducing risks for biofilm-associated pathogen exposure in drinking water and NRND water systems (*34*). In addition, improved surveillance and reporting of biofilm-associated illnesses could lead to the timely detection and investigation of outbreaks and inform disease prevention activities. Interdisciplinary partnerships among public health agencies and industries that use NRND water are pivotal to reduce incidences of waterborne diseases. For drinking water and NRND water systems, addressing factors that promote biofilm growth (stagnation, temperature, or lack of disinfection) could reduce growth of biofilm-associated pathogens. Facilities that serve persons at increased risk for infections, such as healthcare facilities, should review water system design and operations to decrease risks from biofilm-associated pathogens. Additional research on the roles of pipe material, water chemistry, and optimal water distribution system management could provide insights into improving prevention actions. As climate change continues to place increased stress on water systems, improved prevention and maintenance strategies should be developed to prevent illness from all types of water exposure.

Acknowledgments

We thank Jennifer Collins, Patricia M. Griffin, Noelle-Angelique Molinari, and Logan C. Ray for reviewing this manuscript and for their subject matter expertise.

About the Author

Ms. Gerdes is an epidemiologist in the Division of Foodborne, Waterborne, and Environmental Diseases, National Center for Emerging and Zoonotic Infectious Diseases, Centers for Disease Control and Prevention, Atlanta, Georgia, USA. Her research interests focus on data analysis and translating epidemiologic findings and works to improve surveillance systems for waterborne disease and wastewater.

References

1. Collier SA, Deng L, Adam EA, Benedict KM, Beshearse EM, Blackstock AJ, et al. Estimate of burden and direct healthcare cost of infectious waterborne disease in the United States. Emerg Infect Dis. 2021;27:140–9. https://doi.org/10.3201/eid2701.190676
2. Benedict KM, Reses H, Vigar M, Roth DM, Roberts VA, Mattioli M, et al. Surveillance for waterborne disease outbreaks associated with drinking water—United States, 2013–2014. MMWR Morb Mortal Wkly Rep. 2017;66:1216–21. https://doi.org/10.15585/mmwr.mm6644a3
3. Craun GF, Brunkard JM, Yoder JS, Roberts VA, Carpenter J, Wade T, et al. Causes of outbreaks associated with drinking water in the United States from 1971 to 2006. Clin Microbiol Rev. 2010;23:507–28. https://doi.org/10.1128/CMR.00077-09
4. Cutler D, Miller G. The role of public health improvements in health advances: the twentieth-century United States. Demography. 2005;42:1–22. https://doi.org/10.1353/dem.2005.0002
5. US Global Change Research Program. The impacts of climate change on human health in the United States. A scientific assessment, 2016. Chapter 6. Climate impacts on water-related illness [cited 2023 Feb 7]. https://health2016.globalchange.gov/high/ClimateHealth2016_FullReport.pdf
6. US Geological Survey. Estimated use of water in the United States in 2015. Circular 1441, 2018 [cited 2023 Jan 15]. https://pubs.er.usgs.gov/publication/cir1441

7. Wallender EK, Ailes EC, Yoder JS, Roberts VA, Brunkard JM. Contributing factors to disease outbreaks associated with untreated groundwater. Ground Water. 2014;52:886–97. https://doi.org/10.1111/gwat.12121
8. Environmental Protection Agency. Community water system survey 2000. Volume 1: overview [cited 2022 Dec 11]. https://nepis.epa.gov/Exe/ZyPDF.cgi?Dockey=20001ZK5.txt
9. National Research Council. Drinking water distribution systems: assessing and reducing risks. Washington: National Academies Press; 2006.
10. Falkinham JO 3rd, Hilborn ED, Arduino MJ, Pruden A, Edwards MA. Epidemiology and ecology of opportunistic premise plumbing pathogens: *Legionella pneumophila*, *Mycobacterium avium*, and *Pseudomonas aeruginosa*. Environ Health Perspect. 2015;123:749–58. https://doi.org/10.1289/ehp.1408692
11. Graciaa DS, Cope JR, Roberts VA, Cikesh BL, Kahler AM, Vigar M, et al. Outbreaks associated with untreated recreational water—United States, 2000–2014. MMWR Morb Mortal Wkly Rep. 2018;67:701–6. https://doi.org/10.15585/mmwr.mm6725a1
12. Vanden Esschert KL, Mattioli MC, Hilborn ED, Roberts VA, Yu AT, Lamba K, et al. Outbreaks associated with untreated recreational water—California, Maine, and Minnesota, 2018–2019. MMWR Morb Mortal Wkly Rep. 2020;69:781–3. https://doi.org/10.15585/mmwr.mm6925a3
13. Messner M, Shaw S, Regli S, Rotert K, Blank V, Soller J. An approach for developing a national estimate of waterborne disease due to drinking water and a national estimate model application. J Water Health. 2006;4:201–40. https://doi.org/10.2166/wh.2006.024
14. Reynolds KA, Mena KD, Gerba CP. Risk of waterborne illness via drinking water in the United States. Rev Environ Contam Toxicol. 2008;192:117–58. https://doi.org/10.1007/978-0-387-71724-1_4
15. Verhougstraete M, Reynolds KA, Pearce-Walker J, Gerba C. Cost-benefit analysis of point-of-use devices for health risks reduction from pathogens in drinking water. J Water Health. 2020;18:968–82. https://doi.org/10.2166/wh.2020.111
16. Colford JM Jr, Roy S, Beach MJ, Hightower A, Shaw SE, Wade TJ. A review of household drinking water intervention trials and an approach to the estimation of endemic waterborne gastroenteritis in the United States. J Water Health. 2006;4:71–88. https://doi.org/10.2166/wh.2006.018
17. DeFlorio-Barker S, Wing C, Jones RM, Dorevitch S. Estimate of incidence and cost of recreational waterborne illness on United States surface waters. Environ Health. 2018;17:3. https://doi.org/10.1186/s12940-017-0347-9
18. Dorevitch S, Pratap P, Wroblewski M, Hryhorczuk DO, Li H, Liu LC, et al. Health risks of limited-contact water recreation. Environ Health Perspect. 2012;120:192–7. https://doi.org/10.1289/ehp.1103934
19. Beshearse E, Bruce BB, Nane GF, Cooke RM, Aspinall W, Hald T, et al. Attribution of illnesses transmitted by food and water to comprehensive transmission pathways using structured expert judgment, United States. Emerg Infect Dis. 2021;27:182–95. https://doi.org/10.3201/eid2701.200316
20. van Asperen IA, de Rover CM, Schijven JF, Oetomo SB, Schellekens JF, van Leeuwen NJ, et al. Risk of otitis externa after swimming in recreational fresh water lakes containing *Pseudomonas aeruginosa*. BMJ. 1995;311:1407–10. https://doi.org/10.1136/bmj.311.7017.1407
21. Hajjartabar M. Poor-quality water in swimming pools associated with a substantial risk of otitis externa due to *Pseudomonas aeruginosa*. Water Sci Technol. 2004;50:63–7.
22. Wade TJ, Sams EA, Beach MJ, Collier SA, Dufour AP. The incidence and health burden of earaches attributable to recreational swimming in natural waters: a prospective cohort study. Environ Health. 2013;12:67. https://doi.org/10.1186/1476-069X-12-67
23. Calderon R, Mood EW. An epidemiological assessment of water quality and "swimmer's ear". Arch Environ Health. 1982;37:300–5. https://doi.org/10.1080/00039896.1982.10667583
24. Centers for Disease Control and Prevention. Model Aquatic Health Code, 3rd edition. 2018 [cited 2022 Dec 20]. https://www.cdc.gov/mahc/editions/previous.html
25. Hlavsa MC, Aluko SK, Miller AD, Person J, Gerdes ME, Lee S, et al. Outbreaks associated with treated recreational water—United States, 2015–2019. MMWR Morb Mortal Wkly Rep. 2021;70:733–8. https://doi.org/10.15585/mmwr.mm7020a1
26. Centers for Disease Control and Prevention. Healthy swimming. April 28, 2022 [cited 2022 May 16]. https://www.cdc.gov/healthywater/swimming/index.html
27. Hlavsa MC, Cikesh BL, Roberts VA, Kahler AM, Vigar M, Hilborn ED, et al. Outbreaks associated with treated recreational water—United States, 2000–2014. MMWR Morb Mortal Wkly Rep. 2018;67:547–51. https://doi.org/10.15585/mmwr.mm6719a3
28. Centers for Disease Control and Prevention. Estimated burden of acute otitis externa—United States, 2003–2007. MMWR Morb Mortal Wkly Rep. 2011;60:605–9.
29. Centers for Disease Control and Prevention. Healthcare-associated infections (HAIs). August 12, 2019 [cited 2022 Jun 16]. https://www.cdc.gov/hai/organisms/ntm/health-departments.html
30. Shih DC, Cassidy PM, Perkins KM, Crist MB, Cieslak PR, Leman RL. Extrapulmonary nontuberculous mycobacterial disease surveillance—Oregon, 2014–2016. MMWR Morb Mortal Wkly Rep. 2018;67:854–7. https://doi.org/10.15585/mmwr.mm6731a3
31. Grigg C, Jackson KA, Barter D, Czaja CA, Johnston H, Lynfield R, et al. Epidemiology of pulmonary and extrapulmonary nontuberculous mycobacteria infections at 4 US emerging infections program sites: a six-month pilot. Clin Infect Dis. 2023 Apr 21 [Epub ahead of print]. https://doi.org/10.1093/cid/ciad214
32. American Society of Heating, Refrigerating and Air-Conditioning Engineers. ANSI/ASHRAE standard 188–2018, legionellosis: risk management for building water systems. Peachtree Corners (Georgia, USA): The Society; 2018.
33. Centers for Disease Control and Prevention. Healthcare-associated infections. Reduce risk from water. September 11, 2019 [cited 2022 Nov 29]. https://www.cdc.gov/hai/prevent/environment/water.html
34. Clopper BR, Kunz JM, Salandy SW, Smith JC, Hubbard BC, Sarisky JP. A methodology for classifying root causes of outbreaks of Legionnaires' disease: deficiencies in environmental control and water management. Microorganisms. 2021;9:89. https://doi.org/10.3390/microorganisms9010089
35. Centers for Disease Control and Prevention. Safe water program. 2022 [cited 2022 Sep 13]. https://www.cdc.gov/nceh/ehs/water/index.html
36. Centers for Disease Control and Prevention. Developing a water management program to reduce Legionella growth and spread in buildings. A practical guide to implementing industry standards. June 24, 2021 [cited 2022 May 19]. https://www.cdc.gov/legionella/downloads/toolkit.pdf

37. Centers for Disease Control and Prevention. Toolkit for controlling *Legionella* in common sources of exposure. 2021 [cited 2022 Dec 3]. https://www.cdc.gov/legionella/wmp/control-toolkit/index.html
38. Centers for Disease Control and Prevention. Reduce risk from water, from plumbing to patients [cited 2023 Mar 16]. https://www.cdc.gov/hai/prevent/environment/water.html
39. Kanamori H, Weber DJ, Rutala WA. Healthcare outbreaks associated with a water reservoir and infection prevention strategies. Clin Infect Dis. 2016;62:1423–35. https://doi.org/10.1093/cid/ciw122
40. Gamage SD, Ambrose M, Kralovic SM, Roselle GA. Water safety and health care: preventing infections caused by opportunistic premise plumbing pathogens. Infect Dis Clin North Am. 2021;35:667–95. https://doi.org/10.1016/j.idc.2021.04.007
41. Decker BK, Palmore TN. The role of water in healthcare-associated infections. Curr Opin Infect Dis. 2013;26:345–51. https://doi.org/10.1097/QCO.0b013e3283630adf
42. Williams MM, Armbruster CR, Arduino MJ. Plumbing of hospital premises is a reservoir for opportunistically pathogenic microorganisms: a review. Biofouling. 2013;29:147–62. https://doi.org/10.1080/08927014.2012.757308
43. Donohue MJ, Vesper S, Mistry J, Donohue JM. Impact of chlorine and chloramine on the detection and quantification of *Legionella pneumophila* and *Mycobacterium* species. Appl Environ Microbiol. 2019;85:e01942-19. https://doi.org/10.1128/AEM.01942-19
44. Loret JF, Dumoutier N. Nontuberculous mycobacteria in drinking water systems: a review of prevalence data and control means. Int J Hyg Environ Health. 2019;222:628–34. https://doi.org/10.1016/j.ijheh.2019.01.002
45. Centers for Disease Control and Prevention. Preventing waterborne germs at home. February 11, 2022 [cited 2022 May 19]. https://www.cdc.gov/healthywater/drinking/preventing-waterborne-germs-at-home.html
46. DeFlorio-Barker S, Wade TJ, Jones RM, Friedman LS, Wing C, Dorevitch S. Estimated costs of sporadic gastrointestinal illness associated with surface water recreation: a combined analysis of data from NEEAR and CHEERS studies. Environ Health Perspect. 2017;125:215–22. https://doi.org/10.1289/EHP130
47. Greco SL, Drudge C, Fernandes R, Kim J, Copes R. Estimates of healthcare utilisation and deaths from waterborne pathogen exposure in Ontario, Canada. Epidemiol Infect. 2020;148:e70. https://doi.org/10.1017/S0950268820000631

Address for correspondence: Megan E. Gerdes, Centers for Disease Control and Prevention, 1600 Clifton Rd NE, Mailstop H24-9, Atlanta, GA 30329-4027, USA; email: qou5@cdc.gov

Highly Pathogenic Avian Influenza Virus (H5N1) Clade 2.3.4.4b Introduced by Wild Birds, China, 2021

Jingman Tian,[1] Xiaoli Bai,[1] Minghui Li,[1] Xianying Zeng,[1] Jia Xu, Peng Li, Miao Wang, Xingdong Song, Zhiguo Zhao, Guobin Tian, Liling Liu, Yuntao Guan, Yanbing Li, Hualan Chen

Highly pathogenic avian influenza (HPAI) subtype H5N1 clade 2.3.4.4b virus has spread globally, causing unprecedented large-scale avian influenza outbreaks since 2020. In 2021, we isolated 17 highly pathogenic avian influenza H5N1 viruses from wild birds in China. To determine virus origin, we genetically analyzed 1,529 clade 2.3.4.4b H5N1 viruses reported globally since October 2020 and found that they formed 35 genotypes. The 17 viruses belonged to genotypes G07, which originated from eastern Asia, and G10, which originated from Russia. The viruses were moderately pathogenic in mice but were highly lethal in ducks. The viruses were in the same antigenic cluster as the current vaccine strain (H5-Re14) used in China. In chickens, the H5/H7 trivalent vaccine provided complete protection against clade 2.3.4.4b H5N1 virus challenge. Our data indicate that vaccination is an effective strategy for preventing and controlling the globally prevalent clade 2.3.4.4b H5N1 virus.

The hemagglutinin (HA) gene of highly pathogenic avian influenza subtype H5 viruses has evolved into multiple clades (clades 0–9), and some clades are further divided into subclades. Of the 2 dominant clades, 2.3.2.1 has been further categorized into 7 (2.3.2.1a–g) and 2.3.4.4 have been further categorized into 8 (2.3.4.4a–h) subclades (*1*–*3*). The World Organisation for Animal Health reported that >8,000 outbreaks of highly pathogenic avian influenza (HPAI) subtype H5N1 clade 2.3.4.4b occurred in birds during October 2020–October 2022. Massive numbers of birds across 4 continents (Europe, Asia, Africa, and North America) were humanely killed directly or indirectly by infection with clade 2.3.4.4b H5 HPAI viruses (*4*).

H5 HPAI viruses of several clades have spread intercontinentally through global migration of wild birds. In 2005, clade 2.2 H5N1 virus spread by wild birds caused numerous outbreaks in wild birds and domestic poultry in countries throughout Asia, the Middle East, Europe, and West Africa (*5*,*6*). In 2009, clade 2.3.2 H5N1 virus caused problems mainly in Asia and eastern Europe (*7*,*8*). In 2014, both clade 2.3.4.4b H5N8 and clade 2.3.2.1c H5N1 viruses spread and circulated in Eurasia, the Middle East, and Africa (*9*–*11*). At the beginning of 2014, a clade 2.3.4.4c H5N8 virus emerged in South Korea and then circulated in Eurasia and Africa. In 2015, that same virus spread to North America and reassorted with local low pathogenicity avian influenza (LPAI) viruses to produce subtype H5N2, which circulated in the United States during 2015–2016 (*12*,*13*). At the beginning of 2020, clade 2.3.4.4b H5N8 virus caused disease outbreaks and destroyed poultry across Europe, after which it spread to many countries in Asia (*14*,*15*). The H5N8 virus reassorted with different viruses and formed several other subtypes of H5 viruses (e.g., H5N1, H5N2, H5N3, H5N4, H5N5, and H5N6) in different countries and regions. Among them, H5N1 became the globally predominant variant (*16*,*17*). In late 2021, the virus was carried across the Atlantic Ocean to North America (*18*). The viruses caused huge ongoing outbreaks in Europe and North America and led to massive destruction of poultry and wild bird populations (*4*,*19*,*20*).

Author affiliations: State Key Laboratory for Animal Disease Control and Prevention, Harbin Veterinary Research Institute, Chinese Academy of Agricultural Sciences, Harbin, China (J. Tian, X. Bai, M. Li, X. Zeng, X. Song, Z. Zhao, G. Tian, L. Liu, Y. Guan, Y Li, H. Chen); Preventive and Control Center for Animal Disease of Heilongjiang Province, Harbin (J. Xu, P. Li, M. Wang)

DOI: https://doi.org/10.3201/eid2907.221149

[1]These authors contributed equally to this article.

Clade 2.3.4.4b H5 viruses have crossed the bird–mammal barrier to infect humans and other mammals. Since the beginning of 2020, human infection with influenza A(H5N1) clade 2.3.4.4b viruses has been detected in Spain, the United Kingdom of Great Britain and Northern Ireland, the United States, China, and Vietnam and reported to the World Health Organization (*21*). Seven human infections caused by influenza A(H5N8) virus were reported in the Russian Federation (*22*), and some infections caused by H5N6 virus were reported in China in those 3 years (2020–2022) (*23*). In addition, fatal 2.3.4.4b H5N1 infection of some carnivorous mammals (e.g., foxes, otters, red foxes, skunks, coyotes, bobcats) and marine mammals (e.g., harbor seals, dolphins) has been reported in Europe and North America (*24*).

Clade 2.3.4.4b H5N1 virus has become a new threat to the global poultry industry and to public health. To learn more about its spatial transmission and biological properties, we performed extensive phylogeographic and epidemiologic analyses of the globally circulating H5N1 viruses detected during 2020–2022, evaluated the pathogenicity of H5N1 from China in mammalian and waterfowl hosts, compared H5N1 antigenicity with that of the updated vaccine candidate, and assessed the protective efficacy of the current H5-Re14 vaccine against challenge with H5N1 isolates.

All studies with live viruses were conducted in a Biosafety Level 3 laboratory approved for such use by the Harbin Veterinary Research Institute of the Chinese Academy of Agricultural Sciences. All experiments using animals were conducted in strict accordance with recommendations in the Guide for the Care and Use of Laboratory Animals of the Ministry of Science and Technology of the People's Republic of China. The protocol was approved by the Committee on the Ethics of Animal Experiments of the Harbin Veterinary Research Institute of the Chinese Academy of Agricultural Sciences (approval nos.: duck, 211015-01; mouse, 211231-02; chicken, 211112-01).

Materials and Methods

Sample Collection and Virus Isolation

During 2020–2021, we collected 7,421 fresh fecal samples, 507 swab samples, and 6 tissue samples from wild birds in accordance with the regular surveillance of wild birds in China (Table). The samples were amplified in specific-pathogen–free (SPF) chicken embryos, and the HA subtype was identified by using the hemagglutinin inhibition (HI) test with a panel of H1–H16 reference serum. We verified the neuraminidase (NA) subtype by using reverse transcription PCR analysis with a panel of N1–N9 subtype primers (reference serum and primer sequences available on request). We identified host species by using DNA barcoding with the cytochrome C oxidase I mitochondrial gene (*25*).

Genome Sequencing and Phylogenic and Phylodynamic Analyses

We extracted total influenza A virus RNA from the allantoic fluid of virus-infected chicken embryos by using the QIAmp Viral RNA Mini Kit (QIAGEN, https://www.qiagen.com). We performed reverse transcription PCR by using a panel of gene-specific primers and sequenced the products by using an Applied Biosystems DNA analyzer (primers available on request). The genetic information collected from January 1, 2020, to October 17, 2022, was downloaded from GISAID (https://www.gisaid.org) on October 17, 2022 (Appendix 1, https://wwwnc.cdc.gov/EID/

Table. Avian influenza viruses isolated from wild bird samples collected in China, January 2020–December 2021*

		Sample			Virus		
Date	Province	Feces	Swab	Tissue	No. strains	Subtype	Pathotype†
2020							
Jan	Shanxi	700	0	0	2	H5N3	Low
Jan	Heilongjiang	980	394	2	0	NA	NA
Nov	Anhui	1,017	0	0	17	Multiple‡	Low
Nov	Ningxia	600	0	4	1	H5N2	Low
2021							
Mar	Anhui	700	0	0	0	NA	NA
Mar	Liaoning	600	0	0	0	NA	NA
Apr	Ningxia	450	0	0	0	NA	NA
Apr	Heilongjiang	750	0	0	0	NA	NA
Oct	Heilongjiang	324	113	0	2	H5N1	High
Dec	Shanxi	500	0	0	4	H5N1	High
Dec	Henan	800	0	0	11	H5N1	High

*NA, not applicable.
†Pathotype is determined by the cleavage motif of its hemagglutinin gene.
‡The 17 low pathogenicity viruses are 1 H2N3, 1 H3N8, 9 H4N6, 3 H5N8, 1 H6N2, 1 H6N8, and 1 H12N2 strains.

article/29/7/22-1149-App1.pdf). We aligned sequences by using MAFFT version 7.475 with default settings (*26*) and ran neighbor-joining trees by using MEGA version 11 for 1,000 ultrafast bootstraps (*27*). To categorize the groups of each segment in the phylogenetic trees, we used a sequence identity cutoff of >95%. We constructed a maximum-clade credibility time-scaled phylogenetic tree of HA sequences from clade 2.3.4.4b H5N1 viruses by using the SRD06 nucleotide substitution model and an uncorrelated lognormal relaxed clock model (*28*). To investigate the transmission patterns of the clade 2.3.4.4b H5N1 viruses, we performed a phylogeographic analysis by using an asymmetric model with Bayesian stochastic search variable selection implemented in BEAST version 1.10.4 (*28*,*29*). We grouped the sequences from 1,529 isolates into 11 distinct geographic categories (Appendix 2 Table 3, https://wwwnc.cdc.gov/EID/article/29/7/22-1149-App2.pdf). To summarize the diffusion rates, we used the Bayesian stochastic search variable selection, and to estimate Bayes factors, we used SpreaD3 version 0.9.6 (https://rega.kuleuven.be/cev/ecv/software/SpreaD3) (Appendix 2 Table 4).

Animal Studies

We selected 2 representative isolates, A/mandarin duck/Heilongjiang/HL-1/2021 (MD/HLJ/HL-1/2021) and A/whooper swan/Henan/14/2021 (WS/HeN/14/2021), to test in mice and ducks. The 50% lethal dose (LD_{50}) for mice was tested in groups of five 6-week-old female BALB/c mice (Vital River, https://www.vitalriver.com). The mice were intranasally inoculated with a $10^{1.0}$ to $10^{6.0}$ 50% egg infectious dose (EID_{50}) of virus in a volume of 50 μL and then monitored daily for weight loss and death for 14 days. LD_{50} values for mice were calculated according to the Reed-Muench method (*30*). To evaluate virus replication, we tested 3 more mice in the $10^{6.0}$ EID_{50} group and humanely killed them on postinoculation day 3 to assess virus titers in their nasal turbinates, lungs, brains, kidneys, and spleens.

Among the ducks, we inoculated groups of eight 3-week-old SPF ducks (Jinding duck, a local breed; National Poultry Laboratory Animal Resource Center, Harbin, China) intranasally with $10^{6.0}$ EID_{50} of H5N1 virus in a volume of 0.1 mL; at 24 h after inoculation, 3 contact ducks were put in the same cage. On postinoculation day 3, we randomly selected 3 of 8 infected ducks, humanely killed them, and collected their organs (brain, spleen, kidneys, pancreas, cecal tonsil, bursa of Fabricius, thymus, lungs, and larynx) for virus titration. We observed the remaining 5 infected ducks and 3 contact ducks for 2 weeks and collected oropharyngeal and cloacal swab samples on postinoculation days 3 and 5 to detect virus shedding.

Antigenic Analysis

We used HI to perform antigenic analysis (*31*). We generated chicken antiserum of H5 vaccine seed viruses (H5-Re11, H5-Re12, H5-Re13, and H5-Re14) (Appendix 2 Table 7) by inoculating 5-week-old SPF chickens with 0.3 mL of the oil-emulsified inactivated viruses (*32*).

Challenge Study of Clade 2.3.4.4b H5N1 Virus in Chickens

We vaccinated groups of ten 3-week-old white leghorn SPF chickens (National Poultry Laboratory Animal Resource Center) with a 0.3-mL intramuscular injection of the trivalent H5/H7 vaccine previously reported by Zeng et al. (*32*,*33*) (Harbin Weike Biotechnology Co., http://www.hvriwk.com) or with phosphate-buffered saline as a control. Three weeks after vaccination, we challenged the chickens intranasally with 10^5 EID_{50} of MD/HLJ/HL-1/2021 in a volume of 0.1 mL. We collected oropharyngeal and cloacal swab samples on postchallenge days 3 and 5 to detect the virus and observed birds for disease and death for 2 weeks after challenge.

Results

Clade 2.3.4.4b H5N1 Virus Detection

As part of regular surveillance of wild birds during 2020–2021, we collected 7,934 samples, from which we detected 17 H5N1 HPAI viruses and 20 LPAI viruses of multiple subtypes (Table). To determine the evolution of the H5N1 viruses, we sequenced the whole genomes of the 17 HPAI viruses, deposited the sequences in the GISAID database (accession nos. EPI2070071–0206), and performed phylogenic analysis of these viruses together with global clade 2.3.4.4b HPAI H5 viruses submitted to GISAID from January 1, 2020, to October 17, 2022.

The HA genes of the 17 H5N1 viruses shared 98.3%–100% identity at the nucleotide level, and the NA genes shared 97.45%–100% identity (Appendix 2 Figure 2, Figure 3, panel A). The HA genes of the clade 2.3.4.4b H5 strains formed 2 branches—East Asia and Eurasia/Africa—in the phylogenetic tree (Appendix 2 Figures 1, 2); 2 H5N1 viruses isolated in Heilongjiang Province in this study belonged to the East Asia branch, whereas the other 15 viruses belonged to the Eurasia/Africa branch. The NA genes of the 17

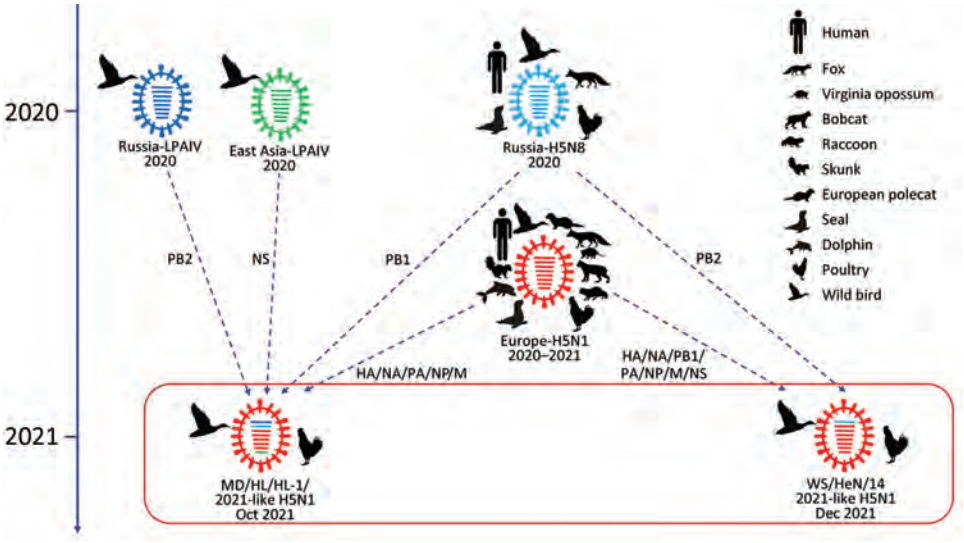

Figure 1. Formation of 2 representatives of avian influenza (H5N1) virus from China. Viral particles are represented by colored ovals containing horizontal bars representing the 8 gene segments (from top to bottom: PB2, PB1, PA, HA, NP, NA, M, and NS). Gene segments of the reassortants are colored according to their corresponding source virus. HA, hemagglutinin; LPAIV, low pathogenicity avian influenza virus; M, matrix; NA, neuraminidase; NP, nucleoprotein; NS, nonstructural protein; PA, polymerase acidic; PB, polymerase basic.

viruses all belonged to the group Europe H5N1 2020 (Appendix 2 Figure 3, panel A). Identity at the nucleotide level was 94.12%–100% for the polymerase basic (PB) 2 genes, 92.96%–100% for the PB1 genes, 97.3%–100% for the polymerase acidic (PA) genes, 97.6%–100% for the nucleoprotein (NP) genes, 98.7%–100% for the matrix (M) genes, and 95.65%–100% for the nonstructural protein (NS) genes of the 17 H5N1 viruses, and they formed multiple groups in their phylogenetic trees (Appendix 2 Figure 3). Diversity of the internal genes of clade 2.3.4.4b H5N1 viruses was greater than that of the HA and NA genes. Of note, the 8 genes of the MD/HLJ/HL-1/2021 and MD/HLJ/HL-2/2021 viruses were similar, and the 8 genes of the other 15 viruses were similar, indicating that these 17 viruses formed 2 different genotypes.

Complex Reassortment of the H5N1 Wild Bird Viruses

To investigate the formation of the 17 H5N1 HPAI viruses, we used MD/HLJ/HL-1/2021 and WS/HeN/14/2021 as representatives of the 2 branches and conducted BLAST analysis (https://platform.epicov.org/epi3/frontend#27b74d) of the highest homology viruses to the 8 segments of 2 reference viruses from GISAID. The data showed that both representatives were reassortants (Figure 1; Appendix 2 Table 2). Seven genes of WS/HeN/14/2021 (PB1, HA, NA, PA, NP, M, and NS) were closely related to those of the H5N1 HPAI viruses in Europe during 2020–2021; the PB2 gene of WS/HeN/14/2021 was provided by the H5N8 HPAI virus in Russia in 2020. MD/HLJ/HL-1/2021 had 5 genes (HA, NA, PA, NP, and M) closely related to those of the H5N1 HPAI viruses in Europe during 2020–2021; its PB1 gene was closely related to the H5N8 HPAI virus in Russia during 2020, whereas its PB2 and NS genes were from the LPAI viruses that circulated in Russia during 2020. Our analysis thus demonstrates that clade 2.3.4.4b H5N1 viruses have undergone complex reassortment with LPAI viruses in different geographic sites since 2020.

Genotypic Analysis and Spread of Clade 2.3.4.4b H5N1 Viruses

Cui et al. analyzed 233 strains of clade 2.3.4.4b H5N1 viruses that were detected globally from October 1, 2020, to April 1, 2022, and revealed 16 genotypes (G01–16) (*17*). The 2 H5N1 viruses from Heilongjiang in this study belonged to G07, whereas the other 15 H5N1 viruses belonged to G10 (Appendix 2 Figure 1). Within 2 months of their detection in wild birds, viruses of these 2 genotypes spread to and were detected in domestic waterfowl in China (*17*).

Because the viruses are still spreading globally, we sought to gain further insight into the large-scale cross-continental transmission and reassortment patterns of clade 2.3.4.4b H5N1 viruses. To that end, we analyzed the sequences of 1,296 viruses that became available from April to October 2022 and detected an additional 19 genotypes (Appendix 1; Appendix 2 Table 3, Figure 4), including 5 in western Europe (G21, G28, G33, G34, and G35), 2 in eastern and central Europe (G19 and G20), 1 in Russia (G17), 1 in Africa (G18), and 10 in North America (G22, G23, G24, G25, G26, G27, G29, G30, G31, and G32) (Appendix 2 Table 3, Figure 5). We further grouped the available isolates into 11 distinct geographic

regions, performed a phylogeographic analysis of their HA genes (Appendix 2 Table 3, Figure 5), and identified 22 spread pathways of clade 2.3.4.4b H5N1 viruses. Of note, 4 of those pathways were decisively supported with Bayes factors >1,000: 2 pathways showed G01 spreading from eastern and central Europe to Russia and from western Europe to North America; 1 showed G04 spreading from western Europe to southern Europe; and the fourth showed G07 spreading from eastern Asia to China (Appendix 2 Table 4). Those data indicate that Europe was the epidemic source for the global spread of clade 2.3.4.4b H5N1 viruses.

Amino Acid Residues of Clade 2.3.4.4b H5N1 Viruses

All 17 H5N1 viruses had residues 137A and 192I and did not have the glycosylation site at positions 158–160 in their HA (H3 numbering) (Appendix 2 Table 5), which have been reported to increase the affinity of avian influenza viruses for human-type receptors (*34*,*35*). The viruses also carried critical virulence-increasing residues, including 66S in PB1-F2 in 15 viruses; 30D, 43M, and 215A in M1 and 42S, 103F, and 106M in NS1 of all 17 viruses (*36*–*41*) (Appendix 2 Table 5). Therefore, clade 2.3.4.4b H5N1 viruses may have the capacity to infect and be virulent in humans.

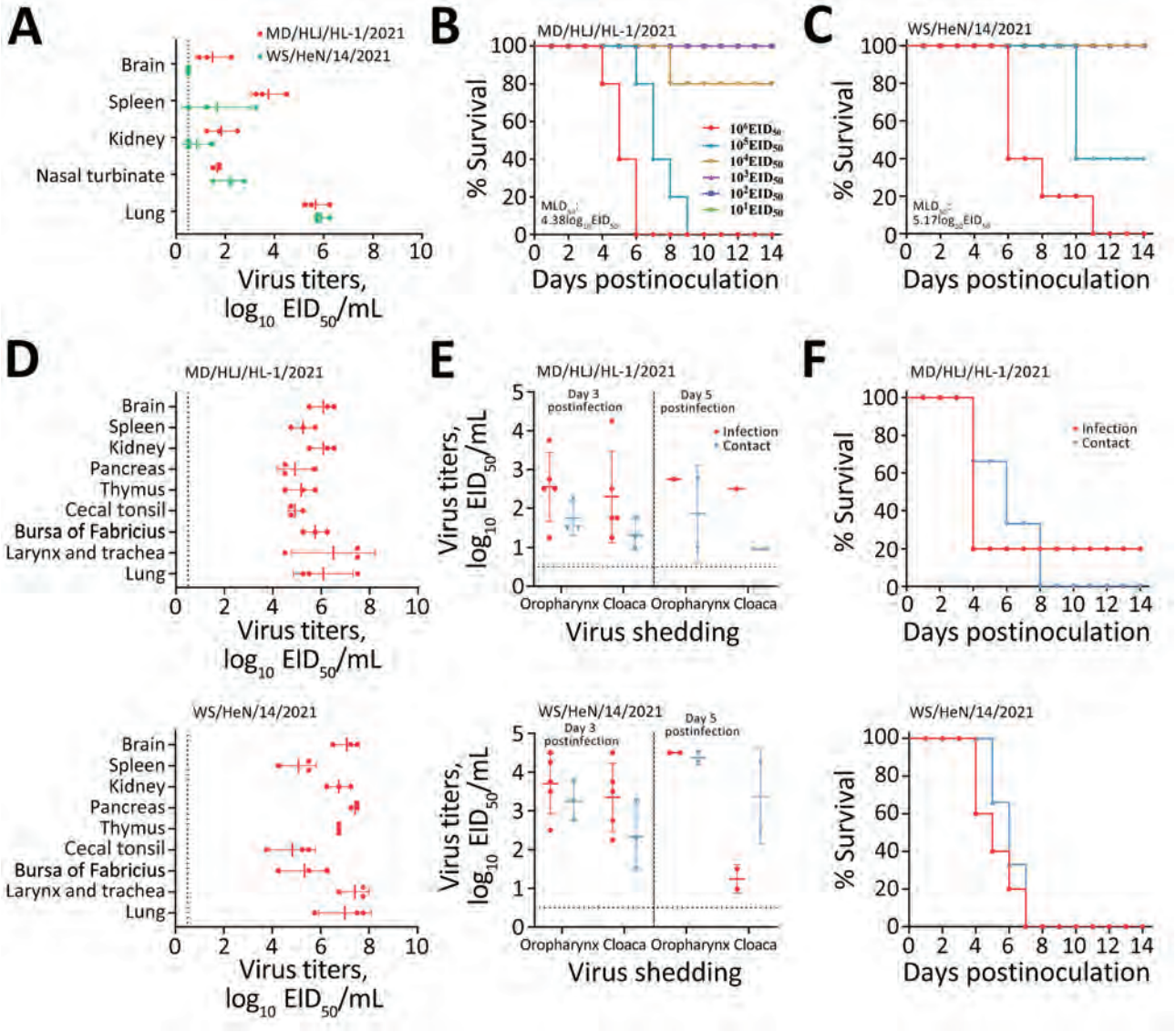

Figure 2. Replication and virulence of representative highly pathogenic avian influenza virus (H5N1) viruses in mice and ducks. A) Virus titers in organs of mice that were humanely killed on postinfection day 3 with 10^6 EID_{50} of the test viruses. B, C) MLD_{50} of the indicated viruses. D) Virus titers in organs of ducks that were killed on day 3 post inoculation with 10^6 EID_{50} in 0.1 mL of the indicated viruses. E) Virus shedding from ducks on the indicated days after inoculation. F) Death pattern of ducks in the infected and control groups. EID_{50}, 50% egg infectious dose; MLD_{50}, 50% lethal dose for mice.

Virulence of H5N1 Wild Bird Viruses in Mice

In several countries, clade 2.3.4.4 H5 viruses have caused infections in humans and other mammals, including terrestrial small carnivores and marine mammals (Appendix 1). To evaluate the replication and virulence of wild bird H5N1 viruses in mammals, we tested 2 representative strains in BALB/c mice: MD/HLJ/HL-1/2021 in G07 and WS/HeN/14/2021 in G10. We found that both viruses replicated systemically and were detected in the nasal turbinates, lungs, spleens, and kidneys of the mice; MD/HLJ/HL-1/2021 was also detected in the brains of the mice (Figure 2, panel A). The LD_{50} value of MD/HLJ/HL-1/2021 in mice was 4.38 $\log_{10}$ EID_{50} and of WS/HeN/14/2021 was 5.17 $\log_{10}$ EID_{50} (Figure 2, panels B, C), indicating that H5N1 wild bird viruses are moderately pathogenic in mice (*1*,*5*,*7*,*9*).

Lethality of H5N1 Wild Bird Viruses in Ducks

Many H5 viruses that are highly pathogenic to galliformes (e.g., chickens, quail, and turkeys) may still be of low pathogenicity to waterfowl (*1*,*15*). To investigate the replication and virulence of clade 2.3.4.4b H5N1 virus in waterfowl, we tested MD/HLJ/HL-1/2021 and WS/HeN/14/2021 in SPF ducks. We found that the 2 viruses replicated efficiently in ducks and were detected in all 9 investigated organs of ducks that were humanely killed on postinoculation day 3 (Figure 2, panel D). We detected virus shedding in oropharyngeal and cloacal swab samples from the infected ducks and contact ducks on postinoculation days 3 and 5 (Figure 2, panel E). MD/HLJ/HL-1/2021 led to the death of 4 of 5 inoculated and 3 contact ducks, whereas WS/HeN/14/2021 led to the death of all 5 inoculated and 3 contact ducks (Figure 2, panel F). Those data indicate that the 2 clade 2.3.4.4b H5N1 viruses we isolated from wild birds are lethal to ducks.

Antigenic Matching of the H5 Vaccine Seed Virus Re14 with the H5N1 Wild Bird Viruses

To evaluate the antigenic difference between the emerged clade 2.3.4.4b of H5N1 viruses and the H5 vaccine strains, we generated antiserum in SPF chickens against 4 H5 vaccine strains (H5-Re11 [clade 2.3.4.4h], H5-Re12 [clade 2.3.2.1f], H5-Re13 [clade 2.3.4.4h], and H5-Re14 [clade 2.3.4.4b]) and tested their cross-reactive HI antibody titers to 4 representative viruses detected in this study: A/mandarin duck/Heilongjiang/HL-1/2021, A/whooper swan/Shanxi/608/2021, A/whooper swan/Henan/14/2021, and A/mandarin duck/Henan/426/2021 (Appendix 2 Table 7). We found that the 4 viruses reacted well with the antiserum of H5-Re14, with titers ranging from 64 to 128, less than 4-fold to the homologous titer, but reacted poorly with the antiserum of the other 3 vaccine strains (Figure 3, panel A; Appendix 2 Table 7).

We further evaluated the protective efficacy of the H5/H7 trivalent vaccine in chickens against challenge with a clade 2.3.4.4b H5N1 virus. Three weeks

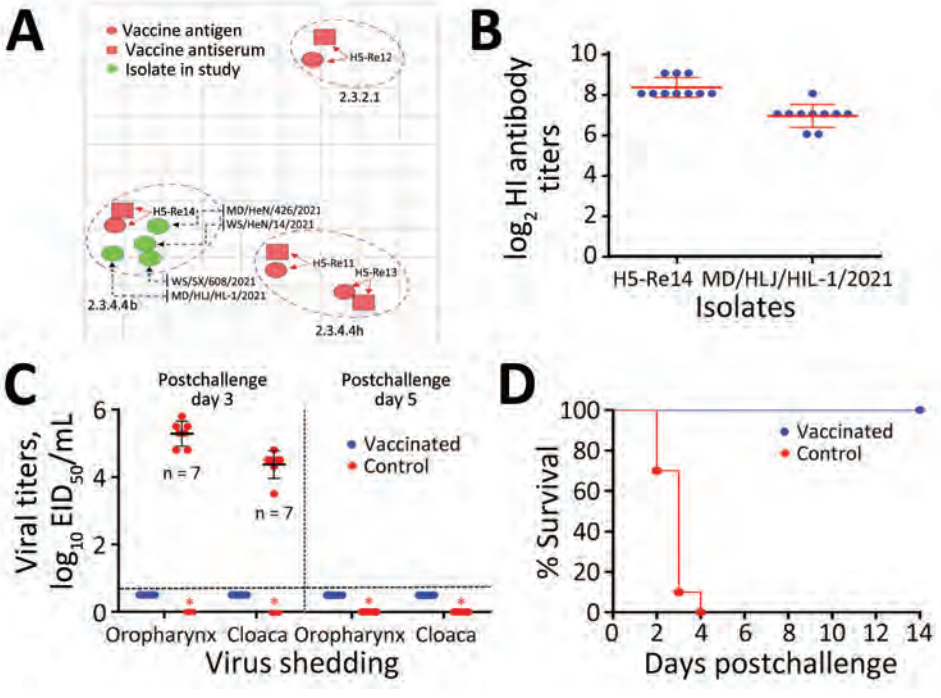

Figure 3. Antigenic difference of avian influenza (H5N1) virus isolates with H5 vaccine strains and protective efficacy of H5 vaccine against the challenge of H5N1 virus. A) Antigenic cartography of H5N1 viruses. The map was generated by using Antigenic Cartography software (https://acmacs-web.antigenic-cartography.org); 1 unit (grid) represents a 2-fold change in the HI assay results (Appendix 2 Table 7, https://wwwnc.cdc.gov/EID/article/29/7/22-1149-App2.pdf). B) HI antibody titers of vaccinated chickens against the vaccine seed virus and the challenge strain. C) Virus shedding from chickens on postchallenge days 3 and 5. D) Survival patterns of chickens in the vaccinated and control groups after challenge with the indicated H5N1 virus. EID_{50}, 50% egg infectious dose; HI, hemagglutination inhibition.

after vaccination, high titers of HI antibody to vaccine strain H5-Re14 and the H5N1 wild bird virus MD/HLJ/HL-1/2021 developed in the chickens (Figure 3, panel B). The vaccinated chickens were completely protected against MD/HLJ/HL-1/2021, with no virus shedding, and all chickens survived during the 14-day observation period (Figure 3, panels C, D); however, all control chickens died within 4 days of challenge, and the 7 chickens that were alive on post-challenge day 3 shed high titers of virus (Figure 3, panels C, D). Those data indicate that the vaccine currently used in China could provide solid protection against the clade 2.3.4.4b H5N1 viruses.

Discussion

Clade 2.3.4.4b H5N8 virus caused massive outbreaks in poultry and wild birds in Europe, Africa, and Asia from January 2020 to October 2021 (*15*,*17*). During that time, the virus reassorted in countries or regions with different viruses and generated H5N1, H5N2, H5N3, H5N4, H5N5, and H5N6 viruses bearing the clade 2.3.4.4b HA gene (*4*,*14*,*16*,*17*,*23*). Among those new subtypes, only H5N1 viruses were widely spread by the movement of migratory birds and have caused thousands of outbreaks in Europe, Africa, Asia, and North America since their generation in the Netherlands in October 2020 (*4*,*14*,*17*). Our study revealed that the widely circulating H5N1 viruses have undergone complex reassortment with other LPAI viruses and formed ≥35 genotypes. Of those novel genotypes of H5N1 viruses, 10 were generated in North America since December 2021, when clade 2.3.4.4b H5N1 virus was first introduced to that region from western Europe (*18*). Given that the H5N1 reassortants found in Europe and North America have infected multiple wild mammals, their threat to public health should be carefully monitored and assessed.

Many countries in Europe and North America control HPAI by culling infected and suspected domestic birds, whereas China controls HPAI by using a massive vaccination strategy. The key to the success of the vaccination strategy is timely updates of vaccine strains (*15*,*32*,*33*). The currently used H5/H7 trivalent inactivated vaccine was updated and has been applied since January 2022; it is produced with 3 seed viruses: H5-Re13, targeting clade 2.3.4.4h H5 viruses; H5-Re14, targeting clade 2.3.4.4b H5 viruses; and H7-Re4, targeting H7N9 viruses (*33*). The antigenic assay in our study demonstrated that the H5-Re14 seed virus antigenically matches well with the recently emerged H5N1 wild bird viruses in China. The vaccine protective efficacy test also demonstrated that the novel H5/H7 trivalent vaccine provides solid protection against challenge with an emerging H5N1 isolate. The success of the mandatory vaccination policy for preventing and controlling HPAI virus in China is an example of a high-risk country using a vaccine to protect the poultry industry and of how vaccinating poultry can prevent and eliminate human infections with avian influenza virus, as evidenced by the successful control of H7N9 influenza (*32*,*33*,*42*). Therefore, we strongly recommend the use of vaccines to protect poultry from globally circulating 2.3.4.4b H5N1 viruses.

Acknowledgments

We thank the authors and laboratories who submitted sequences to the GISAID EpiFlu database.

This work was supported by the National Key Research and Development Program of China (grant no. 2021YFD1800200) and the earmarked fund for CARS-41).

About the Author

Dr. Tian works at the Harbin Veterinary Research Institute, Chinese Academy of Agricultural Sciences, China, with a research focus on avian influenza virus surveillance.

References

1. Cui Y, Li Y, Li M, Zhao L, Wang D, Tian J, et al. Evolution and extensive reassortment of H5 influenza viruses isolated from wild birds in China over the past decade. Emerg Microbes Infect. 2020;9:1793–803. https://doi.org/10.1080/22221751.2020.1797542
2. Li Y, Li M, Li Y, Tian J, Bai X, Yang C, et al. Outbreaks of highly pathogenic avian influenza (H5N6) virus subclade 2.3.4.4h in swans, Xinjiang, western China, 2020. Emerg Infect Dis. 2020;26:2956–60. https://doi.org/10.3201/eid2612.201201
3. World Health Organization/World Organisation of Animal Health/Food and Agriculture Organization of the United Nations/H5N1 Evolution Working Group. Continued evolution of highly pathogenic avian influenza A (H5N1): updated nomenclature. Influenza Other Respir Viruses. 2012;6:1–5. https://doi.org/10.1111/j.1750-2659.2011.00298.x
4. World Organisation for Animal Health. Latest animal disease events [cited 2022 May 3]. https://wahis.woah.org/#/home
5. Chen H, Li Y, Li Z, Shi J, Shinya K, Deng G, et al. Properties and dissemination of H5N1 viruses isolated during an influenza outbreak in migratory waterfowl in western China. J Virol. 2006;80:5976–83. https://doi.org/10.1128/JVI.00110-06
6. Scotch M, Mei C, Makonnen YJ, Pinto J, Ali A, Vegso S, et al. Phylogeography of influenza A H5N1 clade 2.2.1.1 in Egypt. BMC Genomics. 2013;14:871. https://doi.org/10.1186/1471-2164-14-871
7. Li Y, Shi J, Zhong G, Deng G, Tian G, Ge J, et al. Continued evolution of H5N1 influenza viruses in wild birds, domestic poultry, and humans in China from 2004 to 2009. J Virol. 2010;84:8389–97. https://doi.org/10.1128/JVI.00413-10

8. Islam MR, Haque ME, Giasuddin M, Chowdhury EH, Samad MA, Parvin R, et al. New introduction of clade 2.3.2.1 avian influenza virus (H5N1) into Bangladesh. Transbound Emerg Dis. 2012;59:460–3. https://doi.org/10.1111/j.1865-1682.2011.01297.x
9. Li Y, Liu L, Zhang Y, Duan Z, Tian G, Zeng X, et al. New avian influenza virus (H5N1) in wild birds, Qinghai, China. Emerg Infect Dis. 2011;17:265–7. https://doi.org/10.3201/eid1702.100732
10. Kwon JH, Lee DH, Swayne DE, Noh JY, Yuk SS, Erdene-Ochir TO, et al. Highly pathogenic avian influenza A(H5N8) viruses reintroduced into South Korea by migratory waterfowl, 2014–2015. Emerg Infect Dis. 2016;22:507–10. https://doi.org/10.3201/eid2203.151006
11. Shittu I, Meseko CA, Gado DA, Olawuyi AK, Chinyere CN, Anefu E, et al. Highly pathogenic avian influenza (H5N1) in Nigeria in 2015: evidence of widespread circulation of WA2 clade 2.3.2.1c. Arch Virol. 2017;162:841–7. https://doi.org/10.1007/s00705-016-3149-4
12. Bevins SN, Dusek RJ, White CL, Gidlewski T, Bodenstein B, Mansfield KG, et al. Widespread detection of highly pathogenic H5 influenza viruses in wild birds from the Pacific Flyway of the United States. Sci Rep. 2016;6:28980. https://doi.org/10.1038/srep28980
13. Dargatz D, Beam A, Wainwright S, McCluskey B. Case series of turkey farms from the H5N2 highly pathogenic avian influenza outbreak in the United States during 2015. Avian Dis. 2016;60:467–72. https://doi.org/10.1637/11350-121715-Reg
14. Engelsma M, Heutink R, Harders F, Germeraad EA, Beerens N. Multiple introductions of reassorted highly pathogenic avian influenza H5Nx viruses clade 2.3.4.4b causing outbreaks in wild birds and poultry in The Netherlands, 2020-2021. Microbiol Spectr. 2022;10:e0249921. https://doi.org/10.1128/spectrum.02499-21
15. Cui P, Zeng X, Li X, Li Y, Shi J, Zhao C, et al. Genetic and biological characteristics of the globally circulating H5N8 avian influenza viruses and the protective efficacy offered by the poultry vaccine currently used in China. Sci China Life Sci. 2022;65:795–808. https://doi.org/10.1007/s11427-021-2025-y
16. Lewis NS, Banyard AC, Whittard E, Karibayev T, Al Kafagi T, Chvala I, et al. Emergence and spread of novel H5N8, H5N5 and H5N1 clade 2.3.4.4 highly pathogenic avian influenza in 2020. Emerg Microbes Infect. 2021;10:148–51. https://doi.org/10.1080/22221751.2021.1872355
17. Cui P, Shi J, Wang C, Zhang Y, Xing X, Kong H, et al. Global dissemination of H5N1 influenza viruses bearing the clade 2.3.4.4b HA gene and biologic analysis of the ones detected in China. Emerg Microbes Infect. 2022;11:1693–704. https://doi.org/10.1080/22221751.2022.2088407
18. Bevins SN, Shriner SA, Cumbee JC Jr, Dilione KE, Douglass KE, Ellis JW, et al. Intercontinental movement of highly pathogenic avian influenza A(H5N1) clade 2.3.4.4 virus to the United States, 2021. Emerg Infect Dis. 2022;28:1006–11. https://doi.org/10.3201/eid2805.220318
19. Miller BJ. Why unprecedented bird flu outbreaks sweeping the world are concerning scientists. Nature. 2022;606:18–9. https://doi.org/10.1038/d41586-022-01338-2
20. Stokstad E. Deadly flu spreads through North American birds. Science. 2022;376:441–2. https://doi.org/10.1126/science.abq7228
21. World Health Organization. Cumulative number of confirmed human cases for avian influenza A(H5N1) reported to WHO, 2003–2022, 11 November 2022 [cited 11 Nov. 2022]. https://www.who.int/publications/m/item/cumulative-number-of-confirmed-human-cases-for-avian-influenza-a(h5n1)-reported-to-who-2003-2022-11-nov-2022
22. Pyankova OG, Susloparov IM, Moiseeva AA, Kolosova NP, Onkhonova GS, Danilenko AV, et al. Isolation of clade 2.3.4.4b A(H5N8), a highly pathogenic avian influenza virus, from a worker during an outbreak on a poultry farm, Russia, December 2020. Euro Surveill. 2021;26:2100439. https://doi.org/10.2807/1560-7917.ES.2021.26.24.2100439
23. Gu W, Shi J, Cui P, Yan C, Zhang Y, Wang C, et al. Novel H5N6 reassortants bearing the clade 2.3.4.4b HA gene of H5N8 virus have been detected in poultry and caused multiple human infections in China. Emerg Microbes Infect. 2022;11:1174–85. https://doi.org/10.1080/22221751.2022.2063076
24. Food and Agriculture Organization of the United Nations. Global avian influenza viruses with zoonotic potential situation update [cited 2022 Oct 15]. https://www.fao.org/animal-health/situation-updates/global-aiv-with-zoonotic-potential/en
25. Lee DH, Lee HJ, Lee YJ, Kang HM, Jeong OM, Kim MC, et al. DNA barcoding techniques for avian influenza virus surveillance in migratory bird habitats. J Wildl Dis. 2010;46:649–54. https://doi.org/10.7589/0090-3558-46.2.649
26. Katoh K, Standley DM. MAFFT multiple sequence alignment software version 7: improvements in performance and usability. Mol Biol Evol. 2013;30:772–80. https://doi.org/10.1093/molbev/mst010
27. Tamura K, Stecher G, Kumar S. MEGA11: Molecular Evolutionary Genetics Analysis version 11. Mol Biol Evol. 2021;38:3022–7. https://doi.org/10.1093/molbev/msab120
28. Suchard MA, Lemey P, Baele G, Ayres DL, Drummond AJ, Rambaut A. Bayesian phylogenetic and phylodynamic data integration using BEAST 1.10. Virus Evol. 2018;4:vey016. https://doi.org/10.1093/ve/vey016
29. Hill V, Baele G. Bayesian estimation of past population dynamics in BEAST 1.10 using the Skygrid coalescent model. Mol Biol Evol. 2019;36:2620–8. https://doi.org/10.1093/molbev/msz172
30. Reed L, Muench H. A simple method of estimating fifty per cent endpoints. Am J Hyg (Lond). 1938;27:493–7.
31. World Health Organization. Manual for the laboratory diagnosis and virological surveillance of influenza [cited 2022 Dec 15]. https://apps.who.int/iris/handle/10665/44518
32. Zeng X, Chen X, Ma S, Wu J, Bao H, Pan S, et al. Protective efficacy of an H5/H7 trivalent inactivated vaccine produced from Re11, Re12, and H7-Re2 strains against challenge with different H5 and H7 viruses in chickens. J Integr Agric. 2020;19:2294–300. https://doi.org/10.1016/S2095-3119(20)63301-9
33. Zeng X, He X, Meng F, Ma Q, Wang Y, Bao H, et al. Protective efficacy of an H5/H7 trivalent inactivated vaccine (H5-Re13, H5-Re14, and H7-Re4 strains) in chickens, ducks, and geese against newly detected H5N1, H5N6, H5N8, and H7N9 viruses. J Integr Agric. 2022;21:2086–94. https://doi.org/10.1016/S2095-3119(22)63904-2
34. Yamada S, Suzuki Y, Suzuki T, Le MQ, Nidom CA, Sakai-Tagawa Y, et al. Haemagglutinin mutations responsible for the binding of H5N1 influenza A viruses to human-type receptors. Nature. 2006;444:378–82. https://doi.org/10.1038/nature05264
35. Gao Y, Zhang Y, Shinya K, Deng G, Jiang Y, Li Z, et al. Identification of amino acids in HA and PB2 critical for

the transmission of H5N1 avian influenza viruses in a mammalian host. PLoS Pathog. 2009;5:e1000709. https://doi.org/10.1371/journal.ppat.1000709
36. Centers for Disease Control and Prevention. H5N1 genetic changes inventory: a tool for influenza surveillance and preparedness [cited 2022 Oct 20]. https://www.cdc.gov/flu/avianflu/h5n1-genetic-changes.htm
37. Suttie A, Deng YM, Greenhill AR, Dussart P, Horwood PF, Karlsson EA. Inventory of molecular markers affecting biological characteristics of avian influenza A viruses. Virus Genes. 2019;55:739–68. https://doi.org/10.1007/s11262-019-01700-z
38. Kamal RP, Kumar A, Davis CT, Tzeng WP, Nguyen T, Donis RO, et al. Emergence of highly pathogenic avian influenza A(H5N1) virus PB1-F2 variants and their virulence in BALB/c mice. J Virol. 2015;89:5835–46. https://doi.org/10.1128/JVI.03137-14
39. Fan S, Deng G, Song J, Tian G, Suo Y, Jiang Y, et al. Two amino acid residues in the matrix protein M1 contribute to the virulence difference of H5N1 avian influenza viruses in mice. Virology. 2009;384:28–32. https://doi.org/10.1016/j.virol.2008.11.044
40. Nao N, Kajihara M, Manzoor R, Maruyama J, Yoshida R, Muramatsu M, et al. A Single amino acid in the M1 protein responsible for the different pathogenic potentials of H5N1 highly pathogenic avian influenza virus strains. PLoS One. 2015;10:e0137989. https://doi.org/10.1371/journal.pone.0137989
41. Jiao P, Tian G, Li Y, Deng G, Jiang Y, Liu C, et al. A single-amino-acid substitution in the NS1 protein changes the pathogenicity of H5N1 avian influenza viruses in mice. J Virol. 2008;82:1146–54. https://doi.org/10.1128/JVI.01698-07
42. Yin X, Deng G, Zeng X, Cui P, Hou Y, Liu Y, et al. Genetic and biological properties of H7N9 avian influenza viruses detected after application of the H7N9 poultry vaccine in China. PLoS Pathog. 2021;17:e1009561. https://doi.org/10.1371/journal.ppat.1009561

Address for correspondence: Yanbing Li and Hualan Chen, Harbin Veterinary Research Institute, CAAS, 678 Haping Rd, Harbin 150069, China; email: liyanbing@caas.cn and chenhualan@caas.cn

etymologia revisited

Salmonella

[sal′′mo-nel′ə]

Originally published in December 2020

Named in honor of Daniel Elmer Salmon, an American veterinary pathologist, *Salmonella* is a genus of motile, gram-negative bacillus, nonspore-forming, aerobic to facultatively anaerobic bacteria of the family Enterobacteriaceae. In 1880, Karl Joseph Eberth was the first to observe *Salmonella* from specimens of patients with typhoid fever (from the Greek *typhōdes* [like smoke; delirious]), which was formerly called *Eberthella typhosa* in his tribute. In 1884, Georg Gaffky successfully isolated this bacillus (later described as *Salmonella* Typhi) from patients with typhoid fever, confirming Eberth's findings. Shortly afterward, Salmon and his assistant Theobald Smith, an American bacteriologist, isolated *Salmonella* Choleraesuis from swine, incorrectly assuming that this germ was the causative agent of hog cholera. Later, Joseph Lignières, a French bacteriologist, proposed the genus name *Salmonella* in recognition of Salmon's efforts.

References:

1. Dorland's Illustrated Medical Dictionary. 32nd ed. Philadelphia: Elsevier Saunders; 2012.
2. Gossner CM, Le Hello S, de Jong B, Rolfhamre P, Faensen D, Weill FX, et al. Around the world in 1,475 Salmonella geo-serotypes [Another Dimension]. Emerg Infect Dis. 2016;22:1298–302.
3. Issenhuth-Jeanjean S, Roggentin P, Mikoleit M, Guibourdenche M, de Pinna E, Nair S, et al. Supplement 2008-2010 (no. 48) to the White-Kauffmann-Le Minor scheme. Res Microbiol. 2014;165:526–30.
4. Salmon DE. The discovery of the germ of swine-plague. Science. 1884; 3:155–8.
5. Su LH, Chiu CH. Salmonella: clinical importance and evolution of nomenclature. Chang Gung Med J. 2007;30:210–9.

Systematic Review of Hansen Disease Attributed to *Mycobacterium lepromatosis*

Simon M. Collin, Amanda Lima, Stéfano Heringer, Vinícius Sanders, Hugo Aborghetti Pessotti, Patrícia Deps

In 2008, bacilli from 2 Hansen disease (leprosy) cases were identified as a new species, *Mycobacterium lepromatosis*. We conducted a systematic review of studies investigating *M. lepromatosis* as a cause of HD. Twenty-one case reports described 27 patients with PCR–confirmed *M. lepromatosis* infection (6 dual *M. leprae*/*M. lepromatosis*): 10 case-patients in the United States (7 originally from Mexico), 6 in Mexico, 3 in the Dominican Republic, 2 each in Singapore and Myanmar, and 1 each in Indonesia, Paraguay, Cuba, and Canada. Twelve specimen surveys reported 1,098 PCR–positive findings from 1,428 specimens, including *M. lepromatosis* in 44.9% (133/296) from Mexico, 3.8% (5/133) in Colombia, 12.5% (10/80) in Brazil, and 0.9% (2/224) from the Asia-Pacific region. Biases toward investigating *M. lepromatosis* as an agent in cases of diffuse lepromatous leprosy or from Mesoamerica precluded conclusions about clinicopathologic manifestations and geographic distribution. Current multidrug treatments seem effective for this infection.

Since the pioneering work of Gerhard Armauer Hansen in the late 19th Century, Hansen disease (HD; also known as leprosy) has been attributed to *Mycobacterium leprae*. In 2008, bacilli from 2 cases of HD manifesting as diffuse lepromatous leprosy (DLL; also known as Lucio's leprosy or diffuse leprosy of Lucio and Latapi), with signs of Lucio's phenomenon (LP, erythema necroticans), were identified as a second causal agent of HD, *M. lepromatosis* (*1*). The *M. lepromatosis* genome has been sequenced and its evolution and genomic features in relation to *M. leprae* described elsewhere (*2*–*5*). Analyses indicated a most recent common ancestor ≈13.9 million years ago and a 9% overall difference in nucleotide sequence identity (7% in protein-coding genes, 18% in pseudogenes), differentiating *M. lepromatosis* as a separate species from *M. leprae* (*3*,*4*). Functional similarities, such as conservation of genes encoding for laminin binding and phenolic glycolipid 1 adhesin systems involved in Schwann cell invasion, outweigh differences, such as the presence of the hemN gene only in *M. lepromatosis* (*3*,*4*). Whether the 2 species differ systematically in clinicopathologic manifestations in humans has not yet been established, but validated real-time quantitative PCR assays based on unique repetitive elements in *M. lepromatosis* and *M. leprae* are now available (*6*).

DLL is a severe form of HD at the lepromatous pole of the spectrum characterized by an ineffective cellular immune response and high multibacillary load (*7*). Patients with DLL manifest diffuse nonnodular lesions and can develop LP, a severe reactional state in which recurrent crops of large and sharply demarcated ischemic or necrotic skin develop; the lesions often becoming ulcerated or even generalized, particularly on the legs, leading to secondary infection and, in some cases, fatal sepsis (*8*). DLL represents a higher proportion of HD cases in Mexico and the Caribbean than elsewhere, and studies reporting *M. lepromatosis* have tended to describe patients who originate from the region with that form of HD (*9*). However, dual *M. leprae*/*M. lepromatosis* and *M. lepromatosis*–only infections have also been reported beyond the Americas, principally in Asia.

Worldwide occurrences and clinical characteristics of HD attributed to *M. lepromatosis* infection since the species was identified have not been systematically reviewed. There is a clinical and scientific imperative to clarify the contribution of *M. lepromatosis* to a disease that greatly affects patient and public health. We report the results of a systematic review of reported HD cases with PCR–confirmed *M. lepromatosis* infection and data from surveys of archived PCR–tested specimens from persons affected by HD.

Author affiliation: Universidade Federal do Espírito Santo, Vitória, Espírito Santo, Brazil

DOI: https://doi.org/10.3201/eid2907.230024

Methods

Review Protocol and Searches

The protocol for this systematic review was defined in advance and registered with PROSPERO, an international prospective register of systematic reviews (CRD42021239268). Database searches were performed on October 4, 2022 (Appendix, https://wwwnc.cdc.gov/EID/article/29/7/23-0024-App1.xlsx). We imposed no date, language, or publication type restrictions. We manually searched bibliographies of all included studies.

Screening, Inclusion/Exclusion, and Quality Assessment

We conducted initial screening by title and abstract. We included references if a primary research study or clinical case report reported human infection with *M. lepromatosis* investigated using laboratory testing of current or archived specimens, irrespective of whether those specimens were positive for *M. lepromatosis*. We excluded animal studies and studies from before 2008, predating identification of *M. lepromatosis*. We excluded reviews and opinion pieces after manually checking bibliographies. Pairs of reviewers in parallel performed qualitative assessments to rate the methodologic quality of each included study as good, fair, or poor (Appendix). Reviewers used the Joanna Briggs Institute Critical Appraisal Tool for Case Reports (https://jbi.global/critical-appraisal-tools) and, for specimen surveys, a 9-item quality assessment tool adapted from the National Institutes of Health's Quality Assessment Tool for Observational Cohort and Cross-Sectional Studies (https://www.nhlbi.nih.gov/health-topics/study-quality-assessment-tools) (*10*).

Data Extraction and Analysis

Pairs of reviewers in parallel transferred extracted data into predefined templates. Data extracted from case reports were date and geographic location of testing, patient demographics, medical history, diagnostic methods and findings, treatment, and outcome. Data extracted from surveys were case information, test methods, source and type of specimens, and how many specimens provided DNA and tested positive for *M. lepromatosis*, *M. leprae*, or both.

Results

Database searches identified 495 references (Figure 1; Appendix). We identified no additional studies through bibliographic screening, but for completeness, we did include 2 case reports published after our database searches (*9*,*11*). After de-duplication and screening by title and abstract, we retained 58 studies, all published in peer-reviewed journals, for full text review; we extracted data from 33 (21 case reports, 12 specimen surveys). We excluded 1 because it was a retrospective review of 9 cases (*12*) that reported only 1 *M. lepromatosis* case that was also described in another source (*13*). Similarly, we excluded a review of cases among refugees and migrants in Italy during 2009–2018 (*14*) that reported PCR testing of 24 cases, 16 positive for *M. leprae* and 1 for *M. lepromatosis*, because the *M. lepromatosis* case was described in more detail in a case report (*15*).

Among the 21 case report studies, 14 studies described just 1 case, 6 described 2, and 1 described 6, yielding 32 PCR–positive cases: 21 *M. lepromatosis*–only, 5 *M. leprae*–only, and 6 dual infections (Table 1; Appendix 1). Of patients with *M. lepromatosis*, 10/27 resided in the United States (7 originally from Mexico), 6 in Mexico, 3 in the Dominican Republic, 2 each in Singapore and Myanmar, and 1 each in Indonesia, Paraguay, Cuba, and Canada. One study from Mexico reported 4 family cases, but only 2 were PCR–confirmed to be *M. lepromatosis* (*9*). Twenty-two cases occurred in the Americas and 5 in Asia; Mexico was the country of origin or residence for 13/27 case-patients. One source mentioned 2 case-patients from Costa Rica living in the United States but provided no details (*23*). Median age of case-patients was 41 years (range 21–86 years) and 63.0% (17/27) were male.

We assessed 13/21 studies as good and 8/21 as fair quality (Appendix). Eight studies did not provide detailed PCR methods (*11*,*15*,*22*,*24*–*26*,*28*,*29*), but 7 of these referred to laboratories (National Hansen's Disease Programme; US Centers for Disease Control and Prevention; Ecole Polytechnique Fédérale de Lausanne; Japan Leprosy Research Centre) or involved authors with documented experience in *M. lepromatosis* diagnostic methods (*11*,*22*,*24*–*26*,*28*,*29*).

The case-patient from the study in which *M. lepromatosis* was first identified (*1*) was a patient originally from Mexico residing in the United States who had died from DLL with LP. PCR sequencing of the ≈1,500 bp 16S rRNA gene in acid-fast bacilli from frozen liver autopsy specimens showed that the strain, designated FJ924, matched most closely with *M. leprae* (BLAST analysis [https://blast.ncbi.nlm.nih.gov/Blast.cgi] of 16S rRNA gene, 1,475/1,506 bp, 97.9% identity) and next most closely with *M. haemophilum* (1,465/1,505 bp, 97.3%). The researchers obtained archived biopsy specimens from a second patient originally from Mexico, also with DLL and LP, who had

Table 1. Case reports and case series investigating *Mycobacterium lepromatosis* as a cause of Hansen disease*

Ref.	YOP	Pt residence (origin)	Pt age, y/sex	Case description	Specimen source†	PCR-confirmed infection	Remarks
(*1*)	2008	USA (Mexico)	53/M	DLL + LP	Autopsy‡	*M. lepromatosis*	Fatal. *M. lepromatosis* strain FJ924.
		USA (Mexico)	31/M	DLL + LP	Archive	*M. lepromatosis*	Fatal. Archived lymph node tissue (2002).
(*16*)	2011	Mexico	86/F	DLL + LP	Archive	*M. lepromatosis*	Died at 3 mo. Strain Mx1-22 (100% identical with FJ924).
(*17*)	2012	Singapore	61/M	DLL	Archive	Dual	Fatal. Archived skin biopsy tissue (1999).
		Singapore	72/M	DLL	Archive	Dual	Fatal. Archived skin biopsy tissue (1999).
(*18*)	2012	Canada	72/M	Leprosy-like§	Patient¶	*M. lepromatosis*	Died (lung cancer) at 5 mo. Some travel to Florida, no other risk factors.
(*19*)	2013	USA (Mexico)	32/M	LL + ENL	Archive	*M. lepromatosis*	Archived lymph node tissue (2005).
		USA (Mexico)	50/F	DLL + LP	Archive	*M. lepromatosis*	Archived lymph node tissue (1963).
(*20*)	2015	Mexico	43/F	DLL + ENL	Patient	*M. lepromatosis*	Armadillo meat eaten in community but not by patient.
(*22*)	2016	Colombia	37/F	HIV+, LL + LP	Archive	*M. leprae*	LP possible IRIS because of ART.
(*23*)	2016	USA (Mexico)	25/M	BL + T1R >ENL#	Archive	*M. lepromatosis*	Patient reported handling/eating armadillo in Mexico. Syphilis (borderline positive ANA).
		USA (Mexico)	41/F	BL + ENL	Patient	*M. lepromatosis*	Manifested 2012, sibling of 25 y M (2007 case), cohabited with brother for 12 mo after arrival in USA (2003).
(*24*)	2016	Mexico	49/M	DLL + ENL >LP#	Patient	*M. lepromatosis*	None
(*25*)	2017	USA (Mexico)	31/M	DLL + ENL	Patient	*M. lepromatosis*	Patient reported hunting/eating armadillo in Mexico.
(*13*)	2017	USA	59/M	LL	Patient**	*M. lepromatosis*	Rheumatoid arthritis for 2 y (prednisone + methotrexate).
(*26*)	2018	Myanmar	68/M	LL	Patient	*M. lepromatosis*	Patient had HD 20 y previously (treated with dapsone).
		Myanmar	24/M	LL + ENL	Patient	*M. lepromatosis*	BI 5+ at 24 mo, resistance suspected but no DRDR mutations.
(*21*)	2019	Indonesia	41/F	DLL + LP	Patient	Dual	HD 28 y previous (treatment not reported).
(*27*)	2020	Paraguay	21/F	LL + ENL >LP#	Patient	Dual	Vasculitis had been suspected related to drug use.
(*28*)	2020	USA (Nepal)	43/F	BB + T1R >LP#	Patient	*M. leprae*	None
(*15*)	2020	Italy (Cuba)	42/F	DLL + LP	Patient††	*M. lepromatosis*	Necrotic cutaneous vasculitis 4 y previous, partial resolution with corticosteroids.
(*29*)	2020	USA	58/M	LL + ENL	Patient	*M. lepromatosis*	Patient had 12 y history of poor wound healing refractory to immunosuppressive treatment, connective tissue disease (scleroderma) and bilateral acro-osteolysis with amputated digits.
(*30*)	2021	Mexico	32/F	DLL + ENL	Patient	*M. lepromatosis*	None
(*31*)	2022	DR	40/M	LL	Patient	*M. lepromatosis*	None
		DR	35/M	LL	Patient	Dual	None
		DR	26/F	LL	Patient	Dual	Contact of family case-patient. Pregnant at diagnosis; MDT initiated after delivery.
		DR	48/M	BL	Patient	*M. leprae*	Contact of family case-patient
		DR (Haiti)	27/M	LL	Patient	*M. leprae*	Contact of family case-patient
		DR	39/F	LL	Patient	*M. leprae*	None
(*9*)	2022	Mexico	27/M	DLL + LP	Patient‡‡	*M. lepromatosis*	ENL at 3 y treated with thalidomide. No regrowth of eyelashes or eyebrows. Alcoholism, drug, and solvent abuse.
		Mexico	49/F	DLL	Patient	*M. lepromatosis*	Follow up to 2021; no regrowth of eyelashes or eyebrows.
(*11*)	2022	USA	51/M	DLL + LP	Patient	*M. lepromatosis*	Acute kidney injury/glomerulonephritis

*ART, antiretroviral therapy; BB, midborderline (borderline borderline); BI, bacillary index; BL, borderline lepromatous; DLL, diffuse lepromatous; DR, Dominican Republic; ENL, erythema nodosum leprosum (type 2 reaction); IRIS, immune reconstitution inflammatory syndrome; LL, lepromatous; LP, Lucio's phenomenon (erythema necroticans); MDT, multidrug therapy; Pt, patient; ref., reference; T1R, type 1 reaction; YOP, year of publication.
†Patient indicates the case was identified in the study cited.
‡First case identified as *M. lepromatosis* based on the 16S rRNA (strain FJ924) unique 19bp sequence TAATACTTAAACCTATTAA that compared poorly with the corresponding unique *M. leprae* 16bp sequence AAAAAATC—TTTTTTAG.
§No bacilli detected in nerves.
¶Based on report by Han et al. (*1*), 16S rRNA sequencing was repeated from archived specimens and found to match 100% with *M. lepromatosis*
#Right-arrow (>) indicates clinical progression or later development of reactional states.
**One of 3 cases tested by PCR as described in a retrospective clinic review of 9 cases (the other 2 cases were *M. leprae*) (*12*).
††One of 24 cases in Italy tested by PCR as described in a retrospective review of 55 cases (16 cases were *M. leprae.* 7 were PCR–negative) (*23*).
‡‡Index case believed infected by grandfather (LL in 1993, age 60 y, died 2004); infected mother (PCR-confirmed *M. lepromatosis*), and sibling (BL in 2014, age 25 y, MDT 12 mo, cured and followed up to 2021).

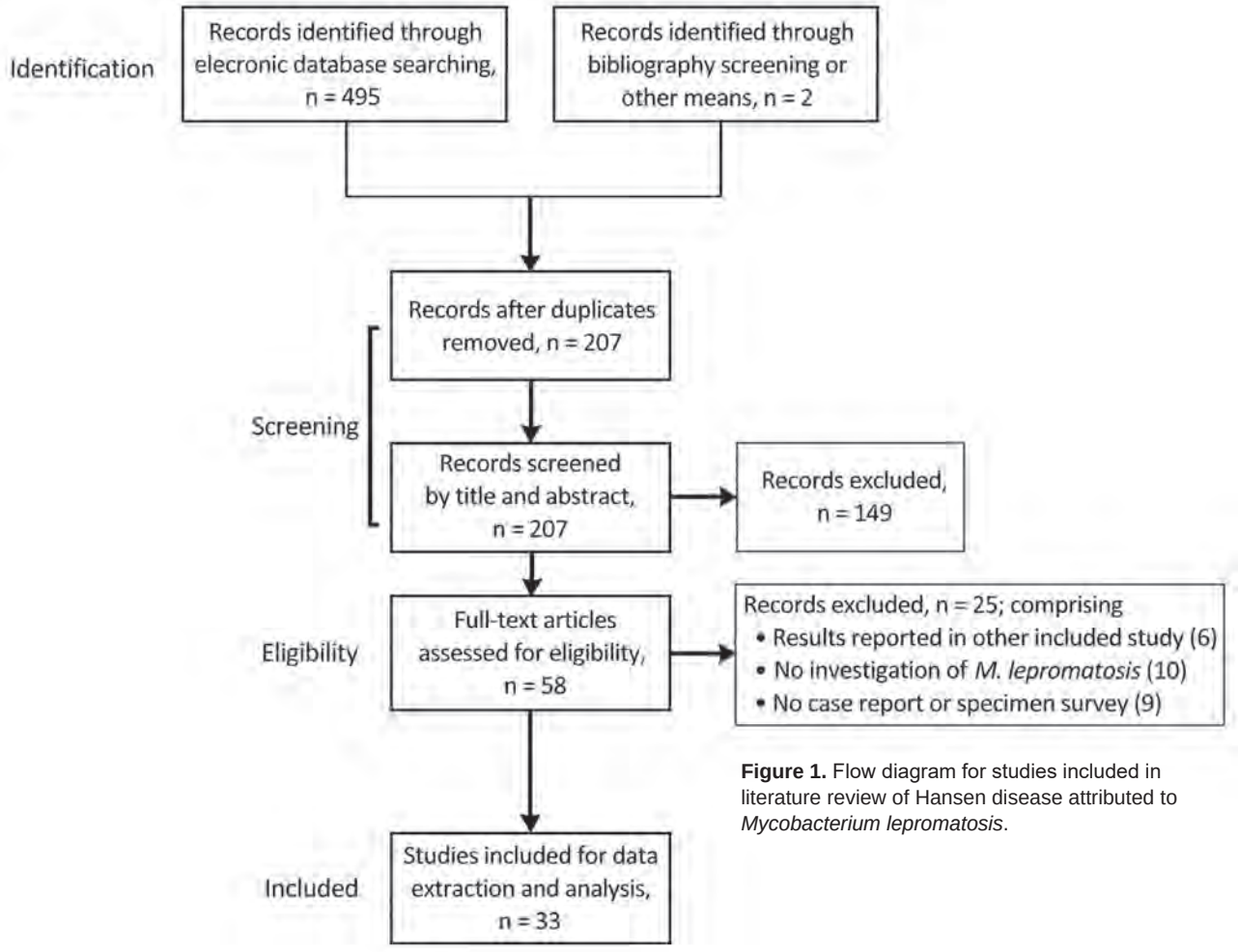

Figure 1. Flow diagram for studies included in literature review of Hansen disease attributed to *Mycobacterium lepromatosis*.

died 5 years earlier. Gene sequences from that earlier case, including from the 16S rRNA gene, matched 100% with strain FJ924. On the basis of those findings, the researchers proposed a new species, *M. lepromatosis*, as a second causal agent of DLL, while speculating that it might also cause lepromatous (LL) and borderline lepromatous (BL) forms of HD (*1*). The researchers also obtained archived specimens from 2 fatal cases of DLL in Singapore (both case-patients died in 1999) with dual *M. lepromatosis*/*M. leprae* infection identified using a mix of species-specific and nonspecific primers matched to GenBank sequences (*17*).

In another study from Mexico, a sample, Mx1-22, taken from an 86-year-old patient with DLL and LP had *rrs*, *rpoB*, *sigA*, and *hsp65* gene sequences identical to FJ924 (*16*). Subsequent studies used a range of species-specific primers and sequencing, 7 targeting 16S rRNA (*13*,*18*–*21*,*23*,*30*), 2 *hemN* (*27*,*31*), and 1 the LPMREP repetitive element (*9*) to confirm *M. lepromatosis* infection (Table 1). The oldest archived specimen in which *M. lepromatosis* was identified was from a US-resident patient originally from Mexico, 50 years of age, treated in Carville, Louisiana, USA, who was diagnosed with DLL with LP in 1963 (*19*). That patient, who initially sought treatment for a soft tissue sarcoma in the right lower leg, developed overt signs of DLL and LP after radiotherapy and amputation of the leg. Histopathologic review identified chronic HD lesions in the skin, vessels, and nerves surrounding the sarcoma, consistent with DLL. The patient survived to 85 years of age.

Of the 27 *M. lepromatosis* case-patients, 15 (55.6%) had DLL, 9 of whom also had LP; 10 had LL, 1 had LP, and 2 had BL (Figure 2). Among those cases, type 2 erythema nodosum leprosum (ENL) HD reactions were reported in 3 cases each of DLL and LL and in both BL cases. Male patients comprised 8/15 DLL and 1/2 BL case-patients but a higher proportion (8/10) of LL case-patients (Figure 3). Median time of evolution from initial symptoms to HD diagnosis was 2 years (range 8 months–12 years); 2 patients had been diagnosed with HD 20 and 28 years earlier.

Two patients reported direct contact (hunting, handling, or eating) with armadillos in Mexico (*23*,*25*); a third came from a village in Mexico where armadillo meat was consumed, but the patient had not eaten it (*20*). Two patients in the United States had no known risk factors or exposures other than travel, including to Florida (*18*), worldwide travel including to Asia, the Caribbean, and the Middle East, and 2 trips to the Pacific coast of Mexico that were short but occurred consistent with a 7–8 year incubation period for HD manifestation (*13*).

Concomitant or differential diagnoses discussed in the case reports included sarcoidosis (initially treated with steroids) (*19*), syphilis (borderline positive antinuclear antibodies, treated initially with intramuscular penicillin) (*23*), rheumatoid arthritis (treated with prednisone and methotrexate 2 years earlier) (*13*), cutaneous vasculitis (treated with azathioprine and prednisone for >5 years) (*30*), vasculitis related to drug abuse (*27*), and acute kidney injury (*11*). All cases were otherwise consistent with the clinical and histopathologic picture of DLL (*32*): insidious onset with violaceous erythema developing on the face and lower extremities (may or may not be anesthetic); myxoedema-like aspect with smooth, tense, alopecic skin, progressing to madarosis; earlobe infiltration; rhinitis; nasal septal defects; hypohidrosis; xerotic and scaly skin with ichthyosiform appearance on lower limbs; areas of hypoesthesia and hyperesthesia associated with hypopigmented, atrophic plaques; and impaired sensation in the hands and feet becoming more generalized because of progressive nerve involvement. Histologically, dense histiocytic infiltration in skin and nerves was observed, advancing to endothelial proliferation with thickening of vascular walls, leading to occlusion of small arteries, and invasion of internal organs, indicated by hepatomegaly and splenomegaly.

All multibacillary HD case-patients were treated with multidrug therapy, typically with rifampicin, clofazimine, and dapsone (sometimes substituted with minocycline, clarithromycin, moxifloxacin, or oxfloxacin) for 12 or 24 months, plus corticosteroids (mainly prednisone), thalidomide, or both for ENL and LP. Treatment outcomes were favorable for 10/27 patients at time of reporting, although that group included 2 patients who had no regrowth of eyelashes or eyebrows at 3-year follow-up, 1 of whom also experienced ENL at 3 years (*9*). One patient whose mild neurologic deficits had resolved at 7 years was still taking thalidomide and prednisone because of new, although sparse, ENL lesions (*23*).

Eight patients were still receiving treatment or had just completed treatment at time of reporting. Most studies did not assess or report grade of disability. Six deaths were reported, of which 4 were attributed to DLL or sepsis secondary to DLL (*1*,*17*). One patient who died was a woman, 86 years of age, who improved after 10 days of treatment and was discharged after 2 weeks in stable condition but then died of unknown causes at home 3 months later (*16*). A man, 72 years of age, died from lung cancer after 5 months; he was described as having leprosy-like illness because, although 16S rRNA sequencing found a 100% match to *M. lepromatosis* and the patient manifested neurologic and dermatologic symptoms of LL and rhinorrhea, histopathology did not confirm mycobacteria within peripheral nerves (*18*).

Five case-patients tested positive only for *M. leprae*: One was a woman, 43 years of age, a United States resident originally from Nepal, diagnosed with midborderline HD with possible type 1 reaction and possible LP because of an erythematous geographic skin plaque which ulcerated, but was not biopsied (*28*). Another was a woman, 37 years of age, from Colombia, HIV-positive, diagnosed with LL and LP; the

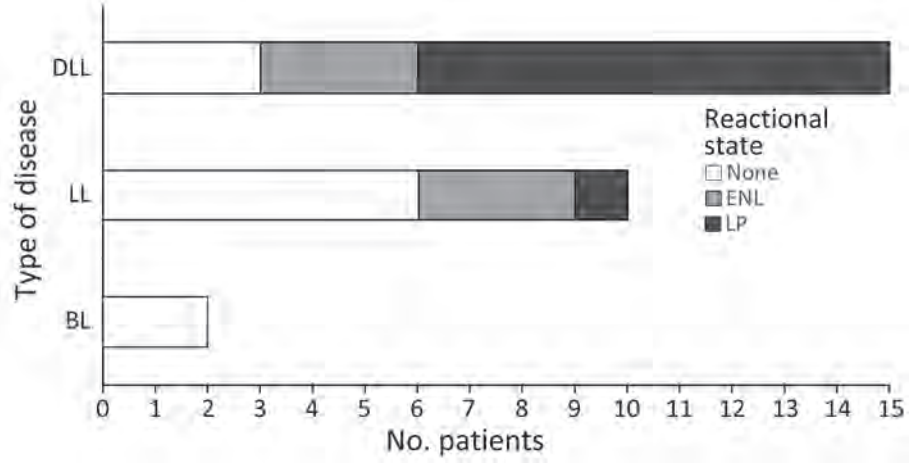

Figure 2. Types of Hansen disease and reactional states in reports included in literature review of PCR-confirmed cases attributed to *M. lepromatosis*. BL, borderline lepromatous leprosy; DLL, diffuse lepromatous leprosy; ENL, erythema nodosum leprosum (type 2 reaction); LL, lepromatous leprosy; LP, Lucio's phenomenon (erythema necroticans, type 3 reaction)

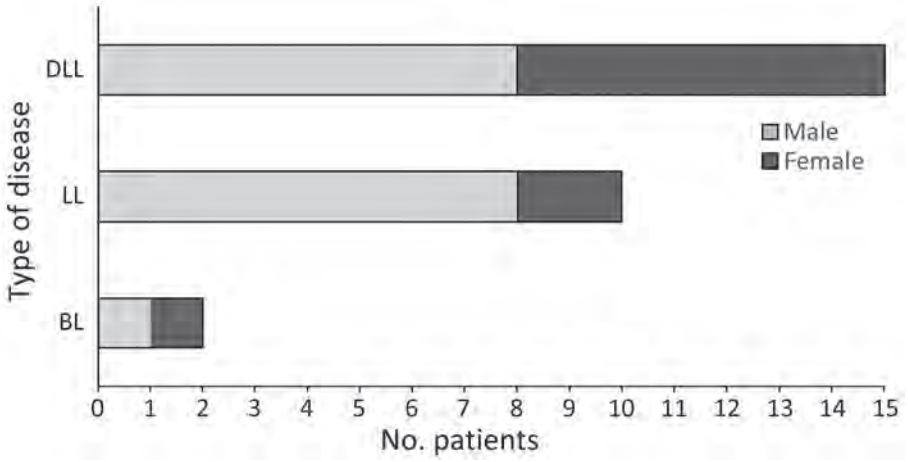

Figure 3. Types of Hansen disease by case-patient sex in reports included in literature review of PCR-confirmed cases attributed to *M. lepromatosis*. BL, borderline lepromatous leprosy; DLL, diffuse lepromatous leprosy; LL, lepromatous leprosy.

LP was potentially triggered as immune reconstitution inflammatory syndrome following initiation of antiretroviral therapy (*22*). The remaining 3 patients, from the Dominican Republic, 2 with LL and 1 with BL, were from a series of 6 cases that also included 1 *M. lepromatosis*–only and 2 dual-infection cases (*31*).

Quality assessment rated 7/12 specimen survey studies as good and 5/12 as fair quality. All but 1 study (*42*) reported details of PCR methods. Nine studies (*34*–*42*) used skin lesion or biopsy or tissue samples, 2 used both skin and lesion biopsy and skin slit smear specimens (*6*,*33*), and 1 did not explicitly state the sources of specimens (Table 2; Appendix) (*3*). Overall, surveys dated 1968–2020 reported 1,098 PCR–positive *M. lepromatosis*–only, *M. leprae*–only, or dual-infection findings from 1,428 specimens. *M. lepromatosis* was identified in 44.9% (133/296, 26 dual infection) of PCR–positive specimens from patients in Mexico or in the United States but originally from Mexico, 3.8% (5/133, 5 dual infection) of patients from Colombia, 12.5% (10/80, 3 dual infection) of patients from Brazil, and 0.9% (2/224) of patients from the Pacific-Asia region; all 157 specimens from China, 50 from Africa (Mali, Uganda), and 77 from Venezuela were positive only for *M. leprae*. For patients from Mexico, excluding those resident in the United States, *M. lepromatosis* was detected in 43.9% (116/264) of PCR–positive specimens, including 25 dual infections. For patients resident in the United States from any country of origin, *M. lepromatosis* was detected in 16.7% (20/120) of PCR–positive specimens, including 1 dual infection.

The distribution of HD types among 116 *M. lepromatosis*–only and 13 dual-infection patients was tuberculoid in 7 (5.4%); borderline tuberculoid, midborderline, or borderline lepromatous in 20 (15.5%); LL in 73 (56.6%); and DLL in 29 (22.5%). LP was reported in relation to 14/27 specimens from patients in Mexico or in the United States but originally from Mexico. One patient from Mexico with LL who provided a specimen positive for *M. lepromatosis* had consumed armadillo meat (*40*).

Discussion

Our systematic review identified 27 case reports of HD attributed to PCR–confirmed *M. lepromatosis* infections. In addition, surveys of specimens from current patients and archived material uncovered 153 cases of *M. lepromatosis* HD. Most of those infections (60% of case reports, 87% of surveyed specimens) occurred in patients resident in Mexico or in the United States but originally from Mexico. Most (70%) of the case reports described patients with DLL, among whom half manifested LP.

Our findings appear to substantiate the hypothesis that *M. lepromatosis* is the predominant HD pathogen in Mesoamerica and the Caribbean, and particularly in Mexico, and that it has a strong tendency to cause the DLL form of HD and, indirectly, severe LP reaction. However, there are some important caveats. First, DLL and LP were identified in Mexico in the late 19th Century by physicians Lucio Nájera and Ygnacio Alvarado and were further characterized by Fernando Latapí in 1938 (*43*,*44*). Discovery of *M. lepromatosis* in fatal cases of DLL with LP in 2 patients in the United States who were originally from Mexico (*1*), combined with the high proportion of HD cases in Mexico that were DLL, with or without LP, might have resulted in disproportionate publication of case reports and specimen surveys focused on this form of HD in this region. Laboratory expertise and resources for detecting *M. lepromatosis* are also more readily available in Mexico and the United States. However, Mexico is not an HD-endemic country, reporting an

average of <200 newly detected cases per year during 2005–2021 (*45*), mostly in the states of Guerrero, Jalisco, Oaxaca, Sinaloa, and Michoacán (*46*). Although this annual average represents a relatively small number of cases, in the context of HD elimination, it is a matter of public health concern. In addition, *M. lepromatosis* has a tendency to cause severe forms including DLL, which with its nonnodular manifestation is prone to diagnosis at later stages; therefore, there remains an immense personal impact on persons affected by the disease.

Current HD multidrug therapies appear to be effective treatments, except in the most severe cases in which patients are at risk of secondary infection. However, evidence on the apparent effectiveness of current multidrug therapy regimens in treating HD caused by *M. lepromatosis* is constrained by the small number of cases described, their clinical complexity and severity, and lack of follow-up data to characterize long-term outcomes, including permanent disabilities.

Our review showed that *M. lepromatosis*–caused HD occurs in other countries in the Americas and, sporadically, in Asia and the Pacific. Most notably, 1 in 8 specimens from the south of Brazil were identified as *M. lepromatosis*. Brazil is an HD-endemic country with ≈20,000 newly detected cases per year. Also, the survey data in our review showed that, when type of HD was reported, a higher percentage of cases attributed to *M. lepromatosis* were LL (57%) than DLL (23%). Even a small fraction of HD cases in Brazil caused by *M. lepromatosis* would

Table 2. Specimen surveys investigating *Mycobacterium lepromatosis* as a cause of Hansen disease*

Ref.	Country (origin)	Specimen date range	Specimens	PCR results					HD types (remarks)
				Neg	Pos	*M. lepromatosis*	Dual infection	*M. leprae*	
(*3*)	Mexico	Not reported	64 type not reported	0	64	6	0	58	DLL 2
	Venezuela	Not reported	77 type not reported	0	77	0	0	77	
	Brazil	Not reported	33 type not reported	0	33	0	0	33	
	Mali	Not reported	48 type not reported	0	48	0	0	48	
	Others	Not reported	5 type not reported	0	5	0	0	5	
(*6*)	Mexico	Not reported	47 skin lesion biopsy	11	36	15	2	19	
	United States	2017	218 type not reported	146	72	3	0	69	
	Philippines		180 sss	0	180	0	0	180	
	United States (all but 1 born in Mexico)	1968–1994	15 skin biopsy sections	0	10	5	1	4	LL 2, DLL 4 (all originally from Mexico)
(*33*)	Colombia†	2006–2016	67 skin lesion, 25 earlobe sss	0	92	0	5	87	
(*34*)	Colombia (Cartagena, Bolívar)	2015–2020	41 skin biopsy	7	41	0	0	34	
(*35*)	Mexico	1988–2007	120 skin biopsy	33	87	55	14	18	B 12, LL 41, DLL 16
(*36*)	Brazil (Curitiba and southern Brazil)	2004–2010	52 skin biopsy	6	46	7	3	36	TT7, LL 3
	Myanmar	2007–2008	9 skin biopsy	3	6	2	0	4	LL 2
	Malaysia (19), Indonesia (3), Nepal (1), Myanmar (1)	2003–2011	31 skin biopsy	4	27	0	0	27	
	Uganda	1979–1990	4 skin biopsy	2	2	0	0	2	
(*37*)	Mexico	Current	19 skin biopsy	9	10	2	1	7	LL 2, not determined 1
(*38*)	United States (various countries of origin)‡	2011–2021	38 tissue	0	38	11	0	27	LL 11 (all originally from Mexico)
(*39*)	Mexico§	1994–2014	41 skin biopsy	12	29	8	8	13	BL 6, LL 6, DLL 4
(*40*)	Mexico	Current patients	38 skin biopsy	0	38	5	0	33	BL 1, LL 1, DLL 3
(*41*)	China	Current patients	171 skin biopsy	86	85	0	0	85	
(*42*)	China (Shandong province)	Not reported	85 skin biopsy	13	72	0	0	72	

*B, borderline (BT, BB or BL); BB, mid-borderline (borderline borderline); BL, borderline lepromatous; BT, borderline tuberculoid; DLL, diffuse lepromatous leprosy; ENL, erythema nodosum leprosum (type 2 reaction); LL, lepromatous leprosy; LP, Lucio's phenomenon (erythema necroticans); neg, negative; pos, positive; ref, reference; sss, skin slit smear; TT, tuberculoid.
†Provinces of Atlántico, Antioquia, Bolívar, Chocó, Cesar, Cundinamarca, Magdalena, Santander, Norte de Santander, Sucre, and Tolima.
‡Mexico (22), Philippines (6), Vietnam (1), India (1), Myanmar (1), Marshall Islands (2), El Salvador (2), Brazil (1), United States (2).
§Yucatan (16), Guerrero (8), Michoacán (6), Guanajuato (3), Morelos (2), 1 each from Campeche, Ciudad de Mexico, Estado de Mexico, Oaxaca, Puebla, and Quintana Roo.

represent a large number of cases. The clear implication is that a national survey of current and newly detected HD cases in Brazil is needed, ideally using the recently validated *M. lepromatosis*/*M. leprae* diagnostic assay (*6*). Parallel studies in neighboring countries where *M. lepromatosis* and DLL are perhaps more prevalent, would yield sequence data that could be used to investigate the distribution of *M. lepromatosis* variants and lineages, including drug-resistant strains, to achieve the same level of understanding as for *M. leprae* (*5*,*47*). Whether *M. lepromatosis* has a pathogenic tendency toward causing DLL and whether certain population groups are more susceptible to developing this form of HD can be investigated by pathogen and host genomic testing across the HD spectrum and in different populations. From a One Health perspective, we know that zoonotic transmission of *M. leprae* presents a risk to human health (*48*), and *M. lepromatosis* has been detected in red squirrels (*Sciurus vulgaris*) from the British Isles, including Ireland (*49*). Given that 4 case-patients with HD caused by *M. lepromatosis* in our review had direct or indirect contact with wild armadillos, a survey of archived specimens or specimens from freshly caught armadillos in Mexico and Brazil is warranted (*50*).

The narrowly focused scope, sensitivity, and specificity of lepromatosis as a search term and the relatively few references included in our review give us confidence that all relevant studies were identified. Quality of reporting was good in 61% of included studies and fair in the remainder. The tendency of studies to focus on DLL in Mesoamerica, possibly resulting in observational and publication biases for case reports and sampling bias for surveys, were the main sources of bias in our review, although there were several large studies from other regions with null findings for *M. lepromatosis*. A key quality item considered for this review was adequate description of PCR methods, which most, but not all, studies provided. Specimen surveys more consistently described PCR methods, including targets and primers, than did case reports, some of which covered time periods during which those methods were still being developed. *M. lepromatosis* does not manifest only as DLL, but most specimen surveys did not provide clinical data for the patients sampled. Even when HD type was stated, misclassification was possible unless HD specialists or reference centers were involved in diagnosis. Although we cannot entirely preclude the possibility of double counting, we identified only a few cases that were reported twice and contacted the authors of 2 studies when geography and time span suggested that possibility to confirm that there was no overlap (*33*,*34*).

It is perhaps remarkable that a new species causing an endemic disease of major public health impact has not prompted larger-scale studies to determine its true prevalence. Even if options for patient management are determined by clinical manifestations of HD rather than its etiologic agents, understanding disease attribution and distribution of a highly pathogenic species are clearly important, and the availability of validated PCR methods enables large-scale epidemiologic studies to be conducted.

In conclusion, clinicians need to be aware that Hansen disease of various forms can be caused by either *M. leprae* or *M. lepromatosis*. Current multidrug therapy regimens appear to be effective regardless of infecting species.

About the Author

Dr. Collin is a public health epidemiologist in England, with expertise in epidemiology of infectious diseases, and a visiting professor at the Federal University of Espírito Santo, Brazil.

References

1. Han XY, Seo YH, Sizer KC, Schoberle T, May GS, Spencer JS, et al. A new *Mycobacterium* species causing diffuse lepromatous leprosy. Am J Clin Pathol. 2008;130:856–64. https://doi.org/10.1309/AJCPP72FJZZRRVMM
2. Han XY, Sizer KC, Thompson EJ, Kabanja J, Li J, Hu P, et al. Comparative sequence analysis of *Mycobacterium leprae* and the new leprosy-causing *Mycobacterium lepromatosis.* J Bacteriol. 2009;191:6067–74. https://doi.org/10.1128/JB.00762-09
3. Singh P, Benjak A, Schuenemann VJ, Herbig A, Avanzi C, Busso P, et al. Insight into the evolution and origin of leprosy bacilli from the genome sequence of *Mycobacterium lepromatosis.* Proc Natl Acad Sci U S A. 2015;112:4459–64. https://doi.org/10.1073/pnas.1421504112
4. Silva FJ, Santos-Garcia D, Zheng X, Zhang L, Han XY. Construction and analysis of the complete genome sequence of leprosy agent *Mycobacterium lepromatosis.* Microbiol Spectr. 2022;10:e0169221. https://doi.org/10.1128/spectrum.01692-21
5. Avanzi C, Singh P, Truman RW, Suffys PN. Molecular epidemiology of leprosy: an update. Infect Genet Evol. 2020;86:104581. https://doi.org/10.1016/j.meegid.2020.104581
6. Sharma R, Singh P, McCoy RC, Lenz SM, Donovan K, Ochoa MT, et al. Isolation of *Mycobacterium lepromatosis* and development of molecular diagnostic assays to distinguish *Mycobacterium leprae* and *M. lepromatosis.* Clin Infect Dis. 2020;71:e262–9. https://doi.org/10.1093/cid/ciz1121
7. Scollard DM. Pathogenesis and pathology of leprosy. In: Scollard DM, Gillis TP, editors. International textbook of leprosy. 2018 . https://www.internationaltextbookofleprosy.org/chapter/pathology
8. Frade MAC, Coltro PS, Filho FB, Horácio GS, Neto AA, da Silva VZ, et al. Lucio's phenomenon: a systematic literature review of definition, clinical features,

histopathogenesis and management. Indian J Dermatol Venereol Leprol. 2022;88:464–77. https://doi.org/10.25259/IJDVL_909_19
9. Romero-Navarrete M, Arenas R, Han XY, Vega-Memije ME, Castillo-Solana AD. Leprosy caused by *Mycobacterium lepromatosis.* Am J Clin Pathol. 2022;158:678–86. https://doi.org/10.1093/ajcp/aqac110
10. National Heart Lung and Blood Institute. Quality assessment tool for observational cohort and cross-sectional studies [cited 2019 May 24]. https://www.nhlbi.nih.gov/health-topics/study-quality-assessment-tools
11. Norman T, Zikry J, Worswick S, Kim G, Ochoa MT. Lucio phenomenon with concomitant necrotizing fasciitis and acute kidney injury. Dermatol Online J. 2022;28. https://doi.org/10.5070/D328357784
12. Bezalel SA, Onajin O, Gonzalez-Santiago TM, Patel R, Pritt BS, Virk A, et al. Leprosy in a midwestern dermatology clinic: report of 9 patients. Mayo Clin Proc. 2019;94:417–23. https://doi.org/10.1016/j.mayocp.2018.11.022
13. Virk A, Pritt B, Patel R, Uhl JR, Bezalel SA, Gibson LE, et al. *Mycobacterium lepromatosis* lepromatous leprosy in US citizen who traveled to disease-endemic areas. Emerg Infect Dis. 2017;23:1864–6. https://doi.org/10.3201/eid2311.171104
14. Beltrame A, Barabino G, Wei Y, Clapasson A, Orza P, Perandin F, et al. Leprosy in refugees and migrants in Italy and a literature review of cases reported in Europe between 2009 and 2018. Microorganisms. 2020;8:1113. https://doi.org/10.3390/microorganisms8081113
15. Trave I, Barabino G, Cavalchini A, Parodi A. Long-term ulcerations caused by *Mycobacterium lepromatosis.* Int J Mycobacteriol. 2020;9:223–5. https://doi.org/10.4103/ijmy.ijmy_40_20
16. Vera-Cabrera L, Escalante-Fuentes WG, Gomez-Flores M, Ocampo-Candiani J, Busso P, Singh P, et al. Case of diffuse lepromatous leprosy associated with "*Mycobacterium lepromatosis.*" J Clin Microbiol. 2011;49:4366–8. https://doi.org/10.1128/JCM.05634-11
17. Han XY, Sizer KC, Tan HH. Identification of the leprosy agent *Mycobacterium lepromatosis* in Singapore. J Drugs Dermatol. 2012;11:168–72.
18. Jessamine PG, Desjardins M, Gillis T, Scollard D, Jamieson F, Broukhanski G, et al. Leprosy-like illness in a patient with *Mycobacterium lepromatosis* from Ontario, Canada. J Drugs Dermatol. 2012;11:229–33.
19. Han XY, Jessurun J. Severe leprosy reactions due to *Mycobacterium lepromatosis.* Am J Med Sci. 2013;345:65–9. https://doi.org/10.1097/MAJ.0b013e31826af5fb
20. Han XY, Quintanilla M. Diffuse lepromatous leprosy due to *Mycobacterium lepromatosis* in Quintana Roo, Mexico. J Clin Microbiol. 2015;53:3695–8. https://doi.org/10.1128/JCM.01951-15
21. Widiatma RR, Sukanto H. Diffuse lepromatous leprosy caused by dual infection of *Mycobacterium leprae* and *Mycobacterium lepromatosis*: a case report. Dermatol Rep. 2019;11:180–2. https://doi.org/10.4081/dr.2019.8094
22. Serrano-Coll HA, Beltrán-Alzate JC, Buitrago SM, Cardona-Castro N. Lepromatous leprosy and human immunodeficiency virus co-infection associated with phenomenon of Lucio versus immune reconstitution inflammatory syndrome. Infectio. 2016;20:272–5. https://doi.org/10.1016/j.infect.2015.10.011
23. Sotiriou MC, Stryjewska BM, Hill C. Two cases of leprosy in siblings caused by *Mycobacterium lepromatosis* and review of the literature. Am J Trop Med Hyg. 2016;95:522–7. https://doi.org/10.4269/ajtmh.16-0076
24. Velarde-Félix JS, Alvarado-Villa G, Vera-Cabrera L. "Lucio's phenomenon" associated with *Mycobacterium lepromatosis.* Am J Trop Med Hyg. 2016;94:483–4. https://doi.org/10.4269/ajtmh.15-0439
25. Cleary LC, Suraj S, Haburchak D, Turrentine JE. The armadillo factor: lepromatous leprosy. Am J Med. 2017;130:1163–6. https://doi.org/10.1016/j.amjmed.2017.06.001
26. Htet L, Kai M, Miyamoto Y. New etiology of leprosy in Myanmar: another two patients. Lepr Rev. 2018;89:316–8. https://doi.org/10.47276/lr.89.3.316
27. Aldama Olmedo OM, Escobar M, Martínez MJ, Aldama M, Montoya Bueno C, Celias LF, et al. Necrotizing erythema nodosumin lepromatous leprosy associated with mixed infection by *Mycobacterium lepromatosis* and *Mycobacterium leprae* [in Spanish]. Rev Nac (Itauguá). 2020;12:107–15. https://doi.org/10.18004/rdn2020.dic.02.107.115
28. Oo YM, Paez A, Brown R. Leprosy: a rare case of infectious peripheral neuropathy in the United States. IDCases. 2020;20:e00765. https://doi.org/10.1016/j.idcr.2020.e00765
29. Watson W, Vassantachart JM, Luke J. Clinicopathological challenge: acute blistering and dermal papules in a patient with scleroderma. Int J Dermatol. 2020;59:e99–101. https://doi.org/10.1111/ijd.14571
30. Flores-Suárez LF, Fernández-Sánchez M, Ahumada-Topete VH, Rodríguez M, Charli-Joseph Y. After all, still a magnificent impersonator. Rheumatology (Oxford). 2021;60:e245–6. https://doi.org/10.1093/rheumatology/keab077
31. Fernández JDP, Pou-Soarez VE, Arenas R, Juárez-Duran ER, Luna-Rojas SL, Xicohtencatl-Cortes J, et al. *Mycobacterium leprae* and *Mycobacterium lepromatosis* infection: a report of six multibacillary cases of leprosy in the Dominican Republic. Jpn J Infect Dis. 2022;75:427–30. https://doi.org/10.7883/yoken.JJID.2021.709
32. Kumar DP, Uprety S, Dogra S. Clinical diagnosis of leprosy. In: Scollard DM, Gillis TP, editors. International textbook of leprosy. 2018 [cited 2023 Jan 8]. https://www.internationaltextbookofleprosy.org/chapter/diagnosis-leprosy
33. Cardona-Castro N, Escobar-Builes MV, Serrano-Coll H, Adams LB, Lahiri R. *Mycobacterium lepromatosis* as cause of leprosy, Colombia. Emerg Infect Dis. 2022;28:1067–8. https://doi.org/10.3201/eid2805.212015
34. Fragozo-Ramos MC, Cano-Pérez E, Sierra-Merlano RM, Camacho-Chaljub F, Gómez-Camargo D. Clinical, histopathological, and molecular characterization of leprosy in an endemic area of the Colombian Caribbean. Int J Mycobacteriol. 2021;10:155–61.
35. Han XY, Sizer KC, Velarde-Félix JS, Frias-Castro LO, Vargas-Ocampo F. The leprosy agents *Mycobacterium lepromatosis* and *Mycobacterium leprae* in Mexico. Int J Dermatol. 2012;51:952–9. https://doi.org/10.1111/j.1365-4632.2011.05414.x
36. Han XY, Aung FM, Choon SE, Werner B. Analysis of the leprosy agents *Mycobacterium leprae* and *Mycobacterium lepromatosis* in four countries. Am J Clin Pathol. 2014;142:524–32. https://doi.org/10.1309/AJCP1GLCBE5CDZRM
37. Kai M, Fafutis-Morris M, Miyamoto Y, Mukai T, Mayorga-Rodriguez J, Rodriguez-Castellanos MA, et al. Mutations in the drug resistance-determining region of *Mycobacterium lepromatosis* isolated from leprosy patients in Mexico. J Dermatol. 2016;43:1345–9. https://doi.org/10.1111/1346-8138.13483
38. Khan S, Adler BL, Armstrong AW, Lahiri R, Ochoa MT. Impact of *Mycobacterium leprae* and *Mycobacterium lepromatosis* on immune reactions and clinical outcomes in Hansen's disease: a single-center retrospective analysis.

J Am Acad Dermatol. 2023;88:722–4. https://doi.org/10.1016/j.jaad.2022.09.030
39. Torres-Guerrero E, Sánchez-Moreno EC, Atoche-Diéguez CE, Carrillo-Casas EM, Arenas R, Xicohtencatl-Cortes J, et al. Identification of *Mycobacterium leprae* and *Mycobacterium lepromatosis* in formalin-fixed and paraffin-embedded skin samples from Mexico. Ann Dermatol. 2018;30:562–5. https://doi.org/10.5021/ad.2018.30.5.562
40. Vera-Cabrera L, Escalante-Fuentes W, Ocampo-Garza SS, Ocampo-Candiani J, Molina-Torres CA, Avanzi C, et al. *Mycobacterium lepromatosis* infections in Nuevo León, Mexico. J Clin Microbiol. 2015;53:1945–6. https://doi.org/10.1128/JCM.03667-14
41. Yuan Y, Wen Y, You Y, Xing Y, Li H, Weng X, et al. Characterization of *Mycobacterium leprae* genotypes in China—identification of a new polymorphism C251T in the 16S rRNA gene. PLoS One. 2015;10:e0133268. https://doi.org/10.1371/journal.pone.0133268
42. Zhang Y, Sun Y, Wang C, Liu D, Chen M, Fu X, et al. Failure to detect *Mycobacterium lepromatosis* as a cause of leprosy in 85 Chinese patients. Indian J Dermatol Venereol Leprol. 2015;81:499–500. https://doi.org/10.4103/0378-6323.162326
43. Saúl A, Novales J. Lucio-Latapí leprosy and the Lucio phenomenon. Acta Leprol. 1983;1:115–32.
44. Vargas-Ocampo F. Diffuse leprosy of Lucio and Latapí: a histologic study. Lepr Rev. 2007;78:248–60. https://doi.org/10.47276/lr.78.3.248
45. World Health Organization. The Global Health Observatory. Geneva: The Organization; 2022 [cited 2023 Jan 8]. https://www.who.int/data/gho
46. Larrea MR, Carreño MC, Fine PE. Patterns and trends of leprosy in Mexico: 1989-2009. Lepr Rev. 2012;83:184–94. https://doi.org/10.47276/lr.83.2.184
47. Aubry A, Sammarco Rosa P, Chauffour A, Fletcher ML, Cambau E, Avanzi C. Drug resistance in leprosy: an update following 70 years of chemotherapy. Infect Dis Now. 2022;52:243–51. https://doi.org/10.1016/j.idnow.2022.04.001
48. Deps P, Antunes JMAP, Collin SM. Zoonotic risk of Hansen's disease from community contact with wild armadillos: a systematic review and meta-analysis. Zoonoses Public Health. 2021;68:153–64. https://doi.org/10.1111/zph.12783
49. Avanzi C, Del-Pozo J, Benjak A, Stevenson K, Simpson VR, Busso P, et al. Red squirrels in the British Isles are infected with leprosy bacilli. Science. 2016;354:744–7. https://doi.org/10.1126/science.aah3783
50. Deps P, Collin SM. *Mycobacterium lepromatosis* as a second agent of Hansen's disease. Front Microbiol. 2021;12:698588. https://doi.org/10.3389/fmicb.2021.698588

Address for correspondence: Patrícia Deps, Universidade Federal do Espírito Santo, Vitória, Espírito Santo, Brazil; email: patricia.deps@ufes.br

etymologia revisited

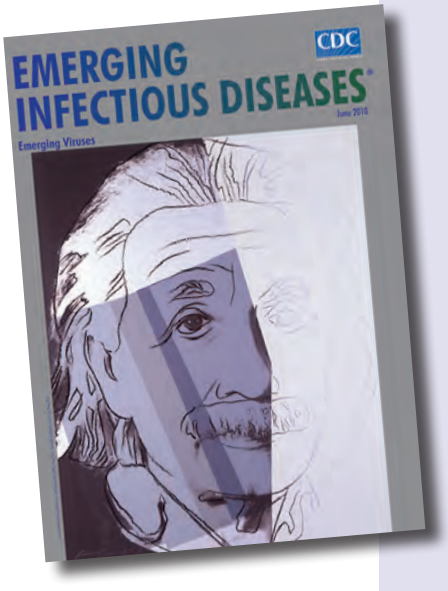

Originally published in June 2010

Lassa Virus

[lah sə] virus

This virus was named after the town of Lassa at the southern end of Lake Chad in northeastern Nigeria, where the first known patient, a nurse in a mission hospital, had lived and worked when she contracted this infection in 1969. The virus was discovered as part of a plan to identify unknown viruses from Africa by collecting serum specimens from patients with fevers of unknown origin. Lassa virus, transmitted by field rats, is endemic in West Africa, where it causes up to 300,000 infections and 5,000 deaths each year.

References:

1 Frame JD, Baldwin JM Jr, Gocke DJ, Troup JM. Lassa fever, a new virus disease of man from West Africa. I. Clinical description and pathological findings. Am J Trop Med Hyg. 1970;19:670–6
2. Mahy BW. The dictionary of virology, 4th ed. Burlington (MA): Elsevier; 2009.

https://wwwnc.cdc.gov/eid/article/16/6/et-1606_article

Sensitivity to Neutralizing Antibodies and Resistance to Type I Interferons in SARS-CoV-2 R.1 Lineage Variants, Canada

Rajesh Abraham Jacob, Ali Zhang,[1] Hannah O. Ajoge,[1] Michael R. D'Agostino,[1] Kuganya Nirmalarajah, Altynay Shigayeva, Wael L. Demian, Sheridan J.C. Baker, Hooman Derakhshani, Laura Rossi, Jalees A. Nasir, Emily M. Panousis, Ahmed N. Draia, Christie Vermeiren, Jodi Gilchrist, Nicole Smieja, David Bulir, Marek Smieja, Michael G. Surette, Andrew G. McArthur, Allison J. McGeer, Samira Mubareka, Arinjay Banerjee, Matthew S. Miller, Karen Mossman

Isolating and characterizing emerging SARS-CoV-2 variants is key to understanding virus pathogenesis. In this study, we isolated samples of the SARS-CoV-2 R.1 lineage, categorized as a variant under monitoring by the World Health Organization, and evaluated their sensitivity to neutralizing antibodies and type I interferons. We used convalescent serum samples from persons in Canada infected either with ancestral virus (wave 1) or the B.1.1.7 (Alpha) variant of concern (wave 3) for testing neutralization sensitivity. The R.1 isolates were potently neutralized by both the wave 1 and wave 3 convalescent serum samples, unlike the B.1.351 (Beta) variant of concern. Of note, the R.1 variant was significantly more resistant to type I interferons (IFN-α/β) than was the ancestral isolate. Our study demonstrates that the R.1 variant retained sensitivity to neutralizing antibodies but evolved resistance to type I interferons. This critical driving force will influence the trajectory of the pandemic.

SARS-CoV-2 continues to evolve and generate new variants. Since the beginning of the COVID-19 pandemic, Canada has encountered 8 waves of infections. Although the first 2 waves were dominated by ancestral viruses, each subsequent wave had a surge in escape variants (*1*,*2*). Mutations in the SARS-CoV-2 genome and within the spike glycoprotein alter the transmission dynamics, severity of disease, and sensitivity to neutralizing antibodies for each new variant (*3*). Thus, continuously isolating and characterizing emerging SARS-CoV-2 variants is critical for developing updated vaccines and drug regimens.

We isolated SARS-CoV-2 R.1 lineage variants from an outbreak in persons facing housing insecurity in Hamilton, Ontario, Canada. In Canada, the circulation of R.1 lineage variants corresponded with the third wave of the pandemic and was preceded by previously circulating variants of concern (VoC), B.1.1.7 (Alpha) and B.1.351 (Beta). Globally, the R.1 lineage began to increase in frequency in December 2020, peaked in April 2021, became rare by June 2021, and was last reported in December 2021 (*4*). In April 2021, the World Health Organization positioned R.1 lineage variants under the variant under monitoring (VuM) category to prioritize monitoring the variants because of distinct mutations in their genome. Most infections with R.1 variants have been reported in Japan and the United States (*5*,*6*). In Canada, 66 R.1 lineage sequences were recorded, according to GISAID (https://www.gisaid.org), during December 2020–

Author affiliations: McMaster University, Hamilton, Ontario, Canada (R.A. Jacob, A. Zhang, H.O. Ajoge, M.R. D'Agostino, W.L. Demian, S.J.C. Baker, L. Rossi, J.A. Nasir, E.M. Panousis, A.N. Draia, D. Bulir, M. Smieja, M.G. Surette, A.G. McArthur, M.S. Miller, K. Mossman); Sunnybrook Research Institute, Toronto, Ontario, Canada (K. Nirmalarajah, S. Mubareka); University of Toronto, Toronto (A. Shigayeva, C. Vermeiren, A.J. McGeer, S. Mubareka, A. Banerjee); University of Manitoba, Winnipeg, Manitoba, Canada (H. Derakhshani); Research Institute of St. Joe's Hamilton, Hamilton (J. Gilchrist, N. Smieja, D. Bulir); Vaccine and Infectious Disease Organization, Saskatoon, Saskatchewan, Canada (A. Banerjee); University of Saskatchewan, Saskatoon (A. Banerjee); University of Waterloo, Waterloo, Ontario, Canada (A. Banerjee); University of British Columbia, Vancouver, British Columbia, Canada (A. Banerjee)

DOI: https://doi.org/10.3201/eid2907.230198

[1]These authors contributed equally to this article.

November 2021 (*4*). Of those, 63 originated from Ontario, 1 each originated from Quebec and British Columbia, and 1 originated from an unknown province or territory. However, data on the immune-evasive properties of this lineage variant are limited.

The type I interferon (IFN) response constitutes the first line of defense against many viruses (*5*,*6*), triggering activation of several IFN-stimulated genes (ISGs) and establishing an antiviral state (*5*). SARS-CoV-2 proteins are involved in IFN evasion either by directly suppressing production or by acting downstream of the host response machinery (*6*,*7*). A recent study compared multiple type I IFNs against diverse SARS-CoV-2 VoC, demonstrating increased IFN resistance (*8*). Furthermore, SARS-CoV-2–infected persons with genetic defects in IFN signaling are at higher risk for severe COVID-19 (*9*). Taken together, characterizing IFN-resistant SARS-CoV-2 variants is critical, given their potential to enhance transmission kinetics and result in viral evolution. Therefore, we evaluated the sensitivity of SARS-CoV-2 R.1 lineage isolates from patients in Canada to neutralizing antibodies and type I interferons.

Methods

Cells and Viruses

Vero E6 cells and Calu-3 cells were cultured in complete media (Appendix, https://wwwnc.cdc.gov/EID/article/29/7/23-0198-App1.pdf). We isolated and purified study isolate SB3 as described previously (*10*) and isolated the R.1 lineage variant from patient nasopharyngeal swab samples (Appendix). We obtained the B.1.351 (Beta) VoC isolate from BEI Resources (https://www.beiresources.org).

Human Donors

We obtained informed consent for the collection of convalescent serum samples from 39 patients with quantitative reverse transcription PCR (qRT-PCR)–confirmed SARS-CoV-2 infection (Appendix). This study was approved by the institutional review board for Sunnybrook Research Institute (approval no. 2218) and Sinai Health System (approval nos. 02-0118-U and 05-0016-C).

SARS-CoV-2 Sequencing and Phylogenetic Tree

We performed sequencing of SARS-CoV-2 genomes from RNA extracts and subsequent bioinformatics analysis following the steps detailed in Kotwa et al. (*11*) (Appendix). We constructed a maximum-likelihood phylogenetic tree using a dataset of study sequences (R.1 645, R.1 646, and SB3), Los Alamos National Laboratories full-length variant reference alignment from GISAID (*12*), and randomly sampled Alpha, Beta, and Gamma variant sequences (Appendix).

Detection of SARS-CoV-2–Specific Binding Antibodies and Neutralization Assay

We determined the IgG targeting the receptor-binding domain (RBD) and spike S1 region by using ELISA (BioLegend, https://www.biolegend.com) (Appendix). We performed neutralization assays by incubating serially diluted serum samples (heat inactivated) with SARS-CoV-2 (15,000, 1,500, or 150 PFU/well) at 37°C for 1 h before adding them to preplated Vero E6 cells. Five days after infection, we quantified luminescence with CellTiter-Glo 2.0 Reagent (Promega, https://www.promega.com) by using a BioTek Synergy H1 microplate reader (Appendix).

Molecular Detection of SARS-CoV-2 $N_{501}Y$ Mutation

Diagnostic nasopharyngeal or midturbinate swab specimens were collected from patients for SARS-CoV-2 testing and $N_{501}Y$ screening at Shared Hospital Laboratory (Toronto, Canada). We performed RNA extraction and qRT-PCR to detect SARS-CoV-2 as previously described (*13*) (Appendix).

Interferon Treatment and Quantitative PCR

Calu-3 cells were either mock-infected or SARS-CoV-2–infected (1 h exposure, 50,000 PFU/well), washed twice with sterile 1× phosphate-buffered serum, and treated with 1 ng/mL or 10 ng/mL of recombinant IFN-α (Sigma-Aldrich, https://www.sigmaaldrich.com) or IFNβ (PeproTech, https://www.peprotech.com). We quantified SARS-CoV-2 RNA and ISGs 72 h postinfection by using qRT-PCR (Appendix).

Viability Assay, Microscopy, and Statistical Analysis

We assessed cell viability of SARS-CoV-2–infected Calu-3 cells by using CellTiter-Glo 2.0 Reagent (Promega) (Appendix) and imaged SARS-CoV-2–infected Calu-3 cells for cytopathic elects using an EVOS M5000 microscope (ThermoFisher Scientific, https://www.thermofisher.com) with the 10× objective. We performed all statistical analyses by using GraphPad Prism (https://www.graphpad.com) (Appendix).

Results

R.1 Lineage Variant Virus Isolation and Lineage Determination

We isolated 2 SARS-CoV-2 isolates belonging to the R.1 lineage (R.1 645, R.1 646) from 2 patients from Hamilton, Ontario, Canada, in March 2021, corresponding to the third wave of the COVID-19

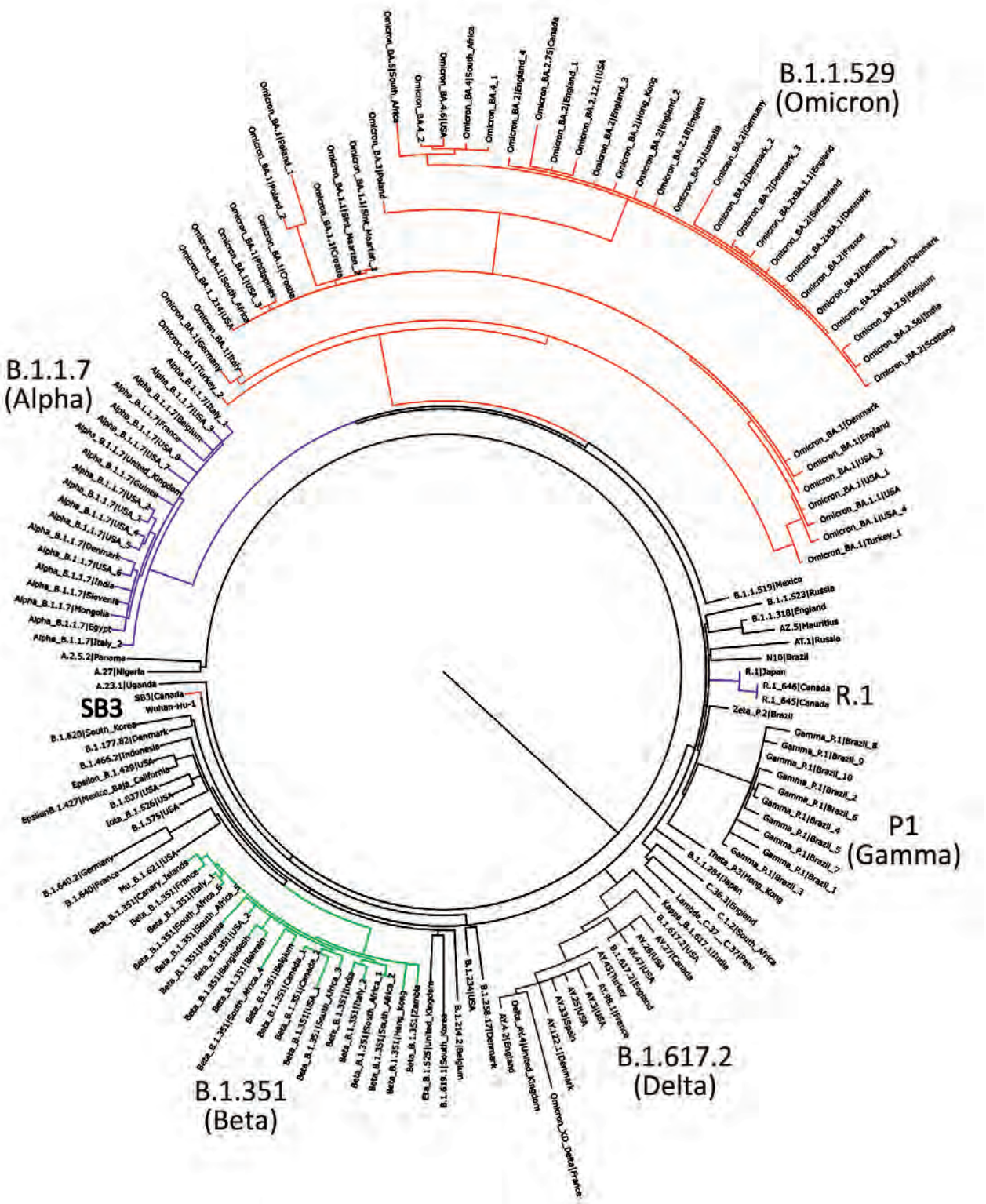

Figure 1. Phylogenetic confirmation that SARS-CoV-2 isolates belong to R.1 lineage in study of sensitivity to neutralizing antibodies and resistance to type I interferons in SARS-CoV-2 R.1 lineage variants, Canada. Tree constructed by using maximum-likelihood estimations by executing 1,000 rapid bootstrap inferences and a thorough search with the general time reversible model of nucleotide substitution. Blue indicates R1 isolates (R.1 645, R.1 646) and red SB3 isolate. Variants are highlighted in magenta (Alpha), green (Beta), brown (Delta), mocha (Gamma), and orange (Omicron). The tree was visualized using FigTree version 1.4.2 (http://tree.bio.ed.ac.uk/software/figtree).

pandemic in Canada. The 2 R.1 isolates were purified from nasopharyngeal samples from SARS-CoV-2–specific qRT-PCR–positive persons by using Vero clone E6 cells as described previously (*10*). We determined the viral whole-genome sequences and deposited them into GISAID (accession nos. EPI_ISL_16641180 and EPI_ISL_16641181). We performed phylogenetic analysis to confirm clustering with the R.1 lineage. The R.1 isolates clustered on their own distinctly from B.1.1.7 (Alpha), B.1.351 (Beta), B.1.617.2 (Delta), P.1 (Gamma), and B.1.1.529 (Omicron) variants (Figure 1). Sequencing of both R.1 isolates revealed multiple mutations in spike ($W_{152}L$, $S_{255}F$, $E_{484}K$, $D_{614}G$, $G_{769}V$), nonstructural protein (NSP) 2 ($P_{129}L$, $A_{247}V$), NSP3 ($S_{1656}A$), NSP12 ($P_{323}L$), NSP13 ($G_{439}R$, $P_{323}L$), NSP14 ($P_{412}H$), ORF3a ($R_{134}H$), membrane ($F_{28}L$), and the nucleocapsid ($S_{187}L$, $R_{203}K$, $G_{204}R$, $Q_{418}H$) regions critical to immune evasion (*14*).

Wave 1 and Wave 3 Serum Samples

We next characterized the R.1 isolates to identify potential effects on the epidemiology of COVID-19. We assessed the susceptibility of R.1 isolates to neutralizing antibodies after SARS-CoV-2 infection in a cohort of patients who had recovered from laboratory-confirmed COVID-19 by collecting convalescent serum samples from 39 unvaccinated donors during the first (n = 26) and third (n = 13) waves of the pandemic in Canada. The cohort consisted of 20 men and 19 women with a median age of 58. Wave 1 consisted of 13 men and 13 women with a median age of 63. Wave 3 consisted of 7 men and 6 women with a median age of 53. Samples were collected a median of 42 days after the first qRT-PCR–positive test. Most patients were symptomatic and more than one third were hospitalized; a subset of hospitalized patients was admitted to the intensive care unit (Table 1).

Wave 1 (March–June 2020) was dominated by infection with the SARS-CoV-2 ancestral strain, whereas wave 3 (March–May 2021) was dominated by infection with the B.1.1.7 (Alpha) VoC (*2*,*15*). A key amino acid change in the RBD of the B.1.1.7 (Alpha) VoC was the $N_{501}Y$ substitution (*16*). We initially used qRT-PCR screening to confirm the presence of the $N_{501}Y$ mutation in the 13 clinical samples from wave 3 patients. The $N_{501}Y$ substitution enhances the affinity of RBD to the angiotensin-converting enzyme 2 receptor (*17*,*18*) and is present in the B.1.1.7 (Alpha), B.1.351 (Beta), P.1 (Gamma), and B.1.1.529 (Omicron) lineages but not in the R.1 lineage variants (*19*–*21*). Whole-genome sequencing confirmed that the wave 3 variant with the $N_{501}Y$ substitution belonged to the B.1.1.7 (Alpha) VoC. For this investigation, we elicited antibodies from wave 1 serum samples (n = 26) by infection with viruses harboring the ancestral SARS-CoV-2 spike, whereas we elicited antibodies from wave 3 serum samples (n = 13) by viruses harboring the B.1.1.7 (Alpha) VoC spike.

Determination of SARS-CoV-2 Spike- and RBD-Binding Antibodies

Initially, we determined the binding ability of waves 1 and 3 serum samples to SARS-CoV-2 ancestral antigens using ELISA. We detected binding antibodies targeting the SARS-CoV-2 spike (S1 subunit) and RBD. Plates coated with either the ancestral S1 or the ancestral RBD were used to detect binding IgG. Antibodies from waves 1 and 3 serum samples bound the ancestral S1 and ancestral RBD (Figure 2, panels A, B). IgG levels from wave 1 serum samples were comparable

Table 1. Clinical summary of patients from study of sensitivity to neutralizing antibodies and resistance to type I interferons in SARS-CoV-2 R.1 lineage variants, Canada*

Characteristic	Value
Total no. samples	39
No. samples, wave 1	26
No. samples, wave 3	13
Median age, total (IQR)	58 (46–68)
Median age, wave 1 (IQR)	63 (55–71)
Median age, wave 3 (IQR)	53 (33–56)
Sex, total	
M	20
F	19
Sex, wave 1	
M	13
F	13
Sex, wave 3	
M	7
F	6
Median no. days to sampling from first COVID-19 positive test (IQR)	42 (25–71)
Hospital admission	14 (36)
Median days from symptom onset to admission (IQR)	6 (2–10)
Symptoms	
Asymptomatic	1 (2)
Fever	17 (43)
Cough	19 (54)
Shortness of breath	8 (20)
Comorbidities	
Diabetes	9 (23)
Cardiac illnesses	4 (10)
Vascular illnesses	13 (33)
Pulmonary illnesses	3 (8)
Renal illnesses	2 (5)
Neuromuscular illnesses	0 (0)
Liver illnesses	0 (0)
Gastrointestinal illnesses	0 (0)
Cancer conditions	3 (7)
Rheumatologic illnesses	1 (2)
Mental health diagnosis	3 (7)
Immunocompromised	0 (0)
ICU admission	4 (10)
Intubation	2 (5)

*Values are no. (%) except as indicated. ICU, intensive care unit; IQR, interquartile range.

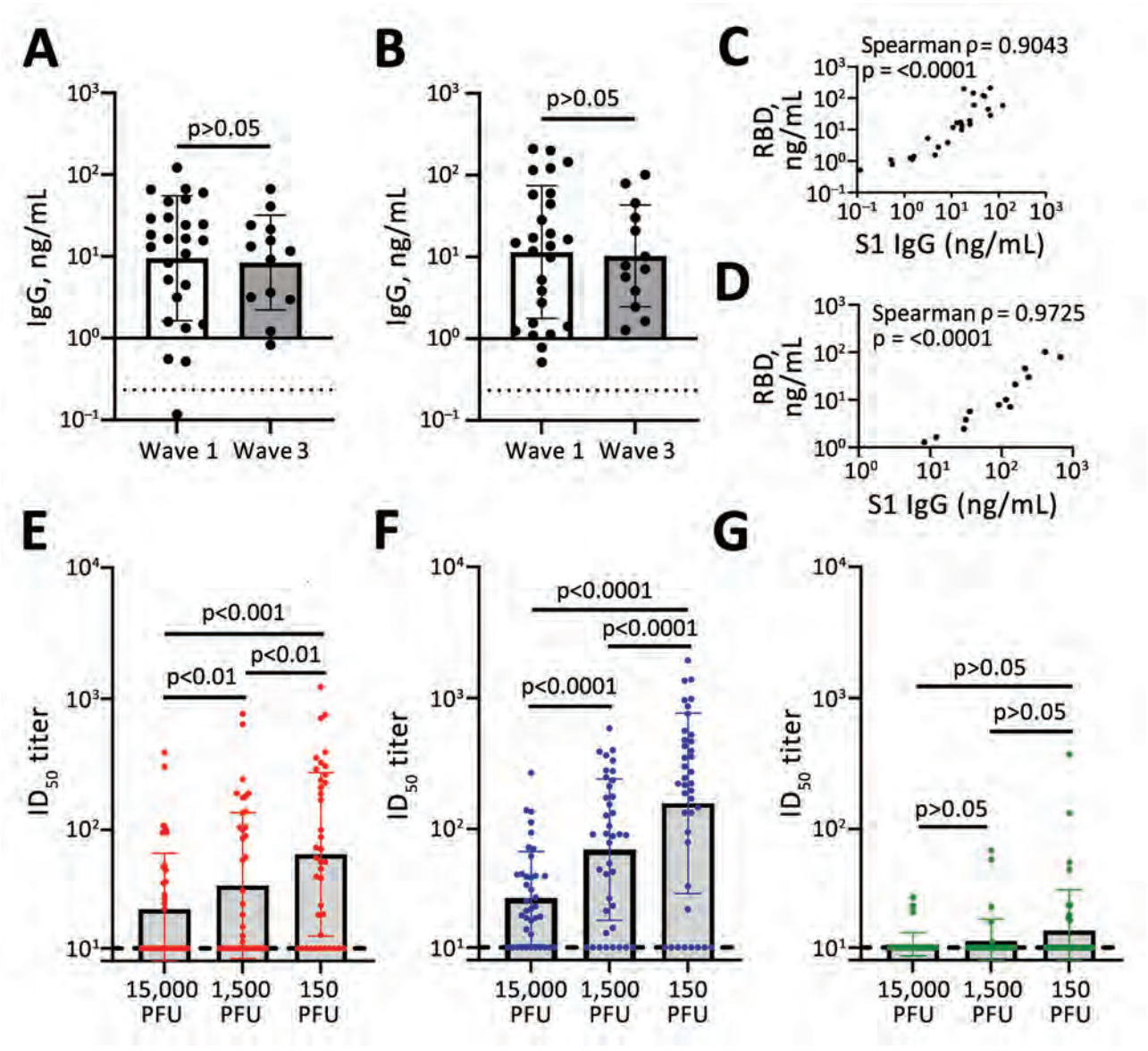

Figure 2. Antibody detection in study of sensitivity to neutralizing antibodies and resistance to type I interferons in SARS-CoV-2 R.1 lineage variants, Canada. A, B) S1 (A) and RBD (b) binding IgG determined by using a sandwich ELISA format. Dashed line indicates the limit of detection. C, D) Correlation between S1 and RBD binding IgG for wave 1 (C) and wave 3 (D). E–G) ID50 titers for SB3 (E), R.1 645 (F), and B.1.351 (Beta) VoC (E). Error bars in panels A, B and E–G indicate SD. Statistical significance was calculated by using an unpaired t test for panels A and B and by using 1-way analysis of variance with Tukey multiple comparisons test for panels E–G. ID_{50}, 50% inhibitory dilution; PFU, plaque-forming units; RBD, receptor-binding domain; S1, spike.

to wave 3 serum samples for both the S1 (geometric mean 9.51 vs. 8.42 ng/mL) and the RBD (geometric mean 11.47 vs. 10.30 ng/mL) (Figure 2, panels A and B). This observation indicates that binding antibodies generated by the B.1.1.7 (Alpha) VoC in wave 3 were cross-reactive with the ancestral S1 and ancestral RBD.

Next, we investigated the correlation between S1-targeting IgG and the RBD-targeting IgG. The S1 and the RBD targeting IgG correlated well; for both wave 1 (Spearman ρ = 0.9043; p<0.0001) and wave 3 serum samples (Spearman ρ = 0.9725; p<0.0001) (Figure 2, panels C. D). This correlation indicates that for both wave 1 and wave 3 serum samples, the ancestral S1 and RBD antigens were equally available for binding.

Neutralization of SB3, R.1 645, and B.1.351 (Beta) VoC

Next, we assessed the antibody function by using a neutralization assay for the entire cohort. We compared the neutralization sensitivity of the R.1 isolates with SB3 and B.1.351 (Beta) VoC. Live SARS-CoV-2

isolates were used for the neutralization assay. SB3 is an ancestral isolate purified from a SARS-CoV-2–infected patient in early 2020 from Toronto, Canada (*10*). B.1.351 is a highly neutralization-resistant isolate that was first detected in late 2020 from Eastern Cape, South Africa (*22*). B.1.351 has extensive mutations in the spike region ($L_{18}F$, $D_{80}A$, $D_{215}G$, $\Delta_{242-244}$, $K_{417}N$, $E_{484}K$, $N_{501}Y$, $D_{614}G$, and $A_{701}V$), conferring resistance to antibodies from both convalescent and vaccinated persons (*22*–*26*).

To establish a robust readout for neutralization, we tested 3 different plaque-forming unit (PFU) levels (15,000, 1,500, and 150) per well for all 3 isolates (SB3, R.1 645, and B.1.351 [Beta] VoC). We generated neutralization profiles for SB3 (Appendix Figure 1, panels A–C), R.1 645 (Appendix Figure 1, panels D–F), and B.1.351 (Appendix Figure 1, panels G–I) and derived 50% inhibitory dilution (ID_{50}) values. For SB3, we observed a significant difference in ID_{50} between the 3 different PFUs tested; 150 PFU/well was the most neutralization sensitive and 15,000 PFU/well the most resistant (Figure 2, panel E). The geometric means of ID_{50} titers were 24.9 for 15,000 PFU/well, 37.7 for 1,500 PFU/well, and 65.2 for the 150 PFU/well (Figure 2, panel E). As for SB3, the geometric mean of R.1 645 ID_{50} titers increased from 29.7 for 15,000 PFU/well to 69.6 for 1,500 PFU/well and 156.9 for 150 PFU/well (Figure 2, panel F). However, for B.1.351, we noticed no significant difference among the 3 PFUs tested. The geometric mean of ID_{50} titers remained very low: 13.2 for 15,000 PFU/well, 14.0 for 1,500 PFU/well, and 16.9 for 150 PFU/well (Figure 2, panel G), corroborating previous data that B.1.351 is highly resistant to neutralization (*23*–*25*). This neutralization profile shows that the serum samples have diverse neutralizing abilities; titers significantly increased as the number of viral particles decreased for SB3 and R.1 645 but not for the highly resistant B.1.351.

Sensitivity of R.1 645 and R.1 646 to Neutralizing Antibodies

Next, we determined whether the 2 R.1 isolates (R.1 645, R.1 646) had similar sensitivity to neutralizing antibodies by screening a subset of the serum samples (n = 19 from wave 1 and 3) on R.1 646 (Appendix Figure 2, panels A–C). The Spearman rank correlation coefficient (ρ) values remained high for 15,000 (Spearman $\rho = 0.8333$; $p<0.0001$), 1,500 (Spearman $\rho = 0.9262$; $p<0.0001$), and 150 (Spearman $\rho = 0.8677$; $p<0.0001$) PFU/well (Appendix Figure 2, panels D–F), indicating that the R.1 isolates were similarly neutralized by the serum samples.

Binding IgG as a Prediction of SARS-CoV-2 Neutralization

We next assessed whether binding antibodies are predictive of SARS-CoV-2 neutralization. We used a linear regression model to predict whether the RBD and spike (S1) targeting IgG could neutralize SB3, R.1 645, and B.1.351 (Beta) VoC, using only the 150 PFU/well condition because it had the highest neutralization titers. RBD-binding IgG were a weak predictor of SB3 ($R^2 = 0.3819$; $p<0.0001$) and R.1 645 ($R^2 = 0.2225$; $p = 0.0024$) neutralization, but we noted no significance for B.1.351 (Beta) VoC ($R^2 = 0.05892$; $p>0.05$) (Appendix Figure 3, panel A). In contrast to RBD, the neutralization prediction was moderately improved for S1-binding IgG for SB3 ($R^2 = 0.5148$; $p<0.0001$) and R.1 645 ($R^2 = 0.6025$; $p<0.0001$) but weak for B.1.351 ($R^2 = 0.1308$; $p<0.0001$) (Appendix Figure 3, panel B). Those data suggest that S1-targeting antibodies outside the RBD are markedly involved in neutralization.

Neutralization of R.1 Isolate by Wave 1 Serum Samples

Next, we determined whether the R.1 isolate (R.1645) that emerged during wave 3 was sensitive to neutralizing antibodies elicited by the ancestral virus from wave 1. To test this possibility, we compared the neutralization susceptibility of R.1 645 with SB3 and B.1.351 (Beta) VoC. We observed no significant difference in the ID_{50} titers between SB3 and R.1 645 at higher PFUs (15,000 and 1,500) (Figure 3, panels A, B). However, R.1 645 was significantly more sensitive than SB3 at 150 PFU/well; we noted a 1.6-fold increase in the geometric mean of the ID_{50} titers (Figure 3, panel C). Furthermore, R.1 645 was significantly more sensitive than B.1.351 at all 3 PFUs tested (Figure 3, panels A–C). A 2.2-fold, 4.5-fold, and 8.2-fold increase in the geometric mean of ID_{50} titers was noted for R.1 645 in comparison to B.1.351 (Figure 3, panels A–C). SB3 also remained significantly more sensitive than B.1.351 at lower PFUs (3.3-fold increase in geometric mean of ID_{50} titers at 1,500 PFU/well and 5-fold increase at 150 PFU/well) (Figure 3, panels B, C). This observation indicates that the R.1 isolate, despite having spike mutations, remains sensitive to antibodies from wave 1 serum samples (Table 2).

Neutralization of R.1 Isolate by Wave 3 Serum Samples

Subsequently, we analyzed whether the antibodies elicited by the B.1.1.7 (Alpha) VoC during wave 3 of the pandemic can neutralize the R.1 isolate. A significant increase in the ID_{50} titers was notable between SB3 and R.1 645 at all the PFUs tested (Figure 3, panels D–F). We noted 1.6-fold, 3.5-fold, and 5.1-fold increases in the geometric mean of the ID_{50} titers for R.1 645 in

Table 2. Summary of neutralization of SARS-CoV-2 isolates from study of sensitivity to neutralizing antibodies and resistance to type I interferons in SARS-CoV-2 R.1 lineage variants, Canada

SARS-CoV-2 isolates	Sensitive isolate	Adjusted p value
Wave 1: 15,000 PFU		
SB3 vs. R.1 645	NA	NS
SB3 vs. B.1.351	NA	NS
R.1 645 vs. B.1.351	R.1645	0.0186
Wave 1: 1,500 PFU		
SB3 vs. R.1 645	NA	NS
SB3 vs. B.1.351	SB3	0.0243
R.1 645 vs. B.1.351	R.1 645	0.0011
Wave 1: 150 PFU		
SB3 vs. R.1 645	R.1 645	0.0141
SB3 vs. B.1.351	SB3	0.0066
R.1 645 vs. B.1.351	R.1 645	0.0022
Wave 3: 15,000 PFU		
SB3 vs. R.1 645	R.1 645	0.0391
SB3 vs. B.1.351	NA	NS
R.1 645 vs. B.1.351	R.1 645	0.0385
Wave 3: 1,500 PFU		
SB3 vs. R.1 645	R.1 645	0.0079
SB3 vs. B.1.351	NA	NS
R.1 645 vs. B.1.351	R.1 645	0.0093
Wave 3: 150 PFU		
SB3 vs. R.1 645	R.1 645	0.0038
SB3 vs. B.1.351	NA	NS
R.1 645 vs. B.1.351	R.1 645	0.0053

*NA, not applicable; NS, not significant; PFU, plaque-forming units.

comparison to SB3. This observation indicates that the antibodies triggered by the B.1.1.7 (Alpha) VoC could neutralize R.1 645 better than SB3. Neutralization titers of R.1 645 also remained high compared with B.1.351 (Beta) VoC, indicating that B.1.351 is significantly resistant to wave 3 serum samples (Figure 3, panels D–F). We noted 2.3-fold, 6.1-fold, and 11.9-fold increases in the geometric mean of ID_{50} titers for R.1 645 in comparison to B.1.351 (Figure 3, panels D–F). However, unlike wave 1 serum samples, we noted no significant difference in the ID_{50} titers between SB3 and B.1.351 for wave 3 serum samples (Figure 3, panels D–F). Those data indicate that the antibody repertoire evolved over time resulting in a substantial loss of neutralization breadth to the ancestral isolate. Of note, the antibody repertoire that evolved in response to the B.1.1.7 (Alpha) VoC during wave 3 could still neutralize the R.1 645 isolate (Table 2).

Sensitivity of R.1 Isolates to Type I Interferons

Next, we investigated the sensitivity of R.1 isolates to type I IFNs. We infected Calu-3 cells with SB3 or one of the 2 R.1 isolates. One hour after absorption, we treated cells with IFN-α or IFN-β (1 ng/mL or 10 ng/mL) for 72 hours. We monitored SARS-CoV-2 RNA levels by using qRT-PCR after isolating total RNA from infected Calu-3 cells to determine the amounts of virus produced 72 hours after infection. As expected, we observed a drop in virus replication with recombinant IFN-α and IFN-β treatment (at both 1 ng/mL and 10 ng/mL concentration) (Figure 4, panels A, B). The R.1 isolates were significantly more resistant to both IFN-α and IFN-β than were SB3 (Figure 4, panels A, B). We observed no significant difference in SARS-CoV-2 RNA levels in the untreated controls. This finding indicates that R.1 isolate resistance to type I IFNs is not caused by differences in the level of incoming virus or inherent replication capacity.

We have previously shown that SARS-CoV-2 is a poor inducer of type I IFN and ISGs (*27*), and others have shown that SARS-CoV-2 can evade the type I IFN machinery (*28*,*29*). Because our R.1 isolates were significantly more resistant to type I IFNs, we examined differences in the expression of 2 ISGs: interferon-induced protein with tetratricopeptide repeats (IFIT1) and interferon regulatory factor 7 (IRF7). We compared the ability of the R.1 isolates to block IFIT1 and IRF7 production in response to IFN to that of SB3. We noted a dose-responsive increase in the transcript levels of *IFIT1* and *IRF7* for both IFN-α– and IFN-β–treated conditions in mock-infected cells (Figure 4, panels C–F). In the presence of SARS-CoV-2, we noted significant suppression of the IFN-α– and IFN-β–mediated activation of *IFIT1* and *IRF7* (Figure 4, panels C–F).). However, we did not observe a significant difference in *IFIT1* or *IRF7* transcript levels between SB3 and the 2 R.1 isolates. We performed a viability assay to confirm that the difference in ISG signal is not caused by SARS-CoV-2–induced cell death (Appendix Figure 4, panels A, B). The absence of SARS-CoV-2–induced

cytopathic effect corroborates our viability data (Appendix Figure 5, panels A, B) and is consistent with other studies (*30*,*31*). This observation implies that the resistance of the R.1 isolates to type-I IFNs is not inherently dependent on ISG modulation.

Discussion

We demonstrate that R.1 isolates are sensitive to neutralizing antibodies induced after natural SARS-CoV-2 infection (Figure 3). These results are encouraging and add to our understanding of the sensitivity of VuMs to neutralizing antibodies. We further demonstrate that the R.1 lineage isolates, in contrast to the B.1.351 (Beta) VoC, retain neutralization sensitivity to antibodies generated early and later during the pandemic (Figure 3). Using a pseudovirus-based neutralization assay, a recent study demonstrated that mutations in R.1 lineage drive resistance to neutralizing antibodies compared with the wild type (*32*). Although a good correlation was observed between pseudovirus and live virus assay for antibody neutralization (*33*), a live virus assay more accurately represents spike protein density, epitope exposure, and replication kinetics of SARS-CoV-2. We observed a significant evolution in the breadth of neutralization with wave 3 antibodies, which resulted in a higher neutralization of R.1 isolates compared with the

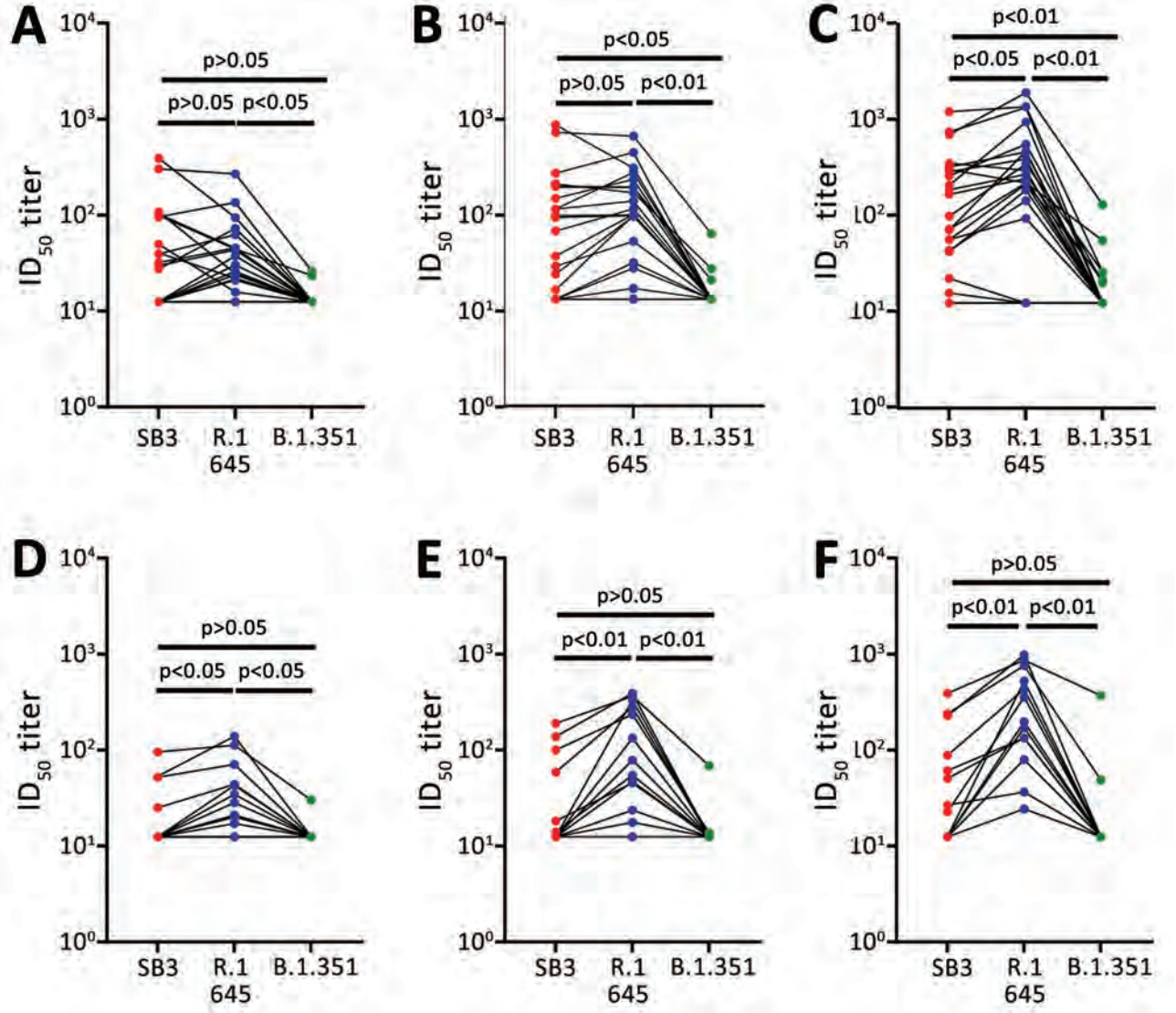

Figure 3. Sensitivity of SARS-CoV-2 lineage variants to neutralizing antibodies, Canada. A–C) Sensitivity of SB3, R.1 645, and B.1.351 (Beta) variants to neutralizing antibodies from patients infected with the ancestral virus (wave 1 samples). D–F) Sensitivity of SB3, R.1 645, and B.1.351 (Beta) VoC to neutralizing antibodies from patients infected with the B.1.1.7 (Alpha) VoC (wave 3 samples). For each isolate, we tested 3 different PFU per well: 15,000 (A, D), 1,500 (B, E), and 150 (C, F). Statistical significance was calculated using 1-way analysis of variance with Tukey multiple comparisons test. ID_{50}, 50% inhibitory dilution; PFU, plaque-forming units.

ancestral isolate (Figure 3, panels D–F). Of the 5 mutations in the spike region of our R.1 isolates, 3 are unique and not found in the B.1.351 (Beta) VoC. These include $W_{152}L$ and $S_{255}F$ substitutions in the N terminal domain of the S1 spike region and the $G_{769}V$ substitution in the S2 domain. A report that investigated key SARS-CoV-2 spike substitutions demonstrated that $W_{152}L$ alone does not confer neutralization resistance (*34*).

We established that the continuum of antibody-mediated neutralization is dependent on the virus

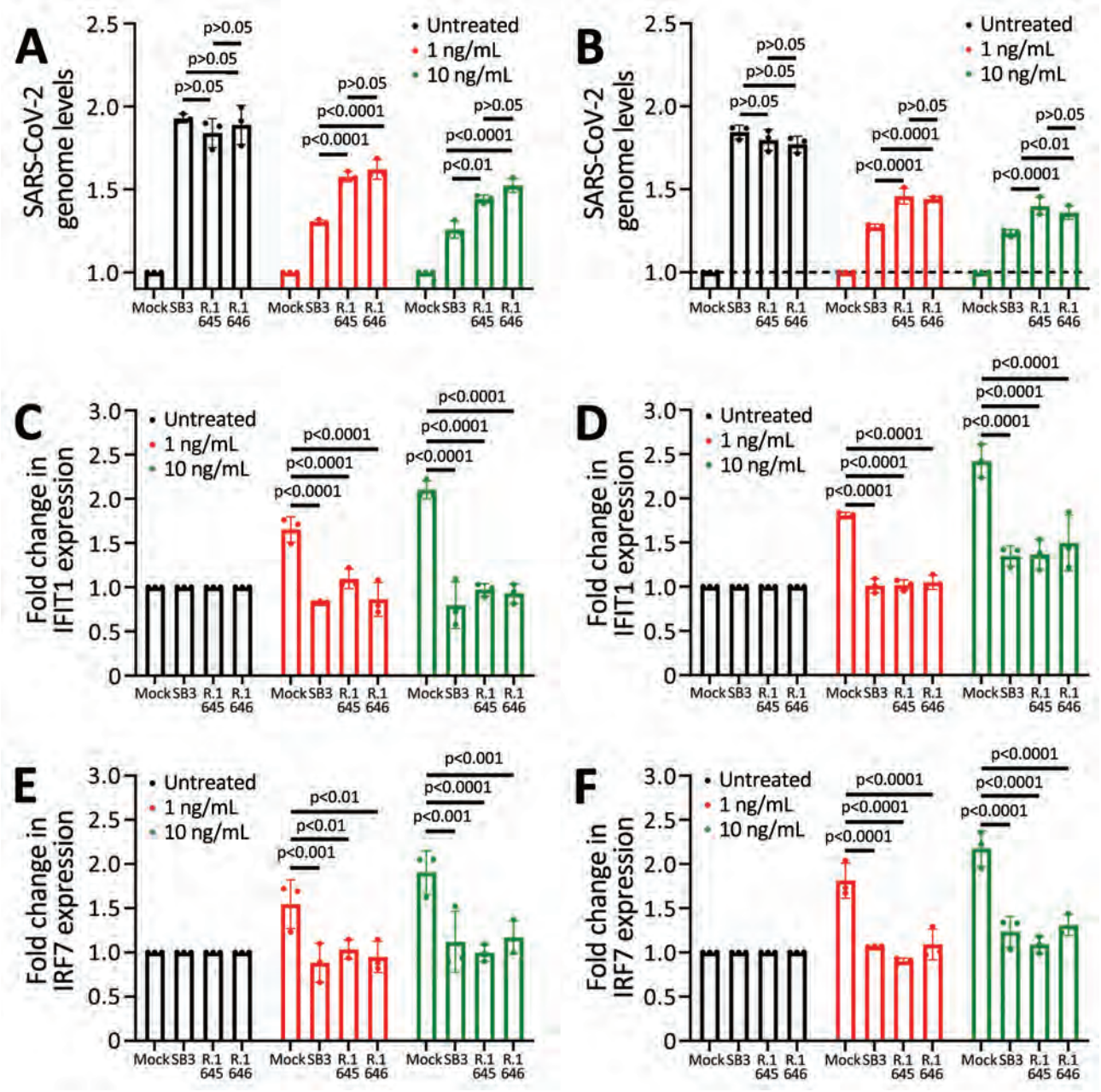

Figure 4. Resistance to type I interferons in SARS-CoV-2 R.1 lineage variants, Canada. A) Sensitivity of SB3, R.1 645, and R.1 646 to IFN-α. B) Sensitivity of SB3, R.1 645, and R.1 646 to IFN-β. C, D) Fold change in *IFIT1* transcript levels in response to IFN-α (C) or IFN-β (D) treatment. E, F) Fold change in *IRF7* transcript levels in response to IFN-α (E) or IFN-β treatment (F). ISG transcript levels were normalized to *GAPDH* transcript levels. For testing, Calu-3 cells were either mock-infected or infected with SARS-CoV-2 (50,000 PFU/well) for 1 hour followed by treatment with recombinant IFN (1 or 10 ng/mL). Total RNA was extracted after 72 hours and SARS-CoV-2 RNA levels were determined using quantitative reverse transcription PCR. 1/ΔCT values are represented after normalizing to mock-infected cells. Statistical significance was calculated using 2-way analysis of variance with Tukey multiple comparisons test. GAPDH, glyceraldehyde 3-phosphate dehydrogenase; IFIT1, interferon-induced protein with tetratricopeptide repeats; IFN, interferon; IRF7, interferon regulatory factor 7; ISG, IFN-stimulated gene.

inoculum (Figure 2, panels E, F) and that different levels of virus inoculum are neutralized differentially for SB3 and R.1 645. A significant drop in the ID_{50} titers was observed as we exponentially increased the number of SARS-CoV-2 particles. Those data imply that the threshold of neutralizing antibody titers necessary for protection is dependent on the exposure dose of virus particles. This finding indicates that a potent humoral response is critical for SARS-CoV-2 protection in vaccinated or naturally infected persons.

Our data show resistance of SARS-CoV-2 variants to type I IFNs, which in turn can influence viral evolution. An increased IFN resistance in SARS-CoV-2 was reported recently (*8*). Our R.1 isolates were significantly resistant to both IFNα and IFNβ treatment within lung epithelial cells (Figure 4, panels A, B). However, whether mutations accumulated in ORF1ab, ORF3, M, and N regions are causing the observed IFN resistance is unclear; this question will be vital in future studies. IFN resistance of R.1 isolates can potentially lead to higher viral loads, thereby accelerating virus shedding and transmission. Although the World Health Organization recategorized R.1 lineage isolates as formerly monitored variants in November 2021, data are limited on the transmission potential and disease severity of the formerly monitored variants. Our finding that R.1 lineage isolates are neutralization sensitive but concurrently IFN resistant indicates that IFN resistance will be a strong driving force in the generation of new variants. Overall, data from this study further advance our knowledge of how virus evolution can influence the trajectory and characteristics of a pandemic.

This work was supported by a COVID-19 response grant to K.M. from the Canadian Institutes of Health Research (CIHR), with sequencing efforts additionally supported by Genome Canada CanCOGeN funding to A.G.M. M.S.M. is supported by a tier 2 Canada Research Chair in Viral Pandemics, a CIHR COVID-19 rapid response grant, a CIHR new investigator award, and an Ontario early researcher award. A.G.M. holds McMaster's inaugural David Braley Chair in Computational Biology, generously supported by the family of the late David Braley. J.A.N. was supported by a Fred and Helen Knight Enrichment Award. Convalescent serum sample collection was supported by a COVID-19 response grant to A.M. and S.M. from CIHR (#439999). Computational support was provided by the McMaster Service Lab and Repository computing cluster, supplemented by hardware donations and loans from Cisco Systems Canada, Hewlett Packard Enterprise, and Pure Storage. Research within A.B.'s laboratory is supported by the Natural Sciences and Engineering Research Council of Canada, CIHR, Saskatchewan Health Research Foundation, and the Coronavirus Variants Rapid Response Network. V.I.D.O. receives operational funding for its CL3 facility (InterVac) from the Canada Foundation for Innovation through the Major Science Initiatives. V.I.D.O. also receives operational funding from the Government of Saskatchewan via Innovation Saskatchewan and the Ministry of Agriculture.

The following reagent was obtained through BEI Resources, NIAID, NIH: SARS-Related Coronavirus 2, Isolate hCoV-19/USA/MD-HP01542/2021 (Lineage B.1.351), in Homo sapiens Lung Adenocarcinoma (Calu-3) Cells, NR-55282, contributed by Andrew S. Pekosz. Homo sapiens lung adenocarcinoma, Calu-3 (HTB-55) and Vero E6 cells (CRL-1586) were obtained from ATCC.

About the Author

Dr. Jacob is a postdoctoral fellow at McMaster University, Hamilton, Canada, and the scientific coordinator for the Canadian Consortium of Academic Biosafety Level 3 Laboratories. His overall research focus is characterizing the molecular and immunological mechanisms underlying virus-host interactions.

References

1. Layton AT, Sadria M. Understanding the dynamics of SARS-CoV-2 variants of concern in Ontario, Canada: a modeling study. Sci Rep. 2022;12:2114. https://doi.org/10.1038/s41598-022-06159-x
2. Tuite AR, Fisman DN, Odutayo A, Bobos P, Allen V, Bogoch II, et al. COVID-19 hospitalizations, ICU admissions and deaths associated with the new variants of concern. Science Briefs of the Ontario COVID-19 Science Advisory Table. 2021 Mar 29 [cited 2023 Feb 1]. https://covid19-sciencetable.ca/sciencebrief/covid-19-hospitalizations-icu-admissions-and-deaths-associated-with-the-new-variants-of-concern
3. Harvey WT, Carabelli AM, Jackson B, Gupta RK, Thomson EC, Harrison EM, et al.; COVID-19 Genomics UK (COG-UK) Consortium. SARS-CoV-2 variants, spike mutations and immune escape. Nat Rev Microbiol. 2021; 19:409–24. https://doi.org/10.1038/s41579-021-00573-0
4. Khare S, Gurry C, Freitas L, Schultz MB, Bach G, Diallo A, et al. GISAID's role in pandemic response. China CDC Wkly.|2021;3:1049–51. https://doi.org/10.46234/ccdcw2021.255
5. Hare D, Mossman KL. Novel paradigms of innate immune sensing of viral infections. Cytokine. 2013;63:219–24. https://doi.org/10.1016/j.cyto.2013.06.001
6. Sa Ribero M, Jouvenet N, Dreux M, Nisole S. Interplay between SARS-CoV-2 and the type I interferon response. PLoS Pathog. 2020;16:e1008737. https://doi.org/10.1371/journal.ppat.1008737
7. Lamers MM, Haagmans BL. SARS-CoV-2 pathogenesis. Nat Rev Microbiol. 2022;20:270–84. https://doi.org/10.1038/s41579-022-00713-0
8. Guo K, Barrett BS, Morrison JH, Mickens KL, Vladar EK, Hasenkrug KJ, et al. Interferon resistance of emerging SARS-CoV-2 variants. Proc Natl Acad Sci U S A. 2022; 119:e2203760119. https://doi.org/10.1073/pnas.2203760119

9. Zhang Q, Bastard P, Liu Z, Le Pen J, Moncada-Velez M, Chen J, et al.; COVID-STORM Clinicians; COVID Clinicians; Imagine COVID Group; French COVID Cohort Study Group; CoV-Contact Cohort; Amsterdam UMC Covid-19 Biobank; COVID Human Genetic Effort; NIAID-USUHS/TAGC COVID Immunity Group. Inborn errors of type I IFN immunity in patients with life-threatening COVID-19. Science. 2020;370:eabd4570. https://doi.org/10.1126/science.abd4570
10. Banerjee A, Nasir JA, Budylowski P, Yip L, Aftanas P, Christie N, et al. Isolation, sequence, infectivity, and replication kinetics of severe acute respiratory syndrome coronavirus 2. Emerg Infect Dis. 2020;26:2054–63. https://doi.org/10.3201/eid2609.201495
11. Kotwa JD, Jamal AJ, Mbareche H, Yip L, Aftanas P, Barati S, et al. Surface and air contamination with severe acute respiratory syndrome coronavirus 2 from hospitalized coronavirus disease 2019 patients in Toronto, Canada, March–May 2020. J Infect Dis. 2022;225:768–76. https://doi.org/10.1093/infdis/jiab578
12. Elbe S, Buckland-Merrett G. Data, disease and diplomacy: GISAID's innovative contribution to global health. Glob Chall. 2017;1:33–46. https://doi.org/10.1002/gch2.1018
13. Kandel CE, Young M, Serbanescu MA, Powis JE, Bulir D, Callahan J, et al. Detection of severe acute respiratory coronavirus virus 2 (SARS-CoV-2) in outpatients: a multicenter comparison of self-collected saline gargle, oral swab, and combined oral-anterior nasal swab to a provider collected nasopharyngeal swab. Infect Control Hosp Epidemiol. 2021;42:1340–4. https://doi.org/10.1017/ice.2021.2
14. Carabelli AM, Peacock TP, Thorne LG, Harvey WT, Hughes J, Peacock SJ, et al.; COVID-19 Genomics UK Consortium. SARS-CoV-2 variant biology: immune escape, transmission and fitness. Nat Rev Microbiol. 2023;21:162–77. https://doi.org/10.1038/s41579-022-00841-7
15. Detsky AS, Bogoch II. COVID-19 in Canada: experience and response to waves 2 and 3. JAMA. 2021;326:1145–6. https://doi.org/10.1001/jama.2021.14797
16. Liu Y, Liu J, Plante KS, Plante JA, Xie X, Zhang X, et al. The N501Y spike substitution enhances SARS-CoV-2 infection and transmission. Nature. 2022;602:294–9. https://doi.org/10.1038/s41586-021-04245-0
17. Luan B, Wang H, Huynh T. Enhanced binding of the N501Y-mutated SARS-CoV-2 spike protein to the human ACE2 receptor: insights from molecular dynamics simulations. FEBS Lett. 2021;595:1454–61. https://doi.org/10.1002/1873-3468.14076
18. Laffeber C, de Koning K, Kanaar R, Lebbink JHG. Experimental evidence for enhanced receptor binding by rapidly spreading SARS-CoV-2 variants. J Mol Biol. 2021;433:167058. https://doi.org/10.1016/j.jmb.2021.167058
19. Plante JA, Mitchell BM, Plante KS, Debbink K, Weaver SC, Menachery VD. The variant gambit: COVID-19's next move. Cell Host Microbe. 2021;29:508–15. https://doi.org/10.1016/j.chom.2021.02.020
20. Tao K, Tzou PL, Nouhin J, Gupta RK, de Oliveira T, Kosakovsky Pond SL, et al. The biological and clinical significance of emerging SARS-CoV-2 variants. Nat Rev Genet. 2021;22:757–73. https://doi.org/10.1038/s41576-021-00408-x
21. Gu H, Chen Q, Yang G, He L, Fan H, Deng YQ, et al. Adaptation of SARS-CoV-2 in BALB/c mice for testing vaccine efficacy. Science. 2020;369:1603–7. https://doi.org/10.1126/science.abc4730
22. Tegally H, Wilkinson E, Giovanetti M, Iranzadeh A, Fonseca V, Giandhari J, et al. Detection of a SARS-CoV-2 variant of concern in South Africa. Nature. 2021;592:438–43. https://doi.org/10.1038/s41586-021-03402-9
23. Planas D, Bruel T, Grzelak L, Guivel-Benhassine F, Staropoli I, Porrot F, et al. Sensitivity of infectious SARS-CoV-2 B.1.1.7 and B.1.351 variants to neutralizing antibodies. Nat Med. 2021;27:917–24. https://doi.org/10.1038/s41591-021-01318-5
24. Wang P, Nair MS, Liu L, Iketani S, Luo Y, Guo Y, et al. Antibody resistance of SARS-CoV-2 variants B.1.351 and B.1.1.7. Nature. 2021;593:130–5. https://doi.org/10.1038/s41586-021-03398-2
25. Cele S, Gazy I, Jackson L, Hwa SH, Tegally H, Lustig G, et al.; Network for Genomic Surveillance in South Africa; COMMIT-KZN Team. Escape of SARS-CoV-2 501Y.V2 from neutralization by convalescent plasma. Nature. 2021;593:142–6. https://doi.org/10.1038/s41586-021-03471-w
26. Banerjee A, Lew J, Kroeker A, Baid K, Aftanas P, Nirmalarajah K, et al. Immunogenicity of convalescent and vaccinated sera against clinical isolates of ancestral SARS-CoV-2, Beta, Delta, and Omicron variants. Med. 2022;3:422–432.e3. https://doi.org/10.1016/j.medj.2022.04.002
27. Banerjee A, El-Sayes N, Budylowski P, Jacob RA, Richard D, Maan H, et al. Experimental and natural evidence of SARS-CoV-2-infection-induced activation of type I interferon responses. iScience. 2021;24:102477. https://doi.org/10.1016/j.isci.2021.102477
28. Lowery SA, Sariol A, Perlman S. Innate immune and inflammatory responses to SARS-CoV-2: implications for COVID-19. Cell Host Microbe. 2021;29:1052–62. https://doi.org/10.1016/j.chom.2021.05.004
29. Diamond MS, Kanneganti TD. Innate immunity: the first line of defense against SARS-CoV-2. Nat Immunol. 2022;23:165–76. https://doi.org/10.1038/s41590-021-01091-0
30. Chu H, Chan JF, Yuen TT, Shuai H, Yuan S, Wang Y, et al. Comparative tropism, replication kinetics, and cell damage profiling of SARS-CoV-2 and SARS-CoV with implications for clinical manifestations, transmissibility, and laboratory studies of COVID-19: an observational study. Lancet Microbe. 2020;1:e14–23. https://doi.org/10.1016/S2666-5247(20)30004-5
31. Mellott DM, Tseng CT, Drelich A, Fajtová P, Chenna BC, Kostomiris DH, et al. A clinical-stage cysteine protease inhibitor blocks SARS-CoV-2 infection of human and monkey cells. ACS Chem Biol. 2021;16:642–50. https://doi.org/10.1021/acschembio.0c00875
32. Mathema B, Chen L, Wang P, Cunningham MH, Mediavilla JR, Chow KF, et al. Genomic epidemiology and serology associated with a SARS-CoV-2 R.1 variant outbreak in New Jersey. MBio. 2022;13:e0214122. https://doi.org/10.1128/mbio.02141-22
33. Sholukh AM, Fiore-Gartland A, Ford ES, Miner MD, Hou YJ, Tse LV, et al. Evaluation of cell-based and surrogate SARS-CoV-2 neutralization assays. J Clin Microbiol. 2021;59:e0052721. https://doi.org/10.1128/JCM.00527-21
34. Lusvarghi S, Wang W, Herrup R, Neerukonda SN, Vassell R, Bentley L, et al. Key substitutions in the spike protein of SARS-CoV-2 variants can predict resistance to monoclonal antibodies, but other substitutions can modify the effects. J Virol. 2022;96:e0111021. https://doi.org/10.1128/JVI.01110-21

Address for correspondence: Karen Mossman, McMaster University, MDCL 5026, 1280 Main St W, Hamilton, ON L8S4K1, Canada; email: mossk@mcmaster.ca

Long-Term Epidemiology and Evolution of Swine Influenza Viruses, Vietnam

Jonathan Cheung, Anh Ngoc Bui, Sonia Younas, Kimberly M. Edwards, Huy Quang Nguyen, Ngoc Thi Pham, Vuong Nghia Bui, Malik Peiris,[1] Vijaykrishna Dhanasekaran[1]

Influenza A viruses are a One Health threat because they can spill over between host populations, including among humans, swine, and birds. Surveillance of swine influenza virus in Hanoi, Vietnam, during 2013–2019 revealed gene pool enrichment from imported swine from Asia and North America and showed long-term maintenance, persistence, and reassortment of virus lineages. Genome sequencing showed continuous enrichment of H1 and H3 diversity through repeat introduction of human virus variants and swine influenza viruses endemic in other countries. In particular, the North American H1-δ1a strain, which has a triple-reassortant backbone that potentially results in increased human adaptation, emerged as a virus that could pose a zoonotic threat. Co-circulation of H1-δ1a viruses with other swine influenza virus genotypes raises concerns for both human and animal health.

Influenza A viruses (IAVs) pose a persistent One Health threat because of their ability to spill over into new host populations (*1*). Because pigs are susceptible to both avian and mammalian IAVs, they play an important role as mixing vessels in the generation of reassortant viruses (*2*). The 2009 influenza (H1N1) pandemic was caused by a reassortant H1N1 virus (pH1N1) containing gene segments from classical swine virus, Eurasian avian-like swine virus, and human seasonal virus lineages (*3*). Three different IAV subtypes (H1N1, H3N2, and H1N2) circulate in swine worldwide (*4*), with regional variation in antigenic characteristics. Contemporary swine influenza virus (swIV) lineages include H1N1, H1N2, and H3N2 triple-reassortant (TR) viruses that originated through reassortment of classical swine, avian, and human influenza viruses in the 1990s (*1*,*5*), European avian-like H1N1 swIV introduced into pigs during the 1970s, and several human H1N1- and H3N2-derived viruses, including pH1N1, pre-2009 H1N1, and H3N2-variant viruses (*4*). The increasing genetic diversity of IAVs in swine presents a pandemic concern (*4*,*6*). Human infections of emerging swIV are most frequently reported in the United States, where all nonhuman influenza viruses are nationally notifiable, with recurring outbreaks at agricultural fairs (*7*,*8*); however, sporadic human cases due to swIVs have been recently reported in Asia (*9*,*10*), Europe (*11*), and Australia (*12*).

In 2013, swIV surveillance was established at a collective slaughterhouse in Hanoi, Vietnam, that sourced pigs from 23 local provinces (*13*) (Table 1). During 2013 and 2014, cocirculation of multiple swIVs was detected, including viruses originating from pH1N1, H1N2 (with pre-2009 seasonal influenza–derived H1 hemagglutinin [HA]), H3N2 derived from human seasonal influenza, and TR H1N2 and H3N2 viruses (*13*). For this study, we extended virologic surveillance to 2019 and serologic surveillance from 2013 to 2019 in this slaughterhouse to characterize swIV evolution.

Materials and Methods

Surveillance and Virus Isolation

We examined 150 paired serum and nasal swab specimens collected from monthly convenience sampling at the Van Phuc slaughterhouse, the main collective swine slaughterhouse in Hanoi, Vietnam. We recorded the province of origin for each sampled pig. We report, in this study, findings from serum samples collected May 7, 2013–August 28, 2019. Virus isolation and sequence

Author affiliations: The University of Hong Kong, Hong Kong, China (J. Cheung, S. Younas, K.M. Edwards, M. Peiris, V. Dhanasekaran); National Institute of Veterinary Research, Hanoi, Vietnam (A.N. Bui, H.Q. Nguyen, N.T. Pham, V.N. Bui); Centre for Immunology & Infection, Hong Kong (M. Peiris).

DOI: http://doi.org/10.3201/eid2907.230165

[1]These senior authors contributed equally to this article.

Table 1. Summary of swine influenza virus isolates, by province, from samples collected at Van Phuc slaughterhouse in Vietnam during 2010–2019*

Province of origin	No. samples	No. (%) positive
Ha Noi	2,178	52 (2.39)†
Ha Nam	855	10 (1.17)
Hai Phong	61	7 (11.48)
Bac Ninh	51	4 (7.84)
Thai Nguyen	199	3 (1.51)
Ninh Binh	22	1 (4.55)
Nghe An	51	1 (1.96)
Hung Yen	96	1 (1.04)
Vinh Phuc	215	1 (0.47)
Hoa Binh	465	2 (0.43)
Phu Tho	301	1 (0.33)
Bac Giang	200	0
Yen Bai	150	0
Thanh Hoa	45	0
Thua Thien Hue	31	0
Nam Dinh	29	0
Dien Bien	2	0
Thai Binh	135	0
Tuyen Quang	27	0
Dong Nai, SV	195	11 (5.64)
Binh Duong, SV	16	0
Binh Dinh, SV	10	0
Kieu Ninh, SV	7	0
Location not specified	509	20 (3.93)
Total	5,850	114 (1.95)†

*SV, southern Vietnam.
†Includes 1 mixed infection of H1N2 and H3N2.

data from swab samples collected May 7, 2013–May 19, 2016, were reported previously (*13*); virus isolation and sequence data from swab samples collected June 30, 2016–August 28, 2019, are reported in this study. We cultured samples for virus isolation in MDCK cells at the National Institute of Veterinary Research Laboratory in Hanoi using described methods (*13*).

Whole-Genome Sequencing and Assembly

We amplified the influenza genome from RNA extracted from virus isolates using a multisegment reverse transcription PCR (RT-PCR) with universal primers (*14*,*15*) and sequenced by using Nextera DNA library preparation and MiSeq (PE300) sequencer (Illumina, https://www.illumina.com), as previously described (*13*). We removed adapters and low-quality reads by using Trimmomatic version 0.36 (USADEL LAB, http://www.usadellab.org), and we performed de novo assembly by using IVA version 0.8.1 (*16*). We mapped the assembled contiguous sequences to the reference sequence using Geneious Prime version 2019.2.1 (Geneious, https://www.geneious.com) and generated consensus sequences by merging overlapping contigs. We submitted to GISAID (https://www.gisaid.org) the Vietnam swIV genome sequences and associated metadata (Appendix 1, https://wwwnc.cdc.gov/EID/article/29/7/23-0165-App1.xlsx). We used BLAST (https://blast.ncbi.nlm.nih.gov/Blast.cgi) to analyze sequences generated in this study with other closely related influenza viruses from the GenBank and GISAID databases, including vaccine strains of human seasonal influenza H1N1. We classified H1 clades according to a phylogeny-based global nomenclature system (*17*).

Phylogenetic Analysis and Genotypic Diversity

We aligned gene segments individually by using MAFFT version 7.490 (*18*) and constructed maximum-likelihood phylogenetic trees by using IQ-TREE version 2.1.4 on the basis of the best-fit nucleotide substitution model determined by ModelFinder (IQ-TREE, http://www.iqtree.org), estimating branch supports by using an approximate likelihood ratio (SH-like) test (*19*). We determined genotypes of swIVs by assigning each segment to specific lineages on the basis of maximum-likelihood phylogenies and characterizing the genotype based on the clade distribution of its internal segments (*20*). We inferred time-scaled phylogenies calibrated by sample collection dates by using the maximum-likelihood method in IQ-TREE version 2.1.4, implementing a least-square dating algorithm (*21*). We visualized trees in FigTree version 1.4.4. (http://tree.bio.ed.ac.uk/software/figtree).

Serologic Assays

We randomly selected 10 pig serum samples from each monthly sampling visit to the same slaughterhouse (*13*). In total, we tested 760 pig serum samples collected during May 2013–August 2019 by using the hemagglutination inhibition (HI) assay against 3 swine H1 subtype influenza virus strains and 1 swine H3-subtype influenza virus strain isolated in this study, as well as pH1N1 virus. Those viruses were A/California/04/2009 (pH1N1), A/swine/Hanoi/7-305/2016 (H1-TR, H1N2), A/swine/Hanoi/11-260/2019 (H1-like, H1N2), A/swine/Hanoi/12-276/2019 (H1-δ1a, H1N2) and A/swine/Hanoi/10-984/2018 (2004/05 human H3N2-origin). We grew the viruses in MDCK cells and used them as antigens. The HI tests were carried out according to the World Health Organization's standard protocol for animal influenza diagnosis (*22*), with details as previously described (*13*).

Results

Incidence of swIVs and Subtype Diversity

No clear pattern of seasonality was detected from the 150 paired swab and serum specimens collected during June 2016–August 2019, nor from previous

studies conducted during 2010–2016 (Figure 1, panels A, B). The abattoir sourced swine from 23 provinces in Vietnam (Figure 1, panel C); most samples (87%) originated from provinces in northern Vietnam, 4% of samples originated from southern provinces, and location data were missing for the remaining samples (9%). Most swIV-positive samples originated from Hanoi (46%), Ha Nam (9%), and Hai Phong (6%) in northern Vietnam and Dong Nai (10%) in southern Vietnam (Table 1; Figure 1, panel C). There were 114 influenza-positive nasal swab samples with 1 mixed-subtype infection among the 5,850 swabs tested, yielding 115 viruses for study, for an isolation rate of 1.95%.

Subtyping of the 115 swIV isolates showed the circulation of 3 virus subtypes, H1N1 (n = 16), H1N2 (n = 46), and H3N2 (n = 53); 1 H1N2 and H3N2 co-infection was detected. Our previous study in the same abattoir during 2013–2014 yielded the same 3 virus subtypes, H1N1 (n = 16), H1N2 (n = 35), and H3N2 (n = 26) (*13*). Of note, we observed a high genetic similarity of viruses collected during each sampling at the Van Phuc slaughterhouse, suggesting that viruses were not maintained in the abattoir but were repeatedly introduced from sourced populations.

Phylogenetic Relationships of the HA Genes

We conducted a maximum-likelihood phylogenetic analysis of the HA genes of 145 swIVs collected during 2016–2019 in Vietnam, together with virus sequences from previous studies from the same abattoir during 2013–2019 and 390 swIVs collected in Vietnam by other studies (Figure 2, panel A). HA sequence data revealed the circulation of 4 distinct H1 lineages and 2 distinct H3 lineages over various time points (Figure 2, panel B; Appendix 2 Figure 1). The H1 subtype viruses included human-derived pH1N1 (n = 122), classical swine-derived H1-TR (n = 84), and pre-2009 seasonal H1N1 (n = 69), which we further classified into H1-δ–like (n = 60) and H1-δ1a (n = 9). In addition, 2 viruses of the H1N2 subtype collected in December 2016 by Takemae et al. (*23*) belong to the Eurasian avian-like

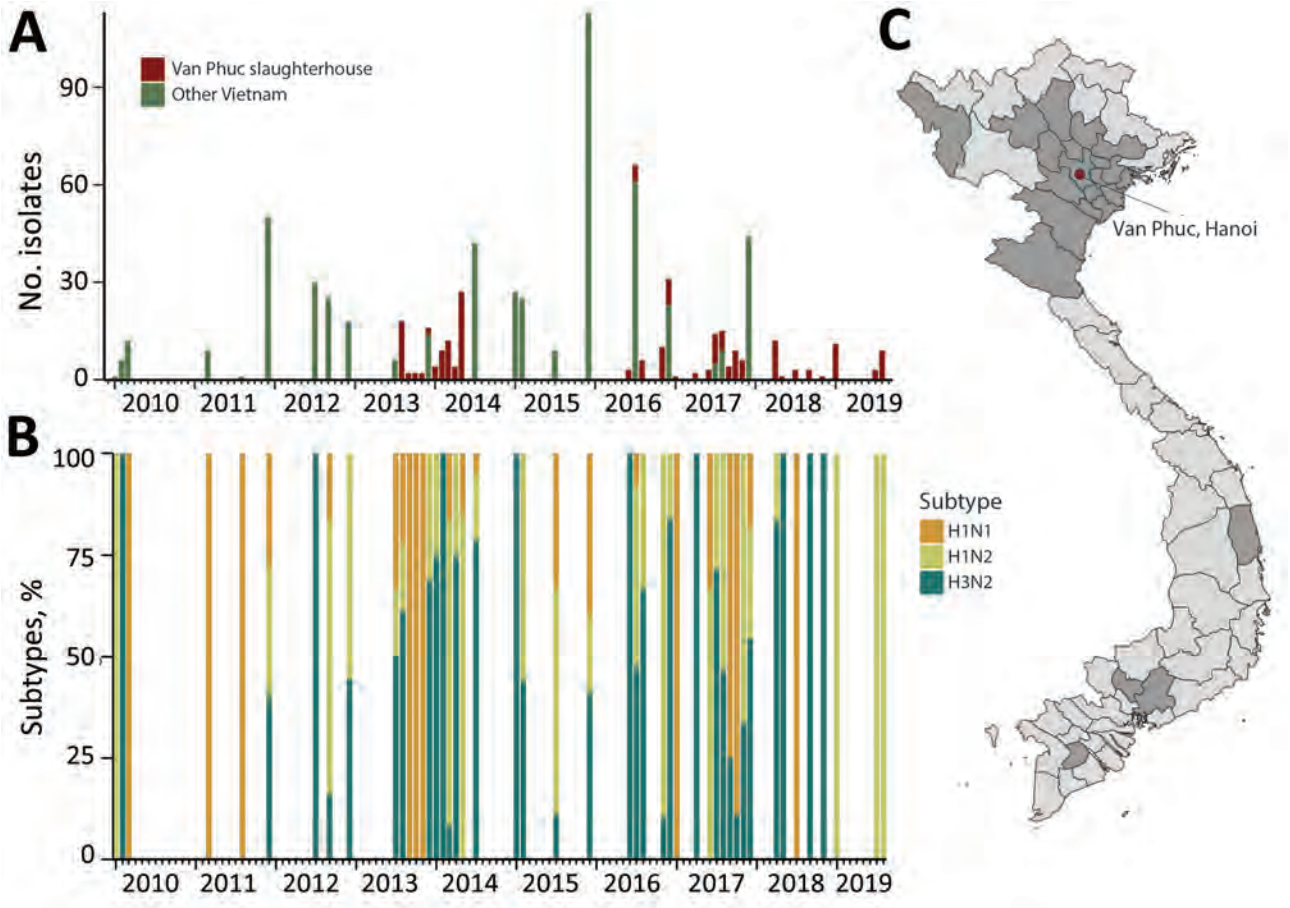

Figure 1. Swine influenza virus detection in Vietnam during 2010–2019. A) Number of swine Influenza viruses isolated from Van Phuc slaughterhouse in Hanoi during 2013–2014 (*13*,*26*) and 2016–2019, alongside other surveillance studies in Vietnam (*23*,*27*,*28*). B) Percentages of swine influenza virus subtypes detected. C) Provincial origins (gray shading) of pigs sampled at Van Phuc slaughterhouse during 2016–2019.

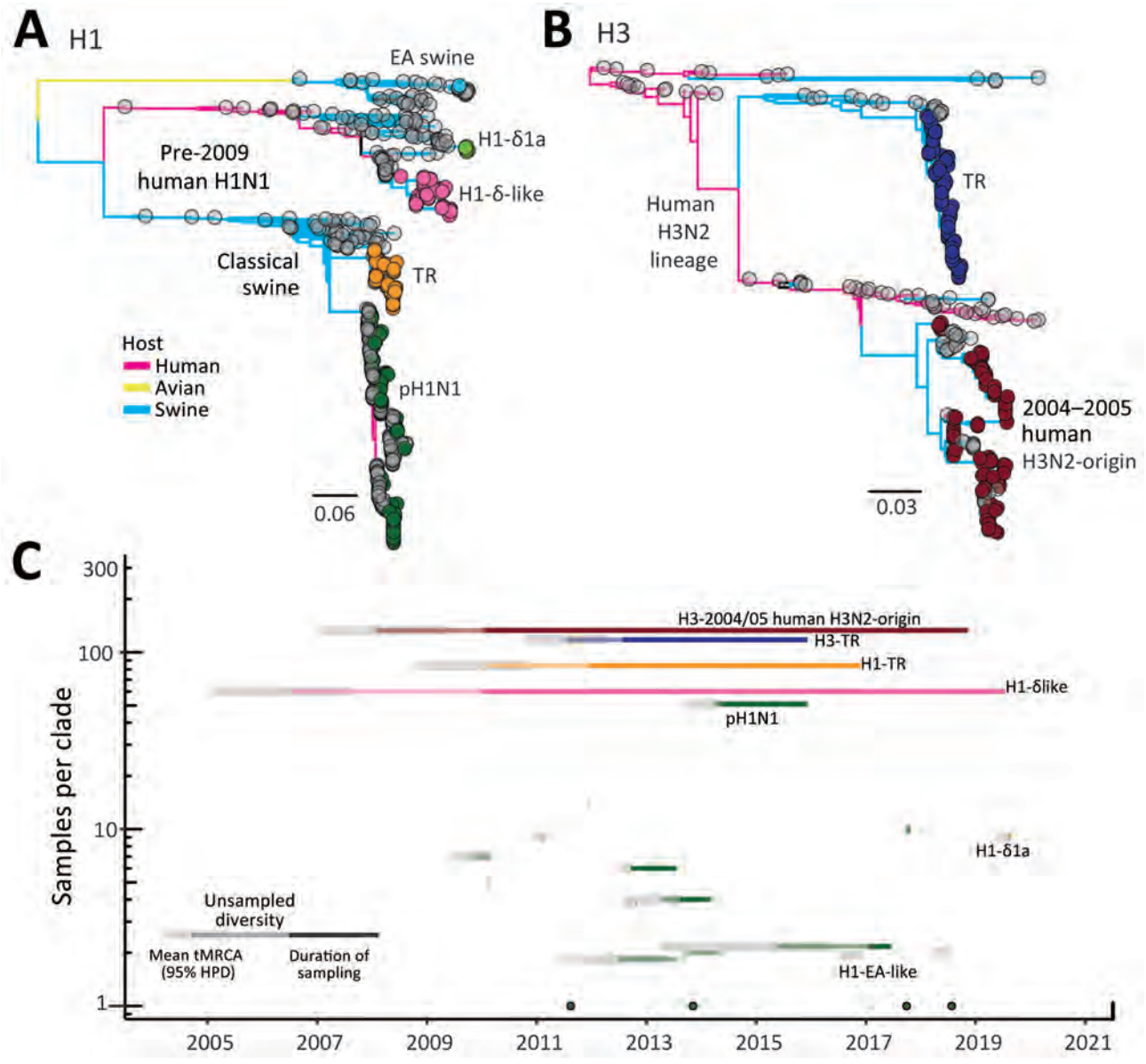

Figure 2. Genomic epidemiology of swine influenza viruses in Vietnam. A, B) Maximum-likelihood phylogeny of the H1 (A) and H3 (B) hemagglutinin genes of swine influenza viruses. Branch tips are colored by lineage origin and branches by host. C) Persistence of independent hemagglutinin lineages of swine influenza viruses detected in Vietnam. EA, Eurasian avian; HPD, highest posterior density; tMRCA, time to most recent common ancestor; TR, triple reassortant.

swine H1 HA lineage. The H3-HA phylogeny indicates swIVs in Vietnam belong to either the swine-origin North American TR lineage or the 2003/04 human H3N2-origin swIV first detected in Vietnam in 2010 (Figure 2, panel B; Appendix 2 Figure 1).

HA phylogenies identified the circulation of 21 independent transmission lineages in swine in Vietnam since 2010, including 4 singletons (Figure 2, panel B). Those lineages were all identified elsewhere in the world and were likely introduced by imported swine or by humans through reverse zoonosis. Of the 21 transmission lineages, 17 independent transmission lineages of pH1N1 virus were detected at various time points. Most introductions were limited to 1–14 samples collected during 1–3 contiguous sampling months and were most closely related to spillover of contemporary human pH1N1 viruses. Two closely related pH1N1 reassortants detected in January and June 2017, A/swine/Hanoi/7_619/2017 and A/swine/Hanoi/8_463/2017, derived HA and neuraminidase (NA) genes from humans around 2013 and polymerase basic (PB) 2, PB1, or nonstructural

genes from TR swIVs from China. Long branches in the HA and NA phylogenetic trees suggest circulation in swine for >3 years.

In addition to recurrent detections of pH1N1 during 2014–2017 (n = 53), a single lineage of H1 TR virus (n = 84), closely related to swIV in Guangxi Province, China, during 2010–2011, was maintained during 2010–2019, and an H1-δ-like lineage (n = 60) was derived independently from pre-2009 human seasonal H1N1 viruses that circulated in 2004–2006. Nine virus sequences collected on the last sampling occasion (in August 2019) belonged to the H1-δ1a lineage and were most closely related to H1N2 swIVs circulating in the United States during 2015–2016 (Appendix 2 Figure 3). The H1-δ1a originated from human seasonal H1N1 viruses circulating in humans during 2002 and 2003 (*24*,*25*) and was previously found only in swine in the United States (*17*).

Two major H3-HA lineages originated from North America. One belongs to the TR lineage that circulated during 2012–2015 in northern Vietnam (n = 132) (*13*,*26*,*27*), and the other belongs to the 2004/05 human H3N2-origin swIV (n = 133) that circulated during 2010–2018 (Figure 2, panel B). The 2004/05 human H3N2-origin lineage clustered with viruses circulating in southern China and Cambodia during 2011–2012 and a zoonotic case reported in Vietnam (A/Ho Chi Minh/459-6/2010 [H3N2]). The 2004/05 human H3N2-origin viruses have been further classified into 2 divergent lineages, NV and SV, based on detection in north and south Vietnam. SV viruses have not been detected since 2015, and NV viruses were detected up to 2018. Taken together, our results indicate a recent bottleneck in overall HA diversity; H1 and H3 TR lineages have not been detected since 2016, and detections of new human pH1N1 viruses have been declining. However, H1-δ viruses became predominant by 2018 and 2019.

Temporal phylogenies of the H1 and H3 HA genes of Vietnam swIVs (Figure 2, panel B; Figure 3, panel A) show long branches of unsampled diversity leading up to the H1-δ–like virus and the 2004/05 human H3N2-origin swIV, which was before initiation of swine surveillance in Vietnam. The pH1N1 virus lineage we described circulated for ≈4 years before detection, and within the swIV clades from Vietnam, long branches of unsampled diversity span 4 to 5 years. A sublineage of the 2004/05 human H3N2-origin virus that diverged before 2010 was only detected in 2016–2019. Similarly, recent viruses belonging to 2 H1-δ sublineages appear to have been sampled after 4 years.

Genotypes of swIV in Vietnam during 2010–2019

Phylogenetic analysis of each gene segment from 2010–2019 showed that the swIV gene pool in Vietnam includes genes from pH1N1 virus, pre-2009 human-derived H1 viruses (further subdivided into H1-δ–like and H1-δ1a), Eurasian avian-like H1 virus, and TR viruses of H1 and H3 subtype (Figure 3). Of the combined 537 swIVs, 111 H1N1 swIVs derived entirely from pH1N1 (genotype 1), 2 H1N1 (genotypes 2–3), 161 H1N2 (genotypes 4–20), and 263 H3N2 (genotypes 21–28) viruses were reassortants (Figure 3). Among the 426 reassortant H1N2 and H3N2 swIVs, we detected several preferred genetic constellations (Figure 3, panel B). We identified 28 swIV gene constellations, designated as genotypes, whereas 1–28, from the 2010 to 2019 time frame, of which 17 were previously reported (*13*,*26*-*28*). Of those, only genotypes 1, 4, and 25 continued to be detected during 2016–2019. Genotypes 1 and 4 were detected in both northern and southern Vietnam; the others were found in either northern or southern Vietnam (Figure 3; Appendix 2 Figure 1).

In each year, we observed the cocirculation of multiple genotypes; few genotypes were maintained across multiple years (Figure 3, panel C). Most of the swIVs detected in Vietnam were genotype 1, which had all 8 gene segments originating from human pH1N1 viruses (n = 111) (Figure 3; Appendix 2 Figure 1). Genotype 1 was dominant in Vietnam during 2010–2015 and 2017–2018, followed by genotypes 23, 7, 24, and 10, found during 2010–2019 (Figure 3, panel C). We found that pH1N1 viruses with PB2, PB1, nucleoprotein (NP), and nonstructural genes from TR viruses and N2-NA genes from human H3N2-derived swIV (genotypes 2, 3, and 13) were detected sporadically (Figure 3). The NA and internal genes of swine pH1N1 viruses were not monophyletic but interspersed between human-origin virus sequences. All potential spillover events were closely related to human viruses, not limited to human viruses in Vietnam.

In contrast to the predominance of a single pH1N1 virus genotype, the H1N2 TR viruses repeatedly acquired internal genes from pH1N1 viruses (genotypes 5, 6, 8, 9, and 14); the most recent H1N2 TR viruses contained all internal genes of pH1N1 viruses. Two H1N2 swIV sequences (genotype 16) contain Eurasian avian-like surface proteins and pH1N1 internal genes. Similarly, the genotype 8 H1N2 viruses, with H1-δ HAs and all other segments from TR viruses, repeatedly gained pH1N1 genes to form genotypes 7, 12, 15, and 20. The most recent H1N2 TR viruses collected in 2019 contain TR N2 and pH1N1 internal segments (genotype 7). However, H1-δ genotype 4 viruses with no pH1N1

genes continued to be detected until 2019. Furthermore, H1-δ1a viruses (genotype 10) isolated in August 2019 contained North American TR internal and NA genes with only the matrix protein (M) gene from pH1N1. Those viruses have not been seen anywhere other than the United States and now Vietnam, suggesting that those swIVs likely spread to Vietnam directly from the United States.

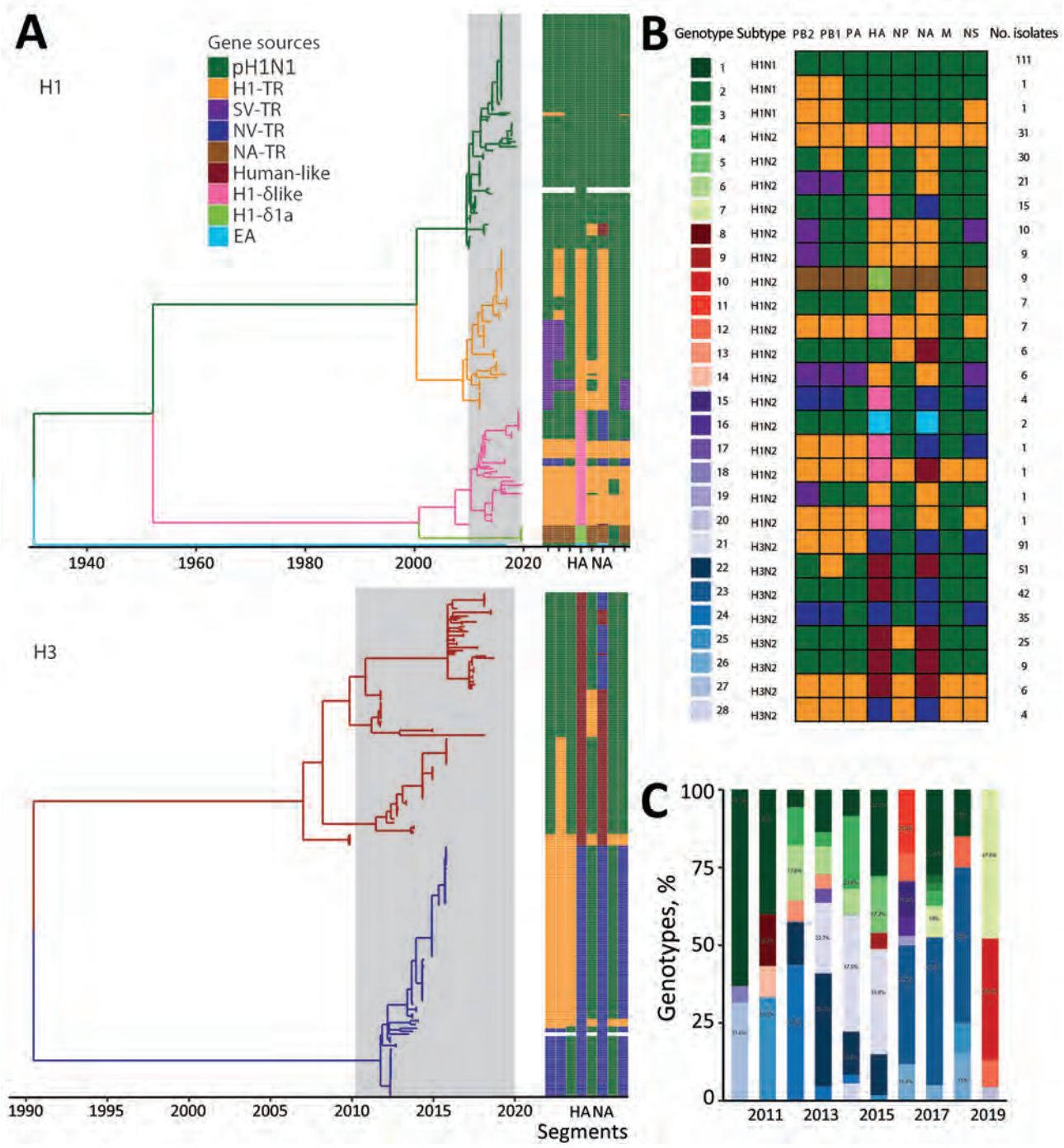

Figure 3. H1 and H3 swine influenza virus genotypes in Vietnam, 2010–2019. A) Temporal phylogeny of HA genes. Branches are colored by lineage of origin. Heatmap illustrates gene segment origins. B) Genotypes identified in Vietnam during 2010–2019. Box shading denotes lineage of origin by color grouping, as shown in panel A. C) Annual percentages of genotypes identified. Colors are as shown in panel B. C-TR, Chinese triple reassortant; EA, Eurasian avian; H1-δ, pre-2009-human H1-δ; H1-δ1a, pre-2009 human H1-δ1A; HA, hemagglutinin; M, matrix; NA, neuraminidase; NA-TR, North American triple reassortant; NP, nucleoprotein; NS, nonstructural; NV-TR, northern Vietnam triple reassortant; PA, polymerase acidic; PB, polymerase basic; SV-TR, southern Vietnam triple reassortant.

We detected 8 distinct H3N2 swIV constellations (genotypes 21–28). The H3 TR viruses that circulated in northern Vietnam during 2012–2015 were initially detected with all genes of TR lineage (genotype 28) or with polymerase acidic, NP, and M genes derived from pH1N1 viruses (genotype 24). However, H3 TR viruses detected during 2014–2015 contained only NP and M genes from pH1N1 (genotype 21). The 2004/05 human H3N2-derived viruses, initially identified in 2010 with all internal genes from TR lineages (genotype 27), gained pH1N1 gene segments with or without maintaining TR PB1 (genotype 22) or NP (genotype 25) genes. However, the most recent viruses of this H3 lineage (detected in 2017–2018) contained the TR N2 and pH1N1 internal genes (genotype 23). Taken together, our findings show that swIV lineages of all subtypes collected in recent years in Vietnam have acquired the pH1N1 internal genes, except 2 divergent H1-δ viruses (genotype 4 and 10) that appear to have become predominant in Vietnam in recent years.

Seroprevalence of swIV in Northern Vietnam

Of swine serum samples tested by HI assay, 41% (309/760) showed antibody titers ≥40 against at least 1 of 5 representative virus antigens tested (Table 2). Seroprevalence of 2004/05 human H3N2-origin virus in 2016–2019 (15.3%) was broadly comparable to that for 2013–2014 (15.9%), whereas H1 lineage seroprevalence varied over time. Seroprevalence of pH1N1 and H1-TR virus decreased, and H1-δ–like virus seroprevalence increased from 13% in 2013–2014 to 20% in 2016–2019. H1-δ1a antibodies were only detected in 2016–2019; the first seropositive samples were collected in March 2016 (Appendix 2 Table 1) and showed limited cross-reactivity to other H1 swIV lineages (Appendix 2 Table 2) (*29*,*30*). Despite continuous detection of an H1-TR lineage during 2013–2017 (Figure 2, panel B), overall seropositivity against the H1-TR reference strain, A/swine/Hanoi/7_305/2016(H1N2), remained low at 2.4% (Table 2). H1-TR seropositive samples displayed elevated HI titers against pH1N1 (2- to 3-fold increase; Appendix 2 Table 3). This result suggests H1-TR reactive antibodies are likely the result of cross-reactivity with pH1N1.

Discussion

Our study, conducted during 2016–2019, provides insights into the evolution and epidemiology of swIV in Vietnam, a major pork-producing country in Asia. Through longitudinal surveillance at a central slaughterhouse in Hanoi, which sourced pigs from across the country, we found H1N1, H1N2, and H3N2 swIVs co-circulating. This finding is consistent with surveillance conducted in 2013–2014 (*13*,*26*) and with other studies in Vietnam (*23*,*27*,*28*), indicating that the swIV subtypes circulating in Vietnam are similar to those found across Asia and globally (*31*–*34*).

We found that the genetic diversity of swIV in Vietnam since 2010 is attributable to the persistence of several swine-origin H1N2 and H3N2 viruses, first reported in other countries in Asia and North America and likely imported via swine trade. We also identified repeat introductions of human pH1N1 viruses through reverse zoonosis. We found extensive reassortment of major swIV lineages, including H1N2 and H3N2 frequently acquiring pH1N1 internal genes and only rare acquisition of other swIV internal genes by pH1N1 lineage viruses. As a result, most recent swIVs from Vietnam contain pH1N1 internal genes. However, 2 divergent H1-δ virus lineages (originally derived from pre-2009 seasonal H1N1 viruses), detected in our most recent sample from 2019, maintained the TR lineage NA and internal genes (genotypes 10, 12, and 20) (Figure 3, panel B).

Although repeated introductions of pH1N1 into swine is consistent with previous swine surveillance from Vietnam (*13*) and southern China (*35*,*36*), the frequency of detections of new human pH1N1 virus lineages in swine in Vietnam has tapered off since 2015. Although onward transmission of pH1N1 was not sustained for most introductions, 1 lineage, first detected in northern Vietnam during 2013–2014 (*13*), persisted in swine for >4 years and reassorted with other prevailing swIV lineages. When introduced as components of reassortants, pH1N1-origin gene segments tend to be maintained in pigs (*27*), whereas viruses whose genomes are entirely derived from pH1N1 tend not to be sustained in the pig population. This phenomenon has been observed globally and in southern China and Hong Kong surveillance studies, which showed that viruses from purely pH1N1 failed to sustain the pig population after each introduction (*36*). Similar evidence of pH1N1 being sustained within swine populations has been reported from the United States (*37*) and Australia (*38*).

Pre-2009 seasonal H1N1 influenza-derived swine viruses (classified under H1-δ) are potentially gaining predominance in swine in Vietnam. Of note, an H1N2 H1-δ1a virus lineage with limited cross-reactivity to other H1 swIV lineages was detected in 2019, and serosurveillance showed evidence of circulation since March 2016. The increasing prevalence of H1-δ–like lineages increases the risk for zoonotic transmission. Previous studies demonstrated significant antigenic distance between pH1N1-like viruses and H1-δ cluster viruses (H1-δ–like and H1-δ1a) (*29*,*30*), and current

Table 2. Seroprevalence against representative swine influenza A viruses isolated from Van Phuc slaughterhouse in Vietnam, 2010–2019*

HA lineage	Reference antigen	No. (%) seropositive†		
		2013–2015, n = 320	2016–2019, n = 440	Overall, n = 760
2009 pandemic H1N1	A/California/04/2009 (H1N1)	57 (17.8)	61 (13.9)	118 (15.5)†
Pre-2009 human seasonal H1-δ–like	A/swine/Hanoi/11-260/2019 (H1N2)	43 (13.4)	89 (20.2)	132 (17.4)†
Pre-2009 human seasonal H1-δ1a	A/swine/Hanoi/12-276/2019 (H1N2)	0	36 (8.2)	36 (4.7)
H1-TR	A/swine/Hanoi/7-305/2016 (H1N2)	10 (3.1)	8 (1.8)	18 (2.4)
2004/05 human H3N2-origin	A/swine/Hanoi/10-984/2018 (H3N2)	49 (15.3)	70 (15.9)	119 (15.7)
Total positive		126 (39.4)	183 (41.6)	309 (40.7)

*Seropositivity defined as hemagglutination inhibition assay titer ≥40. HA, hemagglutinin; TR, triple reassortant.
†A total of 30 serum samples were positive for both A/California/04/2009 (H1N1) and A/swine/Hanoi/11–260/2019 (H1N2). Because cross reactivity between these viruses is low, this result likely indicates sequential infections.

seasonal influenza vaccines do not elicit protection against H1-δ swIVs (*39*–*41*). It is therefore important to ascertain whether current diagnostics can distinguish pre-2009 H1 viruses from currently circulating human seasonal H1 strains.

H1-δ1a viruses likely entered Vietnam via imported swine, demonstrating the role of trade in the global dissemination of swIVs (*42*). East and Southeast Asia countries, including China, Thailand, and Vietnam, which produce >50% of pork globally, are hotspots for emerging infectious diseases from swine (*43*,*44*). Vietnam ranks second in Asia for pork production, producing 19.62 million heads in 2019 (*45*). In addition, pork consumption in Vietnam has risen rapidly, from 12.8 kg/head/year in 2001 to 31.4 kg/head/year in 2018 (*46*), mostly in the form of fresh pork. Vietnam has also been importing breeding hogs from the United States since 1996. On average, 553 breeding hogs were imported each year from the United States during the 2010s, with a peak in 2014–2015 (Appendix 2 Figure 2) (*47*). The H1-δ1a lineage may have been introduced to Vietnam by imported breeding hogs in early 2016, as was seen in mainland China in the early 1990s (*48*).

In each of the swIV lineages detected in Vietnam, we discovered evidence of localized circulation, as evidenced by periods of unsampled diversity and long phylogenetic branches, likely at the provincial level. Despite the limited mixing of swine populations in Vietnam before slaughter (*44*), the infrequent detection of persistent lineages in the central slaughterhouse suggests that the genetic diversity of swIV in Vietnam may be high. This diversity is likely driven by factors such as livestock density and turnover. In comparison, swine in the United States are exposed to a greater degree of mixing during their lifespan because they are transported across long distances for feeding and fattening, which results in replacement by advantageous swIV lineages (*37*).

Our findings indicate that the swIV gene pool in Vietnam is continually enriched by importations from North America and from other countries in Asia. Those viruses include a novel cluster of H1-δ1a (genotype 10) viruses, which may pose a zoonotic threat (*49*). As the H1-δ1a virus was found only during the last sample collection, its persistence is uncertain. Recurrent transmission of pH1N1 viruses from humans to swine and reassortment with other swIV lineages have increased genetic diversity. Hence, to limit further introductions and diversification of the swIV gene pool in Vietnam, it is important to actively monitor both local swine herds and imported swine.

Acknowledgments

We gratefully acknowledge the staff from the originating laboratories responsible for obtaining the specimens and from the submitting laboratories where the genome data were generated and shared via GISAID (Appendix 1).

This study was supported by the National Institute of Allergy and Infectious Diseases, US National Institutes of Health (contract no. 75N93021C00016). The funding bodies had no role in the design of the study and collection, analysis, and interpretation of data and writing of the manuscript.

About the Author

Dr. Cheung is a researcher at the University of Hong Kong School of Public Health. His research interests are the molecular evolutionary virology and epidemiology of zoonotic influenza viruses.

References

1. Van Reeth K, Vincent AL. Influenza viruses. In: Leman AD, Straw JW, Mengeling WL, Taylor DJ, Zimmerman SD, editors. Diseases of swine. New York: John Wiley & Sons; 2019. p. 576–93. https://doi.org/10.1002/9781119350927.ch36
2. Scholtissek C. Pigs as 'mixing vessels' for the creation of new pandemic influenza a viruses. Med Princ Pract. 1990;2:65–71. https://doi.org/10.1159/000157337
3. Smith GJD, Vijaykrishna D, Bahl J, Lycett SJ, Worobey M, Pybus OG, et al. Origins and evolutionary genomics of the 2009 swine-origin H1N1 influenza A epidemic. Nature. 2009;459:1122–5. https://doi.org/10.1038/nature08182

4. Lewis NS, Russell CA, Langat P, Anderson TK, Berger K, Bielejec F, et al.; ESNIP3 consortium. The global antigenic diversity of swine influenza A viruses. eLife. 2016;5:e12217. https://doi.org/10.7554/eLife.12217
5. Olsen CW. The emergence of novel swine influenza viruses in North America. Virus Res. 2002;85:199–210. https://doi.org/10.1016/S0168-1702(02)00027-8
6. Sun H, Xiao Y, Liu J, Wang D, Li F, Wang C, et al. Prevalent Eurasian avian-like H1N1 swine influenza virus with 2009 pandemic viral genes facilitating human infection. Proc Natl Acad Sci U S A. 2020;117:17204–10. https://doi.org/10.1073/pnas.1921186117
7. Jhung MA, Epperson S, Biggerstaff M, Allen D, Balish A, Barnes N, et al. Outbreak of variant influenza A(H3N2) virus in the United States. Clin Infect Dis. 2013;57:1703–12. https://doi.org/10.1093/cid/cit649
8. Bowman AS, Walia RR, Nolting JM, Vincent AL, Killian ML, Zentkovich MM, et al. Influenza A(H3N2) virus in swine at agricultural fairs and transmission to humans, Michigan and Ohio, USA, 2016. Emerg Infect Dis. 2017;23:1551–5. https://doi.org/10.3201/eid2309.170847
9. Li X, Guo L, Liu C, Cheng Y, Kong M, Yang L, et al. Human infection with a novel reassortant Eurasian-avian lineage swine H1N1 virus in northern China. Emerg Microbes Infect. 2019;8:1535–45. https://doi.org/10.1080/22221751.2019.1679611
10. Yang JR, Kuo CY, Yu IL, Kung FY, Wu FT, Lin JS, et al. Human infection with a reassortant swine-origin influenza A(H1N2)v virus in Taiwan, 2021. Virol J. 2022;19:63. https://doi.org/10.1186/s12985-022-01794-2
11. Andersen KM, Vestergaard LS, Nissen JN, George SJ, Ryt-Hansen P, Hjulsager CK, et al. Severe human case of zoonotic infection with swine-origin influenza A virus, Denmark, 2021. Emerg Infect Dis. 2022;28:2561–4. https://doi.org/10.3201/eid2812.220935
12. Deng YM, Wong FYK, Spirason N, Kaye M, Beazley R, Grau MLL, et al. Locally acquired human infection with swine-origin influenza A (H3N2) variant virus, Australia, 2018. Emerg Infect Dis. 2020;26:143–7. https://doi.org/10.3201/eid2601.191144
13. Baudon E, Chu DKW, Tung DD, Thi Nga P, Vu Mai Phuong H, Le Khanh Hang N, et al. Swine influenza viruses in Northern Vietnam in 2013–2014. Emerg Microbes Infect. 2018;7:123. https://doi.org/10.1038/s41426-018-0109-y
14. Hoffmann E, Stech J, Guan Y, Webster RG, Perez DR. Universal primer set for the full-length amplification of all influenza A viruses. Arch Virol. 2001;146:2275–89. https://doi.org/10.1007/s007050170002
15. Zhou B, Donnelly ME, Scholes DT, St George K, Hatta M, Kawaoka Y, et al. Single-reaction genomic amplification accelerates sequencing and vaccine production for classical and swine origin human influenza A viruses. J Virol. 2009;83:10309–13. https://doi.org/10.1128/JVI.01109-09
16. Hunt M, Gall A, Ong SH, Brener J, Ferns B, Goulder P, et al. IVA: accurate de novo assembly of RNA virus genomes. Bioinformatics. 2015;31:2374–6. https://doi.org/10.1093/bioinformatics/btv120
17. Anderson TK, Macken CA, Lewis NS, Scheuermann RH, Van Reeth K, Brown IH, et al. A phylogeny-based global nomenclature system and automated annotation tool for h1 hemagglutinin genes from swine influenza A viruses. MSphere. 2016;1:e00275–16. https://doi.org/10.1128/mSphere.00275-16
18. Katoh K, Standley DM. MAFFT multiple sequence alignment software version 7: improvements in performance and usability. Mol Biol Evol. 2013;30:772–80. https://doi.org/10.1093/molbev/mst010
19. Guindon S, Dufayard JF, Lefort V, Anisimova M, Hordijk W, Gascuel O. New algorithms and methods to estimate maximum-likelihood phylogenies: assessing the performance of PhyML 3.0. Syst Biol. 2010;59:307–21. https://doi.org/10.1093/sysbio/syq010
20. Feng Z, Zhu W, Yang L, Liu J, Zhou L, Wang D, et al. Epidemiology and genotypic diversity of Eurasian avian-like H1N1 swine influenza viruses in China. Virol Sin. 2021;36:43–51. https://doi.org/10.1007/s12250-020-00257-8
21. To TH, Jung M, Lycett S, Gascuel O. Fast dating using least-squares criteria and algorithms. Syst Biol. 2016;65:82–97. https://doi.org/10.1093/sysbio/syv068
22. World Health Organization. Manual for the laboratory diagnosis and virological surveillance of influenza. Geneva: The Organization; 2011.
23. Takemae N, Nguyen PT, Le VT, Nguyen TN, To TL, Nguyen TD, et al. Appearance of reassortant European avian-origin H1 influenza A viruses of swine in Vietnam. Transbound Emerg Dis. 2018;65:1110–6. https://doi.org/10.1111/tbed.12849
24. Karasin AI, Carman S, Olsen CW. Identification of human H1N2 and human-swine reassortant H1N2 and H1N1 influenza A viruses among pigs in Ontario, Canada (2003 to 2005). J Clin Microbiol. 2006;44:1123–6. https://doi.org/10.1128/JCM.44.3.1123-1126.2006
25. Vincent AL, Ma W, Lager KM, Gramer MR, Richt JA, Janke BH. Characterization of a newly emerged genetic cluster of H1N1 and H1N2 swine influenza virus in the United States. Virus Genes. 2009;39:176–85. https://doi.org/10.1007/s11262-009-0386-6
26. Baudon E, Poon LL, Dao TD, Pham NT, Cowling BJ, Peyre M, et al. Detection of novel reassortant influenza A (H3N2) and H1N1 2009 pandemic viruses in swine in Hanoi, Vietnam. Zoonoses Public Health. 2015;62:429–34. https://doi.org/10.1111/zph.12164
27. Takemae N, Harada M, Nguyen PT, Nguyen T, Nguyen TN, To TL, et al. Influenza A viruses of swine (IAV-S) in Vietnam from 2010 to 2015: Multiple introductions of A (H1N1) pdm09 viruses into the pig population and diversifying genetic constellations of enzootic IAV-S. J Virol. 2017;91:e01490-16. https://doi.org/10.1128/JVI.01490-16
28. Ngo LT, Hiromoto Y, Pham VP, Le HT, Nguyen HT, Le VT, et al. Isolation of novel triple-reassortant swine H3N2 influenza viruses possessing the hemagglutinin and neuraminidase genes of a seasonal influenza virus in Vietnam in 2010. Influenza Other Respir Viruses. 2012;6:6–10. https://doi.org/10.1111/j.1750-2659.2011.00267.x
29. Rajao DS, Anderson TK, Kitikoon P, Stratton J, Lewis NS, Vincent AL. Antigenic and genetic evolution of contemporary swine H1 influenza viruses in the United States. Virology. 2018;518:45–54. https://doi.org/10.1016/j.virol.2018.02.006
30. Lorusso A, Vincent AL, Harland ML, Alt D, Bayles DO, Swenson SL, et al. Genetic and antigenic characterization of H1 influenza viruses from United States swine from 2008. J Gen Virol. 2011;92:919–30. https://doi.org/10.1099/vir.0.027557-0
31. Walia RR, Anderson TK, Vincent AL. Regional patterns of genetic diversity in swine influenza A viruses in the United States from 2010 to 2016. Influenza Other Respir Viruses. 2019;13:262–73. https://doi.org/10.1111/irv.12559
32. Danilenko DM, Komissarov AB, Fadeev AV, Bakaev MI, Ivanova AA, Petrova PA, et al. Antigenic and genetic characterization of swine influenza viruses identified in

the European region of Russia, 2014–2020. Front Microbiol. 2021;12:662028. https://doi.org/10.3389/fmicb.2021.662028
33. Encinas P, Del Real G, Dutta J, Khan Z, van Bakel H, Del Burgo MAM, et al. Evolution of influenza A virus in intensive and free-range swine farms in Spain. Virus Evol. 2022;7(2):veab099
34. Saito T, Sakuma S, Mine J, Uchida Y, Hangalapura BN. Genetic diversity of the hemagglutinin genes of influenza A virus in Asian swine populations. Viruses. 2022;14:747. https://doi.org/10.3390/v14040747
35. Vijaykrishna D, Smith GJD, Pybus OG, Zhu H, Bhatt S, Poon LLM, et al. Long-term evolution and transmission dynamics of swine influenza A virus. Nature. 2011;473:519–22. https://doi.org/10.1038/nature10004
36. Liang H, Lam TT, Fan X, Chen X, Zeng Y, Zhou J, et al. Expansion of genotypic diversity and establishment of 2009 H1N1 pandemic-origin internal genes in pigs in China. J Virol. 2014;88:10864–74. https://doi.org/10.1128/JVI.01327-14
37. Nelson MI, Stratton J, Killian ML, Janas-Martindale A, Vincent AL. Continual reintroduction of human pandemic H1N1 influenza A viruses into swine in the United States, 2009 to 2014. J Virol. 2015;89:6218–26. https://doi.org/10.1128/JVI.00459-15
38. Deng Y-M, Wong FYK, Spirason N, Kaye M, Beazley R, Grau MLL, et al. Locally acquired human infection with swine-origin influenza A(H3N2) variant virus, Australia, 2018. Emerg Infect Dis. 2020;26:143–7. https://doi.org/10.3201/eid2601.191144
39. Kimble JB, Souza CK, Anderson TK, Arendsee ZW, Hufnagel DE, Young KM, et al. Interspecies transmission from pigs to ferrets of antigenically distinct swine H1 influenza A viruses with reduced reactivity to candidate vaccine virus antisera as measures of relative zoonotic risk. Viruses. 2022;14:2398. https://doi.org/10.3390/v14112398
40. Anderson TK, Chang J, Arendsee ZW, Venkatesh D, Souza CK, Kimble JB, et al. Swine influenza A viruses and the tangled relationship with humans. Cold Spring Harb Perspect Med. 2021;11:a038737. https://doi.org/10.1101/cshperspect.a038737
41 Venkatesh D, Anderson TK, Kimble JB, Chang J, Lopes S, Souza CK, et al. Antigenic characterization and pandemic risk assessment of North American H1 influenza A viruses circulating in swine. Microbiol Spectr. 2022;10:e0178122. https://doi.org/10.1128/spectrum.01781-22
42. Nelson MI, Viboud C, Vincent AL, Culhane MR, Detmer SE, Wentworth DE, et al. Global migration of influenza A viruses in swine. Nat Commun. 2015;6:6696. https://doi.org/10.1038/ncomms7696
43. Trevennec K, Cowling BJ, Peyre M, Baudon E, Martineau GP, Roger F. Swine influenza surveillance in East and Southeast Asia: a systematic review. Anim Health Res Rev. 2011;12:213–23. https://doi.org/10.1017/S1466252311000181
44. Baudon E, Fournié G, Hiep DT, Pham TTH, Duboz R, Gély M, et al. Analysis of swine movements in a province in northern Vietnam and application in the design of surveillance strategies for infectious diseases. Transbound Emerg Dis. 2017;64:411–24. https://doi.org/10.1111/tbed.12380
45. Statista. Pig production in Vietnam from 2005 to 2021 [cited 2023 June 9]. https://www.statista.com/statistics/661016/vietnam-pig-production/#statisticContainer
46. Asian Agribiz (2023) [cited 2023 June 9]. https://www.asian-agribiz.com/2022/06/22/consumers-in-vietnam-switch-from-pork-to-poultry/
47. US Department of Agriculture Economic Research Service. Livestock and Meat International Trade data [cited 2023 June 9]. https://www.ers.usda.gov/data-products/livestock-and-meat-international-trade-data/livestock-and-meat-international-trade-data/#Zipped%20CSV%20files
48. Zhu W, Yang S, Guo Y, Yang L, Bai T, Yu Z, et al. Imported pigs may have introduced the first classical swine influenza viruses into Mainland China. Infect Genet Evol. 2013;17:142–6. https://doi.org/10.1016/j.meegid.2013.03.007
49. Vandoorn E, Leroux-Roels I, Leroux-Roels G, Parys A, Vincent A, Van Reeth K. Detection of H1 swine influenza A virus antibodies in human serum samples by age group. Emerg Infect Dis. 2020;26:2118–28. https://doi.org/10.3201/eid2609.191796

Address for correspondence: Malik Peiris, School of Public Health, No 7 Sassoon Rd, The University of Hong Kong, Hong Kong, China; email: malik@hku.hk

Lumpy Skin Disease Virus Infection in Free-Ranging Indian Gazelles (*Gazella bennettii*), Rajasthan, India

Shashi Bhushan Sudhakar, Niranjan Mishra, Semmannan Kalaiyarasu, Khusboo Ahirwar, Suchismita Chatterji, Omprakash Parihar, Vijendra Pal Singh, Aniket Sanyal

Near a zoo in Bikaner, India, 2 free-ranging Indian gazelles (*Gazella bennettii*) displayed nodular skin lesions. Molecular testing revealed lumpy skin disease virus (LSDV) infection. Subsequent genome analyses revealed LSDV wild-type strain of Middle Eastern lineage. Evidence of natural LSDV infection in wild gazelles in this area indicates a broadening host range.

Lumpy skin disease (LSD), caused by lumpy skin disease virus (LSDV) of the genus *Capripoxvirus*, is a notifiable transboundary disease of domestic cattle and has recently spread from eastern Europe and Russia to South, East, and Southeast Asia (*1*). Although cattle are the principal hosts, natural LSDV infection has been reported sporadically in wildlife in Africa and Asia (*2*–*5*).

The Indian gazelle (*Gazella bennettii*), a free-ranging ungulate (family *Bovidae*, subfamily *Antilopinae*), is native to the arid regions of India, Pakistan, Iran, and Afghanistan; most live in the Rajasthan state of India (*6*). Recently, lethal LSDV infection was reported in a captive giraffe (*Giraffa camelopardalis*) in Vietnam (*5*), and clinical disease was reported in wildlife in Thailand (*7*). However, the epidemiologic role of wildlife has not been elucidated, and LSDV infection previously has not been detected in Indian gazelles. In addition, information on clinical disease and genetic profile of LSDV from wildlife is scarce. We report detection and genetic characterization of LSDV from wild Indian gazelles in Rajasthan, India.

Author affiliations: ICAR-National Institute of High Security Animal Diseases, Bhopal, India (S.B. Sudhakar, N. Mishra, S. Kalaiyarasu, K. Ahirwar, V.P. Singh, A. Sanyal); Regional Disease Diagnostic Centre, Bikaner, India (S. Chatterji, O. Parihar)

DOI: https://doi.org/10.3201/eid2907.230043

The Study

In August 2022, two free-ranging female Indian gazelles with skin lesions resembling LSD were rescued and quarantined for veterinary care at a zoo in Bikaner, Rajasthan, India. The animals had high fever, vesicles in the mouth, nasal discharge, ocular and oral discharge, and generalized skin nodules all over the body, including the neck and face (Figure 1). Skin and whole blood samples from the affected animals were investigated by PCR and real-time PCR. Both the animals died under veterinary care after 3 days but could not be necropsied for histology and further analysis.

We performed various real-time PCRs and PCRs using DNA extracted from skin lesions and blood by using a capripoxvirus-screening real-time PCR (*8*). Results for skin samples were LSDV-positive but for blood samples were LSDV-negative (Appendix Figure 1, panel A, https://wwwnc.cdc.gov/EID/article/29/7/23-0043-App1.pdf). We performed real-time PCR specific for LSDV wild-type strain (*9*), which showed positive results for skin samples, confirming natural LSDV infection (Appendix Figure 1, panel B). PCR of skin and blood samples were negative for bovine herpes virus type 2, buffalopox virus, cowpox virus, pseudo-cowpox virus, and bovine papular stomatitis virus (*10*). Although the exact cause of death of the 2 Indian gazelles could not be ascertained, LSDV-associated death is likely because the animals tested negative for other related cattle viral pathogens.

To determine the genetic profile of the LSDV strains, we conducted PCR amplification for 3 complete LSDV genes, the LSDV011 G-protein-coupled-chemokine-like receptor (GPCR), LSDV036 RNA polymerase 30-kDa polypeptide (RPO30), and LSDV126 extracellular enveloped virus (EEV), as

Figure 1. Clinical observations of lumpy skin disease virus infection in free-ranging Indian gazelles (*Gazella bennettii*), Rajasthan, India. Photograph shows a female Indian gazelle with multiple circumscribed skin nodules of varying sizes over the entire body, including the face and neck region.

described in our previous study (*11*). We also analyzed skin tissues of 2 LSDV-positive domestic cattle from the nearby area in Rajasthan for comparison. We determined the GPCR, RPO30, and EEV full gene sequences by Sanger sequencing and deposited the sequences in GenBank (accession nos. OP893954–65). We performed phylogenetic analysis by using MEGA version 7.0 (*12*). We found that LSDV sequences from both the gazelles and 2 domestic cattle were identical and subjected 1 sequence from each animal to further genetic analysis.

The GPCR nucleotide sequence alignment showed that the LSDV strains from the Indian gazelles and local cattle had a 12-nt deletion, as previously seen in LSDV wild-type strains of the SG-1 lineage from the Middle East, Europe, and the Balkans (Table**)**. In contrast, all LSDVs reported in India since 2019 had a 12-nt insertion, as observed in ancestral wild-type strains of SG-2 lineage from Kenya. Those results suggest the emergence of LSDV SG-1 lineage in India. In addition, the phylogenetic tree analysis of GPCR showed that LSDV from the Indian gazelles clustered with the LSDV wild-type strains (Appendix Figure 2).

Table. Results of GPCR nucleotide sequence alignment of lumpy skin disease virus infection in free-ranging Indian gazelles (*Gazella bennettii*), Rajasthan, India*

Sample no.	Virus strain	GenBank accession no.	12-nt deletion of in GPCR (96–107)
1	Indian Gazelle/IND/LSDV/BKN-6/2022	OP893960	Y
2	Cattle/IND/LSDV/BKN-2	OP893958	Y
3	Cattle/IND/LSDV/L06/2022	SRX17592135	N
4	Cattle/IND/LSDV/L09/2022	SRX17592137	N
5	Cattle/LSDV/IND/ODI/5RK_LT/2019	MW452639	N
6	Cattle/LSDV/IND/ODI/77BP-LT/2019	MW452646	N
7	Cattle/LSDV/IND/WB/JS9_LT/2019	MW452649	N
8	Cattle/LSDV/Bangladesh/Dhaka/2019	MT448698	N
9	Cattle/LSDV/Kenya/KSGP-O240/Kenyavac	KJ818281	N
10	Cattle/LSDV/Turkey/Pendik/2014	MN995838	Y
11	Cattle/LSDV/Serbia/Bujanovac/2016	KY702007	Y
12	Cattle/LSDV/Kazakhstan/Kubash/2016	MN642592	Y
13	Cattle/LSDV/Greece/Evros/2015	KY829023	Y
14	Cattle/ South Africa/OBP vaccine	KX764645	N
15	Cattle/South Africa/Herbivac vaccine	KX764644	N
16	Cattle/LSDV/South Africa/SIS-Lumpyvax Vaccine	KX764643	N
17	Cattle/LSDV/Russia/Saratov/2017	MH646674	N
18	Cattle/LSDV/Russia/Udmurthiya/2019	MT134042	N
19	Cattle/LSDV/ Kenya/1958	MNO72619	N
20	Cattle/LSDV/Russia/Dagestan/2015	MH893760	Y
21	Springbok/LSDV/South Africa/RSA/06/2011	FJ869374	Y
22	Cattle/LSDV/Kenya/Neethling Warmaths LW	AF409137	Y
23	Cattle/LSDV/Egypt/AHRI21/2019	MN271744	Y
24	Cattle/LSDV/Kenya/Neethling/2490	AF325528	N
25	Cattle/LSDV/China/Xinjiang/2019	MN598006	N
26	Cattle/LSDV/Kenya/KS-1	KJ818283	N
27	Giraffe/LSDV/Vietnam/2021	MZ966326	N
28	SPPVaccine/India/Ranipet vaccine	KF495236	N
29	SPPV/Turkey/Vaccine	MN072631	N
30	GTPV/India/ Uttarkashi/Vaccine	KF495242	N
31	GTPV/Iran/Gorgan/Vaccine	KX576657	N

*Samples 1 and 2 were those from this study. Multiple sequence alignment was conducted by using MEGA version 7.0 (*12*). GTPV, goatpox virus; GPCR, G-protein-coupled-chemokine-like receptor (LSDV011); SPPV, sheeppox virus.

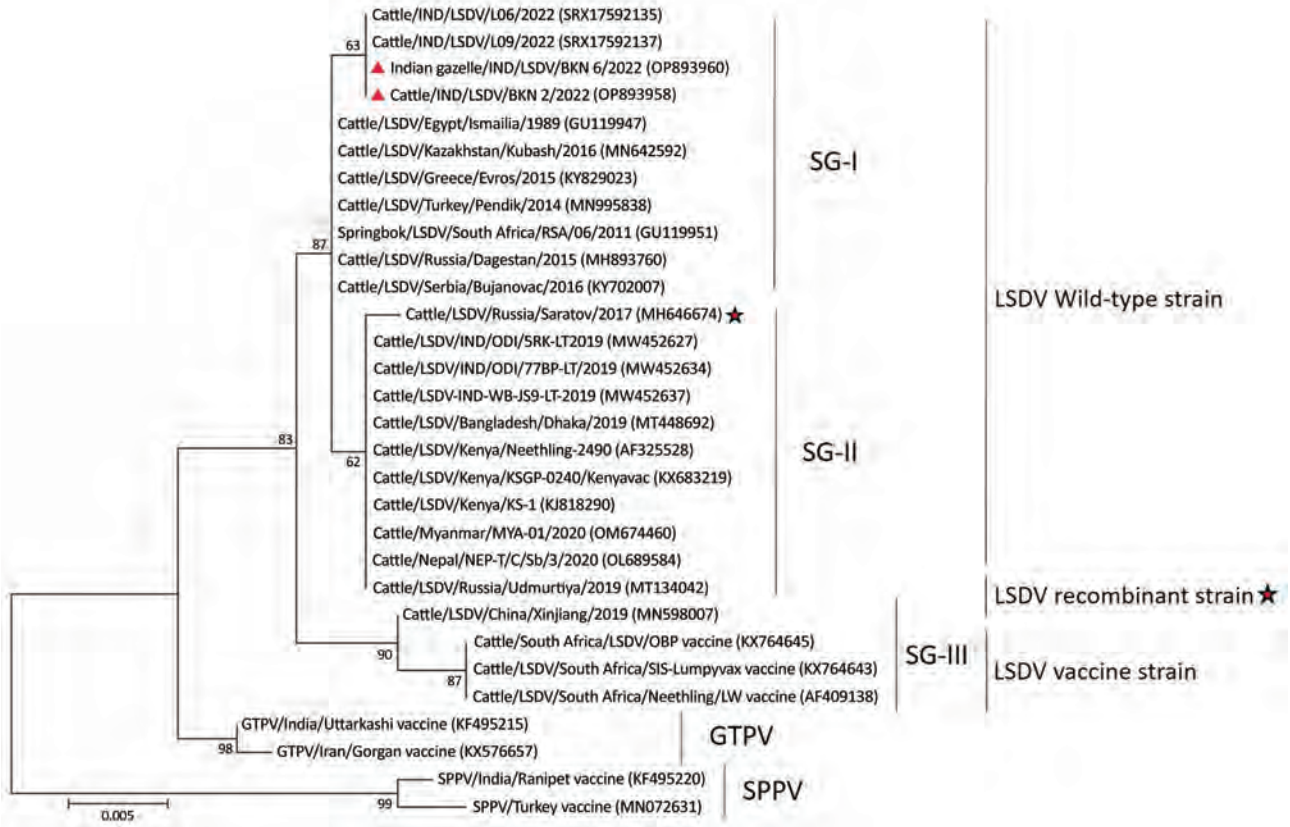

Figure 2. Phylogenetic tree of LSDV from infected free-ranging Indian gazelles (*Gazella bennettii*), Rajasthan, India, compared with reference strains from GenBank. LSDV tree is based on complete LSDV036 RNA polymerase 30-kDa polypeptide (RPO30) gene sequences using maximum-likelihood analysis combined with 1,000 bootstrap replicates. LSDV from Indian gazelle clustered with LSDV wild-type strains from Africa, the Middle East, and Europe. Triangles indicate sequences obtained from this study; stars indicate sequences of LSDV recombinant strains from GenBank. Scale bar indicates nucleotide substitutions per site. GenBank accession numbers are provided. GTPV, goatpox virus; LSDV, lumpy skin disease virus; SPPV, sheeppox virus.

Further phylogenetic analysis of the complete RPO30 gene, commonly used for LSDV genetic tree calculations, showed that LSDV from the gazelles and local cattle in a 2022 LSD outbreak clustered with the LSDV wild-type strains of SG-1 lineage, but they diverged from the main branch in a separate cluster (Figure 2). Those data confirmed emergence of LSDV variants of SG-1 lineage in India, indicating a change in the genetic makeup of recent LSDV wild-type strains. This finding also was supported by our results of EEV nucleotide sequence alignment, which showed that LSDVs from the gazelles had 1 unique mutation (G253A) and 2 mutations (G178A and A459G) that are similar to other wild-type strains of LSDV SG-1 lineage (Appendix Figure 3). In addition, the EEV phylogenetic analysis showed that LSDV from the gazelles clustered with LSDV SG-1 lineage (Appendix Figure 4).

Conclusions

We detected LSDV in 2 diseased free-ranging Indian gazelles in Rajasthan, India. The 2 gazelles eventually died. The clinical manifestations of their disease were akin to those for LSD in domestic cattle. The findings demonstrated emergence of LSD in wildlife in India and susceptibility of the wild *G. bennetti* species to natural LSDV infection. To our knowledge, LSDV-associated death has not been reported in free-ranging wildlife, and most LSDV infections in wildlife are asymptomatic, despite sporadic reports of clinical disease (*5*–*7*) and a single report of death in a captive giraffe (*5*). However, further investigations are needed to assess effects of LSDV infection in the Indian gazelle population and other susceptible wildlife.

Genetic and phylogenetic analysis of LSDV GPCR, RPO30, and EEV sequences revealed that the LSDV from the Indian gazelles clustered with the LSDV wild-type strains of SG-1 lineage commonly circulating in the Middle East, the Balkans, and Europe (*13*). In contrast, since its emergence in India in 2019, all the LSDV strains circulating in domestic cattle have belonged to the ancestral LSDV wild-type strains of SG-2 lineage from Kenya (*10*,*11*). Hence, our

findings suggest a new introduction of LSDV of exotic origin into India.

In conclusion, we found LSDVs in Indian gazelles and local domestic cattle that were phylogenetically similar, reinforcing the hypothesis that susceptible wildlife can become infected with LSDV circulating in cattle in the region, as reported in previous studies (*5*,*14*,*15*). Our findings demonstrate that the host range of LSDV is expanding and free-ranging wildlife in Asia is susceptible to LSDV. Minimizing contacts between wildlife and cattle during LSD outbreaks might help limit cross-species transmission. Continued monitoring is needed to assess the impact of LSDV on gazelles and other wild and domestic ruminants in India.

This study was supported by a grant from Department of Animal Husbandry & Dairying, Ministry of Fisheries, Animal Husbandry and Dairying, New Delhi, India (grant no. CDDL1005235).

About the Author

Dr. Sudhakar is a senior scientist at the ICAR-National Institute of High Security Animal Diseases, Bhopal, India. His primary research interests are epidemiology and diagnosis of animal viruses, including capripoxviruses.

References

1. Tuppurainen ESM, Venter EH, Shisler JL, Gari G, Mekonnen GA, Juleff N, et al. Review: capripoxvirus diseases: current status and opportunities for control. Transbound Emerg Dis. 2017;64:729–45. https://doi.org/10.1111/tbed.12444
2. Hedger RS, Hamblin C. Neutralising antibodies to lumpy skin disease virus in African wildlife. Comp Immunol Microbiol Infect Dis. 1983;6:209–13. https://doi.org/10.1016/0147-9571(83)90012-7
3. Fagbo S, Coetzer JAW, Venter EH. Seroprevalence of Rift Valley fever and lumpy skin disease in African buffalo (*Syncerus caffer*) in the Kruger National Park and Hluhluwe-iMfolozi Park, South Africa. J S Afr Vet Assoc. 2014;85:e1–7. https://doi.org/10.4102/jsava.v85i1.1075
4. Greta A, Gourreau JM, Vassart M, Nguyen-Ba-Vy, Wyers M, Lefevre PC. Capripoxvirus disease in an Arabian oryx (*Oryx leucoryx*) from Saudi Arabia. J Wildl Dis. 1992;28:295–300. https://doi.org/10.7589/0090-3558-28.2.295
5. Dao TD, Tran LH, Nguyen HD, Hoang TT, Nguyen GH, Tran KVD, et al. Characterization of lumpy skin disease virus isolated from a giraffe in Vietnam. Transbound Emerg Dis. 2022;69:e3268–72. https://doi.org/10.1111/tbed.14583
6. Dookia S, Rawat M, Jakher G, Dookia B. Status of Indian gazelle (*Gazella bennettii* Sykes, 1831) in the Thar Desert of Rajasthan, India. In: Sivaperuman C, Baqri QH, Ramaswamy G, Naseema M, editors. Faunal ecology and conservation of the Great Indian Desert. Berlin: Springer; 2009. p. 193–207. https://doi.org/10.1007/978-3-540-87409-6_15
7. World Organization for Animal Health. Frequently asked questions (FAQ) on lumpy skin disease [cited 2022 Jun 9]. https://www.woah.org/en/document/faq-on-lumpy-skin-disease-lsd
8. Bowden TR, Babiuk SL, Parkyn GR, Copps JS, Boyle DB. Capripoxvirus tissue tropism and shedding: a quantitative study in experimentally infected sheep and goats. Virology. 2008;371:380–93. https://doi.org/10.1016/j.virol.2007.10.002
9. Pestova YE, Artyukhova EE, Kostrova EE, Shumoliva IN, Kononov AV, Sprygin AV. Real time PCR for the detection of field isolates of lumpy skin disease virus in clinical samples from cattle. Agric Biol. 2018;53:422–9. https://doi.org/10.15389 /agrobiology.2018.2.422eng
10. Sudhakar SB, Mishra N, Kalaiyarasu S, Jhade SK, Hemadri D, Sood R, et al. Lumpy skin disease (LSD) outbreaks in cattle in Odisha State, India in August 2019: epidemiological features and molecular studies. Transbound Emerg Dis. 2020;67:2408–22. https://doi.org/10.1111/tbed.13579
11. Sudhakar SB, Mishra N, Kalaiyarasu S, Jhade SK, Singh VP. Genetic and phylogenetic analysis of lumpy skin disease viruses (LSDV) isolated from the first and subsequent field outbreaks in India during 2019 reveals close proximity with unique signatures of historical Kenyan NI-2490/Kenya/KSGP-like field strains. Transbound Emerg Dis. 2022;69:e451–62. https://doi.org/10.1111/tbed.14322
12. Kumar S, Stecher G, Tamura K. MEGA7: Molecular evolutionary genetics analysis version 7.0 for bigger datasets. Mol Biol Evol. 2016;33:1870–4. https://doi.org/10.1093/molbev/msw054
13. Manić M, Stojiljković M, Petrović M, Nišavić J, Bacić D, Petrović T, et al. Epizootic features and control measures for lumpy skin disease in south-east Serbia in 2016. Transbound Emerg Dis. 2019;66:2087–99. https://doi.org/10.1111/tbed.13261
14. Le Goff C, Lamien CE, Fakhfakh E, Chadeyras A, Aba-Adulugba E, Libeau G, et al. Capripoxvirus G-protein-coupled chemokine receptor: a host-range gene suitable for virus animal origin discrimination. J Gen Virol. 2009;90:1967–77. https://doi.org/10.1099/vir.0.010686-0
15. Molini U, Boshoff E, Niel AP, Phillips J, Khaiseb S, Settypalli TBK, et al. Detection of lumpy skin disease virus in an asymptomatic eland (*Taurotragus oryx*) in Namibia. J Wildl Dis. 2021;57:708–11. https://doi.org/10.7589/JWD-D-20-00181

Address for Correspondence: Niranjan Mishra, ICAR-National Institute of High Security Animal Diseases, Bhopal 462 022, Madhya Pradesh, India; email: nmishra@hsadl.nic.in

Sexually Transmitted *Trichophyton mentagrophytes* Genotype VII Infection among Men Who Have Sex with Men

Arnaud Jabet, Sarah Dellière, Sophie Seang, Aziza Chermak, Luminita Schneider, Thibault Chiarabini, Alexandre Teboul, Geoffroy Hickman, Alizée Bozonnat, Cécile Brin, Marion Favier, Yanis Tamzali, François Chasset, Stéphane Barete, Samia Hamane, Mazzouz Benderdouche, Alicia Moreno-Sabater, Eric Dannaoui, Christophe Hennequin, Arnaud Fekkar, Renaud Piarroux, Anne-Cécile Normand, Gentiane Monsel

Transmission of dermatophytes, especially *Trichophyton mentagrophytes* genotype VII, during sexual intercourse has been recently reported. We report 13 such cases in France. All patients were male; 12 were men who have sex with men. Our findings suggest sexual transmission of this pathogen within a specific population, men who have sex with men.

Dermatophytes are keratinophilic fungi responsible for frequent skin infections. They are transmitted either by direct contact from an infected host (human or animal) to a receptive host or from the environment. In 2002, two surveys reported cases of tinea cruris infection in sex workers, raising the hypothesis of sexual transmission of dermatophytes (*1*,*2*). In 2009, transmission of *Trichophyton mentagrophytes*, responsible for tinea genitalis, between a heterosexual couple was reported (*3*). Subsequently, a specific internal transcribed spacer (ITS) genotype of *T. mentagrophytes*, genotype VII (TMVII), was reported for cases of suspected sexual transmission, most frequently tinea genitalis (*4*–*7*). In some cases, a temporal association was demonstrated between the appearance of lesions and sexual intercourse between occasional partners, especially sex workers in Southeast Asia (*4*,*8*). Moreover, similar lesions were repeatedly documented in sex partners of infected patients (*4*,*6*). Unlike other *T. mentagrophytes* genotypes, TMVII has not been reported in association with dermatophytosis in children in contact with animals (*9*). We report 13 cases of TMVII infections, highly suspected of being sexually transmitted, diagnosed in 3 large tertiary care hospitals in Paris, France, in men who have sex with men.

Author affiliations: Assistance Publique-Hôpitaux de Paris, Paris, France (A. Jabet, S. Dellière, S. Seang, A. Chermak, L. Schneider, T. Chiarabini, A. Teboul, G. Hickman, A. Bozonnat, C. Brin, M. Favier, Y. Tamzali, F. Chasset, S. Barete, S. Hamane, M. Benderdouche, A. Moreno-Sabater, E. Dannaoui, C. Hennequin, A. Fekkar, R. Piarroux, A.-C. Normand, G. Monsel); Université de Paris, Paris, France (S. Dellière, E. Dannaoui); Sorbonne Université, Paris, France (F. Chasset, A. Moreno-Sabater, C, Hennequin, A. Fekkar, R. Piarroux)

DOI: https://doi.org/10.3201/eid2907.230025

The Study

During January 2021–September 2022, for all strains that could correspond to *T. mentagrophytes* or *T. indotineae* that were isolated at La Pitié-Salpêtrière and Saint-Antoine Hospitals in Paris, we sequenced the ITS1–5.8S-ITS2 region for species identification and genotype determination (*10*). At Saint-Louis Hospital in Paris, sequencing was limited to the isolates responsible for widespread dermatophytosis. For all cases of confirmed TMVII infection, we retrieved the medical records.

Of the 13 cases of TMVII infection, the first was detected in March 2021, and 9 were diagnosed during June–September 2022. All patients were male; median age was 39 (22–59) years (Table 1). Five patients had a single skin lesion, and others had multiple lesions. One patient had inguinal papules and nodules suggestive of Majocchi granulomas, 2 had highly inflammatory folliculitis of the beard (kerion), and the others had typical erythemato-squamous lesions with an active border (Figure).

Of the 13 patients, 11 reported having sexual relations exclusively with men and 1 reported having

Table 1. Main epidemiologic and clinical features of 13 cases of *Trichophyton mentagrophytes* genotype VII infections diagnosed in Paris, France, 2021–2022*

Pt no.	Age, y	HIV+	PrEP	STI history	Travel	Tinea genitalis	Tinea glutealis	Tinea corporis	Tinea faciei/barbae	Prior treatment	*T. mentagrophytes* treatment
1†	45	No	Yes	Ng, Ct, Mg	No	No	Yes	Yes	Yes	No	TRB 1 mo
2	34	No	Yes	Ng	EE	No	Yes	Yes	Yes	ECZ, TS	TRB 5 d, then ITR 200 mg 1 mo, then ITR 100 mg 1 mo
3	28	No	No	ND	ND	Yes	No	Yes	No	No	TRB 4 mo + BFZ 1 mo
4	59	Yes	NA	Ng, Ct, Mg, Tp, HCV	No	Yes	Yes	Yes	Yes	No	TRB 2 mo + ECZ
5‡	39	Yes	NA	Tp	ND	Yes	Yes	Yes	Yes	No	TRB + CPX 3 wk
6‡	41	Yes	NA	Tp	ND	No	Yes	Yes	Yes	No	TRB + CPX 3 wk
7	40	No	Yes	Ng, Ct, Tp	No	No	No	No	Yes	PRI + MPC	TRB 6 wk
8	48	Yes	NA	Ng, Ct, Tp, Ss	No	No	No	Yes	No	No	CPX 4 wk
9‡	26	Yes	NA	Ng, Ct, Tp	ND	Yes	Yes	Yes	No	No	ECZ 6 wk
10‡§	35	No	Yes	Tp	ND	No	No	Yes	No	No	ECZ 6 wk
11§	22	No	Yes	Ng, Ct, Tp	DE	No	Yes	Yes	Yes	AMX then FLC	TRB 4 wk
12	35	Yes	NA	Ng,Tp	IN	No	No	Yes	No	TS then CPX	BFZ 4 wk
13	46	Yes	NA	Ng, Ct, Tp, Ss	ES	No	No	No	Yes	FCD + TS then FCD alone then PRI then AMX/CLAV	ITR 100 mg 2 d, then IV VRC 10 d, then TRB

*AMX, amoxicillin; BFZ, bifonazole; CLAV, clavulanic acid; CPX, ciclopirox olamine; Ct, *Chlamydia trachomatis*; DE, German; ECZ, econazole; EE, Estonia; ES, Spain; FCD, fucidin; FLC, fluconazole; HCV, hepatitis C virus; IN, India; ITR, itraconazole; Mg, *Mycoplama genitalium*; MPC, mupirocin; NA, not applicable; ND, no data; Ng; *Neisseria gonorrheae*; PrEP, pre-exposure prophylaxis; PRI, pristinamycin; Pt, patient; Ss, *Sarcoptes scabiei;* Tp, *Treponema pallidum*; TRB, oral terbinafine (250 mg 1×/d); TS, topical steroids; VRC, voriconazole.
†Patient 1 strain was included in a previous survey (*11*).
‡Patients 5 and 6 and patients 9 and 10 were partners.
§Patients 10 and 11 were co-infected with monkeypox virus.

sexual intercourse with men and women. At least 9 had multiple sex partners in the month before lesion onset. Seven patients were HIV positive, and 5 were taking HIV preexposure prophylaxis. Apart from 1 patient who had recently discontinued treatment, all HIV-positive patients were receiving long-term effective antiretroviral treatment. Twelve patients had previously experienced sexually transmitted infections (STIs) other than HIV. STI testing was performed for 8 patients, leading to detection of *Chlamydia trachomatis* DNA in an anal sample for 1 patient and a syphilis diagnosis for 1 patient. Two patients were co-infected with monkeypox virus, and mpox developed in another patient 1 month after the dermatophytosis diagnosis. For 1 patient, TMVII infection and mpox lesions appeared concurrently in the peri-anal region, suggesting transmission of both agents at the same time (Figure).

Four patients denied any travel outside of France, 1 patient was infected in Germany (Munich) where he lived, and for 3 others, lesions developed after they had returned from travel (to Slovenia, Spain, and India). Only 3 patients reported having had contact with animals (cats or dogs). For 2 patients, both sex partners had documented TMVII infection; for 2 others, contamination from sex partners who had similar skin lesions was suspected. Likewise, 2 patients reported secondary appearance of lesions

Figure. Clinical appearance of *Trichohpyton mentagrophytes* genotype VII infections in men in France, 2022. A, B) Swollen lesions of the mustache (A) and beard (kerions) (B). C) Papular and nodular inguinal lesions. D) Peri-anal mpox lesions with associated papules and pustules with central umbilication and a large lesion with a central necrotic crust, surrounded by extensive erythemato-squamous circinate lesions caused by TMVII infection.

Table 2. Cases of *Trichophyton mentagrophytes* genotype VII infections in Europe, 2014–2019*

Reference	Year	Location	Age, y/sex	No. cases	Tinea genitalis	Tinea corporis/ inguinalis	Tinea faciei/ barbae	Tinea glutealis	Comments
(*4*)	2014	Zurich, Switzerland	27/F	NA	Yes	Yes	No	No	Sexual intercourse 1–2 wk before symptom onset, Southeast Asia; similar lesions in 1 sex partner
	2014		24/M	NA	Yes	Yes	No	No	
	2014		31/M	NA	Yes	No	No	No	
(*13*)	2014	St. Petersburg, Russia	ND	NA	No	Yes	No	No	None
(*5*)	ND	Germany	ND/F	NA	Yes	Yes	No	No	Lesions appeared after return from travel in Egypt; indirect transmission was suspected
(*8*)	ND	Germany	ND/M	NA	No	No	Yes	No	Sexual intercourse with female sex workers in Thailand; secondary case in wife's patient (tinea faciei)
(*6*)	2016–2017	Berlin, Germany	20–40/ mostly young men	37	Most frequent presentation was tinea genitalis				4/18 persons traveled in Southeast Asia 5/18 persons had sex partner with similar lesions
(*9*)	2016	Zurich, Switzerland	21/M	NA	Yes	Yes	Yes	No	None
	2016		33/F	NA	Yes	Yes	No	No	
	2018		65/M	NA	No	No	Yes	No	
	2018		50/M	NA	No	No	Yes	No	
(*7*)	2010–2019	Athens, Greece	ND	4	Yes	No	No	No	None

*NA, not applicable; ND, no data.

on the skin of sex partners. However, infection was not medically confirmed.

The median time between lesion appearance and hospital consultation was 28 (range 7–102) days. Five patients had previously received antibiotic, antifungal, or topical steroid treatments. Nine patients received systemic antifungal treatment (terbinafine, itraconazole, or voriconazole) for 3 weeks to 4 months; the others received only topical treatment. One patient with beard kerion and bacterial superinfection (*Klebsiella aerogenes*) was hospitalized. Among the 13 patients, 10 recovered while receiving antifungal therapy, 1 was still receiving treatment at most recent follow-up, and the 2 others were not available for further follow-up. At least 3 patients experienced postinflammatory pigmentation; 2 others had scars or beard hair loss.

During the study period, of 70 strains sequenced, the predominant identified agent was *T. indotineae* (n = 53), followed by TMVII (n = 13) (GenBank accession no. OK632215, ON740661, OP876812–22). The remaining strains corresponded to *T. mentagrophytes* genotype II*.

Conclusions

For most patients in this series, sexually transmitted dermatophytosis was likely. This hypothesis is supported by the sites of the infection (external genitalia, buttocks, face), the high-risk STI profile of the patients, and consistent identification of TMVII. Lack of animal contact for most patients also suggests human-to-human transmission. Moreover, although *T. mentagrophytes* is considered to be a zoophilic species, no animal-to-human transmission has been documented for TMVII and only 1 strain has been isolated from an animal (cat) (*6*). All 13 patients were male, 12 of whom were men who have sex with men. Even if we cannot exclude recruitment bias, the study suggests active circulation of the pathogen within this population. Previous studies reported TMVII infections in men and women whose sexual practices were either heterosexual or not mentioned. Our series demonstrates that TMVII infected the same population of patients as did the monkeypox virus during the 2022 outbreak (*12*). Contrary to previous reports (*4*–*6*), intimate shaving was not associated with TMVII infection in our case series.

Patients might have acquired TMVII infections in France or internationally, supporting the hypothesis of active circulation of TMVII in Europe, in line with the 51 cases reported since 2014 (Table 2). Southeast Asia might have been the starting point of pathogen spread, as suggested by the first reported cases in Europe being associated with travel to that region (*4*–*6*,*8*). Of 37 cases of TMVII infection reported in Berlin, Germany, over 18 months (January 2016–July 2017), only a small proportion of documented cases was associated with travel outside Germany, suggesting that TMVII was already circulating in Europe (*6*).

Our case series is characterized by a substantial delay in diagnosis. Patients with the most inflammatory lesions were initially mistakenly believed to have had bacterial infections (*4*,*8*). Moreover, prolonged systemic antifungal treatments and patient hospitalizations highlight how severe TMVII infections can be (*4*–*6*,*8*). Therefore, healthcare professionals should be aware of the various features of TMVII infection and perform targeted mycological samplings. In contrast to findings for *T. indotineae* (*14*), no terbinafine resistance has been reported for TMVII. Of note, during the study period, *T. indotineae*, which was recently described as an emerging species of dermatophyte in Paris, responsible for difficult-to-treat tinea (*14*), was the main agent of skin dermatophytosis caused by *T. mentagrophytes* complex species.

Transmission of dermatophytes during sexual intercourse is an example of direct human-to-human transmission, as previously described for combat sports (tinea gladiatorum) (*15*). Sexual transmission should be suspected for patients with STI risk factors and tinea corporis, tinea genitalis, tinea glutealis, or tinea faciei. Diagnosis of sexually transmitted dermatophytosis should lead to exhaustive STI screening of patients and their sex partners.

About the Author

Dr. Jabet is a medical mycologist with a specific research interest in emerging fungal infections and dermatophytosis.

References

1. Bakare RA, Oni AA, Umar US, Adewole IF, Shokunbi WA, Fayemiwo SA, et al. Pattern of sexually transmitted diseases among commercial sex workers (CSWs) in Ibadan, Nigeria. Afr J Med Med Sci. 2002;31:243–7.
2. Otero L, Palacio V, Vázquez F. Tinea cruris in female prostitutes. Mycopathologia. 2002;153:29–31. https://doi.org/10.1023/A:1015257320824
3. Mølenberg D, Deleuran M, Sommerlund M. Connubial tinea gladiatorum due to Trichophyton mentagrophytes. Mycoses. 2010;53:533–4. https://doi.org/10.1111/j.1439-0507.2009.01734.x
4. Luchsinger I, Bosshard PP, Kasper RS, Reinhardt D, Lautenschlager S. Tinea genitalis: a new entity of sexually transmitted infection? Case series and review of the literature. Sex Transm Infect. 2015;91:493–6. https://doi.org/10.1136/sextrans-2015-052036
5. Nenoff P, Schubert K, Jarsumbeck R, Uhrlaß S, Krüger C. Tinea genitalis profunda durch Trichophyton mentagrophytes nach Ägypten-Reise. Akt Dermatol. 2017;43:146–53.
6. Kupsch C, Czaika V, Deutsch C, Gräser Y. Trichophyton mentagrophytes—a new genotype of zoophilic dermatophyte causes sexually transmitted infections. J Dtsch Dermatol Ges. 2019;17:493–501. https://doi.org/10.1111/ddg.13776
7. Siopi M, Efstathiou I, Theodoropoulos K, Pournaras S, Meletiadis J. Molecular epidemiology and antifungal susceptibility of Trichophyton isolates in Greece: emergence of terbinafine-resistant Trichophyton mentagrophytes type VIII locally and globally. J Fungi (Basel). 2021;7:419. https://doi.org/10.3390/jof7060419
8. Wendrock-Shiga G, Mechtel D, Uhrlaß S, Koch D, Krüger C, Nenoff P. Tinea barbae profunda due to Trichophyton mentagrophytes after journey to Thailand: case report and review [in German]. Hautarzt. 2017;68:639–48. https://doi.org/10.1007/s00105-017-4008-2
9. Klinger M, Theiler M, Bosshard PP. Epidemiological and clinical aspects of Trichophyton mentagrophytes/Trichophyton interdigitale infections in the Zurich area: a retrospective study using genotyping. J Eur Acad Dermatol Venereol. 2021;35:1017–25. https://doi.org/10.1111/jdv.17106
10. Taghipour S, Pchelin IM, Zarei Mahmoudabadi A, Ansari S, Katiraee F, Rafiei A, et al. Trichophyton mentagrophytes and T interdigitale genotypes are associated with particular geographic areas and clinical manifestations. Mycoses. 2019;62:1084–91. https://doi.org/10.1111/myc.12993
11. Moreno-Sabater A, Normand AC, Bidaud AL, Cremer G, Foulet F, Brun S, et al. Terbinafine resistance in dermatophytes: a French multicenter prospective study. J Fungi (Basel). 2022;8:220. https://doi.org/10.3390/jof8030220
12. Thornhill JP, Barkati S, Walmsley S, Rockstroh J, Antinori A, Harrison LB, et al.; SHARE-net Clinical Group. Monkeypox virus infection in humans across 16 countries—April–June 2022. N Engl J Med. 2022;387:679–91. https://doi.org/10.1056/NEJMoa2207323
13. Pchelin IM, Zlatogursky VV, Rudneva MV, Chilina GA, Rezaei-Matehkolaei A, Lavnikevich DM, et al. Reconstruction of phylogenetic relationships in dermatomycete genus Trichophyton Malmsten 1848 based on ribosomal internal transcribed spacer region, partial 28S rRNA and beta-tubulin genes sequences. Mycoses. 2016;59:566–75. https://doi.org/10.1111/myc.12505
14. Jabet A, Brun S, Normand AC, Imbert S, Akhoundi M, Dannaoui E, et al. Extensive dermatophytosis caused by terbinafine-resistant Trichophyton indotineae, France. Emerg Infect Dis. 2022;28:229–33. https://doi.org/10.3201/eid2801.210883
15. Kermani F, Moosazadeh M, Hosseini SA, Bandalizadeh Z, Barzegari S, Shokohi T. Tinea gladiatorum and dermatophyte contamination among wrestlers and in wrestling halls: a systematic review and meta-analysis. Curr Microbiol. 2020;77:602–11. https://doi.org/10.1007/s00284-019-01816-3

Address for correspondence: Arnaud Jabet, Service de Parasitologie-Mycologie, Hôpital de La Pitié-Salpêtrière, 47-83 Blvd de l'Hôpital, 75013 Paris, France; email: arnaud.jabet@aphp.fr

Pulmonary Nontuberculous Mycobacteria, Ontario, Canada, 2020

Theodore K. Marras, Paul Nelson, Adriana Peci, Melissa Richard-Greenblatt, Sarah Brode, Ashleigh Sullivan, Frances B. Jamieson, Julianne V. Kus

We measured annual prevalence of microbiologically defined nontuberculous mycobacterial lung disease in Ontario, Canada. *Mycobacterium avium* prevalence was 13 cases/100,000 persons in 2020, a 2.5-fold increase from 2010, indicating a large increase in true *M. avium* lung disease. During the same period, *M. xenopi* decreased nearly 50%, to 0.84 cases/100,000 persons.

Nontuberculous mycobacterial (NTM) pulmonary disease (NTM-PD) is increasingly common and difficult to manage (*1*). Thus, understanding its epidemiology is essential but challenging because the diagnosis requires microbiological, radiological, and clinical information (*1*). Because NTM-PD is not reportable in most jurisdictions, data required to study its epidemiology are generally unavailable. Many investigators have thus solely used microbiological criteria as a surrogate disease definition (*2*). We previously observed large increases in *Mycobacterium avium* complex (MAC) isolation in Ontario, Canada, during 1998–2010 (*3*). We report more recent prevalence of NTM-PD in Ontario.

The Study

This retrospective cross-sectional study of persons in Ontario who had pulmonary NTM isolates during 2020 used Public Health Ontario's laboratory records, which capture ≈95% of NTM in Ontario. We prepared cultures by using BACTEC MGIT 960 (Becton Dickinson, https://www.bd.com) and Lowenstein-Jensen slants. We used matrix-assisted laser desorption/ionization time-of-flight mass spectrometry, line-probe assays (GenoType; Hain Lifescience, https://www.hain-lifescience.de), a laboratory-developed MAC real-time PCR, or 16S rDNA sequencing to identify NTM to species/subspecies levels.

Lacking clinical information, we defined surrogate NTM-PD criteria microbiologically, in 3 categories: uncertain (single sputum), standard (guidelines' microbiological definition [*1*]), and strict (additional culture required) (Figure 1). Although standard microbiological criteria demonstrated a 70%–100% positive predictive value (*3*), we created the strict category (subset of standard) because it is unknown whether the diagnostic test characteristics might vary by potentially changing levels of environmental NTM exposure, possibly affecting frequencies of specimen contamination or colonization. Patients who had NTM isolated in 2020 had previous 24-month sample histories reviewed to determine if they reached disease thresholds. W used Statistics Canada population data for calculating prevalence and age- and sex-standardization (https://www150.statcan.gc.ca/t1/tbl1/en/tv.action?pid = 1710000501). We performed analysis by using SAS Enterprise Guide 9.4 (SAS Institute, https://www.sas.com). The Public Health Ontario Ethics Review Board approved this study.

During 2020, the population of Ontario was 14,726,022, and of 41,471 pulmonary samples tested for mycobacteriology, 8,412 (20.3%) grew NTM. All-species prevalence (cases/100,000 population) by NTM-PD definition was as follows: uncertain, 12.9 (n = 1,899); standard, 19.2 (n = 2,824); and strict, 10.9 (n = 1,602), (Table 1, by species). Overall cases of standard (69.2%) and strict (73.1%) microbiological disease were caused mostly by *M. avium* (69.2% and 73.1%), followed by *M. intracellulare* (6.4% and 6.3%), *M .abscessus* (5.8% and 7.1%), and *M. xenopi* (4.4% and 3.9%).

More female than male patients were classified with standard disease (1,507 [53.4%] vs. 1,285 [45.5%]) and strict disease (892 [55.7%] vs. 696 [43.4%]) (Table

Author affiliations: University of Toronto, Toronto, Ontario, Canada (T.K. Marras, M. Richard-Greenblatt, S. Brode, F.B. Jamieson, J.V. Kus); University Health Network and Mount Sinai Hospital, Toronto (T.K. Marras, S. Brode); Public Health Ontario, Toronto (P. Nelson, A. Peci, M. Richard-Greenblatt, A. Sullivan, F.B. Jamieson, J.V. Kus); University of Oxford, Oxford, UK (M. Richard-Greenblatt); West Park Healthcare Centre, Toronto (S. Brode)

DOI: https://doi.org/10.3201/eid2907.230216

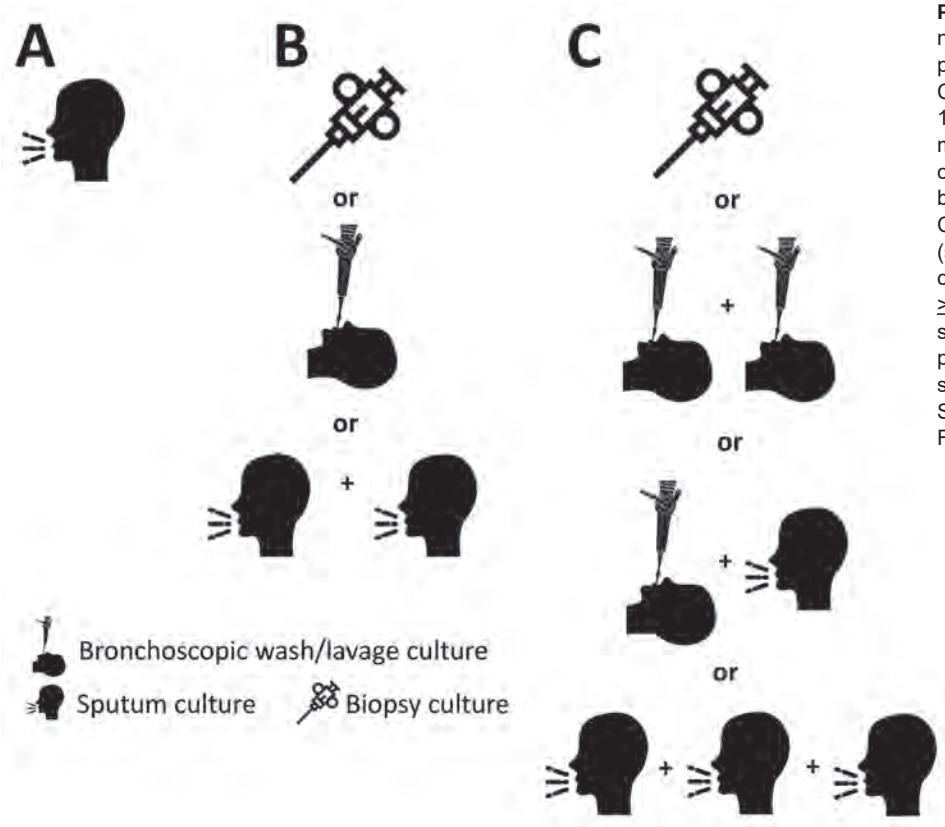

Figure 1. Categories of nontuberculous mycobacteria pulmonary disease, Ontario, Canada, 2020. A) Uncertain state: 1 sputum culture. B) Standard microbiological criteria: ≥2 sputum cultures with the same species, or 1 bronchoscopic or lung biopsy culture. C) Strict microbiological criteria (subset of standard): ≥3 sputum cultures with the same species, or ≥2 bronchoscopic cultures with the same species, or 1 bronchoscopic plus 1 sputum culture with the same species, or 1 lung biopsy culture. Some images were obtained from Flaticon (https://www.flaticon.com).

2). Substantial discrepancies in sex ratio from parity were seen for *M. avium*, *M. intracellulare*, and *M. abscessus*, favoring female patients, and *M. gordonae*, favoring male patients. Adjusting for population sex distribution did not greatly alter those observations.

Depending on species, patients who were ≥60 years of age comprised 63%–85% (74.2% overall) of those with standard disease and 61%–85% (76.9% overall) of those with strict disease (Appendix Table 1, https://wwwnc.cdc.gov/EID/article/29/7/23-0216-

Table 1. Characteristics of pulmonary nontuberculous mycobacterial disease, by microbiological definition, among patients in Ontario, Canada, 2020*

NTM species/subspecies	Standard definition†		Strict definition‡	
	No. (%) patients	Prevalence§	No. (%) patients	Prevalence§
Common MAC species				
M. avium	1,954 (69.2)	13.27	1,171 (73.1)	7.95
M. intracellulare	182 (6.4)	1.24	101 (6.3)	0.69
M. chimaera	39 (1.4)	0.26	18 (1.1)	0.12
M. abscessus and its subspecies				
M. abscessus (total)	164 (5.8)	1.11	114 (7.1)	0.77
subspecies *abscessus*	95 (3.4)	0.65	66 (4.1)	0.45
subspecies *bolletii*	1 (0.04)	0.01	1 (0.06)	0.01
subspecies *massiliense*	52 (1.8)	0.35	38 (2.4)	0.26
subspecies unassigned	16 (0.6)	0.11	9 (0.6)	0.06
Other species				
M. xenopi	123 (4.4)	0.84	63 (3.9)	0.43
M. fortuitum	98 (3.5)	0.67	53 (3.3)	0.36
M. gordonae	117 (4.1)	0.79	26 (1.6)	0.18
Other NTM species	147 (5.2)	1.00	56 (3.5)	0.38
Total	2,824 (100)	19.0	1,602 (100)	10.9

*Counts within each disease definition represent unique patients; some patients fulfilled criteria for >1 species. MAC, *Mycobacterium avium* complex; NTM, nontuberculous myobacteria.
†Standard microbiological criteria: ≥2 sputum cultures with the same species, or 1 bronchoscopic or lung biopsy culture.
‡Strict microbiological criteria (subset of standard): ≥3 sputum cultures with the same species, or ≥2 bronchoscopic cultures with the same species, or 1 bronchoscopic plus 1 sputum culture with the same species, or 1 lung biopsy culture.
§Cases per 100,000 population.

Table 2. Patients with pulmonary NTM, by microbiological definition, *Mycobacterium* species, and patient sex, Ontario, Canada, 2020*

	Standard definition, no. (%) patients†			Strict definition, no. (%) patients‡		
NTM species	Female	Male	Unknown	Female	Male	Unknown
M. avium	1,051 (53.8)	881 (45.1)	22 (1.1)	653 (55.8)	506 (43.2)	12 (1.0)
M. intracellulare	114 (62.6)	65 (35.7)	3 (1.6)	71 (70.3)	28 (27.7)	2 (2.0)
M. chimaera	17 (43.6)	22 (56.4)	0	10 (55.6)	8 (44.4)	0
M. abscessus	102 (62.1)	62 (37.8)	0	68 (59.6)	46 (40.4)	0
M. xenopi	63 (51.2)	57 (46.3)	3 (2.4)	29 (46.0)	34 (54.0)	0
M. fortuitum	47 (48.0)	50 (51.0)	1 (1.0)	26 (49.1)	27 (50.9)	0
M. gordonae	46 (39.3)	70 (59.8)	1 (0.9)	10 (38.5)	16 (61.5)	0
Other NTM	67 (45.6)	78 (53.1)	2 (1.4)	25 (44.6)	31 (55.4)	0
Total	1,507 (53.4)	1,285 (45.5)	32 (1.1)	892 (55.7)	696 (43.4)	14 (0.9)

*Counts within each disease definition represent unique patients; some patients fulfilled criteria for >1 species. NTM, nontuberculous mycobacteria.
†Standard microbiological criteria: >2 sputum cultures with the same species, or 1 bronchoscopic or lung biopsy culture
‡Strict microbiological criteria (subset of standard): >3 sputum cultures with the same species, or >2 bronchoscopic cultures with the same species, or 1 bronchoscopic plus 1 sputum culture with the same species, or 1 lung biopsy culture.

App1.pdf). Younger patients generally represented small minorities. Age-standardized prevalence ratio for all species combined increased from 0.05 in the youngest age group to 4.46 in the oldest age group among patients meeting standard criteria and from 0.07 to 4.56 among patients meeting strict criteria.

We found striking regional heterogeneity in the frequency of NTM-PD (Figure 2; Appendix Table 2). Prevalence of all-species NTM-PD, by standard and strict definitions was lowest in the North West region (3.8 vs. 2.9 cases/100,000 persons) and highest in Toronto (49.8 vs. 28.8 cases/100,000 persons). We compiled selected comparisons between nonoverlapping groups (exclusively standard versus strict definition patients) (Appendix Tables 3, 4).

Conclusions

In this population-based study of NTM-PD in Ontario, we observed high levels by using standard (19.0 cases/100,000 persons) and strict (10.9 cases/100,000 persons) microbiological criteria. *M. avium* comprised most of cases, followed distantly by *M. intracellulare* and *M. abscessus* and less commonly *M. xenopi*. The total NTM-PD prevalence (standard definition) of 19.0 cases/100,000 persons was nearly double the previously reported 9.8 cases/100,000 persons in 2010 (*3*). During the same period, *M. xenopi* prevalence decreased by nearly half, from 1.54 to 0.84 cases/100,000 persons, and *M. abscessus* increased 3.7-fold, from 0.30 to 1.11 cases/100,000 persons (*3*). In our previous study, *M. avium* was not separated from other MAC species, but ≈85% of contemporary Ontario MAC isolates were *M. avium* (*4*). The prevalence of *M. avium* pulmonary disease in Ontario, by standard microbiological definition, increased 2.5-fold, from 5.34 cases/100,000 persons in 2010 (*3*) to 13.27 cases/100,000 persons in 2020, explaining virtually all of the NTM-PD increase.

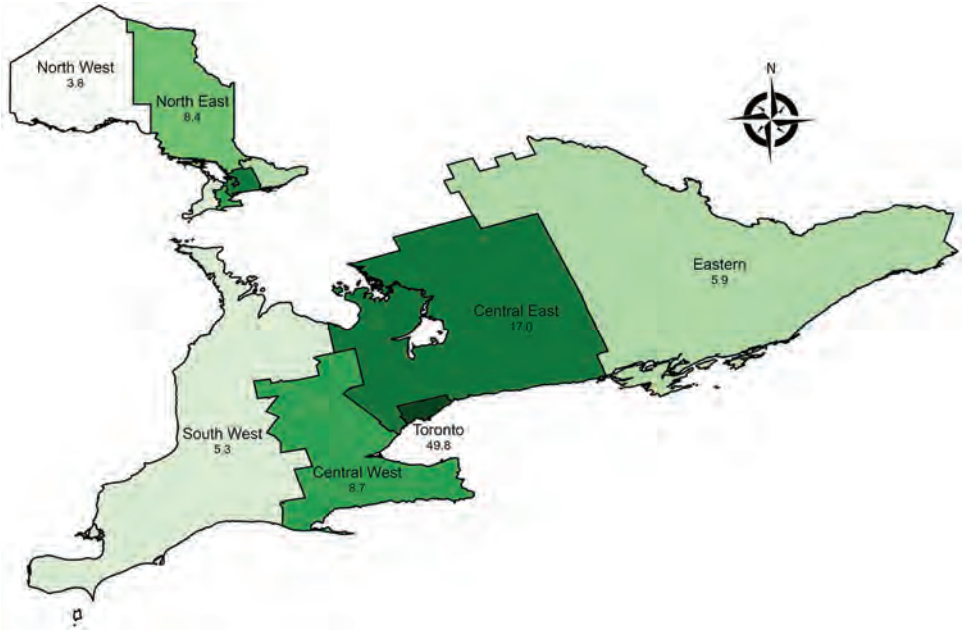

Figure 2. Prevalence of nontuberculous mycobacterial pulmonary disease (standard definition) by Ontario health region, Ontario, Canada, 2020. Numbers below region names indicate number of cases per 100,000 population.

Historically, most population-based studies (*2*) and a recent large managed care study in the United States (*5*) have shown increases in NTM-PD. Trends in NTM species frequencies were reviewed in 8 recent population-based studies that had species-level data (*6*–*13*). In Denmark (1997–2008) (*6*) and Madrid, Spain (2013–2017) (*7*), there were no convincing trends. In Croatia (2006–2010), *M. fortuitum* increased (*8*). The remaining 5 studies demonstrated large increases in MAC (Barcelona/Catalonia in 1994–2014 [*9*]; Queensland, Australia, in 1999–2005 [*10*]; and the United Kingdom in 2007–2012 [*11*]) or specifically *M. avium* (the Netherlands in 2000–2006 [*12*] and Belgium in 2007–2016 [*13*]), without major changes in other species. The Ontario experience is similar, with the exception of the reduction in *M. xenopi*. Most other regions had increases in other species in addition to *M. avium* or MAC. The marked reduction in *M. xenopi* in this study is unexplained but might be related to the increase in *M. avium*. *M. avium* might be outcompeting *M. xenopi* in a common environmental niche or overgrowing the slow-growing *M. xenopi* in culture.

The main limitation of our study is the lack of clinical and radiological information. Defining NTM-PD solely on microbiological criteria overestimates prevalence by misclassifying persons who fulfil microbiological criteria but not clinical/radiological criteria. Although microbiological criteria have good positive predictive values, the diagnostic test characteristics might be unstable (e.g., if there is a major change in NTM exposure). As suggested by hospital NTM pseudo-outbreaks (*14*), increased environmental NTM exposure might increase colonization or contamination of oropharyngeal and airway mucosal secretions and thereby specimens submitted for mycobacterial testing, thus reducing the positive predictive value of microbiological criteria for NTM-PD.

Given our uncertainties, we chose standard and strict for disease definitions, rather than previously used terms such as definite. Regardless, we believe that an increase in environmental NTM exposure, probably contributing to our large increase in *M. avium* isolation, would eventually cause increased disease. There were no changes in laboratory methods explaining the observed *M. avium* increase, and there was no consistent increase in contemporary specimen submission (increased testing bias). Given the absence of laboratory changes, we believe that the increase is related to increased environmental exposures, resulting in increased colonization and disease, or better patient identification for testing by clinicians. Concerning better patient identification for testing, the proportion of culture-positive pulmonary specimens increased from ≈10% in 2010 to 20.3% in 2020 (18.0% in 2018 and 19.3% in 2019). There was a near-linear increase in chest computed tomography (CT) scanning in Ontario during 2007–2016 (*15*), possibly increasing detection because CT scans identify characteristic findings of NTM, accurately driving clinical suspicion. Increased CT use probably contributes to greater detection of true disease, although it could not explain the reduction in *M. xenopi*.

In summary, this study identified a large increase in the prevalence of microbiologically defined *M. avium* lung disease in this region, undoubtedly indicating a large increase in the prevalence of true lung disease caused by *M. avium*. Clinicians should be aware of the causes of this increase and investigators should determine to what extent the increase in microbiologically defined disease reflects true disease.

About the Author

Dr. Marras is an attending staff physician in the Division of Respirology, Department of Medicine, University Health Network and Mount Sinai Hospital, Toronto, and associate professor of medicine, University of Toronto and Director of the Toronto Western Hospital Nontuberculous Mycobacterial Program. His primary research interest is nontuberculous mycobacterial disease, with a particular interest in epidemiology.

References

1. Daley CL, Iaccarino JM Jr, Lange C, Cambau E, Wallace RJ Jr, Andrejak C, et al. Treatment of nontuberculous mycobacterial pulmonary disease: an official ATS/ERS/ESCMID/IDSA clinical practice guideline. Eur Respir J. 2020; 56:2000535. https://doi.org/10.1183/13993003.00535-2020
2. Prevots DR, Marras TK. Epidemiology of human pulmonary infection with nontuberculous mycobacteria: a review. Clin Chest Med. 2015;36:13–34. https://doi.org/10.1016/j.ccm.2014.10.002
3. Marras TK, Mendelson D, Marchand-Austin A, May K, Jamieson FB. Pulmonary nontuberculous mycobacterial disease, Ontario, Canada, 1998–2010. Emerg Infect Dis. 2013;19:1889–91. https://doi.org/10.3201/eid1911.130737
4. Heffer MJ, Al-Ghimlas F, Hoffstein V, Jamieson FB, Mehta M, Chedore P, et al. Mycobacterium avium and Mycobacterium intracellulare: distinct pathogens or just a "complex"? In: Abstracts of the American Thoracic Society 2010 International Conference: New Orleans, Louisiana, May 14–19, 2010. Am J Respir Crit Care Med. 2010;181;A2608.
5. Winthrop KL, Marras TK, Adjemian J, Zhang H, Wang P, Zhang Q. Incidence and prevalence of nontuberculous mycobacterial lung disease in a large U.S. managed care health plan, 2008–2015. Ann Am Thorac Soc. 2020;17:178–85. https://doi.org/10.1513/AnnalsATS.201804-236OC
6. Andréjak C, Thomsen VO, Johansen IS, Riis A, Benfield TL, Duhaut P, et al. Nontuberculous pulmonary mycobacteriosis

in Denmark: incidence and prognostic factors. Am J Respir Crit Care Med. 2010;181:514–21. https://doi.org/10.1164/rccm.200905-0778OC
7. López-Roa P, Aznar E, Cacho J, Cogollos-Agruña R, Domingo D, García-Arata MI, et al. Epidemiology of non-tuberculous mycobacteria isolated from clinical specimens in Madrid, Spain, from 2013 to 2017. Eur J Clin Microbiol Infect Dis. 2020;39:1089–94. https://doi.org/10.1007/s10096-020-03826-7
8. Jankovic M, Samarzija M, Sabol I, Jakopovic M, Katalinic Jankovic V, Zmak L, et al. Geographical distribution and clinical relevance of non-tuberculous mycobacteria in Croatia. Int J Tuberc Lung Dis. 2013;17:836–41. https://doi.org/10.5588/ijtld.12.0843
9. Santin M, Barrabeig I, Malchair P, Gonzalez-Luquero L, Benitez MA, Sabria J, et al. Pulmonary infections with nontuberculous mycobacteria, Catalonia, Spain, 1994–2014. Emerg Infect Dis. 2018;24:1091–4. https://doi.org/10.3201/eid2406.172095
10. Thomson RM; NTM working group at Queensland TB Control Centre and Queensland Mycobacterial Reference Laboratory. Changing epidemiology of pulmonary nontuberculous mycobacteria infections. Emerg Infect Dis. 2010;16:1576–83. https://doi.org/10.3201/eid1610.091201
11. Shah NM, Davidson JA, Anderson LF, Lalor MK, Kim J, Thomas HL, et al. Pulmonary Mycobacterium avium-intracellulare is the main driver of the rise in non-tuberculous mycobacteria incidence in England, Wales and Northern Ireland, 2007–2012. BMC Infect Dis. 2016;16:195. https://doi.org/10.1186/s12879-016-1521-3
12. van Ingen J, Hoefsloot W, Dekhuijzen PN, Boeree MJ, van Soolingen D. The changing pattern of clinical Mycobacterium avium isolation in the Netherlands. Int J Tuberc Lung Dis. 2010;14:1176–80.
13. Soetaert K, Subissi L, Ceyssens P-J, Vanfleteren B, Chantrenne M, Asikainen T, et al. Strong increase of true and false positive mycobacterial cultures sent to the National Reference Centre in Belgium, 2007 to 2016. Euro Surveill. 2019;24:1800205. https://doi.org/10.2807/1560-7917.ES.2019.24.11.1800205
14. D'Antonio S, Rogliani P, Paone G, Altieri A, Alma MG, Cazzola M, et al. An unusual outbreak of nontuberculous mycobacteria in hospital respiratory wards: association with nontuberculous mycobacterial colonization of hospital water supply network. Int J Mycobacteriol. 2016;5:244–7. https://doi.org/10.1016/j.ijmyco.2016.04.001
15. Smith-Bindman R, Kwan ML, Marlow EC, Theis MK, Bolch W, Cheng SY, et al. Trends in use of medical imaging in US health care systems and in Ontario, Canada, 2000–2016. JAMA. 2019;322:843–56. https://doi.org/10.1001/jama.2019.11456

Address for correspondence: Theodore K. Marras, Toronto Western Hospital, 7E-452, 399 Bathurst St, Toronto, ON, M5T 2S8, Canada; email: ted.marras@uhn.on.ca

etymologia revisited

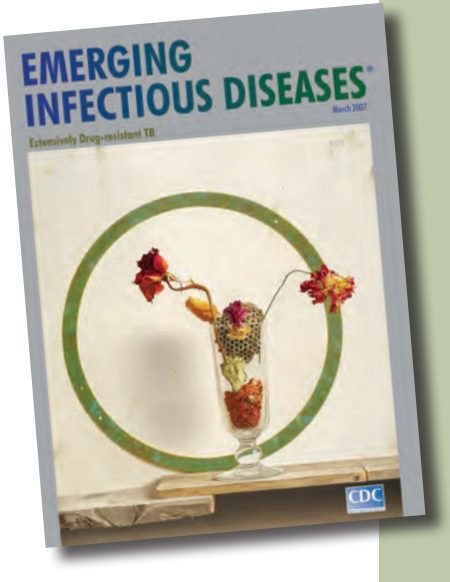

Originally published in March 2007

Norovirus
[nor'-o-vi'rəs]

Genus of viruses that cause viral gastroenteritis. Noroviruses are named after the original strain, "Norwalk virus," which caused an outbreak of acute gastroenteritis among children at an elementary school in Norwalk, Ohio, in 1968. Numerous outbreaks of disease with similar symptoms have been reported since, and the etiologic agents were called "Norwalk-like viruses" or "small round-structured viruses." Noroviruses are transmitted primarily through the fecal-oral route and are highly contagious; as few as 10 viral particles may infect a person.

Source:

1. Mahy BWJ. A dictionary of virology. London: Academic Press; 2001; www.cdc.gov/ncidod/dvrd/revb/gastro/norovirus-qa.htm; www.medicinenet.com/norovirus_infection/article.htm

https://wwwnc.cdc.gov/eid/article/13/3/e1-1303_article

Evolutionary Formation and Distribution of Puumala Virus Genome Variants, Russia

Ekaterina Blinova, Andrei Deviatkin, Marat Makenov, Yulia Popova, Tamara Dzagurova

We analyzed Puumala virus (PUUV) sequences collected from bank voles from different regions of Russia. Phylogenetic analysis revealed PUUV reassortments in areas with the highest hemorrhagic fever with renal syndrome incidence, indicating reassortment might contribute to pathogenic properties of PUUV. Continued surveillance is needed to assess PUUV pathogenicity in Russia.

In Eurasia, hantaviruses cause hemorrhagic fever with renal syndrome (HFRS), which is the most common zoonosis in Russia (*1*). During 2000–2017, a total of 131,590 HFRS cases were reported in Russia (*2*); most (≈98%) HFRS cases are caused by Puumala virus (PUUV) (*2*).

PUUV virions are enveloped particles containing 3 negative-sense single-strand RNA segments (*3*). Those segments vary in length; the large (L) segment is ≈6,550 nt long, the medium (M) segment is ≈3,650 nt, and the small (S) segment is ≈1,828 nt (*4*).

PUUV comprises 8 lineages: Central European, Alpe-Adrian, Danish, South-Scandinavian, North-Scandinavian, Finnish (FIN), Russian (RUS), and Latvian (LAT) (*4*–*6*). Modern PUUV diversity arose from multiple migrations of the viral host, the bank vole (*Clethrionomys glareolus*), during the postglacial period (*7*,*8*); that species also comprises several lineages: Ural, Eastern, Spanish, Italian, Balkan, Western, Carpathian, Basque, and Calabrian (*9*). The LAT, FIN, and RUS PUUV lineages likely had a common ancestor and originated from Eastern refugia (*6*). Those sublineages are carried by *C. glareolus* from Western, Eastern, and Carpathian lineages (*10*,*11*).

The RUS and FIN PUUV lineages are known to exist in Russia (*4*,*8*). Although PUUV-related HFRS has been reported from 54 regions of Russia (*2*), complete protein-coding sequences of the S segment in GenBank are only available from 8 regions: Kursk, Saratov, Samara, Tatarstan, Udmurtia, Bashkortostan, Omsk, and Karelia (Figure 1). Those sequences are mainly from viruses collected in the most epidemiologically active HFRS PUUV hotspots in the Volga region (*2*). PUUV genome variants in 46 other regions of Russia are still unknown. We investigated the distribution of different PUUV genome variants in Russia by obtaining PUUV sequences from bank voles captured in different regions.

The Study

We obtained lung tissue samples from bank voles collected by the territorial Centers of Hygiene and Epidemiology in the Arkhangelsk, Ivanovo, Moscow, Penza, Saratov, Tyumen, Ulyanovsk, and Udmurtia regions (Figure 1). We stored samples, analyzed hantavirus antibodies by immunofluorescence assay (Table 1), extracted RNA, determined samples with high viral RNA content by real-time reverse transcription PCR (Table 1), and sequenced them as described in previous research (*12*).

To determine bank vole sublineages, we obtained sequences of the *cytochrome b* gene by using a previously described protocol (*13*). In all, we obtained PUUV genomic sequences and *cytochrome b* sequences from 17 bank voles (Appendix Table 1, https://wwwnc.cdc.gov/EID/article/29/7/22-1731-App1.pdf). All voles belonged to the Eastern lineage of *C. glareolus* (Appendix Figure 1).

We mapped locations of the newly obtained PUUV sequences and all representative LAT, FIN, and RUS lineage sequences available in GenBank that had complete S segment coding sequences (Figure 1).

Author affiliations: Central Research Institute of Epidemiology, Moscow, Russia (E. Blinova, M. Makenov); Russian Academy of Sciences, Moscow (E. Blinova, Y. Popova, T. Dzagurova); Moscow Institute of Physics and Technology, Dolgoprudny, Russia (A. Deviatkin); Sechenov First Moscow State Medical University, Moscow (A. Deviatkin)

DOI: https://doi.org/10.3201/eid2907.221731

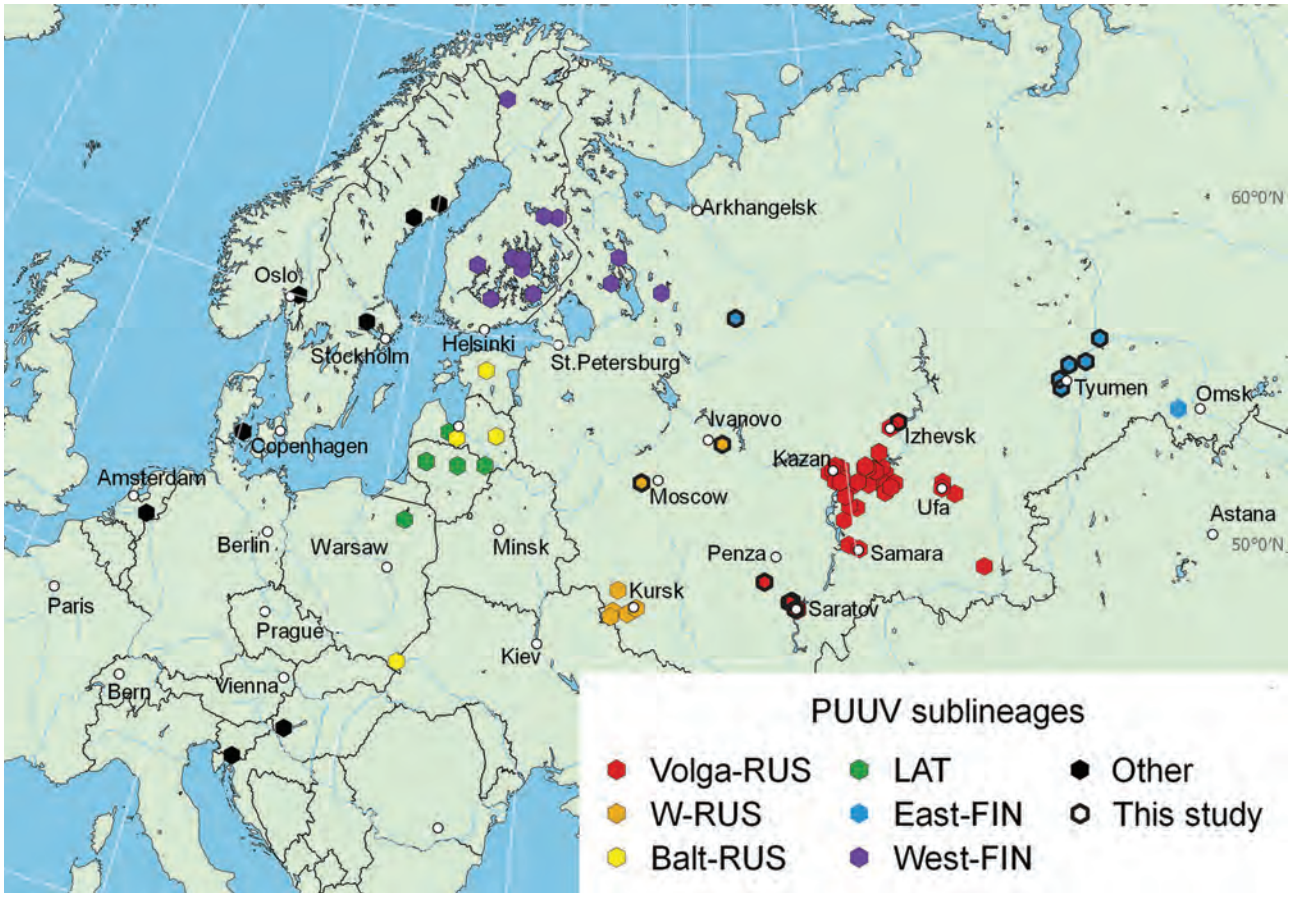

Figure 1. Locations of virus isolation in a study of the evolutionary formation and distribution of Puumala virus genome variants, Russia. The map includes all genome variants belonging to LAT, FIN (West-FIN and East-FIN sublineages), and RUS (W-RUS, Volga-RUS, and Balt-RUS) lineages that had complete coding sequences of the small (S) genome segment available in GenBank as of September 16, 2022. The map was created by using QGIS software (QGIS Development Team, http://qgis.osgeo.org). Color marking for sequences in the map correspond to those in phylogenetic trees (Figure 2). Black frames indicate isolation sites of novel sequences revealed in this study. Because other lineages were not the focus of this study, only a few Puumala virus sequences belonging to other lineages were included. An additional interactive map was generated in R (The R Foundation for Statistical Computing, https://www.r-project.org) by using the leaflet, html widgets, and webshot libraries and is available at https://rpubs.com/andreideviatkin/PUUV_RUS-FIN-LAT_lineages. Balt-RUS, sublineage from the Baltic coast region; East-FIN, sublineage from Siberia and northern Russia; FIN, Finnish lineage; LAT, Latvian lineage; RUS, Russian lineage; Volga-RUS, sublineage from the Volga River Valley; W-RUS, sublineage from western Russia; West-FIN, sublineage from western Finland and Russian Karelia.

We also included representative sequences of other PUUV lineages on the map.

For phylogenetic analysis, we added sequences from this study to GenBank representatives of the LAT, FIN, and RUS lineages. We included representatives of the other PUUV lineages as outgroup (*6*) (Figure 2). According to S-segment phylogeny, we propose dividing the RUS lineage into 3 phylogenetically based sublineages: W-RUS (from western Russia) (*12*), Balt-RUS (from the Baltic coast region), and Volga-RUS (from the Volga River Valley). The percentages of identical nucleotides and amino acids within and between the sublineages did not enable us to establish clear criteria for the delimitation of the sublineages according to the quantitative differences (Table 2).

The topology of our S-segment tree does not match those from previous studies (*12*). The sequences we obtained provide additional information for better resolution of PUUV. L and S segments of PUUV are com-

Table 1. Virus test results for *Clethrionomys glareolus* bank voles captured and tested in study of evolutionary formation and distribution of Puumala virus genome variants, Russia*

Region	No. trapped	No. IFA-positive	No. PCR-positive
Arkhangelsk	43	10	8
Ivanovo	2	2	2
Moscow	61	12	10
Penza	54	28	27
Saratov	44	14	14
Tyumen	110	10	9
Ulyanovsk	98	7	7
Udmurtia	32	9	9

*IFA, immunofluorescence assay.

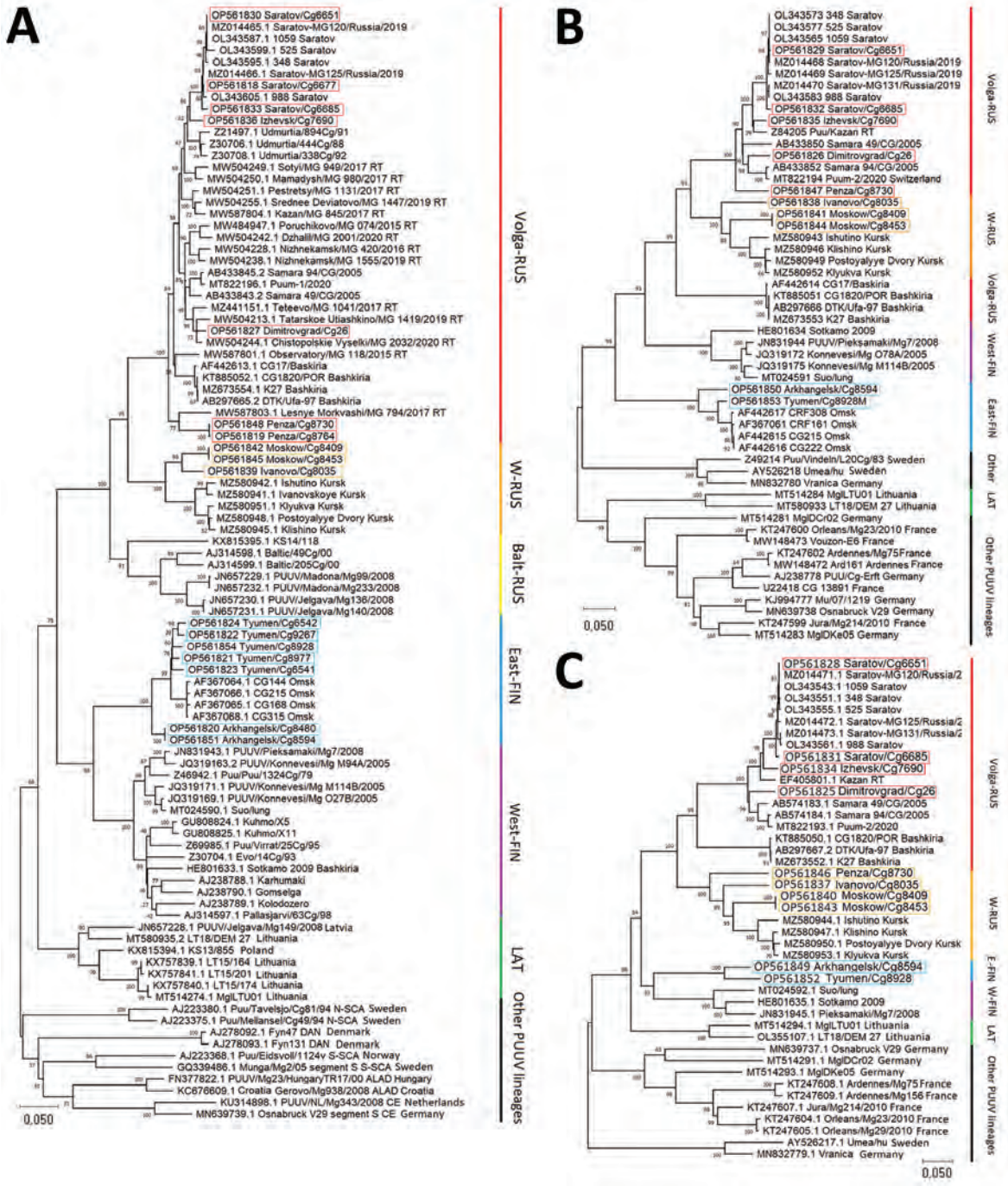

Figure 2. Phylogenetic trees of small (S), medium (M), and large (L) segments in a study of evolutionary formation and distribution of Puumala virus genome variants, Russia. A) S segment based on complete open reading frame (ORF) of 1,302 nt; B) M segment based on partial ORF 2,923 nt (525–3,447 nt of ORF of GenBank accession no. OL343565); C) L segment based on partial ORF 6,405 nt (5–6,409 nt of ORF of GenBank accession no. OL343543). The RUS lineage is divided into 3 large, color-coded subclades: Volga-RUS (red), W-RUS (orange), Balt-RUS (yellow). The FIN lineage is divided into 2 large, color-coded subclades: East-FIN (blue) and West-FIN (purple). Green indicates LAT lineage; black indicates other lineages. Boxes indicated sequences obtained in this study. GenBank accession numbers are provided for all sequences. All alignments and phylogenetic relationships of the sequences were conducted by the MUSCLE algorithm (https://www.ebi.ac.uk/Tools/msa/muscle) and maximum-likelihood method with the general time-reversible model and 1,000 bootstrap by using MEGA version X (https://www.megasoftware.net). The full S segment tree with complete dataset of all available representatives of LAT, FIN, and RUS lineages are available from https://github.com/AndreiDeviatkin/repo/blob/main/S_PUUV.png. Balt-RUS, sublineage from the Baltic coast region; East-FIN, sublineage from Siberia and northern Russia; FIN, Finnish lineage; LAT, Latvian lineage; RUS, Russian lineage; Volga-RUS, sublineage from the Volga River Valley; W-RUS, sublineage from western Russia; West-FIN, sublineage from Finland and Russian Karelia.

Table 2. Percentage identity between sublineages in study of evolutionary formation and distribution of Puumala virus genome variants, Russia*

Sublineage, no. sequences	Volga-RUS, n = 37	W-RUS, n = 8	Balt-RUS, n = 7	East-FIN, n = 11	West-FIN, n = 15	LAT, n = 7
Volga-RUS	97.47–100, 92.93–100	96.77–98.85	95.39–98.16	95.39–97.47	94.01–97.7	95.16–97.24
W-RUS	86.57–90.17	98.62–100, 91.17–100	97.24–98.39	96.77–97.7	94.93–97.93	96.77–97.93
Balt-RUS	85.88–88.86	85.57–88.88	97.93–100, 87.92–100	96.31–97.7	94.70–97.93	96.31–97.93
East-FIN	84.57–86.86	85.17–87.42	85.34–87.39	98.85–100, 94.24–100	96.08–99.08	97.00–97.93
West-FIN	84.27–86.87	85.03–86.77	83.86–86.73	87.02–89.55	96.54–100, 91.01–100	95.39–97.93
LAT	84.38–87.19	85.19–87.27	84.49–86.94	85.93–87.57	84.77–88.23	99.31–100, 89.77–100

*Amino acid and nucleotide identity are shown according to small (S) segment coding sequences. Gray shading indicates nucleocapsid (N) protein calculated by blastp (https://blast.ncbi.nlm.nih.gov), and S complete coding by blastn. Upper triangular matrix indicates identity values based on the complete N protein calculated using the blastp algorithm; lower triangular matrix indicates values based on the S complete coding sequence calculated using the blastn algorithm. Balt-RUS, sublineage from the Baltic coast region; East-FIN, sublineage from Siberia and Russian North; LAT, Latvian lineage; Volga-RUS, sublineage from the Volga River Valley; W-RUS, sublineage from western Russia; West-FIN, sublineage from Finland and Russian Karelia.

parably conservative (Appendix Figure 2), and their phylogenetic trees mostly repeat each other. The M-segment tree was the most distinct (Figure 2, panel B), a finding that corresponds with previous data (*5*). That finding confirms that the M segment is the most variable and most often involved in reassortment events (*14*).

In the M-segment tree, the W-RUS sublineage stood within the Volga-RUS sublineage, but the branch from Bashkiria formed an outgroup (Figure 2, panel B). Almost the entire Volga-RUS sublineage, except for the Bashkir branch, appears to be a product of the exchange of the M segment between ancestors of the W-RUS and the Bashkir branch. The S and L segments are related to the Bashkir branch, and the M segment was obtained from the ancestors of the W-RUS sublineage. Those findings confirm and extend previous results (*12*). Thus, strains from the most epidemiologically active areas have arisen through reassortment. However, whether reassortment has altered the pathogenic properties of those strains remains unclear.

The genome variant from Penza belongs to the group that obtained the M segment by reassortment, as we have described (Figure 2, panel B). On the S-segment tree, Penza/Cg8730 is located on the Volga-RUS sublineage (Figure 2, panel A). However, on the L-segment tree, Penza/Cg8730 belongs to the W-RUS sublineage (Figure 2, panel C). Thus, Penza/Cg8730 likely emerged from a 2-stage reassortment. Although L segment exchange is not a unique event, it occurs much less frequently than exchange among other segments (*14*). Geographically, the Penza region lies west of locations where viruses belonging to the Volga-RUS sublineage were isolated but far from representatives of the W-RUS sublineage. Thus, Penza could be a meeting point of those 2 lineages.

On the S-segment tree, the FIN branch was represented by 2 sublineages: West-FIN from Finland and Karelia and East-FIN from western Siberia (Figure 2). However, on the M-segment tree, West-FIN and East-FIN did not form a common branch (Figure 2, panel B). The current hypothesis generally accepts that the FIN branch split into 2 parts when the territories were recolonized by bank voles after the glacier melted (*8*).

The sequences we obtained from the Arkhangelsk region clustered with sequences of viruses collected in Omsk and Tyumen regions, despite their geographic distance (Figure 1; Appendix Figure 3). According to the phylogenetic trees, the Tyumen and Omsk clades divided after the Arkhangelsk clade split from their common ancestor (Figure 2). Such branching suggests 2 possible paths for spread of the East-FIN subclade: from northwest Russia to the southeast, across the Ural Mountains to western Siberia; or spreading from the Pre-Ural region in 2 directions, to western Siberia and to the Arkhangelsk region. The second possibility supposes a second vole migration wave to the north, after PUUV split off from the East-FIN and West-FIN groups during postglacial period (*8*). PUUV sequences from the area between Arkhangelsk and western Siberia might shed more light on spread of the FIN lineage.

Conclusions

The newly identified viruses from the Tyumen and Arkhangelsk regions of Russia and viruses from Omsk form a common East-FIN branch. This finding raises additional questions about the dispersal routes of the FIN lineage.

Here we considered the RUS lineage as 3 separate sublineages: Volga-RUS, W-RUS, and Balt-RUS. The PUUV genome variants from Tatarstan,

Udmurtia, Samara, and Saratov probably emerged through reassortment because they contained S and L segments related to the Bashkir branch and an M segment derived from ancestors of the W-RUS sublineage. The Penza/Cg8730 genome variant might have arisen from a 2-stage reassortment. Continued surveillance is needed to assess PUUV pathogenicity in Russia, but we found PUUV reassortments in areas with the highest HRFS incidence, indicating reassortment might contribute to pathogenic properties of PUUV.

Acknowledgments

We express our gratitude to the territorial Centers of Hygiene and Epidemiology in the Arkhangelsk, Ivanovo, Moscow, Penza, Saratov, Tyumen, and Ulyanovsk regions, and Udmurtia republic for providing rodent material. We also express our gratitude to Anna Valdokhina and Victoria Bulanenko for sequencing implementation.

Immune diagnostics were funded by the Chumakov Federal Scientific Center for Research and Development of Immune-and-Biological Products of Russian Academy of Sciences internal funds. Reverse transcription PCR, sequencing, and phylogenetic analysis were funded by the Federal Budget Institution of Science Central Research Institute of Epidemiology of The Federal Service on Customers Rights Protection and Human Wellbeing Surveillance internal funds. The other bioinformatic analysis, including mapping virus isolation points on interactive map, isolation by distance, and sliding window analyses, was funded by the Russian Science Foundation (grant no. 22-15-00230).

About the Author

Dr. Blinova is a research associate at Central Research Institute of Epidemiology, Moscow, Russia, and a PhD student in Russian Academy of Sciences, Moscow. Her research interests include epidemiology of Puumala and Dobrava/Belgrade viruses, HFRS incidence, and the course of diseases, phylogenetic diversity, and evolution of viruses.

References

1. Dzagurova TK, Siniugina AA, Ishmukhametov AA, Egorova MS, Kurashova SS, Balovneva MV, et al. Pre-clinical studies of inactivated polyvalent HFRS vaccine. Front Cell Infect Microbiol. 2020;10:545372. https://doi.org/10.3389/fcimb.2020.545372
2. Tkachenko EA, Ishmukhametov AA, Dzagurova TK, Bernshtein AD, Morozov VG, Siniugina AA, et al. Hemorrhagic fever with renal syndrome, Russia. Emerg Infect Dis. 2019;25:2325–8. https://doi.org/10.3201/eid2512.181649
3. Petazzi RA, Koikkarah AA, Tischler ND, Chiantia S. Detection of envelope glycoprotein assembly from old-world hantaviruses in the golgi apparatus of living cells. J Virol. 2021;95:e01238-20. https://doi.org/10.1128/JVI.01238-20
4. Kabwe E, Davidyuk Y, Shamsutdinov A, Garanina E, Martynova E, Kitaeva K, et al. Orthohantaviruses, emerging zoonotic pathogens. Pathogens. 2020;9:775. https://doi.org/10.3390/pathogens9090775
5. Razzauti M, Plyusnina A, Niemimaa J, Henttonen H, Plyusnin A. Co-circulation of two Puumala hantavirus lineages in Latvia: a Russian lineage described previously and a novel Latvian lineage. J Med Virol. 2012;84:314–8. https://doi.org/10.1002/jmv.22263
6. Castel G, Chevenet F, Razzauti M, Murri S, Marianneau P, Cosson JF, et al. Phylogeography of Puumala orthohantavirus in Europe. Viruses. 2019;11:679. https://doi.org/10.3390/v11080679
7. Saxenhofer M, Weber de Melo V, Ulrich RG, Heckel G. Revised time scales of RNA virus evolution based on spatial information. Proc R Soc B Biol Sci. 2017;284(1860):20170857. https://doi.org/10.1098/rspb.2017.0857
8. Sironen T, Vaheri A, Plyusnin A. Molecular evolution of Puumala hantavirus. J Virol. 2001;75:11803–10. https://doi.org/10.1128/JVI.75.23.11803-11810.2001
9. Drewes S, Ali HS, Saxenhofer M, Rosenfeld UM, Binder F, Cuypers F, et al. Host-associated absence of human Puumala virus infections in northern and eastern Germany. Emerg Infect Dis. 2017;23:83–6. https://doi.org/10.3201/eid2301.160224
10. Jeske K, Schulz J, Tekemen D, Balčiauskas L, Balčiauskienė L, Hiltbrunner M, et al. Cocirculation of *Leptospira* spp. and multiple orthohantaviruses in rodents, Lithuania, Northern Europe. Transbound Emerg Dis. 2022;69:e3196–201. https://doi.org/10.1111/tbed.14470
11. Rosenfeld UM, Drewes S, Ali HS, Sadowska ET, Mikowska M, Heckel G, et al. A highly divergent Puumala virus lineage in southern Poland. Arch Virol. 2017;162:1177–85. https://doi.org/10.1007/s00705-016-3200-5
12. Blinova E, Deviatkin A, Kurashova S, Balovneva M, Volgina I, Valdokhina A, et al. A fatal case of haemorrhagic fever with renal syndrome in Kursk Region, Russia, caused by a novel Puumala virus clade. Infect Genet Evol. 2022;102:105295. https://doi.org/10.1016/j.meegid.2022.105295
13. Schlegel M, Ali HS, Stieger N, Groschup MH, Wolf R, Ulrich RG. Molecular identification of small mammal species using novel cytochrome B gene-derived degenerated primers. Biochem Genet. 2012;50:440–7. https://doi.org/10.1007/s10528-011-9487-8
14. Klempa B. Reassortment events in the evolution of hantaviruses. Virus Genes. 2018;54:638–46. https://doi.org/10.1007/s11262-018-1590-z
15. Kumar S, Stecher G, Li M, Knyaz C, Tamura K. MEGA X: molecular evolutionary genetics analysis across computing platforms. Mol Biol Evol. 2018;35(6):1547–9. https://doi.org/10.1093/molbev/msy096

Address for correspondence: Ekaterina Blinova, Federal Service on Customers Rights Protection and Human Wellbeing Surveillance, 3a Novogireevskaya St., Moscow 111123, Russia; email: blinova.e@cmd.su

Candida vulturna Outbreak Caused by Cluster of Multidrug-Resistant Strains, China

Han Du,[1] Jian Bing,[1] Xiaohong Xu,[1,] Qiushi Zheng, Tianren Hu, Yajuan Hao, Shuping Li, Clarissa J. Nobile, Ping Zhan,[2] Guanghua Huang[2]

Candida vulturna belongs to the *Candida haemulonii* species complex and is phylogenetically related to *C. auris*. We report a *C. vulturna* outbreak among persons in Shanxi Province, China, during 2019–2022. Isolates were resistant to multiple antifungal drugs and exhibited enhanced adhesion and biofilm formation properties.

Candida vulturna, a fungal pathogen that is phylogenetically related to *C. haemulonii* and *C. auris*, was isolated from flowers in a taxonomic study of yeasts in 2016 (*1*,*2*). Since then, *C. vulturna* has been sporadically isolated in different countries from clinical specimens such as blood, wounds, and peripherally inserted central catheters (PICCs) (*1*–*4*). *C. vulturna*, *C. haemulonii*, and *C. auris* belong to the *Metschnikowia*/*Candida* clade (*1*,*5*). Antifungal drug resistance, especially to the azoles, is a common feature of species within this clade. During 2009–2022, fungal infections caused by the reportedly rare species *C. haemulonii* and *C. auris* have become more prevalent in clinical settings (*1*,*6*–*10*). The increased occurrence of those infections could be the result of the widespread use of antifungal agents in clinical and agricultural settings, as well as the environmental changes caused by human activities (*10*–*12*).

In China, reports of infections caused by the superbug fungus *C. auris* have been relatively infrequent; however, the prevalence of *C. haemulonii* and associated species in the *C. haemulonii* complex has been steadily increasing in recent years (*8*,*13*). For our study, we analyzed deidentified health records of patients infected with *C. vulturna*, as approved by the ethics committee of a general hospital in Shanxi Province, China.

The Study

We selected a total of 19 patients, 17 male and 2 female, who had been infected with *C. vulturna* during January 1, 2019–October 26, 2022 (Appendix Figure 1, https://wwwnc.cdc.gov/EID/article/29/7/23-0254-App1.pdf). We isolated 16 *C. vulturna* strains directly from the blood through venipuncture and 7 strains from a PICC line tip of the 19 patients (Appendix Table). We initially identified the strains as *C. haemulonii* complex species by growth on CHROMagar *Candida* medium (CHROMagar, https://www.chromagar.com) and confirmed by sequencing of the ribosomal internal transcribed spacer (ITS) region. Most cases were identified in 2019; *C. vulturna* infections were identified in 2 patients during January 1, 2020–January 1, 2022. Enhanced hygiene measures taken at that time may have dampened the spread of *C. vulturna* in the hospital.

On the basis of results of the ITS and multilocus sequence typing for 8 conserved genes, we then performed phylogenetic analyses on the isolates. All strains isolated in this study (CVDH01–19) were closely related by phylogenetic analyses and clustered together in 1 clade (Figure 1; Appendix Figure 2).

The hospital has 1 intensive care unit (ICU). Of the 19 patients we identified as infected with *C. vulturna*, 11 were from the ICU, 4 were from the neuroscience ward, and 4 were from other departments within the hospital. The age range of patients was 13–83 years (median 63 years). Because all patients

Author affiliations: Huashan Hospital, Fudan University, Shanghai, China (H. Du, J. Bing, Q. Zheng, T. Hu, G. Huang); Sinopharm Tongmei General Hospital, Datong, China (X. Xu, Y. Hao, S. Li); University of California, Merced, California, USA (C.J. Nobile); Affiliated Hospital of Jiangxi University of Chinese Medicine, Nanchang, China (P. Zhan)

DOI: https://doi.org/10.3201/eid2907.230254

[1]These first authors contributed equally to this article.

[2]These senior authors contributed equally to this article.

had PICC lines for delivery of medications and *C. vulturna* strains were isolated from the PICC line tips of 7 patients, the use of PICC lines could be a major risk factor for *C. vulturna* infection. Other risk factors could include traumatic injuries, hypertension, cancer, and blood and pulmonary infections (Appendix Table). We also conducted environmental screening assays but were unable to detect or isolate *C. vulturna* from hospital surfaces, including walls, floors, bedside tables, bed sheets, bed frames, blood pressure cuffs, and chairs.

We used 1 representative *C. vulturna* strain from each patient for subsequent antifungal drug susceptibility testing and phenotypic analyses (Appendix Table). Using the breakpoints established for *C. albicans*, we determined that all 19 of the *C. vulturna* strains tested were resistant to azole drugs (Table). All isolates were resistant to amphotericin B (MIC 4 mg/L) but were susceptible to echinocandins (MICs ≤0.125 for caspofungin, ≤0.125 for anidulafungin, ≤0.5 for micafungin), and flucytosine (MIC 0.06).

When grown in liquid media, we observed that the cells from the *C. vulturna* (CVDH) strains isolated in this study formed large aggregates and exhibited enhanced adhesion and biofilm formation abilities. This feature was similar to that of *C. auris* strain SJ01, which formed enhanced biofilms under both in vitro and in vivo conditions (*14*). (Figure 2; Appendix Figure 3).

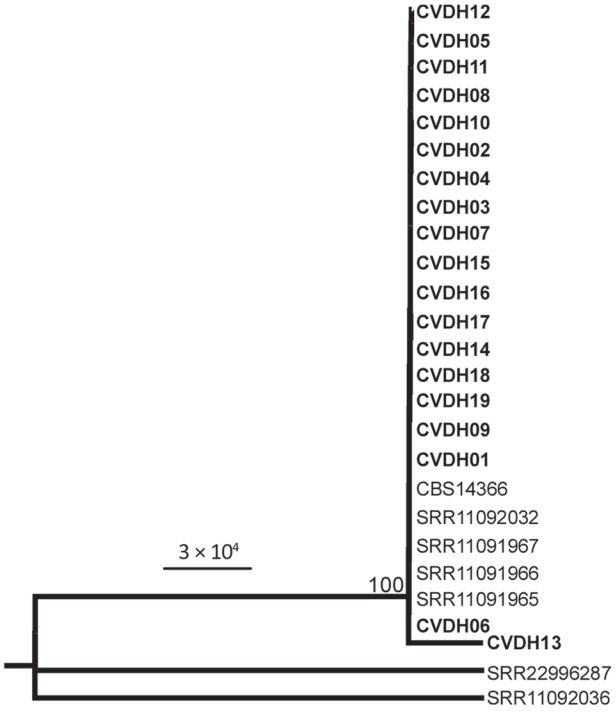

Figure 1. Maximum-likelihood phylogeny analysis of *Candida vulturna* strains from 19 infected patients in Shanxi Province, China, January 1, 2019–October 26, 2022, based on multilocus sequence typing (MLST). Eight genes (*AAT1, ACC1, ADP1, ALA1, ERG11, RPB1, RPB2,* and *ZWF1*) were concatenated and used for phylogenetic analyses. The tree was generated using the program RAxML (https://cme.h-its.org/exelixis/web/software/raxml). The general time reversible model, gamma distribution, 1,000 bootstraps, and midpoint root were adopted. Bold text indicates strains isolated in this study; reference strain data from whole-genome sequencing is from the National Center for Biotechnology Information gene database (accession nos. SRR11091965–67, SRR11092032, SRR11092036, SRR22996287). Sequences for strain CBS14366 were retrieved from its genomic assembly (GenBank accession no. GCA_026585945.1). Strains CVDH01-CVDH19 were isolated from patients of *C. vulturna* infection (cases C1–C19; Table; Appendix Figure 1, https://wwwnc.cdc.gov/EID/article/29/7/23-0254-App1.pdf). Scale bar indicates substitutions per site.

Conclusion

A serious threat to human health is the emergence of new multidrug-resistant fungal species. Both the widespread use of antifungal agents and the reduced susceptibility of these emerging species to antifungal drugs could contribute to the epidemiologic shifts toward multidrug-resistant fungal pathogens that we are increasingly observing in clinical settings. In this study, we report an outbreak of *C. vulturna*, which is phylogenetically closely related to *C. haemulonii* and *C. auris*, in a general hospital in Shanxi Province, China. We observed that the implementation of general enhanced hygiene measures remarkably decreased overall infection rates during the COVID-19 pandemic period (January 1, 2020–January 1, 2022) in this hospital; our findings suggest that the transmission of *C. vulturna* may be preventable through enhanced disinfection methods. Most of the *C. vulturna* isolates we obtained were from patients with bloodstream infections, defined as a single isolation of *C. vulturna* from blood obtained through venipuncture. Phylogenetic analyses indicated that the outbreak strains were closely related (Figure 1; Appendix Figure 2), implying that those strains could have originated from the same ancestor.

Striking characteristics of the *C. vulturna* strains isolated in this study were their enhanced adhesion and biofilm formation abilities. It is conceivable that those characteristics may be key contributors in promoting the spread of *C. vulturna* strains between patients during this outbreak. Consistent with this hypothesis, we observed that the use of PICC lines was a critical risk factor for *C. vulturna* infections. Another notable characteristic of the *C. vulturna* strains isolated in this study was their reduced susceptibilities to azole drugs and amphotericin B (Table), which has

Table. Susceptibility profiles of *Candida vulturna* isolates from 19 infected patients to 9 antifungal drugs, Shanxi Province, China, January 1, 2019–October 26, 2022*

Patient no.	Strain ID	FLC	VOC	ITC	POC	CAS	MFG	AFG	5-FC	AMB
C1	CVDH01	**32**	**32**	**64**	**64**	0.125	0.5	0.125	0.06	**4**
C2	CVDH02	**128**	**32**	**32**	**16**	0.06	0.5	0.125	0.06	**4**
C3	CVDH03	**64**	**32**	**32**	**32**	0.06	0.25	0.125	0.06	**4**
C4	CVDH04	**128**	**32**	**16**	**16**	0.125	0.5	0.06	0.06	**4**
C5	CVDH05	**128**	**32**	**32**	**32**	0.125	0.5	0.06	0.06	**4**
C6	CVDH06	**128**	**32**	**32**	**32**	0.125	0.5	0.125	0.06	**4**
C7	CVDH07	**256**	**64**	**64**	**64**	0.06	0.25	0.125	0.06	**4**
C8	CVDH08	**128**	**32**	**32**	**32**	0.25	0.5	0.125	0.06	**4**
C9	CVDH09	**128**	**32**	**32**	**64**	0.06	0.25	0.25	0.06	**4**
C10	CVDH10	**128**	**32**	**16**	**16**	0.125	0.5	0.125	0.06	**4**
C11	CVDH11	**256**	**64**	**64**	**64**	0.125	0.5	0.125	0.06	**4**
C12	CVDH12	**128**	**32**	**64**	**64**	0.06	0.25	0.125	0.06	**4**
C13	CVDH13	**64**	**32**	**32**	**32**	0.06	0.25	0.125	0.06	**4**
C14	CVDH14	**64**	**16**	**32**	**32**	0.03	0.5	0.03	0.06	**4**
C15	CVDH15	**128**	**64**	**32**	**16**	0.06	0.25	0.125	0.06	**4**
C16	CVDH16	**128**	**32**	**64**	**32**	0.125	0.5	0.125	0.06	**4**
C17	CVDH17	**64**	**32**	**32**	**32**	0.06	0.5	0.06	0.06	**4**
C18	CVDH18	**64**	**8**	**32**	**32**	0.06	0.5	0.06	0.06	**4**
C19	CVDH19	**64**	**32**	**32**	**32**	0.06	0.5	0.06	0.06	**4**

*MIC assays were performed according to Clinical and Laboratory Standards Institute microdilution guidelines. Bold text indicates antifungal resistance (based on the breakpoints for *C. albicans*). AFG, anidulafungin; AMB, amphotericin B; CAS, caspofungin; FLC, fluconazole; ITC, itraconazole; MFG, micafungin; POC, posaconazole; VOC, voriconazole; 5-FC, flucytosine.

also been observed in other species of the *C. haemulonii* complex (*6*,*7*,*13*).

The occurrence of infections caused by fungal species of the *Metschnikowia* clade has become more and more frequent in clinical settings, especially during 2009–2022 (*1*,*6*,*8*,*13*). The widespread use of antifungal drugs in clinical settings and fungicides in agricultural settings could be contributors to the increased emergence of these multidrug resistant fungal pathogens. Given the transmissible, adhesive, and antifungal drug–resistant characteristics of emerging *C. vulturna* clinical isolates, *C. vulturna* could be a serious upcoming threat to hospital infections worldwide.

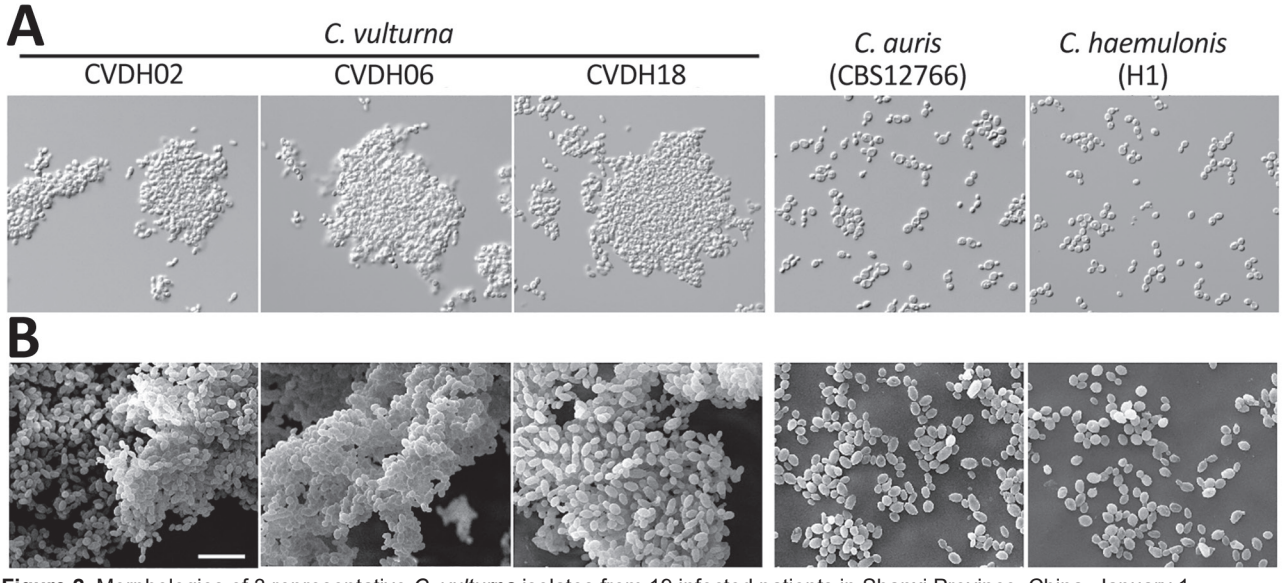

Figure 2. Morphologies of 3 representative *C. vulturna* isolates from 19 infected patients in Shanxi Province, China, January 1, 2019–October 26, 2022. *C. auris* (CBS12766) and *C. haemulonii* (H1) served as reference strains. A) Adhesion phenotypes of *C. vulturna* isolates grown in liquid Lee's glucose medium at 30°C for 24 h. Strains CVDH02, CVDH06, and CVDH18 exhibited strong adhesiveness, whereas the *C. auris* and *C. haemulonii* reference strains grew as separate single cells under the same culture conditions. B) Biofilm formation of *C. vulturna* isolates. *C. auris* (CBS12766) and *C. haemulonii* (G7) served as reference strains. Biofilms were developed on silicone squares at 30°C for 48 h. Lee's glucose medium was used for biofilm growth. Scale bar indicates 10 μm. Morphologies for the other 16 *C. vulturna* isolates and 2 *C. auris* strains are shown in Appendix Figure 3 (https://wwwnc.cdc.gov/EID/article/29/7/23-0254-App1.pdf).

This work was supported by the National Key Research and Development Program of China (grant no. 2021YFC2300400 to G.H. and no. 2022YFC2303000 to H.D. and J.B.), National Natural Science Foundation of China (award nos. 82172290 and 82002123 to H.D., nos. 31930005 and 82272359 to G.H., nos. 32170193 and 32000018 to J.B., and no. 81960367 to P.Z.), Shanghai Municipal Science and Technology Major Project (award no. HS2021SHZX001 to G.H.), Jiangxi Provincial Natural Science Foundation (award no. 20212BAB206060 to P.Z.), the US National Institutes of Health National Institute of General Medical Sciences (grant no. R35GM124594 to C.J.N.), and by the Kamangar family in the form of an endowed chair (to C.J.N.). The content is the sole responsibility of the authors and does not represent the views of the funders. The funders had no role in the design of the study; in the collection, analyses, or interpretation of data; in the writing of the manuscript; or in the decision to publish the results.

C.J.N. is a cofounder of BioSynesis, Inc., a company developing diagnostics and therapeutics for biofilm infections.

About the Author

Dr. Du is an associate professor in the State Key Laboratory of Genetic Engineering, School of Life Sciences, Fudan University, China. Her primary research interest is in the biology of pathogenic fungi.

References

1. Gade L, Muñoz JF, Sheth M, Wagner D, Berkow EL, Forsberg K, et al. Understanding the emergence of multidrug-resistant *Candida*: using whole-genome sequencing to describe the population structure of *Candida haemulonii* species complex. Front Genet. 2020; 11:554. https://doi.org/10.3389/fgene.2020.00554
2. Sipiczki M, Tap RM. *Candida vulturna* pro tempore sp. nov., a dimorphic yeast species related to the *Candida haemulonis* species complex isolated from flowers and clinical sample. Int J Syst Evol Microbiol. 2016;66:4009–15. https://doi.org/10.1099/ijsem.0.001302
3. Zurita J, Paz Y Miño A, Solís MB, Sevillano G. Failed identification of *Candida vulturna* using the updated Vitek 2 yeast identification system, version 9.02 and CHROMagar Candida Plus. New Microbes New Infect. 2022;48:101012. https://doi.org/10.1016/j.nmni.2022.101012
4. Navarro-Muñoz JC, de Jong AW, Gerrits van den Ende B, Haas PJ, Then ER, Mohd Tap R, et al. The high-quality complete genome sequence of the opportunistic fungal pathogen *Candida vulturna* CBS 14366^{T}. Mycopathologia. 2019;184:731–4. https://doi.org/10.1007/s11046-019-00404-0
5. Santos MA, Gomes AC, Santos MC, Carreto LC, Moura GR. The genetic code of the fungal CTG clade. C R Biol. 2011;334:607–11. https://doi.org/10.1016/j.crvi.2011.05.008
6. Kim MN, Shin JH, Sung H, Lee K, Kim EC, Ryoo N, et al. *Candida haemulonii* and closely related species at 5 university hospitals in Korea: identification, antifungal susceptibility, and clinical features. Clin Infect Dis. 2009;48:e57–61. https://doi.org/10.1086/597108
7. Ramos LS, Figueiredo-Carvalho MH, Barbedo LS, Ziccardi M, Chaves AL, Zancopé-Oliveira RM, et al. *Candida haemulonii* complex: species identification and antifungal susceptibility profiles of clinical isolates from Brazil. J Antimicrob Chemother. 2015;70:111–5. https://doi.org/10.1093/jac/dku321
8. Hou X, Xiao M, Chen SC, Wang H, Cheng JW, Chen XX, et al. Identification and antifungal susceptibility profiles of *Candida haemulonii* species complex clinical isolates from a multicenter study in China. J Clin Microbiol. 2016;54:2676–80. https://doi.org/10.1128/JCM.01492-16
9. Jeffery-Smith A, Taori SK, Schelenz S, Jeffery K, Johnson EM, Borman A, et al.; Candida auris Incident Management Team. *Candida auris*: a review of the literature. Clin Microbiol Rev. 2017;31:e00029-17. https://doi.org/10.1128/CMR.00029-17
10. Du H, Bing J, Hu T, Ennis CL, Nobile CJ, Huang G. *Candida auris:* epidemiology, biology, antifungal resistance, and virulence. PLoS Pathog. 2020;16:e1008921. https://doi.org/10.1371/journal.ppat.1008921
11. Jackson BR, Chow N, Forsberg K, Litvintseva AP, Lockhart SR, Welsh R, et al. On the origins of a species: what might explain the rise of *Candida auris*? J Fungi (Basel). 2019;5:58. https://doi.org/10.3390/jof5030058
12. Casadevall A, Kontoyiannis DP, Robert V. On the emergence of *Candida auris*: climate change, azoles, swamps, and birds. MBio. 2019;10:e01397-19. https://doi.org/10.1128/mBio.01397-19
13. Chen XF, Zhang H, Jia XM, Cao J, Li L, Hu XL, et al. Antifungal susceptibility profiles and drug resistance mechanisms of clinical *Candida duobushaemulonii* isolates from China. Front Microbiol. 2022;13:1001845. https://doi.org/10.3389/fmicb.2022.1001845
14. Bing J, Guan Z, Zheng T, Zhang Z, Fan S, Ennis CL, et al. Clinical isolates of *Candida auris* with enhanced adherence and biofilm formation due to genomic amplification of ALS4. PLoS Pathog. 2023;19:e1011239. https://doi.org/10.1371/journal.ppat.1011239

Address for correspondence: Ping Zhan, Dermatology Department, Affiliated Hospital of Jiangxi University of Chinese Medicine, Nanchang, 330006, China; email: zhanping1980@163.com; Guanghua Huang, Department of Infectious Diseases, Huashan Hospital, Shanghai Institute of Infectious Disease and Biosecurity and State Key Laboratory of Genetic Engineering, School of Life Sciences, Fudan University, Shanghai 200438, China; email: huanggh@fudan.edu.cn

Estimates of Serial Interval and Reproduction Number of Sudan Virus, Uganda, August–November 2022

Valentina Marziano, Giorgio Guzzetta, Ira Longini, Stefano Merler

We estimated the mean serial interval for Sudan virus in Uganda to be 11.7 days (95 CI% 8.2–15.8 days). Estimates for the 2022 outbreak indicate a mean basic reproduction number of 2.4–2.7 (95% CI 1.7–3.5). Estimated net reproduction numbers across districts suggest a marked spatial heterogeneity.

On September 20, 2022, Uganda's Ministry of Health declared an Ebola disease outbreak after a case caused by Sudan virus (SUDV) was confirmed in a village in Mubende District (*1*). Suspicious deaths in the same district had occurred earlier in the month. Investigations conducted by the National Rapid Response Team allowed the identification of probable SUDV cases dating back to mid-August 2022 (*2*,*3*). As of November 2, 2022, a total of 149 cases (131 PCR-confirmed and 18 probable) were reported in the country; most cases occurred in the districts of Mubende (63 confirmed, 17 probable), Kassanda (42 confirmed, 1 probable), and Kampala (18 confirmed) (*2*) (Figure 1, panels A–C). On January 11, 2023, the outbreak was declared over with a total of 164 cases (142 confirmed, 22 probable) (*4*).

The Study

We provide 2 estimates of the serial interval distribution (the time elapsed between the symptom onset in an index case-patient and in their secondary case-patients) by using observed serial intervals in infector–infectee pairs as identified during contact-tracing operations conducted in 2 SUDV outbreaks in Uganda, during 2000–2001 (24 pairs) (*5*) and the 2022 outbreak (12 pairs) (*6*). We fitted 3 families of distributions (Weibull, Gamma, and log-normal) with a possible offset (*5*,*6*). We obtained the best fit for the serial interval distribution for both datasets with a Weibull distribution. We estimated the mean serial interval to be 12.0 days (95% CI 10.0–14.2 days) by using the 2000–2001 outbreak data and 11.7 days (95% CI 8.2–15.8 days) by using the 2022 outbreak data.

We then used estimates of the serial interval as a proxy of the generation time to compute the basic (R_0) and net (R_t) reproduction numbers. We defined R_0 as the average number of secondary infections generated by an infectious person in a fully susceptible population. If R_0 <1, transmission is expected to fade out, whereas if R_0 >1, the epidemic has the potential to continue; the larger R_0, the more difficult it is to control the epidemic. We defined R_t as the average number of secondary cases per infectious person at time t; R_t is key to monitor the effectiveness of interventions throughout the epidemic. In the main analysis, we computed R_t and R_0 by using a method based on the renewal equation in the formulation by Cori et al. (*7*). In additional analyses, we used the assumption of exponential (*8*) or subexponential (*9*) growth of the cumulative case incidence curve to compute R_0. We also provided an alternative estimate of R_t obtained by applying a recently proposed approach (*10*) that has been suggested to perform better with low case counts (Appendix, https://wwwnc.cdc.gov/EID/article/29/7/22-1718-App1.pdf).

R_0 of the 2022 outbreak, as estimated from the epidemic curve of Mubende District, was 2.7 (95% CI 1.9–3.5) based on the serial interval distribution from the 2000–2001 outbreak. R_0 was 2.4 (95% CI 1.7–3.3) based on the serial interval distribution from the 2022 outbreak.

Author affiliations: Bruno Kessler Foundation, Center for Health Emergencies, Trento, Italy (V. Marziano, G. Guzzetta, S. Merler); University of Florida, Colleges of Public Health and Health Professions and Medicine, Gainesville, Florida, USA (I. Longini)

DOI: https://doi.org/10.3201/eid2907.221718

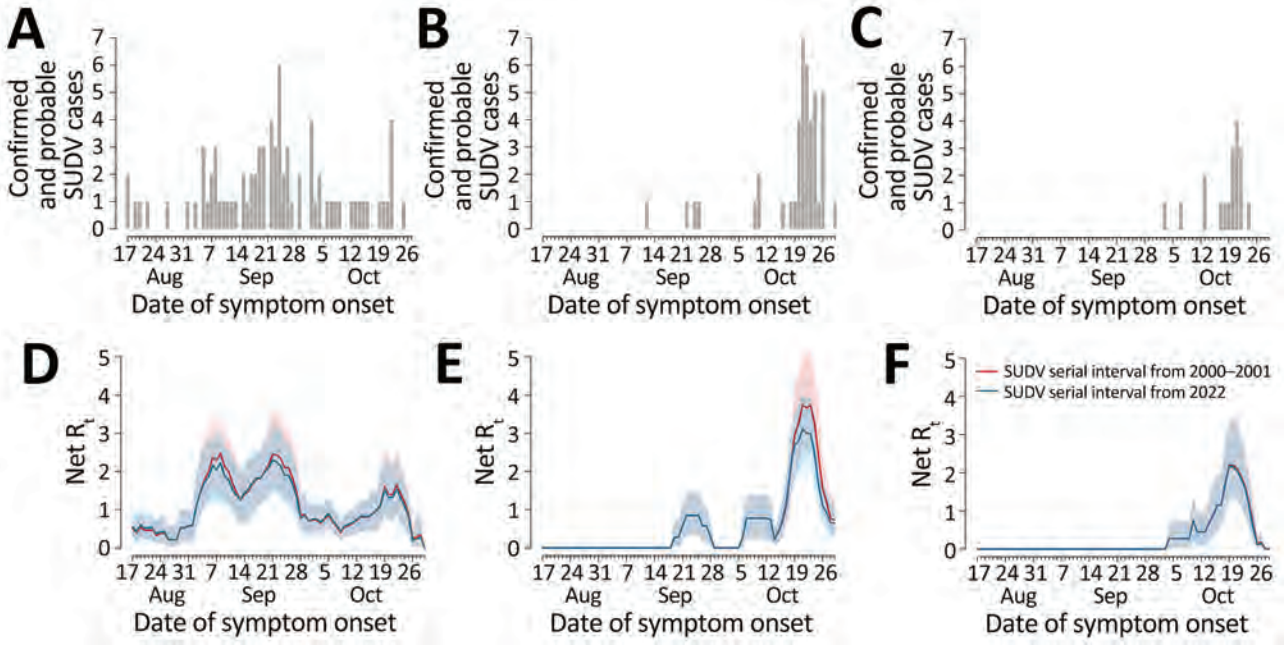

Figure 1. Epidemic curves and reproduction numbers for SUDV outbreaks in Mubende, Kassanda, and Kampala districts, Uganda, August–November 2022. A–C) Number of confirmed and probable cases by date of symptom onset in the 3 considered districts (comprising 95% of cases reported in the whole country, as of November 2, 2022) (*2*): Mubende (A), Kassanda (B), and Kampala (C). D–F). Estimates of the net reproduction number over time in the 3 districts: Mubende (D), Kassanda (E), and Kampala (F). Estimates from the corresponding epidemic curves by date of symptom onset were computed using the serial interval distributions from the 2000–2001 outbreak (*5*) (red) and the 2022 outbreak (*6*) (blue). Shaded areas represent 95% CIs of estimates. We assumed that the first case of the epidemic curve in each district was imported and that all the others were locally transmitted. SUDV, Sudan virus.

We estimated R_t in the 3 districts and according to the 2 estimated serial interval distributions (Figure 1, panels D–F). For convenience and given their similar values, numbers reported hereafter refer to the 2000–2001 serial interval; corresponding numbers for the 2022 serial interval are reported separately (Appendix). In Mubende District, R_t reached a peak during September 21–23, 2022, with an estimated value for R_t that was close to R_0 (mean 2.4 [95% CI 1.5–3.5]). R_t fell rapidly below the epidemic threshold during September 28–October 15 (mean 0.71 [95% CI 0.50–0.91]), possibly because of control interventions and population behavior changes after awareness of the outbreak had increased. In the second half of October, R_t increased again, reaching a peak of 1.34 (95% CI 0.78–2.13) in the week October 18–24. In the districts of Kassanda and Kampala, R_t increased rapidly in the second half of October. In Kassanda, R_t reached a peak of 3.5 (95% CI 2.5–4.9) during October 20–24. In Kampala, the peak R_t value was 2.0 (95% CI 1.3–3.2) during October 18–22.

Estimates of R_t at the national level (Figure 2) are characterized by 2 peaks in September, which were

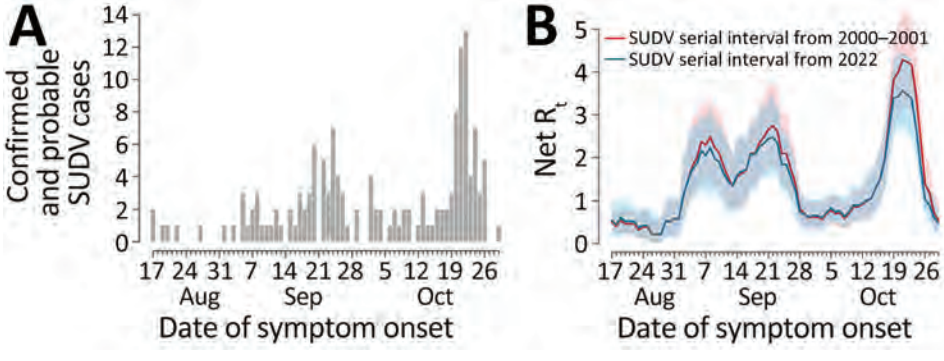

Figure 2. Epidemic curves and reproduction number for SUDV outbreaks, Uganda, August–November 2022. A) Number of confirmed and probable cases, by date of symptom onset, in Uganda as obtained from district-level epidemic curves reported previously (*2*). B) Net reproduction number over time in Uganda, as estimated from the epidemic curve, by date of symptom onset, using the serial interval distributions from the 2000–2001 outbreak (*5*) (red) and from the 2022 outbreak (*6*) (blue). Shaded areas represent 95% CIs of estimates. We assumed that the first case of the epidemic curve was imported and that all the others are locally transmitted. SUDV, Sudan virus.

driven by SUDV transmission in Mubende. A third marked peak that occurred in the second half of October was sustained mainly by increasing transmission in the districts of Kassanda and Kampala, as well as by a resurgence in Mubende.

Conclusions

We estimated the distribution of the serial intervals for SUDV by using 2 different datasets from the 2000–2001 outbreak and from the ongoing outbreak in Uganda, finding similar distributions and an average serial interval of ≈12 days. On the basis of those estimates and publicly available data on the epidemic curve made available by the Ugandan Ministry of Health (*2*), we found the R_0 in Mubende District, the district first and most affected by the current outbreak, was ≈2.4–2.7, although with broad uncertainty (95% CI 1.7–3.5). Those estimates are in line with previous estimates for SUDV, which ranged from 1.3 to 4.1 (*11*), and with estimates obtained using alternative methods (*8*,*9*) (Appendix). After a temporary containment of the outbreak from the end of September until mid-October 2022, with R_t hovering around 0.7, the third week of October marked a resurgence of transmissibility in Mubende (R_t ≈1.3) and the emergence of new outbreaks in the Kassanda (R_t ≈3.5) and Kampala (R_t ≈2.0) districts. The R_0 associated with the national aggregation shows the same temporal features but suggests even higher numbers for the R_0 in the fourth week of October (mean R_0 ≈4), demonstrating the important role played by spatial heterogeneity of transmission in the 2022 outbreak.

Our estimates should be interpreted with caution, considering the following limitations. Estimates of the serial interval distributions are based on small numbers of infector–infectee pairs. Reproduction numbers have a broad uncertainty because of limited case numbers and may be substantially affected by superspreading events, biasing estimate upward with respect to the average transmissibility in the general population. However, the proposed estimates are in line with those obtained using an alternative method that was suggested to be more robust for low case counts (*10*) (Appendix). Moreover, a potential increase in reporting rates of confirmed cases after the discovery of the first cases in each district may inflate the estimate of the reproduction numbers.

Given the geographic expansion of the outbreak, which included urban settings, and the absence of therapeutics and licensed vaccines to treat and prevent SUDV, by the end of October 2022, the World Health Organization assessed the risk for infection at the national level to be very high (*12*). However, the rapid deployment of interventions (including contact tracing, isolation of case-patients, and informational activities to promote community engagement) was sufficient to contain the outbreak, which was declared over on January 11, 2023. Our analysis provides quantitative information on the evolution of SUDV transmissibility in the different districts of Uganda during the 2022 outbreak. Estimates provided for the serial interval may be instrumental in planning control interventions in possible future outbreaks of SUDV.

This research was supported by European Union funding within the NextGeneration EU-MUR PNRR Extended Partnership initiative on Emerging Infectious Diseases (project no. PE00000007, INF-ACT). The funders had no role in study design, data collection and analysis, decision to publish, or preparation of the manuscript.

About the Author

Dr. Marziano is a researcher at the Bruno Kessler Foundation in Trento, Italy. Her primary research interests are mathematical models to investigate the epidemiology of infectious diseases, support public health decisions, and assess the effectiveness of interventions.

References

1. World Health Organization–Uganda. Uganda declares Ebola virus disease outbreak. 2022 [cited 2023 Jun 6]. https://www.afro.who.int/countries/uganda/news/uganda-declares-ebola-virus-disease-outbreak
2. Republic of Uganda Ministry of Health, World Health Organization–Uganda. Ebola virus disease—situation report 42 [cited 2023 Jun 6]. https://www.afro.who.int/sites/default/files/2022-11/Ug_EVD_SitRep%2342.pdf
3. European Centre for Disease Prevention and Control. Ebola disease outbreak caused by Sudan ebolavirus in Uganda, 2022—9 November 2022 [cited 2023 Jun 6]. https://www.ecdc.europa.eu/sites/default/files/documents/ebola-risk-sudan-virus-considered-very-low-risk-assessment.pdf
4. Republic of Uganda Ministry of Health, World Health Organization–Uganda. Ebola virus disease—situation report 93 [cited 2023 Jun 6]. https://www.afro.who.int/sites/default/files/2023-01/Ug_EVD_SitRep%2393.pdf
5. Francesconi P, Yoti Z, Declich S, Onek PA, Fabiani M, Olango J, et al. Ebola hemorrhagic fever transmission and risk factors of contacts, Uganda. Emerg Infect Dis. 2003;9:1430–7. https://doi.org/10.3201/eid0911.030339
6. Republic of Uganda Ministry of Health. Press statement. Update on the Ebola virus disease outbreak and containment measures. 26 October, 2022 [cited 2023 Jun 6]. https://www.health.go.ug/cause/update-on-the-ebola-virus-disease-outbreak-and-containment-measures
7. Cori A, Ferguson NM, Fraser C, Cauchemez S. A new framework and software to estimate time-varying reproduction numbers during epidemics. Am J Epidemiol. 2013;178:1505–12. https://doi.org/10.1093/aje/kwt133
8. Chowell G, Hengartner NW, Castillo-Chavez C, Fenimore PW, Hyman JM. The basic reproductive number of Ebola and the effects of public health measures: the

cases of Congo and Uganda. J Theor Biol. 2004;229:119–26. https://doi.org/10.1016/j.jtbi.2004.03.006
9. Chowell G, Viboud C, Simonsen L, Moghadas SM. Characterizing the reproduction number of epidemics with early subexponential growth dynamics. J R Soc Interface. 2016;13:20160659. https://doi.org/10.1098/rsif.2016.0659
10. Parag KV. Improved estimation of time-varying reproduction numbers at low case incidence and between epidemic waves. PLOS Comput Biol. 2021;17:e1009347. https://doi.org/10.1371/journal.pcbi.1009347
11. Van Kerkhove MD, Bento AI, Mills HL, Ferguson NM, Donnelly CA. A review of epidemiological parameters from Ebola outbreaks to inform early public health decision-making. Sci Data. 2015;2:150019. https://doi.org/10.1038/sdata.2015.19
12. World Health Organization. Ebola disease caused by Sudan Ebola virus—Uganda. 2022 [cited 2023 Jun 6]. https://www.who.int/emergencies/disease-outbreak-news/item/2022-DON421

Address for correspondence: Stefano Merler, Center for Health Emergencies, Bruno Kessler Foundation, Via Sommarive 18, 38123, Trento, Italy; email: merler@fbk.eu

Increased Hospitalizations Involving Fungal Infections during COVID-19 Pandemic, United States, January 2020–December 2021

Jeremy A.W. Gold, Stacey Adjei, Adi V. Gundlapalli, Ya-Lin A. Huang, Tom Chiller, Kaitlin Benedict, Mitsuru Toda

Hospitalizations involving fungal infections increased 8.5% each year in the United States during 2019–2021. During 2020–2021, patients hospitalized with COVID-19–associated fungal infections had higher (48.5%) in-hospital mortality rates than those with non–COVID-19–associated fungal infections (12.3%). Improved fungal disease surveillance is needed, particularly during respiratory virus pandemics.

In the United States, fungal infections impose considerable healthcare costs (≈$6.7 billion during 2018) and cause substantial illness and death (>7,000 deaths during 2021) (*1*,*2*). Fungi causing serious infections include yeasts, such as *Candida*, *Cryptococcus*, and *Pneumocystis* spp.; molds, such as *Aspergillus* spp. and Mucorales; and dimorphic fungi, such as *Blastomycoses*, *Coccidioides*, and *Histoplasma* spp. (*2*). Risk factors vary but generally are associated with environmental exposures; underlying immunocompromising conditions, such as solid organ or stem cell transplantation, cancer, and immunosuppressive medications; and critical illness (*2*–*4*).

COVID-19 infection is a substantial risk factor for certain fungal infections, particularly those caused by invasive molds, likely because of COVID-19–related immune system dysregulation and immunosuppressive therapies, such as corticosteroids or other immunomodulatory medications (*3*). US vital statistics data showed that deaths from fungal infections increased during the COVID-19 pandemic (*2*). However, additional data on fungal infections during the pandemic, including hospitalization rates and healthcare utilization, are lacking because many fungal diseases are not reportable in the United States (https://www.cdc.gov/fungal/fungal-disease-reporting-table.html). Those data might help inform public health planning and clinical practice. Therefore, we analyzed a large healthcare services database to determine rates, patient demographic features, and healthcare utilization for fungal infection–related hospitalizations during the COVID-19 pandemic.

Author affiliation: Centers for Disease Control and Prevention, Atlanta, Georgia, USA

DOI: https://doi.org/10.3201/eid2907.221771

The Study

The Premier Healthcare Database, Special COVID-19 Release (PHD-SR), is a US, hospital-based, all-payer database used by the Centers for Disease Control and Prevention to inform COVID-19 response activities (*5*,*6*). The database contains deidentified records from >1,000 nongovernment, community, and teaching hospitals that contributed inpatient data during the analytic period. We used diagnosis codes from the International Classification of Diseases, 10th Revision, Clinical Modification (ICD-10-CM), listed for each hospitalization and identified hospitalizations involving fungal infections (fungal hospitalizations) and COVID-19 (COVID-19 hospitalizations) during January 1, 2019–December 31, 2021 (Appendix Table 1, https://wwwnc.cdc.gov/EID/article/29/7/22-1771-App1.pdf). We defined COVID-19–associated fungal hospitalizations as those in which both a COVID-19 and fungal infection diagnosis were listed during the same hospitalization.

We estimated annual hospitalization rates (per 10,000 population) by fungal infection type and calculated average annual percentage change during 2019–2021. For COVID-19–associated fungal hospitalizations (2020–2021 only), we calculated hospitalization rates per 10,000 COVID-19 hospitalizations.

We stratified 2020–2021 fungal hospitalizations by COVID-19 association and fungal infection type and compared patient demographics, US hospital census regions and urban–rural classifications (https://www.cdc.gov/nchs/data_access/urban_rural.htm), lengths of hospital stays, intensive care unit (ICU) admissions, invasive mechanical ventilation (IMV) receipt, and in-hospital deaths. We assessed annual trends in fungal hospitalizations by using Cochran-Armitage tests and compared fungal hospitalizations according to COVID-19 status by using χ^2 tests.

During 2019–2021, a total of 59,212 fungal hospitalizations were identified in the PHD-SR. Rates of fungal hospitalizations (per 10,000 hospitalizations) increased from 22.3 in 2019 to 25.0 in 2020 and 26.8 in 2021 (p<0.01), representing an average annual percentage change of 8.5% (Table 1). Average annual rates of hospitalization significantly increased for each fungal infection, except for those caused by *Pneumocystis* spp., *Cryptococcus* spp., and other specified fungi (Table 1).

During 2020–2021, a total of 5,288 (13.4%) of 39,423 fungal hospitalizations were COVID-19–associated. Rates of COVID-19–associated fungal hospitalizations (per 10,000 COVID-19 hospitalizations) increased by 24.9% (43.1% to 57.4%; p<0.01). Annual rates increased significantly for COVID-19–associated fungal hospitalizations involving blastomycosis (0.2 to 0.5 [65.6% change]; p<0.01), aspergillosis (7.9 to 18.9 [58.2% change]; p<0.01), mucormycosis (0.7 to 1.1 [39.8% change]; p = 0.02), histoplasmosis (1.1 to 1.6 [32.1% change]; p = 0.03), pneumocystosis (1.9 to 2.6 [25.4% change]; p = 0.03), and other specified mycoses (1.7 to 2.5 [32.9% change]; p<0.01). Compared with non–COVID-19–associated fungal hospitalizations, COVID-19–associated fungal hospitalizations more frequently involved aspergillosis (27.8% vs. 16.9%; p<0.01), mucormycosis (1.8% vs. 1.4%; p = 0.03), and unspecified mycoses (24.3% vs. 18.5%; p<0.01) and, in general, less frequently involved other fungal infection types (Table 2, https://wwwnc.cdc.gov/EID/article/29/7/22-1771-T2.htm).

Median patient age was 63 (interquartile range [IQR] 52–72) years for COVID-19–associated hospitalizations versus 61 (IQR 46–72) years for non–COVID-19–associated hospitalizations (p<0.01) (Figure). Compared with hospitalizations of patients with non–COVID-19–associated fungal infections, hospitalizations of patients with COVID-19–associated fungal infections more frequently involved those who were male (59.9% vs. 57.5%; p<0.01) and Hispanic/Latino (18.8% vs. 11.7%; p<0.01); occurred in hospitals located in the western United States (29.1% vs. 27.5%; p<0.01); involved longer hospital stays (21 [IQR 11–35] days vs. 9 [IQR 4–17] days; p<0.01); and involved ICU-level care (70.0% vs. 35.5%; p<0.01), IMV receipt (64.4% vs. 22.5%; p<0.01), and increased in-hospital deaths (48.5% vs. 12.3%; p<0.01) (Table 3).

Longer hospital stays, higher ICU admission rates, more IMV receipts, and more deaths were generally observed for hospitalizations caused by COVID-19–associated fungal infections than for non–COVID-19–associated fungal infections, regardless of the specific fungal pathogens involved (Appendix Tables 2, 3). COVID-19–associated fungal hospitalizations with the highest percentages of deaths involved aspergillosis (57.6%), invasive candidiasis (55.4%), mucormycosis (44.7%), and unspecified mycoses (59.0%).

Table 1. Hospitalization rates for invasive fungal infections associated with COVID-19 in study of increased hospitalizations involving fungal infections during COVID-19 pandemic, United States, January 2020–December 2021*

	All fungal hospitalizations, n = 59,212					COVID-19–associated hospitalizations,† n = 5,288			
Fungal pathogen	2019	2020	2021	p value‡	% Change§	2020	2021	p value‡	% Change¶
Pathogenic fungi	22.3	25.0	26.8	<0.01	8.5	43.1	57.4	<0.01	24.9
Candida	4.2	5.3	5.6	<0.01	12.4	11.2	10.9	0.69	−2.4
Aspergillus	4.3	4.2	5.3	<0.01	9.4	7.9	18.9	<0.01	58.2
Coccidioides	3.2	4.0	4.3	<0.01	13.0	6.6	7.4	0.15	10.4
Pneumocystis	2.6	2.4	2.5	0.08	−2.7	1.9	2.6	0.03	25.4
Histoplasma	1.4	1.6	1.6	<0.01	5.6	1.1	1.6	0.03	32.1
Cryptococcus	1.3	1.4	1.2	0.46	−2.0	1.2	1.4	0.48	11.6
Blastomyces	0.3	0.3	0.4	<0.01	11.7	0.2	0.5	<0.01	65.6
Mucorales species	0.3	0.3	0.4	<0.01	17.9	0.7	1.1	0.02	39.8
Other specified fungi	1.5	1.6	1.5	0.38	−1.9	1.7	2.5	<0.01	32.9
Unspecified	4.0	4.9	5.1	<0.01	10.8	12.2	12.7	0.47	4.1

*Rates are per 10,000 hospitalizations. The total number of hospitalizations per year was 8,884,472 in 2019, 7,640,470 in 2020 (424,475 COVID-19–associated), and 7,559,882 in 2021 (601,831 COVID-19–associated). Patients could have >1 fungal infection in a given hospitalization, which occurred for <5% of hospitalizations.
†Hospitalizations of patients with COVID-19–associated fungal infections.
‡Calculated by using Cochran-Armitage tests.
§Average annual percentage change during 2019–2021.
¶Annual percentage change during 2020–2021.

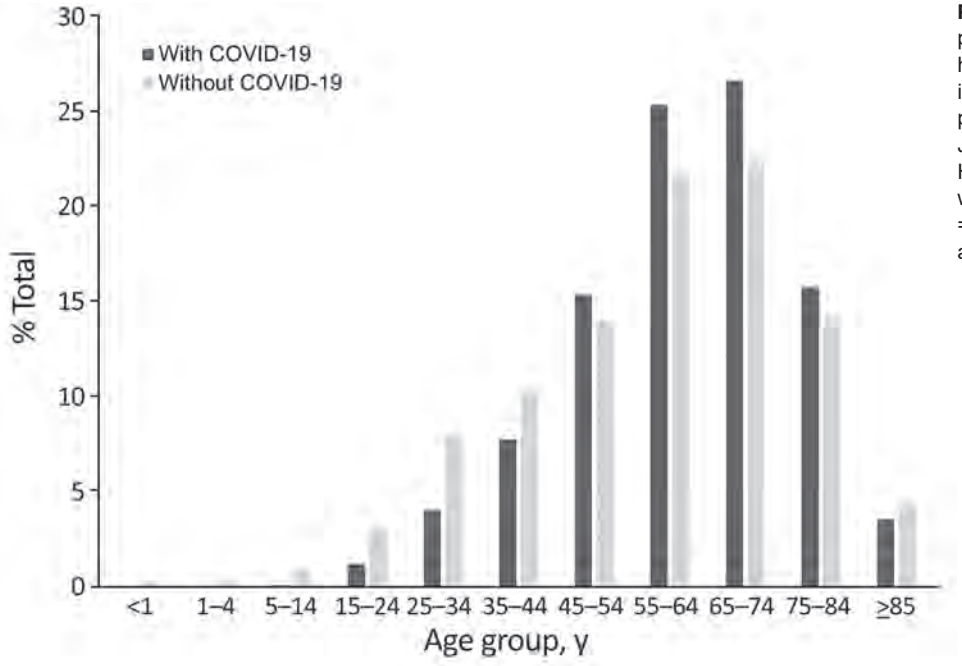

Figure. Age distribution of patients in study of increased hospitalizations involving fungal infections during COVID-19 pandemic, United States, January 2020–December 2021. Hospitalizations for fungal infections were COVID-19–associated (n = 5,288) or non–COVID-19–associated (n = 34,135).

Conclusions

Analysis of a large US healthcare services database indicated that hospitalization rates involving fungal infections increased significantly during 2019–2021, primarily driven by hospitalizations of patients with COVID-19–associated fungal infections. During 2020–2021, a total of 13.4% of fungal hospitalizations were COVID-19–associated, and COVID-19–associated fungal infections were associated with ≈2-fold increase in ICU admission rates and ≈4-fold increase

Table 3. Demographic features and outcomes of patients with fungal infections by COVID-19 status in study of increased hospitalizations involving fungal infections during COVID-19 pandemic, United States, January 2020–December 2021*

Characteristics	Any fungal infection	COVID-19–associated	Non–COVID-19–associated	p value†
Total no. hospitalizations	39,423	5,288	34,135	NA
Median age, y (range)	61 (47–72)	63 (52–72)	61 (46–72)	<0.01
Sex‡				
M	22,779 (57.8)	3,166 (59.9)	19,613 (57.5)	<0.01
F	16,634 (42.2)	2,121 (40.1)	14,513 (42.5)	<0.01
Race/ethnicity				
White, NH	18,359 (46.6)	2,131 (40.3)	16,228 (47.5)	<0.01
Black, NH	5,907 (15.0)	771 (14.6)	5,136 (15.0)	0.38
Hispanic or Latino	5,002 (12.7)	993 (18.8)	4,009 (11.7)	<0.01
Asian, NH	878 (2.2)	106 (2.0)	772 (2.3)	0.24
Other, NH	1,331 (3.4)	210 (4.0)	1,121 (3.3)	0.01
Unknown	7,946 (20.2)	1,077 (20.4)	6,869 (20.1)	0.68
US census region				
South	16,241 (41.2)	2,141 (40.5)	14,100 (41.3)	0.26
West	10,914 (27.7)	1,538 (29.1)	9,376 (27.5)	0.01
Midwest	7,385 (18.7)	943 (17.8)	6,442 (18.9)	0.07
Northeast	4,883 (12.4)	666 (12.6)	4,217 (12.4)	0.62
Urban location	35,938 (91.2)	4,801 (90.8)	31,137 (91.2)	0.31
Healthcare utilization and outcomes				
Median length of stay, d (range)	10 (5–20)	21 (11–35)	9 (4–17)	<0.01
ICU-level care	15,808 (40.1)	3,703 (70.0)	12,105 (35.5)	<0.01
IMV receipt	11,076 (28.1)	3,407 (64.4)	7,669 (22.5)	<0.01
In-hospital death	6,758 (17.1)	2,566 (48.5)	4,192 (12.3)	<0.01

*Values are no. (%) patients except as indicated. ICU, intensive care unit; IMV, invasive mechanical ventilation; NA, not applicable; NH, not Hispanic or Latino.

†p values were calculated by using χ^2 tests for categorical variables or Wilcoxon rank-sum tests for continuous variables, comparing COVID-19–associated and non-COVID-19–associated hospitalizations for fungal infections. Given the heterogeneous nature of fungal infections and their associated risk factors, underlying medical conditions were not analyzed.

‡Sex was unknown for 10 hospitalizations (1 COVID-19–associated, 9 non-COVID-19–associated). Those data were excluded from the χ^2 test calculation.

in in-hospital death rates compared with non–COVID-19–associated fungal hospitalizations. Consistent with national mortality data, hospitalizations of patients with COVID-19–associated (compared with non–COVID-19–associated) fungal infections most often involved invasive candidiasis and aspergillosis and disproportionately occurred among non-White male patients in the western United States (*2*). Racial or ethnic disparities observed for fungal infection–associated hospitalization rates might relate to longstanding inequities in social health determinants, such as lack of access to medical care or occupational exposures, and prevalence of underlying conditions, such as diabetes, that might increase fungal and COVID-19 infection risk among certain minority groups (*2*,*7*–*9*). Also consistent with national mortality data, hospitalization rates for COVID-19–associated aspergillosis and mucormycosis increased from 2020 to 2021 (*2*), likely reflecting a greater burden of COVID-19 during 2021 than 2020 (https://gis.cdc.gov/grasp/covidnet/covid19_5.html), increased clinician awareness and testing for COVID-19–associated mold infections (*10*,*11*), and increased use of corticosteroids for COVID-19 treatment, a major risk factor for aspergillosis and mucormycosis (*4*). Our findings emphasize the importance of maintaining a high index of clinical suspicion for fungal infections in patients at high risk, including those with COVID-19, and the need for increased fungal disease surveillance to detect and evaluate emerging trends.

The first limitation of our study is that, although ICD-10-CM codes for COVID-19 correlate well with SARS-CoV-2 test results in PHD-SR data (*12*), fungal ICD-10-CM codes might be associated with underreporting, misclassification, and nonspecific coding of pathogenic fungi, particularly those causing candidemia and invasive mold disease (*13*–*15*). Second, PHD-SR data are broadly representative of US hospitals, and hospital types remained relatively consistent during the analytic period. However, data might overrepresent certain regions of the country, particularly the South, and participating hospitals can vary over time. Finally, we suspect that most COVID-19–associated fungal infections were secondary complications of COVID-19 because of the natural history of fungal disease in patients with respiratory infections (*3*), but we could not verify this supposition by using PHD-SR data.

Our analysis underscores the substantial burden of patient hospitalizations with fungal infections in the United States and indicates that increased hospitalizations involving fungal infections occurred during the COVID-19 pandemic. As the COVID-19 pandemic evolves, and to increase preparedness for future infectious diseases outbreaks, comprehensive public health surveillance for fungal diseases is needed to characterize disease epidemiology and guide efforts to prevent illness and death.

Acknowledgments

We thank Tegan Boehmer, Lara Bull, Cheryl Cornwell, and Carol Yen-Chin Lin for their guidance and assistance in developing this analytic project.

This activity was reviewed by the Centers for Disease Control and Prevention and conducted in accordance with its policies and applicable federal law (45 C.F.R. part 46, 21 C.F.R. part 56; 42 U.S.C. §241(d); 5 U.S.C. §552a; 44 U.S.C. §3501 et seq.).

About the Author

Dr. Gold is a medical epidemiologist in the Mycotic Diseases Branch, Division of Foodborne, Waterborne, and Environmental Diseases, National Center for Emerging and Zoonotic Infectious Diseases, Centers for Disease Control and Prevention, Atlanta, Georgia, USA. His research interests include the epidemiology and prevention of fungal infections.

References:

1. Rayens E, Norris KA. Prevalence and healthcare burden of fungal infections in the United States, 2018. Open Forum Infect Dis. 2022;9:ofab593. https://doi.org/10.1093/ofid/ofab593
2. Gold JAW, Ahmad FB, Cisewski JA, Rossen LM, Montero AJ, Benedict K, et al. Increased deaths from fungal infections during the coronavirus disease 2019 pandemic—National Vital Statistics System, United States, January 2020–December 2021. Clin Infect Dis. 2023;76:e255–62. https://doi.org/10.1093/cid/ciac489
3. Baddley JW, Thompson GR 3rd, Chen SCA, White PL, Johnson MD, Nguyen MH, et al. Coronavirus disease 2019–associated invasive fungal infection. Open Forum Infect Dis. 2021;8:ofab510. https://doi.org/10.1093/ofid/ofab510
4. Ibrahim AS, Spellberg B, Walsh TJ, Kontoyiannis DP. Pathogenesis of mucormycosis. Clin Infect Dis. 2012;54:S16–22. https://doi.org/10.1093/cid/cir865
5. PINC AI Applied Sciences. PINC AI healthcare data special release: COVID-19. October 2021 [2022 Dec 1]. https://offers.premierinc.com/rs/381-NBB-525/images/PHD_COVID-19_White_Paper.pdf
6. Lawandi A, Warner S, Sun J, Demirkale CY, Danner RL, Klompas M, et al. Suspected severe acute respiratory syndrome coronavirus 2 (SARS-COV-2) reinfections: incidence, predictors, and healthcare use among patients at 238 US healthcare facilities, 1 June 2020 to 28 February 2021. Clin Infect Dis. 2022;74:1489–92. https://doi.org/10.1093/cid/ciab671
7. Bui DP, McCaffrey K, Friedrichs M, LaCross N, Lewis NM, Sage K, et al. Racial and ethnic disparities among COVID-19 cases in workplace outbreaks by industry sector—Utah,

March 6–June 5, 2020. MMWR Morb Mortal Wkly Rep. 2020;69:1133–8. https://doi.org/10.15585/mmwr.mm6933e3
8. Webb Hooper M, Nápoles AM, Pérez-Stable EJ. COVID-19 and racial/ethnic disparities. JAMA. 2020;323:2466–7. https://doi.org/10.1001/jama.2020.8598
9. Rayens E, Rayens MK, Norris KA. Demographic and socioeconomic factors associated with fungal infection risk, United States, 2019. Emerg Infect Dis. 2022;28:1955–69. https://doi.org/10.3201/eid2810.220391
10. Egger M, Bussini L, Hoenigl M, Bartoletti M. Prevalence of COVID-19-associated pulmonary aspergillosis: critical review and conclusions. J Fungi (Basel). 2022;8:390. https://doi.org/10.3390/jof8040390
11. Hoenigl M, Seidel D, Carvalho A, Rudramurthy SM, Arastehfar A, Gangneux JP, et al.; ECMM and ISHAM collaborators. The emergence of COVID-19 associated mucormycosis: a review of cases from 18 countries. Lancet Microbe. 2022;3:e543–52. https://doi.org/10.1016/S2666-5247(21)00237-8
12. Kadri SS, Gundrum J, Warner S, Cao Z, Babiker A, Klompas M, et al. Uptake and accuracy of the diagnosis code for COVID-19 among US hospitalizations. JAMA. 2020;324:2553–4. https://doi.org/10.1001/jama.2020.20323
13. Gold JAW, Revis A, Thomas S, Perry L, Blakney RA, Chambers T, et al. Clinical characteristics, health care utilization, and outcomes among patients in a pilot surveillance system for invasive mold disease—Georgia, United States, 2017–2019. Open Forum Infect Dis. 2022;9:ofac215. https://doi.org/10.1093/ofid/ofac215
14. Benedict K, Gold JAW, Jenkins EN, Roland J, Barter D, Czaja CA, et al. Low sensitivity of International Classification of Diseases, tenth revision coding for culture-confirmed candidemia cases in an active surveillance system: United States, 2019–2020. Open Forum Infect Dis. 2022;9:ofac461. https://doi.org/10.1093/ofid/ofac461
15. Benedict, K, Baggs, J, Wolford J, Jackson, BR, Gold, JAW. Hospitalizations for unspecified mycoses in a large administrative data set and implications for fungal disease burden estimates, United States, 2019–2021. Open Forum Infect Dis. 2023;10:ofad100. https:/doi.org/10.1093/ofid/ofad100

Address for correspondence: Jeremy A.W. Gold, Centers for Disease Control and Prevention, 1600 Clifton Road NE, Mailstop H24-10, Atlanta, GA 30329-4027, USA; email: jgold@cdc.gov

Nonnegligible Seroprevalence and Predictors of Murine Typhus, Japan

Tetsuro Aita, Eiichiro Sando, Shungo Katoh, Sugihiro Hamaguchi, Hiromi Fujita, Noriaki Kurita

To elucidate the epidemiology of murine typhus, which is infrequently reported in Japan, we conducted a cross-sectional study involving 2,382 residents of rickettsiosis-endemic areas in Honshu Island during August–November 2020. *Rickettsia typhi* seroprevalence rate was higher than that of *Orientia tsutsugamushi*, indicating that murine typhus is a neglected disease.

Murine typhus (MT), a fleaborne rickettsiosis caused by the bacterium *Rickettsia typhi*, is a ubiquitous but clinically less recognizable disease than scrub typhus or spotted fever group rickettsioses (*1*). Limited testing because of the infection's nonspecific symptoms and the need for expert laboratories for serodiagnosis makes MT an underrecognized infection. MT occurs worldwide and is endemic to warm urban or coastal regions where the climate is favorable for rats, which can serve as the reservoir of *R. typhi*. However, epidemiologic characteristics and risk factors often vary by region (*1*–*3*). Therefore, accumulating specific and local evidence from each region is required to elucidate the complete picture of MT epidemiology.

In Japan, MT with *Xenopsylla cheopis* fleas as the vector and *Rattus rattus* or *R. norvegicus* rats as the reservoir was endemic before the 1950s (*4*), but the disease has not been notifiable; only a few cases have been reported since then (*5*). As a consequence, the epidemiologic characteristics remain unknown, rendering MT an underrecognized and neglected infection. Clarifying the epidemiologic features of MT in Japan will help clinicians recognize the disease and provide early treatment. We estimate the seroprevalence of rickettsia, primarily of *R. typhi*, in rickettsia-endemic areas of Honshu Island (the largest island of Japan) and characterize the risk factors for MT.

Author affiliations: Fukushima Medical University, Fukushima, Japan (T. Aita, E. Sando, S. Katoh, S. Hamaguchi, N. Kurita); Kita-Fukushima Medical Center, Fukushima (E. Sando, S. Katoh, H. Fujita)

DOI: https://doi.org/10.3201/eid2907.230037

The Study

We conducted a cross-sectional study in 3 sites in the southeastern part of Honshu (Boso Peninsula), endemic areas for scrub typhus and Japanese spotted fever (*6*). We included persons who underwent regular checkups during August–November 2020 (Appendix, https://wwwnc.cdc.gov/EID/article/29/7/23-0037-App1.pdf). Questionnaires were distributed during checkups, and the following data were collected: medical history of rickettsioses; environmental exposure to mountains, agriculture, and bushes; and residential addresses. The respondents were asked through questionnaires whether they resided in or had visited mountainous areas, had visited areas with small trees and weeds, or engaged in agricultural work. In addition, we measured the population density and area of each land use (coasts, forests, farmland, rivers or lakes, and wilderness) within a 500-meter radius of the participant's address (Appendix). The study was approved by the Institutional Review Boards of Nagasaki University and Fukushima Medical University (approval nos. 200305230-2 and 2022-190). Written consent was obtained from all participants.

The primary outcomes were *R. typhi* seroprevalence and ratio of *R. typhi to Orientia tsutsugamushi* seroprevalence. *O. tsutsugamushi* was selected as the comparator outcome because scrub typhus is a notifiable disease and the rickettsiosis most endemic to Japan. Furthermore, we evaluated the seroprevalence of *R. japonica*, the pathogen of Japanese spotted fever, to determine the possibility of an apparently high seroprevalence of *R. typhi* because of cross-reactivity in the genus *Rickettsia* (*7*) (Appendix). We defined seropositivity as a ratio of ≥1:40 and defined *O. tsutsugamushi* seropositivity as a positive result for any of the *O. tsutsugamushi* serotypes. The

sensitivity analyses estimated the seroprevalences at cutoff titers of 1:80 and 1:160.

Because the seropositivity rates of *R. typhi* and *O. tsutsugamushi* were regarded as paired binomial data, we tested the difference in their prevalence by using the McNemar test (*8*) and estimated it using conditional Poisson regression (Appendix). To explore the factors associated with *R. typhi* seropositivity, we fitted a logistic regression model by using the candidate risk factors. We assessed whether there were differences in the seroprevalence ratios across study sites and conducted the imputation of missing values (Appendix).

The median age of all participants was 67 years. *R. typhi*–seropositive participants exhibited a lower population density than *R. typhi*–seronegative participants, showing a similar trend to *O. tsutsugamushi* (Table 1; Appendix Table 1). The residential locations of *R. typhi*–seropositive participants were distributed throughout the Boso Peninsula, and a similar distribution was observed for *O. tsutsugamushi*–seropositive participants (Appendix Figures 1, 2). Although ≈60% of *R. typhi*–seropositive participants had titers of ≤160, 20 participants had titers of ≥1,280, and 4 had titers of ≥40,960 (Table 2). Most *O. tsutsugamushi*–seropositive participants had lower

Table 1. Characteristics and residential geographic features for participants in study of seroprevalence and predictors of murine typhus, by *Rickettsia typhi* IgG seropositivity status, Japan*

Characteristic	*R. typhi*–positive, n = 269	*R. typhi*–negative, n = 2,113	Total, n = 2,382
Sex			
F	123 (45.7)	1,080 (51.1)	1,203 (50.5)
M	146 (54.3)	1,033 (48.9)	1,179 (49.5)
Age group, y			
≤40	2 (0.7)	109 (5.2)	111 (4.6)
41–50	11 (4.1)	269 (12.7)	280 (11.8)
51–60	15 (5.6)	350 (16.6)	365 (15.3)
61–70	71 (26.4)	695 (32.9)	766 (32.2)
71–80	113 (42)	576 (27.2)	689 (28.9)
≥81	57 (21.2)	114 (5.4)	171 (7.2)
Site			
Otaki	180 (66.9)	891 (42.2)	1,071 (45)
Katsuura	42 (15.6)	250 (11.8)	292 (12.2)
Kameda	47 (17.5)	972 (46)	1,019 (42.8)
Medical history			
None	227 (84.4)	1,787 (85)	2,014 (84.9)
Scrub typhus	8 (3.0)	32 (1.5)	40 (1.7)
Japanese spotted fever	2 (0.7)	0	2 (0.1)
Both	0	1 (0.1)	1 (0)
Unknown	32 (11.9)	283 (13.5)	315 (13.3)
Missing	0	10	10
Environmental exposure history			
Mountains			
Yes	70 (26)	456 (21.6)	526 (22.1)
No	199 (74)	1,657 (78.4)	1,856 (77.9)
Agriculture			
Yes	135 (50.2)	766 (36.3)	901 (37.8)
No	134 (49.8)	1,347 (63.7)	1,481 (62.2)
Bushes†			
Yes	141 (52.4)	856 (40.5)	997 (41.9)
No	128 (47.6)	1,257 (59.5)	1,385 (58.1)
Environment surrounding the residence			
Population density, persons/km^2 (5th–95th percentile)	244 (32–1,207)	356 (45–3,354)	306 (44–3,148)
Missing	3	26	29
Coasts, m^2 (5th–95th percentile)	0 (0–235,132)	0 (0–232,102)	0 (0–233,502)
Missing	0	3	3
Forests, m^2 (5th–95th percentile)	307,376 (76,276–664,633)	269,342 (6,023–616,031)	273,757 (7,231–621,401)
Missing	0	3	3
Farmland, m^2 (5th–95th percentile)	236,624 (14,833–458,114)	233,350 (0–486,875)	233,414 (0–483,051)
Missing	0	3	3
Rivers and lakes, m^2 (5th–95th percentile)	17,596 (0–101,103)	13,917 (0–84,788)	14,279 (0–86,124)
Missing	0	3	3
Wilderness, m^2 (5th–95th percentile)	0 (0–27,181)	0 (0–25,095)	0 (0–25,391)
Missing	0	3	3

*Values are no. (%) except as indicated. Continuous and categorical variable data are presented as median (5th–95th percentile) and frequency (%).
†Bushes refer to areas with small trees and weeds.

Table 2. Distribution of antibody titers in *Rickettsia typhi* IgG–positive persons in study of seroprevalence and predictors of murine typhus, Japan

Antibody titer	Seropositive participants, no. (%), n = 269
1:40	53 (19.7)
1:80	33 (12.3)
1:160	80 (29.7)
1:320	37 (13.7)
1:640	46 (17.1)
1:1,280	5 (1.9)
1:2,560	8 (3.0)
1:5,120	2 (0.7)
1:10,240	1 (0.4)
1:20,480	0
≥1:40,960	4 (1.5)

titers, although some exhibited notably high titers (Appendix Table 2).

R. typhi seroprevalence was 11.3% higher than that of *O. tsutsugamushi* (7.9%) (ratio of seropositivity 1.42; 95% CI 1.20–1.68) (Figure 1). Of the 2,382 residents, 204 were *R. japonica* seropositive, for a seroprevalence of 8.6%, lower than that of *R. typhi*. Furthermore, the antibody titer for *R. typhi* was higher than that for *R. japonica* in participants who were seropositive for both *R. typhi* and *R. japonica* (Appendix Table 3). Results of the sensitivity analyses did not show any changes to the predominance of the *R. typhi* seroprevalence over the *O. tsutsugamushi* seroprevalence (Appendix Table 4).

According to the multivariate analysis (Figure 2), the factors associated with *R. typhi* seropositivity were age (per 10-year increase; adjusted odds ratio [aOR] 2.09 [95% CI 1.80–2.42]), low population density (per 1,000 persons/km^2 increase; aOR 0.59 [95% CI 0.40–0.86]), and history of bush exposure (aOR 1.39 [95% CI 1.01–1.92]) (Appendix).

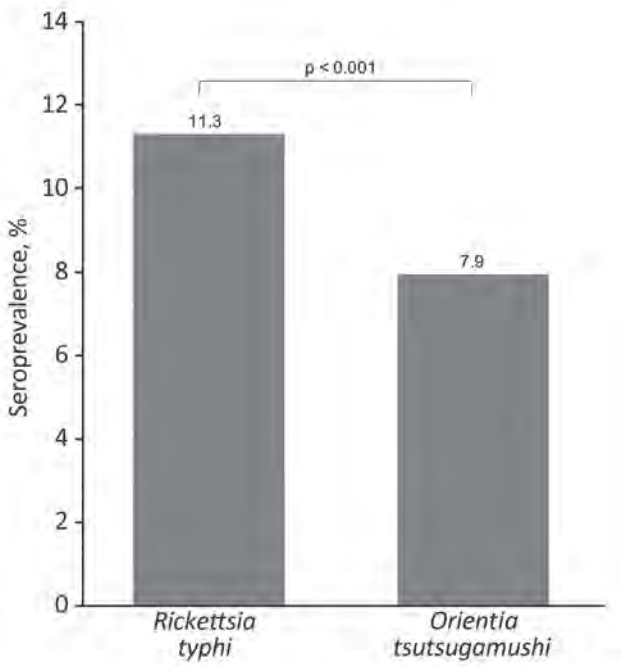

Figure 1. Seroprevalence rates of *Rickettsia typhi* and *Orientia tsutsugamushi* in study of seroprevalence and predictors of murine typhus, Japan. *R. typhi* IgG was detected in 11.3% (95% CI 10.0–12.6) of participants and *O. tsutsugamushi* IgG was detected in 7.9% (95% CI 6.9–9.1) of all participants. The seroprevalence of both infections was compared using the McNemar test. The estimated seropositivity ratio was 1.42 (95% CI 1.20–1.68).

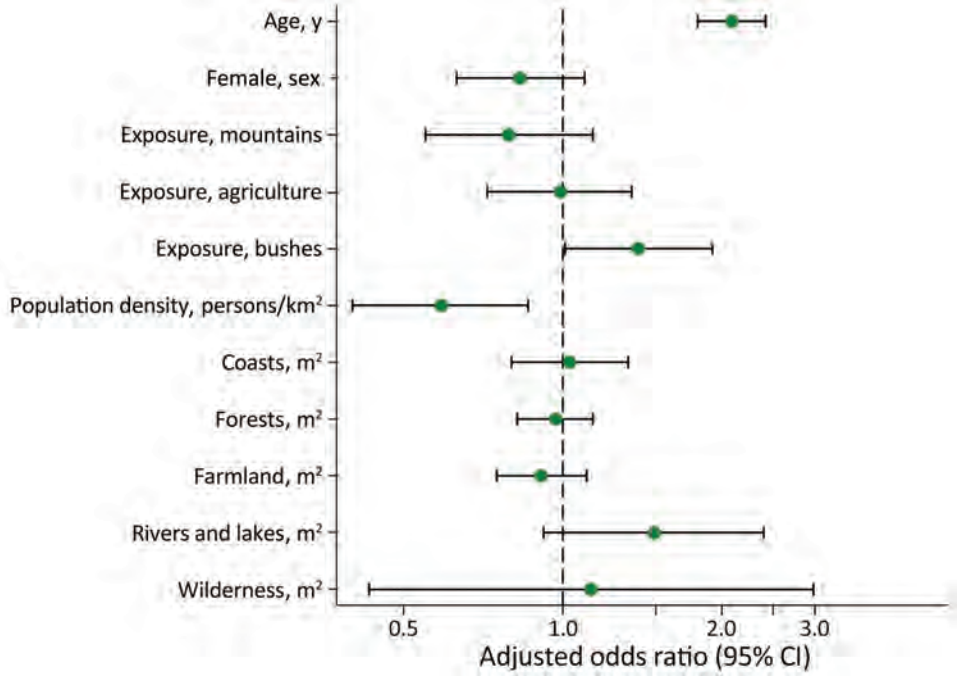

Figure 2. Predictors of *Rickettsia typhi* IgG seropositivity in study of seroprevalence and predictors of murine typhus, Japan. Shown are adjusted odds ratios for age per 10-year increase; population density increase; residential geographic features, such as coasts, forests, farmland, and rivers and lakes; and wilderness per 10-hectare increase. Bushes refer to areas with small trees and weeds.

Conclusions

We demonstrated robust findings of the predominance of *R. typhi* seroprevalence over *O. tsutsugamushi* seroprevalence in rickettsia-endemic areas in Japan. Previously, in those study areas, an epidemiologic study was conducted using now antiquated serologic methods, such as the Weil–Felix test (*4*), which provided unreliable MT and scrub typhus seroepidemiologic data (*9*). Contrary to the previous study's findings, we were able to estimate rickettsiosis seroprevalence and confirm the predominance of MT more precisely using the standard diagnostic test.

This study illustrated that MT is a prevalent and possibly reemerging infection in Japan. Recently, in the United States (*10*), Greece (*11*), and Spain (*12*), the incidence of MT has increased, partly because of improved disease recognition (*10*) and a change in the transmission route (*13*). Thus, given the high seroprevalence of *R. typhi* in Japan, case accumulation is crucial to clarify the possibility of a unique transmission cycle.

The risk factors for *R. typhi* seropositivity in this study differed from those in previous studies. The increase in *R. typhi* seroprevalence with decrease in residential population density contradicts the findings of previous studies that showed urban environment as a risk factor (*2*,*14*). In addition, exposure to weeded areas was identified as a risk factor, but residential environments, including those near coasts, rivers, and lakes, which have been reported as risk factors (*2*,*3*), were not correlated. The differences in risk factors between this study and previous studies might reflect differences in factors related to contact with vectors and reservoirs at each study site.

The first limitation of our study is that seropositivity to *R. typhi* could indicate cross-reactivity to *R. japonica*. However, because *R. typhi* seropositivity was higher than *R. japonica* seropositivity and the cross-reactivity rate to *R. typhi* in confirmed Japanese spotted fever patients is ≈20% (*15*), most patients with *R. typhi* seropositivity have a true MT infection. Second, we did not consider cross-reactivity within the same group (spotted fever or typhus group) in the genus *Rickettsia*. However, other diseases caused by this genus have been reported infrequently, except for Japanese spotted fever and MT in domestic infection cases. Third, this study was conducted in persons undergoing routine checkups and might not represent seroprevalence in the general population.

In summary, *R. typhi* seroprevalence was higher than that of *O. tsutsugamushi* in rickettsia-endemic areas of Japan, indicating that MT is a neglected and underrecognized condition. This study highlights the need to include MT in the differential diagnosis when examining patients with nonspecific infectious symptoms who are residing in rickettsia-endemic areas. Clinicians should consider comprehensive examinations for rickettsial infections, including MT testing, especially in those with a history of residence in sparsely populated areas or exposure to bushes.

Acknowledgments

We thank the staff of the municipal offices in Otaki and Katsuura and Kameda Medical Center for collecting questionnaires and blood samples. We also thank Dr. Fujita, who made great efforts to conduct this research but died before its publication.

This work was supported by JSPS KAKENHI (grant no. JP 19K23972).

About the Author

Dr. Aita is an internist specializing in general internal medicine and clinical epidemiology. He belongs to the Department of General Internal Medicine, Fukushima Medical University as a teaching/research associate, and conducts research on the epidemiology of diseases, diagnostic accuracy, and infections, such as rickettsioses.

References

1. Civen R, Ngo V. Murine typhus: an unrecognized suburban vectorborne disease. Clin Infect Dis. 2008;46:913–8. https://doi.org/10.1086/527443
2. Azad AF. Epidemiology of murine typhus. Annu Rev Entomol. 1990;35:553–69. https://doi.org/10.1146/annurev.en.35.010190.003005
3. Devamani CS, Schmidt WP, Ariyoshi K, Anitha A, Kalaimani S, Prakash JAJ. Risk factors for scrub typhus, murine typhus, and spotted fever seropositivity in urban areas, rural plains, and peri-forest hill villages in South India: a cross-sectional study. Am J Trop Med Hyg. 2020;103:238–48. https://doi.org/10.4269/ajtmh.19-0642
4. Tamiya T. Recent advances in studies of tsutsugamushi disease in Japan. Tokyo: Medical Culture, Inc.; 1962. p. 53–54.
5. Sakaguchi S, Sato I, Muguruma H, Kawano H, Kusuhara Y, Yano S, et al. Reemerging murine typhus, Japan. Emerg Infect Dis. 2004;10:964–5. https://doi.org/10.3201/eid1005.030697
6. Sando E, Suzuki M, Katoh S, Fujita H, Taira M, Yaegashi M, et al. Distinguishing Japanese spotted fever and scrub typhus. Emerg Infect Dis. 2018;24:1633–41. https://doi.org/10.3201/eid2409.171436
7. Uchiyama T, Zhao L, Yan Y, Uchida T. Cross-reactivity of *Rickettsia japonica* and *Rickettsia typhi* demonstrated by immunofluorescence and Western immunoblotting. Microbiol Immunol. 1995;39:951–7. https://doi.org/10.1111/j.1348-0421.1995.tb03298.x
8. Pembury Smith MQR, Ruxton GD. Effective use of the McNemar test. Behav Ecol Sociobiol. 2020;74:133. https://doi.org/10.1007/s00265-020-02916-y

9. Stewart AG, Stewart AGA. An update on the laboratory diagnosis of rickettsia spp. infection. Pathogens. 2021;10:1319. https://doi.org/10.3390/pathogens10101319
10. Ruiz K, Valcin R, Keiser P, Blanton LS. Rise in murine typhus in Galveston County, Texas, USA, 2018. Emerg Infect Dis. 2020;26:1044–6. https://doi.org/10.3201/eid2605.191505
11. Labropoulou S, Charvalos E, Chatzipanagiotou S, Ioannidis A, Sylignakis P, Taka S, et al. Sunbathing, a possible risk factor of murine typhus infection in Greece. PLoS Negl Trop Dis. 2021;15:e0009186. https://doi.org/10.1371/journal.pntd.0009186
12. Rodríguez-Alonso B, Almeida H, Alonso-Sardón M, Velasco-Tirado V, Robaina Bordón JM, Carranza Rodríguez C, et al. Murine typhus. How does it affect us in the 21st century? The epidemiology of inpatients in Spain (1997–2015). Int J Infect Dis. 2020;96:165–71. https://doi.org/10.1016/j.ijid.2020.04.054
13. Penicks A, Krueger L, Morgan T, Nguyen K, Campbell J, Fogarty C, et al. Jumping into the future: an analysis of 50 years of flea data from mammalian wildlife collected during three flea-borne rickettsioses surveys in Orange County, 1967–2017. Proceedings and Papers of the Mosquito and Vector Control Association of California. 2019;87:1.
14. Yao Z, Tang J, Zhan FB. Detection of arbitrarily-shaped clusters using a neighbor-expanding approach: a case study on murine typhus in south Texas. Int J Health Geogr. 2011;10:23. https://doi.org/10.1186/1476-072X-10-23
15. Aita T, Sando E, Katoh S, Hamaguchi S, Fujita H, Kurita N. Serological cross-reactivity between spotted fever and typhus groups of rickettsia infection in Japan. Int J Infect Dis. 2023;130:178–81. https://doi.org/10.1016/j.ijid.2023.03.012

Address for correspondence: Eiichiro Sando, Department of General Internal Medicine and Clinical Infectious Diseases, Fukushima Medical University, 1 Hikarigaoka, Fukushima city, Fukushima, 960-1295, Japan; email: e-sando@fmu.ac.jp

Spotted Fever and Typhus Group Rickettsiae in Dogs and Humans, Mexico, 2022

Ricardo Palacios-Santana,[1] Lihua Wei,[1] Nadia A. Fernandez-Santos,[1] Mario A. Rodriguez-Perez,[1] Sergio Uriegas-Camargo, Nicole L. Mendell, Donald H. Bouyer, Jose Guillermo Estrada-Franco

We found serologic evidence of spotted fever group *Rickettsia* in humans and dogs and typhus group *Rickettsia* in dogs in Reynosa, Mexico. Our investigation revealed serologic samples reactive to spotted fever group *Rickettsia* in 5 community members, which highlights a potential rickettsial transmission scenario in this region.

The spotted fever group (SFG) rickettsiae, which are transmitted primarily by tick bite to rodents, dogs, wild animals, and persons, comprise a phylogenetically discrete clade of the family Rickettsiacae, encompassing ≈30 species. SFG rickettsioses represent a major cause of febrile illness worldwide. This group includes *Rickettsia rickettsii*, the bacterium responsible for Rocky Mountain spotted fever (RMSF), a major pathogen of public health concern linked to severe hemorrhagic illness in humans. SFG rickettsiae are maintained through a tick–vertebrate host cycle; humans are incidental hosts (*1*). The arthropod-borne typhus group (TG) comprises *R. typhi*, the causative agent of murine or endemic typhus, and *R. prowazekii*, the pathogen responsible for epidemic typhus (*2*). *R. typhi* is sustained in enzootic cycles by small mammals, such as rats (*Rattus* spp.) and opossums (*Didelphis* spp.), and by ectoparasites such as the rat flea (*Xenopsylla cheopis*) and cat flea (*Ctenocephalides felis)* (*3*,*4*). Direct transmission of TG rickettsiae to humans is by cross-contamination between mucosal or skin abrasions and *Rickettsia* contained in the feces of either fleas (*R. typhi*) or human body lice (*R. prowazekii*), or simply by inhalation of contaminated dust (*4*). However, a sylvatic cycle of *R. prowazekii* in the United States has been associated with ectoparasites of flying squirrels (*Glaucomys volans*) (*5*). Clinical manifestations of TG rickettsioses start with sudden fever onset and other nonspecific symptoms, including severe headaches, myalgias, arthralgias, nausea, and vomiting.

During 2013–2022, a total of 2,232 RMSF cases were reported in 5 of 6 northern states of Mexico contiguous to the United States (*6*). Endemicity of TG rickettsiae in the southern counties of Texas in the Rio Grande transborder area of the United States (*4*) and seropositivity among blood donors from Mexico City (*7*) and Yucatán (*8*), Mexico, indicate a need to evaluate TG rickettsiae presence in this area. We report a cross-sectional serologic study for SFG and TG rickettsiae conducted in domestic dogs and humans in Reynosa, an urban city in northeastern Mexico. On the basis of previous research in this city (*1*), we hypothesized that dogs are sentinels of infectious disease circulation, as has been reported elsewhere for rickettsiae (*9*,*10*), and therefore are useful in surveillance approaches to monitor rickettsial disease in humans.

The Study

We tested 106 dogs from 71 households in 6 periurban neighborhoods of Reynosa during March 13–July 4, 2022 (Figure). We collected signed, individual informed consents from canine owners and recorded data about the sampled dogs, which included vaccine history, gender, age, and breed. We administered rabies vaccine to unvaccinated dogs. We recruited all household members (n = 36) owning SFG- or TG-seropositive dogs, 16 of whom provided blood

Author affiliations: Instituto Politecnico Nacional, Centro de Biotecnologia Genomica Nacional, Reynosa, Mexico (R. Palacios-Santana, L. Wei, N.A. Fernandez-Santos, M.A. Rodriguez-Perez, J.G. Estrada-Franco); Texas A&M University, College Station, Texas, USA (N.A. Fernandez-Santos); Secretaria de Salud de Tamaulipas, Ciudad Victoria, Mexico (S. Uriegas-Camargo); University of Texas Medical Branch, Galveston, Texas, USA (N.L. Mendell, D.H. Bouyer)

DOI: http://doi.org/10.3201/eid2907.230333

[1]These authors contributed equally to this article.

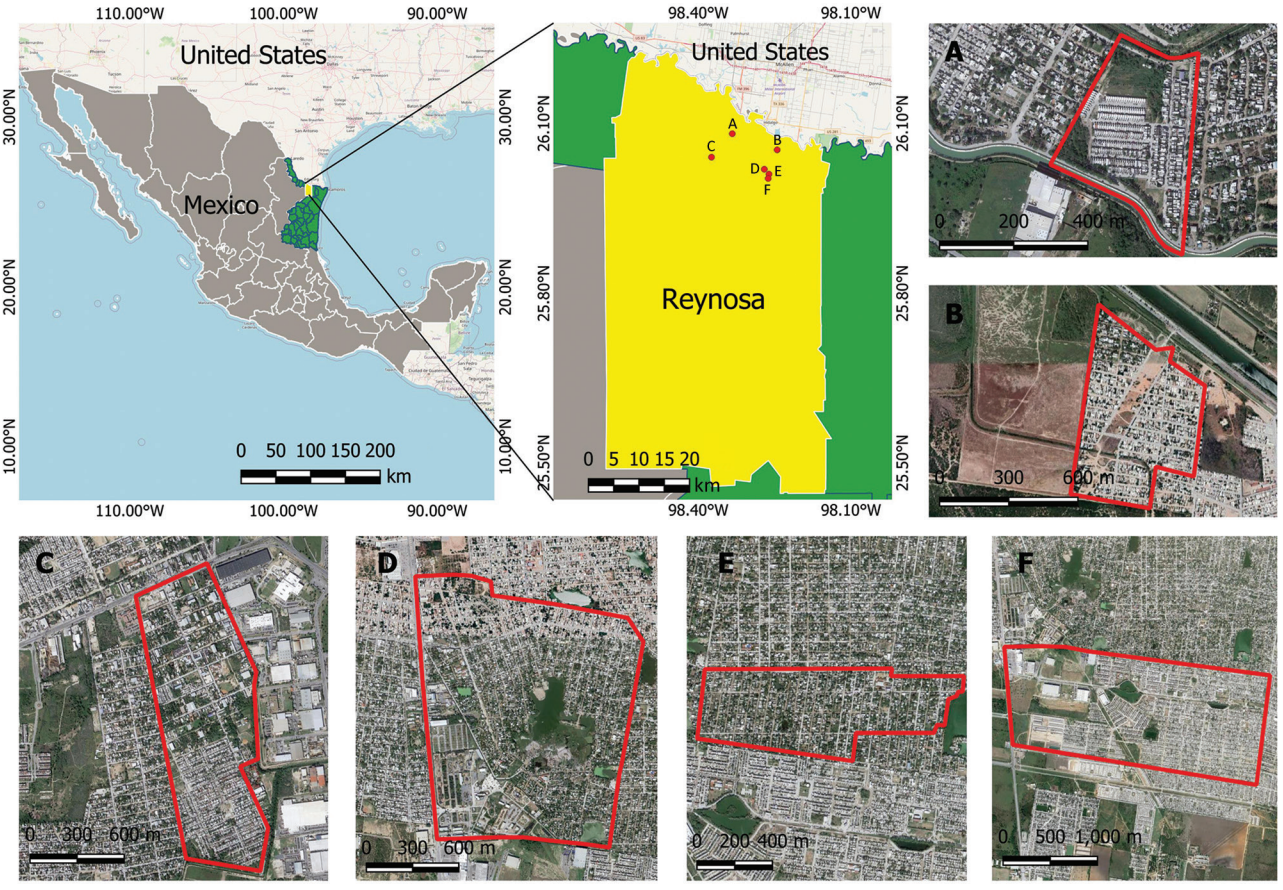

Figure. Sampling locations for study of spotted fever and typhus group rickettsiae in dogs and humans, in Reynosa, Mexico, 2022. Primary maps show location of Reynosa along the Mexico–United States border; neighborhoods sampled (A–F) are labeled and enlarged in the satellite images. Primary maps generated using QGIS 3.28.2 (https://www.qgis.org). Free geographic data of administrative areas of Mexico was downloaded from the National Institute of Statistics and Geography, Mexico (INEGI, https://www.inegi.org.mx/app/mapas). Satellite images and street maps were obtained from Google Maps (https://www.google.com/maps).

samples for further analysis. We collected and processed blood samples (≈3– to 5 mL, dog or human) according to previously reported methods (*1*). We centrifuged blood at 3000 × *g* for 10 min and stored serum samples −80° C until further processing. We tested serum samples for IgG against *R. amblyommatis*, *R. parkeri*, *R. rickettsii*, and *R. typhi* by indirect immunofluorescence assay as previously described (*11*). We recorded serum samples with reciprocal iIgG titers ≥64 or higher as positive and determined endpoint titer of those samples.

Of the dogs sampled, 5 (4.71%, 95% CI 0.68%–8.75%) were positive for SFG *Rickettsia* IgG and 4 (3.77%; 95% CI 0.15%–7.4%) were positive for TG *Rickettsia* IgG antibodies (Appendix Table 1, https://wwwnc.cdc.gov/EID/article/29/7/23-0333-App1.pdf). To further test whether seropositive dogs were sentinels of rickettsial exposure, we collected blood samples from dog owners and their families and questioned them about recent tick bites and clinical history (prior 3 months) associated with signs of rickettsial illness (Appendix Table 2) (*12*). Testing revealed that 5 (32.3%; 95% CI 1.84%–53.9%) of 16 serum samples obtained from owners in households with positive dogs were positive for SFG *Rickettsia* IgG using identical experimental conditions (Appendix Table 1). The Tamaulipas Health Services is conducting a follow-up investigation for the medical evaluation and treatment for the SFG-seropositive persons.

Conclusion

RMSF was described in Mexico in 1943. We report finding antibodies to SFG *Rickettsia* in Reynosa, Mexico, in 2022. Seroevidence of domestic dog exposure to *R. typhi* in Reynosa warrants further investigation, especially given the endemicity of murine typhus in the contiguous Hidalgo County, Texas, USA, that involved >1,000 human cases reported during 2008–2019. Our results validate the theory that dogs can

be sentinels for human diseases and demonstrated their assistance in inferring the temporal and spatial dynamics of some diseases in regions associated with their vectors (*12*).

Metropolitan Reynosa is an industrial center and a reference transborder point area of migration between different demographic groups comprising the Reynosa–Texas–US region, known as Rio Grande Valley. It is a land strip of ≈110 km housing ≈3 million permanent residents, with a large floating population fluctuating in the hundreds to thousands. The entire Mexico–United States transborder region spans 3,141 km, and >286 million crossings are documented annually (*13*).

Historic outbreaks of RMSF along the Mexico–United States border region have been documented, with fatality rates of 30%–80% (*12*). In 2019, an RMSF seroprevalence of 6% (95% CI 4.68%−7.46%; 69/1,136 cases) in dogs was reported from 14 Mexico border cities in the states of Baja California, Sonora, and Coahuila (*14*), which is concordant with the seroprevalence of our study (4.71%; 95% CI 0.68%–8.75%). Human cases of murine typhus have been reported mainly in southeastern Mexico, but rarely in northeastern Mexico. However, endemicity in the Rio Grande Valley has been reported widely on the US side of the border (*4*). In 2022, 23.9% (95% CI 16.9%–31.0%; 34/142 samples) of human serum samples were positive for *R. typhi* IgG in Yucatan, and 15% of those were positive for *R. rickettsii* (*15*). Similarly, first screening of seropositive *Rickettsia* IgG in dogs informed identification of putative human cases, indicating this surveillance strategy is effective (*15*).

Most dogs roam freely in relatively squalid conditions throughout our studied areas. In this context, evidence of TG *Rickettsia* antibodies in dogs did not correspond to the same findings in their owners. On the contrary, SFG-seropositive owners of SFG-seronegative dogs suggests the possibility that the owners may have acquired the infection away from their residence and pets. Although antibody titers of 3 of 5 SFG-reactive human samples suggest *R. parkeri* as the presumptive agent, without paired serum samples, other SFG rickettsiae cannot be excluded. Because of rickettsial cross-reactivity observed by immunofluorescence assay, further studies using cross-absorption techniques to clarify the responsible etiologic agent(s) are warranted. This transborder transmission scenario appears to repeat along Mexico towns contiguous to the US border, where brown dog tick (*Rhipicephalus sanguineus*) infestations are known to be rampant.

Our findings suggest that the epidemiologic fabric of the region is strongly affected by the high incidence of SFG and TG rickettsioses. We hypothesize that improvement of the urban environment, using a One Health approach, along with integrated vector control management of ectoparasites (e.g., dog tick collars, tick trapping, acaricide spraying) would be of utmost importance in reducing the spread of rickettsial diseases in regions such as our study area. Evidence of TG rickettsia exposure of domestic dogs in this study highlights the need for further surveillance to determine the vector phenology and transmission cycle in the region. In conclusion, SFG and TG rickettsiae surveillance and control, by both standard and novel approaches, are urgently needed for areas along the northeastern Mexico–United States border.

Acknowledgments

We thank Victor Moreno Medina for supporting the field work.

This work was supported by funding from the Department of Pathology at University of Texas Medical Branch (to D.H.B.). J.G.E.F. was supported by grants SIP-IPN-20222157, 20221576, 20230712, and 20226932; N.F.S. by grant SIP-IPN 20230712; and M.R.P. by grant 20201174. Graduate studies for R.P.S. were supported by a CONAHCYT Fellow award (CVU 1020234).

Permission to collect samples from canids and humans was approved by Escuela Nacional de Medicina y Homeopatía-IPN (IRB no. CBE/006/2020).

About the Author

Mr. Palacios-Santana is a graduate student at the Centro Biotecnologia Genomica-IPN and is working on vector-borne diseases with a focus on Rocky Mountain spotted fever.

References

1. Salomon J, Fernandez Santos NA, Zecca IB, Estrada-Franco JG, Davila E, Hamer GL, et al. Brown dog tick (*Rhipicephalus sanguineus* sensu lato) infection with endosymbiont and human pathogenic *Rickettsia* spp., in northeastern México. Int J Environ Res Public Health. 2022;19:6249. https://doi.org/10.3390/ijerph19106249
2. Fang R, Blanton LS, Walker DH. Rickettsiae as emerging infectious agents. Clin Lab Med. 2017;37:383–400. https://doi.org/10.1016/j.cll.2017.01.009
3. Walker DH, Ismail N. Emerging and re-emerging rickettsioses: endothelial cell infection and early disease events. Nat Rev Microbiol. 2008;6:375–86. https://doi.org/10.1038/nrmicro1866
4. Azad AF. Epidemiology of murine typhus. Annu Rev Entomol. 1990;35:553–69. https://doi.org/10.1146/annurev.en.35.010190.003005
5. Prusinski MA, White JL, Wong SJ, Conlon MA, Egan C, Kelly-Cirino CD, et al. Sylvatic typhus associated with flying squirrels (*Glaucomys volans*) in New York State, United States. Vector Borne Zoonotic Dis. 2014;14:240–4. https://doi.org/10.1089/vbz.2013.1392

6. Mexico Ministry of Health. General Directorate of Epidemiology [cited 2023 Feb 24] https://www.gob.mx/salud/acciones-y-programas/historico-boletin-epidemiologico
7. Acuna-Soto R, Calderón-Romero L, Romero-López D, Bravo-Lindoro A. Murine typhus in Mexico City. Trans R Soc Trop Med Hyg. 2000;94:45. https://doi.org/10.1016/S0035-9203(00)90432-2
8. Dzul-Rosado K, González-Martínez P, Peniche-Lara G, Zavala-Velázquez J, Zavala-Castro J. Murine typhus in humans, Yucatan, Mexico. Emerg Infect Dis. 2013;19:1021–2. https://doi.org/10.3201/eid1906.121400
9. Bowser NH, Anderson NE. Dogs (Canis familiaris) as sentinels for human infectious disease and application to Canadian populations: a systematic review. Vet Sci. 2018;5:83. https://doi.org/10.3390/vetsci5040083
10. Davila E, Fernández-Santos NA, Estrada-Franco JG, Wei L, Aguilar-Durán JA, López-López MJ, et al. Domestic dogs as sentinels for West Nile virus but not *Aedes*-borne flaviviruses, Mexico. Emerg Infect Dis. 2022;28:1071–4. https://doi.org/10.3201/eid2805.211879
11. Ndip LM, Bouyer DH, Travassos Da Rosa AP, Titanji VPK, Tesh RB, Walker DH. Acute spotted fever rickettsiosis among febrile patients, Cameroon. Emerg Infect Dis. 2004;10:432–7. https://doi.org/10.3201/eid1003.020713
12. Álvarez-Hernández G, Roldán JFG, Milan NSH, Lash RR, Behravesh CB, Paddock CD. Rocky Mountain spotted fever in Mexico: past, present, and future. Lancet Infect Dis. 2017;17:e189–96. https://doi.org/10.1016/S1473-3099(17)30173-1
13. Gutiérrez M, Sánchez-Atondo A, García L, Mungaray-Moctezuma A, Calderón J. Understanding cross-border mobility in medium-small Mexico-US Binational regions. Mexicali-Imperial Valley case study. Transportation Research Interdisciplinary Perspectives. 2021;9:100324. https://doi.org/10.1016/j.trip.2021.100324
14. Pieracci EG, De La Rosa JDP, Rubio DL, Perales MES, Contreras MV, Drexler NA, et al. Seroprevalence of spotted fever group rickettsiae in canines along the United States-Mexico border. Zoonoses Public Health. 2019;66:918–26. https://doi.org/10.1111/zph.12642
15. Torres-Castro M, Reyes-Novelo E, Bolio-González M, Lugo-Caballero C, Dzul-Rosado K, Colunga-Salas P, et al. Epidemiological study of the occurrence of typhus group *Rickettsia* natural infection in domiciliated dogs from a rural community in south-eastern Mexico. Animals (Basel). 2022;12:2885. https://doi.org/10.3390/ani12202885

Address for correspondence: Jose Guillermo Estrada-Franco, Instituto Politecnico Nacional, Centro de Biotecnología Genómica, Reynosa 88710, Mexico; email: jestradaf@ipn.mx; Donald H. Bouyer, Department of Pathology, University of Texas Medical Branch, Galveston, TX 77555, USA; email: dobouyer@utmb.edu

etymologia revisited

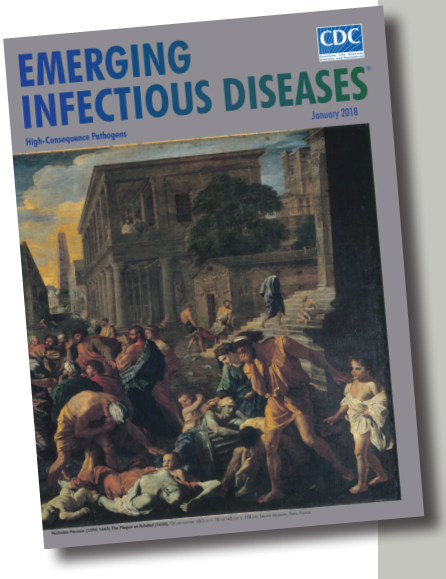

Originally published in January 2018

Plague

[plāg]

Plague (from the Latin *plaga*, "stroke" or "wound") infections are believed to have been common since at least 3000 bce. Plague is caused by the ancestor of current *Yersinia* (named for Swiss bacteriologist Alexandre Yersin, who first isolated the bacterium) *pestis* strains. However, this ancestral *Y. pestis* lacked the critical *Yersinia* murine toxin (*ymt*) gene that enables vectorborne transmission. After acquiring this gene (sometime during 1600–950 bce), which encodes a phospholipase D that protects the bacterium inside the flea gut, *Y. pestis* evolved the ability to cause pandemics of bubonic plague. The first recoded of these, the Justinian Plague, began in 541 ace and eventually killed more than 25 million persons.

References:

1. Alexandre Yersin BW. Etymologia: yersinia. Emerg Infect Dis. 2010;16:496.
2. Centers for Disease Control and Prevention. History of plague [cited 2017 Oct 19]. https://www.cdc.gov/plague/history/index.html.
3. Rasmussen S, Allentoft ME, Nielsen K, Orlando L, Sikora M, Sjögren K-G, et al. Early divergent strains of Yersinia pestis in Eurasia 5,000 years ago. Cell. 2015;163:571–82.

https://wwwnc.cdc.gov/eid/article/24/1/et-2401_article

Cutaneous Pythiosis in 2 Dogs, Italy

Andrea Peano, Anna Rita Molinar Min, Alessandra Fondati, Erica Romano, Chiara Brachelente, Ilaria Porcellato, Andrea Amore, Mario Pasquetti

We report cutaneous pythiosis in 2 dogs in Italy that had recurrent exposure to the same freshwater habitat. Phylogenetic analysis placed the isolates within *Pythium insidiosum* complex cluster IV, corresponding to *P. periculosum*. In Italy, pythiosis should be considered in differential diagnoses by human and veterinary health professionals.

Pythiosis is a granulomatous disease caused by oomycete organisms affecting mainly horses, humans, and dogs, and is historically associated with humid environments (*1*). In India, where the first cases were reported in horses in the late 19th century, pythiosis is known as bursattee, from burus, signifying rain, because infections appeared during the rainy season (*2*). In other countries, pythiosis is known by different names, such as swamp cancer in Australia and the United States and horse leeches in the United States (*2*).

The genus *Pythium* (kingdom Stramenopila) comprises >120 species inhabiting all soil and wet environments. *Pythium* spp. have a saprophytic life cycle, although many are plant pathogens (*3*). *P. insidiosum* has been considered the only species that infects mammals (*2*). In 2003, existence of a cryptic species was suspected on the basis of phylogenetic analyses that indicated *P. insidiosum* is a complex with 3 clusters, 1 (cluster III) of which displays substantial divergence from the other 2 clusters (*4*). Recent studies have revealed a fourth cluster (cluster IV); clusters III and IV form a monophyletic group representing a novel species, *P. periculosum* (*5*). *P. aphanidermatum* has also been reported in 2 cases of human infection (*6*,*7*).

Pythiosis is characterized by the presence of broad, irregular, perpendicular branching hyphae in tissues and cultures that are aseptate in early growth stages or sparsely septate in aged organisms. Biflagellate motile zoospores are the infecting agents, and production in the environment requires free water. The zoospores are attracted by open wounds, encyst on exposed tissue, and develop a germ tube that mechanically penetrates tissue (*2*). The optimal growth temperature range for zoospores is 28°C–37°C (*3*). Pythiosis manifests as rapidly growing granulomatous lesions that might be devastating and life-threatening (*2*). Organs and tissues most affected are the skin, gastrointestinal tract, eyes, and blood vessels (*2*,*3*); disseminated forms are also possible (*3*).

Pythiosis is diffused in warm and humid areas of tropical and subtropical countries, including northeastern Australia, Brazil, Colombia, Costa Rica, India, Thailand, Uruguay, southern and southeastern states of the United States, and Venezuela. The disease has also been reported sporadically in some temperate regions (*3*). A horse with compatible clinical pythiosis features was described in France in 1896 (*8*), whereas confirmed cases have been recently reported in human patients in Spain (*9*,*10*). We describe 2 cases of cutaneous pythiosis in dogs in Italy.

The Study

We evaluated soft tissue swellings in 2 unrelated dogs that lived 30 km apart in Rome province of central Italy in October 2022 (case 1) and January 2023 (case 2) (Figure 1). The animals had never been outside of Italy before onset of skin lesions and were otherwise healthy. We collected anamnesis and clinical manifestation data (Table).

Histopathologic results of lesion punch biopsies showed multifocal to coalescing (pyo)granulomatous and eosinophilic dermatitis and panniculitis with intralesional, irregular branching hyphae (Figure 2, panel A). The hyphae were positive for Grocott methenamine silver stain, appearing dark brown (Figure 2, panel B), whereas they were negative after staining with periodic acid Schiff stain. Culturing on Sabouraud dextrose agar (for fungi)

Author affiliations: Università di Torino, Turin, Italy (A. Peano, A.R. Molinar Min, M. Pasquetti); Veterinaria Trastevere, Rome, Italy (A. Fondati); Ospedale Veterinario Gregorio VII, Rome (E. Romano); Università degli Studi di Perugia, Perugia, Italy (C. Brachelente, I. Porcellato); Ambulatorio Veterinario Cassia, Cesano, Italy (A. Amore)

DOI: https://doi.org/10.3201/eid2907.230320

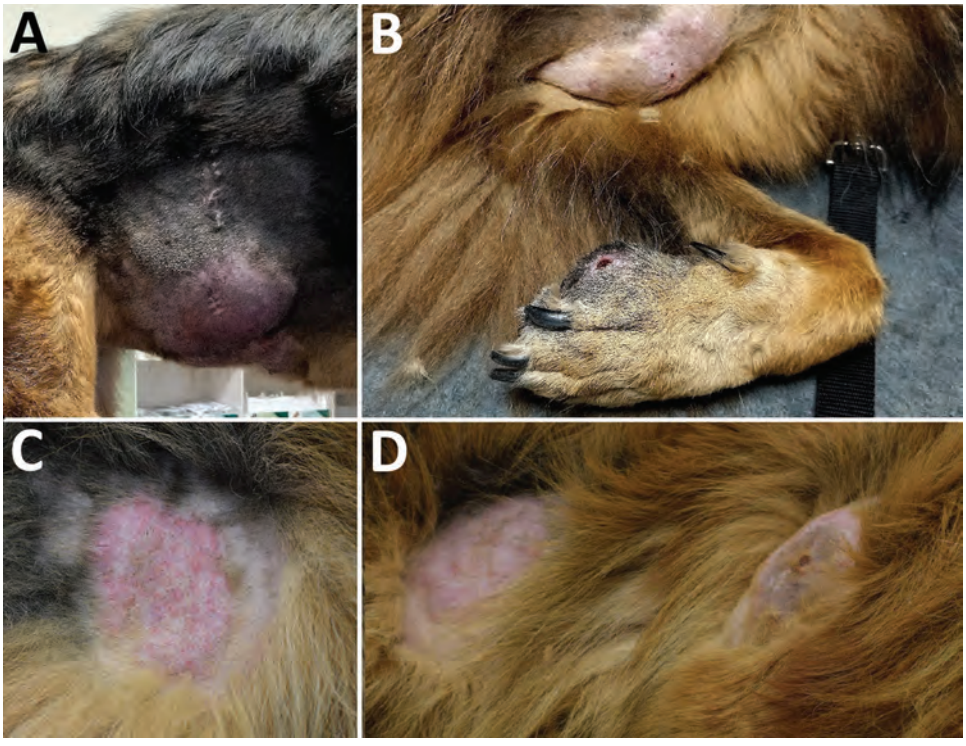

Figure 1. Clinical manifestation of cutaneous pythiosis in 2 dogs, Italy. A, B) Case 1, showing a large mass on the right flank (A) and a large mass on the left axilla and a smaller ulcerated lesion on the first digit of the left forelimb (B). C, D) Case 2, showing detailed image of a plaque (C) and a lateral view of the dog showing 2 plaques on the thorax and thigh (D).

containing chloramphenicol and gentamycin yielded negative results.

To obtain a definitive identification, we extracted genomic DNA from biopsied tissues by using a NucleoSpin Tissue kit (Macherey-Nagel, https://www.mn-net.com). We PCR amplified and sequenced the internal transcribed spacer (ITS) region by using the primer pair ITS4 and ITS5 (*11*). We obtained identical sequences (GenBank accession nos. OQ532907 [case 1] and OQ532908 [case 2]) that were closely related to ITS sequences of *P. insidiosum* from GenBank (compared by using BLASTn, https://blast.ncbi.nlm.nih.gov).

Table. Anamnesis, clinical history, and manifestations in 2 dogs with cutaneous pythiosis, Italy*

Characteristics	Case 1	Case 2
Date of referral visit	October 2022	January 2023
Breed and age	4-year-old neutered female German Shepherd dog	3-year-old male German Shepherd dog
Life habitat	Dog lived in apartment and periodically swam in the Treja river near home (Rome province) and Lake Bracciano (32 km northwest of Rome), especially during hotter months.	Dog lived in a house with another dog (adult Cane Corso without signs of disease) and had outdoor access to a garden. The dog regularly swam in Lake Bracciano.
Travel history	In summer 2019 and 2020, the dog was taken to northwest Italy (Trentino area), where it occasionally swam in mountain lakes. The dog was never outside of Italy before onset of skin problems.	The dog was never outside of Italy before onset of skin problems.
History of skin problems	Since October 2020, several subcutaneous masses, occasionally ulcerated, developed in different body areas and were surgically removed on different occasions. The last intervention was in May 2022 to remove a large mass on the tail base. A caudectomy was necessary because of massive involvement of tail tissue. Several histopathological evaluations over time showed roughly the same pattern of chronic pyogranulomatous dermatitis and panniculitis involving mastocytes, eosinophils, and neutrophils. Infectious organisms were never reported. The dog was treated with different antimicrobial drugs, glucocorticoids, and cyclosporine, which had no or only partial effect on disease evolution.	In November 2022, an abscess formed on the flexor face of the left elbow and was incised to look for a foreign body (not found). The dog was treated with cephalexin and prednisone, then with clindamycin and prednisone, but showed no response. New lesions developed in other body areas.
Clinical manifestations at referral visit	2 large masses (≈10 cm × 12 cm × 10 cm) on the left axilla and right flank; a 3rd smaller mass with a small ulcer on the first digit of the left forelimb.	Multiple dermal and subcutaneous papules and plaques of variable size, some with fistulae yielding serosanguineous exudate.

*Clinical manifestations are shown for both dogs (Figure 1).

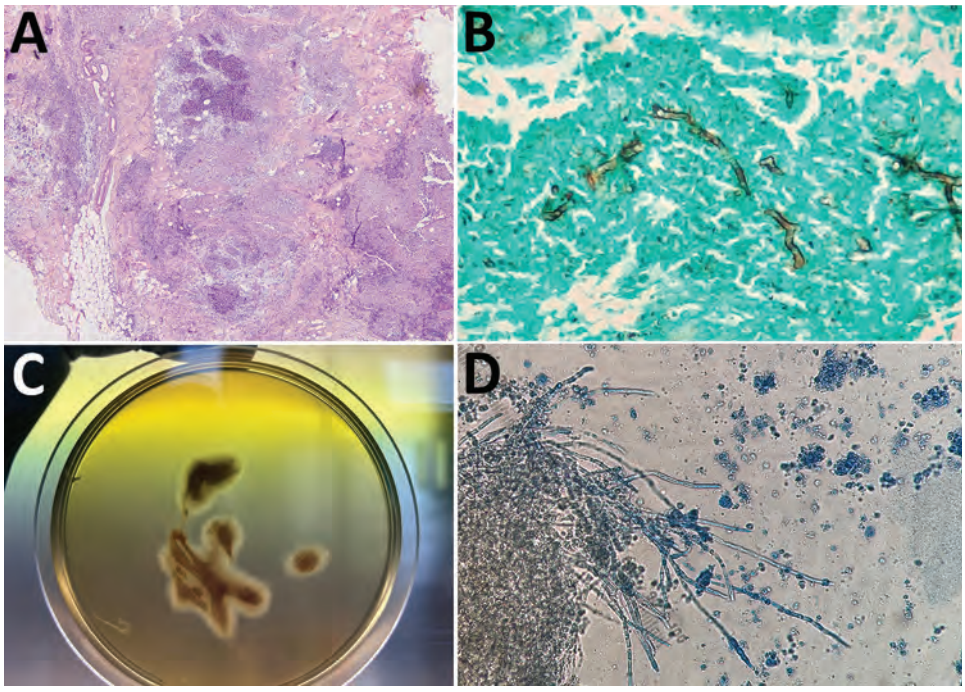

Figure 2. Histological analyses of cutaneous pythiosis in 2 dogs, Italy. A) Section from punch biopsy of cutaneous mass showing confluent pyogranulomatous and eosinophilic granulomas with central necrosis in the deep dermis and panniculus. Hematoxylin and eosin stain; original magnification ×100. B) Section from punch biopsy of cutaneous mass showing broad, irregular branching hyphae. Grocott methenamine silver stain; original magnification ×400. C) Culture (24-hour) of an aspirate from a mass found in case 2. Aspirate was cultured on Sabouraud dextrose agar without antimicrobial drugs, and showed submerged, colorless colonies with irregular radiate patterns. D) Microscopic appearance of the colonies indicating broad (4–10 μm in diameter), hyaline, and sparsely septate hyphae. Original magnification ×250.

We aligned sequences belonging to different clusters within the *P. insidiosum* complex (*5*) by using MEGA11 software (https://www.megasoftware.net). We conducted phylogenetic analysis by using the neighbor-joining method (bootstrap analysis with 1,000 replicates); sequences obtained from the infected dog tissues clustered with *Pythium* cluster IV (Appendix Figure, https://wwwnc.cdc.gov/EID/article/29/7/23-0320-App1.pdf), corresponding to the newly described species *P. periculosum* (*5*).

Although an environmental study would be necessary for confirmation, Lake Bracciano near Rome might have been the infection source (Table). Both dogs regularly swam in the lake, which has vast stagnant waters with stable temperatures of ≈30°C in hotter months, features known to support pathogenic *Pythium* spp. growth (*2*,*3*).

Additional material was collected from the lesion in case 2 through fine-needle aspiration. We suspected the organism failed to grow in previous cultures because of chloramphenicol supplementation (*10*). Therefore, we cultured the aspirate on unsupplemented Sabouraud dextrose agar at 37°C. After a 24-hour incubation, submerged, colorless colonies with irregular radiate patterns developed from the aspirated material (Figure 2, panel C). Microscopically, the hyphae were broad (4–10 μm in diameter), hyaline, and sparsely septate (Figure 2, panel D). Colonies were identified as *P. periculosum* by using the same molecular approach applied to biopsies.

Conclusions

Our cases suggest a geographic distribution of pythiosis broader than previously recognized, aligning with other reports of the disease outside of classical tropical and subtropical areas, such as US regions near the border of Canada, as well as Spain, Israel, Japan, and South Korea (*2*,*3*). Because the average climatic conditions in temperate zones appear unsuitable for the causative oomycete life cycle, cases in those areas likely occur in restricted ecologic niches. Our report illustrates that concept; central Italy has a primarily Mediterranean climate that has mild, sometimes rainy winters and sunny, hot, and usually dry summers. Those features do not fit the description of areas more prone to pythiosis. However, the zone where we suspect the dogs became infected has features of a pythiosis-risk area (warm, humid environment). Increasing reports of pythiosis in nonendemic regions might indicate an expansion of the causative oomycetes because of global climate changes. Another interpretation is that more cases are recognized and published because of increased awareness of healthcare personnel and availability of diagnostic tools (*3*). Environmental and clinical studies will be necessary to address those hypotheses.

The dogs in this report showed signs typically associated with the cutaneous form of pythiosis, including developing multiple masses or dermal plaques over time (*3*). Gastrointestinal pythiosis in dogs is another form of the disease

characterized by weight loss, vomiting, diarrhea, and hematochezia (*3*,*12*).

Genetic variation associated with geographic provenance exists for species within the *P. insidiosum* complex (*4*,*5*). *P. insidiosum* cluster I is mainly found throughout the Americas, whereas *P. insidiosum* cluster II is typically found in Asia and Australia. *P. periculosum* cluster III has been reported mainly in the United States and is sympatric with members of cluster I (*5*). The genotype identified in our cases (*P. periculosum* cluster IV) seems to have a broader distribution; most reports of human cases have been from Thailand and India (*3*). However, *P. periculosum* cluster IV has also been recovered from environmental samples in Brazil and the United States (*13*,*14*) and from human patients in Israel (*15*) and Spain (*10*), which is noteworthy because of the close proximity of Spain to Italy.

In conclusion, from a One Health perspective, our study shows the environmental presence of an unexpected, exotic pathogen that could potentially infect humans in a country with a temperate climate. In Italy, pythiosis should now be considered a differential diagnosis by human and veterinary health professionals, especially in cases where there is a history of exposure to freshwater habitats.

Acknowledgments

We thank the dogs' owners for consenting to the publication of the cases and Gaetano Reggi for referring 1 case.

About the Author

Dr. Peano is an assistant professor at the Department of Veterinary Sciences, Parasitology Section, University of Turin, in northwest Italy. His primary research interests are parasitic and fungal diseases of domestic and wild animals.

References

1. De Cock AW, Mendoza L, Padhye AA, Ajello L, Kaufman L. *Pythium insidiosum* sp. nov., the etiologic agent of pythiosis. J Clin Microbiol. 1987;25:344–9. https://doi.org/10.1128/jcm.25.2.344-349.1987
2. Gaastra W, Lipman LJA, De Cock AW, Exel TK, Pegge RBG, Scheurwater J, et al. *Pythium insidiosum*: an overview. Vet Microbiol. 2010;146:1–16. https://doi.org/10.1016/j.vetmic.2010.07.019
3. Yolanda H, Krajaejun T. Global distribution and clinical features of pythiosis in humans and animals. J Fungi (Basel). 2022;8:182. https://doi.org/10.3390/jof8020182
4. Schurko AM, Mendoza L, Lévesque CA, Désaulniers NL, de Cock AW, Klassen GR. A molecular phylogeny of *Pythium insidiosum*. Mycol Res. 2003;107:537–44. https://doi.org/10.1017/S0953756203007718
5. Miraglia BM, Mendoza L, Rammohan R, Vilela L, Vilela C, Vilela G, et al. *Pythium insidiosum* complex hides a cryptic novel species: *Pythium periculosum*. Fungal Biol. 2022;126:366–74. https://doi.org/10.1016/j.funbio.2022.03.002
6. Calvano TP, Blatz PJ, Vento TJ, Wickes BL, Sutton DA, Thompson EH, et al. *Pythium aphanidermatum* infection following combat trauma. J Clin Microbiol. 2011;49:3710–3. https://doi.org/10.1128/JCM.01209-11
7. Farmer AR, Murray CK, Driscoll IR, Wickes BL, Wiederhold N, Sutton DA, et al. Combat-related *Pythium aphanidermatum* invasive wound infection: case report and discussion of utility of molecular diagnostics. J Clin Microbiol. 2015;53:1968–75. https://doi.org/10.1128/JCM.00410-15
8. Drouin V. Sur une nouvelle mycose du cheval. Rec Med Vet. 1896;30:337–44.
9. Del Castillo-Jiménez MC, Baptista-Díaz N, Montero J, Pascual A. *Pythium insidiosum* ocular infection [in Spanish]. Enferm Infecc Microbiol Clin. 2013;31:118–9. https://doi.org/10.1016/j.eimc.2012.07.012
10. Bernheim D, Dupont D, Aptel F, Dard C, Chiquet C, Normand AC, et al. Pythiosis: case report leading to new features in clinical and diagnostic management of this fungal-like infection. Int J Infect Dis. 2019;86:40–3. https://doi.org/10.1016/j.ijid.2019.06.011
11. White TJ, Bruns T, Lee S, Taylor J. Amplification and direct sequencing of fungal ribosomal RNA genes for phylogenetics. In: Innis MA, Gelfand DH, Sninsky JJ, White TJ, editors. PCR protocols: a guide to methods and applications. San Diego (CA): Academic Press; 1990. p. 315–22.
12. Berryessa NA, Marks SL, Pesavento PA, Krasnansky T, Yoshimoto SK, Johnson EG, et al. Gastrointestinal pythiosis in 10 dogs from California. J Vet Intern Med. 2008;22:1065–9. https://doi.org/10.1111/j.1939-1676.2008.0123.x
13. Paz GSD, Camargo GG, Cury JE, Apolonio EVP, Garces HG, Prado ACD, et al. Outbreak of equine pythiosis in a southeastern region of Brazil: environmental isolation and phylogeny. Transbound Emerg Dis. 2022;69:1617–24. https://doi.org/10.1111/tbed.14135
14. Presser JW, Goss EM. Environmental sampling reveals that *Pythium insidiosum* is ubiquitous and genetically diverse in north central Florida. Med Mycol. 2015;53:674–83. https://doi.org/10.1093/mmy/myv054
15. Tanhehco TY, Stacy RC, Mendoza L, Durand ML, Jakobiec FA, Colby KA. *Pythium insidiosum* keratitis in Israel. Eye Contact Lens. 2011;37:96–8. https://doi.org/10.1097/ICL.0b013e3182043114

Address for correspondence: Andrea Peano, Dipartimento di Scienze Veterinarie, Università di Torino, Largo P. Braccini 2, 10095 Grugliasco, Torino, Italy; email: andrea.peano@unito.it

Nannizzia polymorpha as Rare Cause of Skin Dermatophytosis

Pei-Lun Sun, Ching-Chi Chi, I-Hsin Shih, Yun-Chen Fan

Nannizzia polymorpha is a dermatophyte that rarely infects humans. We describe 2 case-patients from Asia who had an inflammatory type of tinea capitis and tinea manuum caused by infection with this fungus. The diagnosis was confirmed on the basis of the morphologic and molecular characteristics of the microorganism.

Tinea is the most common fungal human skin infection caused by dermatophytes. It is caused by a group of fungi that can digest keratin in the stratum corneum of the skin and affects both humans and animals; animal-to-human transmission is possible. According to current molecular taxonomy, dermatophytes consist of 59 species in 9 genera (*1*). In addition to common pathogens, such as *Trichophyton rubrum* in humans and *Microsporum canis* in companion animals, several cases of sporadic infections caused by lesser-known dermatophyte species have been reported (*2*–*6*). We describe 2 cases of tinea caused by *Nannizzia polymorpha*, which were confirmed by using morphologic characteristics and molecular methods.

The Study

This research has been approved by the Institutional Review Board of Chang Gung Medical Foundation (approval nos. 202001561B0 and 202300067B0). The patient consent was waived by the institutional review board.

Case-patient 1 was a 10-year-old boy who had abrupt onset of a scalp lesion that was 0.5 cm in diameter initially and evolved rapidly over the following 2 days. Physical examination showed a round erythematous plaque studded with multiple pustules and hair loss on his scalp measuring ≈3 cm in diameter. He had no history of animal or soil contact and had not visited a barbershop before the onset.

Author affiliations: Chang Gung Memorial Hospital Linkou Main Branch, Taoyuan, Taiwan (P.-L. Sun, C.-C. Chi, I.-Hsin Shih, Y.-C. Fan); Chang Gung University, Taoyuan (P.-L. Sun, I-Hsin Shih, C.-C. Chi)

DOI: https://doi.org/10.3201/eid2907.230477

On the basis of a clinical diagnosis of tinea capitis, pus was collected for fungal and bacterial cultures, and treatment with oral griseofulvin (500 mg/d) was started. Nine days after treatment started, rashes appeared on the patient's face, ears, trunk, arms, and legs. The treatment was changed to oral terbinafine (250 mg/d) because of a suspected allergic drug reaction. However, the rashes persisted, so his parents stopped treatment after 2 doses of terbinafine. The rashes disappeared thereafter, and the scalp lesion also resolved gradually during the following 2 weeks.

At a follow-up visit, the residual lesion was a round erythematous hairless patch (Figure 1, panel A). Two residual broken hairs were noted by dermoscopy but were negative for fungal spores on microscopy. Fungal culture was performed on a sample collected by using a sterile shampoo brush, but the result was negative.

Case-patient 2 was a 68-year-old woman who had a skin lesion on her right hand that had persisted for >1 month. The lesion had been treated with oral griseofulvin, topical tolnaftate, and econazole at a local clinic but had progressed. The patient had no history of soil or animal contact. The erythematous patch on her right hand had raised borders studded with scales and tiny, itching, nontender pustules along the border (Figure 1, panel B). The diagnosis of tinea manuum was confirmed by the presence of hyaline hyphae and arthroconidia on microscopy. The lesion responded to concomitant treatment with oral terbinafine (250 mg/d) for 2 weeks and topical 1% ciclopirox cream. Mycologic cure was achieved in 4 weeks.

The fungi isolated from both patients were morphologically similar. On potato dextrose agar, the colonies were light yellow with a lanose surface and radiate border (Figure 1, panel C) and an orange-yellow reverse surface (Figure 1, panel D). Microscopy showed abundant polymorphic microconidia and macroconidia (Figure 1, panels E, F). The macroconidia were borne on short conidiophores, moderately thick-walled, cylindrical, clavate, or ellipsoidal, with a rounded tip and tapered base, 1–4-septate, and 9–16 × 15–37.1 μm. The microconidia were sessile or short-stalked, 1-celled or

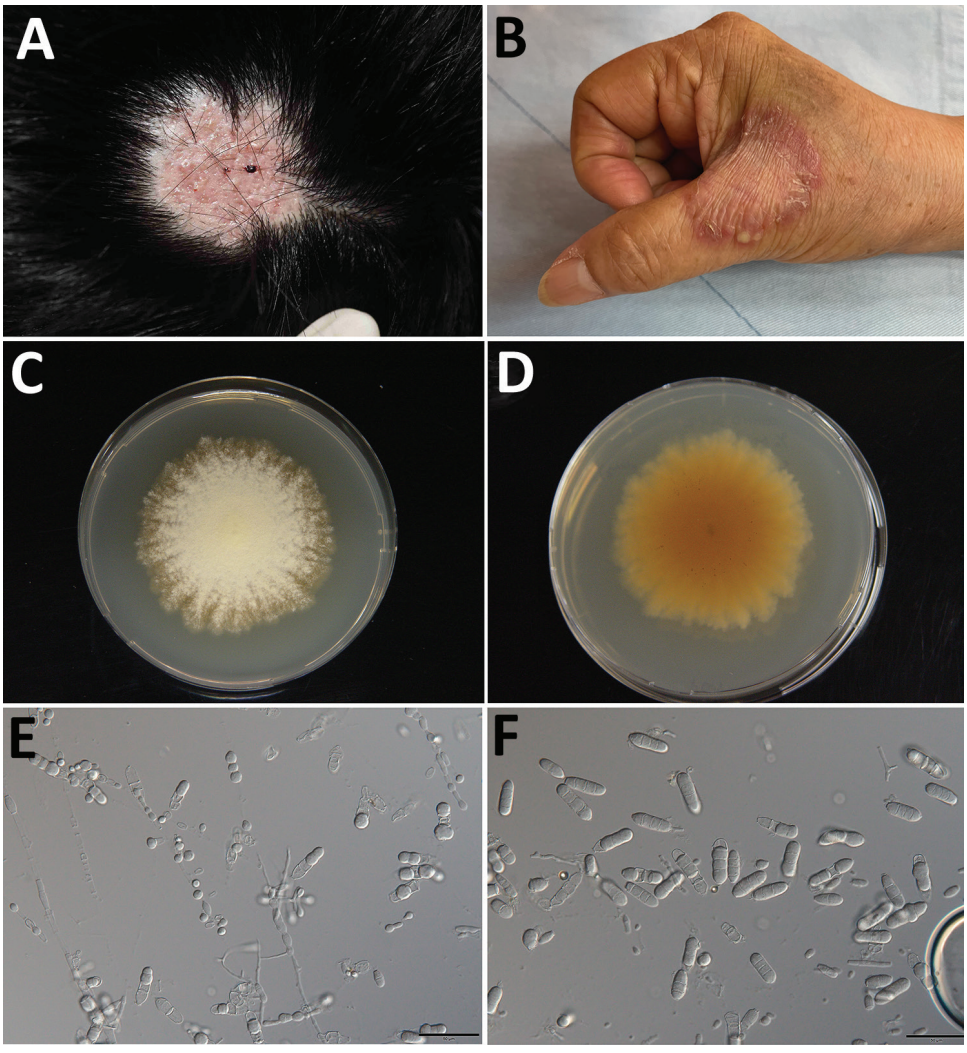

Figure 1. Clinical manifestations in 2 patients with rare cases of skin dermatophytosis caused by *Nannizzia polymorpha*. A) Case-patient 1, with tinea capitis; B) case-patient 2, with tinea manuum. C, D) The colony of isolate CGMHD 3492 isolated from case-patient 1 on potato dextrose agar obverse (C) and reverse (D). E, F) Microscopic features of microconidia (E) and macroconidia (F) (scale bars = 50 μm).

occasionally 2-celled, clavate or tear-shaped with a truncate base, and 2.9–7 × 5–11.5 μm. The abundant intercalary conidia were barrel-shaped, spathulate, or cylindrical. The intercalary chlamydospores were spherical, borne singly, in pairs or occasionally in chains, and 4.9–8.7 μm in diameter.

The sequence of the internal transcribed spacer (ITS) of ribosomal DNA of the isolate had a 99.37% similarity with that of *N. polymorpha* strain CBS 121947. Phylogenetic analysis using ITS alone and multilocus analysis using ITS, large subunit of ribosomal DNA, partial β-tubulin gene, translation elongation factor 3, and 60S ribosomal protein L10 confirmed that both isolates were *N. polymorpha* (Figure 2).

The sequences were deposited into GenBank (accession nos. OQ422181 and OQ427395 for ITS, OQ422485 and OQ427396 for large subunit of ribosomal DNA, OQ538298 and OQ538302 for 60S ribosomal protein L10, OQ538303 and OQ538301 for translation elongation factor 3, and OQ538299 and OQ538300 for partial β-tubulin gene).

We determined the MICs for 8 antifungal agents of the 2 isolates (Table) by using Clinical and Laboratory Standards Institute M38 Reference Method for Broth Dilution Antifungal Susceptibility Testing of Filamentous Fungi protocol for dermatophytes (*7*).

Conclusions

Nannizzia is a genus that had included the sexual stages of certain dermatophytes. In the latest classification of dermatophytes proposed in 2017, it is now the genus name for most geophilic and a few zoophilic fungi from the genus *Microsporum* (*8*). There are currently 13 species in the genus *Nannizzia*. Human infections by *Nannizzia* are opportunistic and result from contact with contaminated soil. Most cases are caused by *N. gypsea* species complex (*N. gypsea*, *N. incurvata*, *N. fulva*), and the clinical manifestations are tinea corporis,

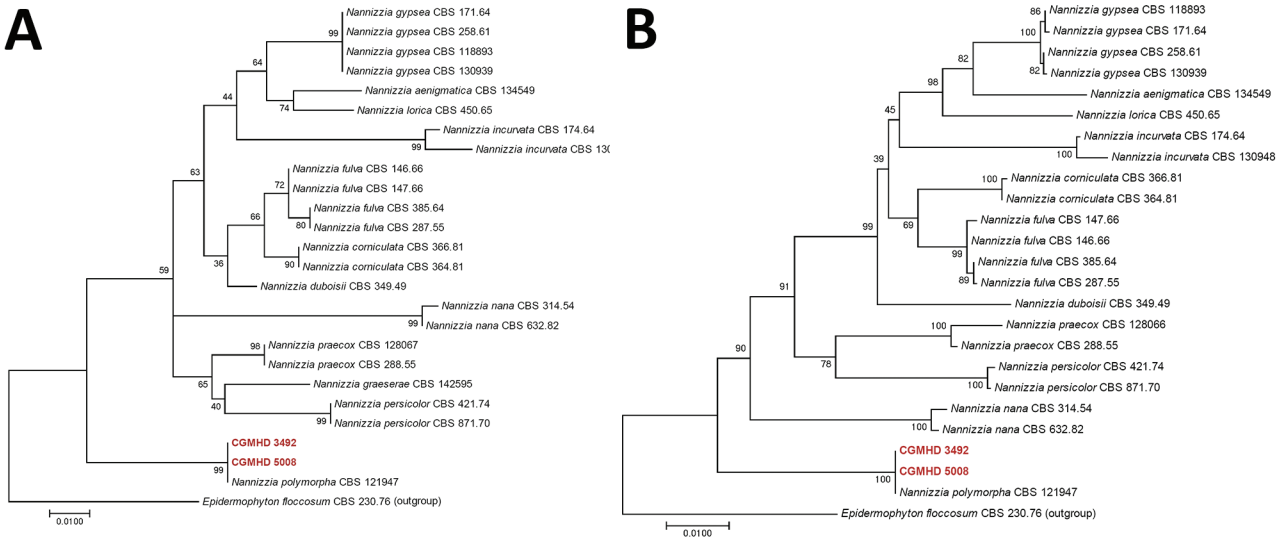

Figure 2. Phylogenetic trees of *Nannizzia polymorpha* in 2 patients with rare cases of skin dermatophytosis caused by this fungus. Trees were constructed by using MEGA 7.0 software (https://www.megasoftware.net) and the maximum-likelihood method on the basis of the internal transcribed spacer region (A) and combined datasets of internal transcribed spacer region, large subunit of ribosomal DNA, partial β-tubulin gene, translation elongation factor 3, and 60S ribosomal protein L10 (B). Red indicate strains isolated in this study. Tamura-Nei was used as a substitution model in both analyses. Numbers at nodes are bootstrap values. Scale bars indicate nucleotide substitutions per site.

tinea capitis, and onychomycosis. Other members of the genus *Nannizzia* that have been reported to cause human infections include *N. aenigmatica* (*9*), *N. duboisii* (*9*), *N. lorica* (*2*), *N. nana* (*4*), *N. perplicata* (*10*), *N. persicolor* (*4*), *N. praecox* (*6*), and *N. polymorpha*.

N. polymorpha is a rare dermatophyte species. The type strain CBS 121947 was originally called *Microsporum amazonicum*. However, later morphologic and phylogenetic studies showed that it was new, and the species name *N. polymorpha* was proposed in 2019 (*8*). The strain was isolated from facial lesions of a patient in Kourou City, French Guiana (*11*). No additional cases or isolation records have been reported to our knowledge.

Case-patient 1 had an infection of the scalp accompanied by a prominent inflammatory reaction and hair loss. Although microscopic examination was not performed initially, the pathogenic role of the fungus in this patient was established by the massive growth of a single pure fungus and the good response to antifungal treatment. Case-patient 2 had tinea manuum and a prominent inflammatory reaction. Both patients responded to short-term antifungal treatment. Although there are currently no clinical breakpoints for antifungal agents against *N. polymorpha*, it is probably susceptible to all 8 antifungal drugs tested because of the low MIC values.

To our knowledge, there have been no reports of environmental isolation or animal infections caused by *N. polymorpha*. Its rarity might be attributable to the paucity of environmental surveys on dermatophytes or because it was only named in 2019. All 3 isolates reported were from patients with skin infections. The inflammatory characteristics of the lesion suggest that it is geophilic. However, further studies are needed to elucidate its ecologic niche.

Laboratory diagnosis of *N. polymorpha* is simple because of the abundant and variable shapes of macroconidia and microconidia and the typical cylindrical macroconidia with a blunt rounded apex. The colony was light yellow and lanose, which differentiated it morphologically from the cinnamon granular surface of species in the *N. gypse*a complex. *N. graeserae* has macroconidia similar to those of *N. polymorpha*; however, the ITS sequences showed only 523/589 (89%) similarity between our strain and *N. graeserae* CBS 142595. *Arthroderma flavescens* also has similar macroconidia, but they are longer than those of *N. polymorpha*, more monotonous, and uniform in shape. When an unidentifiable strain is encountered, DNA sequencing can provide an unequivocal diagnosis.

Table. MICs of antifungal agents for the 2 *Nannizzia polymorpha* isolates implicated in rare cases of skin dermatophytosis

Antifungal agent	MIC, μg/mL
Fluconazole	2–4
Griseofulvin	0.125–0.25
Terbinafine	0.063–0.125
Itraconazole	0.063–0.25
Isavuconazole	0.016–0.031
Voriconazole	0.031–0.063
Efinaconazole	<0.008
Luliconazole	<0.008

About the Author

Dr. Sun is associate professor at the School of Medicine, Chang Gung University, Taoyuan, Taiwan, and physician scientist in the Department of Dermatology, Chang Gung Memorial Hospital, Linkou Medical Center, Taoyuan. His primary research interest is medical mycology, especially dermatophyte infections.

References

1. de Hoog GS, Dukik K, Monod M, Packeu A, Stubbe D, Hendrickx M, et al. Toward a novel multilocus phylogenetic taxonomy for the dermatophytes. Mycopathologia. 2017;182:5–31. https://doi.org/10.1007/s11046-016-0073-9
2. García-Martos P, Gené J, Solé M, Mira J, Ruíz-Henestrosa R, Guarro J. Case of onychomycosis caused by *Microsporum racemosum*. J Clin Microbiol. 1999;37:258–60. https://doi.org/10.1128/JCM.37.1.258-260.1999
3. Krzyściak P, Al-Hatmi AM, Ahmed SA, Macura AB. Rare zoonotic infection with *Microsporum persicolor* with literature review. Mycoses. 2015;58:511–5. https://doi.org/10.1111/myc.12341
4. Porras-López C, Martínez-Herrera E, Frías-De-León MG, Moreno-Coutiño G, Del Rocío Reyes-Montes M, Arenas R, et al. Dermatophytosis caused by *Nannizzia nana*. J Mycol Med. 2021;31:101047. https://doi.org/10.1016/j.mycmed.2020.101047
5. Sitterle E, Frealle E, Foulet F, Cabaret O, Cremer G, Guillot J, et al. *Trichophyton bullosum*: a new zoonotic dermatophyte species. Med Mycol. 2012;50:305–9. https://doi.org/10.3109/13693786.2011.605810
6. Uhrlaß S, Mayser P, Schwarz R, Koch D, Krüger C, Korfmann I, et al. Dermatomycoses due to *Nannizzia praecox* (formerly *Microsporum praecox*) in Germany: case reports and review of the literature. Mycopathologia. 2018;183:391–8. https://doi.org/10.1007/s11046-017-0213-x
7. Alexander BD. Reference method for broth dilution antifungal susceptibility testing of filamentous fungi, 3rd ed. Wayne (PA): Clinical and Laboratory Standards Institute; 2017.
8. Dukik K, de Hoog GS, Stielow JB, Freeke J, van den Ende BG, Vicente VA, et al. Molecular and phenotypic characterization of *Nannizzia* (Arthrodermataceae). Mycopathologia. 2020;185:9–35.
9. Hubka V, Dobiašova S, Dobiaš R, Kolařik M. *Microsporum aenigmaticum* sp. nov. from *M. gypseum* complex, isolated as a cause of tinea corporis. Med Mycol. 2014;52:387–96. https://doi.org/10.1093/mmy/myt033
10. Borman AM, Szekely A, Fraser M, Lovegrove S, Johnson EM. A novel dermatophyte relative, *Nannizzia perplicata* sp. nov., isolated from a case of tinea corporis in the United Kingdom. Med Mycol. 2018.
11. CBS (Fungal Biodiversity Centre). CBS strains database [cited 2023 May 24]. https://wi.knaw.nl/page/fungal_table

Address for correspondence: Pei-Lun Sun, Department of Dermatology, Chang Gung Memorial Hospital, Linkou Branch, No.5, Fushin St, Taoyuan 33305, Taiwan; email: sunfungus@gmail.com

etymologia revisited

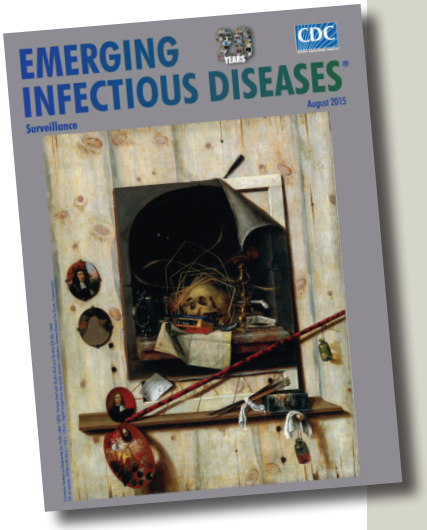

Originally published in August 2015

Escherichia coli

[esh”ə-rik’e-ə co’lī]

A gram-negative, facultatively anaerobic rod, *Escherichia coli* was named for Theodor Escherich, a German-Austrian pediatrician. Escherich isolated a variety of bacteria from infant fecal samples by using his own anaerobic culture methods and Hans Christian Gram’s new staining technique. Escherich originally named the common colon bacillus *Bacterium coli commune*. Castellani and Chalmers proposed the name *E. coli* in 1919, but it was not officially recognized until 1958.

References:

1. Oberbauer BA. Theodor Escherich—Leben und Werk. Munich: Futuramed-Verlag; 1992.
2. Shulman ST, Friedmann HC, Sims RH. Theodor Escherich: the first pediatric infectious diseases physician? Clin Infect Dis. 2007;45:1025–9 .

https://wwwnc.cdc.gov/eid/article/21/8/et-2108_article

Fatal Invasive Mold Infections after Transplantation of Organs Recovered from Drowned Donors, United States, 2011–2021

Karen Wu, Pallavi Annambhotla, Rebecca J. Free, Jana M. Ritter, Brooke Leitgeb, Brendan R. Jackson, Mitsuru Toda, Sridhar V. Basavaraju, Jeremy A.W. Gold

Drowned organ donors can be exposed to environmental molds through the aspiration of water; transplantation of exposed organs can cause invasive mold infections in recipients. We describe 4 rapidly fatal cases of potentially donor-derived invasive mold infections in the United States, highlighting the importance of maintaining clinical suspicion for these infections in transplant recipients.

During 2011–2021, a total of 4,136 organs from 1,272 drowned donors were transplanted in the United States (*1*). Aspiration of water during drowning events can expose victims to environmental molds (e.g., Mucorales and *Scedosporium*) that can cause invasive mold infections (IMIs) in transplant recipients (*2*–*5*).

Solid organ transplant (SOT) recipients are at increased risk for IMIs because of predisposing factors that weaken the immune system (e.g., underlying conditions and immunosuppressive medications taken to prevent organ rejection) (*6*). SOT recipients might acquire IMIs upon reactivation of a dormant infection, progression from colonization to invasive disease, inhalation of environmental molds, or exposure to mold in the transplanted organ (*7*). Previous case reports of donor-derived IMIs involving drowned donors highlight challenges in investigating IMIs in transplant recipients (e.g., ruling out alternative exposures) and high death rates (*4*,*5*,*8*). To inform clinical practice and policies to improve patient outcomes, we describe the donor and recipient characteristics and clinical progression of IMIs determined to be potentially transmitted from drowned donors in the United States during 2011–2021.

Author affiliation: Centers for Disease Control and Prevention, Atlanta, Georgia, USA

DOI: https://doi.org/10.3201/eid2907.230524

The Study

In the United States, suspected transplant-transmitted infections are reported by organ procurement organizations or transplant centers to the Organ Procurement and Transplantation Network for investigation by the Disease Transmission Advisory Committee (DTAC). As a member of DTAC, the Centers for Disease Control and Prevention (CDC) investigates select potential donor-derived IMIs to determine whether transmission occurred through transplantation and prevent further transmission. For this study, we included investigations involving a drowned donor and ≥1 recipient with a posttransplant IMI in which the donated organs were determined to be the potential route of transmission (*9*).

During 2011–2021, CDC conducted 3 investigations involving 3 donors who drowned and 9 SOT recipients who received organs from those donors. Transmission of an IMI potentially occurred to >1 recipient of each donor. We describe these investigations and related findings; information about donors' time spent immersed underwater was unavailable.

For case 1, the donor was a 2-year-old boy who was found unconscious in a pool. Organ procurement occurred ≈6 days after hospital admission. An autopsy revealed congested lung parenchyma consistent with drowning and no findings consistent with IMI; a histopathologic examination was not performed. The recipient of both kidneys (index recipient) was a 23-year-old man with end-stage renal disease caused by lupus nephritis. He experienced graft thromboses after transplantation requiring transplanted kidney removal 8 days posttransplant; histopathologic examination revealed severe mucormycotic emboli. He died 10 days after transplantation. Autopsy revealed massive pulmonary emboli and severe necrosis in the

abdominal and pelvic cavities. The recipient of the liver was a 2-year-old girl with congenital biliary atresia. After transplantation, clinicians noted decreased hepatic artery flow. The patient subsequently underwent transplant hepatectomy 3 days posttransplant. Histopathologic examination revealed thrombosis of multiple vessels, extensive hepatic necrosis, and angioinvasive fungal elements suggestive of mucormycosis. The patient died 4 days after transplantation. No other organs were transplanted.

For case 2, the donor was a 30-year-old man who had cardiac arrest while swimming. Organ recovery occurred 8 days after hospital admission. Autopsy revealed no gross or histopathologic evidence of IMI. The recipient of the liver (index recipient) was a 60-year-old man with cirrhosis caused by hepatitis B and C and hepatocellular carcinoma. Two days after transplantation, clinicians performed a posttransplant liver biopsy, which found no evidence of acute rejection or fungal organisms. Three days later, the patient had worsening hepatic and renal function. Emergency laparotomy revealed liver necrosis with absence of blood flow in the portal vein. The patient died 6 days after transplantation. Autopsy findings noted fungal organisms morphologically consistent with Mucorales in the liver parenchyma and blood vessels. Tissues were further evaluated at CDC, where mucormycetes were identified by immunohistochemical examination (Figure). Two other recipients received the donor's right and left kidneys. Neither recipient received antifungal prophylaxis nor had clinical signs or symptoms consistent with an IMI.

For case 3, the donor was a 41-year-old man who fell into a lake after having a seizure. At the hospital, a large quantity of dark fluid was suctioned from his lungs. On bronchoscopic examination, clinicians noted black particulate matter in the lungs; no leukocytes or organisms were seen in the bronchial washings. Organ procurement occurred ≈5 days after hospital admission. Histopathologic examination of lung tissue at CDC showed severe aspiration pneumonia. Culture and polyfungal immunohistochemical assays on donor lung tissue, performed at CDC after illness in a recipient was reported, were negative for fungal pathogens. The recipient of the liver and right kidney (index recipient) was a 66-year-old man with end-stage liver disease and chronic kidney disease who received a diagnosis of scedosporiosis ≈1 month posttransplant and eventually had brain lesions consistent with fungal abscesses, as previously published (*5*). He died 8 weeks after transplantation. Three other patients received the pancreas, heart, and left kidney. After DTAC notified transplant centers of the index case, all 3 recipients were started on voriconazole prophylaxis; none had onset of scedosporiosis.

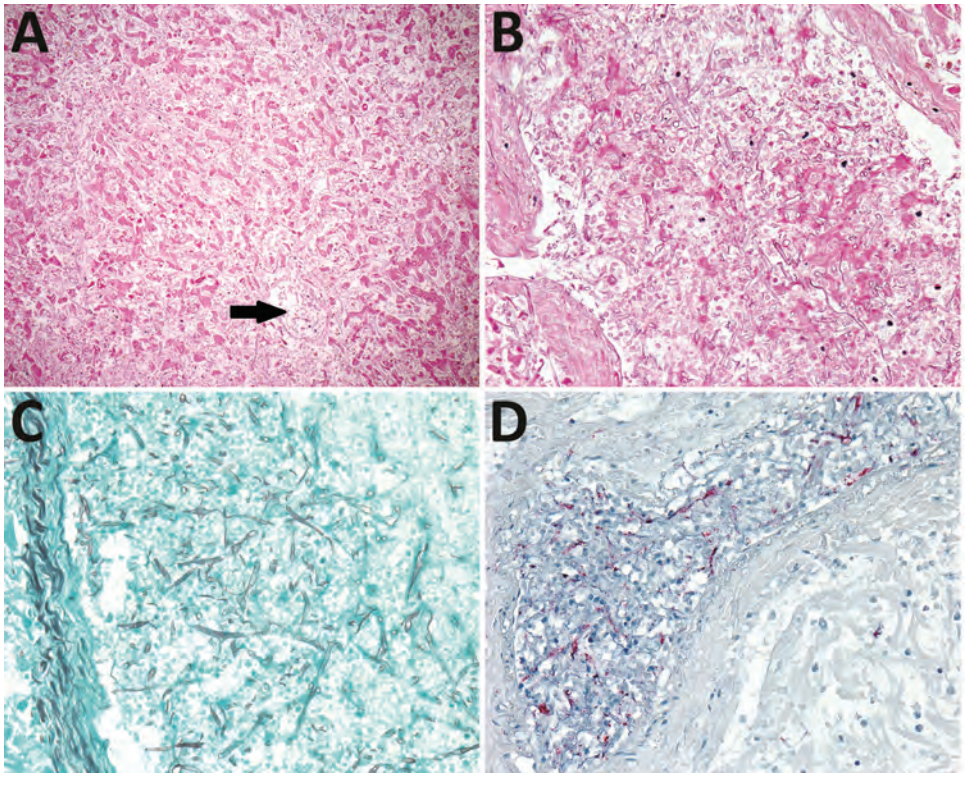

Figure. Invasive fungal infection in transplanted liver from an organ donor who drowned, United States (case 2). A) Centrilobular hepatic necrosis without substantial inflammation; fungal hyphae are in a central vein (arrow) and throughout the sinusoids. Hematoxylin–eosin; original magnification ×100. B) Numerous fungal hyphae are in the lumen and wall of a large hepatic vessel. Hematoxylin–eosin; original magnification ×200. C) Grocott methenamine silver stain highlights ribbon-like, pauciseptate, branching funal hyphae within the hepatic vessel. Original magnification ×200. D) Intravascular fungal hyphae stain red by immunohistochemical assay for mucormycete fungi. Original magnification ×200.

Conclusions

We describe 3 investigations of potentially donor-derived IMIs resulting in 4 fatal organ recipient infections, although IMI was not definitively identified in these drowned donors. The 4 recipients tested positive for fungi a median of 7 days (range 3–26 days) and died a median of 8 days (range 4–55 days) after transplantation. All recipients who tested positive died. Onset of disease and outcomes were faster and more severe than reported in previously published literature on donor-derived IMIs, which described a median time of 21 days (range 9 days–6 months) to disease onset and a death rate of 17%; the shortest time to onset of donor-derived mucormycosis described by Gomes and Singh was from a drowned donor (*3*,*6*). These findings highlight the importance of early diagnosis, timely treatment, and prompt communication among transplant centers to facilitate early prophylaxis, diagnosis, and treatment of other recipients when indicated. Transplant teams can also consider antifungal prophylaxis with drugs active against Mucorales and *Scedosporium* species in SOT recipients receiving organs from drowned donors.

One limitation of our study is that these investigations are neither inclusive nor representative of all potential donor-derived IMIs in the United States, given that DTAC relies on passive reporting. Donor drowning circumstances (e.g., type of water and water temperature) likely affect the probability of an IMI after drowning, but this information was not generally available in the donor medical records. Determining whether an IMI was donor-derived is challenging because SOT recipients can be exposed to molds through multiple sources (e.g., healthcare-associated exposures and community exposures) both before and after transplant. Exposed donors may not have detectable pulmonary disease even in the presence of mold; average incubation periods for IMIs in drowning victims are longer than the time between drowning and organ procurement in the described cases (*10*,*11*). Alternatively, angioinvasive molds could have infiltrated from other exposed mucosa or abrasions, leading to dissemination to extrapulmonary organs before procurement. The relatively short times from organ transplantation to symptom onset and the presence of IMIs among multiple recipients of the same donor support a donor origin for infection; previous reports suggest that IMIs in organ transplant recipients have a median time to onset of ≥180 days (*6*).

Because of the substantial need for organs and considerable mortality rates among persons awaiting transplantation, donors who drowned are considered on a case-by-case basis by transplant clinicians (*12*). Clinicians should maintain clinical suspicion for IMI when caring for SOT recipients receiving organs from drowned donors, communicate concerns about IMIs to other recipient transplant centers in a timely manner, and consider the use of Mucorales- and *Scedosporium*-active antifungal prophylaxis (*13*,*14*).

This work was supported in part by the Health Resources and Services Administration (contract no. HHSH250-2019-00001C).

About the Author

Dr. Wu is an epidemiologist in the Division of Healthcare Quality and Promotion of CDC's National Center for Emerging and Zoonotic Infectious Diseases and previously served as an Epidemic Intelligence Service Officer in the Division of Foodborne, Waterborne, and Environmental Diseases, also of CDC's National Center for Emerging and Zoonotic Infectious Diseases. Her research interests include the epidemiology of healthcare-associated infections and the One Health approach.

References

1. Organ Procurement and Transplantation Network. Data. 2022 [cited 2022 Dec 1]. https://optn.transplant.hrsa.gov/data
2. Ratermann KL, Ereshefsky BJ, Fleishaker EL, Thornton AC, Buch KP, Martin CA. Fulminant invasive pulmonary aspergillosis after a near-drowning accident in an immunocompetent patient. Ann Pharmacother. 2014;48:1225–9. https://doi.org/10.1177/1060028014537611
3. Gomez CA, Singh N. Donor-derived filamentous fungal infections in solid organ transplant recipients. Curr Opin Infect Dis. 2013;26:309–16. https://doi.org/10.1097/QCO.0b013e3283630e4d
4. Kim SH, Ha YE, Youn JC, Park JS, Sung H, Kim MN, et al. Fatal scedosporiosis in multiple solid organ allografts transmitted from a nearly-drowned donor. Am J Transplant. 2015;15:833–40. https://doi.org/10.1111/ajt.13008
5. Leek R, Aldag E, Nadeem I, Gunabushanam V, Sahajpal A, Kramer DJ, et al. Scedosporiosis in a combined kidney and liver transplant recipient: a case report of possible transmission from a near-drowning donor. Case Rep Transplant. 2016;2016:1879529. https://doi.org/10.1155/2016/1879529
6. Pappas PG, Alexander BD, Andes DR, Hadley S, Kauffman CA, Freifeld A, et al. Invasive fungal infections among organ transplant recipients: results of the Transplant-Associated Infection Surveillance Network (TRANSNET). Clin Infect Dis. 2010;50:1101–11. https://doi.org/10.1086/651262
7. Brunet K, Alanio A, Lortholary O, Rammaert B. Reactivation of dormant/latent fungal infection. J Infect. 2018;77:463–8. https://doi.org/10.1016/j.jinf.2018.06.016
8. Alexander BD, Schell WA, Siston AM, Rao CY, Bower WA, Balajee SA, et al. Fatal *Apophysomyces elegans* infection transmitted by deceased donor renal allografts. Am J Transplant. 2010;10:2161–7. https://doi.org/10.1111/j.1600-6143.2010.03216.x

9. Kaul DR, Vece G, Blumberg E, La Hoz RM, Ison MG, Green M, et al. Ten years of donor-derived disease: a report of the disease transmission advisory committee. Am J Transplant. 2021;21:689–702. https://doi.org/10.1111/ajt.16178
10. Inaba K, Branco BC, Lam L, Salim A, Talving P, Plurad D, et al. Organ donation and time to procurement: late is not too late. J Trauma. 2010;68:1362–6. https://doi.org/10.1097/TA.0b013e3181db30d3
11. Katragkou A, Dotis J, Kotsiou M, Tamiolaki M, Roilides E. *Scedosporium apiospermum* infection after near-drowning. Mycoses. 2007;50:412–21. https://doi.org/10.1111/j.1439-0507.2007.01388.x
12. Tullius SG, Rabb H. Improving the supply and quality of deceased-donor organs for transplantation. N Engl J Med. 2018;378:1920–9. https://doi.org/10.1056/NEJMra1507080
13. Farmakiotis D, Kontoyiannis DP. Emerging issues with diagnosis and management of fungal infections in solid organ transplant recipients. Am J Transplant. 2015;15:1141–7. https://doi.org/10.1111/ajt.13186
14. Shoham S, Dominguez EA; AST Infectious Diseases Community of Practice. Emerging fungal infections in solid organ transplant recipients: guidelines of the American Society of Transplantation Infectious Diseases Community of Practice. Clin Transplant. 2019;33:e13525. https://doi.org/10.1111/ctr.13525

Address for correspondence: Karen Wu, Centers for Disease Control and Prevention, 1600 Clifton Rd NE, Mailstop H16-2, Atlanta, GA 30329-4027, USA; email: vom5@cdc.gov

Surveillance and Genomic Characterization of Influenza A and D Viruses in Swine, Belgium and the Netherlands, 2019–2021

Anna Parys, Nick Vereecke, Elien Vandoorn, Sebastiaan Theuns, Kristien Van Reeth

During 2019–2021, we isolated 62 swine influenza A viruses in Belgium and the Netherlands. We also detected influenza D in pigs in the Netherlands. The ever-changing diversity of influenza viruses and the identification of influenza D emphasize the need for more virus surveillance.

Three influenza A virus (IAV) subtypes circulate globally in swine: H1N1, H1N2 and H3N2. Within each subtype, multiple hemagglutinin (HA) and neuraminidase (NA) lineages or clades cocirculate. In Europe, there are 4 swine IAV HA lineages: the HA-1A classical swine lineage including influenza A(H1N1)pdm09 virus (pH1N1), HA-1B human seasonal lineage (H1hu), HA-1C Eurasian avian lineage (H1av), and European human-like H3 lineage (*1*). In addition, there are 4 NA lineages: pH1N1, N1av, A/swine/Scotland/410440/1994-like (N2s), and A/swine/Gent/1/1984-like (N2g). Swine IAV lineages have continued to evolve through exchange of genome segments (reassortment) and mutations in the viral surface proteins (drift); these processes resulted in multiple genotypes with gene segments of swine, avian, and human origin.

A new genus, influenza D virus (IDV), was identified in pigs in Oklahoma in 2011 (*2*). Two IDV lineages, D/swine/Oklahoma/1334/2011 and D/bovine/Oklahoma/660/2013 (D/660), have been identified in swine and cattle in Europe on the basis of the hemagglutinin-esterase fusion protein (HEF). In this study, we identified the prevailing swine IAVs circulating in Belgium and the Netherlands during 2019–2021 and determined their genotypes by whole-genome characterization. Furthermore, we described the isolation and characterization of an emerging swine IDV in the Netherlands.

Author affiliations: Ghent University, Merelbeke, Belgium (A. Parys, E. Vandoorn, K. Van Reeth); Ghent University and PathoSense BV, Lier, Belgium (N. Vereecke, S. Theuns)

DOI: http://doi.org/10.3201/eid2907.221499

The Study

We started with 152 samples that had tested IAV-positive by reverse transcription PCR by Animal Healthcare Flanders (Torhout, Belgium) or through random viral and bacterial metagenomics analysis by PathoSense (Lier, Belgium) (*3*). The samples were submitted to the diagnostic laboratories by the farmer or the veterinarian for an etiologic diagnosis of respiratory signs. Samples were nasal and tracheobronchial swab specimens and lung tissues from pigs in Belgium and the Netherlands, collected during November 2019–December 2021. From those samples, we obtained 62 swine IAVs by virus isolation in MDCK cells. We determined their subtype by hemagglutination inhibition assays with reference antiserum that we obtained by double vaccination with inactivated virus vaccines (Appendix 1 Table, https://wwwnc.cdc.gov/EID/article/29/7/22-1499-App1.xlsx) and a multiplex reverse transcription quantitative PCR, specific for the HA and NA (Table 1; Appendix 1 Table) (*4*). Two of those IAVs originated from pigs in the Netherlands; the other 60 were isolated from pigs in Belgium. Subtyping revealed 34 (54.8%) viruses of the H1N1 subtype, comprising 30 (48.4%) H1avN1av viruses, 3 (4.8%) pH1N1av viruses, and 1 (1.6%) H1huN1av virus. The second most dominant subtype was H1N2 with 27 (43.5%) viruses: 13 (21.0%) H1huN2 viruses, 13 (21.0%) pH1N2 viruses, and 1(1.6%) H1avN2 virus. We isolated 1 (1.6%) H3N2 virus.

We selected 23 of the 62 swine IAV isolates for targeted whole-genome sequencing using nanopore sequencing (Table 2) (*5*–*7*). All sequences are available through GenBank (accession nos. OP445672–

Table 1. Overview of swine influenza A virus isolates from pigs in Belgium and the Netherlands, November 2019–December 2021

Subtype	Lineage	No. isolates/y			Total, N = 62
		2019, n = 4	2020, n = 34	2021, n = 24	
H1N1	H1avN1av	1	17	12	30
	pH1N1av	0	2	1	3
	H1huN1av	0	0	1	1
H1N2	H1huN2	2	8	3	13
	pH1N2	1	5	7	13
	H1avN2	0	1	0	1
H3N2	H3huN2	0	1	0	1

*av, European avian-like; hu, European human-like; p, 2009 pandemic

79, OP445741–812, OP458600–702). Sequencing of HA revealed that the isolates belonged to all 4 lineages reported in Europe: 10 H1av, 8 pH1, 4 H1hu, and 1 H3. For NA, all isolates of the H1N1 subtype had their NA derived from H1av viruses. Within the H1N2 subtype, 2 isolates derived their NA from N2s and 9 from N2g viruses. The 6 internal gene segments were derived from pH1 or H1av viruses or a combination of both. We designated the A/swine/Belgium/Gent-249/2020 genotype, previously reported by Chepkwony et al. (*7*), as AQ; we identified a genotype of isolate A/swine/Belgium/Gent-234/2020 and designated it as AR. The naming of both isolates is in accordance with the nomenclature system introduced by Watson (*8*) and updated by Henritzi (*9*).

For both HA and NA sequences, we performed maximum-likelihood phylogenetic analyses (*10*) (Figures 1, 2). We selected a total of 28 swine and human IAVs as reference viruses, including both historical and contemporary IAVs circulating in pigs as well as humans in Europe and North America; sources isolates were US Department of Agriculture, Worldwide Influenza Centre at Francis Crick Institute, US Centers for Disease Control, the Ploufragan-Plouzané-Niort Laboratory of the French Agency for Food, Environmental and Occupational Health & Safety, and the Istituto Zooprofilattico Sperimentale delle Venezie. This analysis revealed that 8 of 10 H1av isolates belonged to clade 1C.2.2 and 2 isolates to clade 1C.2.1. In contrast, all 4 H1hu isolates belonged to clade 1B.1.2.1 and all 8 pH1 isolates to clade 1A.3.3.2. The NA genes grouped per lineage and the shorter horizontal branches suggest a slower evolution than the HA gene.

Two tracheobronchial swab specimens from swine farms, originating from Belgium and the Netherlands, tested IDV-positive via metagenomics in 2021 (*3*). The pigs had demonstrated mild upper respiratory signs. Cattle were present on both farms. The samples were investigated by virus isolation on swine testicle cells. We isolated IDV from the sample from the Netherlands and performed next-generation whole-genome sequencing. We designated the isolate as D/swine/Netherlands/PS-497/2021 (GenBank accession nos. OP474071–77); phylogenetic analyses of the HEF nucleotide sequence revealed that it belonged to the D/660 lineage and clustered together with recent bovine IDV isolates from Italy (Appendix 2, https://wwwnc.cdc.gov/EID/article/29/7/22-1499-App2.pdf). In addition, a BLAST homology search (http://www.fludb.org) of all gene segments showed no evidence of reassortment and confirmed the close relationship to D/660.

Table 2. Swine influenza A virus genotypes of 23 viruses isolated from pigs in Belgium and the Netherlands, November 2019–December 2021*

Subtype	Genotype	Surface genes		Internal genes						Total
		HA	NA	PB2	PB1	PA	NP	M	NS	
H1N1	M	H1av	N1av	av	av	av	av	p	av	4
	A	H1av	N1av	av	av	av	av	av	av	3
	AB	H1av	N1av	av	av	av	p	av	av	1
	AC	H1av	N1av	av	av	av	av	p	p	1
	S	pH1	N1av	p	p	p	p	p	p	2
	H	H1hu	N1av	av	av	av	av	av	av	1
H1N2	AR	H1av	N2g	av	av	av	av	p	av	1
	R	pH1	N2g	p	p	p	p	p	p	6
	C	H1hu	N2s	av	av	av	av	av	av	1
	AI	H1hu	N2g	av	av	av	av	p	av	1
	AQ	H1hu	N2s	av	av	av	av	p	av	1
H3N2	N	H3g	N2g	av	av	av	av	p	av	1

*Nomenclature as described by Watson et al. (*7*). av, European avian-like; g, A/swine/Gent/1/1984-like; HA, hemagglutinin; hu, European human-like; M, matrix; NA, neuraminidase; NP, nucleoprotein; NS, nonstructural protein; p, 2009 pandemic; PA, polymerase; PB, polymerase basic; s, A/swine/Scotland/410440/1994-like.

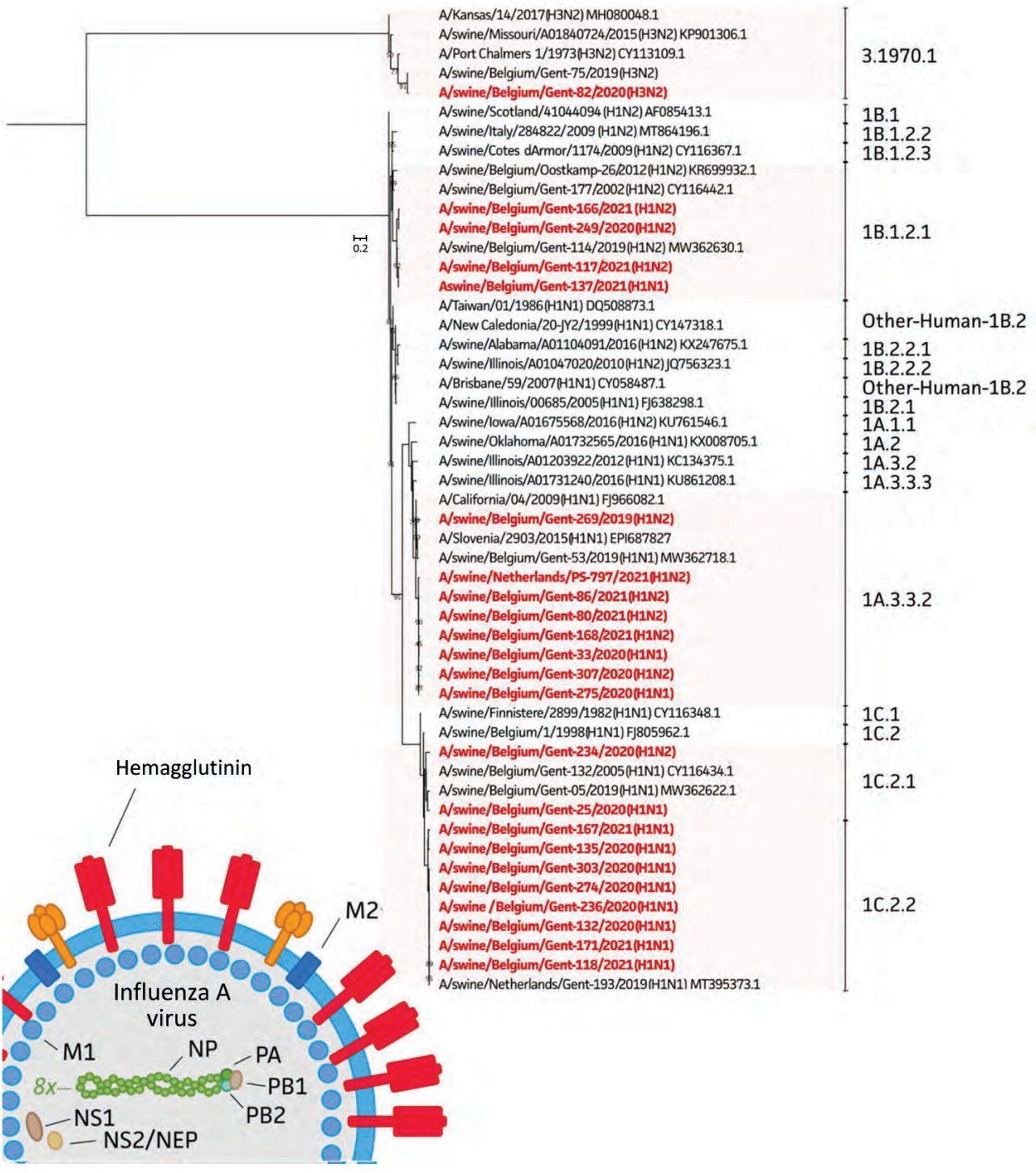

Figure 1. Phylogenetic tree based on the hemagglutinin nucleotide sequences of 23 swine influenza A isolates from pigs in Belgium and the Netherlands, November 2019–December 2021, and 28 swine and human influenza A reference viruses. We generated maximum-likelihood trees using IQ-TREE (http://www.iqtree.org) with the general time reversible plus invariable site plus FreeRate model and 1,000 ultrafast bootstraps. Sequences retrieved from GenBank or GISAID (https://www.gisaid.org) are identified by virus names and accession numbers. Bold text indicates study isolates. The clades of hemagglutinin are indicated; 8x means that 1 of the 8 total segments of the viral genome is shown. Scale bar represents the number of nucleotide substitutions per site per year. M, matrix protein; NEP, nuclear-encoded plastid RNA polymerase; NP, nucleoprotein; NS, nonstructural protein; PA, polymerase acidic; PB, polymerase basic.

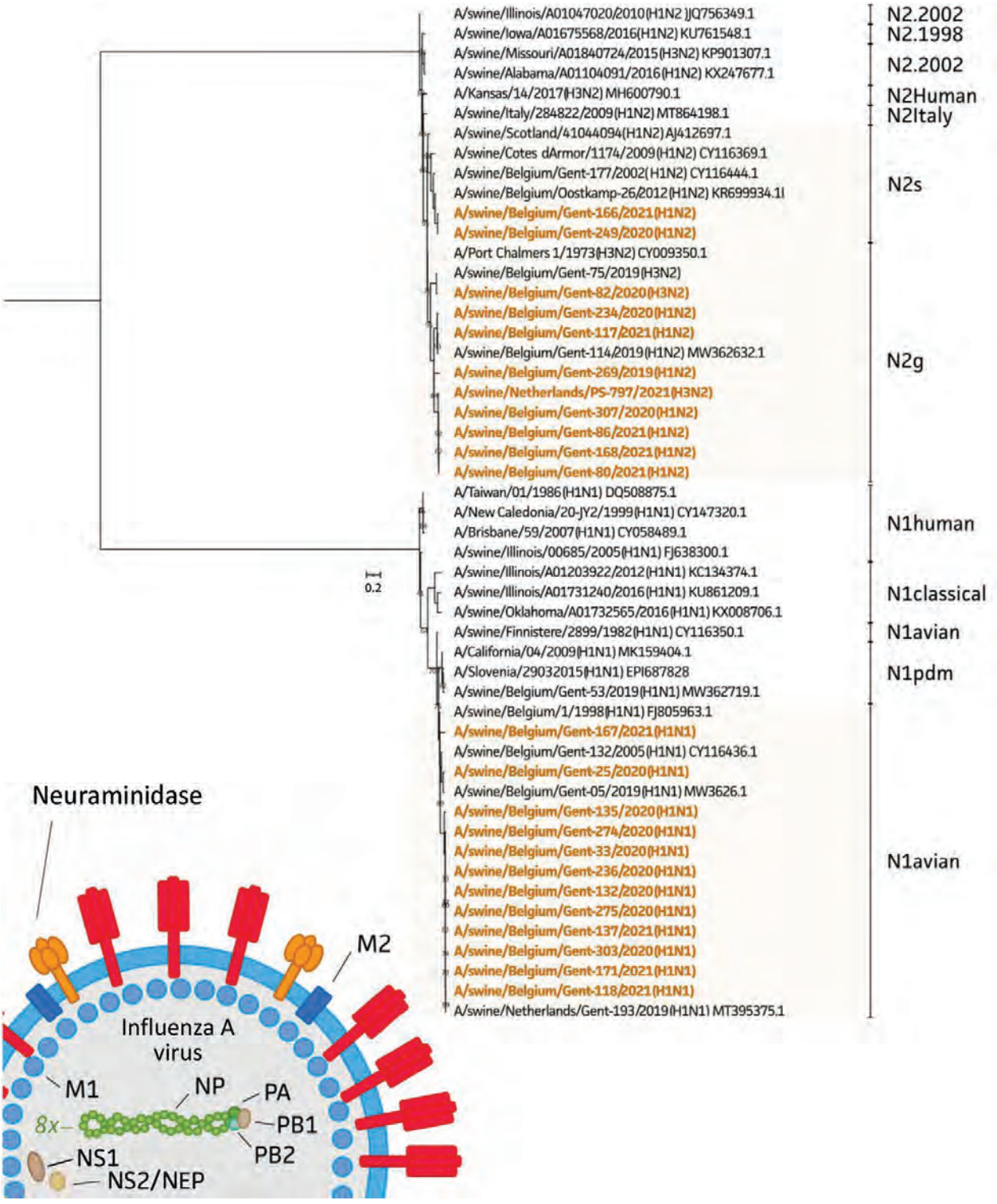

Figure 2. Phylogenetic tree based on neuraminidase nucleotide sequences of 23 swine influenza A isolates from pigs in Belgium and the Netherlands, November 2019–December 2021, and 28 swine and human influenza A reference viruses. We generated maximum-likelihood trees using IQ-TREE (http://www.iqtree.org) with the general time reversible plus invariable site plus FreeRate model and 1,000 ultrafast bootstraps. Sequences retrieved from GenBank or GISAID (https://www.gisaid.org) are identified by virus names and accession numbers. Bold text indicates study isolates. The lineage of neuraminidase is indicated; 8x means that 1 of the 8 total segments of the viral genome is shown. Scale bar represents the number of nucleotide substitutions per site per year. M, matrix protein; NEP, nuclear-encoded plastid RNA polymerase; NP, nucleoprotein; NS, nonstructural protein; PA, polymerase acidic; PB, polymerase basic.

Conclusions

This study is a follow-up of a previous surveillance study in Belgium and the Netherlands during 2014–2019 (*7*). The H1av lineage was predominant in both studies and accounted for roughly half of all swine IAV isolates. A major change, however, was the increase in clade 1C.2.2 isolates from 23.8% in 2014–2019 to 80.0% in 2019–2021 (*7*). Of note, recent serologic investigations of human antibodies against H1 swine IAVs pointed toward a relatively greater zoonotic risk for H1av viruses compared with European H1hu or pH1 viruses (*11*).

The second most predominant lineage was the pH1 lineage (25.8%). Until 2018, this lineage was widespread in the United Kingdom and Poland, whereas prevalence in other countries in Europe was ≈5% (*8*,*9*). Most pH1 viruses in this study were reassortants in which the pN1 was replaced by N2, a trend described previously (*8*). The increased frequency of pH1 swine IAVs explains the emergence of second-generation reassortants between this lineage and the long-existing H1av lineage in swine in Europe as well as in Asia. Some specific reassortant genotypes with H1av surface proteins and pH1 internal genes that have been found in Asia were announced as a pandemic threat (*12*). However, it remains unclear whether they are higher on the pandemic risk scale than other H1av reassortants because of the lack of comparative data. The increase in pH1N2 swine IAVs might also play a role in the low number of H3N2 swine IAVs in Belgium and the Netherlands; this connection was previously described as a possible result of immunity against N2 influencing the prevalence of both virus lineages and favoring the lineage with the greatest genetic diversity in swine (*8*).

In summary, we report IDV isolation in swine in the Netherlands and circulation of lineage D/660 in swine in Europe that is genetically related to bovine IDV. Trombetta et al. previously suggested circulation of the D/660 lineage in swine in Italy, based on the detection of antibodies in swine veterinarians in 2004 (*13*). The finding of bovine-related IDV strains in those pigs is unsurprising because cattle were present on both farms, suggesting a potential interspecies transmission. Although the phylogenetic analysis seems to confirm that the IDV HEF evolutionary rate is slower than that of IAV HA and NA (*2*) (Appendix 2), we note that IDV emerging virus in swine may have zoonotic potential (*13*,*14*). Therefore, this study supports the hypothesis that pigs and swine influenza viruses should be a high priority for surveillance for pandemic threats (*15*).

Acknowledgments

We thank Nele Dennequin, Melanie Bauwens, Marlies Ballegeer, Jonathan Vandenbogaerde, and Joridan Rombaut for excellent technical assistance. We thank Klaas Visscher and David Goussey for their excellent observation skills and the detection of IDV cases in the field.

This study was financed by the Special Research Fund of Ghent University (grant no. 01J102017) and the Belgian Federal Service for Public Health, Food Chain Safety and Environment (Federale overheidsdienst—FOD) under the project "Surveillance of coronaviruses in cattle and swine with emphasis on their zoonotic risk (CORUVA)," grant no. RF 21/6347. N. V. was funded by a grant from the Flemish Agency for Innovation and Entrepreneurship (Baekeland Mandate HBC.2020.2889).

About the Author

Dr. Parys was a PhD student at the Laboratory of Virology, Faculty of Veterinary Medicine, Ghent University, during the study period. She uses the pig as a model for the development of broadly protective influenza A vaccines and has a special interest in the public health implications of swine influenza.

References

1. Anderson TK, Chang J, Arendsee ZW, Venkatesh D, Souza CK, Kimble JB, et al. Swine influenza A viruses and the tangled relationship with humans. Cold Spring Harb Perspect Med. 2021;11:a038737. https://doi.org/10.1101/cshperspect.a038737
2. Liu R, Sheng Z, Huang C, Wang D, Li F. Influenza D virus. Curr Opin Virol. 2020;44:154–61. https://doi.org/10.1016/j.coviro.2020.08.004
3. Theuns S, Vanmechelen B, Bernaert Q, Deboutte W, Vandenhole M, Beller L, et al. Nanopore sequencing as a revolutionary diagnostic tool for porcine viral enteric disease complexes identifies porcine kobuvirus as an important enteric virus. Sci Rep. 2018;8:9830. https://doi.org/10.1038/s41598-018-28180-9
4. Henritzi D, Zhao N, Starick E, Simon G, Krog JS, Larsen LE, et al. Rapid detection and subtyping of European swine influenza viruses in porcine clinical samples by haemagglutinin- and neuraminidase-specific tetra- and triplex real-time RT-PCRs. Influenza Other Respir Viruses. 2016;10:504–17. https://doi.org/10.1111/irv.12407
5. Van Poelvoorde LAE, Bogaerts B, Fu Q, De Keersmaecker SCJ, Thomas I, Van Goethem N, et al. Whole-genome-based phylogenomic analysis of the Belgian 2016-2017 influenza A(H3N2) outbreak season allows improved surveillance. Microb Genom. 2021;7:000643. https://doi.org/10.1099/mgen.0.000643
6. Vereecke N, Kvisgaard LK, Baele G, Boone C, Kunze M, Larsen LE, et al. Molecular epidemiology of porcine parvovirus type 1 (PPV1) and the reactivity of vaccine-induced antisera against historical and current PPV1 strains. Virus Evol. 2022;8:veac053. https://doi.org/10.1093/ve/veac053
7. Chepkwony S, Parys A, Vandoorn E, Stadejek W, Xie J, King J, et al. Genetic and antigenic evolution of H1 swine influenza A viruses isolated in Belgium and the

Netherlands from 2014 through 2019. Sci Rep. 2021;11:11276. https://doi.org/10.1038/s41598-021-90512-z
8. Watson SJ, Langat P, Reid SM, Lam TTY, Cotten M, Kelly M, et al.; ESNIP3 Consortium. Molecular epidemiology and evolution of influenza viruses circulating within European swine between 2009 and 2013. J Virol. 2015;89:9920–31. https://doi.org/10.1128/JVI.00840-15
9. Henritzi D, Petric PP, Lewis NS, Graaf A, Pessia A, Starick E, et al. Surveillance of European domestic pig populations identifies an emerging reservoir of potentially zoonotic swine influenza A viruses. Cell Host Microbe. 2020; 28:614–627.e6. https://doi.org/10.1016/j.chom.2020.07.006
10. Chernomor O, von Haeseler A, Minh BQ. Terrace aware data structure for phylogenomic inference from supermatrices. Syst Biol. 2016;65:997–1008. https://doi.org/10.1093/sysbio/syw037
11. Vandoorn E, Leroux-Roels I, Leroux-Roels G, Parys A, Vincent A, Van Reeth K. Detection of H1 swine influenza A virus antibodies in human serum samples by age group. Emerg Infect Dis. 2020;26:2118–28. https://doi.org/10.3201/eid2609.191796
12. Sun H, Xiao Y, Liu J, Wang D, Li F, Wang C, et al. Prevalent Eurasian avian-like H1N1 swine influenza virus with 2009 pandemic viral genes facilitating human infection. Proc Natl Acad Sci U S A. 2020;117:17204–10. https://doi.org/10.1073/pnas.1921186117
13. Trombetta CM, Montomoli E, Di Bartolo I, Ostanello F, Chiapponi C, Marchi S. Detection of antibodies against influenza D virus in swine veterinarians in Italy in 2004. J Med Virol. 2022;94:2855–9. https://doi.org/10.1002/jmv.27466
14. Borkenhagen LK, Mallinson KA, Tsao RW, Ha SJ, Lim WH, Toh TH, et al. Surveillance for respiratory and diarrheal pathogens at the human–pig interface in Sarawak, Malaysia. PLoS One. 2018;13:e0201295. https://doi.org/10.1371/journal.pone.0201295
15. Borkenhagen LK, Salman MD, Ma MJ, Gray GC. Animal influenza virus infections in humans: a commentary. Int J Infect Dis. 2019;88:113–9. https://doi.org/10.1016/j.ijid.2019.08.002

Address for correspondence: Kristien Van Reeth, Laboratory of Virology, Faculty of Veterinary Medicine, Ghent University, Salisburylaan 133, 9820 Merelbeke, Belgium; email: kristien.vanreeth@ugent.be

etymologia revisited

Streptomycin

strep'to-mi'sin

In the late 1930s, Selman Waksman, a soil microbiologist working at the New Jersey Agricultural Station of Rutgers University, began a large-scale program to screen soil bacteria for antimicrobial activity. By 1943, Albert Schatz, a PhD student working in Waksman's laboratory, had isolated streptomycin from *Streptomyces griseus* (from the Greek *strepto-* ["twisted"] + *mykēs* ["fungus"] and the Latin *griseus*, "gray").

In 1944, Willam H. Feldman and H. Corwin Hinshaw at the Mayo Clinic showed its efficacy against *Mycobacterium tuberculosis*. Waksman was awardeda Nobel Prize in 1952 for his discovery of streptomycin, although much of the credit for the discovery has since been ascribed to Schatz. Schatz later successfully sued to be legally recognized as a co-discoverer of streptomycin.

Originally published in March 2019

References:

1. Comroe JH Jr. Pay dirt: the story of streptomycin. Part I. From Waksman to Waksman. Am Rev Respir Dis. 1978;117:773–81.
2. Wainwright M. Streptomycin: discovery and resultant controversy. Hist Philos Life Sci. 1991;13:97–124.

https://wwwnc.cdc.gov/eid/article/25/3/et-2503_article

Detecting, Quantifying, and Isolating Monkeypox Virus in Suspected Cases, Spain

Marta E. Álvarez Argüelles, Zulema Pérez Martínez, Susana Rojo Alba, Jose María González Alba, Ana María Fernandez-Verdugo, Isabel Costales González, Garbriel Martín Rodríguez, Jose Antonio Boga Riveiro, Mario Margolles Martins, Santiago Melón García

When a monkeypox virus outbreak began in several parts of the world in May 2022, timely and accurate diagnosis became mandatory. In our laboratory, a real-time quantitative PCR was designed and evaluated in several patient samples and compared with isolation results. Genomic viral load was related to virus viability.

After smallpox was eradicated worldwide in 1980 and routine smallpox vaccination subsequently ceased, monkeypox virus (MPXV) emerged as the most consequential orthopoxvirus for public health (*1*). The genetic clades of MPXV are clade I (formerly the Congo Basin [Central African] clade), which is associated with higher virulence and greater mortality rate, and clade II (formerly the West African clade) (*1*,*2*).

In May 2022, the United Kingdom reported an outbreak of mpox (formerly monkeypox) that subsequently spread globally (*3*); Spain was one of the most affected countries (*4*). The rapid increase in mpox cases has challenged clinical laboratories to understand the spread and transmission of MPXV. We sought to detect and isolate MPXV in persons at risk for infection by genomic amplification using a real-time quantitative PCR (qPCR) and isolation in culture cell.

This study did not require research ethics committee approval because it describes analyses that were completed at the public laboratory as part of routine clinical testing and surveillance during the mpox outbreak in Asturias in the northwest of Spain. Therefore, this study was considered public health practice and was exempt from this requirement.

Author affiliations: Hospital Universitario Central de Asturias, Oviedo, Spain (M.E. Álvarez Argüelles, Z. Pérez Martínez, S. Rojo Alba, J.M. González Alba, A.M. Fernandez-Verdugo, I. Costales González, G.M. Rodríguez, J.A. Boga Riveiro, S. Melón García); Epidemiological Surveillance Department, Oviedo (M. Margolles Martins)

DOI: https://doi.org/10.3201/eid2907.221229

The Study

During May 24–July 15, 2022, a total of 66 samples (42 lesion swabs, 20 respiratory samples, and 4 blood samples) belonging to 41 adults (mean age 35.61 ± 11.25, range 17–60 years) and collected within 72 hours of illness onset were submitted in accordance with laboratory requirements (Table 1). All patients were located in a 30-km area around Oviedo, the capital of Asturias. In addition to MPXV, we also tested for herpes simplex virus, varicella zoster virus, enterovirus, human herpesvirus 8, molluscum contagiosum virus, and human papilloma virus, according to clinical manifestations. Samples were processed following laboratory protocols for nucleic acid detection, and 21 were inoculated onto monolayer conventional cell culture (MRC-5 cell, Vero-E6, and A549 and LLC-MK2 cells subcultures).

We extracted nucleic acids by using the automated nucleic acid purifier Magnapure 96 (Roche Diagnostics, https://www.roche.com). We performed orthopoxvirus group PCR (*5*) and specific MPXV in-house real-time qPCR.

For qPCR, we amplified 5 μL of extracted nucleic acids in a final volume of 10 μL, including the Brillant III Ultra-fast QPCR Master MIX (Agilent Technologies, https://www.agilent.com), 1,000 nm of each primer (MPXV-S, TGTTGACGCACCAGCGTCT; MPXV-A, AACAGTGGACCCTTGATGACTGT), and 200 nm of FAM-labeled MGB probe (CAATCCATGGTATTCGA; ABI, CA). We performed qPCR as follows: 95° for 7 min, 45 cycles of 95° for 5 min and 60° for 33 min. In addition, we quantified the human β-globin

Table 1. Characteristics, sample type, and clinical features for patients in study of MPXV detection and isolation, Spain*

Patient no.	Date	Age, y/sex	HIV serostatus	MSM/SP†	Sample type	Clinical features
1	2022 May 24	54/F	–	No	Lesion swab	Rash, fever
2	2022 May 25	17/M	–	NA	Pharyngeal and oral swab	Acute pharyngitis
3	2022 Jun 15	34/M	+	Yes	Lesion swab	Genital lesions
4	2022 Jun 15	34/M	–	Yes	Lesion swab	Lesions, fever, adenopathies
5	2022 Jun 15	49/M	+	Yes	Nasopharyngeal and lesion swab	Perioral lesions
6‡	2022 Jun 17	39/M	+	Yes	Nasopharyngeal and lesion swab	Lip lesion, fever
7	2022 Jun 18 and 21	45/M	+	Yes	Pharyngeal and lesion swabs	Perianal and pharyngeal discomfort, vesicular exanthema
8	2022 Jun 20	25/F	–	No	Nasopharyngeal and lesion swab	Lesion
9	2022 Jun 20	49/M	–	Yes	Lesion swab	Lesion
10	2022 Jun 20 and 24	41/M	–	Yes	Nasopharyngeal and lesion swab	Febrile, pubic lesion
11	2022 Jun 21	45/M	–	Yes	Lesion swab	Folliculitis in the context of scabies
12	2022 Jun 24	43/M	–	Yes	Lesion swab	Odynophagia, folliculitis, genital lesion, fever
13	2022 Jun 30	37/M	–	Yes	Lesion swab	Cutaneus and genital lesions, adenopathies
14	2022 Jul 1	35/M	+	Yes	Nasopharyngeal, lesion swab, blood	Cutaneus and genital lesions, fever, adenopathies
15	2022 Jul 1	29/M	+	Yes	Nasopharyngeal and lesion swab	Vesicular lesions on trunk, palms, and genitals, fever
16	2022 Jul 2	35/M	+	No/Yes	Lesion swab	Odynophagia/cutaneus and genital lesions, fever, adenopathies
17	2022 Jul 2	22/M	–	No/Yes	Lesion swab	Genital lesions
18	2022 Jul 3	47/M	+	No	Lesion swab	Cutaneus and genital lesions
19	2022 Jul 4	30/M	–	Yes	Nasopharyngeal and lesion swab	Lesions, fever
20‡§	2022 Jul 4	26/M	–	Yes	Lesion and rectal swabs, blood	Lesions, fever
21	2022 Jul 5	22/M	–	NA	Lesion swab	Itchy lesions
22	2022 Jul 5	41/M	+	NA	Lesion swab	Lesions¶
23	2022 Jul 5	48/M	–	NA	Lesion swab	Lesions¶
24	2022 Jul 5	30/M	+	NA	Nasopharyngeal and lesion swab	Lesions¶
25	2022 Jul 6	26/M	–	NA	Nasopharyngeal and lesion swab	Lesions¶
26	2022 Jul 7	29/M	–	Yes	Lesion swab	Lesions¶
27	2022 Jul 8	28/M	–	NA	Lesion swab	Lesions¶
28	2022 Jul 8	60/M	–	NA	Pharyngeal and lesion swab	Lesions¶
29	2022 Jul 8	22/M	+	Yes	Pharyngeal and lesion swab, blood	Cutaneus and genital lesions
30	2022 Jul 11	54/M	NA	NA	Lesion swab	Lesions¶
31	2022 Jul 11	47/M	–	Yes	Pharyngeal and lesion swab	Lesions, adenopathies
32	2022 Jul 12	30/M	NA	NA	Lesion swab	Lesions¶
33	2022 Jul 12	32/F	NA	NA	Lesion swab	Lesions¶
34	2022 Jul 12	34/F	–	No	Pharyngeal and lesion swab	Necrotic lesions on forehead
35	2022 Jul 13	19/F	NA	NA	Pharyngeal and lesion swab, blood	Umbilical lesions
36	2022 Jul 13	56/M	NA	NA	Pharyngeal and lesion swab	Lesions¶
37	2022 Jul 13	21/M	–	No	Lesion swab	Lesions¶
38	2022 Jul 13	19/F	–	No	Lesion swab	Lesions¶
39	2022 Jul 14	34/F	–	No	Pharyngeal and lesion swab	Back rash in different stages of evolution
40	2022 Jul 15	42/M	NA	NA	Lesion swab	Lesions¶
41	2022 Jul 15	30/M	+	Yes	Pharyngeal and lesion swab	Lesions, adenopathies

*Gray shading indicates MPXV-infected patients. MPXV, monkeypox virus; MSM, men who have sex with men; NA, not available; SP, high-risk sexual practices; +, positive; –, negative.
†No further information was available regarding attending clinicians' criteria for high-risk sexual practices.
‡Inpatient.

Table 2. Results of days of isolation and average cycle threshold values of samples according to results of culture in study of MPXV detection and isolation, Spain*

Cell	No. positive cultures	Mean days of positivity ±SD (range) [95% CI]	Mean Ct of positive cultures ±SD (range) [95% CI]	No. negative cultures	Mean Ct of negative cultures ±SD (range) [95% CI]	p value
MRC-5 cells	12	5.8 ±2.4 (3–10)† [4.2–7.4]	22.4 ±6.4 (15–34) [18.3–26.5]	9	29.5 ±3.1 (25–34) [27.1–31]	0.0068
VeroE6 cells	16	3.7 ±1.3 (3–7)† [2.9–4.5]	23.4 ±5.8 (15–34) [20.3–26.4]	5	32.02 ±1.1 (31–34) [30.8–33.5]	0.0035
Both lines	17	3.7 ±1.3 (3–7) [2.9–4.5]	23.9 ±5.9 (15–34) [20.8–26.9]	4	32.25 ±1.25 (31–34) [30.2–34.2]	0.0099

*Ct, cycle threshold; MPXV, monkeypox virus.
†p = 0.012.

gene in each sample to evaluate sample quality and to calculate normalized viral load in $\log_{10}$ copies per 10^3 cells (*6*).

We detected MPXV in 23 (56.09%) of the 41 patients studied. All were men; the mean age was 38.13 ± 9.42 years (range 22–56 years). At least 15 stated they had sex with men, and 12 were HIV-positive. We detected herpes simplex virus 1 in 2 persons (1 of whom was co-infected with MPXV) and varicella zoster virus 1 person. MPXV was detected in 25 (96.15%) lesion swab samples with a viral load of 7.58 ± 2.03 (range 3.84–11.71 [95% CI 6.44–8.19]) and in 8 (66.66%) respiratory swab specimens with a viral load of 5.04 ± 1.01 (range 3.5–6.23 [95% CI 4.192–5.88]; p = 0.0041).

We isolated virus in 13 (81.25%) patients out of 16 infected persons inoculated. From those persons, we recovered MPXV in 17 (80%) of 21 samples assayed: 4 (80%) respiratory swab samples (3 from Vero-E6 and 1 from MRC-5 cells) and 13 (81.25%) lesion swab samples (13 from Vero-E6 cells and 11 from MRC-5 cells) (p = 0.68) (Table 2). In 6 subcultures in A549 cells and in LLC-MK2 cells, cytopathic effect was observed and confirmed by PCR (Figure 1).

We characterized the virus using Sanger sequencing method, and we purified then sequenced the PCR product by using BigDye Terminator v1.1 Cycle Sequencing Kit with an ABI PRISM 3700 DNA analyzer (both ThermoFisher Scientific, https://www.thermofisher.com). We analyzed the sequences subsequently

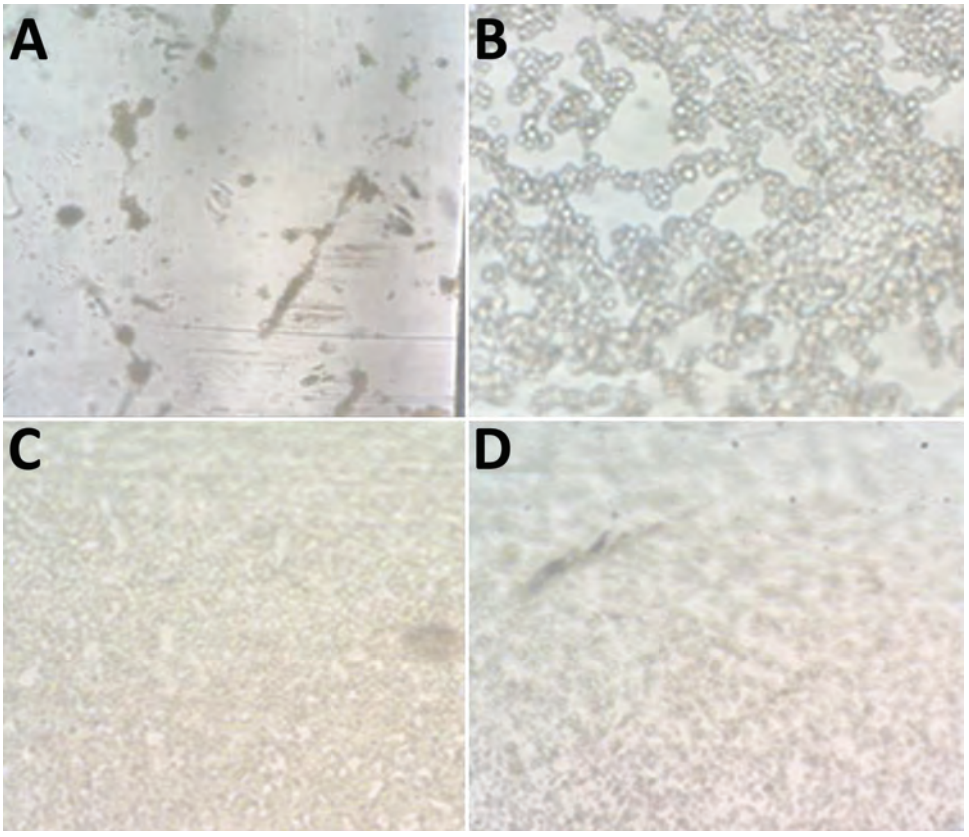

Figure 1. Cytopathic effect in monkeypox virus–infected cells from patients in Asturias, Spain. A) MRC-5; B) Vero E6; C) A549; D) LLC-MK2. Original magnification ×10.

obtained by using IQ-TREE multicore version 2.1.3 (http://www.iqtree.org). We performed tree reconstruction using best-fit model chosen according to Bayesian information criterion. We tested tree branches by the SH-like aLRT method with 1,000 replicates, generating 1,000 samples for ultrafast bootstrap (Figure 2).

Conclusions

In MPXV infection, human-to-human transmission can result from close contact with respiratory secretions, skin lesions of an infected person, or recently contaminated objects (*7*). In this study, all infected patients were men who had skin lesions. In <50% of cases, patients were experiencing fever, adenopathy, or malaise. Fifteen patients stated they had sex with men or engaged in high-risk sexual practices. In this study, 12 HIV-positive patients were infected with MPXV but did not have higher viral load (*4*). Only 2 patients were hospitalized. One patient had fever and severe lymphocytosis. The other was a renal transplant

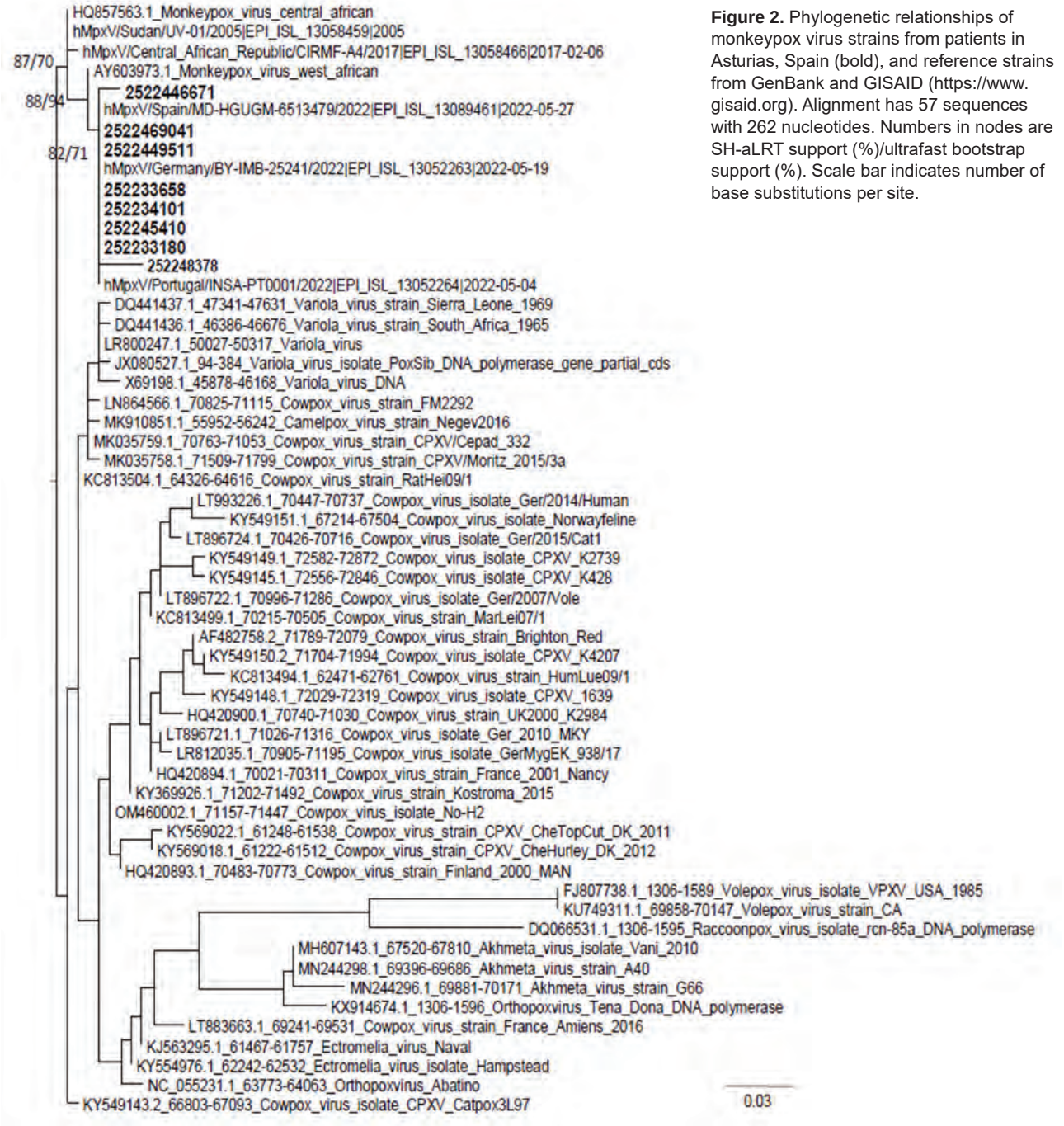

Figure 2. Phylogenetic relationships of monkeypox virus strains from patients in Asturias, Spain (bold), and reference strains from GenBank and GISAID (https://www.gisaid.org). Alignment has 57 sequences with 262 nucleotides. Numbers in nodes are SH-aLRT support (%)/ultrafast bootstrap support (%). Scale bar indicates number of base substitutions per site.

patient hospitalized mainly because of his immunosuppressed state. In that patient, the virus was detected for >1 week. In any case, all the patients had a positive outcome.

All viruses were characterized as clade II, similar to findings from other cases in Spain, suggesting the same focus of infection (S. Buenestado et al., unpub. data, https://virological.org/t/updatetwo-draft-genomes-from-madrid-spain-of-the-monkeypoxvirus-2022-outbreak/848). As expected, the disease followed a self-limited course, and no patients experienced severe complications. DNA sequencing also makes it possible to interpret transmission episodes and confirm the existence of endemic variants (*8*,*9*). Community transmission data were available for 10 cases. Only 2 were considered secondary cases, indicating that transmission in that environment at that point was not common but had started and could spread.

When possible, blood and pharyngeal or nasopharyngeal swabs were collected, per World Health Organization recommendations (*7*,*10*). Blood samples were only collected from 3 patients, and virus was detected in 2 of them at <4 $\log_{10}$ copies/mL. Viremia occurs very early in the course of infection and usually contains a lower viral load than lesions. On the other hand, the normalized viral load was lower in respiratory swab samples than in lesion swab samples, which was to be expected. Patients sought care at a more advanced stage of infection, in which lesions are already present in different phases.

In this study, virus was easily recovered in standard cell culture (VeroE6, MRC-5) from samples with a real-time qPCR cycle threshold of <31 and ≈3.3 $\log_{10}$ copies/10^3 cells, according to a standard curve (*6*). Cytopathic effect appeared in <5 days. In addition, subcultures were achieved in other cell lines commonly used in the laboratory (A549 or LLC-MK2). Those data indicate that at higher viral loads, the virus is complete and transmissible, as has been demonstrated with other viruses such as SARS-CoV-2 (*11*). A limitation of this study was the lack of detailed clinical information for many patients.

In summary, MPXV requires rapid diagnosis and a rapid public health response. The designed real-time qRT-PCR and virus characterization proved very useful in diagnosing mpox and surveillance for MPXV and could aid in controlling the spread of infection and managing outbreaks. Furthermore, the use of culture can help confirm transmission.

This project was partially funded by Grupin IDI/2021/000033.

About the Author

Dr. Álvarez-Argüelles is a researcher and microbiologist dedicated to the field of virology. Her primary research interests are viruses that cause clinical infections and the use and application of virus-detection methods.

References

1. World Health Organization. Monkeypox: experts give virus variants new names [cited 2022 Sep 30]. https://www.who.int/news/item/12-08-2022-monkeypox–experts-give-virus-variants-new-names
2. Adler H, Gould S, Hine P, Snell LB, Wong W, Houlihan CF, et al.; NHS England High Consequence Infectious Diseases (Airborne) Network. Clinical features and management of human monkeypox: a retrospective observational study in the UK. Lancet Infect Dis. 2022;22:1153–62. https://doi.org/10.1016/S1473-3099(22)00228-6
3. World Health Organization. Monkeypox—United Kingdom of Great Britain and Northern Ireland [cited 2022 May 18]. https://www.who.int/emergencies/disease-outbreak-news/item/2022-DON383
4. Jesús IM, Elisa GM, Susana JB, Fernando MM, Alba NJ, Jesús SD, et al. Monkeypox outbreak predominantly affecting men who have sex with men, Madrid, Spain, 26 April to 16 June 2022. Euro Surveill. 2022;27:2200471. PMID 35801519
5. Fedele CG, Negredo A, Molero F, Sánchez-Seco MP, Tenorio A. Use of internally controlled real-time genome amplification for detection of variola virus and other orthopoxviruses infecting humans. J Clin Microbiol. 2006;44:4464–70. https://doi.org/10.1128/JCM.00276-06
6. Álvarez-Argüelles ME, de Oña-Navarro M, Rojo-Alba S, Torrens-Muns M, Junquera-Llaneza ML, Antonio-Boga J, et al. Quantification of human papilloma virus (HPV) DNA using the Cobas 4800 system in women with and without pathological alterations attributable to the virus. J Virol Methods. 2015;222:95–102. https://doi.org/10.1016/j.jviromet.2015.05.016
7. World Health Organization. Laboratory testing for the monkeypox virus. Interim guidance [cited 2022 May 23]. https://apps.who.int/iris/rest/bitstreams/1425052/retrieve
8. Nakazawa Y, Emerson GL, Carroll DS, Zhao H, Li Y, Reynolds MG, et al. Phylogenetic and ecologic perspectives of a monkeypox outbreak, southern Sudan, 2005. Emerg Infect Dis. 2013;19:237–45. https://doi.org/10.3201/eid1902.121220
9. Faye O, Pratt CB, Faye M, Fall G, Chitty JA, Diagne MM, et al. Genomic characterisation of human monkeypox virus in Nigeria. Lancet Infect Dis. 2018;18:246. https://doi.org/10.1016/S1473-3099(18)30043-4
10. Hasso M, Perusini S, Eshaghi A, Tang E, Olsha R, Zhang H, et al. Monkeypox virus detection in different clinical specimen types. Emerg Infect Dis. 2022;28:2513–5. https://doi.org/10.3201/eid2812.221160
11. La Scola B, Le Bideau M, Andreani J, Hoang VT, Grimaldier C, Colson P, et al. Viral RNA load as determined by cell culture as a management tool for discharge of SARS-CoV-2 patients from infectious disease wards. Eur J Clin Microbiol Infect Dis. 2020;39:1059–61. https://doi.org/10.1007/s10096-020-03913-9

Address for correspondence: Santiago Melón García, Hospital Universitario Central de Asturias, Microbiology Av. Roma, s/n., Oviedo, Asturias, ES 33011; email: santiago.melon@sespa.es

Tuberculosis Infection among Non–US-Born Persons and Persons ≥60 Years of Age, United States, 2019–2020

Rachel Woodruff, Roque Miramontes

We examined tuberculosis (TB) infection results for the United States from the 2019–2020 National Health and Nutrition Examination Survey. Over this period, 10% of non–US-born persons and 7% of those ≥60 years of age tested positive for TB infection. These results provide up-to-date information on TB infection among study subpopulations.

Each year, the Centers for Disease Control and Prevention (CDC) collects demographic and clinical data for tuberculosis (TB) disease cases reported from all 50 states and the District of Columbia (*1*). Studies that examined the completeness and accuracy of the national TB surveillance system found that this reporting consistently and accurately captured close to 100% of all diagnosed cases and is therefore highly representative of the burden of TB disease in the United States (*2*–*4*).

The precursor to TB disease, latent TB infection (LTBI), is not a reportable condition in most US states (*5*), so the number of infected persons is not well understood. Beginning in 1970, CDC funded a TB component of several National Health and Nutrition Examination Surveys (NHANES) that provide the primary source of national data on LTBI in the US population (*6*–*8*). Most recently, CDC provided funding for the 2019–2020 NHANES survey to examine LTBI among non–US-born persons ≥6 years of age and all persons ≥60 years of age. The 2019–2020 NHANES protocol was reviewed and approved by the NCHS Ethics Review Board (https://www.cdc.gov/nchs/nhanes/irba98.htm).

NHANES is a series of sequentially run cross-sectional surveys that assess the health of the civilian, noninstitutionalized US population (*9*). To obtain a nationally representative sample, NHANES employs a complex, stratified, multistage probability cluster sampling design (*9*). The sample for the NHANES 2019–2020 survey cycle was intended to be nationally representative and included 30 primary sampling units (*10*). However, 2019–2020 NHANES data collection was suspended in mid-March 2020 because of the COVID-19 pandemic. At that time, data collection had been completed in only 18 of 30 primary sampling units. Because data collection was incomplete, calculating survey weights for that partial cycle was not possible, and the sample was therefore not nationally representative. As a result, only an unweighted partial dataset from the Centers for Disease Control and Prevention's National Center for Health Statistics (NCHS) Research Data Center was available for analysis.

The Study

Non–US-born 2019–2020 NHANES study participants >6 years of age and all study participants ≥60 years of age were eligible to be tested for TB infection using an interferon-gamma release assay (IGRA), QuantiFERON-TB Gold Plus (QIAGEN, https://www.qiagen.com). We selected those specific subpopulations of persons because of their high IGRA test positivity in previous studies (*8*,*11*), the potential for complications of TB disease in the ≥60 age group, and the high risk of LTBI progressing to TB disease among non–US-born persons (*11*). We excluded persons in those subpopulations who did not undergo phlebotomy as part of the routine NHANES exam. Data for coexisting conditions were not available in the 2019–2020 NHANES dataset (*12*). All IGRA test results were provided by a single Clinical Laboratory Improvement Act–certified laboratory. Qualitative results were reported for each IGRA test result based on criteria provided by the manufacturer. We used R statistical software (The R Foundation for Statistical Computing, https://www.R-project.org) to obtain frequencies and percentages of eligible

Author affiliation: Centers for Disease Control and Prevention, Atlanta, Georgia, USA

DOI: https://doi.org/10.3201/eid2907.230324

NHANES participants with positive TB test results by demographic characteristics. Because of NCHS confidentiality policy, Research Data Center results were suppressed for all categories and subcategories that had <5 responses (*13*).

In the 2019–2020 NHANES study, 837 non–US-born participants >6 years of age were tested for TB infection, of whom 85 (10%) had positive TB test results (Table). Among non–US-born study participants who tested positive for TB, 51% (43/85) identified as non-Hispanic Asian and 35% (30) as Hispanic; 79% (67) had been in the United States for ≥5 years. In comparison, among all non–US-born study participants (irrespective of TB test results), 35% (290) identified as non-Hispanic Asian and 43% (356) as Hispanic.

Among the NHANES study participants who were ≥60 years of age (including both US-born and non–US-born persons), 1,123 were tested for TB, among whom 81 (7%) had positive TB test results (Table). Among those who tested positive for TB, 43% (35) identified as non-Hispanic Black. Among study participants ≥60 years of age, those with TB-positive test results were less likely than the overall total to identify as non-Hispanic White (21% vs. 44%), more likely to be living in poverty (17.3% vs. 14.4%), less likely to have at least a high school diploma (32.1% vs. 20.5%), and more likely to have been born outside the United States (29.6% vs. 15.9%).

All TB-positive non–US-born NHANES study participants >6 years of age and TB-positive participants ≥60 years of age were more likely to identify within racial and ethnic minority groups, not have at least a high school diploma, and be living in poverty than overall study participants in each of those subpopulations. In addition, participants ≥60 years of age who tested positive for TB were more likely to have been born outside the United States than overall study participants ≥60 years of age. Although not directly comparable across studies, data from our study about demographic differences between TB-positive and overall study participants for both subpopulations were consistent with previous research (*8,11*).

Comparing data between the 2019–2020 and previous NHANES studies was also limited by a change

Table. Characteristics of non–US-born study participants >6 y of age and all study participants ≥60 years of age who were eligible for TB testing, United States, 2019–2020*

Characteristic	Non–US-born persons ≥6 y, no. (%)		All persons ≥60 y, no. (%)	
	Positive TB test	All	Positive TB test	All
All participants	85 (100.0)	837 (100.0)	81 (100.0)	1,123 (100.0)
Sex				
M	42 (49.4)	408 (48.7)	43 (53.1)	582 (51.8)
F	43 (50.6)	429 (51.3)	38 (46.9)	541 (48.2)
Age group, y				
6–14	NA	65 (7.8)	NA	NA
15–24	NA	72 (8.6)	NA	NA
25–44	28 (32.9)	278 (33.2)	NA	NA
45–59	30 (35.3)	244 (29.2)	NA	NA
≥60	24 (28.2)	178 (21.3)	81 (100.0)	1,123 (100.0)
Race/ethnicity				
Non-Hispanic White	NA	55 (6.6)	17 (21.0)	495 (44.1)
Non-Hispanic Black/African American	NA	113 (13.5)	35 (43.2)	357 (31.8)
Hispanic/Mexican American	30 (35.3)	356 (42.5)	19 (23.5)	177 (15.8)
Non-Hispanic Asian	43 (50.6)	290 (34.6)	NA	55 (4.9)
Other	NA	23 (2.7)	NA	39 (3.5)
Poverty				
At or above poverty level	60 (70.6)	535 (63.9)	51 (63.0)	791 (70.4)
Below poverty level	NA	150 (17.9)	14 (17.3)	162 (14.4)
Unknown	NA	NA	16 (19.8)	170 (15.1)
Education level				
No high school diploma	32 (37.6)	312 (37.3)	26 (32.1)	230 (20.5)
High school graduate	17 (20.0)	133 (15.9)	23 (28.4)	300 (26.7)
Beyond high school	36 (42.4)	391 (46.7)	32 (39.5)	592 (52.7)
Unknown	NA	NA	0	NA
Birthplace				
Within United States	0	0	57 (70.4)	945 (84.1)
Outside United States	85 (100.0)	837 (100.0)	24 (29.6)	178 (15.9)
Time in the United States, y†				
<1	NA	29 (3.5)	NA	NA
1–4	NA	118 (14.1)	NA	6 (33.7)
≥5	67 (78.8)	653 (78.0)	20 (83.3)	162 (91.0)
Unknown	NA	37 (4.4)	NA	6 (33.7)

*NA, not available (data not collected for this subpopulation or not reported because cell size <5).
†Percentages were calculated using the numbers of persons born outside the United States as the denominator.

in the way participants were classified into US-born or non–US-born categories. For the 2019–2020 survey cycle, NHANES study participants were considered US-born if born in a state or the District of Columbia within the United States or in a US-affiliated territory; for the 2011–2012 study, participants born in a US-affiliated territory were considered non–US-born. Because country of birth is one of the most critical stratification factors for examining characteristics of LTBI, defining country of birth consistently will be essential in future NHANES survey cycles that include TB testing.

Conclusions

Although the 2019–2020 NHANES TB test results were not representative of the US population, study data still indicate that TB infection remains a critical health screening consideration among non–US-born persons and persons ≥60 years of age. Therefore, persons in these subpopulations should be prioritized for TB testing and, if TB infection is diagnosed, treated with an appropriate regimen to prevent progression to active TB disease (*14*,*15*). Furthermore, the likely disruption of testing and treatment of TB infection that occurred because of the COVID pandemic suggests we still have much to do if we are to eliminate TB in the United States (*1*).

Acknowledgments

We thank Wanjun Cui for her assistance.

About the Authors

Ms. Woodruff is a health scientist with the Division of Tuberculosis Elimination, National Center for HIV, Viral Hepatitis, STD, and TB Prevention, Centers for Disease Control and Prevention, Atlanta. She works on research and programmatic activities that support TB control and elimination in the United States. Mr. Miramontes is chief of the Data Management, Statistics and Evaluation Branch, Division of Tuberculosis Elimination, National Center for HIV, Viral Hepatitis, STD, and TB Prevention, Centers for Disease Control and Prevention, Atlanta.

References

1. Filardo TD, Feng PJ, Pratt RH, Price SF, Self JL. Tuberculosis—United States, 2021. MMWR Morb Mortal Wkly Rep. 2022;71:441–6. https://doi.org/10.15585/mmwr.mm7112a1
2. Viner K, Johnson CC, Newbern EC, Dickman B, Dettinger L, Waller K, et al.; Centers for Disease Control and Prevention. Assessment of declines in reported tuberculosis cases—Georgia and Pennsylvania, 2009. MMWR Morb Mortal Wkly Rep. 2011;60:338–42.
3. Winston CA, Navin TR, Becerra JE, Chen MP, Armstrong LR, Jeffries C, et al. Unexpected decline in tuberculosis cases coincident with economic recession—United States, 2009. BMC Public Health. 2011;11:846. https://doi.org/10.1186/1471-2458-11-846
4. Yelk Woodruff RS, Pratt RH, Armstrong LR. The US National Tuberculosis Surveillance System: a descriptive assessment of the completeness and consistency of data reported from 2008 to 2012. JMIR Public Health Surveill. 2015;1:e15 https://doi.org/10.2196/publichealth.4991
5. National Library of Medicine. MedlinePlus: reportable diseases [cited 2023 March 6] https://medlineplus.gov/ency/article/001929.htm
6. Engel A, Roberts J. Tuberculin skin test reaction among adults 25–74 years, United States, 1971–72. Vital Health Stat 11. 1977;204:1–40.
7. Bennett DE, Courval JM, Onorato I, Agerton T, Gibson JD, Lambert L, et al. Prevalence of tuberculosis infection in the United States population: the national health and nutrition examination survey, 1999–2000. Am J Respir Crit Care Med. 2008;177:348–55. https://doi.org/10.1164/rccm.200701-057OC
8. Miramontes R, Hill AN, Yelk Woodruff RS, Lambert LA, Navin TR, Castro KG, et al. Tuberculosis infection in the United States: prevalence estimates from the National Health and Nutrition Examination Survey, 2011–2012. PLoS One. 2015;10:e0140881. https://doi.org/10.1371/journal.pone.0140881
9. Akinbami LJ, Chen TC, Davy O, Ogden CL, Fink S, Clark J, et al. National Health and Nutrition Examination Survey, 2017–March 2020 prepandemic file: sample design, estimation, and analytic guidelines. Vital Health Stat. 2022;190:1–36.
10. Centers for Disease Control and Prevention. NHANES 2019–2020 overview [cited 2023 Feb 6]. https://wwwn.cdc.gov/nchs/nhanes/continuousnhanes/overview.aspx?BeginYear=2019
11. Yelk Woodruff R, Hill A, Marks S, Navin T, Miramontes R. Estimated latent tuberculosis infection prevalence and tuberculosis reactivation rates among non-US-born residents in the United States, from the 2011–2012 National Health and Nutrition Examination Survey. J Immigr Minor Health. 2021;23:806–12. https://doi.org/10.1007/s10903-020-01065-8
12. Centers for Disease Control and Prevention. 2019–March 2020 convenience sample limited access data. [cited 2023 Apr 25] https://wwwn.cdc.gov/nchs/nhanes/search/datapage.aspx?Component=LimitedAccess&CycleBeginYear=2019
13. National Center for Health Statistics Research Data Center. Disclosure manual—preventing disclosure: rules for researchers. 2019 [cited 2023 Feb 6] https://www.cdc.gov/rdc/data/b4/Disclosure-Manual-v2.3.pdf
14. Sterling TR, Njie G, Zenner D, Cohn DL, Reves R, Ahmed A, et al. Guidelines for the treatment of latent tuberculosis infection: recommendations from the National Tuberculosis Controllers Association and CDC, 2020. MMWR Recomm Rep. 2020;69(No. RR-1):1–11. https://doi.org/10.15585/mmwr.rr6901a1
15. Mangione CM, Barry MJ, Nicholson WK, Cabana M, Chelmow D, Coker TR, et al.; US Preventive Services Task Force. Screening for latent tuberculosis infection in adults: US Preventive Services Task Force recommendation statement. JAMA. 2023;329:1487–94. https://doi.org/10.1001/jama.2023.4899

Address for correspondence: Rachel Woodruff, Centers for Disease Control and Prevention, 1600 Clifton Road NE, Mailstop H24-4, Atlanta, GA 30329-4027, USA; email: zex5@cdc.gov

Extensively Drug-Resistant *Shigella flexneri* 2a, California, USA, 2022

J.R. Caldera, Shangxin Yang, Daniel Z. Uslan

Author affiliation: David Geffen School of Medicine at University of California, Los Angeles, California, USA

DOI: https://doi.org/10.3201/eid2907.230465

In Los Angeles, California, USA, persistent, refractory shigellosis was diagnosed in an immunocompetent man who has sex with men. Whole-genome sequencing augmented phenotypic antimicrobial susceptibility testing to comprehensively profile bacterial drug resistance and appropriately guide therapy and clear the infection.

Shigellosis is an infectious diarrheal illness traditionally associated with contaminated food and water (*1*). Recent reports, however, have indicated increased transmission through sexual activity, including direct (anal/oral sex) and indirect (use of contaminated objects such as sex toys) sexual contact (*2*). Several outbreaks of extensively drug-resistant (XDR) *Shigella* spp. among men who have sex with men (MSM) have been described (*3*–*5*).

Recently, the emergence of sexually transmitted XDR *Shigella flexneri* serotype 2a was reported among gay, bisexual, and other MSM in England (*4*). The study by the UK Health Security Agency characterized *S. flexneri* isolates harboring $bla_{\text{CTX-M-27}}$ and identified the 2 phylogenetically related clusters, each composed of isolates within 10 single-nucleotide polymorphisms (SNPs). Long-read sequencing elucidated the genomic location of the resistance determinant, and plasmid similarities with XDR *Shigella sonnei* from a current outbreak supported interspecies horizontal acquisition of drug resistance. Those findings underscore the substantial threat of mobilizable genetic elements and their role in propagating antimicrobial resistance (AMR). We describe a case of extensively drug-resistant *S. flexneri* infection in a 36-year-old man in California, USA.

The patient was an HIV-negative man who has sex with men and who had a history of shigellosis (*S. flexneri* type 1) 1.5 years earlier and mpox 4 months earlier. He sought hospital care for fever, abdominal pain, nonbloody watery diarrhea, and mild leukopenia. A fecal culture grew *S. flexneri* type 2, which was treated with ciprofloxacin for 4 days. Antimicrobial susceptibility testing (AST) was not requested. The patient's sign/symptoms and leukocyte count slowly improved, although he continued to have loose bowel movements with mucous. He was referred for outpatient infectious diseases consultation. At that time, the patient's history included frequent anonymous sexual encounters, typically including performing and receiving fellatio, analingus, and insertive anal intercourse; he stated he always wore condoms for intercourse but did not use barrier protection for fellatio or analingus. Testing for other sexually transmitted infections (including gonorrhea, chlamydia, HIV infection, and syphilis) produced negative results. Because his signs/symptoms were persistent, we sent repeat fecal samples to the UCLA Health Clinical Microbiology Laboratory for bacteria and parasites studies, including the BD Max Enteric Bacterial Panel PCR test (BD, https://www.bd.com), and results were again positive for *Shigella* spp. The patient elected to undergo observation only, and no additional treatment was provided.

Table. AST profile for extensively drug-resistant *Shigella flexneri* 2a isolate UCLA_1207, 2023, from patient in California, USA*

Drug	MIC, mcg/mL	Interpretation	Detected AMR gene
Amoxicillin + clavulanate	32	Resistant†	$bla_{\text{OXA-1}}$, $bla_{\text{CTX-M-15}}$
Ampicillin	>32	Resistant†	$bla_{\text{OXA-1}}$, $bla_{\text{CTX-M-15}}$
Azithromycin	32	Resistant	*mph(A)*
Cefazolin	>32	Resistant†	$bla_{\text{OXA-1}}$, $bla_{\text{CTX-M-15}}$
Cefepime	4	Susceptible, dose dependent†	$bla_{\text{CTX-M-15}}$
Ceftazidime	4	Susceptible[1]	$bla_{\text{CTX-M-15}}$
Ceftazidime/avibactam	≤2	Susceptible†	None
Ceftriaxone	64	Resistant†	$bla_{\text{CTX-M-15}}$
Ciprofloxacin	>4	Resistant	*qnrS1*, *gyrA* D87N+S83L
Doxycycline	>16	Resistant†	*tet(B)*
Ertapenem	≤0.25	Susceptible†	None
Imipenem	≤1	Susceptible†	None
Levofloxacin	>8	Resistant†	*qnrS1*, *gyrA* D87N+S83L
Meropenem	≤0.25	Susceptible†	None
Minocycline	4	Susceptible†	*tet(B)*
Piperacillin + tazobactam	≤8	Susceptible†	$bla_{\text{OXA-1}}$, $bla_{\text{CTX-M-15}}$
Trimethoprim/sulfamethoxazole	>4/80	Resistant	*dfrA17*, *sul1*
Fosfomycin	Not performed‡	Not performed‡	Not applicable

*AMR, antimicrobial resistance; AST, antimicrobial susceptibility testing.
†AST not initially included in primary report and performed and reported at physician request.
‡AST not performed because of lack of interpretive guidelines by the Clinical and Laboratory Standards Institute.

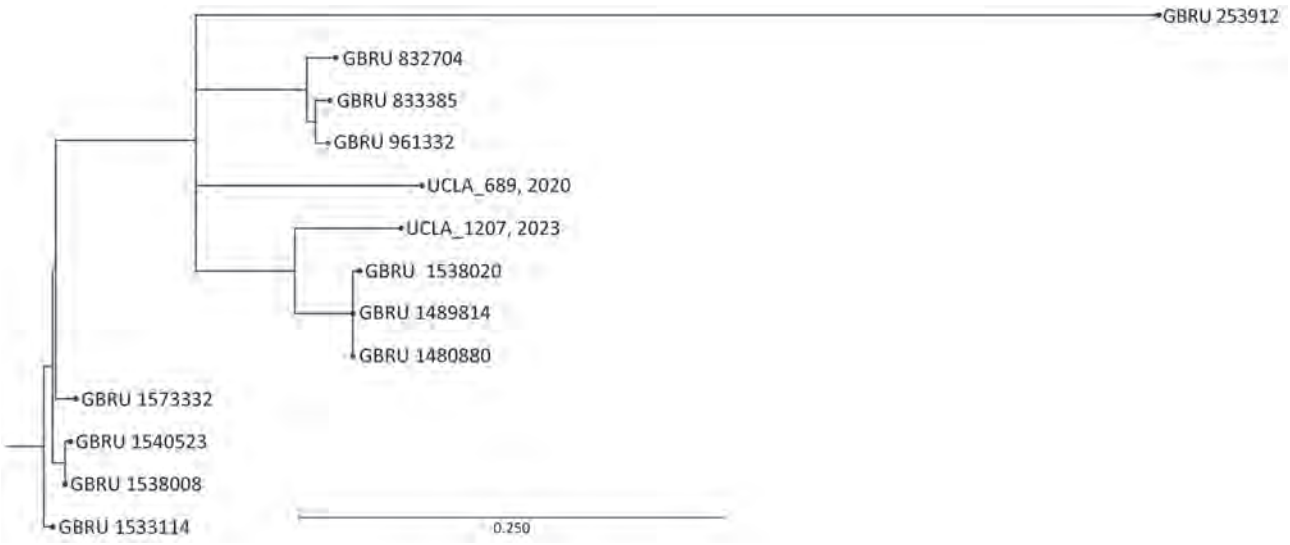

Figure. Maximum-likelihood single-nucleotide polymorphism tree of *Shigella flexneri* strain 2a isolates from California, USA (UCLA_689, 2020, and UCLA_1207, 2023), and the United Kingdom. Analysis was performed by using CLC Genomics Workbench version 22.0.2 (https://www.qiagen.com) single-nucleotide polymorphism analysis for microbial relatedness workflow and using reference strain *Shigella flexneri* 2a strain 981. GBRU, UK Gastrointestinal Bacterial Reference Unit; UCLA, University of California Los Angeles. Scale bar indicates nucleotide substitutions per 100 sites.

Subsequent fecal samples sent several weeks later were again positive for *S. flexneri*, and the Los Angeles County Public Health Laboratory serotyped the cultured isolate as 2a. AST of the most recent isolate identified extensive AMR (Table). The patient was asymptomatic at that time. Because of a lack of other oral antimicrobial options, on the basis of AST results we chose minocycline for initial treatment to avoid parenteral treatment and the associated risks, solely to reduce bacterial shedding.

Ultimately, inconsistencies in AST results together with concerns over the XDR phenotype prompted whole-genome sequencing (WGS) of the isolate with the Illumina MiSeq platform (Illumina, https://www.illumina.com). K-mer–based phylogenic analysis (KmerFinder version 3.2, https://cge.food.dtu.dk/services/KmerFinder) identified *S. flexneri* 2a strain 981 as the most closely related reference, with 99.70% genome coverage and 98.20% pairwise identity (*6*–*8*). We performed further SNP analysis for microbial relatedness against a previously sequenced multidrug-resistant *S. flexneri* 2a isolate (UCLA 2020, which did not carry a CTX-M gene) from man who has sex with men residing in Riverside, California, along with the publicly available sequences from the United Kingdom study, which were all serotype 2a with plasmid-borne $bla_{\text{CTX-M-27}}$ (*4*,*9*). Analysis revealed that the 2 California isolates are closely related to the UK *S. flexneri* strains, which contain <200 SNPs (Figure).

AMR gene analysis performed by using ResFinder version 4.0 (https://cge.food.dtu.dk/services/ResFinder) identified a compendium of AMR genes that not only corroborated the phenotypic AST results but also reconciled the ambiguous or discrepant categorical results within classes of antimicrobials (Table). Specifically, detection of $bla_{\text{CTX-M-15}}$ indicated that an extended-spectrum β-lactamase enzyme had been acquired and suggested resistance to all cephalosporins, which contrasts with the elevated, yet susceptible, MIC for ceftazidime and cefepime. Detection of *tet(B)* indicated that resistance to tetracyclines is not limited to doxycycline but also includes minocycline, again in contrast with the elevated, yet susceptible, MIC determined by AST. Moreover, the absence of detectable fosfomycin resistance–conferring gene(s) provided confidence that fosfomycin was appropriate for patient management.

Thus, with information from the WGS-based genomic characterization, we replaced minocycline treatment with fosfomycin (3 g by mouth every other day for 3 doses). Three weeks after completing treatment with fosfomycin, the patient's PCR result was negative, indicating clearance of *Shigella*.

In summary, persistent shigellosis caused by XDR *S. flexneri* was successfully treated with fosfomycin, as guided by WGS. Moreover, we demonstrate the genetic relatedness of 2 isolates from California to an ongoing outbreak in Europe, although with different CTX-M genes. This case illustrates the clinical value of WGS not only for providing a more comprehensive bacterial

drug resistance profile but also for tracking the global epidemiology of clinically important organisms.

Acknowledgment

We thank Naeemah Logan for her expertise and guidance.

About The Author

Dr. Caldera is a clinical microbiology fellow at the University of California, Los Angeles, California. His primary research interest focuses on the development of diagnostic assays that use advanced molecular and sequencing techniques in clinical microbiology.

References

1. National Institutes of Health, National Institute of Allergy and Infectious Diseases. *Shigellosis* [cited 2023 Mar 23]. https://www.niaid.nih.gov/diseases-conditions/shigellosis
2. Centers for Disease Control and Prevention. Shigella infection among gay, bisexual, and other men who have sex with men [cited 2023 Mar 24]. https://www.cdc.gov/shigella/msm.html
3. Charles H, Prochazka M, Thorley K, Crewdson A, Greig DR, Jenkins C, et al.; Outbreak Control Team. Outbreak of sexually transmitted, extensively drug-resistant *Shigella sonnei* in the UK, 2021–22: a descriptive epidemiological study. Lancet Infect Dis. 2022;22:1503–10. https://doi.org/10.1016/S1473-3099(22)00370-X
4. Thorley K, Charles H, Greig DR, Prochazka M, Mason LCE, Baker KS, et al. Emergence of extensively drug-resistant and multidrug-resistant *Shigella flexneri* serotype 2a associated with sexual transmission among gay, bisexual, and other men who have sex with men, in England: a descriptive epidemiological study. Lancet Infect Dis. 2023;S1473-3099(22)00807-6. https://doi.org/10.1016/S1473-3099 (22)00807-6
5. Lefèvre S, Njamkepo E, Feldman S, Ruckly C, Carle I, Lejay-Collin M, et al. Rapid emergence of extensively drug-resistant *Shigella sonnei* in France. Nat Commun. 2023;14:462. https://doi.org/10.1038/s41467-023-36222-8
6. Hasman H, Saputra D, Sicheritz-Ponten T, Lund O, Svendsen CA, Frimodt-Møller N, et al. Rapid whole-genome sequencing for detection and characterization of microorganisms directly from clinical samples. J Clin Microbiol. 2014;52:139–46. https://doi.org/10.1128/JCM.02452-13
7. Larsen MV, Cosentino S, Lukjancenko O, Saputra D, Rasmussen S, Hasman H, et al. Benchmarking of methods for genomic taxonomy. J Clin Microbiol. 2014;52:1529–39. https://doi.org/10.1128/JCM.02981-13
8. Clausen PTLC, Aarestrup FM, Lund O. Rapid and precise alignment of raw reads against redundant databases with KMA. BMC Bioinformatics. 2018;19:307. https://doi.org/10.1186/s12859-018-2336-6
9. Kamau E, Adamson PC, Crandall J, Mukhopadhyay R, Yang S. Discovery of a novel sub-lineage of multi-drug resistant *Shigella flexneri* in southern California. Int J Infect Dis. 2023;132:1–3. https://doi.org/10.1016/j.ijid.2023.03.039

Address for correspondence: Daniel Z. Uslan, UCLA Division of Infectious Diseases, David Geffen School of Medicine at UCLA, Ste 301, 911 Broxton Ave, Los Angeles, CA 90024, USA; email: duslan@mednet.ucla.edu

Novel Highly Pathogenic Avian Influenza A(H5N1) Clade 2.3.4.4b Virus in Wild Birds, South Korea

Sun-hak Lee, Andrew Y. Cho, Tae-hyeon Kim, Seo-jeong Ahn, Ju Ho Song, Heesu Lee, Yun-Jeong Choi, Nyamsuren Otgontogtokh, Jung-Hoon Kwon, Chang-Seon Song, Dong-Hun Lee

Author affiliations: Konkuk University, Seoul, South Korea (S.-h. Lee, A.Y. Cho, T.-h. Kim, S.-j. Ahn, J.H. Song, H. Lee, Y.-J. Choi, N. Otgontogtokh, C.-S. Song, D.-H. Lee); Kyungpook National University, Daegu, South Korea (J.-H. Kwon)

DOI: https://doi.org/10.3201/eid2907.221893

We isolated 5 highly pathogenic avian influenza A(H5N1) clade 2.3.4.4.b viruses from wild waterfowl feces in South Korea during November 2022. Whole-genome sequencing and phylogenetic analysis revealed novel genotypes produced by reassortment with Eurasian low pathogenicity avian influenza viruses. Enhanced surveillance will be required to improve prevention and control strategies.

Highly pathogenic avian influenza viruses (HPAIVs) have caused major economic losses in the poultry industry and are a major threat to public health. Since the first detection of HPAIV A(H5N1) from a goose in 1996 in Guangdong, China, its descendants have evolved into multiple hemagglutinin (HA) gene-specific clades (H0–H9) and subclades (*1*) causing intercontinental epizootics (*2*). Over several decades, H5 HPAIVs have evolved into multiple subtypes and genotypes generated by reassortment with low pathogenicity avian influenza viruses (LPAIVs), which led to emergence of clade 2.3.4.4 H5Nx HPAIVs in eastern China during 2013–2014 (*3*).

In mid-2016, reassortant H5N8 clade 2.3.4.4b HPAIVs that contained internal genes of LPAIVs from Eurasia were detected in wild birds at Uvs-Nuur Lake in Russia and Qinghai Lake in China (*4*); the viruses caused large outbreaks in Europe during 2016–2017 (*5*). Subsequently, various novel reassortant H5N8 HPAIVs were detected in Eurasia (*5*,*6*). In late 2020, novel reassortant clade 2.3.4.4b H5N1 HPAIVs were detected and became predominant in Europe in poultry and wild birds (*5*).

We isolated 5 H5N1 HPAIVs from wild bird feces collected in South Korea in November 2022 (Appendix 1, https://wwwnc.cdc.gov/EID/

Table 1. Nucleotide sequence identities between gene segments of 5 novel clade 2.3.4.4b highly pathogenic avian influenza A(H5N1) viruses from wild birds in South Korea and nearest homologs in the GISAID Epiflu database*

Isolates	Gene	Virus	Accession no.†	% Identity
All 5 isolates	PB2	A/goose/Hunan/SE284/2022(H5N1)/HPAI	EPI2029895	99.21%
		A/duck/Mongolia/826/2019 (H4N6)/LPAI	EPI1777578	98.33%
	HA	A/turkey/Tyumen/81-96V/2021 (H5N1)/HPAI	EPI1958105	99.47%
		A/chicken/Tyumen/47-79V/2021 (H5N1)/HPAI	EPI1957985	99.41%
	NA	A/goose/Hunan/SE284/2022 (H5N1)/HPAI	EPI2029897	99.22%
		A/duck/Bangladesh/51600/2021 (H5N1)/HPAI	EPI2163444	99.15%
	M	A/ibis/Egypt/RLQP-229S/2022 (H5N1)/HPAI	EPI2201158	99.80%
		A/duck/Bangladesh/19D1817/2021 (H5N1)/HPAI	EPI2062119	99.80%
K22-730-1, K22-742, K22-856-2, K22-862-1‡	PB1	A/Mallard/South Korea/KNU2019-20/2019 (H5N1)/LPAI	EPI1902594	98.77%
		A/duck/Saga/411117/2013 (H6N1)/LPAI	EPI855573	98.72%
	PA	A/duck/Bangladesh/18D1811/2022 (H5N3)/LPAI	EPI1997269	99.44%
		A/duck/Bangladesh/17D1839/2022 (H5N3)/LPAI	EPI1997245	99.44%
	NP	A/Northern Shoveler/South Korea/KNU2021-13/2021 (H11N9)/LPAI	EPI2153438	99.40%
		A/Mallard/South Korea/KNU2019-51/2019 (H5N3)/LPAI	EPI1902887	99.33%
	NS	A/mallard/Yakutia/47/2020 (H7N7)/LPAI	EPI1848197	99.52%
		A/Wild duck/South Korea/KNU2020-31/2020 (H1N1)/LPAI	EPI1931606	99.40%
K22-920§	PB1	A/mallard/Anhui/3-617/2019 (H6N1)/LPAI	EPI1743666	98.46%
		A/Eurasian_Curlew/China/CZ322(7)/2019 (H3N8)/LPAI	EPI1890551	98.46%
	PA	A/common teal/Amur region/92b/2020 (H6N2)/LPAI	EPI1849993	99.26%
		A/mallard/Russia Primorje/94T/2020 (H1N1)/LPAI	EPI1849961	99.21%
	NP	A/Spot-billed duck/South Korea/KNU2020-105/2020 (H3N2)/LPAI	EPI1931651	99.33%
		A/Eurasian teal/South Korea/JB32-15/2019 (H10N7)/LPAI	EPI1903752	98.80%
	NS	A/mallard/Yakutia/47/2020 (H7N7)/LPAI	EPI1848197	99.28%
		A/duck/Bangladesh/39397/2019 (H10N3)/LPAI	EPI1778261	99.28%

*HPAI influenza viruses isolated from wild bird feces in November 2022. HA, hemagglutinin; HPAI, highly pathogenic avian influenza; LPAI, low pathogenicity avian influenza; M, matrix protein; NP, nucleoprotein; NS, nonstructural; PA, polymerase acidic; PB, polymerase basic.
†Accession numbers of nearest homologs as of December 8, 2022, from GISAID (https://www.gisaid.org).
‡Genotype I.
§Genotype II.

article/29/7/22-1893-App1.pdf): A/Spot-billed_duck/Korea/K22-730-1/2022(H5N1) [K22-730-1],A/Wild_bird/Korea/K22-742/2022(H5N1) [K22-742], A/Spot-billed_duck/Korea/K22-856-2/2022(H5N1) [K22-856-2], A/Spot-billed_duck/Korea/K22-862-1/2022(H5N1)[K22-862-1],and A/Spot-billed_duck/Korea/K22-920/2022(H5N1) [K22-920] (Appendix 1 Table 1). To rapidly share the information, we conducted whole-genome sequencing of the isolates and deposited the genome sequences in the GISAID database (https://www.gisaid.org).

All H5N1 isolates were classified as HPAIV on the basis of HA cleavage site amino acid sequences (PLRPKRRKR/G). The 5 isolates shared high nucleotide sequence identities (99.4% to ≈100%) across all 8 influenza genes, except for the K22-920 isolate polymerase basic protein 1 (PB1), polymerase acidic protein (PA), nucleoprotein (NP), and nonstructural (NS) genes (93.0% to ≈99.0%). BLAST (https://blast.ncbi.nlm.nih.gov) search results showed HA, neuraminidase, and matrix (M) protein genes of all isolates had >99.1% identities with 2021–2022 clade 2.3.4.4b HPAIVs (Table 1). PB1, PA, NP, and NS genes of all isolates were highly similar (98.72%–99.52%) to 2019–2022 LPAIVs from East Asia. PB1, PA, NP, and NS genes of K22-920 were similar to 2019–2020 LPAIVs from South Korea, Russia, and Bangladesh (>98.4%–99.3%).

In maximum-likelihood phylogenetic analyses, PB2, HA, neuraminidase, and M genes of the 5 H5N1 viruses from South Korea clustered with those of viruses previously described as genotype G10, identified in China during 2022–2023 (Appendix 1 Figures 1–8); G10 is a natural reassortant H5N1 HPAIV containing the PB2 gene from LPAIVs (*7*). PB1, PA, NP, and NS genes of all H5N1 viruses from South Korea except K22-920 clustered with those of LPAIVs from Asia; those gene segments in K22-920 clustered separately with other LPAIVs from Asia, including South Korea, Russia, and Bangladesh (Appendix 1 Figures 2, 3, 5, 8). Bayesian phylogeny of the HA gene indicated the H5N1 viruses from South Korea formed a well-supported cluster; time to most recent common ancestor was estimated to be August 11, 2022 (95% highest posterior density June 11–October 11, 2022), suggesting those H5N1 HPAIVs most likely emerged 1–2 months before the autumn wild bird migration to South Korea (Figure 1; Appendix 1 Figure 9). The isolates from South Korea shared recent common ancestry with the A/Jiangsu/NJ210/2023(H5N1) virus; time to most recent common ancestor between them was April 12, 2022 (95% highest posterior density December 26, 2021–July 28, 2022), suggesting the ancestral H5N1 HPAIVs had been circulating undetected for ≈7 months.

The H5N1 HPAIVs from South Korea contained amino acids in HA with binding affinity for avian α-2,3-linked sialic acid receptors (T118, V210, Q222, and G224) (H5 numbering) (*8*,*9*). They also had 2 HA amino acid substitutions, S113A and T156A, associated with increased binding affinity to human α-2,6-

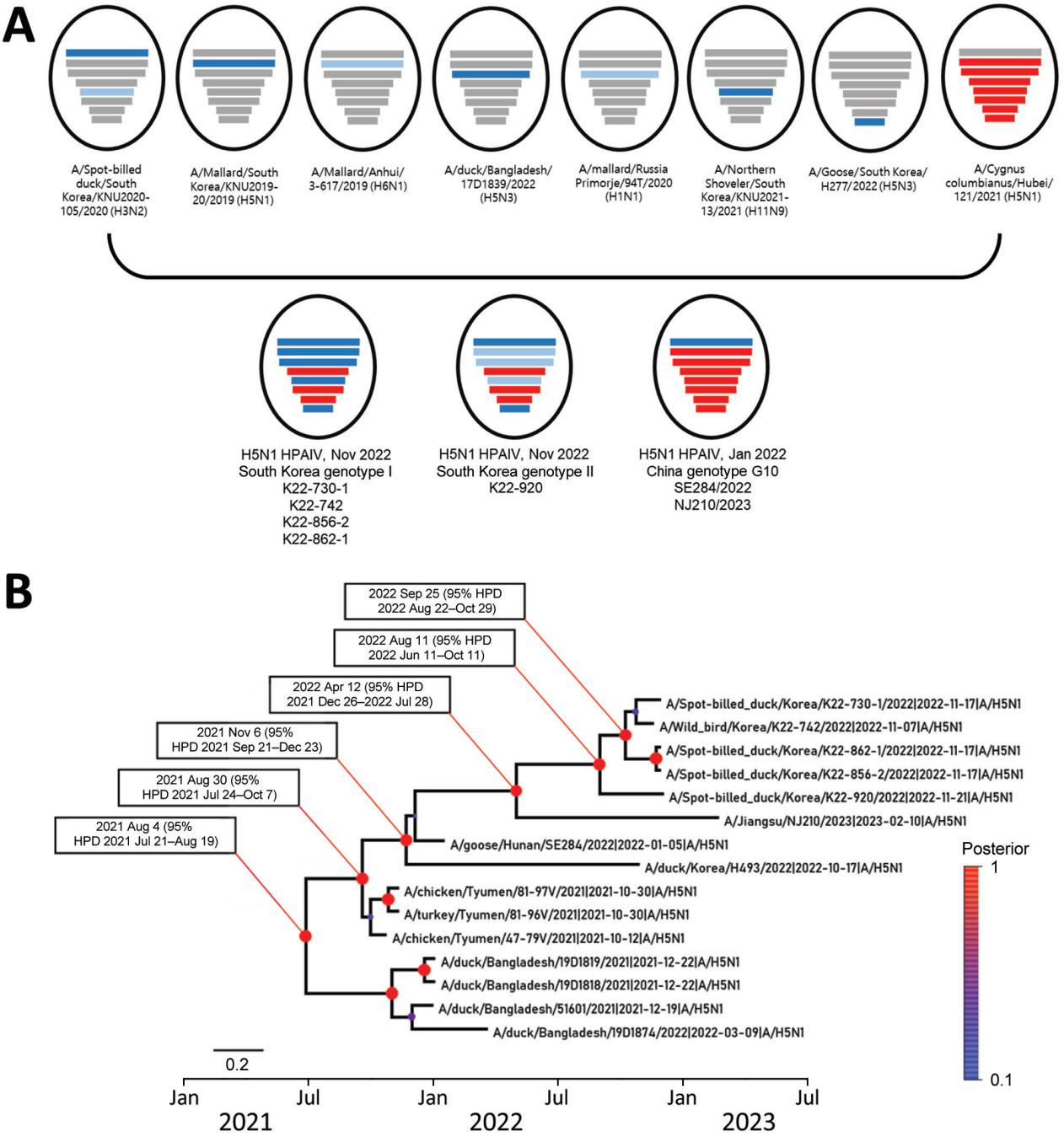

Figure 1. Phylogenetic analysis of novel highly pathogenic avian influenza A(H5N1) clade 2.3.4.4b viruses found in wild bird feces in South Korea, November 2022. A) Schematic representation of origin of virus isolates from South Korea compared with genotype G10 viruses found in China. Bars represent 8 gene segments of avian influenza virus in the following order (top to bottom): polymerase basic 2, polymerase basic 1, polymerase acidic, hemagglutinin, nucleoprotein, neuraminidase, matrix, and nonstructural. Different bar colors indicate different virus origins estimated from maximum-likelihood phylogenetic trees. Gene segments originating from highly pathogenic avian influenza viruses are indicated by red bars. Gene segments originating from low pathogenicity avian influenza viruses are indicated by blue bars. B) Time-scaled maximum clade credibility tree for hemagglutinin gene segments from novel viruses isolated in South Korea (5 viruses at top). Red to blue colored scale on right side indicates posterior clade probabilities at nodes. Scale bar indicates nucleotide substitutions per site. HPD, highest posterior density.

linked sialic acid receptors (Appendix 1 Table 2). All 5 isolates had amino acid substitutions that included A515T in PA, known to increase polymerase activity in mammal cells, and N30D, I43M, T215A in MP1 and L89V in PB2, known to increase virulence in mice (Appendix 1 Tables 2, 3).

The HPAI/LPAI reassortment of H5Nx clade 2.3.4.4b HPAIVs created a diverse genetic pool of H5 clade 2.3.4.4 viruses that continuously emerged in various countries (*1*). Clade 2.3.4.4 H5N8 HPAIV isolated from Uvs-Nuur Lake in Russia had reassorted H3N8 LPAIV genes from Mongolia (*4*). In Europe, HPAIVs identified in 2020 (*5*,*6*) were produced by reassortment between clade 2.3.4.4b HPAIV and LPAIVs from Eurasia. Novel reassortments of clade 2.3.4.4 HPAIV and LPAIVs from Eurasia were also detected in 2016 (*10*), during 2020–2021 (Appendix 1 reference *1*), and in late 2021 (Appendix 1 reference *2*) in South Korea. Considering the continuous emergence and global dissemination of novel reassortant clade 2.3.4.4b HPAI H5Nx viruses, enhanced active surveillance in wild animals and domestic poultry will be required to monitor the introduction, dissemination, and evolution of HPAIVs and provide insight for improved prevention and control strategies.

Acknowledgments

We thank our colleagues worldwide for their laboratory contributions, which are made available through GISAID (Appendix 2, https://wwwnc.cdc.gov/EID/article/29/7/22-1893-App2.xlsx).

This research was supported by the Bio and Medical Technology Development Program of the National Research Foundation, funded by the government of South Korea (grant no. NRF-2018M3A9H405635, and by the National Institute of Wildlife Disease Control and Prevention, South Korea (grant no. 2022-007)..

About the Author

Mr. Lee is a PhD candidate at Konkuk University, Seoul, South Korea. His primary research interests focus on molecular epidemiology and host–pathogen interactions of avian influenza viruses.

References

1. Gu M, Liu W, Cao Y, Peng D, Wang X, Wan H, et al. Novel reassortant highly pathogenic avian influenza (H5N5) viruses in domestic ducks, China. Emerg Infect Dis. 2011;17:1060–3. https://doi.org/10.3201/eid/1706.101406
2. Lee DH, Criado MF, Swayne DE. Pathobiological origins and evolutionary history of highly pathogenic avian influenza viruses. Cold Spring Harb Perspect Med. 2021;11:a038679. https://doi.org/10.1101/cshperspect.a038679
3. Lee Y-J, Kang H-M, Lee E-K, Song B-M, Jeong J, Kwon Y-K, et al. Novel reassortant influenza A(H5N8) viruses, South Korea, 2014. Emerg Infect Dis. 2014;20:1087–9. https://doi.org/10.3201/eid2006.140233
4. Lee DH, Sharshov K, Swayne DE, Kurskaya O, Sobolev I, Kabilov M, et al. Novel reassortant clade 2.3.4.4 avian influenza A(H5N8) virus in wild aquatic birds, Russia, 2016. Emerg Infect Dis. 2017;23:359–60. https://doi.org/10.3201/eid2302.161252
5. Pohlmann A, King J, Fusaro A, Zecchin B, Banyard AC, Brown IH, et al. Has epizootic become enzootic? Evidence for a fundamental change in the infection dynamics of highly pathogenic avian influenza in Europe, 2021. mBio. 2022;13:e0060922. https://doi.org/10.1128/mbio.00609-22
6. Lewis NS, Banyard AC, Whittard E, Karibayev T, Al Kafagi T, Chvala I, et al. Emergence and spread of novel H5N8, H5N5 and H5N1 clade 2.3.4.4 highly pathogenic avian influenza in 2020. Emerg Microbes Infect. 2021;10:148–51. https://doi.org/10.1080/22221751.2021.1872355
7. Cui P, Shi J, Wang C, Zhang Y, Xing X, Kong H, et al. Global dissemination of H5N1 influenza viruses bearing the clade 2.3.4.4b HA gene and biologic analysis of the ones detected in China. Emerg Microbes Infect. 2022;11:1693–704. https://doi.org/10.1080/22221751.2022.2088407
8. Burke DF, Smith DJ. A recommended numbering scheme for influenza A HA subtypes. PLoS One. 2014;9:e112302. https://doi.org/10.1371/journal.pone.0112302
9. Suttie A, Deng YM, Greenhill AR, Dussart P, Horwood PF, Karlsson EA. Inventory of molecular markers affecting biological characteristics of avian influenza A viruses. Virus Genes. 2019;55:739–68. https://doi.org/10.1007/s11262-019-01700-z
10. Kwon JH, Lee DH, Swayne DE, Noh JY, Yuk SS, Erdene-Ochir TO, et al. Reassortant clade 2.3.4.4 avian influenza A(H5N6) virus in a wild mandarin duck, South Korea, 2016. Emerg Infect Dis. 2017;23:822–6. https://doi.org/10.3201/eid2305.161905

Address for correspondence: Dong-Hun Lee, Wildlife Health Laboratory, College of Veterinary Medicine, Konkuk University, Seoul, South Korea; email: donghunlee@konkuk.ac.kr

Long-Term SARS-CoV-2 Antibody Seroprevalence in Blood Donors, Italy

Martina Ferrari, Lorenza Di Marco, Alessandra Pivetti, Stefania Paduano, Chiara Vecchi, Veronica Bernabucci, Rosina Maria Critelli, Simone Lasagni, Monica De Maria, Donatella Venturelli, Monica Pecorari, Giorgia Boaretto, Giulia Fregni Serpini, Dante Romagnoli, Roberto Mantovani, Giovanni Battista Ceccherelli, Erica Villa

Author affiliations: University of Modena and Reggio Emilia and Azienda Ospedaliero-Universitaria di Modena, Modena, Italy (M. Ferrari, L. Di Marco, A. Pivetti, V. Bernabucci, R.M. Critelli, S. Lasagni, E. Villa); Clinical and Experimental Medicine PhD Program, University of Modena and Reggio Emilia, Modena (L. Di Marco, S. Lasagni); University of Modena and Reggio Emilia Modena (S. Paduano); Azienda Ospedaliero-Universitaria di Modena, Modena (C. Vecchi, M. De Maria, D. Venturelli, M. Pecorari, G. Boaretto, G.F. Serpini, D. Romagnoli, G.B. Ceccherelli); Associazione Italiana Volontari Sangue, Modena (R. Mantovani)

DOI: https://doi.org/10.3201/eid2907.221745

We evaluated SARS-CoV-2 antibody response in voluntary blood donors in Italy at different timepoints. Immediately after lockdown easing, 908/25,657 donors (3.5%) had low IgG titers against nucleocapsid. In the next 2 years, titers increased despite few COVID-19 symptoms. On multivariate analysis, allergic rhinitis was associated with reduced risk for symptomatic COVID-19.

Antibodies against different viral epitopes develop in persons infected with SARS-CoV-2 (*1*,*2*). We evaluated SARS-CoV-2 antibody levels and types in a voluntary blood donor (VBD) population in Modena, Italy, at different timepoints from the beginning of the COVID-19 pandemic and examined the effects of clinical and biologic factors, including natural and vaccine-associated SARS-CoV-2 antibody presence, on antibody development and clinical outcomes.

During July–December 2020, a total of 908/25,657 (3.5%) sequential VBDs whose donations were positive for SARS-CoV-2 nucleocapsid IgG were referred to our hospital for clinical evaluation and oronasopharyngeal molecular swab testing. All but 4 (0.4%) were negative for spike IgM. We repeated serologic and swab testing in the same donors after 3 months and 22 months (Figure; Appendix Table 1, https://wwwnc.cdc.gov/EID/article/29/7/22-1745-App1.pdf). Apart from rhinitis (n = 68, 7.5%), obesity (n = 60, 6.6%), and hypertension (n = 98, 10.8%, all in patients taking angiotensin-converting enzyme [ACE] inhibitors), the VBDs were healthy. Symptomatic COVID-19 infection occurred in 9 (9.1%) ACE users and 221 (31.0%) non–ACE users ($p<0.001$ by χ^2 test).

Of the 908 VBDs, 208 (22.9%) reported histories of symptomatic COVID-19 infection in the 3 months before their donation. Apart from fever (5.2%) and asthenia (2.4%), signs and symptoms at initial, 3-month, and 22-month follow-up assessments were minor. Of the 908 VBDs who tested positive for nucleocapsid SARS-CoV-2 IgG at baseline, 27 (2.9%) were also positive by oronasopharyngeal swab test. When tested again 3 months later, 33/908 (3.6%) had a positive oronasopharyngeal swab test. One VBD was positive on both occasions. Very low viral load prevented SARS-CoV-2 subtype lineage identification. No VBD required hospitalization during the study period. Most VBDs received SARS-CoV-2 vaccines beginning in February 2021; 54 (5.9%) did not. Vaccinated VBDs had significantly lower titers of nucleocapsid IgG and significantly higher titers of IgG against the spike protein receptor binding domain and of neutralizing antibodies, compared with the unvaccinated VBDs (Appendix Figure 1).

Titers of SARS-CoV-2 antibody types within vaccinated or unvaccinated VBDs in 2022 were not related to VBDs' prevaccination histories of symptomatic COVID-19. Titer of antibodies against the nucleocapsid was significantly higher in symptomatic cases compared with those who were not symptomatic in 2022; this observation was consistent in both vaccinated and unvaccinated donors ($p<0.001$ by t-test) (Appendix Table 3). Logistic regression revealed that allergic rhinitis was associated independently with a reduced risk for symptomatic COVID-19 (Table).

This 2-year prospective study showed that SARS-CoV-2 seroprevalence in VBDs is a reliable indicator of the epidemiologic situation in the general population. The very low initial percentage (3.5%) of VBDs with SARS-CoV-2 nucleocapsid antibodies mirrored that in the general population in the same province (2.5%) (*3*); the percentage of antibodies was an indicator of natural infection. Nucleocapsid IgG levels were significantly higher (5%–6.4%) in VBDs in nearby regions tested 3 months earlier than ours, reflecting much greater SARS-CoV-2 exposure because of a relaxed containment policy. The policy implemented in the study area was extremely strict, resulting in almost no hospital admission for COVID-19 by the end of the lockdown period (*4*,*5*). In

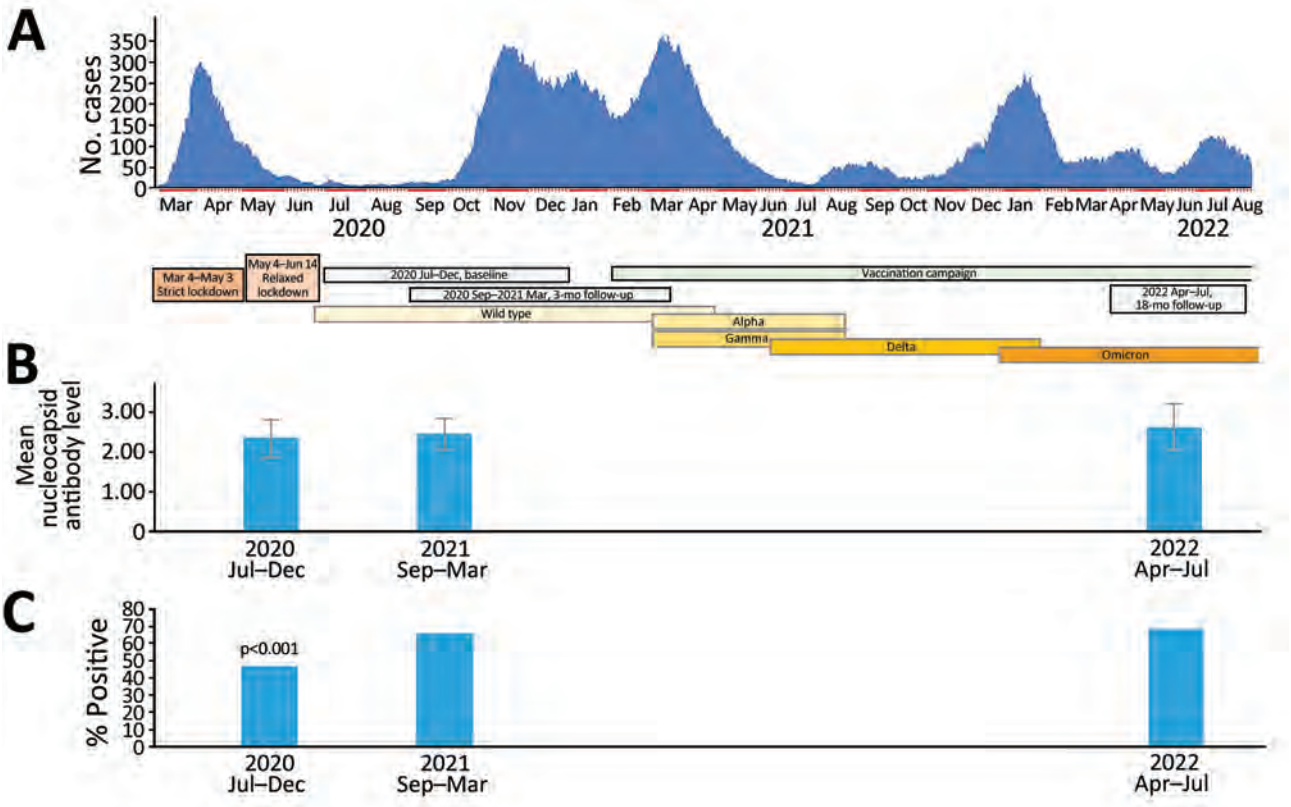

Figure. Study timepoints plotted against hospital admissions for COVID-19 in study of SARS-CoV-2 seroprevalence among voluntary blood donors in Modena, Italy. A) After the first wave of COVID-19 in March 2020–April 2020, which followed 2-month strict and 1-month relaxed lockdown periods, a 4-month period (June 2020–September 2020) of almost no hospital admissions associated with low (3.5%) SARS-CoV-2 antibody seroprevalence ensued. Thereafter, a sequence of intercurrent waves occurred with only a very short period of few admissions in July 2021. Titers of antibodies against the virus nucleocapsid (tested in the same donors at baseline and after 3 and 22 months) increased throughout the observation period although not significantly. Colored horizontal bars indicate prevalent variants throughout the observation periods. B) Mean antibody titers against nucleocapsid among strongly positive donors were significantly higher at the 2nd and 3rd testing points compared with baseline. Error bars indicate standard deviation. C) Percentages of donors with strongly positive antibody response against the nucleocapsid, tested on the whole cohort. p value indicates the comparison of percentages at 2nd and 3rd testing points to percentage at baseline.

towns in the study area close to the Lombardy border, 7.8%–18.8% of the general population carried SARS-CoV-2 antibodies (*6*). Given the extremely strict lockdown policy, however, the general population had marginal immunity against SARS-CoV-2, despite good titers in persons testing positive. The infection rate rose with the easing of lockdown, creating an 8-month-long emergency situation for

Table. Factors associated with the risk of severe COVID-19 development in blood donors, Italy*

	Univariate analysis		Multivariate analysis	
Variable	OR (95% CI)	p value	OR (95% CI)	p value
Age	0.985 (0.973–0.996)	**0.008**	0.984 (0.964–1.005)	0.135
Sex	1.047 (0.755–1.453)	0.783		
Body mass index	1.001 (1.000–1.002)	0.178		
Smoking	0.498 (0.193–1.287)	0.150		
Concurrent conditions	0.600 (0.299–1.205)	0.151		
Allergic rhinitis	0.180 (0.043–0.757)	**0.019**	0.170 (0.40-0.719)	**0.016**
ACE inhibitor use	0.181 (0.089–0.365)	**<0.011**	1.036 (0.452–2.373)	0.933
Chronic therapies	0.793 (0.392–1.602)	0.517		
Influenza vaccination	0.678 (0.276–1.666)	0.397		
Family case of SARS-CoV-2 infection	0.938 (0.407–2.159)	0.880		
Education level	1.248 (0.824–1.892)	0.296		
Municipality of residence	1.011 (0.996–1.027)	0.134		

*Bold text indicates significance. ACE, angiotensin-converting enzyme.

hospitals. The observed stable elevation of titers of antibodies against the nucleocapsid and other epitopes, independent of vaccination, suggests equivalent elevation of viral circulation, as described previously (*7*,*8*), although vaccination reduced COVID-19's clinical severity and lethality.

SARS-CoV-2 infection symptoms in this large VBD cohort were mild, consistent with previous findings (*9*). Univariate analysis indicated that the VBDs' young median age and good health (active, with few concurrent conditions) likely contributed to that outcome. The association of allergic rhinitis with a reduced risk for symptomatic COVID-19 could be linked with the reduction of ACE2 receptors in the epithelial cells of inflamed airways of affected VBDs; we could not rule out a connection between treatment for rhinitis and COVID-19 (*10*).

A limitation of the study is the lack of information on the exact timing of the primary infection; symptoms of COVID-19 were rare, and antibodies against nucleocapsid, which have higher waning than those against the spike protein, were less valuable as indicators of infection. However, the results of this long-term follow-up of the VBD population before and after SARS-CoV-2 vaccination offers an interesting perspective of the epidemiologic events associated with SARS-CoV-2 infection, especially the paradoxical effect of strict lockdown.

This study was supported by a grant from Regione Emilia-Romagna–Bankitalia.

About the Author

Dr. Ferrari has a medicine degree from the University of Modena and Reggio Emilia and is currently a resident physician in geriatrics at Azienda Ospedaliero–Universitaria of Modena. During her university career, she developed an active interest in epidemiologic research, mostly in the field of SARS-CoV-2 infection.

References

1. Burbelo PD, Riedo FX, Morishima C, Rawlings S, Smith D, Das S, et al. Sensitivity in detection of antibodies to nucleocapsid and spike proteins of severe acute respiratory syndrome coronavirus 2 in patients with coronavirus disease 2019. J Infect Dis. 2020:206–13. https://doi.org/10.1093/infdis/jiaa273
2. Schöler L, Le-Trilling VTK, Eilbrecht M, Mennerich D, Anastasiou OE, Krawczyk A, et al. A novel in-cell ELISA Assay allows rapid and automated quantification of SARS-CoV-2 to analyze neutralizing antibodies and antiviral compounds. Front Immunol. 2020;11:573526. https://doi.org/10.3389/fimmu.2020.573526
3. Paduano S, Galante P, Berselli N, Ugolotti L, Modenese A, Poggi A, et al. Seroprevalence survey of anti-SARS-CoV-2 antibodies in a population of Emilia-Romagna region, northern Italy. Int J Environ Res Public Health. 2022;19:7882. https://doi.org/10.3390/ijerph19137882
4. Valenti L, Pelusi S, Cherubini A, Bianco C, Ronzoni L, Uceda Renteria S, et al. Trends and risk factors of SARS-CoV-2 infection in asymptomatic blood donors. Transfusion. 2021;61:3381–9. https://doi.org/10.1111/trf.16693
5. Antonucci F, Fiore JR, De Feo L, Granato T, Di Stefano M, Faleo G, et al. Increased SARS-CoV-2 seroprevalence in healthy blood donors after the second pandemic wave in South-Eastern Italy: evidence for asymptomatic young donors as potential virus spreaders. Infect Dis (Lond). 2022; 54:241–6. https://doi.org/10.1080/23744235.2021.2003856
6. Berselli N, Filippini T, Paduano S, Malavolti M, Modenese A, Gobba F, et al. Seroprevalence of anti-SARS-CoV-2 antibodies in the Northern Italy population before the COVID-19 second wave. Int J Occup Med Environ Health. 2022;35:63–74. https://doi.org/10.13075/ijomeh.1896.01826
7. Alzaabi AH, Ahmed LA, Rabooy AE, Zaabi AA, Alkaabi M, AlMahmoud F, et al. Longitudinal changes in IgG levels among COVID-19 recovered patients: a prospective cohort study. PLoS One. 2021;16:e0251159. https://doi.org/10.1371/journal.pone.0251159
8. Al-Naamani K, Al-Jahdhami I, Al-Tamtami W, Al-Amri K, Al-Khabori M, Sinani SA, et al. Prevalence and persistence of SARS-CoV2 antibodies among healthcare workers in Oman. J Infect Public Health. 2021;14:1578–84. https://doi.org/10.1016/j.jiph.2021.09.006
9. Kaspersen KA, Hindhede L, Boldsen JK, Mikkelsen S, Vestergaard LS, Berthelsen AN, et al. Estimation of SARS-CoV-2 infection fatality rate by age and comorbidity status using antibody screening of blood donors during the COVID-19 epidemic in Denmark. J Infect Dis. 2022;225:219–28. https://doi.org/10.1093/infdis/jiab566
10. Wakabayashi M, Pawankar R, Narazaki H, Ueda T, Itabashi T. Coronavirus disease 2019 and asthma, allergic rhinitis: molecular mechanisms and host-environmental interactions. Curr Opin Allergy Clin Immunol. 2021;21:1–7. https://doi.org/10.1097/ACI.0000000000000699

Address for correspondence: Erica Villa, CHIMOMO Department, University of Modena & Reggio Emilia, Via del Pozzo 71, Modena, 41121, Italy; email: erica.villa@unimore.it

Reemergence of Dengue Virus Serotype 3, Brazil, 2023

Felipe Gomes Naveca,[1] Gilberto A. Santiago,[1] Rodrigo Melo Maito, Cátia Alexandra Ribeiro Meneses, Valdinete Alves do Nascimento, Victor Costa de Souza, Fernanda Oliveira do Nascimento, Dejanane Silva, Matilde Mejía, Luciana Gonçalves, Regina Maria Pinto de Figueiredo, Ana Cecília Ribeiro Cruz, Bruno Tardelli Diniz Nunes, Mayra Marinho Presibella, Nelson Fernando Quallio Marques, Irina Nastassja Riediger, Marcos César Lima de Mendonça, Fernanda de Bruycker-Nogueira, Patricia C Sequeira, Ana Maria Bispo de Filippis, Paola Resende, Tulio Campos, Gabriel Luz Wallau, Tiago Gräf, Edson Delatorre, Edgar Kopp, Andrea Morrison, Jorge L. Muñoz-Jordán,[2] Gonzalo Bello[2]

Author affiliations: Fundação Oswaldo Cruz, Rio de Janeiro, Brazil (F.G. Naveca, M.C.L. Mendonça, F. de Bruycker-Nogueira, P.C. Sequeira, A.M.B. de Filippis, P. Resende, G. Bello); Centers for Disease Control and Prevention, San Juan, Puerto Rico, USA (G.A. Santiago, J.L. Muñoz-Jordán); Laboratório Central de Saúde Pública de Roraima, Boa Vista, Brazil (R.M. Maito, C.A.R. Meneses); Fundação Oswaldo Cruz, Manaus, Brazil (F.G. Naveca, V.A. Nascimento, V.C. Souza, F.O. do Nascimento, D. Silva, M. Mejía); Fundação de Vigilância em Saúde–Dra. Rosemary Costa Pinto, Manaus (L. Gonçalves); Fundação de Medicina Tropical–Dr Heitor Vieira Dourado, Manaus (R.M.P. Figueiredo); Seção de Arbovirologia, Instituto Evandro Chagas, Ananindeua, Brazil (A.C.R. Cruz, B.T.D. Nunes); Laboratório Central de Saúde Pública do Paraná, Curitiba, Brazil (M.M. Presibella, N.F.Q. Marques, I.N. Riediger); Fundação Oswaldo Cruz, Recife, Brazil (T. Campos, G.L. Wallau); Bernhard Nocht Institute for Tropical Medicine Department of Arbovirology, Hamburg, Germany (G.L. Wallau); Fundação Oswaldo Cruz, Curitiba (T. Gräf); Universidade Federal do Espírito Santo, Alegre, Brazil (E. Delatorre); Florida Department of Health, Tampa, Florida, USA (E. Kopp, A. Morrison)

DOI: https://doi.org/10.3201/eid2907.230595

We characterized 3 autochthonous dengue virus serotype 3 cases and 1 imported case from 2 states in the North and South Regions of Brazil, 15 years after Brazil's last outbreak involving this serotype. We also identified a new Asian lineage recently introduced into the Americas, raising concerns about future outbreaks.

[1]These first authors contributed equally to this article.

[2]These senior authors contributed equally to this article.

Dengue virus serotype 3 (DENV-3) consists of 5 distinct genotypes (I–V). Genotype III (GIII) is the most widespread and was associated with large outbreaks in Asia, Africa, and the Americas (*1*). DENV-3 GIII probably emerged in the Indian subcontinent around the mid-1970s and was first introduced into the Americas in the 1990s. This introduction established an endemic lineage that evolved separately from the Asian lineage for >20 years (GIII-American-I lineage) and has been extensively transmitted across the continent in subsequent years (*2*). The most recent DENV-3 GIII-American-I lineage sequences were reported in Mexico in 2021 (GenBank accession nos. OM417340 and OM417341).

The first autochthonous case of DENV-3 GIII-American-I lineage in Brazil was reported in December 2000 in Rio de Janeiro state (Southeast Region) (*3*,*4*). This lineage caused a massive dengue outbreak in Rio de Janeiro state in 2002, and subsequent outbreaks were reported in Brazil throughout the 2000s, highlighting its rapid spread (*5*). Multiple importations of the GIII-American-I lineage from the Lesser Antilles (Caribbean) into Brazil occurred through the 2000s. The Southeast and North regions of Brazil were the most important dissemination hubs (*6*,*7*). In contrast, public data reveals that DENV-3 represented a small fraction (<1%) of total dengue cases in Brazil since 2010 (Appendix Figure, https://wwwnc.cdc.gov/EID/article/29/7/23-0595-App1.pdf), and few cases have been confirmed by sequencing. Thus, DENV-3 transmission has not been reported for the last few years, suggesting that the DENV-3 GIII-American-I lineage may have become extinct in Brazil.

We describe the genetic characterization of 4 DENV-3 cases detected in Brazil in 2023. Three autochthonous cases were detected in Roraima State by the Roraima State Central Laboratory during January 3–March 4, and 1 case imported from Suriname was detected in Paraná State by the Paraná State Central Laboratory on March 12. Serum samples were sent for sequencing at Fundação Oswaldo Cruz Amazônia (Manaus, Brazil), part of the Fundação Oswaldo Cruz Genomics Surveillance Network Consortium of Brazil's Ministry of Health. We obtained 4 complete DENV-3 genomes by using the Viral Surveillance Panel (Illumina, https://www.illumina.com), aligned them with DENV-3 sequences sampled worldwide, and analyzed them for genotyping and spatiotemporal diffusion reconstruction (Appendix).

We classified the 4 complete DENV-3 genomes detected in Brazil in 2023 as GIII according to the Flavivirus Genotyping Tool (https://www.rivm.nl/mpf/typingtool/flavivirus). Phylogenetic analysis of the

DENV-3 GIII dataset revealed that the new GIII sequences detected in Brazil branched together with sequences sampled in Puerto Rico and Florida (USA) in 2022 from both autochthonous cases and cases imported from Cuba (Figure, panel A). The new monophyletic clade consisting of DENV-3 sequences detected in the Americas during 2022–2023 (GIII-American-II lineage) nested among sequences sampled in Asia belonging to the Asian lineage of GIII over the last decade and outside the GIII-American-I lineage that consists of sequences sampled in the Americas during 1994–2021 (Figure, panel A). Thus, the identified GIII-American-II

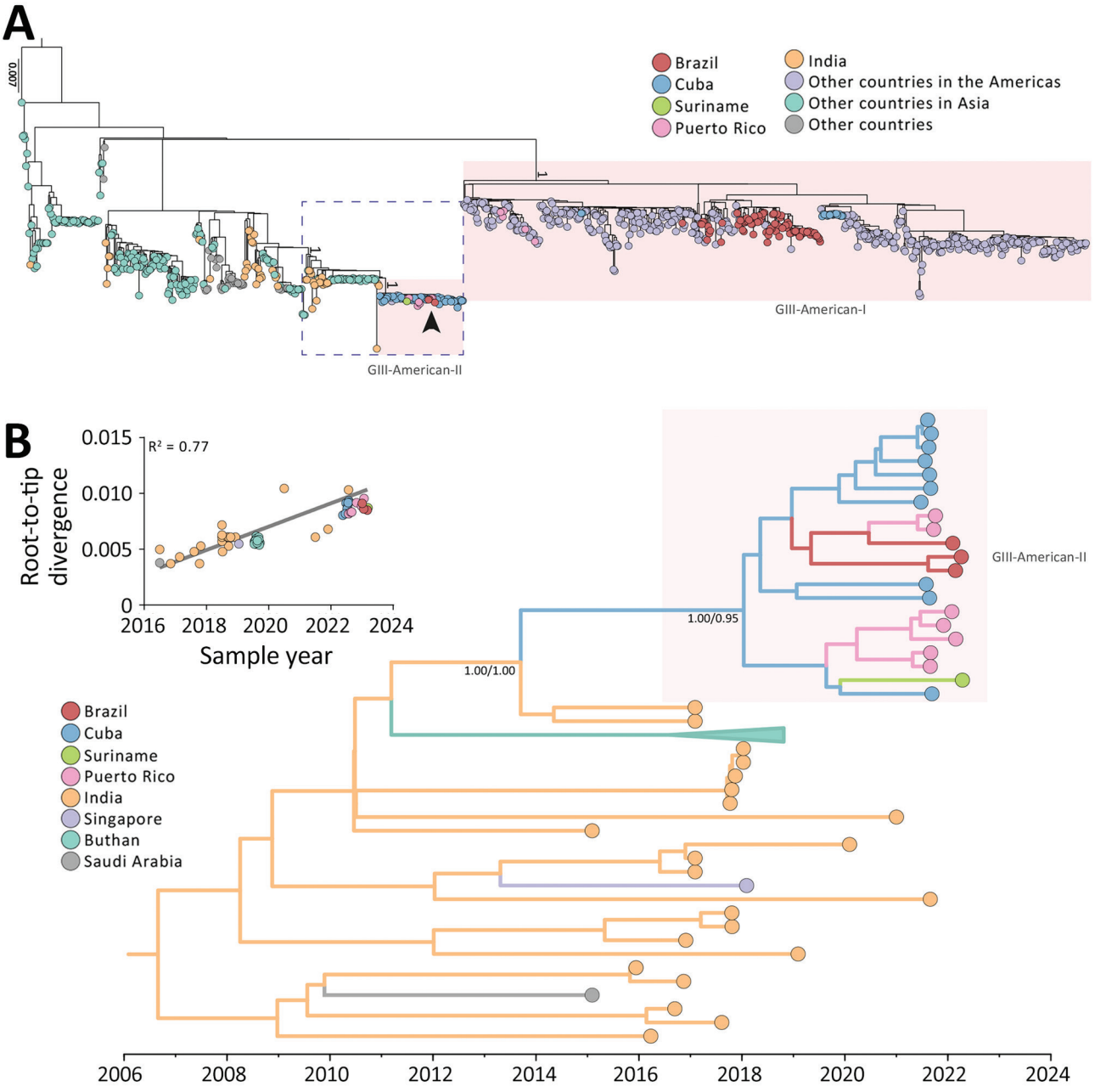

Figure. Evolutionary analysis for dengue virus serotype 3 (DENV-3) genotype III, Brazil. A) Rooted tree shows the evolutionary relationships of the complete genome sequences from the DENV-3 genotype III identified in Roraima state, Brazil (arrow), and 979 publicly available sequences from GenBank. Colors represent different sampling locations. Red highlighting shows the 2 DENV-3 GIII American lineages. The dashed blue rectangle indicates the area enlarged in panel B. Scale bar indicates nucleotide substitutions per site. B) Time-resolved maximum clade credibility tree showing the enlarged area from panel A. Colors indicate geographic sampling location. To improve visualization, the monophyletic clade for Bhutan has been collapsed. Posterior probability/posterior state probability values at key nodes show support for branching structure. Inset shows the plot of the root-to-tip genetic distance against sampling time.

lineage was not a reemergence of the GIII-American-I lineage previously established in the continent but a new introduction of GIII from Asia. The dissemination of a new DENV-3 lineage in a large and populous country like Brazil is concerning because many inhabitants may lack immunity against this serotype. Brazil has not faced recent outbreaks by this serotype; therefore, there is an increased risk for epidemics. Moreover, the endemicity of other DENV serotypes may increase the likelihood of an upsurge of severe cases.

The phylogeographic tree estimated for a subset of GIII-American-II sequences and the most closely related GIII Asian sequences (Appendix) indicates that this new American lineage was most probably introduced from the Indian subcontinent (posterior state probability 1) in 2019 (Bayesian credible interval 2018–2020) and infers that it could have circulated cryptically for ≈3 years before being detected in 2022 (Figure, panel B). Our phylogeographic analysis points to Cuba as the most probable (posterior state probability 0.95) introduction point of the GIII-American-II lineage (Figure, panel B). However, this result is probably biased by the absence of DENV-3 genomes representative of other Caribbean countries. Of note, the estimated onset date of the new GIII-American-II lineage coincides with a severe DENV-3 epidemic described in Jamaica during 2018–2019, the largest dengue outbreak reported on this Caribbean island in 40 years (*8*). Those observations support the hypothesis that the DENV-3 GIII-American-II lineage might have been introduced from India into the Caribbean Region around 2018–2019 and was more recently disseminated from the Caribbean to Brazil, Suriname, and Florida during 2022–2023.

In conclusion, our findings confirm the detection of DENV-3 GIII in the Northern Region of Brazil in 2023, associated with a new introduction of this genotype from the Indian subcontinent into the Americas. The >15-year absence and lack of widespread recent transmission of DENV-3 in Brazil might have rendered the population highly susceptible to infection by this serotype, highlighting the i mportance of early detection and the need for continuous monitoring of DENV-3 spread in Brazil and other countries in the Americas.

Author contributions: F.G.N., A.M.B.F., G.A.S., J.L.M.J., and G.B. conceived and designed the study and contributed to data analysis. R.M.M. and C.A.R.M. contributed to diagnostics, patients, and public health surveillance data analysis from Roraima State. M.M.P., N.F.Q.M., and I.N.R. contributed to diagnostics, patient, and public health surveillance data analysis from Paraná State. G.A.S., J.L.M.J., E.K., and A.M. contributed to diagnostics, patient, and sequence data from Puerto Rico and Florida, USA. G.A.S., V.A.N., V.C.S., F.O.N., D.S., M.M., and L.G. contributed with sequencing and data analysis. T.C. contributed to HPC software environment configuration and raw sequencing data analysis. F.G.N., A.M.B.F., and G.B. contributed to laboratory management and obtaining financial support. F.G.N., G.A.S., J.L.M.J., R.M.P.F., A.C.R.C., B.T.D.N., M.C.L.M., F.B.-N., P.C.S., P.R., G.L.W., E.D., T.G., and G.B. contributed to epidemiologic and phylogenetic data analysis. F.G.N, V.A.N., G.L.W., T.G., E.D., and G.B. wrote the first draft, and all authors contributed and approved the final manuscript.

About the Author

Dr. Naveca is a public health researcher at Brazil's Fundação Oswaldo Cruz, working in Rio de Janeiro and Amazonas state. His primary research interest lies in diagnostics, molecular epidemiology, and the evolution of emergent and reemergent viruses, mainly arboviruses.

References

1. Messer WB, Gubler DJ, Harris E, Sivananthan K, de Silva AM. Emergence and global spread of a dengue serotype 3, subtype III virus. Emerg Infect Dis. 2003;9:800–9. https://doi.org/10.3201/eid0907.030038
2. Araújo JM, Nogueira RM, Schatzmayr HG, Zanotto PM, Bello G. Phylogeography and evolutionary history of dengue virus type 3. Infect Genet Evol. 2009;9:716–25. https://doi.org/10.1016/j.meegid.2008.10.005
3. Miagostovich MP, dos Santos FB, de Simone TS, Costa EV, Filippis AM, Schatzmayr HG, et al. Genetic characterization of dengue virus type 3 isolates in the State of Rio de Janeiro, 2001. Braz J Med Biol Res. 2002;35:869–72. https://doi.org/10.1590/S0100-879X2002000800002
4. Nogueira RM, Miagostovich MP, de Filippis AM, Pereira MA, Schatzmayr HG. Dengue virus type 3 in Rio de Janeiro, Brazil. Mem Inst Oswaldo Cruz. 2001;96:925–6. https://doi.org/10.1590/S0074-02762001000700007
5. Nogueira RM, Schatzmayr HG, de Filippis AM, dos Santos FB, da Cunha RV, Coelho JO, et al. Dengue virus type 3, Brazil, 2002. Emerg Infect Dis. 2005;11:1376–81. https://doi.org/10.3201/eid1109.041043
6. de Araújo JM, Bello G, Romero H, Nogueira RM. Origin and evolution of dengue virus type 3 in Brazil. PLoS Negl Trop Dis. 2012;6:e1784. https://doi.org/10.1371/journal.pntd.0001784
7. Campos TL, Durães-Carvalho R, Rezende AM, de Carvalho OV, Kohl A, Wallau GL, et al. Revisiting key entry routes of human epidemic arboviruses into the mainland Americas through large-scale phylogenomics. Int J Genomics. 2018;2018:6941735. https://doi.org/10.1155/2018/6941735
8. Lue AM, Richards-Dawson MEH, Gordon-Strachan GM, Kodilinye SM, Dunkley-Thompson JAT, James-Powell TD, et al. Severity and outcomes of dengue in hospitalized Jamaican children in 2018-2019 during an epidemic surge in the Americas. Front Med (Lausanne). 2022;9:889998. https://doi.org/10.3389/fmed.2022.889998

Address for correspondence: Felipe Gomes Naveca, Instituto Leônidas e Maria Deane (Fiocruz), Amazonas, Brazil, 476 Teresina St, Adrianópolis, Manaus 69057-070, Brazil; email: felipe.naveca@.fiocruz.br

Candida auris–Associated Hospitalizations, United States, 2017–2022

Kaitlin Benedict, Kaitlin Forsberg, Jeremy A.W. Gold, James Baggs, Meghan Lyman

Author affiliation: Centers for Disease Control and Prevention, Atlanta, Georgia, USA

DOI: https://doi.org/10.3201/eid2907.230540

Using a large US hospital database, we describe 192 *Candida auris*–associated hospitalizations during 2017–2022, including 38 (20%) *C. auris* bloodstream infections. Hospitalizations involved extensive concurrent conditions and healthcare use; estimated crude mortality rate was 34%. These findings underscore the continued need for public health surveillance and *C. auris* containment efforts.

Candida auris is a highly transmissible and frequently drug-resistant emerging fungal pathogen capable of causing severe infections. *C. auris* can colonize skin, leading to infection and transmission in healthcare settings. In the United States, reported clinical cases increased by 95% during 2020–2021 (*1*). US data on *C. auris* come primarily from case series and outbreak investigations and are geographically limited, and national surveillance data lack detail on patients' underlying conditions, healthcare use, and outcomes. Therefore, we used a large healthcare services database to describe features of hospitalized patients with *C. auris* infection or colonization.

The PINC-A1 Healthcare Database (PHD) (https://offers.premierinc.com/rs/381-NBB-525/images/PINC_AI_Healthcare_Data_White_Paper.pdf) is a hospital-based all-payer database that contains healthcare use, financial, and pharmacy data from >1,000 US hospitals. Laboratory data are available from ≈25% of those hospitals. We identified all hospitalizations with a culture positive for *C. auris* from any specimen type during 2017–2022. We used diagnosis codes from the International Classification of Diseases 10th Revision, Clinical Modification, to identify underling conditions and complications (Appendix Table, https://wwwnc.cdc.gov/EID/article/29/7/23-0540-App1.pdf) and billing data to identify medical devices. We assessed features of *C. auris* hospitalizations and compared those with versus those without bloodstream infection (BSI) by using χ^2, Fisher exact, and Wilcoxon tests ($\alpha = 0.05$).

A total of 192 *C. auris* hospitalizations (38 [20%] with BSI) occurred in 42 hospitals. *C. auris* hospitalizations primarily occurred among older adults (median age 68 years [range 21–89 years]), male patients (54%), and non-Hispanic White patients (60%). Non-Hispanic Black patients more frequently had BSI than did other races/ethnicities (39% vs. 29%; p = 0.022) (Table). The first positive *C. auris* specimen was collected within 2 days of admission for 63% of bloodstream and 48% of nonbloodstream *C. auris* hospitalizations. Among hospitalizations with bloodstream *C. auris*, 58% also had another positive specimen type. Among hospitalizations without bloodstream *C. auris*, the most common positive specimen types were axilla (38%) and urine (34%).

Underlying conditions and complications were similar for patients with bloodstream and nonbloodstream *C. auris* and most commonly were sepsis (64%), diabetes (55%), chronic kidney disease (44%), and pneumonia (43%). Compared with nonbloodstream *C. auris*, bloodstream *C. auris* hospitalizations more frequently involved central venous catheters (CVC) (76% vs. 53%; p = 0.010) and tracheostomies (29% vs. 12%; p = 0.008). Echinocandin use was more frequent for bloodstream (76%) versus nonbloodstream (25%) hospitalizations; median time from first positive culture to echinocandin use was 2 days (interquartile range 1–3 days).

Most (75.5%) hospitalizations involved an intensive care unit stay; mechanical ventilation was used in 43% of hospitalization. Median hospitalization length was 13 days (range, 1–209 days). In-hospital mortality rate was 21%; discharge locations included hospice (13%), skilled nursing facility (28%), and long-term acute care (15%). Estimated crude mortality rates were 47% for bloodstream *C. auris* vs. 31% for nonbloodstream.

This analysis of a large convenience sample of *C. auris*–associated hospitalizations provides information about clinical features that are currently unavailable through national public health surveillance. Our results support smaller previous investigations showing that infection and colonization with *C. auris* occurs most commonly in patients with complex medical conditions (*2*–*5*). The proportion of *C. auris* cases involving BSI (20%) was comparable to the 9%–28% BSI rate among clinical and screening cases found in previous state-specific studies (*2*,*6*). Including in-hospital deaths and discharges to hospice, the overall estimated crude mortality rate of 34% (47% for BSI) was similar to the 30-day mortality rate from a previous study in New York (27% overall and 39% for BSI) (*2*).

Table. Characteristics of hospitalizations involving *Candida auris,* United States, 2017–2022*

Characteristics	Total, n = 192	Bloodstream infection,† n = 38	Nonbloodstream infection,‡§ n = 154	p value
Mean, median age, y (range)	66.0, 68.0 (21–89)	61.8, 66.5 (32–86)	67.0, 68.0 (21–89)	0.042
Age category, y				0.264
<45	22 (11.5)	§	§	
45–64	52 (27.1)	11 (28.9)	41 (26.6)	
≥65	118 (61.5)	20 (52.6)	98 (63.6)	
Sex				0.193
M	104 (54.2)	17 (44.7)	87 (56.5)	
F	88 (45.8)	21 (55.3)	67 (43.5)	
Race/ethnicity, n = 186				0.022
Non-Hispanic Black	45 (24.2)	14 (38.9)	31 (20.7)	
All other races/ethnicities¶	141 (75.8)	22 (61.1)	119 (79.3)	
Payer				0.483
Medicare	128 (66.7)	25 (65.8)	103 (66.9)	
Medicaid	35 (18.2)	§	§	
Private health insurance	20 (10.4)	§	§	
Other	§	§	§	
Clinical features				
Mean, median time from admission to first positive *C. auris* specimen collection, d (range)	8.6, 2.0 (1–187)	8.7, 1.0 (1–53)	8.6, 3.0 (1–187)	0.997
Within 2 d	98 (51.0)	24 (63.2)	74 (48.1)	
≥2 d	94 (49.0)	14 (36.8)	80 (51.9)	
Systemic antifungal use on or after first positive *C. auris* culture				
Echinocandin	68 (35.4)	29 (76.3)	39 (25.3)	<0.001
Fluconazole	20 (10.4)	§	§	0.081
Amphotericin B	§	§	§	0.016
Underlying conditions and complications				
Sepsis	123 (64.1)	25 (65.8)	98 (63.6)	0.804
Diabetes	106 (55.2)	20 (52.6)	86 (55.8)	0.721
Chronic kidney disease	85 (44.3)	17 (44.7)	68 (44.2)	0.949
Pneumonia	83 (43.2)	17 (44.7)	66 (42.9)	0.834
Chronic respiratory failure	61 (31.8)	15 (39.5)	46 (29.9)	0.255
Liver disease	29 (15.1)	§	§	0.099
COVID-19	24 (12.5)	§	§	0.891
Solid organ malignancy	21 (10.9)	§	§	0.502
Hematologic malignancy	§	§	§	1.000
HIV	§	§	§	0.486
Neutropenia	§	§	§	1.000
Transplant and complications	§	§	§	0.585
Medical devices				
Central venous catheter	111 (57.8)	29 (76.3)	82 (53.2)	0.010
Mechanical ventilation	83 (43.2)	18 (47.4)	65 (42.2)	0.565
Tracheostomy	29 (15.1)	11 (28.9)	18 (11.7)	0.008
Feeding tube	16 (8.3)	§	§	0.913
Urinary catheter	17 (8.9)	§	§	0.297
Total parenteral nutrition	17 (8.9)	§	10 (6.5)	0.021
Outcomes				
Mean, median length of hospitalization, d (range)	18.6, 13 (1–209)	22.5, 16.5 (1–65)	17.6, 12.0 (1–209)	0.212
Intensive care unit stay	145 (75.5)	30 (78.9)	115 (74.7)	0.583
Discharge status				0.046
In-hospital death or discharged to hospice#	65 (33.9)	18 (47.4)	47 (30.5)	0.123
Discharged to skilled nursing facility	53 (27.6)	§	§	
Discharged to long-term care acute hospital	28 (14.6)	§	§	
Other	46 (24.0)	§	§	

*Values are no. (%) patients except as indicated. Data were from the PINC-A1 Healthcare Database (PHD) (https://offers.premierinc.com/rs/381-NBB-525/images/PINC_AI_Healthcare_Data_White_Paper.pdf). Most *C. auris* hospitalizations were in the South (76.6%) or the Midwest (21.4%) regions; <10 *C. auris* hospitalizations were in the Northeast or the West regions; >95% of hospitals were in urban locations. A total of 35.4% of *C. auris* hospitalizations were from 2022, 51.0% were from 2021, and 13.5% were from 2017–2020. We found 0 *C. auris* hospitalizations for 2012–2016.
†A total of 22 (57.9%) patients also had *C. auris* isolated from another specimen type; among those, 81.8% had both specimens collected on the same day, and the remainder had the bloodstream specimen collected first.
‡Specimen types: 59 axilla, 53 urine, 18 wound, 13 respiratory, 21 other or unspecified.
§Nonzero number <10 or cell that would enable calculation of another cell <10.
¶Includes 112 (60.2%) non-Hispanic White and 21 (11.3%) Hispanic.
#Forty (20.8%) in-hospital deaths and 25 (13.0%) discharged to hospice.

Consistent with candidemia treatment guidelines, most BSI hospitalizations involved echinocandin use, and treatment lag was typical (*7*). Hospitalizations involving *C. auris* BSI were associated with non-Hispanic Black race, similar to those for non–*C. auris* candidemia (*8*). The association between CVC use and *C. auris* BSI is not surprising, given that CVC use is a well-documented risk factor for candidemia and is common among patients with *C. auris*, because extensive healthcare exposure, intensive care unit stays, and use of medical devices are key factors in *C. auris* acquisition (*2*,*9*). Many BSI patients were probably admitted with *C. auris,* based on first positive blood specimens occurring soon after admission, similar to finding from a New York case series (*3*). However, we could not assess previous healthcare exposures and prehospitalization laboratory data, which are major considerations because patients with *C. auris* usually acquire it in healthcare settings and can remain colonized for months (*9*).

Other limitations of our study include lack of antifungal susceptibility testing data, possible underdetection of cases caused by potential incompleteness of 2022 data, and underrepresentation of the West and the Northeast regions in PHD laboratory data (*10*), which is particularly relevant because those regions report high case counts (https://www.cdc.gov/fungal/candida-auris/tracking-c-auris.html). PHD laboratory data also underrepresent rural, smaller hospitals (*10*), potentially further biasing this convenience sample of *C. auris* cases. In conclusion, this analysis of hospitalization data supports previous targeted reports and demonstrates a need for strengthened national surveillance and further studies to identify risk factors for *C. auris* infection and colonization.

This activity was reviewed by the Centers for Disease Control and Prevention (CDC) and was conducted consistent with applicable federal law and CDC policy (e.g., 45 C.F.R. part 46.102(l)(2), 21 C.F.R. part 56; 42 U.S.C. §241(d); 5 U.S.C. §552a; 44 U.S.C. §3501 et seq.). PHD data are fully deidentified; thus, this analysis was not subject to review by the CDC institutional review board. No specific funding was received for this work.

About the Author

Ms. Benedict is an epidemiologist in the Mycotic Diseases Branch, Division of Foodborne, Waterborne, and Environmental Diseases, National Center for Emerging and Zoonotic Infectious Diseases, Centers for Disease Control and Prevention, Atlanta, Georgia, USA. Her research interests include the epidemiology and prevention of fungal infections.

References

1. Lyman M, Forsberg K, Sexton DJ, Chow NA, Lockhart SR, Jackson BR, et al. Worsening spread of *Candida auris* in the United States, 2019 to 2021. Ann Intern Med. 2023;176:489–95.
2. Adams E, Quinn M, Tsay S, Poirot E, Chaturvedi S, Southwick K, et al.; Candida auris Investigation Workgroup. *Candida auris* in healthcare facilities, New York, USA, 2013–2017. Emerg Infect Dis. 2018;24:1816–24. https://doi.org/10.3201/eid2410.180649
3. Park JY, Bradley N, Brooks S, Burney S, Wassner C. Management of patients with *Candida auris* fungemia at Community Hospital, Brooklyn, New York, USA, 2016–2018. Emerg Infect Dis. 2019;25:601–2. https://doi.org/10.3201/eid2503.180927
4. Prestel C, Anderson E, Forsberg K, Lyman M, de Perio MA, Kuhar D, et al. *Candida auris* Outbreak in a COVID-19 specialty care unit—Florida, July–August 2020. MMWR Morb Mortal Wkly Rep. 2021;70:56–7. https://doi.org/10.15585/mmwr.mm7002e3
5. Simon SP, Li R, Silver M, Andrade J, Tharian B, Fu L, et al. Comparative outcomes of *Candida auris* bloodstream infections: a multicenter retrospective case–control study. Clin Infect Dis. 2023;76:e1436–43. https://doi.org/10.1093/cid/ciac735
6. Pacilli M, Kerins JL, Clegg WJ, Walblay KA, Adil H, Kemble SK, et al. Regional emergence of *Candida auris* in Chicago and lessons learned from intensive follow-up at 1 ventilator-capable skilled nursing facility. Clin Infect Dis. 2020;71:e718–25. https://doi.org/10.1093/cid/ciaa435
7. Gold JA, Seagle EE, Nadle J, Barter DM, Czaja CA, Johnston H, et al. Treatment practices for adults with candidemia at 9 active surveillance sites, United States, 2017–2018. Clin Infect Dis. 2021;73:1609–16. https://doi.org/10.1093/cid/ciab512
8. Toda M, Williams SR, Berkow EL, Farley MM, Harrison LH, Bonner L, et al. Population-based active surveillance for culture-confirmed candidemia—four sites, United States, 2012–2016. MMWR Surveill Summ. 2019;68:1–15. https://doi.org/10.15585/mmwr.ss6808a1
9. Southwick K, Adams EH, Greenko J, Ostrowsky B, Fernandez R, Patel R, et al. New York State 2016–2018: progression from *Candida auris* colonization to bloodstream infection. Open Forum Infect Dis. 2039;5(Suppl 1):S594–5. https://doi.org/10.1093/ofid/ofy210.1695
10. Benedict K, Baggs J, Wolford H, Jackson BR, Gold JA. Hospitalizations for unspecified mycoses in a large administrative dataset and implications for fungal disease burden estimates, United States, 2019–2021. Open Forum Infect Dis. 2023;10:d100. https://doi.org/10.1093/ofid/ofad100

Address for correspondence: Kaitlin Benedict, Centers for Disease Control and Prevention, 1600 Clifton Rd NE, Mailstop H24-9, Atlanta, GA 30329-4027 USA; email: jsy8@cdc.gov

Isolation of *Elizabethkingia* spp. from Diagnostic Specimens from Dogs and Cats, United States, 2019–2021

J. Scott Weese, Kurtis E. Sobkowich, Zvonimir Poljak, Theresa M. Bernardo

Authors affiliation: University of Guelph, Guelph, Ontario, Canada

DOI: https://doi.org/10.3201/eid2907.230218

We retrospectively reviewed *Elizabethkingia* spp. culture and susceptibility results from 86 veterinary diagnostic laboratory results from US dogs and cats. We noted 26 *E. menigoseptica*, 1 *E. miricola*, and 59 unspeciated *Elizabethkingia* isolates from 9 US states (2–22 isolates per state). *Elizabethkingia* infections in animals might increase risks to humans.

Elizabethkingia is a genus of environmental gram-negative bacteria that can cause severe opportunistic infections in humans. The 3 main *Elizabethkingia* species are *E. meningoseptica*, the most common cause of disease; *E. miricola*; and *E. anophelis* (*1*). Human infections are rare—5–10 infections are reported annually per state in the United States (*2*)—but mortality rates can be high, 24%–41% (*1*,*3*,*4*).

Elizabethkingia infections have rarely been reported in domestic animals; 1 case was reported in a dog in Portugal (*5*), and 2 isolates were reported from horses in the United States (*6*). We describe *Elizabethkingia* spp. isolated from specimens from dogs and cats submitted to a US diagnostic veterinary laboratory for bacterial culture and susceptibility testing.

We evaluated bacterial culture results from specimens from dogs and cats that were submitted to IDEXX Laboratories (https://www.idexx.com) in the United States during 2019–2021. Available metadata included year collected, state, county, animal species, animal age, anatomic sample site, and antimicrobial susceptibility. Isolates were identified by using MALDI Biotype matrix-assisted laser desorption/ionization time-of-flight mass spectrometry (Bruker Corporation, https://www.bruker.com). Antimicrobial susceptibility was determined by using Clinical and Laboratory Standards Institute (CLSI) breakpoints for non-Enterobacterales bacteria (*7*).

In all, we investigated 86 *Elizabethkingia* spp. isolates: 26 (30%) were *E. meningoseptica*, 1 was *E. miricola*, and 59 (69%) were only identified to the genus level. All isolates were from individual animals; 71 (83%) were from dogs and 15 (17%) were from cats. Twenty-one (24%) isolates were identified in 2019, 36 (42%) in 2020, and 29 (34%) in 2021. Isolates were from 9 states, each of which had 2 (South Carolina, Tennessee) to 22 (Washington) isolates (Table 1). The most common specimen sites were skin and soft tissue infection (25; 29%), abscesses (20; 23%), ears (12; 14%), lower respiratory tract (10; 12%), nasal (6; 7.0%), and surgical site infections (3; 3.5%). We also assessed antimicrobial susceptibility data (Table 2).

Table 1. *Elizabethkingia* spp. isolated from diagnostic specimens from dogs and cats, United States, 2019–2021

State	No. isolates
Washington	22
Virginia	13
Pennsylvania	13
Oregon	11
Texas	11
Wisconsin	9
California	3
South Carolina	2
Tennessee	2

We assessed clustering at the county level over time. We noted 19 counties that had multiple isolates; 4 pairs of isolates at the county level were from specimens submitted within the same month, and another pair of isolates was submitted from a single county in subsequent months.

Although reports of *Elizabethkingia* spp. infections in animals have been limited, our data indicate that this bacterium is rare but extant in clinical specimens from dogs and cats in the United States. Noninvasive infections predominated; skin infections, abscesses,

Table 2. Antimicrobial susceptibility of *Elizabethkingia* spp. isolated from 71 dog and 15 cat diagnostic specimens, United States, 2019–2021*

Antimicrobial drug	No. tested	No. (%) susceptible
Amikacin	84	13 (15)
Amoxicillin	57	4 (7.0)
Amoxicillin-clavulanic acid	57	5 (8.8)
Cefotaxime	46	6 (13)
Cefovecin	57	5 (8.8)
Cefpodoxime	57	7 (12)
Ceftazidime	86	6 (7.0)
Ceftiofur	53	9 (17)
Cephalexin	57	3 (5.3)
Chloramphenicol	64	9 (14)
Doxycycline	59	39 (66)
Enrofloxacin	86	73 (85)
Gentamicin	85	17 (20)
Imipenem	86	7 (8.1)
Marbofloxacin	86	75 (87)
Trimethoprim/sulfamethoxazole	54	48 (89)

*Antimicrobial susceptibility testing performed according to Clinical and Laboratory Standards Institute guidelines (*7*) at IDEXX Laboratories (https://www.idexx.com).

and wound infections accounted for >50% of isolates. The distribution of infection sites is consistent with an environmental opportunist, for which infection would develop after environmental contamination of compromised sites, particularly after skin barrier damage. Those animal infections contrast with human infections, in which meningitis and bacteremia are most common (*1*,*3*). Whether those differences are because of a true difference in disease distribution or because human data are biased due to more testing of high-risk populations, such as infants and immunocompromised persons, publication biases toward reporting severe disease, or both, remains unclear.

Isolates were from multiple states. Geographic distribution of infection in humans is not well reported in the United States; however, Wisconsin was the site of a notable high incidence outbreak in humans during 2015–2016 (*8*). Further study of geographic patterns in humans and domestic animals is warranted.

Most isolates appeared to be from sporadic infections. In a few instances, 2 isolates were from the same county in the same or subsequent months. Because clinic-level data were not available, whether those isolates were from the same clinics or had any epidemiologic links is unclear. Therefore, although clustering in clinics is possible, as seen in human healthcare facilities, we could not determine whether any of these infections were linked. Because clinical data were not available, we could not determine whether *Elizabethkingia* was the cause of disease or was a clinical contaminant.

The zoonotic risks posed by animals with *Elizabethkingia* spp. infections are unknown; however, 2 equine-origin *E. anopheles* isolates clustered within a clade of human isolates in 1 instance (*6*), and another instance had a similar overlap between isolates from a frog and a human (*9*). Those findings are not unexpected for infections that likely originate in the environment but do not clarify whether zoonotic transmission can occur once an animal has a clinical infection.

Elizabethkingia isolates tend to have intrinsic resistance to multiple antimicrobial drugs (*10*). The high prevalence of susceptibility to potentiated sulfonamides (89%) and fluoroquinolones (85%–87%) for samples from dogs and cats in this study is consistent with human data (*10*), as would be expected if a common environmental source was involved.

Although rare, *Elizabethkingia* spp. were identified in dogs and cats in multiple US states. Because *Elizabethkingia* is an environmental pathogen, human and animal exposures presumably are from similar environmental sources. Thus, an understanding of infections in animals might have relevance for assessing risks to humans and for identifying potential animal health risks.

Acknowledgments

The authors thank IDEXX Laboratories for providing the data and supporting Dr. Bernardo's IDEXX Chair in Emerging Technologies and Preventive Healthcare.

About the Author

Dr. Weese is a professor at the Ontario Veterinary College, University of Guelph, Guelph, Ontario, Canada, director of the University of Guelph Centre for Public Health and Zoonoses, and chief of infection control at the Ontario Veterinary College Health Sciences Centre. His primary research interests include emerging infectious diseases in animals, zoonotic diseases, antimicrobial resistance, and antimicrobial stewardship.

References

1. Dziuban EJ, Franks JL, So M, Peacock G, Blaney DD. *Elizabethkingia* in children: a comprehensive review of symptomatic cases reported from 1944 to 2017. Clin Infect Dis. 2018;67:144–9. https://doi.org/10.1093/cid/cix1052
2. US Centers for Disease Control and Prevention. About *Elizabethkingia* [cited 2022 Dec 16]. https://www.cdc.gov/elizabethkingia/about/index.html
3. Lau SK, Chow WN, Foo CH, Curreem SO, Lo GC, Teng JL, et al. *Elizabethkingia anophelis* bacteremia is associated with clinically significant infections and high mortality. Sci Rep. 2016;6:26045. https://doi.org/10.1038/srep26045
4. Lee DH, Patel RH, Mehra I, Shenoy R, Nanjappa S, Greene J. A case series of *Elizabethkingia meningosepticum* bacteremia in the cancer population. Cureus. 2021;13:e18627. https://doi.org/10.7759/cureus.18627
5. Bordelo J, Viegas C, Coelho C, Poeta P. First report of bacteremia caused by *Elizabethkingia meningoseptica* in a dog. Can Vet J. 2016;57:994.
6. Johnson WL, Ramachandran A, Torres NJ, Nicholson AC, Whitney AM, Bell M, et al. The draft genomes of *Elizabethkingia anophelis* of equine origin are genetically similar to three isolates from human clinical specimens. PLoS One. 2018;13:e0200731. https://doi.org/10.1371/journal.pone.0200731
7. Clinical and Laboratory Standards Institute. Performance standards for antimicrobial susceptibility testing; thirty-first informational supplement (M100-S31). Wayne (PA): The Institute; 2021.
8. Perrin A, Larsonneur E, Nicholson AC, Edwards DJ, Gundlach KM, Whitney AM, et al. Evolutionary dynamics and genomic features of the *Elizabethkingia anophelis* 2015 to 2016 Wisconsin outbreak strain. Nat Commun. 2017;8:15483. https://doi.org/10.1038/ncomms15483
9. Hu R, Zhang Q, Gu Z. Whole-genome analysis of the potentially zoonotic *Elizabethkingia miricola* FL160902 with two new chromosomal MBL gene variants. J Antimicrob Chemother. 2020;75:526–30. https://doi.org/10.1093/jac/dkz480
10. Comba IY, Schuetz AN, Misra A, Friedman DZP, Stevens R, Patel R, et al. Antimicrobial susceptibility of *Elizabethkingia* species: report from a reference laboratory. J Clin Microbiol. 2022;60:e0254121. https://doi.org/10.1128/jcm.02541-21

Address for correspondence: J. Scott Weese, Department of Pathobiology, Ontario Veterinary College, University of Guelph, Guelph, ON N1G2W1, Canada; email: jsweese@uoguelph.ca

Detection of *Mycobacterium angelicum* in Human Urinary Tract, French Polynesia

Mohamed Lamine Keita,[1] Madjid Morsli,[1] Marc Levy, Grégoire Basse, Cécile Verrier, Michel Drancourt

Author affiliations: Aix-Marseille University, Marseille, France (M.L. Keita, M. Morsli, M. Drancourt); Institut Hospitalo-Universitaire Méditerranée Infection, Marseille (M.L. Keita, M. Morsli, M. Drancourt); Bacterial Virulence and Chronic Infections, INSERM U1047, Department of Microbiology and Hospital Hygiene, CHU Nîmes, University of Montpellier, Nîmes, France (M. Morsli); Centre Hospitalier de Polynésie Française, Papeete, French Polynesia (M. Levy, G. Basse, C. Verrier)

DOI: https://doi.org/10.3201/eid2907.221864

We definitively characterized *Mycobacterium angelicum*, an aquatic zoonotic opportunistic pathogen of the *M. szulgai* complex, using a polyphasic approach that included whole-genome sequencing. The sequence was obtained on the island of Tahiti, French Polynesia, from a urine specimen collected from a patient experiencing a urinary tract infection.

Mycobacterium angelicum, a slow-growing mycobacterium associated with animals living in freshwater environments, was delineated within the *M. szulgai* complex by 16S rRNA gene sequencing after its initial isolation from a freshwater angelfish (*Pterophyllum scalare*) in 2003 (*1*). In line with international recommendations (*2*), *M. angelicum* was formally described in 2015 as a new species including the seminal 2003 isolate, 2 additional isolates from freshwater fish, and a fourth isolate recovered from a freshwater tank containing tortoises (*1*). Meanwhile, another isolate was identified in Benin from the rodent *Crocidura olivieri* (*3*). A clinical isolate recovered from a respiratory tract sample taken from a patient in Northern Ireland was also tentatively identified as *M. angelicum* on the basis of 16S rRNA gene sequencing (*4*). We report another clinical isolate identified as *M. angelicum* on the basis of a polyphasic identification approach including whole-genome sequencing (WGS).

A middle-aged patient sought care for active struvite urolithiasis in the left kidney at the main hospital in Papeete, French Polynesia, 18 years after a right nephrectomy for obstructive pyonephrosis. We were unable to follow up with the patient beyond this medical episode. Of 3 successive urine samples collected over 3 consecutive days, which all lacked acid-fast bacilli after Ziehl-Neelsen staining, we successfully cultured 1 urine sample on MGIT (Becton, Dickinson and Company, https://www.bd.com) in 11 days. Culture on Löwenstein Jensen medium (Becton Dickinson) at 37°C under aerobic conditions remained negative after 3 months' incubation. This isolate positively stained by Ziehl-Neelsen staining; it exhibited rod-shaped, pink-stained bacteria measuring 3.225 ± 0.858 µm by 0.717 ± 0.048 µm under electron microscopy observation using a SU5000 SEM electron microscope (Hitachi, https://www.hitachi.com). Matrix-assisted laser desorption/ionization time-of-flight mass spectrometry using a Microflex spectrometer and software (Bruker Daltonics, https://www.bruker.com), as previously described (*5*), yielded a noninformative score of 1.31; a derived dendrogram clustered the isolate within the *M. szulgai* group. We conducted WGS concatenating Illumina (https://www.illumina.com) and Nanopore (https://nanoporetech.com) reads using Spades software version 3.15.4, as previously described (*6*); this process yielded 66.4% guanine-cytosine content, 0.23% gap ratio, and a 6,673,592-bp sequence distributed into 51 contigs encoding for 5,707 proteins, 56 tRNA, 3 rRNA, and 2 CRISPRs with a 90.5% total coding ratio. We deposited the sequence into GenBank (submission identification no. 2639860). As a first step, BLAST analysis (https://blast.ncbi.nlm.nih.gov/Blast.cgi) of the 1,326,459-bp longest contig yielded 98% coverage and 99.3% similarity with an environmental *M. angelicum* isolate strain DSM 45057 WGS (GenBank accession no. NZ_MVHE01000100) (*1*) and a 98.6% DNA–DNA hybridization using the Type Strain Genome Server (Leibniz Institute DSMZ, https://www.dsmz.de). As a second step, we used the Orthologous Average Nucleotide Identity tool version 0.93.1 (*7*); the isolate clustered with the best BLAST hit *M. angelicum* isolate with 99.73% genome similarity, whereas further genome sequence similarity values were 93.25% with *M. szulgai*, 93.01% with *M. riyadhense*, and >85% with other mycobacteria (Figure). Those data identified our isolate as the *M. angelicum* Tahiti strain; we deposited it into the Collection de Souches de l'Unité des Rickettsies (CSUR Q5816). No antimicrobial resistance–encoding sequences were predicted in the *M. angelicum* Tahiti strain genome. In agreement with the qualification of *M. angelicum* as a human pathogen by the Center for Genomic Epidemiology online platform (http://www.genomicepidemiology.org), 24 pathogenicity-associated genes were identified in the *M. angelicum* Tahiti strain, all highly conserved in

[1]These authors contributed equally to this article.

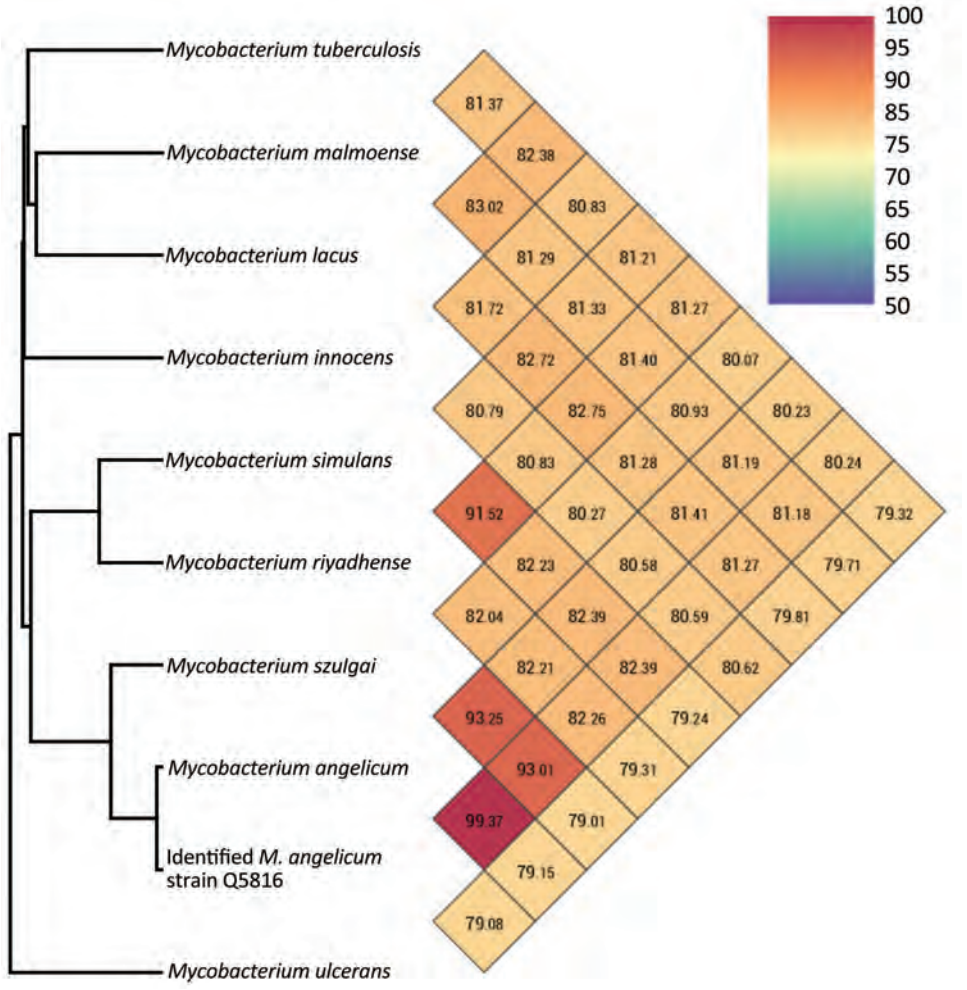

Figure. Whole-genome sequence–based clusterization of a *Mycobacterium angelicum* strain from a human urinary tract, French Polynesia. The strain clustered within the *M. szulgai* complex, based on orthoANI calculations (*7*).

Mycobacterium species (Appendix, https://wwwnc.cdc.gov/EID/article/29/7/22-1864-App1.pdf). The location of the *Clp*S gene in 74,165–74,377, its 97.14% sequence similarity with the homologous gene in *Mycobacterium*, and encoding an ATP-dependent Clp protease were predicted as nonpathogenicity factors affecting antimicrobial metabolism and rifampin resistance to protect the *Mycobacterium* cell wall against various stresses (*8*,*9*).

We identified the Tahiti strain as *M. angelicum* by combining WGS with phenotypic data in the presence of controls. The identification pathway was an opportunity to make a clinical *M. angelicum* WGS available; 1 *M. angelicum* partial genome sequence (GenBank NZ_MVHE01000100.1) derived from a freshwater angelfish isolate had been described previously (*1*). We did not find reports of *M. angelicum* as a contaminant in that study, in a urine collection device, or as a laboratory contaminant. Furthermore, we did not find previous reports of *M. angelicum* analysis in either of the 2 laboratories that handled this patient's urine or the strain itself; we concluded that this *M. angelicum* isolate was not a contaminant. This isolate was the only microorganism we were able to isolate by culture from a urine sample; however, its role in the complex urinary tract pathology of this patient remained putative.

Previously, an isolate of *M. angelicum* was identified from a bronchoalveolar sample collected from a patient with chronic obstructive pulmonary disease in Northern Ireland; identification was based on 100% partial identity (817-bp) 16S rRNA gene sequencing with the reference (*3*). Our study underscores the need for WGS sequencing of bacterial pathogens not identified by first-line phenotypic schemes, including appropriate matrix-assisted laser desorption/ionization time-of-flight mass spectrometry (*5*).

Acknowledgments

According to French law, anonymous case report does not require specific ethical approval when the patient does not oppose reporting.

M.L.K. is supported by the Fondation Meditérranée Infection. This work was supported by Microbes, Evolution, Phylogeny and Infections, Aix Marseille University, Institut de Recherche pour le Développement.

Authors' contributions: M.L.K. and M.M.: data collection, data cleaning, design of the study, data interpreting, validation and writing of the manuscript. M.L., G.B., and C.V.: clinical examination, data collection, validation, interpretation, and writing of the manuscript. M.D.: design of the study, data interpretation, validation, funding, critical review of the manuscript, coordination and direction of the work. All authors declare that they have read and approved the manuscript.

About the Authors

Mr. Keita is a PhD student in the Institut Hospitalo-Universitaire Méditerranée Infection, Marseille, France. His primary research interest is in the clinical microbiology of mycobacteria of tropical sources, including *Mycobacterium ulcerans*. Dr. Morsli is an expert in the genomics and metagenomics of mycobacteria, working at the Centre Hospitalier Universitaire, Nîmes, France.

References

1. Pourahmad F, Pate M, Ocepek M., Borroni E, Cabibbe AM, Capitolo E, et al. *Mycobacterium angelicum* sp. nov., a non-chromogenic, slow-growing species isolated from fish and related to *Mycobacterium szulgai*. Int J Syst Evol Microbiol. 2015;65:4724–4729. https://doi.org/10.1099/ijsem.0.000642
2. Christensen H, Bisgaard M, Frederiksen W, Mutters R, Kuhnert P, Olsen JE. Is characterization of a single isolate sufficient for valid publication of a new genus or species? Proposal to modify recommendation 30b of the Bacteriological Code (1990 revision). Int J Syst Evol Microbiol. 2001;51:2221–5. https://doi.org/10.1099/00207713-51-6-2221
3. Durnez L, Suykerbuyk P, Nicolas V, Barrière P, Verheyen E, Johnson CR, et al. Terrestrial small mammals as reservoirs of *Mycobacterium ulcerans* in Benin. Appl Environ Microbiol. 2010;76:4574–7. https://doi.org/10.1128/AEM.00199-10
4. Davies E, Wieboldt J, Stanley T, Maeda Y, Smyth M, Stanley S, et al. Isolation and identification of '*Mycobacterium angelicum*' from a patient with type II respiratory failure: suggested reporting guidelines to molecular clinical laboratories. Br J Biomed Sci. 2012;69:134–6. https://doi.org/10.1080/09674845.2012.12069140
5. Robinne S, Saad J, Morsli M, Hamidou ZH, Tazerart F, Drancourt M, et al. Rapid identification of *Mycobacterium tuberculosis* complex using mass spectrometry: a proof of concept. Front Microbiol. 2022;13:753969. https://doi.org/10.3389/fmicb.2022.753969
6. Morsli M, Boudet A, Kerharo Q, Stephan R, Salipante F, Dunyach-Remy C, et al. Real-time metagenomics-based diagnosis of community-acquired meningitis: a prospective series, southern France. EBioMedicine. 2022;84:104247. https://doi.org/10.1016/j.ebiom.2022.104247
7. Lee I, Ouk Kim Y, Park SC, Chun J. OrthoANI: an improved algorithm and software for calculating average nucleotide identity. Int J Syst Evol Microbiol. 2016;66:1100–3. https://doi.org/10.1099/ijsem.0.000760
8. Adilijiang G, Feng S, Mi K, Deng H. Quantitative proteomics analysis of ClpS-mediated rifampicin resistance in *Mycobacterium* [in Chinese]. Sheng Wu Gong Cheng Xue Bao. 2014 Jul;30:1115–27.
9. Marsee JD, Ridings A, Yu T, Miller JM. *Mycobacterium tuberculosis* ClpC1 N-terminal domain is dispensable for adaptor protein-dependent allosteric regulation. Int J Mol Sci. 2018;19:3651. https://doi.org/10.3390/ijms19113651

Address for correspondence: Michel Drancourt, MEPHI, IHU Méditerranée Infection, 19-21, Blvd Jean Moulin, 13005 Marseille CEDEX 05, France; email: michel.drancourt@univ-amu.fr

Low Susceptibility of Pigs against Experimental Infection with HPAI Virus H5N1 Clade 2.3.4.4b

Annika Graaf, Ronja Piesche, Julia Sehl-Ewert, Christian Grund, Anne Pohlmann, Martin Beer, Timm Harder

Author affiliation: Friedrich-Loeffler-Institut, Greifswald–Insel Riems, Germany

DOI: http://doi.org/10.3201/eid2907.230296

We found that nasal and alimentary experimental exposure of pigs to highly pathogenic avian influenza virus H5N1 clade 2.3.4.4b was associated with marginal viral replication, without inducing any clinical manifestation or pathological changes. Only 1 of 8 pigs seroconverted, pointing to high resistance of pigs to clade 2.3.4.4b infection.

Spread of highly pathogenic avian influenza (HPAI) virus H5N1 clade 2.3.4.4b of the goose/Guangdong (gs/GD) lineage, has exacerbated since early 2022 into a panzootic (*1*). Regional enzootic status in wild bird populations in Europe and North America, with lethal courses of HPAI virus infection in some species, produced large numbers of wild bird carcasses, easy prey for raptors and scavengers. Exposure of

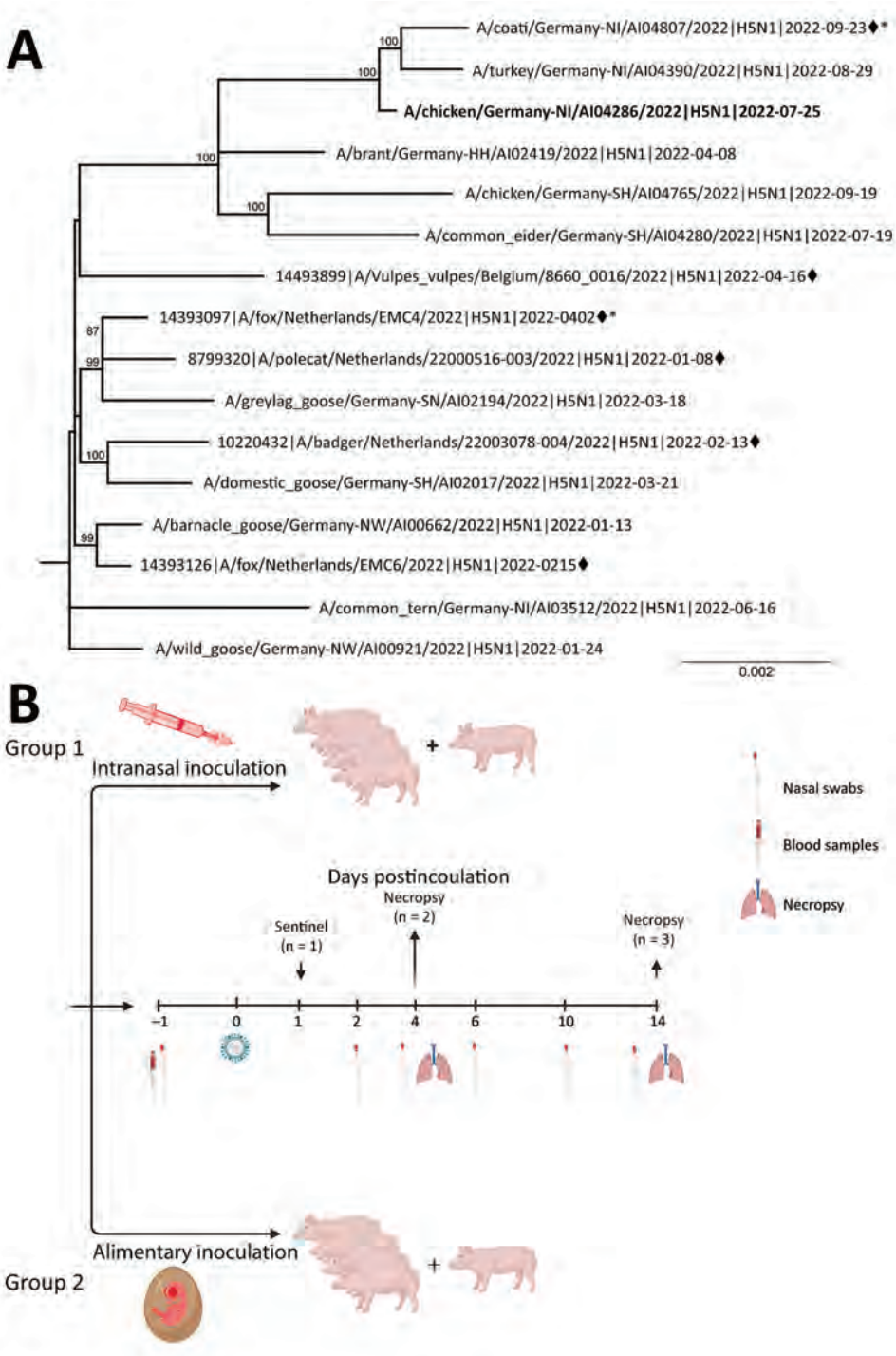

Figure. Phylogeny and experimental design for study of susceptibility of pigs against experimental infection with highly pathogenic avian influenza (HPAI) (H5N1) virus clade 2.3.4.4b. A) Maximum-likelihood phylogenetic tree (RAxML, https://cme.h-its.org/exelixis/web/software/raxml) based on 8 concatenated genome segments of selected recent HPAI H5N1 viruses from naturally infected avian hosts and from mammalian hosts (black diamonds) in Europe. Bold indicates study isolate A/chicken/Germany/AI04286/2022. Asterisks (*) indicate sequences with polymerase basic 2 E627K mutations. B) Scheme of the experimental setting of HPAI H5N1 virus infection of pigs. Four pigs, 4 months of age, were inoculated with 10^6 $TCID_{50}$ in 2 mL using mucosal atomization devices. Four pigs were each fed with 1 HPAI H5N1 virus–infected embryonated chicken egg, carrying ≈10^8–10^9 $TCID_{50}$/mL of allantoic fluid. Each pig was offered an egg, separately, in a trough and observed to complete consume it. Ten-day-old eggs were inoculated with 0.2 mL of clarified amnio-allantoic fluid of egg passage 1 and incubated for 3 days or until embryonic death was evident. Eggs were chilled until fed to pigs. Panel B created with BioRender.com and licensed by the company (agreement no. UC258UM8J3). $TCID_{50}$, 50% tissue culture infectious dose.

terrestrial carnivores and marine mammals resulted in sporadic infections, some of those terminating with fatal encephalitis (2). Frequent spill-over events, rather than consistent mammal-to-mammal transmission, were at the basis of these cases (Figure, panel A). However, recently reported HPAI outbreaks among sea lions along the Pacific coast of South America and an outbreak in a mink farm in Spain (3) may constitute first examples of avian-independent transmission chains and increase public health concerns about zoonotic transmissions of this virus. Still, the total of 11 human cases globally reported for the currently dominating H5N1 2.3.4.4b lineage did not point toward increased zoonotic propensity (4).

Possible adaption of avian influenza virus (AIV) to mammalian livestock hosts and subsequent

Table. Detection of seroconversion and of influenza A viral loads in tissues and nasal swabs of experimentally infected pigs exposed by intranasal or alimentary inoculation with HPAI virus H5N1 clade 2.3.4.4b virus*

Infection route	Day postinoculation	Animal ID	GEq, by qRT-PCR							NP-ELISA Seroconversion
			Nasal swabs†	Conchae nasalis	Trachea	Lung	Ileocaecal tonsil	Colon	Brain	
Intranasal	4	1	30	–	–	–	–	–	–	–
	4	2	150	–	–	–	–	–	–	–
	14	3	30	10	–	–	–	–	–	–
	14	4	10	60	–	10	170	200	350	+
	14	Sentinel	–	–	–	–	–	–	–	–
Alimentary	4	1	–	–	5	–	–	–	–	–
	4	2	30	–	–	–	–	–	–	–
	14	3	20	–	–	–	–	–	–	–
	14	4	140	–	–	–	–	–	–	–
	14	Sentinel	–	–	–	10	–	–	–	–
Intranasal positive control‡	4	1	300,000	10,000	860,000	5,400	NA	NA	NA	–
	4	2	83,000	35,000	56,000	1,500	NA	NA	NA	–
	4	3	750,000	4,300	1,600,000	1,500	NA	NA	NA	–
	4	4	710,000	29,000	520,000	1,100	NA	NA	NA	–

*Shown are only tissues for which >1 animal has tested positive. GEq, genome copy equivalents per 0.1 mL calculated on the basis of qRT-PCR quantification of cycle values; HPAIV, highly pathogenic avian influenza; ID, identification; NA, not applicable; qRT-PCR, quantitative reverse transcription PCR; +, positive; –, negative.
†Nasal swabs positive at day 2 postinfection for the intranasal group and day 4 postinfection for the alimentary group.
‡Four pigs, infected with the same device and dose of a swine-adapted influenza A virus strain (subtype H1avN1, clade 1C2.1) of a former study are included for comparison (*11*). Pigs were sacrificed at day 4 post infection when no seroconversion was to be expected; gastrointestinal tissues and brain were not examined.

human exposure is of particular concern. In this respect, the role of pigs as a "mixing vessel" for HPAI viruses is largely unresolved. AIV can potentially be transmitted to pigs, and further reassortment with swine influenza A viruses (swIAVs) may contribute to the emergence of pandemic strains. Rare and subclinical infections of pigs with gs/GD HPAI virus have been confirmed serologically in Vietnam, Thailand, and France (*5*) and virologically in Indonesia (clades 2.1.1 and 2.1.3), Nigeria (clade 2.3.2.1c), China (clade 2.3.4), and Italy (clade 2.3.4.4.b) (*6*–*8*).

For our study, we purchased 4-month-old pigs (6 male, 4 female) from a conventional pig holding in Germany and exposed them nasally or by the alimentary route to high doses of the recent avian-derived HPAI virus H5N1 2.3.4.4b isolate A/chicken/Germany/AI04286/2022 (genotype Ger-10.21-N1.5). The egg-grown isolate was closely related to a mammal case but lacked any mammalian-adaptive mutations (Figure, panel A). We inoculated 2 groups of 4 pigs each intranasally or by feeding 1 infected embryonated chicken egg per animal. One sentinel pig per group was associated at day 1 postinoculation to assess the transmission by direct contact to those inoculated (Figure, panel B).

After exposure, HPAI virus H5N1 detection by real-time RT-PCR was limited to day 2 (intranasal group) and day 4 (oral group) postinoculation, with a range of 10–150 genome copy equivalents per 0.1 mL (Table). An avian-derived, swine-adapted H1avN1 strain intranasally inoculated into naïve pigs at the same dose and by the same device produced 3–4 $\log_{10}$ levels greater nasal excretion in comparison (Table) (*9*). It cannot be excluded that HPAI virus H5N1 detected in nasal swabs at day 2 postinoculation still represents residual inoculum. Correspondingly, except for 1 alimentary inoculated that showed tracheal viral loads at day 4 postinoculation close to the detection limit, samples from the remaining 3 pigs euthanized at day 4 postinoculation gave no indication of viral replication in respiratory or gut tissues, regardless of the inoculation route. Only in 1 intranasally inoculated animal, euthanized at day 14 postinoculation, was viral RNA detected at low levels in organ samples. In addition to samples from the respiratory and alimentary tracts, minute amounts of RNA were found also in a brain sample of that pig. The virus could not be isolated using chicken hepatoma cells and MDCK-II cells, and histologic and immunohistochemical investigations gave no evidence for inflammatory reactions or presence of viral antigen. Low viral loads in this pig impeded sequence analysis of eventual mutants. Nonetheless, this pig was the only animal that seroconverted at 14 dpi. In agreement with the virologic findings, none of the pigs showed any clinical signs or fever within 14 days of observation.

In conclusion, only 1 of 8 pigs inoculated intranasally with HPAI virus H5N1 underwent transient, low-level infection that resulted in the presence of viral RNA in several tissue specimens and seroconversion at 14 dpi. In naturally infected wild mammals, this virus was prominently detected in the brain (*2*).

Given the detection of viral RNA in the brain of 1 intranasally inoculated pig, it cannot be excluded that longer observation might have revealed continuing viral replication in the brain of this animal. Sialic acid α2,3-gal receptors dominate on porcine brain cells, which might have fostered replication of α2,3-adapted viruses, such as HPAI virus H5N1 (*10*).

Overall, we conclude that pigs are unlikely vehicles in transmitting this genotype of HPAI virus H5N1 clade 2.3.4.4b among pigs and across interfaces. However, considering the ongoing massive panzootic of this virus, a plethora of new genotypes of the circulating strain is emerging, with possibly higher permissiveness for pigs. Therefore, swine populations need to be part of HPAI virus surveillance programs, and periodic reassessment of prepandemic propensity of circulating HPAI virus H5N1 genotypes in the swine model is required.

Acknowledgments

We acknowledge the originating and submitting laboratories that provided sequences available in the GISAID EpiFlu database (http://www.gisaid.org). We are grateful to animal keepers Doreen Fiedler, Frank Klipp, Christian Lipinski, and Steffen Kiepert.

Animal experiments were approved by the State Office for Agriculture, Food Safety and Fishery, in the Federal State of Mecklenburg-Western Pomerania, Germany (LALFF M-V 7221.3-2-010/18). All animals were kept under BioSafety Level 3 conditions in the corresponding animal facilities at Friedrich-Loeffler-Institute, Greifswald–Insel Riems, Germany.

About the Author

Dr. Graaf is a veterinary virologist at the International (World Organisation for Animal Health/Food and Agriculture Organization of the United Nations) and National Reference Laboratory for Avian Influenza at the Institute of Diagnostic Virology at the Friedrich-Loeffler-Institute. Her research interests focus on avian and swine influenza A virus surveillance in Germany.

References

1. Alkie TN, Lopes S, Hisanaga T, Xu W, Suderman M, Koziuk J, et al. A threat from both sides: Multiple introductions of genetically distinct H5 HPAI viruses into Canada via both East Asia-Australasia/Pacific and Atlantic flyways. Virus Evol. 2022;8:veac077. https://doi.org/10.1093/ve/veac077
2. Bordes L, Vreman S, Heutink R, Roose M, Venema S, Pritz-Verschuren SBE, et al. Highly pathogenic avian influenza H5N1 virus infections in wild red foxes (*Vulpes vulpes*) show neurotropism and adaptive virus mutations. Microbiol Spectr. 2023;11:e0286722. https://doi.org/10.1128/spectrum.02867-22
3. Agüero M, Monne I, Sánchez A, Zecchin B, Fusaro A, Ruano MJ, et al. Highly pathogenic avian influenza A(H5N1) virus infection in farmed minks, Spain, October 2022. Euro Surveill. 2023;28:5–10. https://doi.org/10.2807/1560-7917.ES.2023.28.3.2300001
4. Centers for Disease Control and Prevention. Ask the expert: highly pathogenic avian influenza A (H5N1) viruses [cited 2023 Apr 14]. https://www.cdc.gov/flu/avianflu/spotlights/2022-2023/avian-flu-highly-pathogenic.htm
5. Choi YK, Nguyen TD, Ozaki H, Webby RJ, Puthavathana P, Buranathal C, et al. Studies of H5N1 influenza virus infection of pigs by using viruses isolated in Vietnam and Thailand in 2004. J Virol. 2005;79:10821–5. https://doi.org/10.1128/JVI.79.16.10821-10825.2005
6. He L, Zhao G, Zhong L, Liu Q, Duan Z, Gu M, et al. Isolation and characterization of two H5N1 influenza viruses from swine in Jiangsu Province of China. Arch Virol. 2013;158:2531–41. https://doi.org/10.1007/s00705-013-1771-y
7. Meseko C, Globig A, Ijomanta J, Joannis T, Nwosuh C, Shamaki D, et al. Evidence of exposure of domestic pigs to highly pathogenic avian influenza H5N1 in Nigeria. Sci Rep. 2018;8:5900. https://doi.org/10.1038/s41598-018-24371-6
8. Nidom CA, Takano R, Yamada S, Sakai-Tagawa Y, Daulay S, Aswadi D, et al. Influenza A (H5N1) viruses from pigs, Indonesia. Emerg Infect Dis. 2010;16:1515–23. https://doi.org/10.3201/eid1610.100508
9. Graaf A, Petric PP, Sehl-Ewert J, Henritzi D, Breithaupt A, King J, et al. Cold-passaged isolates and bat-swine influenza a chimeric viruses as modified live-attenuated vaccines against influenza a viruses in pigs. Vaccine. 2022;40:6255–70. https://doi.org/10.1016/j.vaccine.2022.09.013
10. Nelli RK, Kuchipudi SV, White GA, Perez BB, Dunham SP, Chang KC. Comparative distribution of human and avian type sialic acid influenza receptors in the pig. BMC Vet Res. 2010;6:4. https://doi.org/10.1186/1746-6148-6-4

Address for correspondence: Annika Graaf, Friedrich-Loeffler-Institute, Suedufer 1017493, Greifswald–Insel Riems, Germany; email: annika.graaf@fli.de

Challenges in Forecasting Antimicrobial Resistance

Mamoon A. Aldeyab, William J. Lattyak

Author affiliations: University of Huddersfield, Huddersfield, UK (M.A. Aldeyab); Scientific Computing Associates Corp., River Forest, Illinois, USA (W.J. Lattyak)

DOI: https://doi.org/10.3201/eid2907.230489

To the Editor: We read with interest the article by Pei et al. (*1*), which discussed challenges in forecasting antimicrobial resistance (AMR) and emphasized the need for improved AMR predictive intelligence. We complement the authors on their findings and share our experience with a threshold-logistic modeling concept that we recently introduced to improve understanding of the relationship between antimicrobial drug use thresholds and incidence of resistant pathogens and a threshold transfer function model that can be used to project AMR prevalence (*2*,*3*).

AMR modeling and forecasting are challenging because of the evolutionary ability of pathogens to adapt to changing environmental conditions. To be useful, a model should address time-varying effects of explanatory variables on response function and changes in the structural relationship between predictor and target variables. Concepts such as threshold transfer function modeling that includes autoregressive moving average components can partially address those issues. Model recalibration is essential and dictated by breakdown in predictive ability. Model parameters can be reestimated after recording new observations. Model structure does not change, but parameter estimates are updated to reflect new information. If statistical significance of a parameter falls below a defined confidence level, model structure might need modification. In practice, model estimation and assessment can be automated. Forecasting model accuracy can also be automated by comparing ongoing performance to baseline accuracy. When model or predictive performance degradation is flagged, a more comprehensive model recalibration is dictated. The time between model calibrations is unknown and depends on the stability of identified relationships in the model and degree to which evolutionary changes in AMR are observed. Further real-world testing is required to determine other factors that can explain resistance and define thresholds, find optimal interventions to reduce antimicrobial drug use to identified thresholds, and assess feasibility of implementing those interventions in daily clinical practice.

References

1. Pei S, Blumberg S, Vega JC, Robin T, Zhang Y, Medford RJ, et al.; CDC MIND-Healthcare Program. Challenges in forecasting antimicrobial resistance. Emerg Infect Dis. 2023;29:679–85. https://doi.org/10.3201/eid2904.221552
2. Aldeyab MA, Bond SE, Conway BR, Lee-Milner J, Sarma JB, Lattyak WJ. Identifying antibiotic use targets for the management of antibiotic resistance using an extended-spectrum β-lactamase-producing *Escherichia coli* case: a threshold logistic modeling approach. Antibiotics (Basel). 2022;11:1116. https://doi.org/10.3390/antibiotics11081116
3. Aldeyab MA, Bond SE, Conway BR, Lee-Milner J, Sarma JB, Lattyak WJ. A threshold logistic modelling approach for identifying thresholds between antibiotic use and methicillin-resistant *Staphylococcus aureus* incidence rates in hospitals. Antibiotics (Basel). 2022;11:1250. https://doi.org/10.3390/antibiotics11091250

Address for correspondence: Mamoon A Aldeyab, Department of Pharmacy, School of Applied Sciences, University of Huddersfield, Huddersfield HD1 3DH, UK; email: m.aldeyab@hud.ac.uk

In Response: Real-time evaluation of predictive models for antimicrobial resistance (AMR) is critical for real-world applications, as indicated in our recently published article (*1*). Aldeyab and Lattyak introduced a threshold-logistic regression model that links antimicrobial drug use to AMR prevalence in hospital settings (*2*). The authors advocate implementing and testing this model in hospitals to assess operational utility. I agree that this is a practical starting point to challenge time-series model use for real-time AMR predictions. Most time-series models have been validated in retrospective analyses. Translational research is needed to promote the use of those models for real-world AMR control.

The authors mention several practical considerations when applying time-series models in real time, including stationarity of both predictor and target variables and criteria for model recalibration. Evaluating methods to address those issues is crucial to achieve desirable performance in hospital settings. In addition to those technical challenges, several broader questions remain regarding model design and utility. First, how much AMR prevalence variation can be explained by antimicrobial drug use? Are there other essential factors (e.g., community introduction) that should be included in the model? Second, how will healthcare providers and hospitals use AMR forecasts? What policies will be informed by forecasts, and what are the downstream effects? Answers to those questions will help determine the eventual real-world utility of predictive models.

Evaluating real-time AMR prediction is a complicated task. By drawing experience from computer vision (*3*) and forecasts for other infectious diseases (*4*–*6*), open-access challenges with transparent and fair evaluation methods run in a common task framework (*7*) can substantially stimulate the advance of predictive methods and might produce robust application models. Such collaborative efforts are needed to evaluate existing methods, identify difficulties and solutions, and push the operational use of AMR predictive models forward.

Acknowledgments

This work was supported by the US Centers for Disease Control and Prevention, grant nos. U01CK000592 and 75D30122C14289.

References

1. Pei S, Blumberg S, Vega JC, Robin T, Zhang Y, Medford RJ, et al.; CDC MIND-Healthcare Program. Challenges in forecasting antimicrobial resistance. Emerg Infect Dis. 2023;29:679–85. https://doi.org/10.3201/eid2904.221552
2. Aldeyab MA, Lattyak WJ. Challenges in forecasting antimicrobial resistance. Emerg Infect Dis. 2023 Jul [*date cited*]. https://doi.org/10.3201/eid2907.230489
3. Russakovsky O, Deng J, Su H, Krause J, Satheesh S, Ma S, et al. ImageNet large scale visual recognition challenge. Int J Comput Vis. 2015;115:211–52. https://doi.org/10.1007/s11263-015-0816-y
4. Cramer EY, Ray EL, Lopez VK, Bracher J, Brennen A, Castro Rivadeneira AJ, et al. Evaluation of individual and ensemble probabilistic forecasts of COVID-19 mortality in the United States. Proc Natl Acad Sci USA. 2022;119:e2113561119. https://doi.org/10.1073/pnas.2113561119
5. Reich NG, Brooks LC, Fox SJ, Kandula S, McGowan CJ, Moore E, et al. A collaborative multiyear, multimodel assessment of seasonal influenza forecasting in the United States. Proc Natl Acad Sci USA. 2019;116:3146–54. https://doi.org/10.1073/pnas.1812594116
6. Johansson MA, Apfeldorf KM, Dobson S, Devita J, Buczak AL, Baugher B, et al. An open challenge to advance probabilistic forecasting for dengue epidemics. Proc Natl Acad Sci USA. 2019;116:24268–74. https://doi.org/10.1073/pnas.1909865116
7. Donoho D. 50 years of data science. J Comput Graph Stat. 2017; 26:745–66. https://doi.org/10.1080/10618600.2017.1384734

Address for correspondence: Sen Pei, Department of Environmental Health Sciences, Mailman School of Public Health, Columbia University, New York, NY 10032, USA; email: sp3449@cumc.columbia.edu

Sen Pei

Author affiliations: Columbia University, New York, New York, USA

DOI: https://doi.org/10.3201/eid2907.230617

Dangerous Medicine: The Story Behind Human Experiments with Hepatitis

Sydney Halpern

Yale University Press, 2021, New Haven, Connecticut, USA; ISBN-10: 030025962; ISBN-13: 978-0300259629; Pages: 304; Price: $30.00

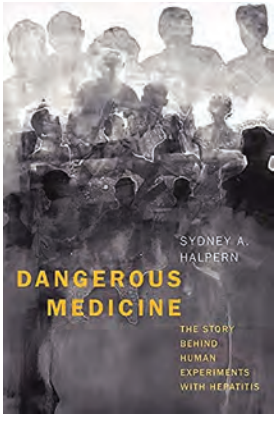

Does the good of the public ever outweigh individual risk? What responsibility do scientists, research sponsors and the government have for clinical study participants, particularly those from vulnerable populations?

Dr. Sydney Halpern tackles these fundamental questions in *Dangerous Medicine: The Story Behind Human Experiments with Hepatitis*, as she tells the compelling and largely hidden story of the hepatitis experiments that took place in the United States during World War II and most of the Cold War. Those experiments involved infecting persons, primarily prisoners, conscientious objectors, and institutionalized, developmentally disabled children, with hepatitis. Throughout most of the experiments, scientists had not yet identified the distinct hepatitis viruses. Thus, while they justified their studies as the pursuit of ending hepatitis epidemics through development of a vaccine, they didn't realize that they were infecting persons with a mix of hepatitis A, B, and C viruses. They also didn't fully understand the ramifications; both hepatitis B and C could lead to chronic, lifelong infections that would increase a person's lifetime liver cancer risk by as much as 40%.

The author does an excellent job of setting up the sociopolitical climate that fostered the hepatitis experiments and of highlighting the roles that politics, media, the scientific elite, and wartime sentiment played. Science in the name of national defense created a moral imperative for persons who were not doing their duty as Americans (i.e., war objectors and prisoners) to contribute to society by volunteering their health. The recruitment of institutionalized children had a different, but still highly troubling, narrative, one of coercion and misinformation. Dr. Halpern expertly guides readers in an exploration of who controls the narrative, and thus the power.

The hepatitis studies played an important role in the rise of bioethics and creation of federal oversight of clinical research. Dr. Halpern discusses the complexities of informed consent and coercion and the ethics of research among vulnerable populations. The reader is asked to consider the responsibility (or lack thereof) that researchers and research sponsors hold to mitigate the long-term impacts of participating in clinical studies. She points out that we have not yet adequately explored the extent of the harms of the hepatitis experiments. We must continue to wrestle with the fundamental ethical questions inherent in clinical research to prevent creating such harmful situations now and into the future.

This book is important to read at any time, but perhaps no more so than today. As we face new infectious challenges like SARS-CoV-2, we run the risk of conducting clinical research in the dark, without knowing the actual risks and harms of studies to induce infection. A for-the-greater-good mentality is a slippery slope, which erroneously justifies deliberate risk in the face of public health crisis.

Dr. Halpern provides comprehensive detail throughout the book without losing sight of the narrative, and she weaves in perspectives from study participants themselves. In doing so, she crafts a well-balanced, authoritative, engaging story that will be appreciated by researchers, clinicians, public health professionals, and anyone interested in the history of science and bioethics.

Chari Cohen

Author affiliation: Hepatitis B Foundation, Doylestown, Pennsylvania, USA

DOI: http://doi.org/10.3201/eid2907.230064

Address for correspondence: Chari Cohen, Hepatitis B Foundation, 3805 Old Easton Rd, Doylestown, PA 18902-8400, USA; email: chari.cohen@hepb.org

Biho Takashi (active ca. 1890–1930). *Bat in Moon*, ca. 1905. Color woodblock print on paper, 9 1/4 in × 9 9/16 in/23.5 cm × 24.3 cm. Brooklyn Museum, Brooklyn, New York, USA. Gift of the Estate of Dr. Eleanor Z. Wallace, 2007.32.4

"On the Bat's Back I Do Fly after Summer Merrily"

Byron Breedlove

The only mammals that can fly, bats play a vital role in maintaining healthy ecosystems. They devour large amounts of insect pests; pollinate hundreds of species of fruit, including avocados, bananas, and mangoes; and spread seeds of a number of plants, including cacao, figs, and nuts. This month's cover image, *Bat in Moon* by Biho Takashi, portrays a soaring bat silhouetted across a full moon. A fitting caption can be taken from Ariel's words in Act V, Scene I, of *The Tempest* by William

Author affiliation: Centers for Disease Control and Prevention, Atlanta, Georgia, USA

DOI: https://doi.org/10.3201/eid2907.AC2907

Shakespeare: "On the bat's back I do fly after summer merrily."

Little is known about the artist Biho Takashi. Even his actual name cannot be verified. Woodblocks attributed to Takahashi Bihō or Hirose Bihō bear signatures identical to his. The Five Colleges and Historic Deerfield Museum Consortium in western Massachusetts offers that Biho "was a designer of kachō-e, or 'animal and flower pictures' and that he used a gradient effect known as bokashi in many of his works."

Biho's skill with bokashi is revealed by the textures of the bat's wings, its folded legs visible as creases in the taut wing membranes and its whiskers, claws, wingtips, and tail crisply revealed. The night sky lightens in the bottom third of the image, and its blankness refocuses attention to the bat and moon. The viewer can appreciate the grace and form of an animal that contributes to healthy ecosystems but is also sometimes vilified because of superstition and its role as a host for pathogens that can infect humans. Bats are hosts for a number of viruses that affect humans, and their droppings, when present in large quantity, can potentially infect humans with the fungal disease histoplasmosis.

Researchers James Wynne and Lin-Fa Wang wrote, "In many respects, bats represent the perfect reservoir for emerging zoonotic pathogens. They often live in large colonies or roosts; they can, through flight, travel and disseminate viruses over considerable distances; and they enjoy remarkable longevity for their body size." However, some of those same attributes that enable bats to be effective reservoirs for viral infections, including their living in large colonies, have had deadly consequences for some bat species.

During the past 2 decades across North America, bat populations have been declining precipitously because of *Pseudogymnoascus destructans*, commonly known as white-nose syndrome fungus. Bats infected with this emerging fungus were first detected in the United States in 2006 in a cave frequented by tourists near Albany, New York. Veterinary pathologist Lisa Farina and wildlife pathologist Julie Lankton have stated that an estimated 6 million bats died from this infection within a decade after its discovery and that it "may represent the largest mammalian wildlife mortality event in recorded history."

Although this fungus also exists in bats in Europe, it has not proven to cause extensive mortality among those populations. No current evidence suggests this pathogen can infect humans, but circumstantial evidence suggests that, because *P. destructans* survives on shoes, clothing, or gear, humans may have transmitted it to that New York hibernaculum after visiting caves in European locales.

As the Centers for Disease Control and Prevention notes, "Disease spread by fungi are a One Health issue—fungi that cause human diseases live in the environment and some can spread between animals and people." Perhaps the appearance of *P. destructans* in bats and *Batrachochytrium dendrobatidis,* a waterborne fungal pathogen that causes chytridiomycosis in amphibians, were bellwether events regarding the emergence of infectious fungal diseases.

In October 2022, the World Health Organization issued a report stating, "Fungal pathogens are a major threat to public health as they are becoming increasingly common and resistant to treatment with only four classes of antifungal medicines currently available, and few candidates in the clinical pipeline. Most fungal pathogens lack rapid and sensitive diagnostics and those that exist are not widely available or affordable globally." That report categorized 19 fungal pathogens as priorities and ranked four as critical for public health: *Cryptococcus neoformans*, *Candida auris*, *Aspergillus fumigatus*, and *Candida albicans.* Factors driving the emergence and spread of fungal diseases include climate change, human migration and mass transit, and environmental contamination with antifungal agents. The World Health Organization report explains that among those at highest risk for developing fungal infections are immunocompromised persons, including patients with chronic obstructive pulmonary disease, liver or kidney disease, and viral respiratory tract infections. The report also notes, "The coronavirus disease (COVID-19) pandemic has been associated with an increase in the incidence of comorbid invasive fungal infections."

Worldwide, fungal infections impose significant healthcare costs and cause substantial morbidity and mortality. In this issue of EID, researchers Jeremy A.W. Gold and colleagues state, "In the United States, fungal infections impose considerable healthcare costs (≈$6.7 billion during 2018) and cause substantial illness and death (>7,000 deaths during 2021)." Other articles document the range and variety of fungal infections affecting humans, including significant increases of severe infections from *C. auris* in healthcare settings in Israel and, from the United States, unusual cases of coccidioidomycosis affecting patient's ears and incidents of patients who died of fatal invasive mold infections after receiving transplanted organs from drowned donors. Tackling the problems posed by infectious fungal diseases requires public health resources for researchers to develop new antifungal medicines and improve surveillance and diagnostics. Takashi's *Bat in Moon* serves as an emblematic reminder of the value of scientific research at the One Health intersection of human, animal, and environmental health.

Bibliography

1. Campana MG, Kurata NP, Foster JT, Helgen LE, Reeder DM, Fleischer RC, et al. White-nose syndrome fungus in a 1918 bat specimen from France. Emerg Infect Dis. 2017;23:1611–2. https://doi.org/10.3201/eid2309.170875
2. Eskew EA, Todd BD. Parallels in amphibian and bat declines from pathogenic fungi. Emerg Infect Dis. 2013;19:379–85. https://doi.org/10.3201/eid1903.120707
3. Farina LL, Lankton JS. Chiroptera. In: Terio KA, McAloose, St. Leger DJ, editors. Pathology of Wildlife and Zoo Animals. New York: Academic Press; 2018. p. 607−33. https://doi.org/10.1016/B978-0-12-805306-5.00025-0
4. Five Colleges and Historic Deerfield Museum Consortium. Hirose Bihō; Hirose Yoshikuni [cited 2023 May 4]. https://museums.fivecolleges.edu/detail.php?museum=&t=objects&type=exact&f=&s=aii&record=6
5. Gold JA, Adjei JS, Gundlapalli AV, Huang YL, Chiller T, Benedict K, et al. Increased hospitalizations involving fungal infections during COVID-19 pandemic, United States, January 2020–December 2021. Emerg Infect Dis. 2023;29:1433–7.
6. Lorch JM, Palmer JM, Lindner DL, Ballmann AE, George KG, Griffin K, et al. First detection of bat white-nose syndrome in western North America. mSphere. 2016;1:e00148–16. https://doi.org/10.1128/m9Sphere.00148-16
7. Merritt H, Yamada N. Bihō. In: Merritt H, Yamada N, editors. Guide to modern Japanese woodblock prints. Honolulu: University of Hawaii Press; 1992.
8. US Department of the Interior. 13 awesome facts about bats [cited 2023 May 30]. https://www.doi.gov/blog/13-facts-about-bats
9. World Health Organization. Fungal priority pathogens list to guide research, development and public health action [cited 2023 Jun 6]. https://www.who.int/publications/i/item/9789240060241
10. Wibbelt G, Kurth A, Hellmann D, Weishaar M, Barlow A, Veith M, et al. White-nose syndrome fungus (*Geomyces destructans*) in bats, Europe. Emerg Infect Dis. 2010;16:1237–43. https://doi.org/10.3201/eid1608.100002
11. Wynne JW, Wang L-F. Bats and viruses: friend or foe? PLoS Pathog. 2013;9:e1003651. https://doi.org/10.1371/journal.ppat.1003651

Address for correspondence: Byron Breedlove, EID Journal, Centers for Disease Control and Prevention, 1600 Clifton Rd NE, Mailstop H16-2, Atlanta, GA 30329-4027, USA; email: wbb1@cdc.gov

etymologia revisited

Scrapie

[skra'pe]

Scrapie is a fatal neurodegenerative disease of sheep and goats that was the first of a group of spongiform encephalopathies to be reported (1732 in England) and the first whose transmissibility was demonstrated by Cuille and Chelle in 1936. The name resulted because most affected sheep develop pruritis and compulsively scratch their hides against fixed objects. Like other transmissible spongiform encephalopathies, scrapie is associated with an alteration in conformation of a normal neural cell glycoprotein, the prion protein. The scrapie agent was first described as a prion (and the term coined) by Stanley Prusiner in 1982, work for which he received the Nobel Prize in 1997.

Originally published in June 2020

References:

1. Brown P, Bradley R. 1755 and all that: a historical primer of transmissible spongiform encephalopathy. BMJ. 1998;317:1688–92.
2. Cuillé J, Chelle PL. The so-called "trembling" disease of sheep: is it inoculable? [in French]. Comptes Rendus de l'Académie Sciences. 1936;203:1552.
3. Laplanche J-L, Hunter N, Shinagawa M, Williams E. Scrapie, chronic wasting disease, and transmissible mink encephalopathy. In: Prusiner SB, editor. Prion biology and diseases. Cold Spring Harbor (NY): Cold Spring Harbor Laboratory Press; 1999. p. 393–429.
4. Prusiner SB. Novel proteinaceous infectious particles cause scrapie. Science. 1982;216:136–44.

https//wwwnc.cdc.gov/eid/article/26/6/et-2606_article

EMERGING INFECTIOUS DISEASES®

Upcoming Issue • Unexpected Hazards

- Clinical Characteristics of *Corynebacterium ulcerans* Infection, Japan
- Waterborne Infectious Diseases Associated with Exposure to Tropical Cyclonic Storms, United States
- Economic Evaluation of Wastewater Surveillance Combined with Clinical COVID-19 Screening Tests, Japan
- Prospecting for Zoonotic Pathogens by Using Targeted DNA Enrichment
- Genome-Based Epidemiologic Analysis of VIM/IMP Carbapenemase-Producing *Enterobacter* spp., Poland
- Elimination of *Dirofilaria immitis* Infection in Dogs, Linosa Island, Italy, 2020–2022
- Predicting COVID-19 Incidence Using Wastewater Surveillance Data, Denmark, October 2021–June 2022
- Emerging *Corynebacterium diphtheriae* Species Complex Infections, Réunion Island, France, 2015–2020
- Soft Tissue Infection of Immunocompetent Man with Cat-Derived *Globicatella* Species
- Infected Aneurysm Caused by *Desulfovibrio desulfuricans* Infection
- Chromosome-Borne CTX-M-65 Extended-Spectrum β-Lactamase–Producing *Salmonella enterica* Serovar Infantis, Taiwan
- Multidrug Resistant *Shigella sonnei* Bacteremia among Persons Experiencing Homelessness, Vancouver, British Columbia, Canada
- Human Fecal Carriage of *Streptococcus agalactiae* ST283, Thailand
- SARS-CoV-2 Variants and Age-Dependent Infection Rates among Household and Nonhousehold Contacts.
- Fatal Meningitis from Shiga Toxin–Producing Escherichia coli in 2 Full-Term Neonates, France
- Case of Extensively Drug-Resistant *Shigella sonnei* Infection, United States
- Longitudinal Association of COVID-19 Hospitalization and Death with Online Search for Loss of Smell or Taste
- Rio Negro Virus Infection, Bolivia, 2021
- Rapid Serologic Test for Diagnosis of Yaws in Patients with Suspicious Skin Ulcers
- Healthcare-Associated Infections Caused by *Mycolicibacterium neoaurum*

Complete list of articles in the August issue at https://wwwnc.cdc.gov/eid/#issue-301

Earning CME Credit

To obtain credit, you should first read the journal article. After reading the article, you should be able to answer the following, related, multiple-choice questions. To complete the questions (with a minimum 75% passing score) and earn continuing medical education (CME) credit, please go to http://www.medscape.org/journal/eid. Credit cannot be obtained for tests completed on paper, although you may use the worksheet below to keep a record of your answers.

You must be a registered user on http://www.medscape.org. If you are not registered on http://www.medscape.org, please click on the "Register" link on the right hand side of the website.

Only one answer is correct for each question. Once you successfully answer all post-test questions, you will be able to view and/or print your certificate. For questions regarding this activity, contact the accredited provider, CME@medscape.net. For technical assistance, contact CME@medscape.net. American Medical Association's Physician's Recognition Award (AMA PRA) credits are accepted in the US as evidence of participation in CME activities. For further information on this award, please go to https://www.ama-assn.org. The AMA has determined that physicians not licensed in the US who participate in this CME activity are eligible for AMA PRA Category 1 Credits™. Through agreements that the AMA has made with agencies in some countries, AMA PRA credit may be acceptable as evidence of participation in CME activities. If you are not licensed in the US, please complete the questions online, print the AMA PRA CME credit certificate, and present it to your national medical association for review.

Article Title

Clinical and Mycologic Characteristics of Emerging Mucormycosis Agent *Rhizopus homothallicus*

CME Questions

1. Your patient is a 46-year-old man with mucormycosis. On the basis of the retrospective review of consecutive mucormycosis cases from a tertiary care center in India by Shivaprakash and colleagues, which one of the following statements about the proportion of *Rhizopus homothallicus* infection and clinical characteristics, including 30-day mortality in rhino-orbital mucormycosis (ROM) from *R. homothallicus* vs *Rhizopus arrhizus*, of emerging *R. homothallicus* is correct?

A. *R. homothallicus* accounted for 18% of mucormycosis cases
B. *R. homothallicus* infection was independently associated with worse survival than R arrhizus infection
C. Mortality of subjects with ROM from *R. homothallicus* was significantly worse for COVID-19-associated mucormycosis (CAM) vs non-CAM subgroups
D. Mean age for patients with R arrhizus ROM was significantly higher than for those with *R. homothallicus* ROM

2. On the basis of the retrospective review of consecutive mucormycosis cases from a tertiary care center in India by Shivaprakash and colleagues, which one of the following statements about the mycological characteristics, including antifungal susceptibility testing and amplified fragment length polymorphism analysis, of emerging *R. homothallicus* is correct?

A. 18S gene sequencing and amplified length polymorphism revealed distinct clustering of *R. homothallicus*
B. Minimum inhibitory concentrations for *R. homothallicus* were high for itraconazole and posaconazole
C. *R. homothallicus* antifungal susceptibility testing showed amphotericin B resistance
D. Clades among isolates of *R. homothallicus* differed significantly in patients with CAM vs non-CAM

3. According to the retrospective review of consecutive mucormycosis cases from a tertiary care center in India by Shivaprakash and colleagues, which one of the following statements about clinical implications of the clinical and mycological characteristics of emerging *R. homothallicus* is correct?

A. The study revealed why *R. homothallicus* emerged in India during the COVID-19 pandemic
B. *R. homothallicus* is an important agent of mucormycosis with epidemiological and clinical significance
C. Compared with *R. arrhizus*, *R. homothallicus* may be more virulent or present later in the course of infection
D. Identifying *R. homothallicus* from macroscopic and microscopic appearance is challenging

Earning CME Credit

To obtain credit, you should first read the journal article. After reading the article, you should be able to answer the following, related, multiple-choice questions. To complete the questions (with a minimum 75% passing score) and earn continuing medical education (CME) credit, please go to http://www.medscape.org/journal/eid. Credit cannot be obtained for tests completed on paper, although you may use the worksheet below to keep a record of your answers.

You must be a registered user on http://www.medscape.org. If you are not registered on http://www.medscape.org, please click on the "Register" link on the right hand side of the website.

Only one answer is correct for each question. Once you successfully answer all post-test questions, you will be able to view and/or print your certificate. For questions regarding this activity, contact the accredited provider, CME@medscape.net. For technical assistance, contact CME@medscape.net. American Medical Association's Physician's Recognition Award (AMA PRA) credits are accepted in the US as evidence of participation in CME activities. For further information on this award, please go to https://www.ama-assn.org. The AMA has determined that physicians not licensed in the US who participate in this CME activity are eligible for AMA PRA Category 1 Credits™. Through agreements that the AMA has made with agencies in some countries, AMA PRA credit may be acceptable as evidence of participation in CME activities. If you are not licensed in the US, please complete the questions online, print the AMA PRA CME credit certificate, and present it to your national medical association for review.

Article Title

Rising Incidence of *Sporothrix brasiliensis* Infections, Curitiba, Brazil, 2011–2022

CME Questions

1. You are advising a tropical medicine practice about cat-transmitted sporotrichosis (CTS). On the basis of the medical record review of 216 sporotrichosis cases diagnosed during 2011 to 2022 in Curitiba, Brazil, by Cognialli and colleagues, which one of the following statements about CTS disease incidence, demographics, and clinical and laboratory findings is correct?

A. Proven sporotrichosis was established in one quarter of sporotrichosis cases
B. Ocular was the main clinical form of sporotrichosis
C. CTS was more frequent in males than females
D. 11% of patients had occupational risk factors

2. On the basis of the medical record review of 216 sporotrichosis cases diagnosed during 2011 to 2022 in Curitiba, Brazil, by Cognialli and colleagues, which one of the following statements about CTS incidence trends and geographic distribution is correct?

A. Incidence rate rose from 0.3 cases per 100,000 outpatient visit-years (OPVY) in 2011 to 21.4 cases per 100,000 OPVY in 2021
B. CTS was associated with zoonotic transmission in three quarters of cases
C. The first substantial increase in the number of cases and incidence was in 2020
D. Critical CTS hotspots were mostly in affluent areas of the city

3. According to the medical record review of 216 sporotrichosis cases diagnosed during 2011 to 2022 in Curitiba, Brazil, by Cognialli and colleagues, which one of the following statements about clinical and public health implications of CTS disease incidence, clinical syndromes, and geographic distribution is correct?

A. A One Health approach is unlikely to help control CTS
B. CTS control depends primarily on veterinarians
C. Development of anti-CTS vaccines, specifically for cats, is needed to help control CTS
D. Recent stabilization of sporotrichosis incidence indicates successful efforts to prevent CTS transmission